Organic chemistry and mineral interactions in the solar system

Thesis

Organic Chemistry and Mineral Interactions in the Solar System

Michael David Goodyear

BSc (Open) 2007
MA (Cambridge) 1979
PhD (Manchester) 1978
BA (Cambridge) 1975

This thesis is submitted for the degree of
Doctor of Philosophy

Department of Physical Sciences
The Open University

Submitted September 2013

Abstract

The objective of this project was to develop methods to detect meteoritic organic compounds *in situ*, and to determine whether any associations exist between specific classes of compound and co-located minerals, thus indicating a possible common origin. Carbonaceous chondrites, (which comprise a small proportion of meteorites), contain a few per cent of organic material, heterogeneously distributed within their structure, the major part being macromolecular ("insoluble organic material", IOM). Model compounds were covalently bonded to "molecular tags", atoms or groups not normally present in meteorites, enabling easier detection against background signals when using analytical methods suitable for use *in situ*, such as Raman spectroscopy or SEM. Also, extra functionality was introduced to model compounds by ozone treatment, allowing a greater density of tags to be attached. Following development work with terrestrial models, meteorite samples were exposed to ozone, but oxalic acid was formed instead of the expected oxygenated IOM derivative. To determine if this result was due to an effect of the minerals present, whole rock samples and demineralised IOM were analysed, both before and after exposure to ozone. Isolated IOM behaved differently from that still *in situ*. Fresh samples of IOM were isolated (using two literature methods), and their reactions and properties compared. The evidence obtained indicated that the structure of IOM had been modified on isolation, and that the modifications caused by the two methods were different. This shows that any data generated from isolated IOM does not necessarily directly relate to organic material still present within a meteorite. Using the data obtained in this study, and that previously reported, two-component models for the structure of IOM, and scenarios for its formation, were discussed.

Table of Contents

List of Figures

List of Schemes and Equations

List of Tables

Acknowledgements

David Hope, the former Archbishop of York, retired in 2005 and for a while, became a parish priest. At the time he said that he wanted to get back to his roots, taking services, carrying out christenings and weddings and suchlike, rather than being an Archbishop. I often thought that would be an interesting model for scientist managers late in their careers, to go back into the lab and work at the bench again, so when my former employers decided that I would be given that opportunity, after thinking about it for a bit, that's what I decided to do. Most people I spoke to thought it was a great idea, so I must thank Vic Pearson and Iain Gilmour for letting me have a go at carrying out basic research again, although in a very different field from my previous career.

It's certainly been different, and I'd like to thank Vic especially for all her suggestions and advice (well, most of it), and all the others who have helped me get to grips with all the lab and instrument work which was so unfamiliar. In particular, that's Ian Franchi, Mabs and Iain Gilmour, Diane Johnson, Imran Janmohamed, Taff Morgan, Diane Turner and Sasha Verchovsky, but also all the other staff and students who I've met and worked with over the last four years.

It's been very interesting to try to work out something about what was going on four and a half billion years ago, by studying tiny bits of space rock, struggling to push back our knowledge and understanding back to the beginning of the Solar system.

So, we beat on, boats against the current, borne back ceaselessly into the past.

Chapter 1 Introduction

1.1. Organic Compounds and the Origins of Life

In the infancy of the science of chemistry, it was believed there was a fundamental difference between the chemical compounds formed within living organisms, and those synthesised by other means, (such as in a laboratory, or as minerals found in rocks) (Jaffe, 1976). Life somehow bestowed a "vital force" into the former, which were known as "organic" compounds, the others being described as "inorganic". This distinction was eventually disproved by a number of examples, the most famous of which was by Wöhler in 1828 (Schütt, 2003) who converted an "inorganic" salt (ammonium cyanate) into an "organic" compound (urea) in the laboratory, without any involvement of life processes. Thus it became accepted that organic compounds, although the basis of the chemistry of life, can have an origin totally removed from any life process.

Carbon is the essential element of organic compounds, and it is upon these frameworks that all known forms of life are based. Although a simple definition is hard to construct, organic compounds can be best described as those containing usually more than one atom of carbon, along with hydrogen, oxygen and a few other common elements.

It is very unlikely indeed that the extremely complex molecules (such as proteins), which now make up living organisms, could arise by random interactions of single atoms. Life therefore must have arisen from simpler compounds, with molecular complexity increasing over time (Bada and Lazcano, 2003; Szathmáry, 2005). An example of such a simple compound is formamide. This has been detected in extraterrestrial environments (Rubin *et al.*, 1971), and mechanisms for its formation

from even-simpler precursors (such as water and hydrogen cyanide), followed by reactions (catalysed by minerals) to give more complex molecular species, have recently been proposed (Saladino *et al.*, 2011; Saladino *et al.*, 2012a; Saladino *et al.*, 2012b; Leyton, 2012). Of course, this original biochemical evolution need not have occurred solely on the Earth, and theories have been proposed that these simple molecules (or indeed life itself) originated elsewhere and were somehow delivered to the Earth (for example, on comets (Wickramasinghe, 2009)). Although discussion of mechanisms of formation of complex molecules on the early Earth began some time ago (for example, Bernal, 1957), research still continues (Bada, 2004; Parker *et al.*, 2011).

What is clear, however, is that the predecessors to life must have been relatively-simple organic compounds, acting as the precursors from which molecules of some complexity could be built. Determining which compounds formed under abiotic conditions, and by what mechanisms, is a necessary precursor to understanding how they subsequently interacted to form early biological systems; the study of these primitive materials is the purpose of the work described in this thesis.

Finding any terrestrial materials dating from the early history of the Earth is extremely difficult. Everything more than about four billion years old has been reworked by tectonic and erosional processes; the oldest known materials surviving from that time being zircons, dated to about 4.4 Gya, although found in younger rocks (Wilde 2001); no traces remain of any organic materials that may have existed on or within the Earth during its earliest history. The exact date of the oldest-preserved fossil evidence of life processes is still not agreed (Javaux *et al.*, 2010), but

is most probably derived from cellular organisms, *i.e.* already developed to some considerable degree of complexity.

To obtain information on organic materials formed prior to the emergence of life, it is necessary therefore to investigate non-terrestrial systems. We are able to remotely observe other planetary systems in their early stages of formation; for example, organic compounds have been detected in a disk surrounding AA Tauri, a star in the T Tauri class, which is less than a few million years old (Carr and Najita, 2008). However, it is difficult to untangle the multiplicity of signals seen in the spectra of such stars, and definitive identification of the carbon compounds present is limited to only a few major components, for example, carbon monoxide and dioxide, hydrogen cyanide and acetylene. Furthermore, conditions prevailing in these remote planetary systems may be greatly different from those in the developing Solar System, and so a local source of material is required for study.

1.2. Meteorites as Sources of Pre-biotic Organic Compounds

Having never accreted into large planetary-sized bodies, asteroids (and comets) comprise the left-overs from the formation of the Solar System. Instrumental data and images have been returned by spacecraft from the neighbourhood of comets and asteroids (such as Giotto flying by 1P/ Halley, or Dawn, orbiting 4 Vesta), but to date, no spacecraft has delivered large samples from asteroids or comets to Earth. Small grains have been returned (from 25143 Itokawa by Hayabusa in 2010 (Yurimoto *et al.*, 2011), and 81P/ Wild 2 by Stardust in 2006 (Sandford *et al.*, 2006)) but the small sample size has restricted the work possible, and samples from Itokawa have been found to be essentially free of organic content (Kitajima *et al.*, 2011).

There is, however, a source of suitable materials which is available for study. Meteorites are the remains of extraterrestrial bodies which enter the atmosphere, and fall to Earth. From studies of the spectral properties of meteorites and reconstructions of their orbits prior to impact on Earth, most have been shown to be fragments of asteroids, and perhaps comets, these sources being termed "parent bodies" (McSween, 1999), which, following some orbit-altering event, were deflected into Earth-impact trajectories. Importantly, a small proportion of meteorites found on Earth (known as carbonaceous chondrites, and discussed in more detail in section 1.3.1) contain organic materials, in high enough concentrations to allow extensive study (Pizzarello, 2006). Carbonaceous chondrites have radiometric ages much older than any terrestrial materials (Krot and Bizzarro, 2009). They pre-date the emergence of life, and contain samples of the pre-biotic organic materials described in section 1.1, the identification and analysis of which is described in section 1.4.

The mode of formation of the organic materials found in carbonaceous chondrites remains poorly understood. They may have been formed prior to the meteorite parent body, incorporated during its accretion, either remaining largely unchanged over time, or being modified subsequently. Alternatively, they may have been formed *in situ*, from much simpler precursors. Such reactions, occurring within the parent body of the meteorite, may have involved an interaction between organic compounds and the mineral components of the asteroid, which could have acted either as catalysts, or reagents, and clearly, similar processes may have operated on or within the early Earth. The work described in this thesis forms part of an on-going study into the nature, if any, of this interaction. By studying the formation of organic compounds present within meteorites, it may be possible to infer if similar processes

operated on the early Earth, and, ultimately, how life originally formed from these simple precursors.

1.3. Meteorites and Asteroids

As discussed in the previous section, asteroids are the remains of the materials which eventually formed the Solar system, with meteorites being fragments derived from them which have been delivered to Earth. In this section, the classification systems used for meteorites (and, briefly, for asteroids) are discussed, highlighting the links between them.

1.3.1. Meteorite Classification

Meteorites are categorised into three broad groups, based on their overall composition (McSween, 1999).

- **Stones** are primarily rocks, that is made up of assemblages of minerals
- **Stony-irons**, a small group, contain metal and minerals, in similar amounts
- **Irons** are composed mostly of metal, namely iron and nickel

The meteorites required for this study are those containing organic compounds. Meteorites containing carbon compounds (both organic and inorganic) comprise a small subgroup of the stones, known as carbonaceous chondrites. (Chondrites are a meteorite type containing chondrules, small, sub-millimetre-sized igneous spherules (Mason, 1962)). Classification systems have been developed for the other groups, but further discussion of those meteorites, which lack any organic content, is outside the scope of this project.

Carbonaceous chondrites were later divided into three sub-groups, based on carbon and volatile content (Wiik, 1956), and subsequently defined by Mason as being "stony meteorites containing an appreciable amount of carbon, other than free carbon

(diamond and graphite)" (Mason, 1963). Mason reviewed data relating to the organic components obtained by extraction with solvents, or of the residue following acid-mediated demineralisation (as well as the minerals). Methods reported were largely limited to elemental analysis or other non-specific techniques, although some mass spectrometric data was included (Nagy *et al.*, 1961). The data presented was grouped according to the three categories previously proposed by Wiik (1956). This classification was incorporated in to the comprehensive system subsequently proposed by van Schmus and Wood (1967), extending the number of groups to six, and later to eight (Krot *et al.*, 2005), correlated with the degree of aqueous or thermal alteration, and based largely on petrological categorisation, and not on any classification of organic content. With the addition of a letter to designate the type specimen for each group, and a number to indicate the type and degree of alteration, this system is still in use today, and is summarised in Figure 1-1.

Class	Type specimen	Petrological sub-types					
		Increasing aqueous ⟸ alteration			Increasing thermal ⟹ metamorphism		
		1	2	3	4	5	6
CI	Ivuna	100					
CM	Mighei	10	90				
CR	Renazzo	5	90	5			
CB	Bencubbin			100			
CV	Vigarano			100			
CO	Ornans			100			
CK	Karoonda			10	60	25	5
CH	ALHA85085			100			

Figure 1-1: The classification of carbonaceous chondrites (adapted from Scott and Krot, 2005; the degree of shading, and numbers within each cell indicate the approximate percentages of each sub-type)

One CM meteorite, Murchison, which fell in 1969, has been extensively studied. The total mass of this meteorite was around 100 kg (Fuchs *et al.*, 1973), and thus

provides ample material for experimentation. Samples of this meteorite were used for all the studies described in this thesis.

1.3.2. Asteroid Classification

Most asteroids orbit the Sun in a region known as the asteroid belt, located mainly between the orbits of Mars and Jupiter. They form a number of families, with similar orbital characteristics, with some in orbits which cross that of the Earth (McSween, 1999). Their surfaces have been studied using infra-red (IR) spectrometry, generating spectra diagnostic of their surface composition (Gaffey and McCord, 1979). Based on the spectra obtained, asteroids have been assigned to classes, using a number of classification systems, most commonly that of Tholen (Barucci and Fulchignoni, 1989). A full discussion of asteroid classification is outside the scope of this thesis but the most populous classes are S (stony, which show spectra dominated by signals due to minerals, such as olivine or pyroxene), M (metallic) and C (carbonaceous, which give spectra containing features diagnostic of organic materials). By comparison of the spectra of meteorites with those of asteroids, meteorites can be associated with asteroid groups, and thus potential links to parent bodies can be established (Chapman, 1976; Lodders and Osborne, 1999). For example, C-type asteroids are likely to be the source of many carbonaceous chondrites.

The distribution of asteroid classes within the belt is not random, with each class occupying a particular region of the belt (McSween, 1999). S-type asteroids are found mainly in the inner part of the asteroid belt, where the degree of solar heating is high, resulting in higher temperatures. Those found in the middle to outer belt, such as C-type, experience less solar heating, and so their components are less likely

to have been thermally altered. Thus organic materials contained within them may be subjected to environments conducive to organic reactions taking place (that is, environments not far removed from that found on Earth today). Clearly, however, beyond a certain critical distance (the "snow line") temperatures would not exceed 0°, and so liquid water could not exist, greatly reducing the scope for aqueous alteration, although reactions could still occur in solvents of lower freezing-point (as discussed in section 1.5.6).

The temperature, and thus the environment, will also vary within an asteroid, at least during the earlier stages of its formation. Heat may be generated internally (from the decay of short-lived radio-isotopes) or derive from accretion, but will eventually be lost by radiation. Until equilibrium with its surroundings has been reached, within an asteroid, temperature will increase with depth (apart from a surface layer heated by the Sun, depending on the location of the asteroid within the belt). It is possible therefore that different degrees of thermal processing would occur at different depths within the parent body, with the result that the compounds found in meteorites would depend on its original location within the parent body.

1.3.3. Meteorite Mineralogy and its Role in Organic Synthesis

The petrography and mineralogy of meteorites of all types have been studied intensively, and is reviewed in detail by Papike (1998). Murchison, as for other CM chondrites, has been subject to aqueous alteration, but not thermal metamorphism. Its chondrules contain mainly forsterite, and aqueous alteration has converted some forsterite into phyllosilicates which have a complex mineralogy (Fuchs *et al.*, 1973). Metal grains are not common. Sulfur is present, both as the free element, and as troilite. Chondrules are often coated with fine-grained rims, the origin of which is

not clear (Bunch and Chang, 1980; Metzler *et al.*, 1992), and are discussed in section 1.5.5. The matrix between the chondrules is composed largely of phyllosilicates of complex composition, such as cronstedite (Zolensky *et al.*, 1993, Barber, 1981), and a "poorly-characterised phase", (PCP) (Fuchs *et al.*, 1973;, Bunch and Chang, 1980). Other minerals, such as calcite and gypsum are also present.

If minerals are involved in the synthesis of meteoritic organic materials, they may act as catalysts, resulting in the formation of compounds which could not otherwise form. Alternatively, they may act to influence a reaction to proceed in one possible direction rather than another, in particular to influence the formation of one isomer of a product over another. Of special importance is the possibility that mineral catalysis may alter the ratio of optical isomers formed (discussed later in this section).

Of these minerals, phyllosilicates are the most likely candidates for possible involvement in the formation of organic compounds. Various clays (such as montmorillonite) are well-known as catalysts in organic synthesis (Wallis *et al.*, 2009; Varma, 2002), whereas simpler silicates (such as forsterite) are not. Clays possess open crystalline structures containing reactive anions (such as hydroxide and fluoride), into which small molecules can enter. If these minerals are associated with the synthesis of organic materials in some way, and provided there has not been significant redistribution of materials by fluid flow, then the minerals and the organic reaction products are likely to remain co-located within the structure of the meteorite. The degree of fluid flow within parent bodies has been the subject of much research (for example, see a discussion in Brearley, 2005). Systems effectively isolated from their surroundings (for example by lack of matter or energy transfer) are known as "closed" (the opposite being "open"). In this context, meteorites having minimal

internal fluid flow are named "closed" in contrast to those with significant flow, named "open". Although modelling studies indicate the likelihood of open systems (Travis and Schubert, 2005), other mineralogical and petrological studies indicate large-scale fluid-mediated redistribution to be minimal (Morlok *et al.*, 2006; Bland *et al.*, 2009) favouring the presence of closed systems. However, co-location is not necessarily an indicator of a genetic connection between the formations of the two components. Minerals and organic compounds could be formed separately, and only come together at the time of the accretion of the parent body.

Although altered by aqueous processes, the mineralogy of CM carbonaceous chondrites such as Murchison shows no evidence for major thermal alteration (which would have also resulted in decomposition of organic materials). Murchison is therefore an excellent source of samples for this study.

On Earth, many organic compounds of biogenic origin, if they contain appropriately-substituted carbon atoms, exist in only one of the two (or more) asymmetric molecular forms possible. This is a result of the enzymatically-mediated synthesis of such molecules, where only one form is correctly configured for binding within the enzyme. Some compounds, most notably amino acids, have been detected in meteorites with an excess of the same isomer as found in terrestrial systems (Pizzarello *et al.*, 2012). This could indicate an extraterrestrial, biogenic origin, or be a result of terrestrial contamination. However, other explanations have been proposed (after ruling out contamination). For example, some other asymmetric catalytic system (inorganic in nature) may have facilitated the synthesis of one isomer over another. Alternatively, both isomers may have been synthesised originally, but one may have been preferentially destroyed. Many mechanisms have

been proposed for these alternatives, but to date, no conclusive evidence to support any hypothesis has been identified (see, for example, Breslow, 2011; Holmlid, 2009; Cataldo *et al.*, 2005). Identifying evidence of a possible role of inorganic (mineral) meteoritic materials in the abiotic synthesis of optically-active organic compounds, (by finding an association of the reaction products with specific minerals) would greatly help resolve this problem.

There is therefore potential for an interaction to exist between the minerals present in carbonaceous chondrites and organic materials, resulting in the formation of the compounds now found to be present. The petrology and mineralogy of carbonaceous chondrites has already been described; the nature of the organic content of carbonaceous chondrites has also been the study of much investigation; the results of these studies are reviewed in the next section.

1.4. The Detection and Analysis of Organic Compounds in Meteorites

1.4.1. Early Work

Witnesses to meteorite falls (such as those in California in 2011 and in Russia in 2013) often report noticing a distinctive smell, reminiscent of bitumen, or other organic materials (for a description of early investigations into such meteorites, see Gaines *et al.*, 2009). The Orgueil meteorite (type CI1, which fell in 1864) was investigated by Louis Pasteur, (see Nagy *et al.*, 1961), but only basic scientific work on the organic content of meteorites was reported; techniques capable of true analysis of such materials (such as chromatography and spectroscopy) had not yet been developed. By the middle of the twentieth century, organic materials had been isolated from meteorite samples by extraction with organic solvents, and some components identified (such as hydrocarbons and acids identified by Briggs and

Mamikunian (1963)), who also noted that substantial organic material was not removed by extraction, but little valuable information was deduced concerning its nature or composition.

The analysis of meteoritic organic materials was by reviewed by Hayes (1967). The analytical techniques used in the papers he reviewed included Infra-red (IR) and Ultra-violet (UV) spectroscopy, as well as some Mass Spectrometry (MS), but no modern spectroscopic techniques, such as Nuclear Magnetic Resonance spectroscopy (NMR). Analyses had often been conducted on mixtures (such as fractions isolated using column chromatography), so the value of the data presented is limited. Material losses during sample preparation and analysis (for example, during solution concentration) would lead to inaccuracies in quantitative calculations. The fraction of extractable content, which, if calculated by weight alone (and often quoted as being up to 30%), is almost certainly an over-estimate, as it likely contains extractable components other than organic compounds. For example, some minerals (e.g. gypsum) have appreciable water solubility, and sulfur is readily-soluble in many organic solvents, and so there is much scope for solvent extracts to contain inorganic, as well as organic, materials. As Hayes himself noted, these data need to be "taken with a grain of salt".

Soon after Hayes published his review, the falls (both in 1969) of the Murchison and Allende carbonaceous chondrites provided the community with hundreds of kilograms (data relating to meteorites is listed in "Metbase", (http://www.metbase.de/home.html) of organic-rich meteorite of known provenance and limited terrestrial exposure, leading to an explosion in the amount of research carried out. With the development of modern analytical methods in the following

years, the amount of data available has increased enormously, in both quantity and quality.

The early work described above had led to the understanding that the organic material present in carbonaceous chondrites was of two types, that which could be extracted into organic solvents, and that which could not. Analysis of these two components is discussed separately in the following two sections.

1.4.2. Soluble Organic Compounds

With the advent of modern separatory methods such as High Performance Liquid Chromatography (HPLC) and capillary Gas Chromatography (GC), as well as more sensitive analytical technology (especially mass spectrometry), it is now possible to separate, detect and identify much smaller amounts of material than was the case at the time of Hayes's review. The soluble organic fraction, those compounds which can easily be extracted from a meteorite using solvents, were the initial targets of study, being more amenable to analysis by the methods available at that time.

Soluble compounds present are extracted using one or more solvents, and the resulting solutions analysed using techniques such as gas chromatography-mass spectrometry (GC-MS). This may be qualitative (limited to identification of the components) or, if appropriate standards are used, include quantification of each component. The proportions of different classes of soluble compounds found in Murchison are shown graphically, in Figure 1-2, and summarised in Table 1-1.

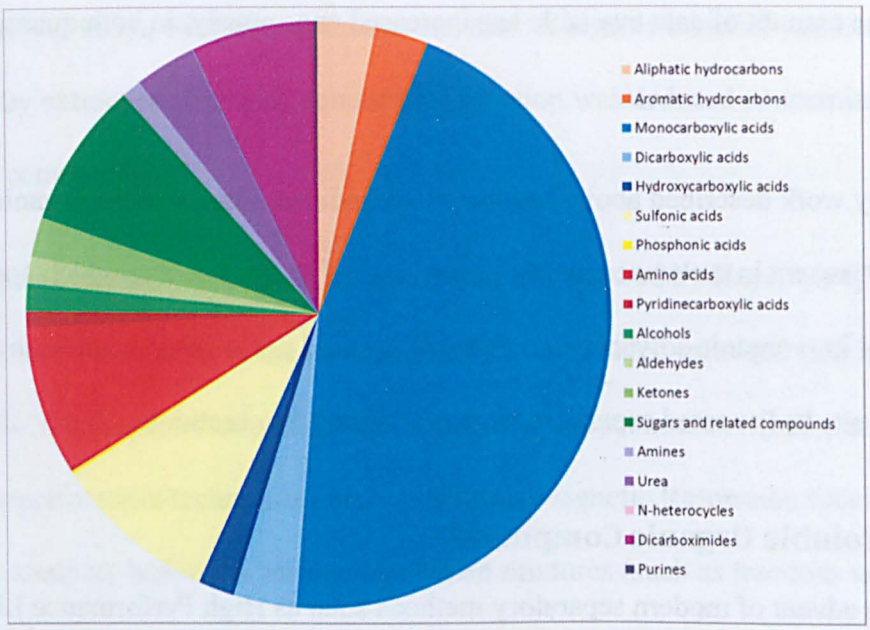

Figure 1-2: Proportions of classes of soluble organic compounds found in Murchison (data taken from Gilmour, 2005)

Functionality	% of total	Colour group in Figure 1-2
Hydrocarbons	8	Oranges
Nitrogenous acids	9	Reds
Carboxylic acids	50	Blues
Other acids	9	Yellows
Other oxygen-containing groups	13	Greens
Nitrogen-containing groups	11	Purples

Table 1-1: Summary of proportions of functional groups found in soluble organic compounds extracted from Murchison (data taken from Gilmour, 2005)

This data has been compiled from a number of separate studies, each focused on determination of the presence of particular individual chemical classes (for example carboxylic acids). No example has been found of a study in which the total organic content of a meteorite sample (or set of samples) has been extracted and quantified.

The data shows that organic acids form the major part of the soluble component, which may result in part from the extractive procedures used. For example, if a base is used to extract acids, then hydrolysis of compounds such as amides or esters is also likely, resulting in them not be detected, and the acid content increased (for example, Yuen and Kvenvolden, 1973). This factor (the effect of the isolation

process on the material being prepared for analysis) is often overlooked in reports of the analysis of meteoritic organic materials. For example, after extraction with a solvent, it is usually necessary to concentrate the solution by evaporation to provide sufficient material for analysis. If this concentration process is not carefully controlled (for example, by fractional distillation) then volatile components will be lost, leading to an underestimate of their content.

A more-recent study employing extraction with a series of solvents, followed by analysis with very high resolution mass spectrometry, showed that the range of compounds present was very large indeed, with all possible structural isomers of each compound often being present (Schmitt-Kopplin *et al.*, 2010). The technique allowed detection of extremely small quantities of material, hence the detection and identification of so many individual compounds, although it did not allow quantification of the components. The results of this study suggested that the extractable component is a mixture of very many types of organic compound, formed in a totally random way.

Some studies have, by correcting for any co-extraction of inorganic materials, and the use of appropriate standards, determined absolute levels of classes of soluble organic materials and individual components. If results from these (separate) studies are combined, the total content of soluble organic materials are typically much less than 1% of the meteorite mass. For example, Sephton (2002) lists about twenty categories of organic compound found in Murchison, with the total amounting to about 750-800 ppm (*i.e.* 0.08%). When data is presented for individual compounds, the abundance of each is generally below 50 ppm (Lawless and Yuen, 1979; Martins *et al.*, 2006), with most compounds being substantially less than this. Only the lower

molecular weight compounds (such as formic, acetic or propionic acids) are more abundant. Several other reviews have been published in the last few years (Botta and Bada, 2002; Watson *et al.*, 2004; Gilmour, 2005; Sephton, 2005; Pearson *et al.*, 2009), and none lists total quantities above 0.1% or so. As the total organic content of carbonaceous chondrites is typically in the range 2-5% of the weight of the meteorite, but the soluble compounds together amount to no more than 0.1%, the proportion of soluble organic material must only represent about 5% of the total organic content, with the remaining minimum of 95% comprising insoluble material. These more modern studies do not support the estimate given by Hayes in 1967 (Hayes, 1967) that the soluble component forms about 30% of the total organic content, which must have been inflated by other extractable components, but whatever the actual proportion of soluble materials, the remaining, major part is insoluble, and its analysis is discussed in the following section.

1.4.3. Insoluble Organic Material

Insoluble materials pose a much greater challenge to the analyst as the range of suitable methods is much reduced. Nevertheless, significant progress has been made in the study of the insoluble organic material (IOM) found in meteorites, as discussed in the following section.

Analysis

In contrast to the soluble fraction, IOM, being insoluble and involatile, has proved difficult to analyse. Any technique which requires material in solution cannot be used, and so one is limited to solid-state methodology, for example, NMR (Cody and Alexander, 2005), IR (Quirico and Bonal, 2004) or Raman spectroscopy (Kebukawa *et al.*, 2010a). IOM can be isolated from a meteorite sample by removal

of the mineral components and collecting the insoluble organic material which remains. In this procedure, silicate minerals, which make up the majority of the meteorite sample, are converted into soluble fluorosilicates using aggressive reagent systems, such as hydrofluoric and hydrochloric acids, and subsequently removed. As with the soluble organic fraction, the possibility that the molecular structure of IOM may be altered during its isolation, (by reaction with these reagents) must not be ignored. As the structure and composition of IOM is not accurately known, it is difficult to assess *a priori* what these alterations might be.

IOM can also be analysed by degradative techniques, such as pyrolysis, in which large molecules are thermally broken down into smaller ones, which can then be analysed by, for example, GC-MS (*e.g.* Sephton *et al.*, 2005). The results can be complex; small molecules detected could have been physically retained within the IOM and released by heat, or be the result of pyrolytic bond breaking, or formed by decomposition (or other reactions) of other molecules generated during pyrolysis. Chemical modification in conjunction with pyrolysis has also yielded some useful information, *e.g.* methylation, hydrogenation or hydrolysis (Watson *et al.*, 2005b; Watson *et al.*, 2005a), although the chemistry occurring in these experiments is no doubt even more complex and difficult to interpret.

Nomenclature

This material is often referred to in the literature as "kerogen", or "polymeric" or "macromolecular" material. These terms are not interchangeable, and the first two are incorrect. "Kerogen" refers to high molecular-weight, organic material, of a terrestrial origin, derived from biological sources. The organic material in meteorites may *resemble* kerogen, particularly if it has been exposed to heat or pressure, but it must be quite different. Kerogen has a biological origin, being formed from the

remains of plants, algae *etc.* for example, cell walls These are often composed of repeating molecular sub-units, and are often highly oxygenated, alicyclic or aromatic systems (which would not be expected for material with an abiotic origin). However, both meteoritic material and kerogen will be converted to graphite under extremes of temperature and pressure, (Quirico *et al.*, 2003) and so although meteoritic and terrestrial materials of high metamorphic grade may be superficially similar, their origins cannot be the same.

The phrase "polymeric material" is also incorrect. A polymer is a molecule of high molecular weight formed by the linking together of many identical sub-units (monomers) to form a molecule of regular, repeating structure. These can include biogenically-derived compounds such as chitin and starch, but there is no evidence that this meteoritic material has such an ordered structure.

Thus the high molecular weight material present in meteorites is neither of these, and so could be referred to simply as "high molecular weight material" or "macromolecular material" (indicating it is formed of very large molecules, but without being specific as to what they are). As this material is insoluble in common organic solvents (that is, those used to dissolve the extractable organic fraction, without inducing any chemical change), the abbreviation IOM (insoluble organic material)is thus appropriate, and is used throughout this work. Such solvents would include hydrocarbons, esters, alcohols etc., but not, for example, mineral acids or alkalis.

Structure

Analytical data generated supports likely compositional differences for IOM isolated from different meteorite classes (Cody and Alexander, 2005; Gardinier *et al.*, 2000).

Spectroscopic studies indicate the basic structure contains both aliphatic and aromatic components, with the latter forming the major part, composed of up to about four aromatic rings. The nature of the substituents and linking groups is still unclear, but degradative analysis shows the presence of branched aliphatic systems containing fewer than ten carbon atoms (for example Derenne *et al.*, 2002; Kebukawa *et al.*, 2011; Cody *et al.*, 2011; Cody and Alexander, 2005; Huang *et al.*, 2007; Remusat *et al.*, 2005a).

Derenne and Robert (2010) have reviewed the analytical data available (^{1}H and ^{13}C NMR, EPR and FTIR spectroscopies, HR-TEM, XANES, elemental analysis and GC-MS following oxidative or pyrolytic degradation) and suggested a typical structure, shown in Figure 1-3.

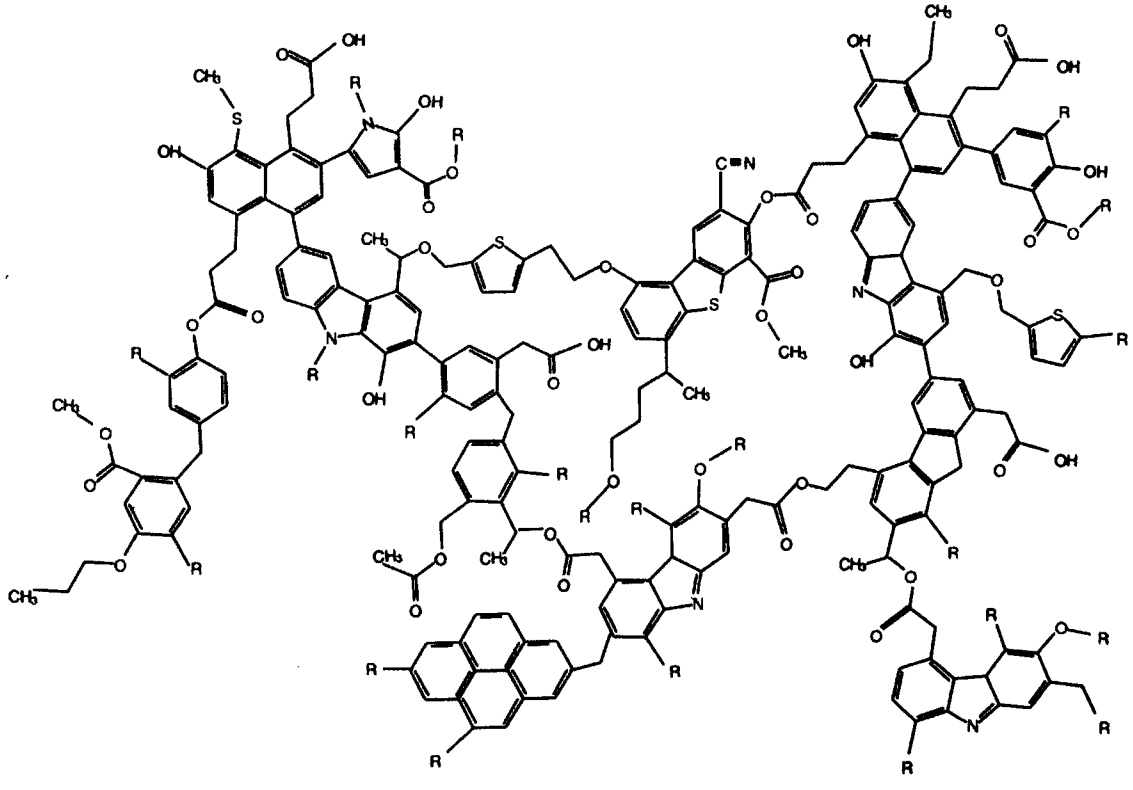

Figure 1-3: Representation of the structure of IOM (based on a review of analytical data, and proposed by Derenne and Robert, 2010)

The structure shown in the Figure is intended to be an average representation of the typical structure of IOM; considerable variation will exist in the actual structures of individual IOM molecules. It depicts a macromolecular structure, formed from aromatic sub-units consisting of a few rings, linked together by short, branched aliphatic chains, and containing various other functional groups, such as ethers, esters and nitriles. Heterocyclic rings include fused pyrroles and thiophenes. The structure as depicted is macrocyclic, although the authors do not comment on this feature, but would result from a cyclisation of a linear chain of substituted aromatic sub-units. The actual structure may also include cross-linking groups (either aliphatic or aromatic.

1.5. Extraterrestrial Organic Synthesis

For organic (or any other) compounds to be formed (in any environment), three conditions have to be satisfied.

- A suitable supply of raw materials must be available, at reasonable concentration.
- The environment must deliver the necessary amount of energy, *i.e.* the temperature must be sufficient
- There must be a viable mechanism to enable the raw materials to be converted into products. This mechanism will be specific for the raw materials available.

The last point is important; just because a chemical equation can be written for a reaction, it doesn't follow that such a reaction can occur (possibly whatever the prevailing reaction conditions). There has to be a reasonable mechanism to enable the reagents to interact and generate the desired product; it is not enough just to supply the required atoms in the right atomic ratio, and expect them to combine in a specific way to generate a complex compound.

The organic compounds present in meteorites could have formed in a number of environments over the lifetime of the meteorite, its parent body, or before. The elements making up these compounds, other than hydrogen, were formed inside stars, in environments where temperatures were too high for any compounds to form. As conditions became less severe, elements were able to combine to form compounds, which could themselves interact and react. As this process continued, clouds of dust and gas were produced, which eventually led to the formation of planetary systems (such as our Solar System). Thus elements and compounds formed and then combined and reacted in a series of environments, under a variety of conditions (of temperature and pressure). These environments include

- Stellar neighbourhoods
- The diffuse interstellar medium
- Denser, collapsing molecular clouds from which planetary systems form
- In the Solar Nebula, in the gas phase or on grains
- Within the parent body of a meteorite
- In the remnants of a fragmented parent body, before, during and after arrival on Earth

The formation of organic compounds in these environments, and the potential interactions of these compounds with other materials present, are considered in turn in this section.

1.5.1. Nucleosynthesis Following the Big Bang

In the first few minutes after the Big Bang, protons, neutrons and electrons formed (Mackintosh *et al.*, 2005). Temperatures high enough to enable them to combine together *via* nuclear reactions, persisted for only about an hour (Alpher *et al.*, 1948), giving rise to deuterium and helium nuclei, along with a very small proportion of lithium and beryllium, but practically nothing else. After that time, temperatures fell

to a level such that nuclear reactions no longer occurred, and then eventually (after several hundreds of thousands of years) to a point low enough to enable nuclei and electrons to combine, to form atoms. Any changes to these original atomic proportions, and formation of all the other elements, have occurred since that original nucleosynthetic phase. Thus, at the point of recombination, to a good approximation, the universe consisted of hydrogen and helium, with a smattering of deuterium and lithium, and so these elements were the only raw materials available to form the first generation of stars.

1.5.2. Stars as Sources of Heavier Elements

The first generation of stars were formed by gravitational collapse of clouds of hydrogen and helium. Jeans (1902) showed that if such clouds possess sufficient mass or density, they will collapse spontaneously, contracting and heating up until the temperature is sufficient for nuclear fusion to occur, forming a star. Within the central regions of stars, where these high temperatures are found, hydrogen is converted to helium, followed by a series of reactions, depending on the mass of the star, forming heavier elements, up to iron (Burbidge *et al.*, 1957).

In low-mass stars, such as the Sun, temperatures are only sufficiently high to form elements with low atomic numbers, such as carbon, nitrogen and oxygen. As the stellar mass increases, so elements with higher atomic numbers, such as sodium, magnesium, neon, silicon, titanium, zirconium, and iron, can form (Cameron, 1955; Merrill, 1952). As the star reaches the end of its life cycle, these elements are delivered to the interstellar medium (ISM) by a variety of energetic processes, such as violent stellar winds, formation of planetary nebulae, or supernovae (Ryan *et al.*, 2002). The nature of these processes depends on the mass of star involved. For

lower-mass stars, the latter stages of its life-cycle are much less violent, and conditions in the stellar vicinity can be sufficiently mild to enable atoms to form, and to combine, *i.e.* for chemistry to occur. In contrast, massive stars end their lives as a supernova, during which the elements formed in the star (such as high atomic number elements, including many short-lived nuclei) are distributed explosively into the ISM; it is only during a supernova (or, possibly during the merger of subsequently-formed neutron stars (Goriely *et al.*, 2011)), that elements heavier than iron are synthesised. Thus, as successive generations of stars form, evolve and die, the cosmic abundances of these heavier elements increase with time, with shorter-lived radionuclides decaying to daughter products. In contrast, within stars, deuterium is rapidly destroyed, so its current abundance in the universe is now lower than the primordial value, (Tytler *et al.*, 2000; Pettini and Bowen, 2001), the exact amount being used as a test of Big Bang models.

Carbon is the fourth most abundant element in the universe, formed in stars as described above. In the absence of other elements with which it can form compounds, elemental carbon exists in several stable solid-state configurations, known as allotropes (polymorphic forms of free elements). Two of these, diamond and graphite, have been known since antiquity, but more recently others, such as buckminsterfullerene (Kroto *et al.*, 1985), nanotubes and graphene (Novoselov *et al.*, 2005; Geim and Novoselov, 2007), have been identified, with fullerenes also having been detected in extraterrestrial environments (Gielen *et al.*, 2011).

1.5.3. Stellar Neighbourhoods

Elements available for chemistry around stars

As a low-to-medium mass star (such as the Sun) reaches maturity, those elements formed in the core (mainly carbon and oxygen) are brought to the surface during convective, "dredge-up" phases. As the star expands, and the outer layers cool and become less-well gravitationally-bound, significant quantities of gas are lost to the ISM *via* strong stellar winds. The specific materials released to the ISM depend on the composition of the star, and in particular, its carbon-to-oxygen (C/O) ratio (Lodders and Fegley, 1999). The major elements (excluding helium) present in stellar atmospheres (or circumstellar envelopes, CSEs) are hydrogen, carbon and oxygen. Carbon and oxygen readily combine to form carbon monoxide, and whichever of those two elements is present in a limiting amount will essentially be consumed, leaving an excess of the other to react with any other elements present. Thus, if the C/O ratio is less than one, all the carbon will be consumed, and the chemistry of the CSE will be dominated by compounds of oxygen with other elements, such as silicon, iron and magnesium. If however, the C/O ratio is greater than one, then the reaction consumes all the oxygen, and the chemistry of the outer parts of the star is dominated by carbon compounds (Helling *et al.*, 1996; Frenklach and Feigelson, 1989), particularly those with hydrogen, known as hydrocarbons.

Low C/O stars

The compounds formed in the outflows of low-carbon, red giant stars consist of a fairly small number of simple inorganic compounds (usually termed minerals, (Hazen *et al.*, 2008)) formed from low atomic number elements, *e.g.* silicon, nitrogen, oxygen, magnesium, aluminium and iron, (see reviews by Zinner, 2005; Bernatowicz *et al.*, 2006). These include binary compounds (*e.g.* corundum or rutile)

or simple silicates such as olivine or pyroxene, as listed in Table 1-2. At this stage, the range of minerals is small, limited to those which can form by simple interatomic combination. Very close to a star, where the temperature is high, only the most refractory substances can form, but with increasing distance, and decreasing temperature, so minerals condense in a well-established sequence (Ebel, 2006). Compounds of oxygen with non-metals, such as carbon dioxide and monoxide, or sulfur dioxide, form molecules with much weaker intermolecular forces, and so only condense at much lower temperatures.

Mineral	Formula
Rutile	TiO_2
Corundum	Al_2O_3
Osbornite	TiN
Nierite	α-Si_3N_4
Troilite	FeS
Spinel	$MgAl_2O_4$
Hibonite	$CaAl_{12}O_{19}$
Forsterite	Mg_2SiO_4
Perovskite	$MgSiO_3$

Table 1-2: Names and formulas of minerals formed in outflows from low C/O stars (taken from Hazen *et al.*, 2008)

Iron or iron-nickel particles can also condense, along with other metals, but compounds of carbon are largely absent, as most carbon has reacted with oxygen to form carbon monoxide. However, signals indicative of fullerenes and other polycyclic aromatic hydrocarbons, (PAHs, for examples, see Figure 1-5) have been detected in these environments (Gielen *et al.*, 2011).

Other inorganic materials which form in this environment are ices and gases. Ices include compounds existing as gases and liquids under normal terrestrial conditions, but frozen at the low temperatures of the interstellar environment, and include water,

carbon monoxide, and ammonia. More volatile elements, such as neon, krypton and xenon may also be present, either frozen or in the gaseous state (Allamandola *et al.*, 1999).

High C/O stars

In high C/O stars, the amount of oxygen available for reaction with other elements is much less, and so their outflows are dominated by carbon as the free element, or as compounds with elements other than oxygen, notably hydrogen, forming hydrocarbons. Depending on the structure, the ratio of hydrogen to carbon in hydrocarbons can range from 4 (in methane) to essentially zero, in extended graphene sheets, with only minimal bond termination by hydrogen at the edges of the molecule. Hydrocarbons have been observed spectroscopically in the outflows of carbon-rich stars (Pascoli and Polleux, 2000), where temperatures are often around 1000 K, and, under these conditions, many such molecules are stable (Kwok, 2004). These hydrocarbons take many different forms, depending on the degree of reaction, (cyclisation and hydrogenation) of the small carbon-containing molecules that are needed to generate more complex structures.

Polyynes are one-dimensional chains of carbon atoms, linked by alternating single and triple bonds and are usually terminated by hydrogen (to give a stable molecule), as shown in Figure 1-4. Cyclic structures, such as the PAHs shown in Figure 1-5 can be formed from these small linear units by progressively adding two-carbon fragments, such as acetylene, followed by cyclisation.

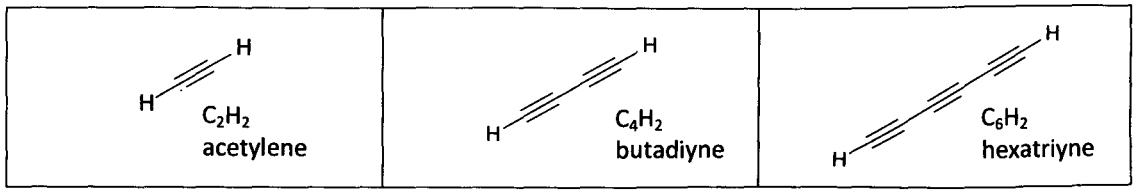

Figure 1-4: Structures and formulas of simple linear polyynes

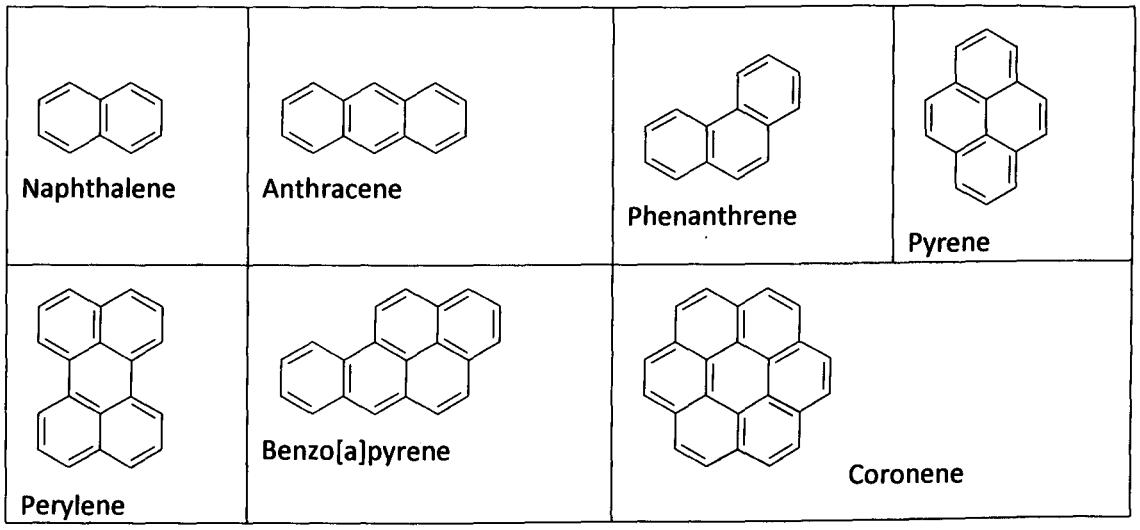

Figure 1-5: Examples of polycyclic aromatic hydrocarbons (PAHs)

These rings can then be linked, and elaborated by further similar reactions, eventually forming large structures such as that shown in Figure 1-6 proposed by Kwok (2004). Functionalisation could occur by reaction of the exposed parts of these structures with reactive atoms, radicals or small molecules to give aromatic molecules containing a range of functional groups. Linking these together will form large molecules such as that proposed as the structure of IOM (shown in Figure 1-3). These structures, although similar, differ in the proportions of extended carbocyclic ring systems to smaller, functionalised aromatic sub-units. The structure in Figure 1-6 is mainly composed of carbocyclic rings (with other functionality (a minor component) highlighted), whereas that in Figure 1-3 (shown again below, for comparison) contains only functionalised, small-ring systems, linked by aliphatic chains.

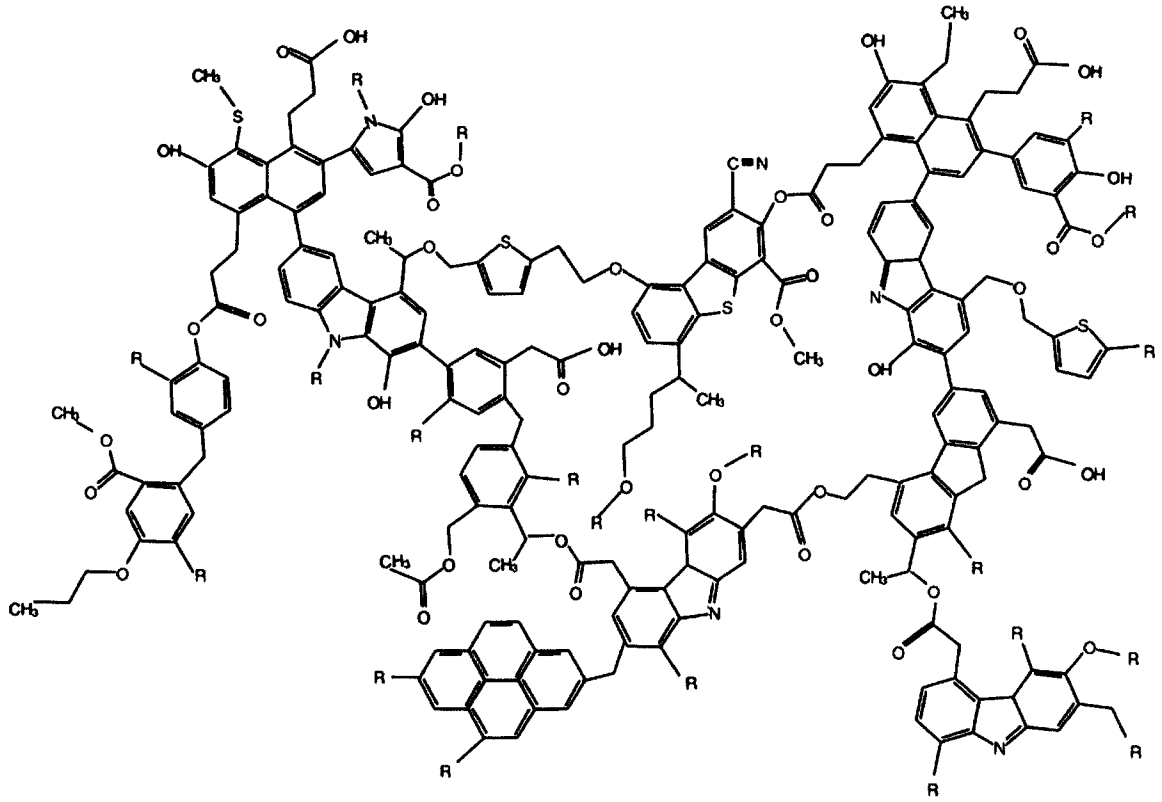

Figure 1-3: Representation of the structure of IOM (based on a review of analytical data, and proposed by Derenne and Robert, 2010)

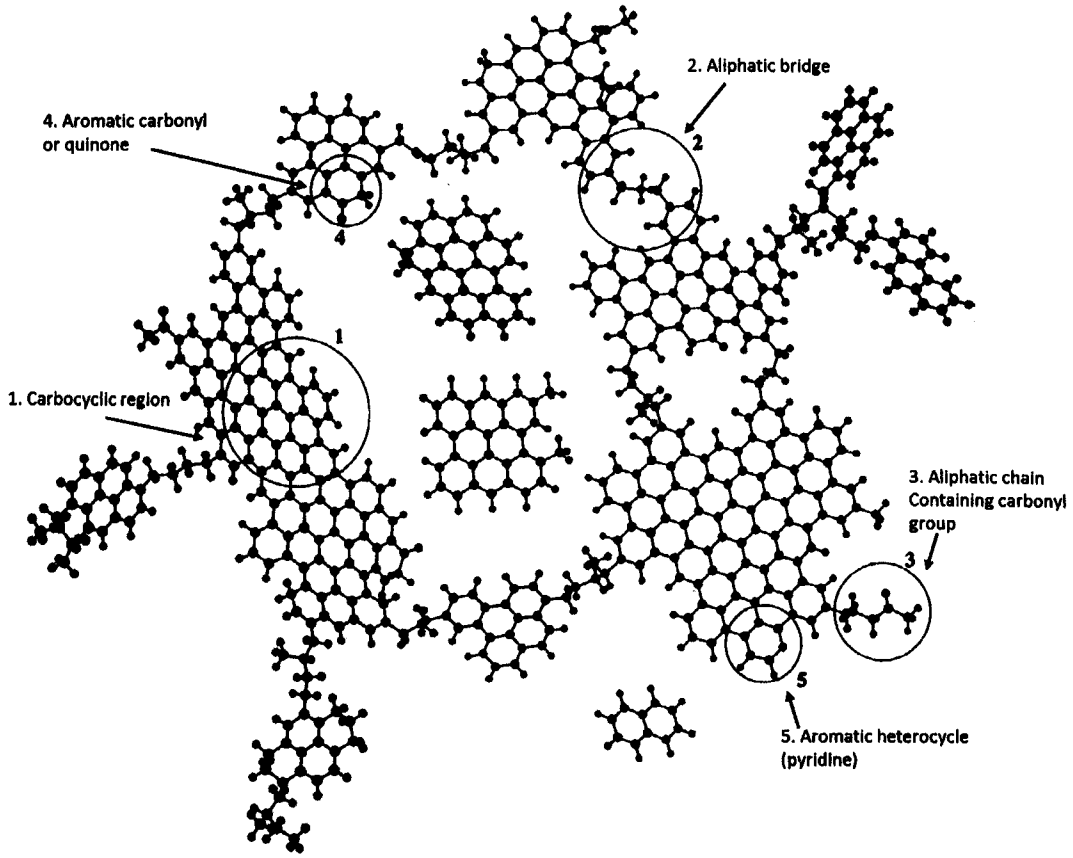

Figure 1-6: Extended carbon network formed in stellar outflows (taken from Kwok, 2004), with functionalised regions circled and labelled.

As stellar outflows are ejected at high speed (up to tens of km/sec), the residence time of these materials in the peristellar environment is only a few years, but as temperatures and pressures are high, many reactions are able to occur generating many kinds of small molecules, such as ammonia, nitriles, and other compounds of common elements (Lodders, 2008). As these materials recede from the star into the ISM, and the temperature and pressure both decrease, so these synthetic reactions effectively stop.

1.5.4. The Interstellar Medium (ISM)

Diffuse clouds

Elements formed inside stars are propelled into the space between the stars, the ISM, mixing with pre-existing hydrogen and helium and the compounds formed in the stellar vicinity, to form large diffuse interstellar clouds. These clouds are initially very cold (*ca.* 10-20 K) and very tenuous (10^9-10^{12} particles/m^3), and composed mostly of hydrogen and helium, with other components, namely dust grains, ices and other gases, amounting to less than 1% of the cloud mass (Boss and Goswami, 2006). The conditions within the clouds forming the ISM cover a range of densities, temperatures and pressures, ranging from diffuse to (relatively) dense, and the reactions that occur reflect these conditions, generally increasing in rate with increasing temperature and pressure as the ISM evolves over time, as described in this section.

The components of diffuse clouds can react with each other to form more complex molecules, either in the gas phase, or on the surfaces of mineral or ice grains (see reviews by Herbst, 1995; Nuth *et al.*, 2006), discussed in turn in the following paragraphs.

Gas-phase chemistry

Reactions in the gas phase are controlled by the likelihood of one atom or molecule approaching another close enough to form a bond. However, the low temperatures and the tenuous nature of this medium cause the reaction rates to be very low. In addition, the major part of a diffuse cloud is made up of hydrogen (plus the unreactive helium), and so the chance of forming complex molecules with atoms of other elements is vanishingly small. A further problem is that even if atoms (such as hydrogen) do interact, the molecule initially formed is too energetic to survive; it cannot relax into a lower energy state, and so immediately decomposes (Duley and Williams, 1984). Furthermore, the high levels of interstellar UV flux tend to decompose any molecules which had formed (Tielens, 2005), as the tenuous nature of the clouds allows UV radiation to penetrate deep into their interior. The gas phase of the diffuse ISM is therefore not an environment in which substantial organic synthesis can occur.

Nevertheless, a number of molecules (*e.g.* methanol, formaldehyde, and hydrogen cyanide) have been detected spectroscopically in diffuse clouds (Sandford, 1996; Sellgren *et al.*, 1995; Chiar *et al.*, 2000). It is possible though, that compounds detected in the ISM could have been formed elsewhere. As previously stated, levels of UV flux within the ISM can be high, but PAHs, formed in the outflows of stars, are able to absorb this radiation *via* their extended conjugated structure, and so are able to survive to some extent (Siebenmorgen and Krügel, 2010). Other compounds can escape into the gas phase from grains, following their formation there as described below.

Evolution of minerals and grains

Apart from gas and ice, the other component of the ISM is dust; small grains of minerals formed by the reaction of metallic elements such as iron and magnesium with silicon and oxygen. In interstellar space, this dust is continually fragmented by shock waves (*e.g.* from supernovae) or by radiation, or collisions. The lifetime of a dust particle before its destruction is calculated as less than its residence time in the ISM, and, as dust is known to exist in that environment from observations (Sandford, 1996), it must also be formed there, by re-condensation of the tiny fragments generated in the destruction processes (Jones, 1997; Draine and Salpeter, 1979). In this environment therefore, grains and molecules are continuously destroyed and re-formed, recycling and mixing materials many times (Ehrenfreud and Charnley, 2000). It is not only the basic components of the grains (*e.g.* their constituent minerals) which are mixed, but also any other materials present on the grains, such as frozen gases and ices, and any organic materials which had formed there.

Chemistry on grains: The formation of complex organic materials

As described above, the diffuse interstellar medium is cold and tenuous, and the rates of bimolecular (or higher-order) chemical reactions are low. Reaction rates will be much higher if the reactions can occur on the surfaces of grains, where atoms are physically adsorbed, and held in close proximity to one another, thus greatly increasing the probability of reaction. For example, two hydrogen atoms can combine to form a hydrogen molecule on the surface of a grain (the excess energy being lost into the grain), whereas this process is very unlikely in the gas phase (Duley and Williams, 1984; Hasegawa *et al.*, 1992).

Modelling (d'Hendecourt *et al.*, 1985; Shalabiea and Greenberg, 1994) has shown that it is possible to form many simple molecules, radicals and ions (such as water,

carbon monoxide and cyanide), supported on grains, of which many have been detected spectroscopically (for reviews, see Herbst, 1995; Sandford, 1996). As ices build up on the surface of a grain, forming a layer, or mantle, they can provide a medium for further reactions (still in the solid state), as shown graphically in Figure 1-7. Molecules are adsorbed onto the grain, depending on the chemical makeup of the cloud. Reactions can occur to generate new molecules, which, following evaporation or grain disruption, can be released back into the cloud.

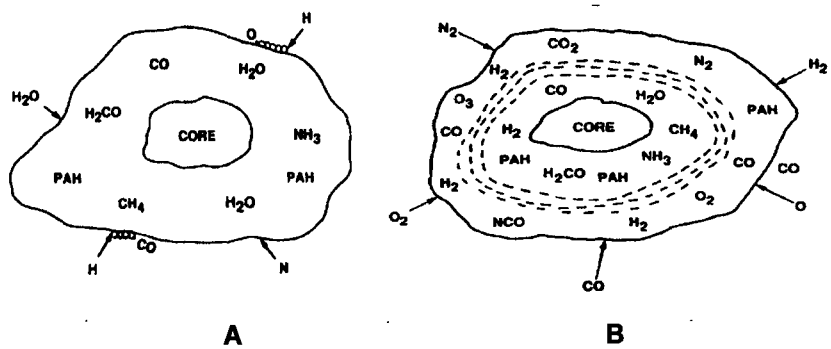

Building up a grain in reducing (A) and oxidising (B) environments

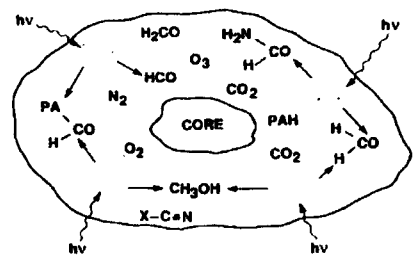

Subsequent reactions of simple molecules increasing molecular complexity

Figure 1-7: Graphical representation of grains with ice mantles (from Sandford, 1996)

Laboratory simulations have shown that the simple molecules detected in interstellar clouds (provided they are present in sufficient concentrations) can react further under the conditions of temperature and pressure expected (Schutte *et al.*, 1993; Bernstein *et al.*, 1995; Simakov *et al.*, 2002; Simakov and Kuzicheva, 2005) generating relatively complex organic molecules. Studies also predict the functionalisation of polycyclic aromatic hydrocarbons (Bernstein *et al.*, 2003), *via* the addition of reactive radicals, resulting in for example, the introduction of hydroxyl and carbonyl

groups. This reaction has also been demonstrated in the laboratory, by exposing simple compounds to interstellar-like conditions, resulting in generation of material similar to that found in meteorites (Wdowiak *et al.*, 1995b).

Features of the spectra of interstellar clouds which are still unexplained are the "diffuse interstellar bands" (DIBs), that is, absorption lines which do not easily relate to specific compounds. Although there is no firm agreement on the source (or sources) of these features, more complex organic molecules, such as functionalised PAHs, have been suggested as possibilities (Snow, 2001).

Dense molecular clouds and hot molecular cores

For a cloud of gas of given size, once the mass is greater than a certain critical value, it will undergo spontaneous self-gravitational contraction (Jeans, 1902). A stable cloud of interstellar gas with density initially below the critical value can be locally compressed by some external shock, such as a supernova, or radiation pressure from hot, energetic stars, to give regions where both the density and temperature are higher than the diffuse ISM, but still not dense or massive enough to be able to collapse to form a solar system (Messenger *et al.*, 2006). These regions, where formation of complex molecules is more favourable (due to the higher temperature and density), are known as dense molecular clouds.

The increased particle density within such a cloud decreases its transparency to radiation, and although the rates of chemical reaction are not much greater than in the diffuse ISM, the rate of radiative decomposition is much reduced. As the lifetimes of compounds are longer, there is much more chance that they can go on to react further, resulting in the formation of complex molecules (hence the name "molecular cloud"). The chemistry and properties of such clouds are described in several

reviews (Herbst, 1985; Herbst, 1995; Irvine *et al.*, 1985; van Dishoeck *et al.*, 1993). Modelling studies show that formation of a large range of organic compounds is possible (Graedel *et al.*, 1982; Prasad and Huntress, 1980b; Prasad and Huntress, 1980a; Prasad and Huntress, 1982), and as the quality of observational data increases, so the presence of these molecules is confirmed (for example, van Dishoeck, 2004). Lists of extraterrestrial molecules tend to use a rather wide definition of the word "molecule", and usually include radicals and ions in the total, as well as inorganic species. At the time of writing, published lists contain *ca.* 180 discrete structures (for example, http://www.astro.uni-koeln.de/cdms/molecules, accessed 20 April 2013), of which about 50 are true organic molecules (that is uncharged carbon compounds, lacking any unpaired electrons), including hydrocarbons, ethers, esters, alcohols, nitriles *etc.*

Mechanisms of formation of organic compounds in these clouds are the same as in the diffuse ISM; chemistry can occur both on the surface of grains and, less so, in the gas phase, with materials formed on grains being evaporated into the gas phase over time (Ehrenfreud and Charnley, 2000; Allamandola, 2008).

Dense molecular clouds are massive, containing considerably more than a solar mass, so it is quite reasonable that a portion of the cloud may be heterogeneous, containing volumes of relatively-high density, or parts be compressed more than others, possibly in response to a second shock event, and thus be able to begin the process of gravitational contraction (Boss and Goswami, 2006). These denser regions are known as hot molecular cores, and form the stage intermediate between dense molecular clouds, and a proto-planetary nebula, or accretion disk (Shu *et al.*, 1987; van Dishoeck, 2004; Lada and Lada, 2003; Cassen and Boss, 1988; Williams

et al., 2000). Such cores have a density of 10^{10}-10^{12} particles/m^3, and are significantly warmer than the rest of the cloud, with a temperature in the range 50-300 K, and here, synthesis will be correspondingly more favoured.

As the cloud contracts, gravitational energy is converted to heat. The cloud warms up (André *et al.*, 2000), and the icy mantles of grains evaporate into the gas phase, where the materials released can mix and react. The rates of chemical reactions will increase both due to the greater energy of the constituent molecules (due to the increased temperature), and the greater probability of interaction (due to the higher density), and therefore there is potential for extensive organic chemistry to occur (Langer *et al.*, 2000; Irvine and Knacke, 1989). Molecules of some complexity can be formed, for example, dimethyl ether (Ehrenfreud and Charnley, 2000), propionitrile, and ethyl formate have all been detected (Belloche *et al.*, 2009).

1.5.5. Cloud Collapse and Planetary System Formation

The process of cloud collapse, and subsequent formation of a planetary system was described in detail by Cameron (1962), and updated more recently by Cameron and others (Shu *et al.*, 1987; Cameron, 1995; Nichols, 2006). Continued collapse of a dense molecular core can be prevented by turbulence and other factors, but if these fail to act, then the cloud will collapse under its own gravitation (for models see Jin and Sui, 2010; Boss, 2004; Sandford, 1996).

The collapsing cloud forms a rotating disc of dust and gas, over a period of about 10^5 y (Boss and Goswami, 2006). As the collapse proceeds, so the central portions are heated further, more-volatile materials evaporate, and eventually, the temperature reaches that at which nuclear fusion can occur, (Tytler *et al.*, 2000) and a new star is formed. Accretion inwards continues, driven by gravitational collapse, and residual

gas is blown away by the developing stellar wind. The pressure of the radiation generated by the star halts the collapse of the disk, and an equilibrium results. The remaining phases of planetary system evolution are thus a balance between material falling inwards, and radiation and gas flowing outwards (see the reviews listed in the previous paragraph).

A temperature and pressure gradient is set up through the nebula, and so as the environment changes with distance from the developing star, so do the processes which the nebular components undergo, and therefore the products which result from those processes (Boss, 2004). The end result of this phase of stellar system development is a proto-planetary system, namely a dusty disk, surrounding a protostar, with a thermal gradient established. The temperature ranges from that which would cause total decomposition of organic materials, in the centre, to a level low enough to give no change at all at the periphery (Boss, 1998).

Chemical evolution within a developing planetary system

The raw material for the formation of a planetary system, apart from hydrogen and helium (and other gases in low concentration), is a variety of minerals, as dust grains, coated to varying degrees with volatile compounds, frozen as ices, and organic compounds, including polymeric materials, of variable composition (Sandford, 1996; Alexander, 2001; Huss, 1988; Palme and Jones, 2005; Anders and Ebihara, 1982).

As cloud material falls inwards, both the pressure and temperature increase, and eventually, the temperature at the centre of the disk increases to a point where all organic molecules are decomposed. In contrast to inorganic minerals (which will also be volatilised), cooling the resulting vapour will not result in re-condensation of the input materials, but only of the products of their decomposition (Boss, 2004),

thus the degree to which extant organic materials are preserved depends strongly on the temperature profile of the disk, and the degree of mixing of materials within it. If mixing is sufficient, and temperatures high enough, then all organic material formed prior to formation of the planetary system would be destroyed; all organic materials found today would therefore be products of Solar System processes (Nuth and Johnson, 2012), with no pre-solar material remaining.

Various models for disk formation give different profiles, ranging from complete volatilisation and mixing (Cassen and Boss, 1988), to no significant radial mixing, with stratified temperatures throughout the disk. Some models show a temperature gradient with high temperatures in the inner parts sufficient to cause complete volatilisation (Wood and Morfill, 1988), but colder in the outer parts, allowing survival of volatile materials in the solid state. Laboratory studies have been carried out to model the effects of a range of conditions (Mendybaev *et al.*, 2002), and using this information, phase diagrams can be constructed to show how the physical composition of a defined chemical mixture will change with variations in pressure and temperature (Prinn, 1993).

The presence of materials (of appropriate thermal stability) which can be proved to have formed before the Solar System would show that this mixing and heating cannot have been complete. As such evidence has been found in meteorites (for example, the presence of noble gases in nanodiamonds (Alexander, 2001), or increased levels of deuterium in organic-containing grain mantles (Huss, 1988)) and assuming that these are true interstellar signatures (and no alternative mechanism of formation is possible), then complete mixing cannot have occurred. It is therefore

possible that some organic materials may have survived from before the formation of the disc.

Chemistry in the developing nebula employs similar mechanisms to that in the ISM, namely occurring either in the gas phase, or on the surfaces of grains. Temperatures and pressures are higher in the nebula, and particles will increase in size as the grains accrete together; increasing temperatures will cause more volatilisation of grain ices and volatiles into the gas phase, but compounds formed in this phase of the development of a planetary system will still be those typical of the gas or solid phase.

For volatile materials frozen onto a grain, reactions would be similar to those in the ISM (described in section 1.5.4). There would be little scope for reactions between organic compounds and mineral surfaces, particularly if the mineral were an unaltered, relatively unreactive species (such as olivine). Previously, it had been believed that hydrated minerals, such as clays could have condensed directly from the nebula (Grossman and Larimer, 1974); later work indicates this is not likely (Prinn and Fegley, 1987), and so these minerals would not be expected to be present at this stage.

At intermediate temperatures (up to *ca.* 800°), a range of reactions can occur (Mennella *et al.*, 1999; Blanco *et al.*, 1999) including processing of small molecules, such as acetylene, to give macromolecular compounds (Morgan *et al.*, 1991; Geiss and Reeves, 1981). This chemistry on grain surfaces, is still similar to that occurring in the ISM, but operating at higher rates due to the higher temperatures. Thus, it is possible that the evolution of organic materials in the early Solar System may mirror that in the ISM, only faster, generating a similar range of compounds but over a much shorter time.

In a nebula, temperatures range from over 1000° at distances less than 1 AU, to that of interstellar space at the extreme edge (Boss, 1993), thus providing a range of conditions under which chemistry can occur. Although only decomposition will occur at the highest temperatures near the developing star, there is scope for the simple compounds formed in the cold, tenuous interstellar environment to react together in other regions, further from the star, in a number of ways, to give molecules of significant complexity. For example, aldehydes (formed by homologation of carbon, followed by carbonylation), can react with ammonia and hydrogen cyanide, followed by hydrolysis, to give amino acids; dicarboxylic acids could be formed by oxidative fragmentation of PAHs linked by aliphatic chains and so on. The amino acid glycine was reported as having been detected in interstellar space (Kuan *et al.*, 2003), but this discovery is now in doubt (Snyder *et al.*, 2005), despite laboratory simulations indicating the possibility of synthesis induced by UV radiation of ices (Lee *et al.*, 2009). Nevertheless, this molecule has also been detected in cometary samples returned by Stardust (Elsila *et al.*, 2009).

Chondrules and CAIs

In very energetic environments, such as close to a star, aggregations of dust can be melted to form chondrules, approximately spherical structures typically 0.2-2mm in diameter, mostly composed of relatively high-melting point anhydrous minerals, such as olivine or pyroxene. The exact mechanism of formation of chondrules is not known (Boss, 1996), and discussion is outside the scope of this project. Other refractory objects formed in the early nebula are calcium-aluminium-rich inclusions, or CAIs. These are small particles, typically 1-2 mm in size, containing very high-melting point minerals, and so, as for chondrules, must have formed in a high-

temperature part of the Solar Nebula (MacPherson, 2005), in an environment where all organic compounds would be destroyed.

However, chondrules or CAIs can become coated with dust, prior to further aggregation, forming rims of different mineralogy around them (being that of the dust particles, and unrelated to the chondrules or CAIs themselves), and this process could be facilitated by the presence of coatings of sticky ices or organic materials on the dust grains. Evidence has been found (Kring, 1991) that rims can be composed of several distinct mineral assemblages, that is, formation from essentially primordial, but different, dust reservoirs within the nebula, or from those that have undergone alteration. These rims would retain the organic materials present in the dust, which could have been formed in any of the previously-discussed environments. Any chemistry within the rims of chondrules or CAIs would be expected to be similar to that occurring on grains, that is, in the solid state.

Rims around chondrules are often described as "accretionary" (Metzler *et al.*, 1992), supposing an origin in the nebula where the chondrules accreted a dusty coating. Although there is scope for this coating to be altered (possibly in the presence of organic materials) prior to accretion, or once the chondrules have been incorporated into a parent body (Hua *et al.*, 2002), it is also possible that it is uncoated chondrules that form parent bodies, and their surfaces are altered during consolidation and lithification of the parent body (Sears *et al.*, 1993), forming these rims. This is discussed in the next section. As the organic materials found in fine-grained rims (Pearson *et al.*, 2007b) may have their origins in any of these scenarios; untangling the history of the rims surrounding chondrules is one of the ultimate objectives of the work described in this thesis.

1.5.6. Chemistry on Planetesimals and Meteorite Parent Bodies

Formation of planetesimals

As the remnants of the Solar Nebula circulated around the early Sun, dust particles collided and coalesced, forming progressively larger particles which eventually merged, over one or two million years, forming the planets and other bodies of the Solar System (Weidenschilling, 2011). Being composed of numerous small grains, the set of compounds present in these developing planetesimals is potentially much greater than on a single grain, and so much more complex chemistry is possible, particularly as, due to higher temperatures and pressures, liquids may be present. The key difference in this environment is therefore the ability of compounds present to mix, and to react together, in solution, as discussed in this section.

The temperature of these growing rocky bodies depends on their distance from the Sun, and their size. Clearly, the closer to the Sun, the warmer they will be, so that within certain distances, volatile compounds will be melted or vaporised, but beyond that, these compounds would remain frozen. The temperature of an accreted body will also depend on its size. All planetesimals will contain a certain proportion of short-lived radio-isotopes, such as ^{26}Al or ^{60}Fe, (injected into the molecular cloud by a nearby supernova), the decay of which will generate heat (Hevey and Sanders, 2006). The larger the body, the less heat is lost to the surroundings, so the more is retained, and the hotter the body will become. For small bodies, such as asteroids, this heating will result in the melting of ices, vaporisation of volatiles, and thermolysis of organic compounds. For larger bodies, temperatures will be such that minerals will melt, resulting in gravitationally-driven differentiation, forming planets and other achondritic bodies. Under those circumstances, organic compounds will

not survive. Thus it is within the smaller bodies, the parent bodies of meteorites that solution chemistry is most likely to occur.

Solution chemistry within asteroids

As ices supported on small grains melt, the resulting liquids are exposed to vacuum and will evaporate, as the pressure is very low. In contrast, liquids forming deeper within larger rocky bodies may not be able to escape into space, particularly in closed systems, where permeability is low, and extensive fluid flow cannot occur. Thus, pressures will rise, allowing liquids to continue to exist and be retained within those bodies. As the temperature rises further, and less-volatile ices melt, environments of different temperatures and polarities are formed, as shown in Table 1-3 below. The much more polar environment in solution provided by these higher-melting ices enables new chemistry to occur, which was not possible in the previous environments. Thus the set of compounds which could be formed is expanded, possibly facilitating extensive multi-molecular chemistry. For example, compounds insoluble in non-polar solvents at low temperatures could now dissolve, and react. This phase in the lifetime of a meteorite clearly offers the environment capable of generating the largest variety of organic materials.

Compound	Liquid range (K)	Dielectric constant (ε)
Carbon monoxide	68 - 82	1
Methane	91-112	2
Ammonia	195-240	22
Water	273-373	80

Table 1-3: Physical properties of solvents formed from ices

If the temperature rises high enough to melt water ice, an aqueous environment will be produced, where water will dissolve soluble salts, and then enable hydrolysis of

other materials, both organic and inorganic. In the presence of liquid water, silicates, such as olivine and pyroxene undergo hydrolysis to generate hydrated sheet silicates (phyllosilicates) and clays. Clays are known to exert a catalytic effect on many chemical reactions (Wallis *et al.*, 2009; Varma, 2002), and so clearly there is an opportunity for interactions between the mineral and organic components of these bodies. The extent of this possible interaction is currently not known, but could represent a major pathway for the synthesis of organic compounds. As discussed in section 1.2, understanding the formation of organic compounds by abiotic processes, possibly involving interactions with co-located minerals, which then provide the feedstock for the development of life (on the early Earth) is the ultimate purpose of this study.

Anhydrous minerals present in the accreted parent body will react with water (and other solvents) in ways that depend on their structure. These reactions may also vary, depending on the nature of any organic materials present in their vicinity. In the absence of significant fluid flow throughout a meteorite (as demonstrated by Bland *et al.*, 2009), and therefore without thorough mixing by solution flow, the organic heterogeneity may be considerable, depending both on the original organic, and inorganic compounds present.

Within the matrix of the meteorite, the fine-grained minerals present, possibly with coats of dust and ices, may well react in a very complex manner once the ices melt, as the number of potentially-reacting species is high. This may result in a complex mixture of organic materials existing in close proximity to matrix grains.

A similar consideration applies to the fine-grained rims surrounding chondrules (as discussed in the previous section). Their nature could form a key part of

understanding the relationships between organic and inorganic materials. Alteration of the minerals making up the rims may have been contemporaneous with the formation of the organic materials currently co-located (either before, or after accretion). Alternatively, those organic materials may have migrated into the rim assisted by local fluid flow, having been formed elsewhere, such as in neighbouring regions of matrix. If the minerals making up the rims could be shown to cause catalytic formation of the organic materials, then a genetic link would be much more likely. The nature of the organic materials themselves could help identify the time of their formation, if for example, their structures are diagnostic of chemistry occurring in the solid-phase (supported on icy grains) or in solution (post accretion). To enable this potentially complex history to be understood, it is necessary to understand which organic materials are found located with which minerals. Once those associations are understood, it may be possible to unravel the history of the chemical processes which have occurred.

It is not just the formation of small organic molecules which may be linked with minerals. The site of IOM formation is also not known, and although it may form in peristellar environments (as discussed in section 1.5.3), and be accreted either as discrete carbonaceous grains, or as a coating on minerals, it is possible that it formed by condensation reactions of small molecules, within the parent body. The mechanism for such chemistry is not clear, complicated by the uncertainties around the structure of IOM. Nevertheless, understanding its location within the structure of the meteorite, and the nature of co-located minerals can only help understand its mechanism of formation.

Lithification

In the absence of lithification, accreted bodies would remain unconsolidated, and liable to further disruption. They could be cemented together by impacts, melting material between grains and clasts, with lithification on cooling (Consolmagno, 2000), or else by mineralogical changes, caused by the action of water (Skinner, 1989). These processes may well have affected the organic components as well as the inorganic. An alternative cementation mechanism could be the organic materials themselves. If the grains and dust are coated with organic materials prior to accretion, then this material can glue the grains together, at first lightly, but if IOM molecules condense further, by reacting together, an extended macromolecular structure may develop within the fabric of the meteorite (as discussed in the previous section). The mineral components might then be bound together with substantial strength (Flynn *et al.*, 2010; Flynn *et al.*, 2008). Again, an understanding of the location of IOM, and of co-located minerals must help in unravelling its history.

1.5.7. Post-Fragmentation Conditions Experienced by Meteorites

In Solar orbit

Whilst still orbiting the Sun, chemistry would be expected to be active within a meteorite parent body whilst that body remained warm enough for liquids to exist. The heat retained in such bodies depends on their size, larger bodies cooling more slowly than small ones (as the surface area to volume ratio increases, increasing radiative heat loss). On fragmentation (for example, following a collision between two parent bodies), heat generated during the collision will cause volatiles to be lost to space, but subsequently, cooling will be accelerated, and synthesis will be slowed significantly. Once the body has re-frozen, then chemistry will be equivalent to that of a frozen grain. Although the surface of the body will be warmed by the Sun

(allowing reactions to occur, and volatiles to escape), within the frozen body, any chemistry would be much slower.

Entry into the Earth's atmosphere

On entry of a meteoroid into the Earth's atmosphere, the outer layers are subjected to heating, but for only a few minutes at most. During that time, the outer surface (which would have experienced solar heating) is ablated away, and only the inner portion will survive to fall to Earth. As these bodies have a very low thermal conductivity, the interior will experience little or no heating. Studies have been carried out to understand the chemistry that may occur during this phase (Wilson, 2009), but for a large body entering the atmosphere, only the outer layers will suffer chemical change; the interior will remain cold and unmodified.

Residence on the surface of the Earth

The final environment in which chemical change can occur is during residence on the Earth, under normal terrestrial conditions. Atmospheric weathering will cause changes to the mineralogy (*e.g.* soluble minerals such as gypsum, will be washed out by rain (Cooper and Jenniskens, 2012)), or minerals can undergo aqueous weathering (forming new minerals). In addition, a meteorite can also absorb terrestrial organic compounds from the environment, and it is important that these are not mistaken for indigenous materials. Although the potential for such contamination was recognised some time ago (for example, Hayes, 1967; Hamilton, 1965), definitive evidence of contamination has been obtained more recently, for example, *via* isotopic analysis of hydrocarbons (Sephton *et al.*, 2001; Watson *et al.*, 2003).

Contaminants can include long-chain hydrocarbons, indicative of terrestrial plant chemistry (Watson *et al.*, 2003), or amino acids with an enantiomeric excess

indicating likely enzymatically-mediated synthesis, and thus a terrestrial origin (Pizzarello *et al.*, 2008).

1.5.8. The Origins of Meteoritic Organic Materials: Summary

Carbonaceous chondrites contain organic materials which originated in one or more of the environments discussed in this section. Those environments fall into three main categories, and can be summarised as:

- Gas phase: The ISM (cold and tenuous) and Solar Nebula (warmer and denser)
- Solid state: On the icy surfaces of grains
- In solution: Within meteorite parent bodies after accretion

Materials capable of formation in either of the first two groups of environments may have been incorporated into the parent body of the meteorite and remained unchanged, or possibly undergone some degree of modification, or they could have been formed there, from simple precursors.

For materials which may have either a nebular or parent-body based origin, then some unique marker of their synthetic origin is required in order to understand where formation occurred. For such a marker to be valid however, it must uniquely define the synthetic conditions. For example, the ratio of deuterium to hydrogen, previously considered as indicative of a pre-solar origin (Millar *et al.*, 1989) has now been postulated as also resulting from ionic reactions within the Solar System, implying a much more recent origin (Remusat *et al.*, 2009). Furthermore, it has also been suggested that hydrogen-deuterium exchange occurs in the chemical extraction of IOM prior to analysis (Kerridge *et al.*, 1988), and the isotope ratios determined are in fact, an artefact of the isolation process. Whilst there is uncertainty in the source of

this isotopic ratio, it cannot be used as an indicator of the origin of the organic material without other evidence.

Assuming no terrestrial contamination, any organic compound found in a meteorite, for which formation in solution is the only viable mechanism, must have formed within the parent body of the meteorite. The presence of a co-located mineral, capable of catalysing its formation would provide strong evidence of formation *in situ*. If its formation can *only* occur *via* such catalysis, then co-location can be taken as evidence that the compound formed in that location only.

The value of meteoritic organic compounds in the search for an understanding of the formation of life on Earth was discussed in sections 1.1 and 1.2; the remaining sections of this chapter set out the objectives of this project, and means by which they might be achieved.

1.6. Project Objectives

As discussed earlier in this chapter, organic compounds (which may have either an interstellar or nebular origin), formed part of the materials which went to make up the asteroids and planets of the Solar System. In smaller bodies, the parent bodies of asteroids, temperatures may not have reached the point where organic materials decompose, but only such that liquids could exist and intermolecular reactions could take place. The compounds which formed, possibly in association with minerals (either extant, or after aqueous alteration) may have a history similar to those that formed on the early Earth. By studying the compounds found in meteorites, which pre-date the emergence of life, in particular, the associations between inorganic and organic compounds, we may learn how the compounds necessary for life formed on Earth.

The objective of this project was therefore to determine whether such associations exist, and if so, to understand the nature of the associations, *i.e.* which minerals were co-located, and genetically linked with which classes of organic compound. To discover if such co-location exists, it is necessary to detect and identify both minerals and organic materials, *in situ*, within the structure of a meteorite sample.

The objectives of the project are therefore

- To develop methodology for the detection of classes of organic materials in situ, within carbonaceous chondrites
- To study the mineralogy of samples of carbonaceous chondrite, in conjunction with the methodology above, to determine the nature of any physical association between organic and inorganic components of the meteorite
- To attempt to understand the nature of any mechanistic link between the formation of these co-located materials

The approach taken to meeting these objectives is discussed in the next section.

1.7. The Detection of Meteoritic Organic Materials *in situ*

1.7.1. Background

Much work has been carried out to determine the mineralogical structure of carbonaceous chondrites, identifying minerals found in the various parts of the meteorite (Papike, 1998). Detection of organic materials, co-located with specific minerals has not been studied to the same extent. Organic materials have been located in relation to mineral components using a non-specific staining reaction (with osmium tetroxide (Pearson *et al.*, 2007b)), but to date, no other methods using bulk samples without preparation (and therefore avoiding possible physical disturbance), or destruction, have been reported.

Most analytical information (such as that discussed in section 1.4) relating to organic materials in meteorites has been obtained using solvent extracts, or from demineralised residues; therefore any information on the original location of the organic materials has been lost. To understand exactly where the organic materials are located within the fabric of the meteorite, and which other materials are also present in that location, methods for detection and analysis *in situ* are needed. The initial aim of this project is therefore to develop such methods.

1.7.2. Constraints

To determine if spatial relationships exist between meteorite components, it is important that these components are not moved relative to one another during sample preparation or analysis. There is a risk that cutting and polishing could redistribute the softer organic materials with respect to mineral grains, thus rendering any spatial relationships which might be detected as meaningless. Such surface smearing has not been widely reported, but has been noticed in the preparation of samples of shale for SEM (Pye and Krinsley, 1984). Similarly, immobilisation by use of epoxy resin must also be avoided, as the resin (containing organic materials) will permeate pores and voids in the meteorite structure and so obscure detection of materials previously in place. Its concentration would also be considerably greater than the organic material originally present. Clearly, use of any solvent, which would dissolve and redistribute soluble materials, must also be avoided. Until surfaces can be analysed before and after these manipulations, and locations of organic materials be shown to be unchanged, then it is prudent to keep any physical manipulation to a minimum.

As the total organic content of a carbonaceous meteorite is, at most, only a few per cent, the organic content per cubic micron is of the order of a few picograms, and

thus methods sampling on a micron scale will only have this quantity of material available to generate some analytical signal. If this were not sufficient, then spatial resolution would have to be lowered to allow a larger area or volume to be sampled.

Any analytical method must be capable of operation under the constraints outlined above, if organic materials are to remain undisturbed in position, and analysed *in situ*.

1.7.3. Methods used for Analysis of Meteoritic Organic Materials

Most of the methods used to generate the data presented in section 1.4 are unsuitable for the generation of data *in situ*. Many spectroscopic methods, for optimum performance, normally require the analyte to be in solution, such as Infra-red (IR) and Ultra-violet (UV) spectroscopy or physically placed within a spectrometer (and so only delivering a result as an average of a bulk sample) such as Nuclear Magnetic Resonance (NMR) or Electron Spin Resonance spectroscopy (ESR). Spectral resolution of such solid state spectroscopy is inferior to that obtained from materials in solution.

Reflectance IR spectra have been obtained from solid samples of meteorites, but the methodology used required a small sample to be flattened or ground flat before analysis (Kebukawa *et al.*, 2007). Nevertheless, areas showing absorptions due to carbonyl-containing organic materials are clearly seen, as shown in Figure 1-8, where signal strength has been rendered as a colour scale. This method would need to be modified before it could be used for *in situ* detection, to enable the use of unprepared samples. Near-field IR spectroscopy, whilst capable of excellent spatial resolution, requires extensive sample preparation, slicing the sample to the required thickness with an ultra-microtome (Kebukawa *et al.*, 2010).

Mass spectrometry (MS), which has been used to generate much data on small samples, requires introduction of a sample in the liquid or gas phase into an ionisation chamber, resulting in its destruction. Using the NanoSIMS instrument (Hoppe, 2006) developed by Cameca , a sample is ionised by bombardment with ions, which are directed into the spectrometer. It can be used to analyse very small regions for specific ions, but requires extensive sample preparation, and cannot be used for unprepared, topologically rough samples.

MS methodologies have been developed in which an ion or laser beam is moved across a sample, vaporising a small region of the surface. The vapour is analysed in a spectrometer, but the region being analysed is destroyed in the process. A dual laser system, where one laser is used to vaporise a portion of the sample, and another to ionise the vapour produced (known as "L^2MS") has also been used to study meteorite samples (Spencer *et al.*, 2008). Although this method also results in destruction of the sample, useful results have been obtained *in situ*, demonstrating the variability of content of organic species across the surface of a sample (Clemmett *et al.*, 2012a). Since the sample is destroyed by the technique, re-analysis using this, or any other method, is not possible. This method is still being developed to enable detection of a range of organic species (individual organic species require a particular laser frequency to ensure selective ionisation), but an example of a map showing the presence of hexane and hexene in a sample of Bells is shown in Figure 1-9.

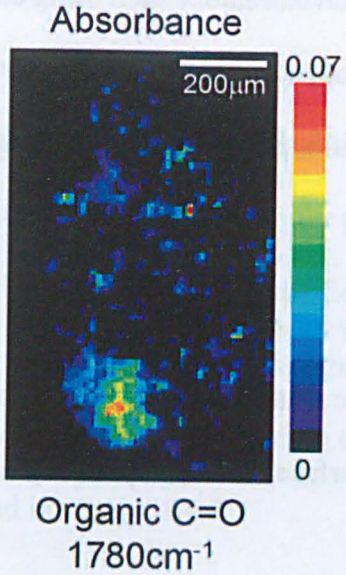

Figure 1-8: Map of strength of IR signals obtained from sample of Tagish Lake showing regions rich in carbonyl-containing compounds (from Kebukawa *et al.*, 2010)

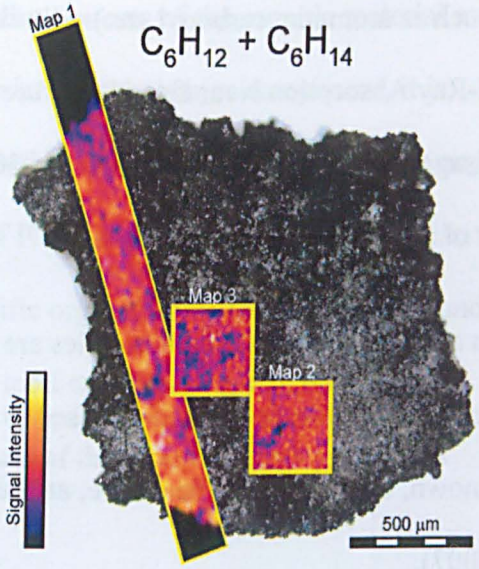

Figure 1-9: Map showing the distribution of hexane and hexene in Bells deduced from the strength of IR signals (from Clemmett *et al.*, 2012b)

Analytical data using a variety of methods has been obtained on thin wafers of meteorite, removed from a sample using an ion beam (this procedure is discussed in section 2.3.2). Although spatial relationships within the wafer can be studied, wider associations, such as across the surface of the sample, cannot. Extraction of a wafer is also dependant on the structural stability of the meteorite sample. Carbonaceous chondrites are not well-cemented, and fragile wafers are prone to disintegration during preparation and handling. Such wafers have however been studied using Transmission Electron Microscopy (TEM) (Zega *et al.*, 2007), in conjunction with NanoSIMS, to identify the location of specific isotopic hotspots.

Electron Energy-Loss Spectroscopy (EELS) can also be used to obtain data on the presence of organic materials in thinned wafers extracted from samples of meteorite (Garvie and Buseck, 2004), although in this technique, spatial resolution is limited by that delivered by the X-ray source used. Nevertheless, the technique can be used to show the presence of elements such as carbon in different chemical environments

(such as aromatic, carbonyl *etc.*). Similar results have been obtained using carbon X-Ray Absorption Near Edge Structure Spectroscopy (XANES), for which disaggregated samples (Wirick *et al.*, 2006), or wafers isolated by ion-milling (Zega *et al.*, 2007) have been used.

In all these methods where samples are isolated by ion-milling, the degree of damage, or chemical change, caused to the organic materials by the ion beam is not known, but is likely to be severe, at least on the surface of the sample (Zega *et al.*, 2007).

X-ray photoelectron spectroscopy has been used to detect the presence of specific elements (such as fluorine) on the surface of a sample, but that study was not intended to generate data showing spatial distribution (Takahagi and Ishitani, 1988).

The methods described above either require sample preparation (or removal of thin samples from the bulk) or result in sample destruction, or use methodology which is under development. The application of Raman Spectroscopy, and Scanning Electron Microscopy-Electron Dispersive Spectroscopy (SEM/EDS) to the generation of *in situ* data are described in more detail in Chapter 2. Both techniques have been previously used to generate surface maps of solid, unprepared samples indicating the presence of elements (by EDS) or organic molecules (Raman).

1.7.4. Increasing the Detectability of Organic Materials *in situ*

The methods described above have all been used to detect organic materials present in meteorites, relying on the ability of the techniques to detect signals due to organic functional groups (such as carbonyl), or elemental carbon against the background of the signals generated by the other components of the meteorite. In particular, inorganic, carbon-containing compounds, such as carbonates, could interfere.

In addition, the soluble and macromolecular components of the organic material may be co-located within the meteorite, and as the latter is the major component, it is likely to dominate any analytical signal. Indeed, it may be impossible to detect any soluble organic compounds in the presence of IOM, unless some feature unique to the soluble fraction can be identified. If specific organic compounds (or compound classes) are to be located (rather than just the total organic material), the quantity available drops further, according to the amount of those components present (as discussed in section 1.4.2).

It is proposed therefore to develop a procedure, satisfying the constraints outlined in section 1.7.2, which increases the detectability of organic materials (particularly of specific classes). This methodology, "molecular tagging", involves attachment (at the molecular level) of some atom or functional group which could be more easily detected than the native, unmodified organic material. The chemical method used to attach tags must avoid the use of solvents, or any physical manipulation which could lead to redistribution of organic materials. The method of detection must be one for which unprepared samples are suitable

The use of this methodology will enable the precise location of organic materials in a sample of meteorite to be determined, and coupled with similar petrological analysis, any associations which may exist between the organic and inorganic components of the meteorite, to be detected.

1.8. Thesis Structure

The initial objective of this project is to develop, and then to demonstrate, methods of molecular tagging suitable for detection and characterisation of meteoritic organic materials *in situ.* These will then be used, in conjunction with established

methodology, for the similar analysis of co-located inorganic compounds, to establish whether any spatial relationships exist between these two components. Work to achieve this objective (and other work subsequently undertaken) is described in the following chapters of this thesis.

The evaluation of analytical methodologies which are suitable for the analysis of tagged meteorite samples is discussed in Chapter 2. Their benefits and limitations are evaluated, in particular discussing the type of information which can be gained from each one. Other analytical methods used in the characterisation of IOM (as described in Chapters 5 to 7) are also discussed.

The development of methodology for molecular tagging is described in Chapter 3. To preserve valuable meteorite samples, terrestrial analogues were used in the development phase; the advantages and disadvantages of different analogues are discussed.

In Chapter 3, the development of a process for the activation of IOM towards tagging is also described. This methodology involves the exposure of samples to ozone with the aim of introducing functional groups which would be more reactive towards the conditions developed for tagging. This work also involves the use of terrestrial analogues, and was progressed in parallel to the development of tagging chemistry. Results obtained from the chemical modification and tagging of meteorite samples are described in Chapter 4, but were not as expected given the structure and reactivity of IOM as described in the literature.

To better understand these reactions of meteoritic organic materials, IOM, isolated by demineralisation of Murchison, using literature methodology, (described in the Appendix) was exposed to the same activation conditions. This work, described in

Chapter 4 showed that isolated IOM did not react in the same way as IOM still contained within the meteorite sample. The implications of the results obtained are also discussed.

To better understand the effects of demineralisation on the structure of IOM, a sample of Murchison was demineralised using two literature methods (described in the Appendix), and the results compared. The first part of the procedure, solvent extraction and acid washing is described in Chapter 6. The subsequent removal of silicates is described in Chapter 7.

It was found that not only did IOM isolated from Murchison by demineralisation behave differently from organic material still in place within the meteorite, but that samples of IOM isolated using the two methods behaved differently from one another as well. The implications of these observations, and their influence on current understanding of the nature of the organic content of carbonaceous chondrites is discussed in Chapter 7, along with future work which could be carried out to resolve remaining uncertainties.

Finally, Chapter 8 contains a summary of the results of this project, the progress towards meeting the project objectives, and proposals for future work to achieve objectives not yet met.

Chapter 2 Analytical Methods

The analytical methods discussed in this chapter are those that were used to collect data in support of the objective of this project, namely to determine precisely where within a sample of a carbonaceous chondrite organic materials are located, and with which minerals, if any, specific classes of organic materials are co-located.

For each method, its theory, advantages and limitations are discussed, focusing on the specific nature of the information that it can (and cannot) deliver in the context of this work. Examples are given for each technique, illustrating the typical data generated.

The first two methods, Raman Spectroscopy and Scanning Electron Microscopy were selected for use to support the development of a methodology for *in situ* analysis (as described in section 1.7). These methods have the advantage that they require little or no surface preparation, and both have been previously used to generate data from samples of meteorites.

Images of sample surfaces were obtained using these two techniques. Although those obtained using SEM were typically of high quality, the limited depth of field of the microscope used in Raman spectroscopy gave images with only a small portion in focus. In addition, as the images generated by SEM and Raman microscopy are visually quite different, it is often difficult to locate a single portion of the sample surface using both techniques. A methodology enabling better recognition of surface features was developed and is described in section 2.3. The remaining methods (Pyrolysis-2D Gas Chromatography-Mass Spectrometry and Stepped Combustion)

are not applicable as *in situ* methods, but were used as part of the work described in Chapters 6 and 7, the investigation into the structure of IOM.

2.1. Raman Spectroscopy

2.1.1. Background

Theory

Raman spectroscopy relies on the phenomenon of the inelastic scattering of photons of light, following an interaction with phonons related to vibrations of chemical bonds in the structure of the substance under test (for an introductory text, see McCreery, 2000). When photons incident on a sample are scattered, the majority do not undergo any change in frequency (this is known as Rayleigh scattering). A small proportion however, *ca.* 10^{-6} are scattered inelastically, and undergo a shift in frequency, both to higher and to lower values, equal to that of the vibration involved in the interaction. Those scattered to lower frequency (Stokes scattering) are of higher intensity than those scattered to higher frequency (anti-Stokes scattering). Only the Stokes signals are used to produce the Raman spectrum. A Raman spectrum therefore consists of a number of signals at the frequencies of chemical bonds present in the sample, as well as combinations and overtones of those frequencies. Raman shift frequencies are usually reported using units of cm^{-1}, as for infra-red spectra, which also originate from vibrations of chemical bonds. Samples require little or no preparation, and this technique is particularly useful for insoluble materials, such as macromolecules or minerals.

Spot spectra

Raman spectra are acquired by directing a laser onto the surface of a sample, and collecting the scattered light. This generates a spectrum relating to the small area of

the sample illuminated by the laser. To obtain data over a surface, the laser is moved from point to point as appropriate, collecting a spectrum at each location. Thus a single point spectrum can be acquired, or a set of spectra can be collected, and compared or processed in some way.

Mapping

An approach which is often more useful is to automate this process, collect a large number of spectra, and then process them to create a map, corresponding to the area over which the spectra were collected. The information of interest (for example, the strength of a particular signal, or the ratio of two sets of signals) is extracted from the spectra and then represented (usually) as a colour scale across the area of the map. If these signals are diagnostic of some surface feature (such as that generated by a particular mineral), then the map generated represents the presence of the mineral within the area sampled. An example is shown in Figure 2-1, generated by Bernard *et al.* (2008). In this image, colours represent signals characteristic of minerals (red-garnet, green-quartz, yellow-aragonite, cyan-calcite), thus clearly showing the spatial relationships between them.

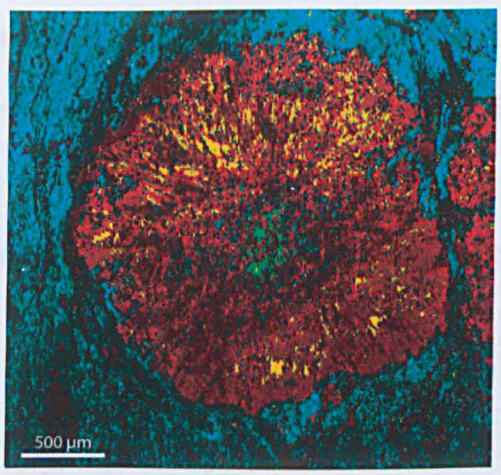

Figure 2-1: Image formed from Raman signals due to minerals present (red-garnet, green-quartz, yellow-aragonite, cyan-calcite (taken from Bernard *et al.*, 2008)

Spectra of terrestrial carbonaceous macromolecular materials

As Raman spectra can easily be obtained from insoluble materials, it has proved useful in the study of the nature of the organic materials which make up coal and oil. Whereas pure carbon, graphite, gives a single sharp signal at 1581 cm^{-1}, coals and oils give two main broad bands, one at around 1570-1600 cm^{-1}, and the other at about 1350-1400 cm^{-1}. These are commonly known as the "G" (Graphite) peak and the "D" (Disorder) peak respectively. An example is shown in Figure 2-2. The spectrum of graphite is shown in Figure 2-2A, beside that from a sample of a carbonaceous phyllite (Figure 2-2B). The G peak arises from the vibrations of perfect graphene sheets (from which graphite is formed) (Novoselov *et al.*, 2005), and the D peak is absent. Deviations away from this perfect structure are described as introducing "disorder", and thus giving rise to the D peak. As the graphite structure is disrupted, extra signals due to substituents at the edges of the graphene sheet are seen, as well as those generated as the graphene structure deviates more and more from the perfect infinite two-dimensional structure (Ferrari *et al.*, 2006). Theoretical studies have shown that the G peak is in fact due to stretching of sp^2 bonds, whereas the D peak is due to breathing modes of six-membered rings (Castiglioni *et al.*, 2001b; Castiglioni *et al.*, 2001a). The latter vibration is Raman-inactive in a perfect graphene sheet, hence the absence of the D peak in pure graphite.

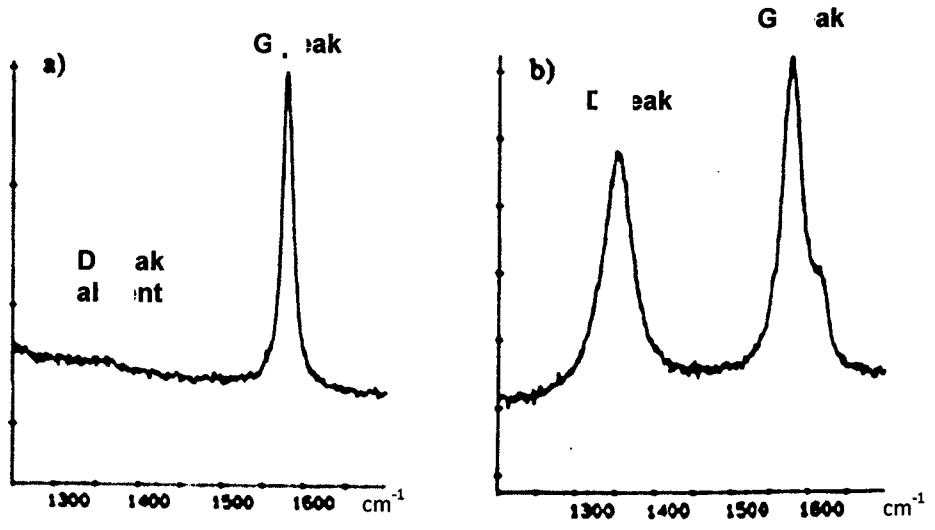

Figure 2-2: Comparison of Raman spectra of a) graphite, showing only G peak, and b) carbonaceous phyllite showing both D and G peaks, (taken from Wopenka and Pasteris, 1993)

Many studies have been carried out investigating the relationship between degree of maturation and/or graphitisation of organic materials, and Raman signal positions and widths (Quirico *et al.*, 2009; Muirhead *et al.*, 2012). For example, by taking samples of coals of differing grades of maturity (as indicated by the vitrinite reflectance value, Rm, which is a measure of the degree of alteration experienced by coal deposits), the effect of maturation on the Raman spectrum can be seen (in Figure 2-3) (Quirico *et al.*, 2009). The differences in the spectra are due to changes in the structure of the carbonaceous materials present, although the exact nature of those changes is not necessarily well-understood. Such spectra can then be used to study the degree of chemical alteration, caused by pressure and heat due to burial at depth under various conditions (Quirico *et al.*, 2005b; Potgieter-Vermaak *et al.*, 2011).

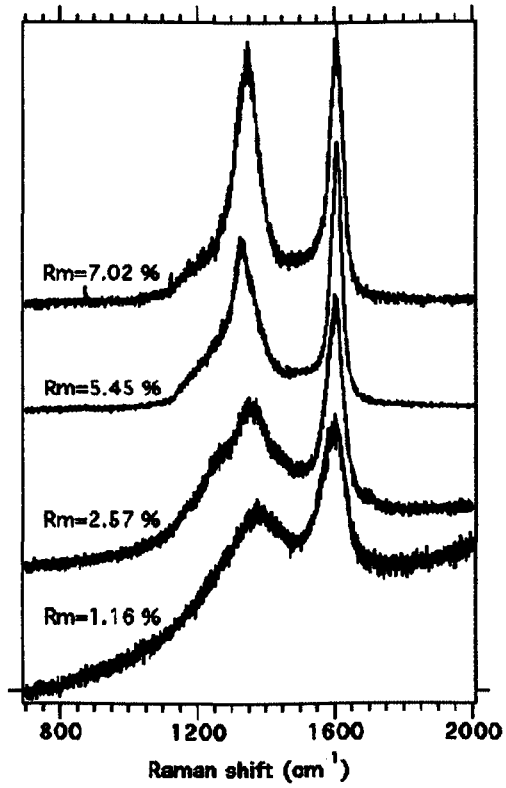

Figure 2-3: Raman spectra of coals of different maturation levels, as defined by Vitrinite Reflectance, Rm (taken from Quirico *et al.*, 2009)

Spectra of meteoritic organic materials

Meteoritic organic material is often compared with that found in terrestrial rocks (as discussed in section 1.4.3). Despite their origins being very different, the Raman spectra of carbonaceous meteorites resemble those of terrestrial coals and other organic-containing rocks, as shown in Figure 2-4, that data being generated in a study of the Raman spectra of a range of meteorite types (Busemann *et al.*, 2007). This showed that the ratio of the D and G peak areas varies between meteorite classes, indicating that the proportions of the parts of the IOM molecules giving rise to these two peaks also vary. Thus, the structure of IOM appears to vary across this set of meteorite samples.

The variation observed by Busemann *et al.* (2007) may indicate a correlation with chemical change of IOM during the alteration history of these meteorites. Other studies using CO and CV meteorites have shown similar differences in the shapes

and peak ratios of the peaks between 1300 and 1700 cm^{-1}, interpreted as modification to the structure of polyaromatic carbonaceous material (Bonal *et al.*, 2006, Bonal *et al.*, 2007). The differences could also indicate an inherent variation in the IOM, due to incorporation of different reservoirs during accretion of the various parent bodies of these meteorites, or possibly both an initial difference in IOM content, and different alteration histories.

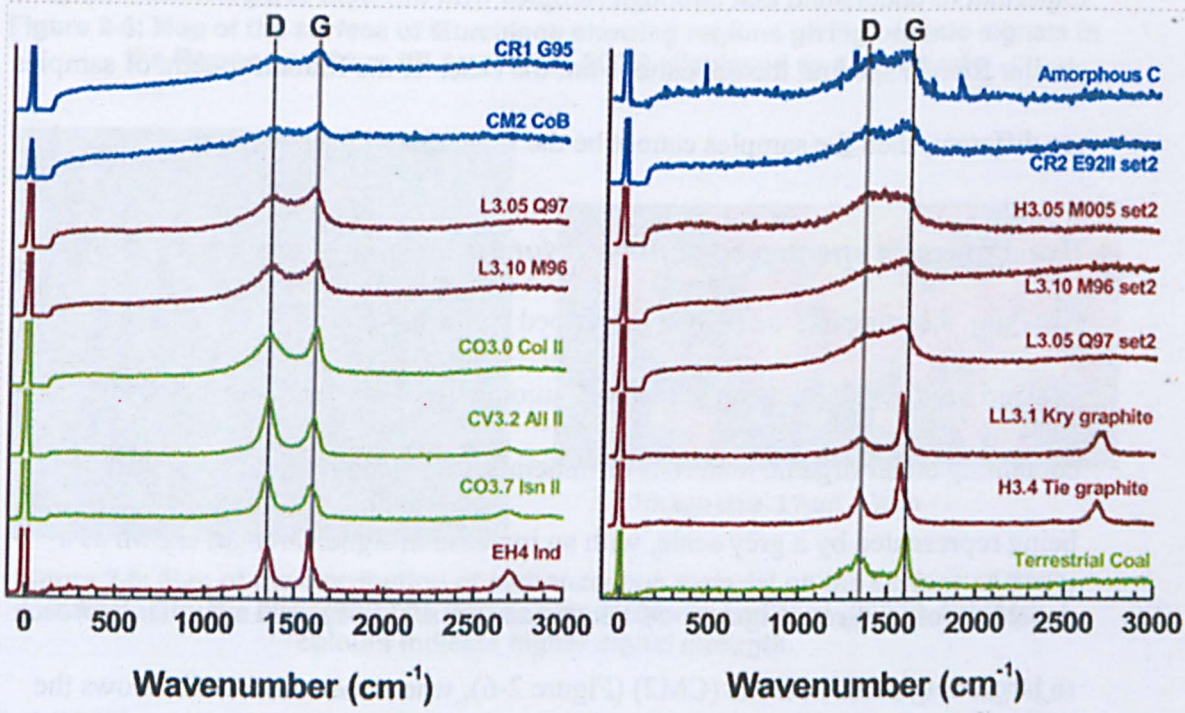

Figure 2-4: Raman spectra of IOM from various meteorites, with D and G peaks highlighted (taken from Busemann *et al.*, 2007). At this scale, differences in the positions of the peaks cannot be determined

As the structure of IOM within these meteorites before any alteration had taken place is not known, it is not possible to determine which of these alternatives is the case. Detailed comparison of the spectra of IOM with that of terrestrial kerogen to attempt to determine IOM alteration histories may not be valid, as the origins, and therefore structures, of these two macromolecular materials are quite different, as well as the effects of pressure and temperature on their structures (see section 1.4.3). It is also important to understand that although samples with different compositions may give similar Raman spectra, the opposite is not the case. If the Raman spectra of samples are different, then the samples cannot be the same material.

Use of Raman spectra to generate surface maps of meteorite samples

Applying the mapping technique (described earlier) to grains of Murchison, El Amri *et al.* (2005) generated low-definition maps showing distinct regions containing either organic materials or minerals, the strength of the organic signal being represented by a grey scale, with an increase in signal strength shown as a darkening of the grey (Figure 2-5). Busemann *et al.* (2007) used a similar approach to larger fragments of Bells (CM2) (Figure 2-6), where the colour scale shows the strength of the signal due to IOM, between 1200 and 1800 cm^{-1}, in this case, the higher the signal strength, the brighter the colour. In both cases, a higher signal strength is correlated with a higher concentration of organic material.

These two figures are examples of non-specific visualisation of the locations of organic materials. The grey- or colour-scales represent the presence of aromatic carbon, with no selectivity between classes of organic compound, soluble or macromolecular.

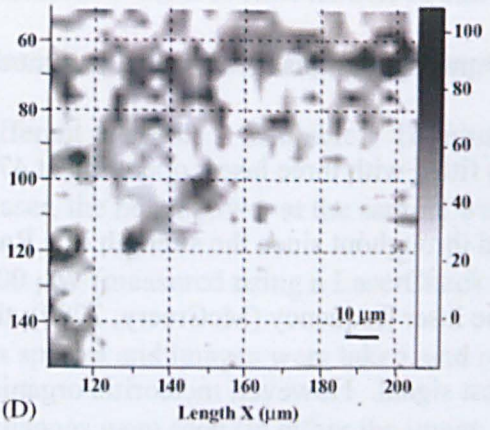

Figure 2-5; Map of the surface of Murchison showing regions giving organic signals in the Raman spectrum (El Amri *et al.*, 2005), displayed as a grey scale

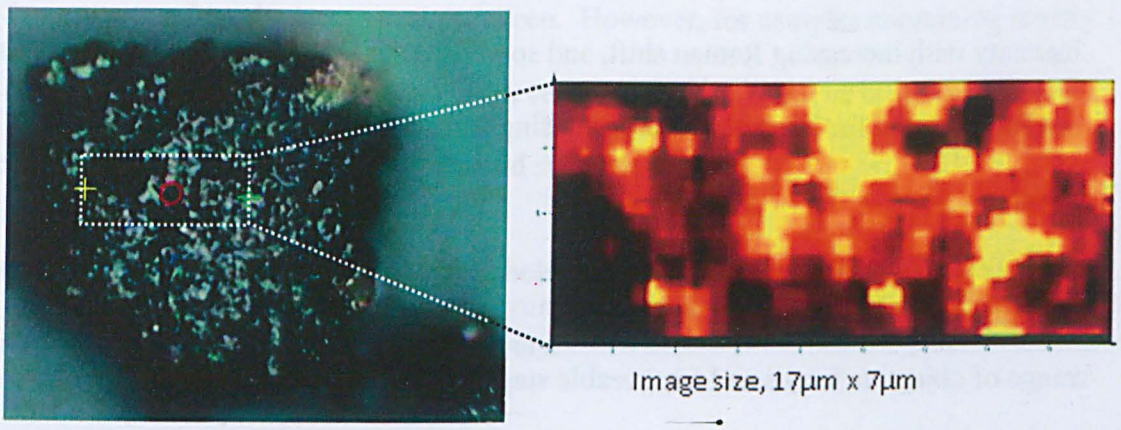

Figure 2-6: Map of the distribution of carbonaceous material on the surface of Bells, indicated by the strength of its Raman signal (Busemann *et al.*, 2007). Brighter colours indicate higher signal strength.

2.1.2. Use of Raman Spectroscopy in this Study

Instrumentation

All spectra were collected using a Jobin Yvon LabRAM HR confocal Raman Spectrometer, supplied by Horiba Scientific. The instrument is controlled using Labspec software (version 5.64.15), which was also used for data processing and spectral manipulation. The instrument contains a Peltier-cooled CCD detector, operating at *ca.* -80°, which delivers a value of photon count for a specific spectral range of scattered light. For the standard settings used, a grating of 600 lines/inch and a spectral range of 2000 cm^{-1}, the output is a series of data points representing

photon counts at intervals of Raman shift of 2 cm^{-1}. Greater resolution could be obtained using a finer grating, but this would result in a much lower signal strength.

The spectrometer was fitted with three lasers operating at 473, 514 and 632 nm. The 473 nm laser was used throughout since the strength of a Raman signal depends on the fourth power of the laser frequency (McCreery, 2000); the shortest wavelength light gives the strongest signal. However, meteoritic organic materials often fluoresce and the overall level of fluorescence increases on irradiation with shorter wavelengths of light. The fluorescence appears as a featureless signal, increasing in intensity with increasing Raman shift, and so gives a steady rise in the baseline. This can be corrected for using the data-processing software, as described later in this section.

The laser beam is directed by a series of mirrors into a microscope, fitted with a range of objective lenses and a moveable stage. The stage can be moved manually, or using the instrument software. During sample set-up, the sample is illuminated with white light. By moving an internal beam deflector, this light is directed through the microscope into a video camera, the output of which is viewed using Labspec software. The white light is turned down, and the beam deflector removed before taking a spectrum.

Spectra were acquired using the x50 lens; when the laser beam is focused on the sample surface, a spot size of about 2 μm diameter was formed, which defines the area of the surface sampled in any one spectrum. This could be reduced by restricting the width of the laser beam, but at the cost of lower signal strength. The laser light reflected and scattered off the sample is directed back through the instrument into the spectrometer (where reflected and Rayleigh scattered light is

blocked out). The amount of laser light incident on a sample is adjusted by altering the output power of the laser itself, and/or by employing a neutral-density filter in the beam path (a range of different densities is available). To minimise possible sample damage by the incident laser, the beam power at the sample was restricted to a maximum of about 40-100 μW (measured using a LaserCheck power meter supplied by Coherent Inc.). When spectra and images were taken, and re-taken of an area using these settings, no changes were seen (in either the image or the spectrum). For organic materials in a rock matrix (such as meteorite whole-rock samples), sample damage caused by the laser was never seen. However, for samples containing mostly organic materials, such as isolated IOM, care needs to be taken, as heat damage was seen when the laser power was increased substantially.

Other instrument parameters (confocal hole diameter and slit width) were not varied, and set at 300 μm and 150 μm respectively.

Before use each day, the spectrometer was zeroed and calibrated using a silicon standard which gives a strong, sharp peak at 520.7 cm^{-1}. When calibration was repeated after continuous use for several hours, or after an overnight run, changes in the position of the calibration signal was found to be no more than 1 cm^{-1}.

Spectra were collected for sufficient time to give a good signal-to-noise ratio, by selecting a suitable irradiation time and number of acquisitions for combination by the software. The instrument manufacturer recommends only a small number of acquisitions (up to five), but extension of the acquisition time if the signal is weak, or noisy. Typically, four acquisitions were used, extending each as necessary (which could be up to *ca.* 500 seconds for an organic-poor sample).

Sample preparation and manipulation

The lack of need for extensive sample preparation for Raman spectroscopy has been stated previously; for this study, samples were not physically prepared in any way. Samples of meteorite or rock chips, or powders were held using the same method as for SEM (see section 2.2), *i.e.* mounted on small aluminium stubs. For acquisition of a Raman spectrum, these stubs were mounted in a holder made from a screw-top vial top, which was placed directly onto the microscope stage. Liquids were placed on a slide using a Pasteur pipette.

In all cases, whilst viewing the sample under low magnification (x10) using the video camera, it was moved into the centre of the field of view, and the microscope manually focused. The magnification was increased to x20 then x50, refocusing each time. The poor depth of field of the microscope (see section 2.1.4) made focusing directly at high magnification very difficult.

Data processing and manipulation

Data was processed using the proprietary software Labspec 5 (version 5.64.15), and spectra were collected singly, or in sets. Single spectra were acquired after visually selecting a specific region or feature for study and aligning it with the laser beam by manually moving the microscope stage.

It was, however, necessary to focus the laser onto the sample, and so if the topography varied by more than a few microns, refocusing was necessary if more than one spectrum was acquired. The software provides a routine to refocus between each sample, based on maximisation of the signal strength within a pre-set range. This Autofocus feature was used in the acquisition of sets of spectra, but added to the total time required per sample (up to a minute per spectrum).

Typical sets of spectra comprised 15-40 spectra, collected over 6-24 h, with the stage movement pre-programmed using the software. A rectangular region of the surface was selected (visually) that appeared to contain the desired features for analysis (for example, organic-rich areas), and points selected with sufficient separation that spectra did not overlap. A typical area might be 50 μm square, with spectra taken every 10 μm, generating 25 spectra.

Average spectral parameters (for example, positions of the D or G peaks) were obtained by acquiring a set of spectra, taken over an area of sample, controlling the instrument using the mapping options. The instrument was set up to collect spectra over a rectangular area of the sample surface, by movement of the microscope stage at pre-programmed intervals.

Spectra were collected over the standard frequency range 200-2200 cm^{-1}, then the regions below 1000 cm^{-1} and above 2000 cm^{-1} discarded during processing when studying the signals due to aromatic carbon. The region between 1000 and 2000 cm^{-1} contained all the signals of interest, and gave a flat baseline after processing. The signal due to fluorescence was subtracted by applying a baseline correction (using a second order polynomial function) to the set of spectra.

The positions of the peaks seen in these spectra were determined in two ways. The Raman spectrometer generates a spectrum calculated by Fourier transform of the signals received at its sensor. These signals, although resembling a continuous spectrum, are in fact a histogram of photon counts over a spread of Raman shifts depending on the diffraction grating selected. The standard grating (600 lines/cm) gives a resolution of 2 cm^{-1}. The Labspec software uses peak-fitting routines to

convert the histogram into a set of smooth, fitted peaks. These routines also return other parameters including peak width and area.

The software attempts to fit a Gaussian or Lorentzian peak, or a combination of the two, to the histogram of data generated by the spectrometer. Whereas this peak-fitting procedure is appropriate to sharp, single peaks, originating in simple molecular systems (such as a pure standard organic compound), its relevance to the analysis of broad bands such as those obtained from IOM should be questioned. IOM is not a simple compound, but a complex mixture of macromolecules (as discussed in section 1.4.3), consisting of numerous interacting and non-interacting vibrational systems. As such, its Raman spectrum is best considered as an envelope over a set of spectra, which could have any peak shape, and could be quite symmetric or very skewed, depending on the nature and ratio of these components. Although the software may be able to generate a small set of overlapping peaks which fit the observed spectrum well, they can have no real physical meaning, such as each being generated by a single vibrational system within the structure of IOM. When this peak fitting is attempted, the position of the maxima of the calculated peaks does not coincide with that of the actual peaks (*i.e.* the position of the G peak is underestimated, and that of the D peak overestimated in all cases). Manual adjustment is therefore required to determine the actual position of peak maximum. When plotted, (as shown in Figure 2-7), a distinct difference between the two sets of values can be seen (illustrated using data obtained from samples of IOM, as discussed in section 5.4).

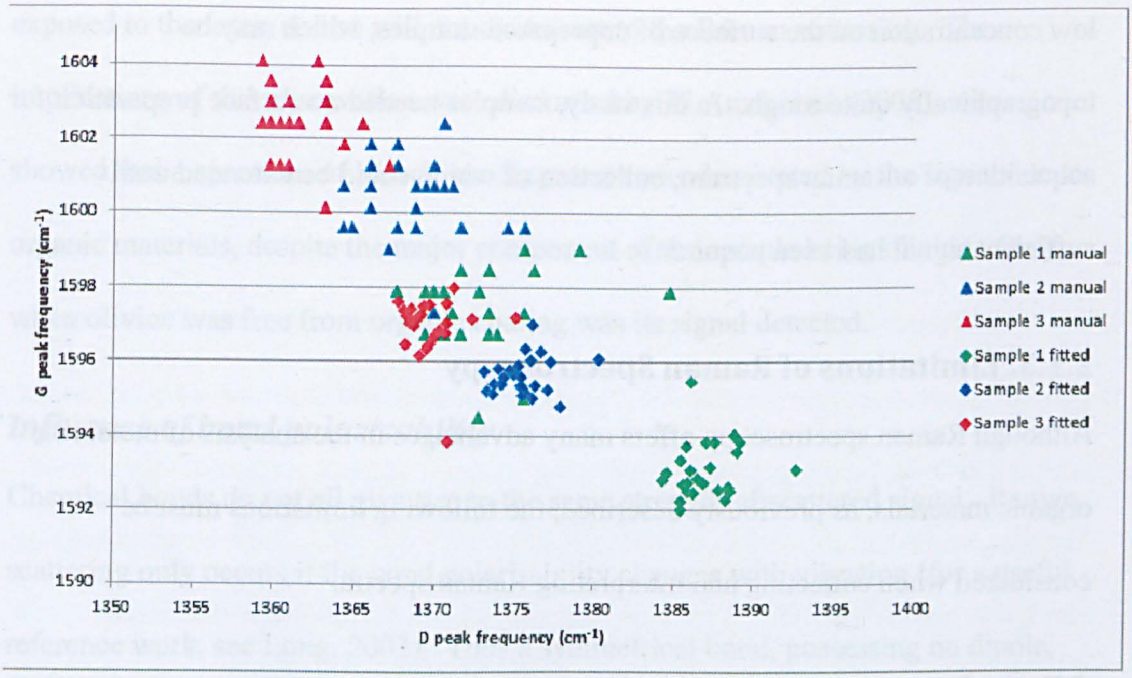

Figure 2-7: Comparison of peak positions obtained by fitting and manual adjustment of spectra obtained from three samples of IOM isolated from Murchison (section 5.4)

The differences measured between each set of fitted and manually adjusted peaks are similar, so, for the purposes of this study, any trends in the relative positions of these peaks are equally apparent from either set of data, although clearly, absolute comparisons must be made like with like. The manually-adjusted data shows a wider spread than that fitted by the software; this uncertainty is estimated as no more than ± 1 cm^{-1}. The wider spread is due to a limitation in the software, which restricts the smooth manual adjustment of peak positions, so in all experiments, the position fitted by the software was used for any comparisons. The data obtained from this procedure was exported into Microsoft Excel, and used to produce the graphs shown in Figure 2-7 and the later sections of this thesis.

Generation of maps

Maps were generated as previously described, using similar methods to those used by Busemann *et al.* (2007), shown in Figure 2-6. In section 1.7.2, the constraints on analysis of solid samples were discussed, namely the need to detect compounds at

low concentration on the surfaces of unprepared samples, which may be topographically quite rough. In this study, samples needed no surface preparation for acquisition of a Raman spectrum, collection of which could be extended until sufficient signal had been acquired.

2.1.3. Limitations of Raman Spectroscopy

Although Raman spectroscopy offers many advantages in the analysis of meteoritic organic materials, as previously described, the following limitations must be considered when collecting and interpreting Raman spectra.

Effect of sample orientation

The strength of a Raman signal depends on the orientation of the vibrating bond to the direction of laser polarisation. For amorphous materials this orientation is randomised across the sample, but for crystalline materials (such as mineral grains) , significant variations in signal strength may result depending on the orientation of the sample, rather than in the concentration of the contributing mineral species. Thus at certain orientations, signals from crystalline mineral grains may be difficult to detect, with the grains not being identified on, for example, surface maps.

Influence of surface opacity

The signal is also affected by the transparency of the sample. For highly transparent substances, the laser may penetrate some distance into the sample before being scattered. For meteoritic organic materials however, being dark and opaque, this is not the case, and the laser will essentially only interact with the surface of the substance under test, penetrating less than a micron. This is an important limitation; for the meteorite samples typically studied in this work, the Raman signal is that of the surface layer alone. Any underlying mineral, or other material, will not be

exposed to the laser, and so will not contribute to the Raman scattering. The implications of this observation were discussed by El Amri *et al.* (2005), who showed that a spectrum of Murchison fragments was dominated by the signal due to organic materials, despite the major component of the sample being olivine. Only when olivine was free from organic coating was its signal detected.

Influence of bond polarisability

Chemical bonds do not all give rise to the same strength of scattered signal. Raman scattering only occurs if the bond polarisability changes with vibration (for a useful reference work, see Long, 2002). Thus a symmetrical bond, possessing no dipole, but with its polarisability changing on vibration, will give a Raman signal. For example, although a carbon-carbon double bond only gives a weak absorption in an IR spectrum (which is generated from changes in dipole during vibration), it shows a strong peak in the Raman spectrum. Although carbonyl bonds are much stronger in IR spectra than in Raman, other bonds due to such functionality (such as carbon-carbon and the carbon-oxygen single bonds of carboxylic acids) would also be expected to give rise to strong Raman signals. It may not be possible to assign each signal observed to a specific functional group, but the set of signals for a specific compound can act as a fingerprint. Changes in this fingerprint are evidence of change in the structure of the compound giving rise to it.

Discontinuity of maps

Mapping also has limitations. A map is built up from a set of signals obtained at discrete locations as the laser beam is tracked across the sample surface, and not from a continuous variation of signal. The laser beam used is focused through a microscope, and at the sample, is only a few microns in diameter. Thus it is only this small region which can generate a signal, and so for mineral grains, or surface

features larger than the laser spot, only a portion will be illuminated and so give rise to a spectrum. To obtain a spectrum from the whole of a large feature, it is necessary to move the laser across the sample, taking many spectra at small intervals. In contrast, for grains or features smaller than the laser spot, many of these may be irradiated at one time, resulting in a composite signal. In such cases, it may be possible to deconvolute the data obtained from many spectra taken at small intervals across a sample, using appropriate software. If the laser spot is moved only a small distance across the surface between each spectrum, then a very large number will be needed to map even a small area of the sample. If larger gaps are left between spectra, then although a larger area can be covered, small features may be missed entirely. As the software blends the set of discrete signals into a continuous map, such small features would therefore not be present.

A significant drawback of the instrument used for Raman spectroscopy is poor depth of field of the microscope. This difficulty is addressed in the next section.

2.1.4. Use of the Raman Microscope for Imaging

Influence of poor depth of field

To select an area for study by Raman spectroscopy, a sample is placed on the microscope stage of the instrument, and viewed *via* the video camera. Using a series of objective lenses (typically x10 to x50), successively higher magnifications are used to home in on the area of interest. However, the depth of field of the microscope is very small, typically less than 5 μm at the highest magnification, making recognition of features of interest very difficult. This problem is particularly acute as rock samples (and all unprepared samples used in this study) are generally topographically rough, and uneven, so that only a small portion is in focus, with the

region of focus moving across the surface as the sample is moved up and down. This region may only be a few microns wide, and so it is very difficult to recognise surface features. An example of an image acquired from a fragment of Murchison is shown in Figure 2-8 (note, Labspec software does not create a scale bar when images are saved as TIFF or JPG files; scale bars attached to these images have been added manually, and are approximate).

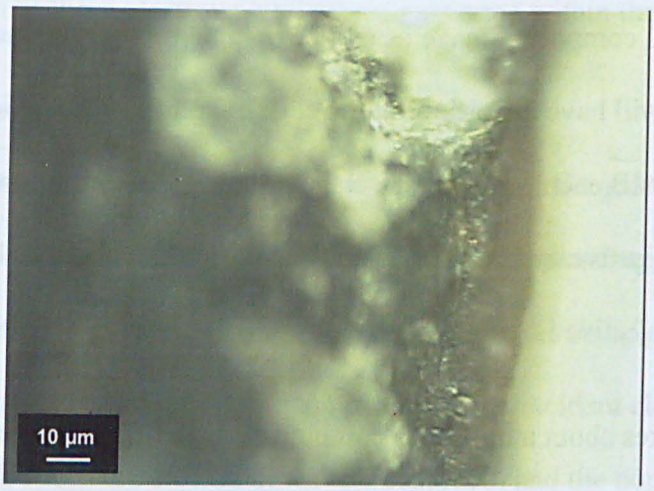

Figure 2-8: Poor depth of field shown in a Raman microscope image of Murchison fragment

Image stacking

By adjusting the microscope stage up and down (in the Z-direction), a series of images can be obtained, each of which shows a small area of the surface in focus. Commercial software is available which can process such a set of images and using various algorithms, select only the areas in focus and combine them together to give a focused image (Piper, 2008). Two programs were evaluated, Helicon Focus (http://www.heliconsoft.com/heliconfocus.html) and Zerene Stacker (http://zerenesystems.com/cms/home). Both programs can be configured to optimise the images produced, and for the purpose of generating in-focus images of chips of meteorites, both gave very similar results (the quality of the images produced was identical by eye). Zerene stacker was chosen for future work, as its configuration

options (although not needed for this project) were more extensive, and may be useful in other work, or for more specialised imaging applications.

Practical considerations

When generating images for stacking, it is important to make sure the sample movement is restricted to the Z-direction. If the sample moves from side to side (in the X and Y directions), then areas at the edge of the sample will not feature in all images, and a full composite image cannot be obtained. The software will generate an image, but it will have distortions at the edges. Images were typically obtained as TIFF files (*ca.* 1MB each), moving the stage up or down 1 μm between each image, when the x50 objective was used. A larger separation can be used if a lower-magnification objective is used.

The software takes about a minute to combine 50 such images generating an image, in focus, of a similar file size to each individual image.

The image shown in Figure 2-9 was compiled from 30 images using Zerene Stacker and covers the same area of the fragment of Murchison as shown in Figure 2-8.

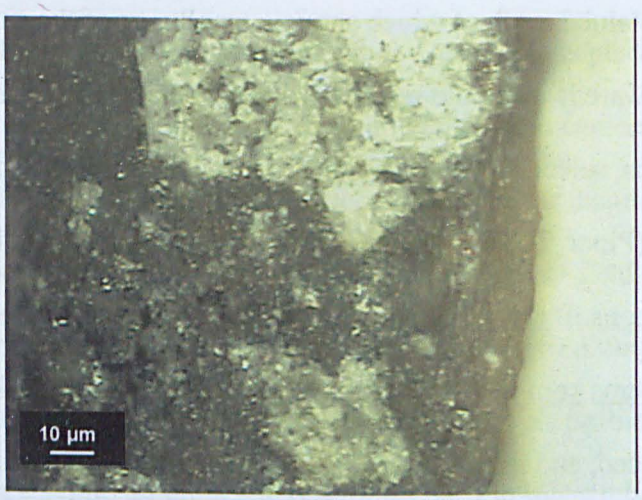

Figure 2-9: Stacked image of Murchison fragment showing improved depth of field compared with unstacked image (Figure 2-8)

2.2. Scanning Electron Microscopy (SEM)

2.2.1. Background

Theory

In a Scanning Electron Microscope, a focused beam of electrons is accelerated towards the sample under study, and swept rapidly across it in a rastering pattern. The electrons interact with the atoms of the sample, being scattered in various ways, and *via* detection of these electrons (and others generated within the sample), images are generated.

As the electron beam penetrates the sample, the electrons undergo many collisions with its atoms, initiating a cascade of secondary electrons spreading out within the sample. The depth of penetration of the electron beam into a sample depends on its elemental composition and density, and the energy of the incident electrons. Eventually, the electrons are slowed down and absorbed, and the portion of the sample within which this occurs is known as the Interaction, or Excitation Volume (see descriptive texts such as Reimer, 1998; Goldstein *et al.*, 1981) and is shown in Figure 2-10.

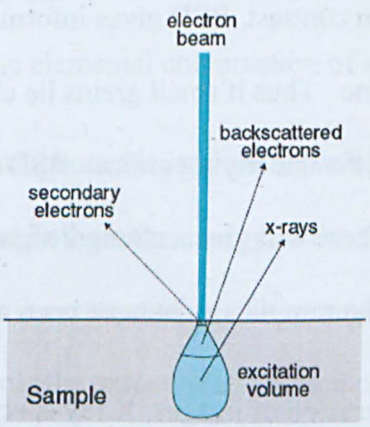

Figure 2-10: Generation of electrons and X-rays using scanning electron microscopy
(Diagram modified from http://www4.nau.edu/microanalysis/microprobe-sem/signals.html)

Secondary electrons are produced by inelastic scattering of the electron beam by the atoms of the sample, especially at low electron energies, when the penetration into the sample is reduced. The probability of electrons escaping the sample decreases exponentially with depth within the sample, so these detectable electrons are largely generated in a layer close to the surface. These electrons are detected by a Secondary Electron Detector (SED). (Secondary electrons are generated throughout the interaction volume, but only those generated close to the surface can escape and reach the detector.)

As the beam penetrates the sample, electrons lose energy and are absorbed. Some however, are scattered back towards the surface (known as backscattered electrons), and these too are captured, in a second detector (a Back Scatter Detector, BSD). The efficiency of creation of these electrons increases with the atomic number (Z) of the atom involved in the scattering.

As the two types of electrons are generated in different parts of the sample, the data generated from them should be interpreted separately. SED gives an image of the surface, with good depth of field, enhanced by shadows in the same manner as images with visible light. In contrast, BSD gives information relating to a substantial part of the interaction volume. Thus if small grains lie close to the surface, BSD will merge data from them with the underlying grains. BSD efficiency is also increased for elements of high Z, so these will give a stronger signal in BSD than in SED (which, if deep enough in the sample, might have been missing completely).

The use of SEM in the generation of images, X-ray spectra and element maps is well-established as a valuable technique in the study of meteorites, and is discussed in the following sections.

Generation of X-Rays

In addition to using an electron beam to produce an image, it can also be used to generate X-rays from a sample. When the accelerated electrons interact with an atom in the sample, another electron can be ejected from an inner electron shell generating an ion. When this ion captures a passing electron, a photon of radiation will be emitted characteristic of the energy levels of the atom concerned. The energy of the X-ray is dependent on the atomic number of the atom (Moseley, 1913), these X-rays forming a series, designated by the letters K, L, M *etc.* By analysing the emitted X-rays using a spectrometer, and measuring their frequencies, the identities of the nuclei can be deduced (for an introductory description, (see Goldstein *et al.*, 1981). The spectrometer used in this study analyses the X-rays by frequency, and is known as an Energy-Dispersive Spectrometer (EDS). The intensity of the radiation depends on the relative quantity of each nucleus present (although differently for each element) and thus, following calibration the relative quantities of each element can be calculated.

As long as the area being sampled is homogenous (*i.e.* for grains larger than the electron beam diameter), this data can be used to calculate the average atomic ratios in a sample, thus allowing the elemental composition of a pure grain to be obtained.

The X-rays are generated throughout the interaction volume (see Figure 2-10). This has dimensions which depend both on the energy of the electrons (*i.e.* the acceleration voltage), and on the composition of the sample, differing from element to element (which also controls the extent of absorption of emerging X-rays by the sample). X-ray spectra generated in this way could be used not only to determine the elemental composition of the sample, but also, following application of a chemical

tag, to detect the presence of organic materials tagged with elements formerly not present.

In common with Raman data, X-rays generated in an SEM can be used in two ways, to obtain spectra at single locations (spot spectra), or to generate surface maps.

Spot spectra.

If an area of the sample is selected by viewing its image (using either SED or BSD), a spot X-ray spectrum can be obtained centred at this region of interest. The signal obtained is generated from a volume a few microns in each dimension, the interaction volume (see Figure 2-10), and not necessarily just from grains visible at the surface. For a sample composed of grains smaller than the interaction volume, or with a surface coating, the resulting X-rays will be related to the average composition of the interaction volume. If the surface coating is relatively thin, its contribution to the overall signal could be very low.

Mapping

Using the instrumental software, element maps can be created by moving the electron beam across a pre-programmed area of the surface, and analysing the resulting X-ray emission as the beam scans the surface. By selecting characteristic X-ray energies relating to elements of interest, then a map of the signal due to that element can be created. Using the instrument software, different elements can be allocated different colours, and so maps of the concentrations of several elements can be constructed. These colour maps can be overlaid on an image of the sample surface, revealing any correspondences with the mineral grains making up the sample. It is important to consider that, whereas the electron image obtained by SED only shows the surface of the sample, the X-ray spectrum is generated in the body of

the sample beneath the surface; if the structure is inhomogeneous, the spectrum may bear little relation to the surface structure.

Application of SEM to extraterrestrial samples

Examples of the use of SEM to generate images and X-ray data are shown in Figure 2-11, derived from a sample of Adrar 003 (an equilibrated ordinary chondrite L/LL3.1)

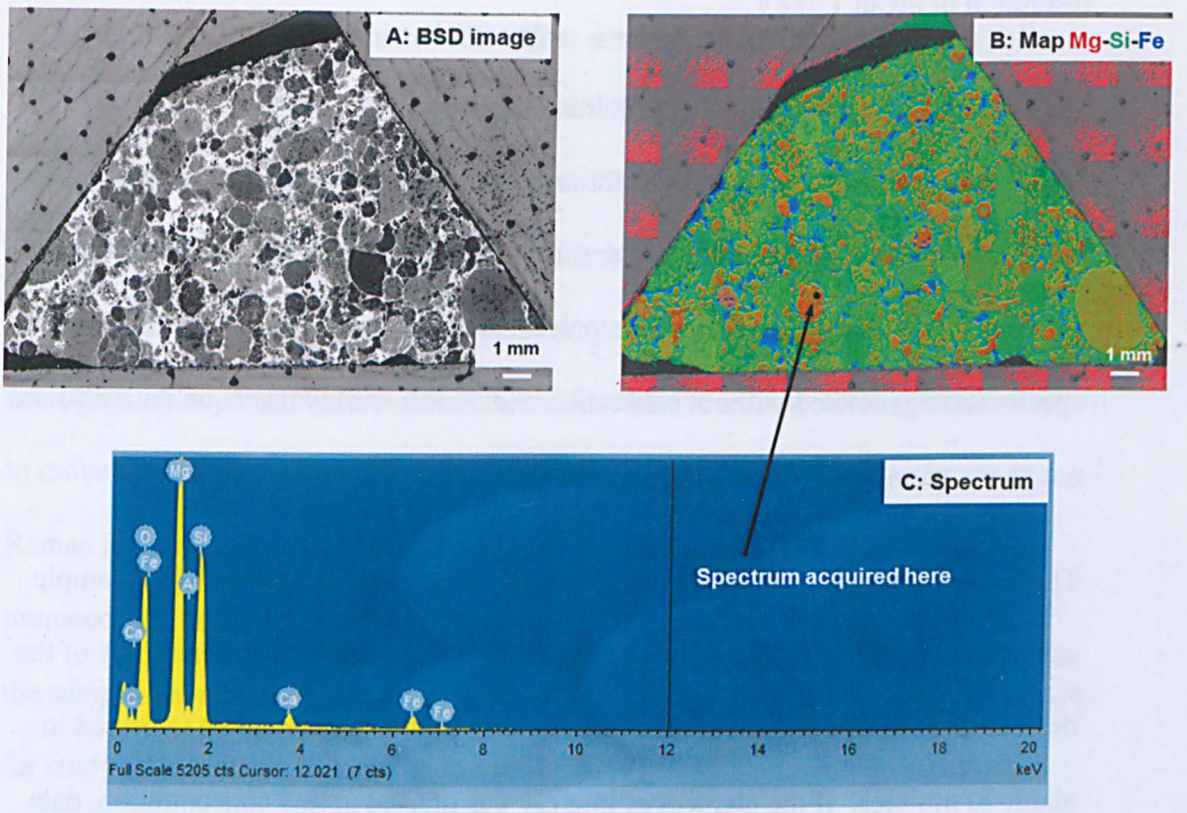

Figure 2-11: A) BSD Image, B) Element map and C) X-ray spectrum obtained from sample of Adrar 003 (unpublished data courtesy of Diane Johnson, Dept. Of Physical Sciences, Open University)

2.2.2. Use of SEM in this Study

Instrumentation

The majority of the work described in this thesis was carried out using a Quanta 200 3D Dual beam FIBSEM (Focused Ion Beam-SEM) instrument, supplied by FEI, using a gallium ion-beam mounted at 52° to the electron beam. The instrument is fitted with an X-Max 80 mm^2 silicon drift EDS spectrometer (Oxford Instruments).

The SEM was typically operated at 20 keV in high-vacuum mode, and the gallium ion-beam at 30 keV. A movable gas injector, containing trimethyl(methyl-cyclopentadienyl)platinum, could be positioned close to the sample to allow ion-beam mediated deposition of platinum.

The EDS detector detects X-rays by generation of photoelectrons as the X-rays strike a silicon target. These are analysed according to their photon energies, with a resolution of about 130 eV.

Data was processed using the Inca Microanalysis Suite (v 4.13) supplied by Oxford Instruments. This provides routines for analysis of X-ray spectra produced from specified locations on the surface. For this study, simple qualitative spectra were acquired, which indicate the elements present within the volume sampled. These spectra were generated without calibration and therefore only used qualitatively, and not to accurately calculate elemental ratios.

The X-rays generated as the electron beam moves across the surface of the sample can also be used to generate a map of elemental composition. The sensitivity of the detector is such that sufficient data to generate a usable map could be collected in about 20 minutes. If the element of interest was present at low concentration, data collection was extended to give a stronger signal. However, if data collection were extended, the signals due to common rock-forming elements become very intense, and if overlaid over a weak signal, could obscure signals from the element of interest.

The software also allows acquisition of images using either electron detector (SED or BSD). These can be taken at any magnification desired, and stitched together either

using Inca, or with other image processing software such as Adobe Photoshop, to produce composite images of large areas.

Some images were acquired using another instrument, a Zeiss Supra 55VP microscope, in which electrons are generated using a Field Emission Gun (and known as a FEGSEM). This instrument generates electrons of lower energy, and was used to create some high-resolution images of fragile materials

Sample preparation, immobilisation and orientation

The aim of this project is to develop methodology for the detection of meteoritic organic materials *in situ.* This is planned to involve chemical modification of the surface of the meteorite, and so it is necessary to develop ways to analyse this surface both before and after treatment, to demonstrate the changes that are occurring. Also, as more than one analytical technique is to be used, it is necessary to move the sample between instruments, and re-locate the area chosen for study. Raman Spectroscopy and SEM are analytical methods with which the samples prepared will be studied, and so it is necessary to find a way to compare images of the samples using these two imaging techniques, and to select portions of the surface for study with both. As described in section 1.7.2, sample preparation must not involve any procedure which could cause organic materials to be moved about the surface, hence any operations involving solvents, mechanical treatment such as polishing or cutting, or embedding in epoxy resin, are not possible. However, in order to return to the same region of the sample for re-analysis (for example, after chemical treatment), some degree of sample immobilisation is required.

Analysis with minimal sample mounting

For analysis by SEM, it is usual to fix a sample to a metal stub (usually aluminium) by means of conducting tape, or a carbon-based adhesive. This restrains the sample against accidental movement (for example, as the sample is moved into view), and also provides a means to prevent charge build-up. (A sample will become negatively-charged during electron impact, giving poor-quality images, unless this excess charge can be conducted to earth.) Charge build-up is often prevented by coating samples with a thin layer of carbon. As the purpose of this project is to detect carbon and its compounds, this method would interfere, creating a permanent background signal, and was not routinely used.

Chips of meteorite or terrestrial rock were placed onto carbon adhesive pads on SEM stubs, and gently pushed into place using tweezers. Powders were sprinkled onto the pad using a spatula. Some samples, chemically treated on glass supports, were not transferred to adhesive pads. In these cases, the glass was fixed to an aluminium stub using conducting tape fixed around its edge.

A sample mounted in this way is also suitable for analysis by Raman spectroscopy; the aluminium stub can be held in any suitable mount and simply placed on the microscope stage (as described in section 2.1.2). The mount also helps fix sample orientation, as the stub can be marked (for example, by scratching) so that its orientation can be easily seen. However, it is possible that methods of fixing samples onto stubs may be affected by any chemical treatments used for tagging organic materials (discussed in section 1.7.2), in that the fixative may react with the reagents employed. This issue is addressed in section 4.2.1.

Very small samples can be placed onto a piece of gold foil (mounted on a special holder) using a micromanipulator, and pressed into it using a special press. Although this will crush and distort the sample, what is formed after the pressing will remain fixed, and is suitable for analysis by both SEM and Raman spectroscopy. These samples were held in a stub, modified to accept the holder containing the gold foil.

Sample orientation and mobilisation

It is easy to move a sample within an SEM; the stage can be moved, tilted and rotated, and so the sample can be set into any orientation desired, in contrast to Raman spectroscopy, for which the microscope stage, on which a sample is placed, cannot be rotated or tilted.

2.2.3. Limitations of Electron Microscopy

A significant limitation of electron microscopy is that the impact of the electron beam on the sample may damage it, in particular, organic materials may be decomposed. Indeed, ion-mediated decomposition of an organic material is the mechanism by which platinum metal is deposited on a sample for FIB milling (as described in section 2.3.2). It is necessary to check samples for changes which may be occurring, for example, visually, or by re-analysis. A situation where damage was significant is discussed in section 5.3.2.

An SEM usually works in a high-vacuum. Under such conditions, volatile compounds will be removed into the vacuum system, but for the study of macromolecular materials, this will not be a problem.

A limitation of X-ray spectroscopy is that the resolution of the spectrometer is limited to about 130 eV. Many X-ray lines lie closer together than this, and so elements giving rise to those lines cannot be completely resolved. If the signals due

to common elements (such as oxygen or silicon) are close to those of the elements used for tagging, the latter will be difficult to detect in low quantities. Consideration of these factors in the selection of elements to use for tagging is discussed in sections 3.2.3 and 3.3.

It is important to remember that X-rays are generated throughout the interaction volume (as are back-scattered electrons) whereas electrons detected with the SED arise in a much thinner layer close to the surface. Data generated by SED is therefore related to this thin layer, whereas that derived from BSD or X-rays relates to the interaction volume. For samples composed of grains smaller than this volume, these data sets will be different.

2.2.4. Use of SEM for Imaging

Obtaining an image by SEM is relatively straightforward. If the instrument is set up correctly, when a sample is placed at the electron beam focus, a good-quality, in-focus image is easy to obtain. The magnification can be adjusted over a wide range (typically x50 to x5000 was used).

Images of a sample of Murchison prior to any treatments or processing, were acquired using both SED and BSD, and are shown in Figure 2-12. Although both images are clear and focused, with good depth of field (in contrast to images obtained using the Raman microscope, discussed previously), features within the meteorite appear quite differently in the two images, which makes initial interpretation of their characteristics difficult. For example, the large feature highlighted appears bright in the SED image (as if it is a mineral grain), whereas in the BSD image it appears as a dark region, seemingly carbonaceous. As the magnification is increased, so the area of the image is reduced, but high quality

images of the whole surface can be obtained by moving the sample at regular intervals, and combining the images so obtained using Inca software (see section 2.2.2) or, for example, Adobe Photoshop. In the image below (Figure 2-13), a set of 71 images taken at magnification of *ca.* x1000 have been stitched together to form a single image, shown reduced in size.

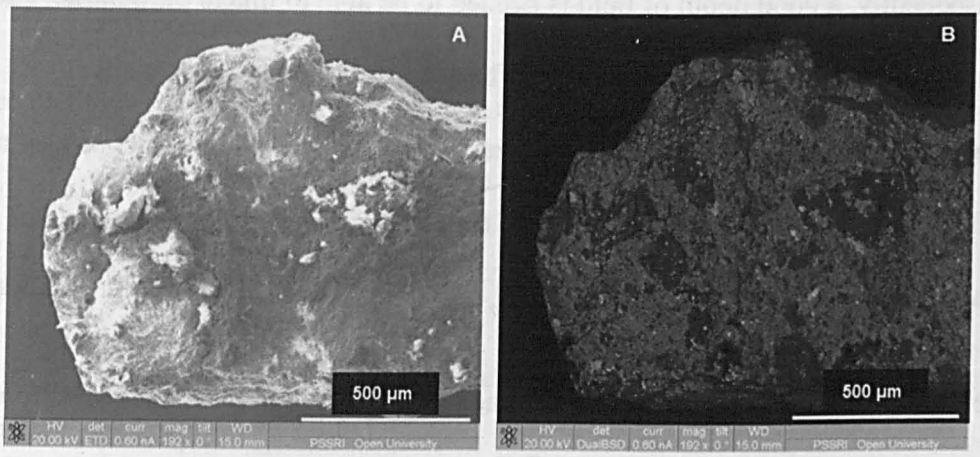

Figure 2-12: Images of a Murchison fragment obtained using A) SED and B) BSD showing difference in appearance using the two detectors

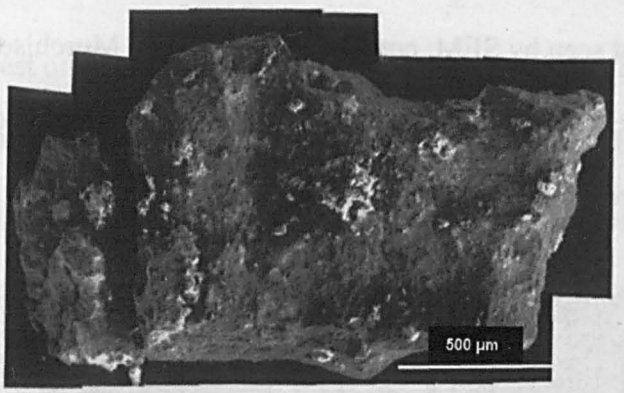

Figure 2-13: Image of a Murchison fragment compiled from many images

2.3. Use of Raman and SEM Imaging in Combination

As discussed in sections 2.1.4 and 2.2.2, useful images can be obtained using both Raman microscopy and SEM. Having been generated in very different ways, the images obtained give complementary information, and so operating both techniques generates more information than either one alone. The main difficulty to be overcome, independent of fixing method, is the need to be able to recognise the area

of sample being analysed, and so obtain images with the two instruments of exactly the same (small) region of a sample surface. Although this sounds trivial, in fact, considerable problems were experienced. The samples of meteorite used to prepare the images above were not mechanically treated, and so possessed considerable surface topography, and at the scale of the instruments being used, are quite rough. Consequently, a good depth of field is needed to be able to image the sample, and to locate the area intended to be analysed. The second difficulty is to be able to recognise features seen using one technique, with the other. Again, this proved more difficult than expected, as the response of the meteorite surface to the analytical techniques proved quite different.

The use of Zerene Stacker to combine images obtained with the Raman spectrometer was discussed in section 2.1.4. Although this software allows the production of good-quality images, the appearance of the surface still appears considerably different from that seen by SEM; comparing images of a Murchison fragment obtained using the two techniques may prove difficult. It is quite difficult therefore to compare features in images merely by eye.

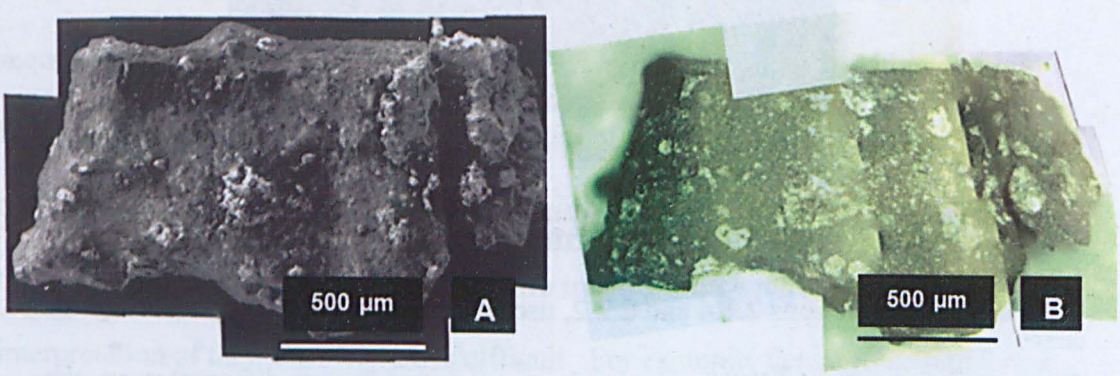

Figure 2-14: Comparison of images of a Murchison fragment obtained *via* A) SEM and B) Raman microscope highlighting the differences in appearance

In order to obtain images of an area of interest using the two methodologies, it is necessary to have a point of reference on the sample, a feature than can be easily seen using both methods. If a distinctive grain or other surface feature is present, it may be possible to use that to locate areas of interest. If such a point of reference is not present, it is necessary to place an artificial marker on the surface, as described in the next section.

Three methods of marking were evaluated and compared:

(i) use of a pre-existing distinctive grain

and, using FIBSEM

(ii) application of a platinum marker, and
(iii) application of a milled marker.

2.3.1. Locating Distinctive Features Using Both SEM and Raman Microscopy

If a region of interest on a sample surface contains, for example, a distinctively-shaped mineral grain, with practice the same region could be found at high magnification using both optical and electron imaging. Using a fragment of Murchison, shown in Figure 2-15, an area of interest was chosen, containing an easily visible feature (the heart-shaped inclusion, highlighted, within the matrix). This region is shown at higher magnification (using the SEM) in Figure 2-17A. The fragment was aligned under the Raman microscope, and an image acquired of the same region (Figure 2-16). The high contrast between the bright inclusion and the dark matrix, as well as the poor depth of field, made comparison of the two images difficult, and at higher magnification, almost impossible. Nevertheless, it is these single images which are needed to find the area over which to acquire the set of images for stacking (it is not practical to acquire sets of images for stacking over the

whole sample, as each image only covers a very small fraction of the whole). Once the area of interest has been located, then a series of images could be acquired, and combined using Zerene Stacker to generate the composite image such as that shown in Figure 2-17B. Although the contrast between the mineral inclusion and the matrix is still high, the image is of good enough quality to allow individual grains to be located. If no suitably-distinctive grain is present in the sample, it is necessary to apply some artificial marker.

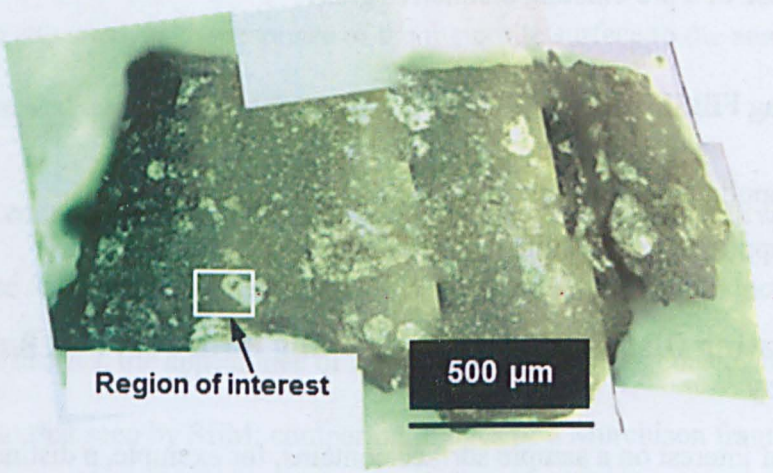

Figure 2-15: Low-magnification image obtained using Raman microscope of a fragment of Murchison, showing heart-shaped inclusion

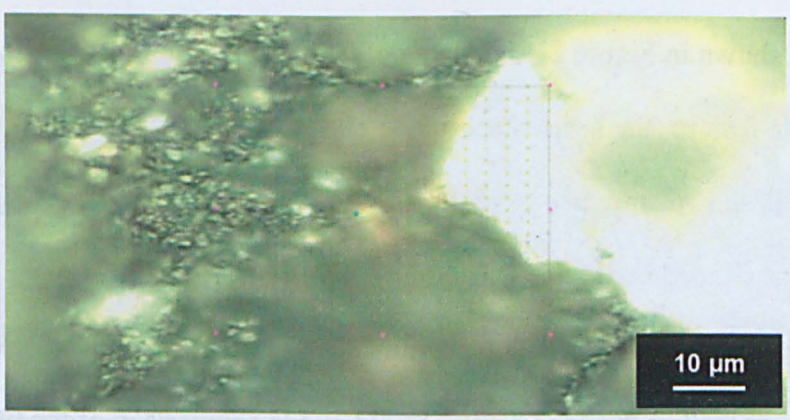

Figure 2-16: Higher-magnification, unprocessed image of the same region of a Murchison fragment as shown in Figure 2-15, obtained using Raman microscope

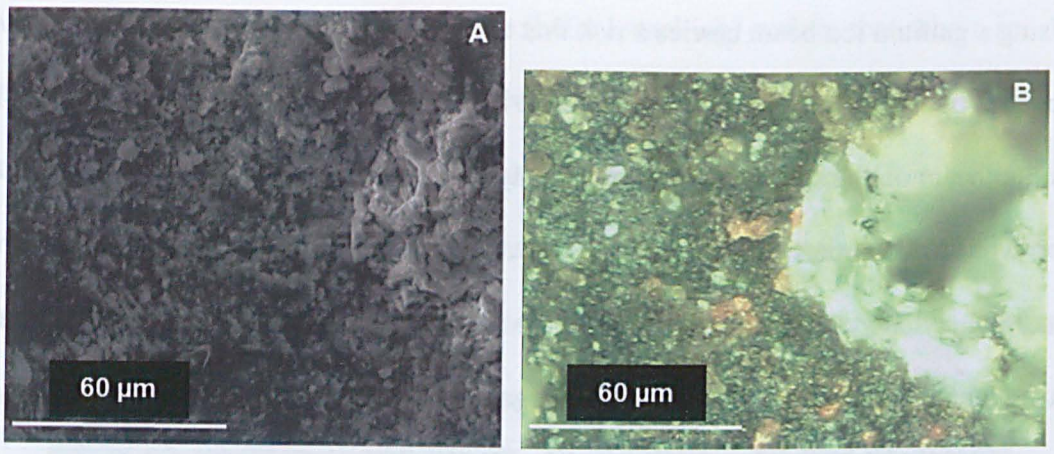

Figure 2-17: A) SEM and B) stacked Raman microscope images of region of Murchison fragment highlighted in Figure 2-15.

2.3.2. Physical Marking of Samples using a Focused Ion Beam (FIB)

Ion milling

The SEM instrument used in this study (described in section 2.2.2) is fitted with a Focused Ion Beam (FIB), mounted at 52° to the axis of the electron beam. This directs a separately-controlled, focused beam of gallium ions at the sample. The gallium ions possess sufficient energy to ablate the sample of the surface, the decomposition products being removed by the SEM vacuum system. By rastering the ions across the sample, material can be removed to give holes and trenches as desired. This methodology (known as ion-milling) is also used to prepare thin wafers of a sample, which can be removed for analysis using other techniques (for a description, see Zega *et al.*, 2007). The ion beam can also be used to decompose a gaseous compound of platinum, introduced close to the sample. The platinum atoms thus liberated are deposited onto the sample. This technique is usually used to protect the sample surface when milling TEM samples, laying down a platinum strap, to enable the thinned sample to be safely extracted and manipulated (Zega *et al.*, 2007). In this study however, this technique was used to apply a marker to the surface.

Using a gallium ion beam carries a risk that the beam may chemically modify the sample, or cause gallium to be incorporated into the minerals present. The impact of an ion beam on the sample surface physically ablates material; organic compounds too will be decomposed and removed. Towards the edges of the beam, where its energy may be too low to cause physical disruption of the surface, there may still be sufficient to cause decomposition of the organic materials present. Material ablated may be redeposited away from the ion-beam, and gallium ions may become embedded within the minerals, altering their structure. As gallium is typically present at very low levels in meteorite samples, any detected after FIB use can be assumed to come from the beam, and ignored. To minimise these effects, the ion beam should be directed as far away as practicable from the area of interest.

Deposition of a platinum marker

The second approach was to use the FIB to deposit a layer of platinum on a sample surface. By directing a gallium ion beam onto the sample surface, whilst applying a stream of a volatile organometallic compound (trimethyl(methylcyclo-pentadienyl)platinum) (Huth *et al.*, 2012) to the same location, platinum atoms (formed from the ion-mediated decomposition of the compound) are implanted into the sample surface. In the example shown in Figure 2-18, the SEM software was used to raster the ion beam across the surface, forming a marker in the shape of an arrow. Two images of a fragment of Murchison are shown in Figure 2-18. The image shows that the platinum arrow (contained within the white box) is not particularly clear, although the contrast between it and the background was much greater using BSD (as shown in Figure 2-19). The area of the arrow was examined using the Raman microscope, but even with image stacking (Figure 2-20), it only showed as an indistinct bright patch. It is necessary to be able to locate the area

which has been marked in a single image (before stacking) such as that shown in Figure 2-16. Only when the area of interest has been located (even if not in focus), is it possible to know where to acquire the set of images to be stacked. (It is impractical to acquire stacked images of such small areas over the whole of the sample). As the arrow proved very difficult to see in the optical image, this approach was not progressed further.

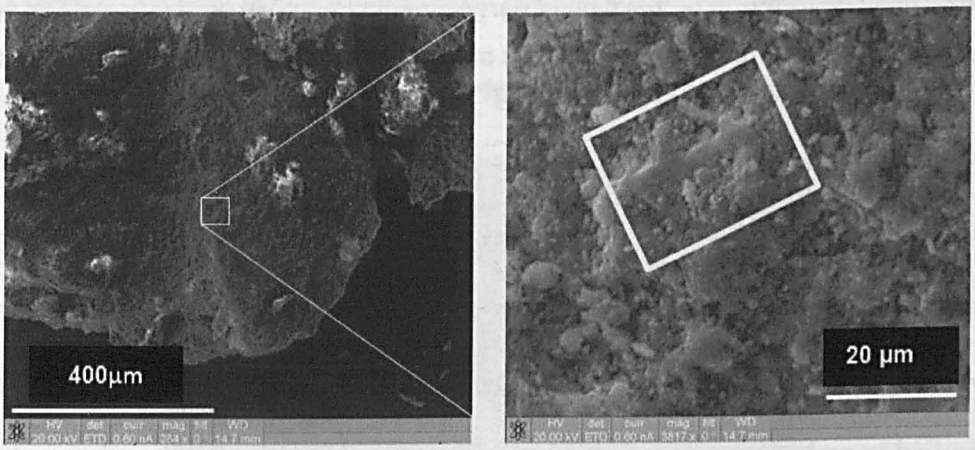

Figure 2-18: SED Images of platinum arrow deposited on a fragment of Murchison. The arrow can clearly be seen

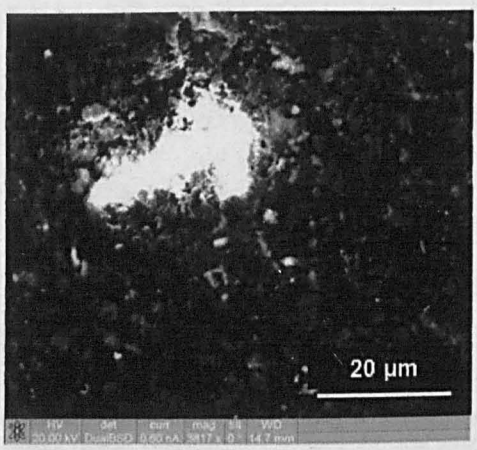

Figure 2-19: BSD image of arrow deposited on a fragment of Murchison. In contrast to the SED-derived image (above), the arrow is indistinct.

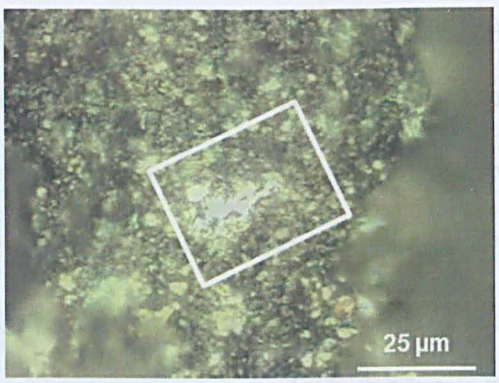

Figure 2-20: Stacked Raman microscope image of the same arrow as shown in Figure 2-19, which is barely visible in visible light.

Cutting a marker using FIB milling

If the gallium ion beam is directed at the sample surface, the ions collide with, and dislodge, the atoms making up the surface molecules, which are then removed by the vacuum system of the SEM (or redeposited elsewhere). By adjusting the ion current to an appropriate level, and directing the beam across the sample surface, it can be controlled to cut a hole in the surface of a sample to the desired shape, size or depth.

An arrow shape was created by milling three small trenches into the sample using the FIB. The results are shown in Figure 2-21, with the arrow being easy to see once its approximate location had been found. When the arrow had been cut out, the sample was removed from the SEM, and mounted on the Raman microscope stage. The approximate area of the sample was searched to find the milled arrow; the location of the arrow had to be found using unprocessed microscope images, before a set of images could be acquired for stacking. However, it was quite difficult to find the arrow owing to the poor depth of field (Figure 2-22). Once the arrow was found however, and a set of images taken and stacked, the arrow can clearly be seen (Figure 2-23). Therefore, provided the marker can be found in unstacked images, cutting a marker using the FIB is a suitable method for physically marking a sample, if distinctive grains are not already present.

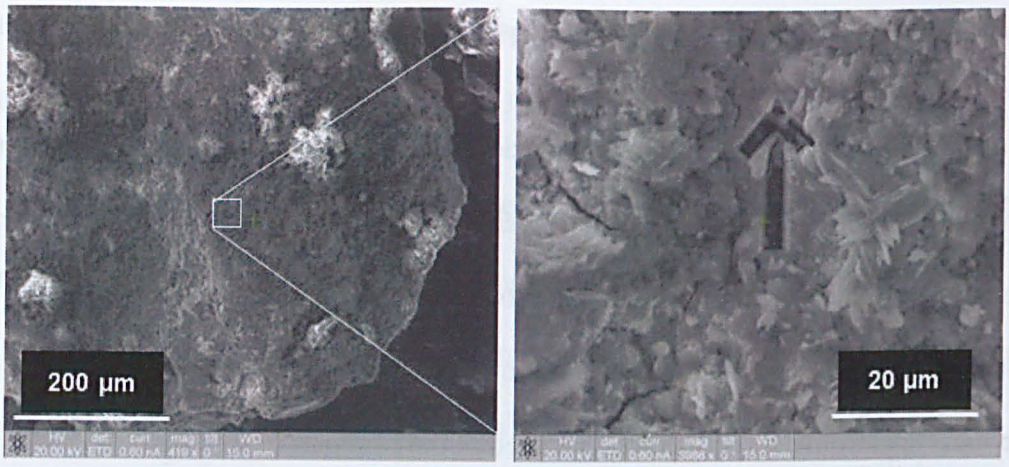

Figure 2-21: SED images of arrow cut into a fragment of Murchison, which is clearly seen

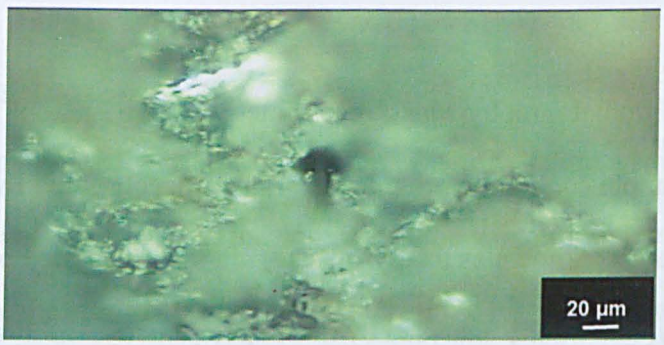

Figure 2-22: Unstacked images of arrow obtained using Raman microscope, needed for approximate location of surface features

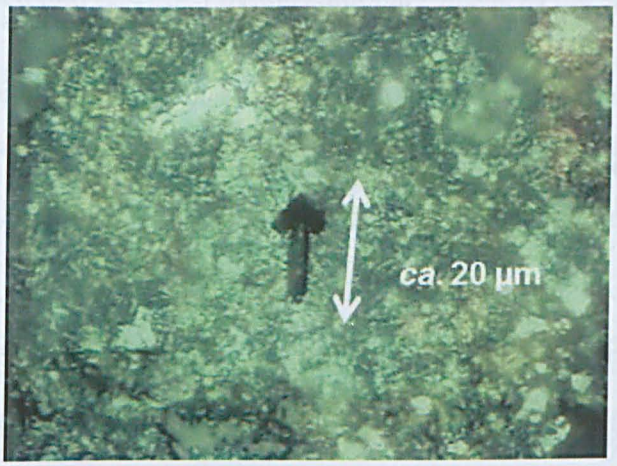

Figure 2-23: Stacked image (x50) obtained using Raman microscope, showing FIB arrow, about 20 µm in length, clearly visible

2.4. Pyrolysis-Gas Chromatography-Mass Spectrometry (Py-GC-MS)

Py-GC-MS has been used previously (as described below) for investigations into the structures of involatile, high molecular weight materials, and so was used as part of the study into the structure of IOM described in chapters 6 and 7. This technique is not suitable for *in situ* work, as the sample must be vaporised before introduction into the mass spectrometer, and so was not used in the first part of this study.

2.4.1. Background

Theory

Pyrolysis-Gas Chromatography-Mass Spectrometry (Py-GC-MS) is a three stage-technique. A sample containing organic materials is decomposed by pyrolysis, the products of pyrolysis (known as the pyrolysate) are then separated by gas chromatography, and finally analysed by mass spectrometry. In this study, the more powerful technique of two-dimensional Gas Chromatography (GCxGC) was used, as detailed below. Time-of-flight Mass Spectrometry (ToF-MS) was used to analyse the pyrolysate, after separation by GCxGC. This combined technique (Py-GCxGC-ToF-MS) is described in the following sections.

Pyrolysis

Pyrolysis is the decomposition of a material by heat, in an inert environment and in the absence of any other reagents (in contrast to combustion (see section 2.5) where organic materials are reacted with oxygen). If an organic compound is heated sufficiently, the energy imparted may be enough to break one or more bonds, depending on the strengths of bonds present. The products of bond-breaking may be stable, may decompose, react with one another, or with remaining unpyrolysed material, and therefore the end-product of pyrolysis is often (but not always) a

complex mixture. The theory of pyrolysis is described in two useful introductory texts (Wampler, 2007; Moldoveanu, 1998).

As a mixture of products is usually obtained from pyrolysis of organic materials, the pyrolysate must be separated into its components (by chromatography) before analysis. Identification of these components can sometimes allow reconstruction of the structure of the structure of the sample undergoing pyrolysis, but if not, the technique can be used to generate a profile of pyrolytic breakdown, to enable comparison of one sample with another.

2D-Gas chromatography (GCxGC)

Gas chromatography involves the vaporisation of a sample into a stream of carrier gas (usually helium), followed by the delivery of the vapour into the end of a long capillary column, the walls of which are coated with a high-boiling oil, known as the stationary phase (the stream of helium is known as the mobile phase). Molecules of analyte are absorbed and desorbed by the stationary phase as the steam of carrier gas flows through the column. Some components are absorbed poorly, others more strongly, depending on their partition coefficients between the two phases. The column is heated *via* a pre-programmed temperature ramp, to increases the elution rate of the analyte. Thus compounds which are more strongly absorbed onto the column are eventually released as the temperature rises. The net effect is to separate out the components of the mixture according to their relative partition between the mobile and stationary phases.

In the two dimensional variant of GC, two columns are used. The gas stream is passed through the first column, *via* a gas-tight coupling into a second column. The two columns are coated with different stationary phases (with different properties),

for which the partition coefficients of the components of the analyte are likely to be different. A common combination is to use a non-polar stationary phase for the primary column (separation is therefore largely dependent on volatility), and a more-polar phase in the secondary column (giving polarity-related separation)

The first few centimetres of the second column are held within a device known as a modulator. In this, alternating jets of cold and hot nitrogen are directed onto the column. This has the effect of condensing the analyte onto the column walls, then releasing it back into the gas stream (twice) before entry into the second column. The modulator was set to hold the analyte stream for a short time (typically 4 sec) before releasing it, thus small packets of eluent are sequentially released into the second column for a second separation. This column is much shorter than the first and of narrower bore, (so the linear flow rate is faster), and elution is very rapid (a few seconds, slightly less than the interval set into the modulator).

The temperature of the second column is programmed to be slightly higher than the first, and, as the elution time is so fast, it is effectively operating in an isothermal mode for each packet of analyte.

Compounds co-eluting from the first column will be separated if their affinities for the second column are different (*i.e.* if they have different polarities). This enables separation, for example, of aliphatic and aromatic hydrocarbons of similar boiling point. Another useful effect is the separation of bleed of the stationary phase from the first column. This material, typically a mixture of silicones, has very low polarity, and emerges rapidly from the second column, usually before any other compounds, and can easily be ignored when processing data. The eluent from the

second column is then directed into a mass spectrometer for analysis. The operation of two-dimensional GC is shown graphically in Figure 2-24.

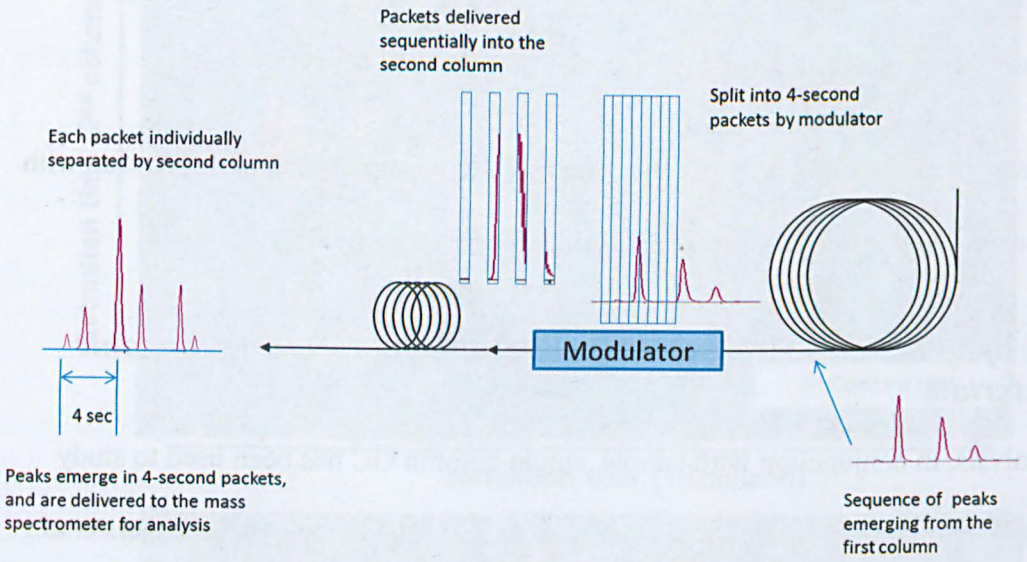

Figure 2-24: Schematic showing the operation of 2D-Gas Chromatography

Time-of-Flight mass spectrometry (ToF-MS)

The eluent from the gas chromatograph is passed into an ionisation chamber, where the molecules in the gas stream are ionised, then accelerated across a high voltage into the mass spectrometer. The ions are characterised by the time of flight from the accelerator to the detector, this time being inversely dependent on the mass of the ion. This type of spectrometer is capable of very rapid analyses; in this case, a spectrum is collected every 5 ms.

The strength of signal generated by the instrument is a measure of the variation in ion current with time. Any ion, or combination, can be selected but a useful measure is the total ion current (TIC). This provides a trace of the whole signal generated by the spectrometer with time, and serves as a fingerprint of the results of the pyrolysis.

Instrumental software is used to further process the data, generating a chromatogram in two dimensions (the two dimensions being the retention times of the two

columns). This can be portrayed as a contour map, or in 3D form, the third dimension being the ion current (of any selected ion, combination of ions, or the total), as shown in Figure 2-25. The exact ways in which this data is manipulated is software-dependant; that used in this study is described in section 2.4.3.

A detailed description of mass spectrometry (and its application in connection with gas chromatography) is given in Watson and Sparkman (2007).

Use of Py-GCxGC-ToF-MS in previous studies of meteoritic organic materials

Pyrolysis, in conjunction with simple, single-column GC has been used to study terrestrial, macromolecular materials, such as those in coal and oil (Hartgers *et al.*, 1994), and has been shown to generate an extremely complex mixture of products, containing hydrocarbons, thiophenes, and other aromatic and aliphatic compounds. The complexity of the pyrolysate was such that GC using a single column did not give complete separation. Similar results were obtained when meteoritic samples were analysed (also using single-column GC) for example, (Murae, 1995) who investigated the pyrolytic decomposition at a range of temperatures and Remusat *et al.*, who generated data for Murchison (Remusat *et al.*, 2005b). Much better separation has been achieved using two-dimensional GC to separate the pyrolysates obtained from CO3 chondrites ((Pearson *et al.*, 2007a), Murchison (Watson *et al.*, 2005a) and Cold Bokkevelt (CM2) (Watson *et al.*, 2007). Chromatograms obtained from Murchison, are shown in Figure 2-25. Part of the chromatogram has been highlighted and annotated (in Figure 2-25A) to identify groups of structurally-related components.

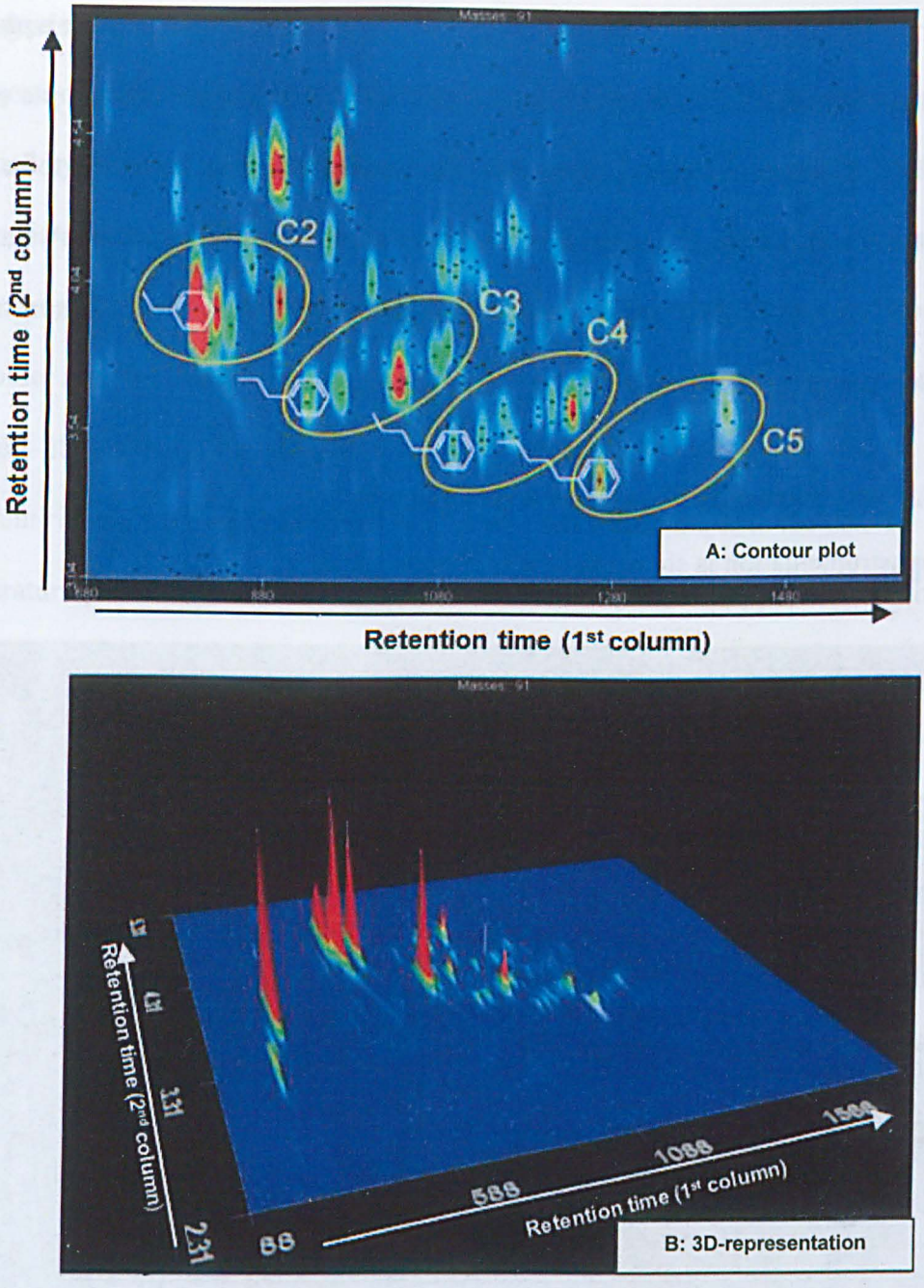

Figure 2-25: 3D-Chromatograms obtained using Py-GCxGC-MS analysis of Murchison, annotated to show elution of alkyl-substituted benzenes (from Watson *et al.*, 2005a)

This analytical method is extremely useful for the identification of the products formed by pyrolysis. However, not only is the structure of the organic material prior to pyrolysis unknown, the reactions that are occurring on pyrolysis are not fully understood.

Despite this difficulty, an advantage of the technique is that it can generate a profile of meteoritic organic material, comparing the data generated from one sample with another. Two samples giving the same result are likely (but not certainly) to be the same, but if the profiles are different, then the samples must be different. A similar approach (using 1D-GC) to the "typing" of organic materials has been demonstrated by Sephton *et al.* (1994).

2.4.2. Instrumentation Used in this Study

The instrumentation is shown below, in Figure 2-26.

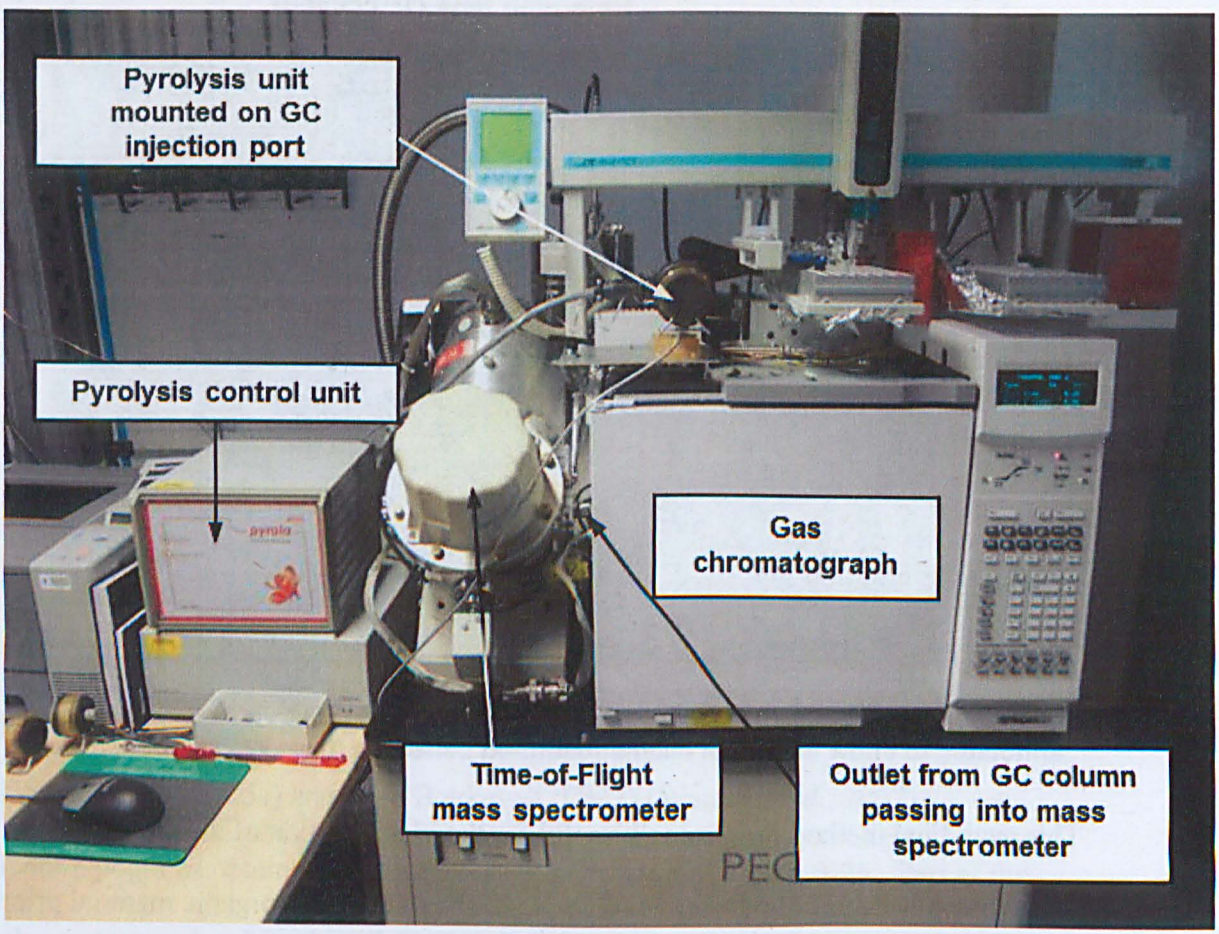

Figure 2-26: Py-GCxGC-ToF-MS instrumentation used in this study, with components annotated

Pyrolysis

Pyrolyses described in this study were carried out using a Pyrola 2000 instrument, supplied by PyroLab AB. The platinum ribbon sample holder is cleaned by briefly heating in a blowtorch flame, then the sample (needing no preparation, and typically about 1 mg) is placed in a small dimple in the ribbon using tweezers or a spatula, and the holder inserted into the pyrolysis unit containing an atmosphere of helium (see Figure 2-28). The instrument delivers two short bursts of electric current to the platinum ribbon, heating it electrically. The first heats the sample to the desired temperature (over a few milliseconds), which is sustained by the application of the second burst, for a programmed time (typically two seconds). The instrument is calibrated by performing a series of experiments, varying the current applied during these two phases of heating until a constant temperature profile, at the desired value is obtained. This procedure is repeated over a range of temperatures, and using the data so obtained, the instrument can vary the current applied to achieve any desired temperature with this range. An example of a profile obtained during calibration is shown in Figure 2-27.

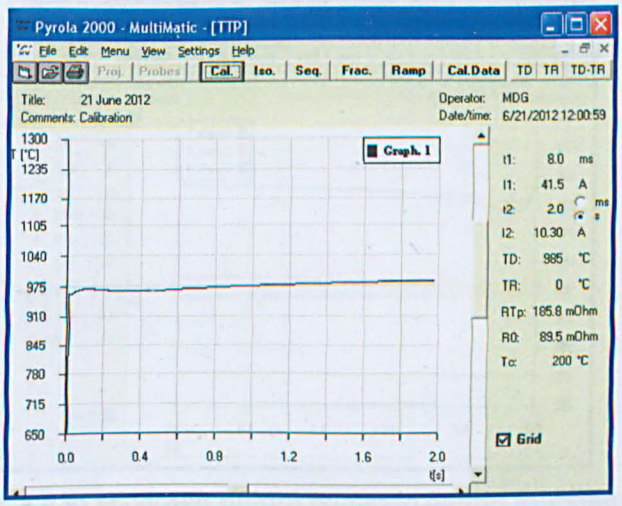

Figure 2-27: Temperature profile obtained during Pyrola calibration, generated using instrument software

The instrument can be programmed to carry out a sequence of pyrolyses at different temperatures. The pyrolysis temperature is measured using a photodiode, which gives accurate readings above 550°. Below this value, the temperature is calculated from the resistance of the ribbon, which is much less accurate.

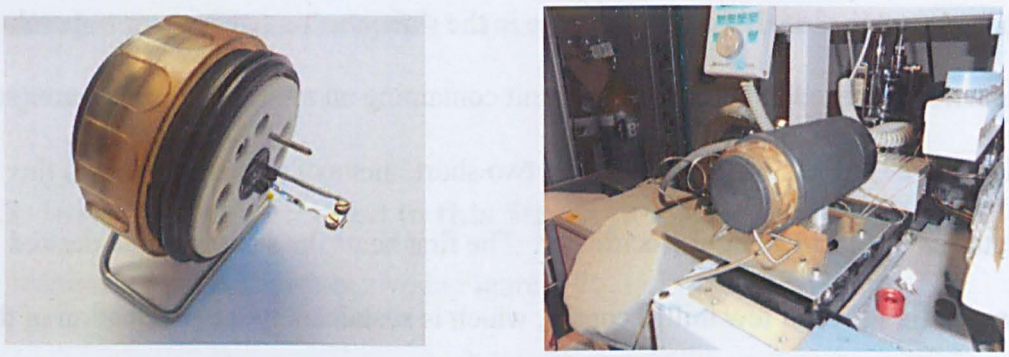

Figure 2-28: Pyrola filament holder (left) and pyrolysis chamber (right)

In this study, pyrolysis was usually carried out using a set of three temperatures (300°, 600° and 900°). Initial heating at 300° is carried out to remove any volatile contaminants and physically-entrained compounds from the sample. These will be volatilised, but most chemical bonds would not be pyrolytically broken at this temperature. A typical profile is shown in Figure 2-29, showing the values obtained using both temperature detectors at the three temperatures.

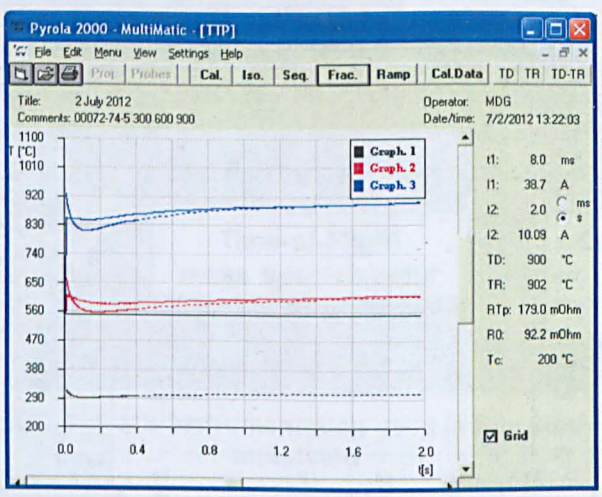

Figure 2-29: Temperature profile obtained during pyrolysis of a sample of Murchison, (900° in blue, 600° in red and 300° in black) from resistance measurement (dashed line) and thermal diode data (solid line-valid only above 550°).

Pyrolytic decomposition occurs during the second heating step. The temperature used in previous studies was typically approximately 600°, (for example, Watson *et al.*, 2010, Sephton *et al.*, 1994), a temperature conveniently achieved in simpler pyrolytic heaters, which used the Curie point of the material making up the sample holder as a temperature control. As the Pyrola device allows accurate temperature control over a wide range, for this study, a range of temperatures was investigated, as described in section 6.3.2. Little difference in pyrolysate profile was seen over the range 500-700°. A temperature of 600° was therefore selected to allow comparability of results with published work

The final phase of heating was carried out at 900°, to sweep out any residual materials contained within the Pyrola apparatus (but not to generate data). A blank chromatogram after every set of three pyrolyses showed that this was successful, and no cross-contamination from previous runs was ever seen.

The products of pyrolysis are carried in the stream of helium into a gas chromatograph, through a needle inserted directly into the GC inlet, on top of which the pyrolysis chamber is mounted, (shown in Figure 2-26).

2D-Gas Chromatography (GCxGC)

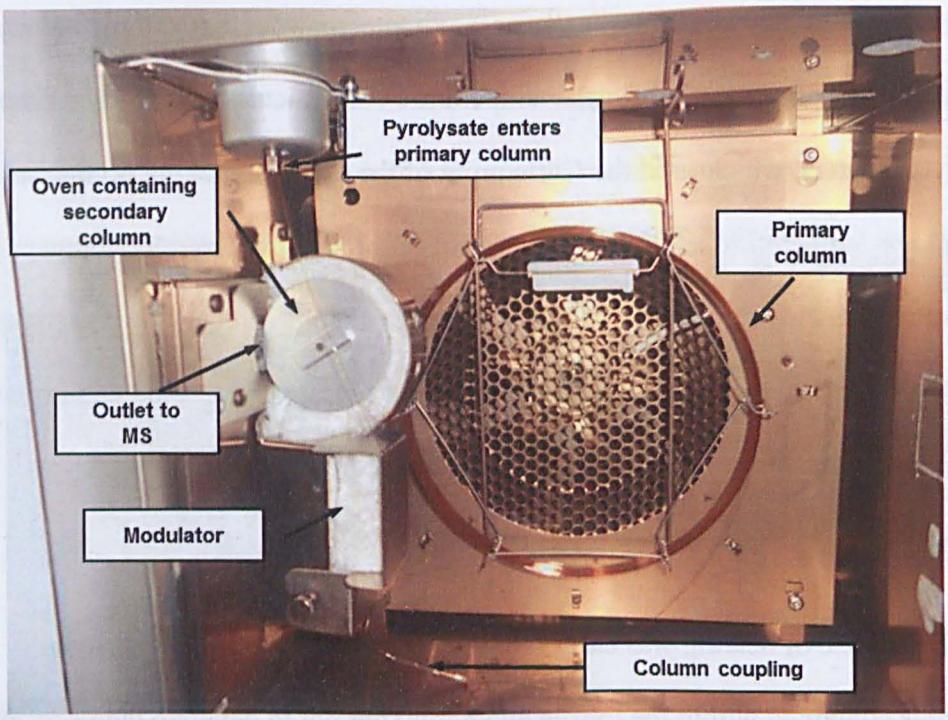

Figure 2-30: Interior of Gas Chromatograph used in this study, operating in 2D Mode

The gas chromatograph used was an Agilent Model 6890N, controlled by ChromaTOF software. The primary oven temperature ramp parameters used were

- Initial temperature, 35°, held for 1.25 min
- ramp rate 5°/min
- maximum temperature of 300°
- held for 1 min.

The secondary oven is maintained 15° higher than the primary oven, and the modulator at 30° higher than the primary oven. The modulator was set to deliver a hot pulse of nitrogen for 0.6 s, followed by a cold pulse for 1.4 s, twice in each cycle of 4 s. The injector was maintained at 250°, and the transfer line to the MS at 280°.

The columns used in this study, for all samples, are described in Table 2-1 below.

	Primary	Secondary
Name	BPX-5	BPX50
Description	5% phenyl/95%methylpolysilphenylene siloxane	50% Phenyl Polysilphenylene-siloxane
Length (m)	30	2 (total, including transfer line)
Bore (μm)	250	100
Coating thickness (μm)	0.25	0.10
Helium flow rate	1 mL/min	

Table 2-1: Details of chromatography columns used in this study

Time-of-Flight mass spectrometry

The mass spectrometer used was a Pegasus IV TOF-MS instrument, supplied by Leco Inc. The data generated by the spectrometer was analysed using the proprietary ChromaTOF software (v4.43.3.0). The instrument collects a mass spectrum (from 33 to 400 mass units) every 5 m, which are stored, and labelled by the time of acquisition, relative to the start of chromatography. The software is able to process this data, generating a chromatogram in two dimensions (the two dimensions being the retention times of the two columns). Using the mass spectra, the software can generate a three-dimensional representation, using the ion current (total, or of any ion or combination of ions) as the Z-coordinate. The software compares the spectra generated against library spectra, to enable identification of the compound being analysed. The software returns a measure of confidence in the match obtained, enabling a manual screening of the results.

Additionally, the ChromaTOF software analyses the mass spectrum generated as each peak emerges. If there is no change during the course of elution of a single peak, it recognises that the peak represents a single compound. If the spectrum does change, however, this indicates that two or more different compounds are eluting with similar retention times, (thus giving overlapping peaks). The software attempts

to separate out the differences in mass spectra, and thus deconvolute the peak into its components.

2.4.3. Data Handling

The amount of data generated from a single pyrolysis using the Py-GCxGC-ToF-MS instrument described above is very large, and some degree of data reduction is essential. The GC programme takes approximately 55 minutes, during which time a mass spectrum is collected every 5 ms, generating over 600 000 spectra per pyrolysis. Even after the software has grouped these into individual compounds, there can be several thousand components identified (many of which are present only in trace amounts). One way to usefully interpret the data is, rather than seeking to identify many individual compounds present, is to look for patterns or groups of compounds which samples have, or do not have, in common.

Total ion current profile

Unprocessed output from the spectrometer (generated from a sample of Murchison) showing the variation of total ion current (TIC) with time is shown in Figure 2-31. This shows a trace of total ion current (although any ion, or combination of ions can be selected) generated by the detector with time. An expanded section is shown in Figure 2-32, covering the elution over a period of 20 seconds. It shows a periodicity of 4 seconds, representing the effect of the modulator in splitting the output from the primary column into 4-second packages. Each peak in any one of these 4-second packages is at least one discrete compound.

Although these traces show a pattern diagnostic of the sample being analysed, the presence of very volatile compounds (e.g. gases) eluting at the start of the chromatogram, and bleed from the columns (eluting as the temperature increases,

and unretained by the secondary column) tends to obscure the compounds generated from the sample on pyrolysis. The large number of data points results in the baseline appearing as a solid band of colour. These undiagnostic peaks can be largely eliminated by processing the data to remove compounds with short retention times in both columns, to give a trace such as that shown in Figure 2-33, which is derived from the same sample as the trace in Figure 2-31. Traces presented in this form can be easily overlaid; comparison of two or more such TIC traces can simply show that samples are, or are not the same, without the need to identify any of the peaks giving rise to the chromatogram (treating it like a fingerprint).

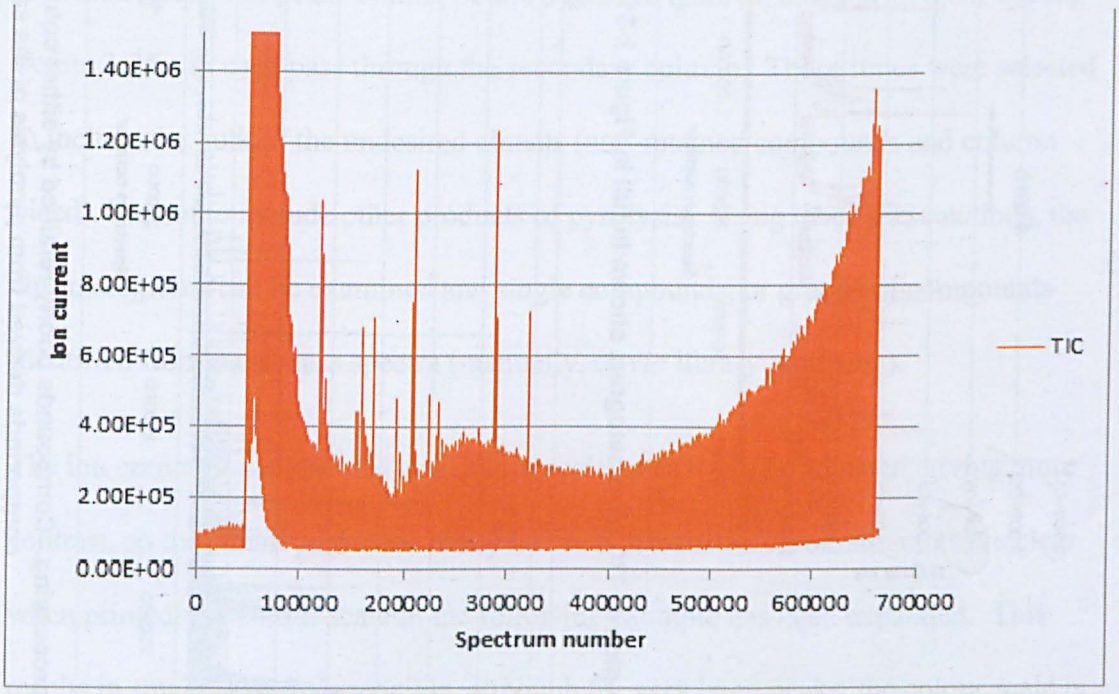

Figure 2-31: Output from GCxGC before processing (showing pyrolysate of a sample of Murchison IOM). Unretained gases give a large peak at the start of the chromatogram, and column bleed gives an apparent rise in the baseline.

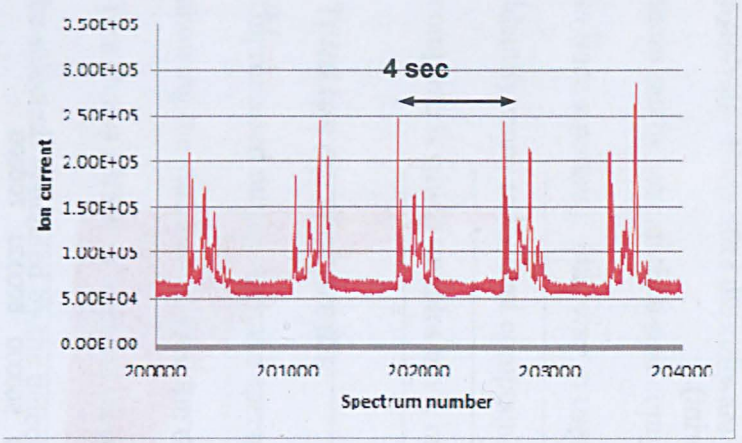

Figure 2-32: Expanded region of TIC chromatogram shown in full in Figure 2-31. The baseline is now less-pronounced.

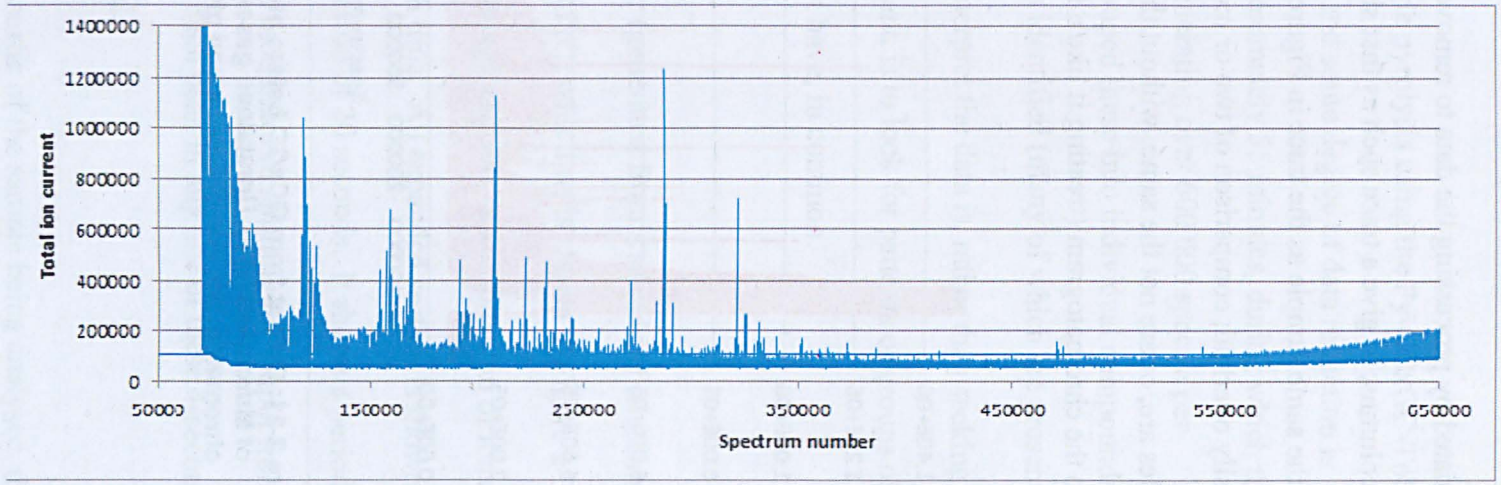

Figure 2-33: GCxGC output after processing. Compounds poorly retained by either column have been removed showing more clearly the compounds derived from pyrolysis of the sample

Two-dimensional GC

Data is returned from the software as a set of mass spectra, each related to a chromatogram peak (the peaks are identified by their coordinates, the two retention times, on the 2D-chromatogram). As for TIC profiles, the 2D-chromatogram can also be plotted using total ion (or any selected ion) current, and shown either as a contour map, or a 3D representation, as shown in Figure 2-34 (the same sample of IOM used to generate the chromatograms shown in the previous two figures). In these examples, the chromatograms have been processed to remove the column bleed from the primary column and the non-retained peak always present at the start of the chromatogram. All peaks eluting before 350 s are ignored, along with those eluting before 1.25 s in each pass through the secondary column. Those times were selected to include the bulk of the undesired eluents (non-retained compounds and column bleed), but not to include other products of pyrolysis. Using these presentations, the chromatograms can be examined and single compounds, or groups of compounds identified from their mass spectra (manually, or *via* library matching).

The ion current is represented as a colour scale, which can be adjusted, giving more contrast, so that small peaks can easily be seen. To ensure chromatograms are clear when printed, the colour scale in the following example has been expanded. This results in small peaks being visible, although for very large peaks, the colour scale is saturated. This is not a problem in this study as few peaks are large.

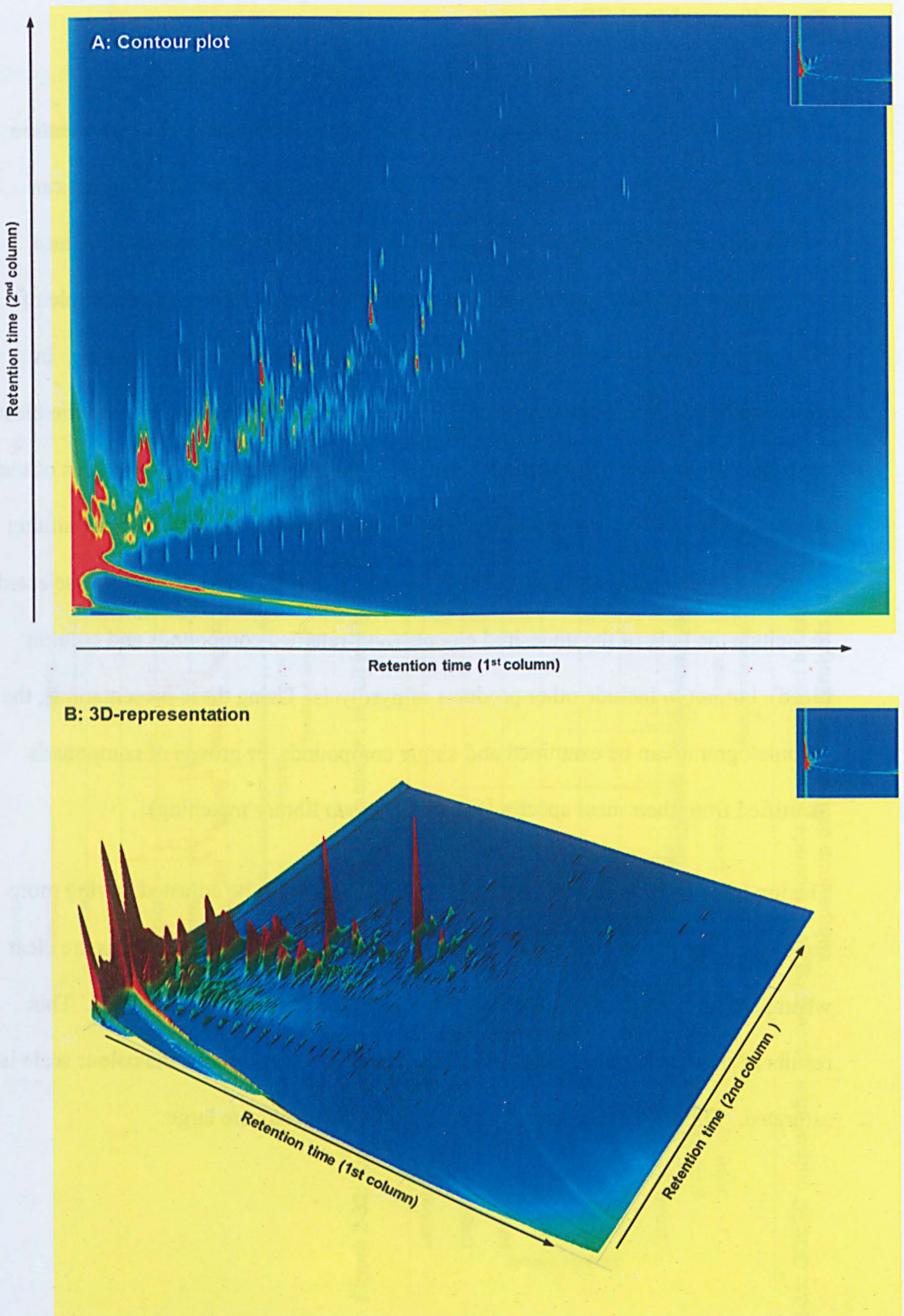

Figure 2-34: 3D-chromatograms obtained from pyrolysis of a sample of Murchison IOM at 600°, showing peaks visualised after software processing

2.4.4. Limitations of this Technique

Although Py-GCxGC-ToF-MS can generate much valuable data, it suffers from some limitations

Sample size

The technique requires only a small amount of material to be pyrolysed. For an inhomogeneous sample (such as a carbonaceous chondrite), different results will be obtained according to the composition of the subsample pyrolysed. To gain meaningful information on the meteorite as a whole, either many subsamples must be analysed, or a large sample finely powdered, to provide an average composition, and thus an average result. As meteorite samples are valuable, work is always carried out using the minimum quantities possible, so the use of homogenised large samples is rarely appropriate. In this study, key samples were analysed in duplicate to ensure sub-sample variation (in these cases) was less of an issue.

Non-quantitative data

The information delivered by the technique is qualitative, not quantitative (ionisation efficiency is not constant). It was found not to be possible to obtain accurate sample weights pre-and post-pyrolysis (as a sufficiently accurate balance, capable of weighing the pyrolysis unit, was not available). It is not known what fraction of the organic material present is responsible for the generation of the pyrolysate. If only a small fraction, differences which appear significant in the results of pyrolysis, may reflect only minor differences in the progenitor organic material.

Detection of analytes

Also, molecular species generated by pyrolysis may not be detected by the spectrometer. Although the column temperature at the end of chromatography is

over 300°, it is possible that some polar materials, such as carboxylic acids, or involatile compounds, such as multi-ringed aromatic structures, may not be eluted, and so remain undetected. Compounds which are eluted may either be only poorly ionised, or ions generated so unstable that they rapidly decompose into small fragments. In both cases, these compounds, although eluted through the GC columns, will not be detected.

Generation and interpretation of mass spectra

Lastly, two factors must be considered when interpreting mass spectra generated by this technique. Firstly, the ionisation energy of the instrument is 70 eV, which is usually more than that required to ionise an organic molecule. The ion generated loses energy by fragmentation, and it is this set of ions (molecular ion, plus daughter ions) which form the mass spectrum. Some classes of molecules (notably aliphatic hydrocarbons) fragment extremely readily and do not give a recognisable molecular ion. For these compounds, a definitive identification is usually not possible.

Secondly, the assignment of structures depends on software algorithms, comparing the spectra generated against libraries. This is usually successful for common compounds, but clearly depends on the quality and extent of the library used. In cases where assignment seems unlikely, or no match is found, it is necessary to attempt to interpret the spectrum manually, which was carried out when required, although for common compounds, assignments, when checked, were found to be correct.

2.5. Stepped Combustion

As for Py-GC-MS, this technique is not suitable for the analysis of organic materials *in situ*, but was used to investigate the structure of IOM, as described in chapters 6 and 7.

2.5.1. Background

Stepped combustion is a technique in which a sample is heated stepwise at increasing temperatures in oxygen, and the gases evolved at each step are collected, quantified and isotopically analysed. The gases include carbon dioxide, generated from oxidation of carbon (elemental or present as compounds with other elements) nitrogen, generated when nitrogenous compounds are decomposed, and inert gases, released when their carriers are destroyed. Carbon dioxide can also be generated when some minerals, in particular carbonates, decompose thermally. The technique has been used to generate profiles of the carbon-containing content of mineral samples, comparing the output with the combustion profiles of pure standards. The profiles shown in Figure 2-35, (taken from Wright and Pillinger, 1988) illustrate the ranges of combustion temperatures obtained. Organic materials generally combust at lower temperatures than inorganic. Most metal carbonates decompose thermally with the evolution of carbon dioxide, over a range of temperatures, from below 300° in the case of lead carbonate, to over 800° for barium carbonate. Those common in meteorites (calcium, iron and magnesium carbonates) decompose in the range 500-650° (Milodowski and Morgan, 1980).

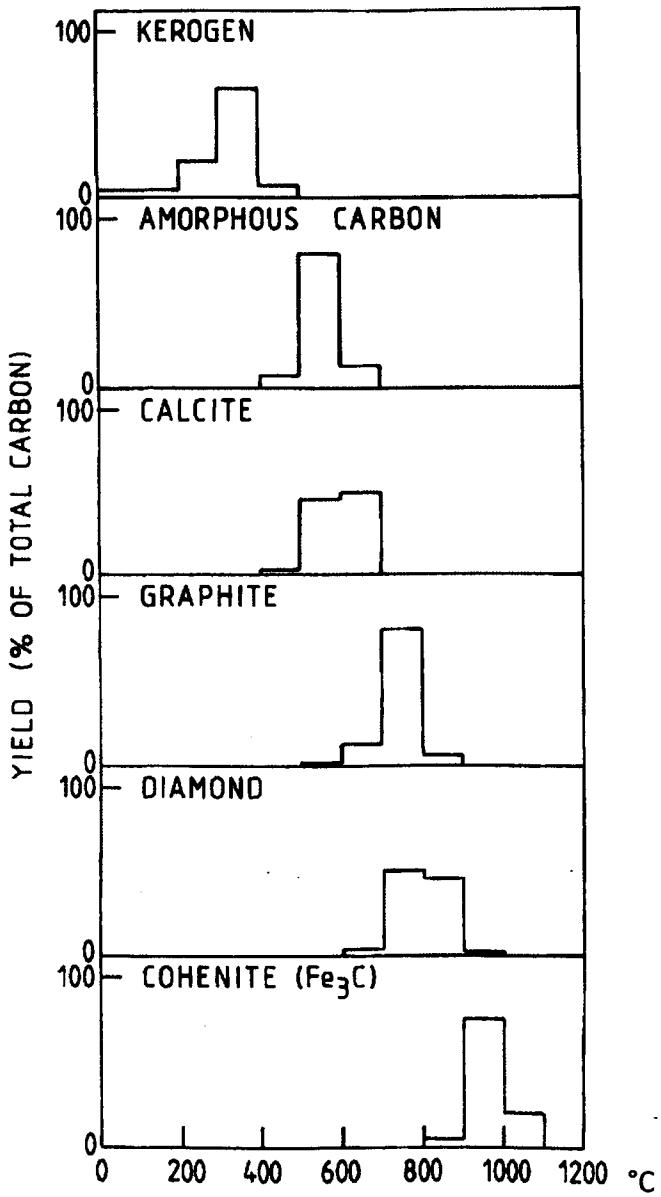

Figure 2-35: Stepped combustion data for standard carbonaceous compounds, showing typical combustion temperatures for carbon-containing species (from Wright and Pillinger, 1988)

Stepped combustion has been used to study a wide range of meteorite samples, in investigations into carbonaceous content (Grady *et al.*, 2002), nitrogen (Wright *et al.*, 1988) and inert gases (Verchovsky *et al.*, 1997; Verchovsky *et al.*, 2012). Another study (Sephton *et al.*, 2003) investigated samples from different meteorites, both of whole rock carbonaceous chondrites and IOM isolated by demineralisation. Organic materials combust over a relatively small temperature range, and this technique has not typically been used to derive information about the structure *per se* of organic

materials. It does however generate useful information regarding the ratios of the broad categories of carbonaceous materials (such as those exemplified in Figure 2-35), especially their presence or absence. In this study it was used to compare one sample with another, in particular noting changes which had occurred during parts of the process of isolation of IOM.

2.5.2. Instrumentation

Stepped combustion was carried out using a bespoke instrument ("Finesse") designed and built at the Open University (Wright *et al.*, 1988; Wright and Pillinger, 1988). A sample, typically about 0.2 - 0.5 mg, wrapped in a piece of pre-cleaned platinum foil, is introduced into a combustion chamber. The sample is heated at a series of increasing temperature steps, and at each step is reacted with oxygen. The oxygen is generated by the thermal decomposition of copper (II) oxide (heated in a separate chamber).

The temperature step size can be varied (typically between 25° and 200°). Smaller steps give higher resolution information about the extent of carbon combustion with increasing temperature. However, the time taken to acquire data for each step is the same, so carrying out a larger number of steps increases the time for data collection proportionally. This then increases the possibility of thermal decomposition of organic materials during the longer residence times inside the furnace. Analysis typically takes around 24 h per sample.

The products of combustion are separated by the instrument (under computer-control), in a series of cooled collection traps. These gases (carbon dioxide and nitrogen) are sequentially released from the traps by controlled heating, and analysed in separate mass spectrometers. The mass of each gas is measured, and its isotopic

composition determined from its mass spectrum, following appropriate calibration of the instrument using gases of known composition. After performing the set of combustion experiments at the desired temperatures, the system is cooled, ready for the next sample.

The data obtained is plotted to show the variation of generated mass and isotopic composition of products of combustion with temperature. Typically, the mass of gas generated rises to a peak, and falls away, as all combustible material is consumed. A typical result is shown in Figure 2-36, showing the evolution of carbon dioxide. Similar traces can be generated for nitrogen, and inert gases, but were not generated for this study. The carbon dioxide generated is also analysed isotopically, and graphs can be overlaid with that data, showing the variation in carbon isotope ratio of carbon dioxide collected with temperature. For example, the trace shown in Figure 2-36 shows that the carbon in Murchison combusting at about 1100° has a much higher proportion of ^{13}C than any of the carbon combusting at other temperatures. Also, this component is not present in the sample of IOM.

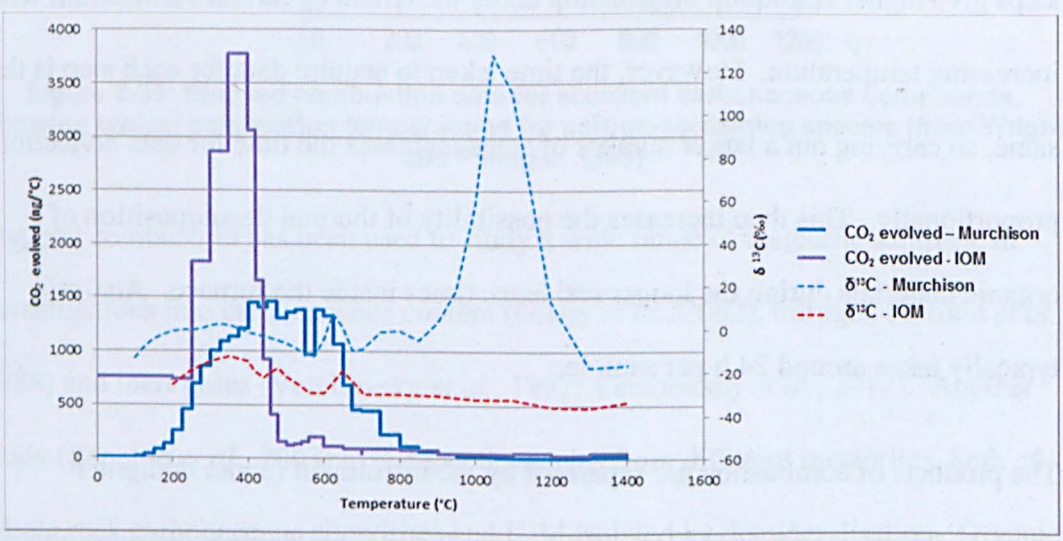

Figure 2-36: Stepped combustion data, obtained from Murchison showing both level of CO_2 evolved (solid lines), and its isotopic composition (dashed lines) (taken from Sephton *et al.*, 2003)

2.5.3. Limitations of Stepped Combustion

The main constraint acting on this technique is similar to that for Py-GCxGC-ToF-MS, namely sample size. The instrument was designed with high sensitivity, to enable accurate analysis of trace amounts of evolved gas, and so, for samples with a high carbon content (especially isolated IOM), very small samples, much less than 1 mg, are required. Consequently, using an inhomogeneous material such as a carbonaceous meteorite, it is difficult to ensure the sample is representative of the whole. Many small samples are needed to ensure that representative data is collected, which can be very time-consuming to collect, especially if analysis using a large number of temperature steps is needed.

A further limitation is the stability of the samples under investigation to the conditions employed. Temperatures during the latter stages of analysis are well in excess of those used for pyrolysis, and so it is very likely that organic materials, even if uncombusted, may decompose thermally, and if not evolving carbon dioxide or nitrogen, will be undetected. This may make accurate interpretation of combustion profiles (for organic materials) difficult.

2.6. Conclusion

The data acquired using the analytical methodologies described in this chapter are presented and discussed in the following chapters of this thesis. Both Raman spectroscopy and SEM/EDS were used successfully in the analysis of meteorite sample surfaces, collecting both images and data, as described in Chapters 3 and 4. All four techniques were subsequently used for the study of IOM (described in Chapters 5 to 7), providing data enabling conclusions on the structure of IOM to be drawn (discussed in Chapter 7).

Chapter 3 Development of Methodology for Tagging Meteoritic Organic Materials

The concept of molecular tagging, that is, the attachment of atoms or functional groups to organic materials present in meteorite samples, in order to increase the detectability of organic compounds, *in situ,* was introduced in section 1.7.4. This chapter describes the development of such a procedure, to tag the organic materials present within carbonaceous chondrites. Methodology was developed to tag both soluble and insoluble organic materials, the latter being the major component of the organic inventory of carbonaceous chondrites, as discussed in section 1.4.

3.1. Precedent for Molecular Tagging

Molecular tagging has been used in many fields of study where it is difficult to detect materials due to low abundance or method sensitivity. In this methodology, the target analyte is rendered more detectable either by attachment of a molecular fragment, containing some more-easily detected component, or substitution of part of the analyte structure with a similarly more-easily detected replacement.

Three types of tag are commonly used

- Isotopes (radioactive or stable),
- Elements, normally either absent, or present at low levels, attached using a suitable reagent
- Functional groups, added by reaction of an analyte with some suitably reactive reagent containing the functional group.

3.1.1. Isotopes

Substitution of one isotope for another is a powerful method of tagging, and is usually termed "isotopic labelling". Substitution of one isotope for another does not affect the reactivity of the analyte, apart from a possible change in reaction rate, and,

with the advent of modern analytical methods, such as NMR or MS, stable isotopes are easy to detect in a wide range of compounds. Isotopic labelling is often used to track organic compounds through a sequence of reactions, such as a biochemical pathways *in vivo*, or a mechanistic investigation *in vitro*, and is now standard chemical laboratory methodology. By following the course of the labelled material (detecting the isotope in reaction products, or intermediates), the pathway or reaction mechanism can be elucidated. For example, substitution, of carbon-13 for carbon-12 has been used to track metabolic pathways, the location of the isotopic label being detected by NMR (for example, see Staunton and Weissman, 2001).

Tracking compounds labelled with radioisotopes is usually carried out by detection of their daughter products. The annihilation of positrons, formed from the decay of isotopes such as carbon-11 and fluorine-18, is used in Positron Emission Tomography (PET) to detect labelled drugs *in situ* within a patient, in order to understand their distribution about the body. In this procedure, the active pharmaceutical molecule is tagged with the appropriate isotope (Kubota, 2001), administered to a patient, and then the location of the drug detected by the gamma rays emitted from the reaction of positrons with electrons.

In the examples discussed above, the isotopes are introduced synthetically, as replacements for one or more atoms normally present within the molecule under study. For this project however, the aim is to attach a tag, by reacting organic materials *in situ* with some reagent capable of introducing a tag, rather than synthesis of an analyte *de novo*, as is the case in stable isotopic labelling.

The use of radioisotopes was outside the scope of this project, and so the methods described below, where a detectable atom or functional group is added to the subject under test, were evaluated as possible methodologies for evaluation.

3.1.2. Elements

In elemental tagging, a reagent, containing an element normally only present at low levels (to avoid an excessive background signal), is reacted with a substrate, thus covalently bonding the element to the compound under investigation. This new element is then detected using any appropriate analytical technique (such as SEM/EDS).

Nanoparticles containing gold, covalently bonded to reactive functionality have been developed to enable tagging of biological substrates. These can then be examined, after addition of the gold nanoparticles, by SEM or (Transmission Electron Microscopy) TEM. These reagents are commercially available, examples including imide derivatives capable of reaction with thiols (such as described by Jeon and Shipley, 2000), or carbamates, which react with amines. Although gold would be a suitable tagging element, these reagents require aqueous solvents for the tagging reactions, and are thus not appropriate for this project; to satisfy the criteria set out in section 1.7.2, reactions avoiding solvents are required.

Reagent systems which can be used in the gas phase have been developed for the study of carbon fibres (Takahagi and Ishitani, 1988), polyethylene films (Everhart and Reilley, 1981) and acrylic polymers (Dickie *et al.*, 1982). In these examples, the functional groups present in the samples under test (alcohols, carboxylic acids and amines) were reacted with one or more volatile reagents containing fluorine. The

presence of that element was detected (in the bulk sample) using X-ray Photoelectron Spectroscopy. The methodology was not intended to detect fluorine *in situ* within the sample, but just to show that it was present, therefore implying the presence of the organic functionality intended to react with the reagents used.

After the work described in this section had been completed, a study of a similar technique to that described later in this chapter was published (Larnøy *et al.*, 2011). This involved the detection of chitosan in wood samples by EDS following its reaction with a chlorine-containing reagent. In this example, chlorine was detected *in situ*, the same methodology as developed in this study.

A tagging method has been developed for organic materials in meteorites using osmium tetroxide (Pearson *et al.*, 2007b). Samples of meteorite were exposed to osmium tetroxide vapour and the incorporation of osmium monitored using EDS. This study showed that incorporation of osmium varied across the surfaces of the samples used, presumably as a result of the variability of organic content, but the specific organic functionality reacting with osmium tetroxide was not identified.

Thus there is good precedent for the use of gaseous reagents, capable of reaction with meteorite samples, to attach atoms, detectable by *in situ* methods, (for example, EDS), to the organic materials present.

3.1.3. Functional groups

Another methodology much used in the past is to convert one functional group into another, with the aim of forming a product much easier to detect than the substrate. This approach is the basis of the use of spray reactions to visualise TLC plates. The spot of material present on a TLC plate is usually non-coloured, but following

exposure to a particular reagent (appropriate to the class of compound being detected), highly-coloured derivatives can be formed, easily detectable visually, or with ultra-violet light. This methodology has been common-place for many years, and a wide range of derivatisation reagents is available commercially (for example, many are listed by Sigma-Aldrich, www.sigmaaldrich.com). An example is in the analysis of amines and amino-acids, which are often not easily detected unless they possess a highly-UV absorbent chromophore. Reaction *in situ* with the reagent fluorescamine generates an intensely-coloured derivative which can be detected at the picomole level (Udenfriend *et al.*, 1972). Biological staining reagents have been used to increase the visibility of biological structures, such as bacteria, which had been believed to be present as the so-called "organised elements" found in some meteorite samples (Fitch and Anders, 1963; Anders and Fitch, 1962); the "organised elements" were later identified as terrestrial contaminants (Anders *et al.*, 1964).

However, this procedure, employing a reagent system in solution still carries a risk of causing mobilisation of the materials being detected, within the sample of meteorite. To avoid any possibility of this occurring, it would be necessary to use a reagent in the gas phase. The use iodine vapour as a visualisation reagent for TLC has been established for many years, and although a non-specific reaction, provides a good precedent for a procedure, using a reagent, in the vapour phase, to react with the substrate in the solid state, converting one or more compounds present into new functionality. The products would then be detected using a method suitable for use in situ, such as Raman spectroscopy, and if the introduced functional groups give sufficiently-strong signals, their presence could be detected and visualised as described in section 2.1.

3.2. Development of Tagging

As described above, the methods of tagging most appropriate to the study of organic materials *in situ* in samples of meteorites, are those which introduce new functionality, or new elements, *via* reactions with gases or vapours, rather than liquids. The following sections contain a review of the chemistry which would be appropriate for this methodology, and the reactions which might be expected to occur.

3.2.1. Target Functionality

The targets for tagging are the organic materials present within carbonaceous chondrites, the nature of which was discussed in section 1.4. The major component of the organic inventory is the insoluble, non-volatile organic material, IOM. Its structure (discussed in section 1.4.3) is believed to be a network of functionalised aromatic groups, linked by branched aliphatic chains, containing various oxygenated functional groups (Derenne and Robert, 2010). Soluble compounds form a few per cent of the total organic material, and contain a wide variety of functionality, with carboxylic and other acids as the major component (see section 1.4.2, and Gilmour, 2005).

Since the major component of the organic content of carbonaceous chondrites, IOM, is macromolecular and insoluble, it may prove relatively unreactive. It was proposed therefore, to attempt to introduce extra functionality into its structure, with the aim of increasing the number of reactive sites available for tagging.

Extra functionality could be created by reaction of the target with ozone and would be expected to introduce oxygen-containing functional groups. These groups, being

also present in the majority of soluble compounds, would be a good target for derivatisation methods, and therefore for tagging. This, therefore, was the objective of this part of the work.

These methods must also meet the constraints outlined in section 1.7.2, specifically not to cause solvent-mediated redistribution of organic materials (either before or after reaction).

3.2.2. Potential Tagging Methods

The tag being attached to each functional group must contain some component which would enable the tagged group to be easily detected. This component should be absent, or present only at a low level before tagging. These components fall into three categories:

- Isotopes
- Elements
- Chemical bonds present in functional groups

Many analytical methods exist for the detection of these components, which could be adapted or employed for use *in situ.* For the reasons outlined in section 3.1.1, the use of isotopes, both stable and radioactive was not pursued. Elements suitable for introduction *via* tagging reagents were reviewed, selecting those which would not normally be present in high concentrations in carbonaceous chondrites, (and thus which would interfere in subsequent analysis). However, introduction of a new functional group, containing an element not previously present in the sample, gives the most flexibility in the detection methods which can be used

The remainder of this chapter describes the selection of appropriate tagging reagents, based on the availability of suitable chemistry, and which meet both the constraints outlined previously, and can be detected *in situ*.

3.2.3. Selection of Elements Suitable for Inclusion in Tags

The graph presented in Figure 3-1 shows the abundances of elements in CI chondrites. Units of abundance are normalised with respect to silicon, which is assigned an arbitrary abundance of 10^6. These meteorites contain elements in a similar ratio to that observed in the Sun (apart from the most volatile elements), and therefore are believed to best represent the average composition of the Solar System at the time of its formation. It is therefore a guide to the likely average composition of the other carbonaceous chondrites, for which alteration was only chemical (not thermal) and believed to be largely isochemical (Bland *et al.*, 2009). Elements with an abundance of 10 000 or more on this scale were defined to be common components of meteorites, and are therefore excluded as potential tags. Gallium and platinum were also excluded, as they are likely to be introduced if samples are marked with platinum, or ion-milled to give features helping locate regions of interest, as described in section 2.3.2. Radioactive elements were also excluded, on grounds of safety and practicality.

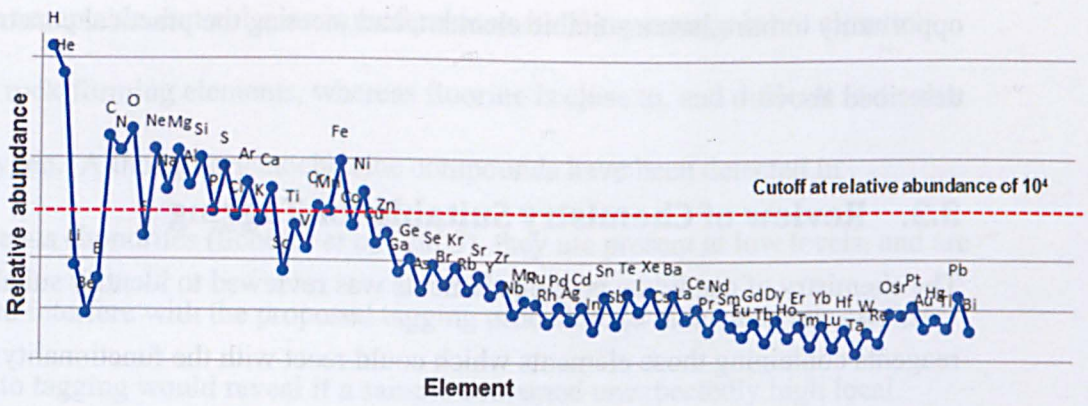

Figure 3-1: Meteoritic elemental abundances (Si = 10^6) (data taken from Lodders, 2003) showing cutoff between common and less-common elements

3.2.4. Constraints on Potential Chemistry

As outlined in section 1.7.2, any method of chemical tagging must not redistribute the organic material contained within the sample, in any way. Apart from the need to avoid physical methods such as cutting and polishing, these constraints also restrict the chemistry that can be employed.

The use of solvents must be avoided, as this would most probably remove any soluble organic materials, either present initially, or formed during the tagging process. Mobilisation of organic material would also be likely if the sample were to be heated. An ideal procedure would be the exposure of a sample to a gas or vapour (the latter formed from a liquid below its boiling point), under ambient conditions, using no solvent, and requiring the minimum of handling.

As described earlier, carbonaceous chondrites contain a wide variety of classes of organic materials, present as both soluble compounds and IOM (listed in detail in section 1.4). The chemistry of the main functional groups present in these compounds was evaluated, to select chemistry applicable to that group and the

opportunity to introduce a suitable element, and meeting the practical constraints described above.

3.3. Review of Chemistry Suitable for Tagging

The chemistry of candidate tagging elements was reviewed to identify suitable reagents containing those elements which could react with the functionality present, under the constraints as described in section 1.7.2. Particular focus was applied to reactive, volatile compounds, which enable reaction in the absence of solvents.

Metallic elements tend to form non-volatile (and therefore unsuitable) binary or complex compounds with non-metals, such as oxides or halides. One exception is osmium, which forms a volatile oxide, which has been (as described earlier) used to tag organic materials (Pearson *et al.*, 2007b). Volatile carbonyls are formed by many metals, but these do not readily react with the functional groups expected to be present in meteoritic organic material, and are usually toxic. Many metals also form volatile organometallic compounds, such as metal alkyls, or coordination compounds such as cyclopentadienyl complexes. These too, do not have the desired reactivity, and many are toxic or pyrophoric. Alkylzinc reagents could potentially be useful as a tag for some carbonyl groups, although alkylzinc reagents can be pyrophoric in the absence of solvent.

Non-metallic elements offer many options as tags, as it is often possible to substitute them into alkyl groups, and thus generate regents with similar properties to the unsubstituted compounds. An example is the halogens; halo-substituted acids or anhydrides can be more reactive than the unsubstituted compound, and thus potentially useful as ways of incorporating these atoms. Both fluorine and chlorine

would be acceptable, but chlorine is preferable as its X-ray energy is not close to common rock-forming elements, whereas fluorine is close to, and difficult to resolve from, oxygen. Although organochlorine compounds have been detected in carbonaceous chondrites (Schöler *et al.*, 2005), they are present at low levels, and are unlikely to interfere with the proposed tagging procedure (a blank analysis carried out prior to tagging would reveal if a sample contained unexpectedly high local concentrations of chlorine).

3.3.1. Unsaturated Carbon-Carbon Bonds

Double bonds and aromatic rings react as nucleophiles with halogens to give derivatives such as those shown in Scheme 3-1.

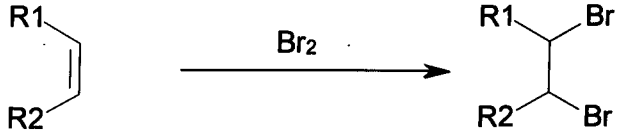

Scheme 3-1: Reaction of unsaturated bonds with halogens (*e.g.* bromine)

As IOM contains many such unsaturated bonds, this reaction is likely to generate a poly-halogenated derivative of some complexity, and may be suitable as a non-specific way to introduce halogen atoms as tags.

The reaction of nucleophilic double bonds with osmium tetroxide was used previously (Pearson *et al.*, 2007b) to introduce osmium atoms, presumably giving either the intermediate osmate ester, or the osmium oxide by-product generated on its hydrolysis (see Scheme 3-2), which can then be detected by EDS. The nature of the osmium by-product will depend on the stoichiometry and reactivity of the unsaturated species present.

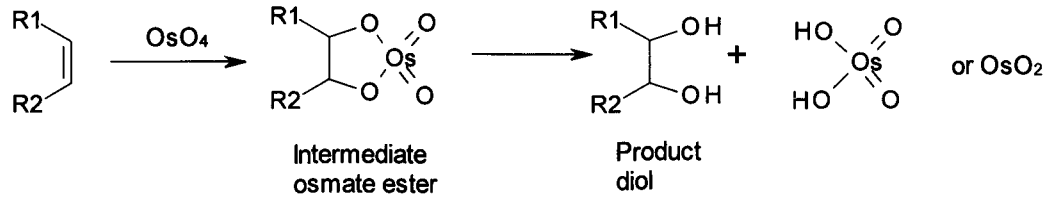

Scheme 3-2: Reaction of unsaturated bonds with osmium tetroxide

3.3.2. Carboxylic Acids

Fluorine and chlorine-containing compounds have long been used to derivatise carboxylic acids (*e.g.* to increase volatility for analysis by gas chromatography (GC) (Deyrup *et al.*, 1985; Brooks *et al.*, 1974; Dickie *et al.*, 1982)). Carboxylic acids can be esterified by formation of a mixed anhydride with trifluoroacetic anhydride (TFAA), followed by treatment with an alcohol (see Scheme 3-3). Alternatively, a reactive intermediate can be formed using a carbodiimide, followed by treatment with an alcohol containing a tag, as shown in

Scheme 3-4. This reaction is commonly used in organic synthesis, is applicable to a wide range of alcohols and carboxylic acids, and gives high yields (Williams and Ibrahim, 1981). To introduce a tagging element, R2 could be an alkyl group substituted with fluorine or chlorine, for example, CF_3– or CCl_3CH_2– groups.

Reactions are commonly carried out using dicyclohexylcarbodiimide (DCC, where R1 = *c*-C_6H_{11}). In this case, removal of the poorly-soluble urea by-product is usually a problem, but for the purposes of this study, it would not interfere with the detection of the product ester by EDS. Diisopropylcarbodiimide (DIC, R1 = *i*-C_3H_7) is a better reagent to use, being less toxic, a liquid at room temperature (and so easier to handle), and having an appreciable vapour pressure. Chemistry can therefore occur in the gas phase, as has been reported recently (Takabayashi *et al.*, 2010). Alcohol

R2OH is selected according to its volatility and reactivity, and the desired tagging element (for physical data of selected compounds, see Table 3-1, section 3.3.6).

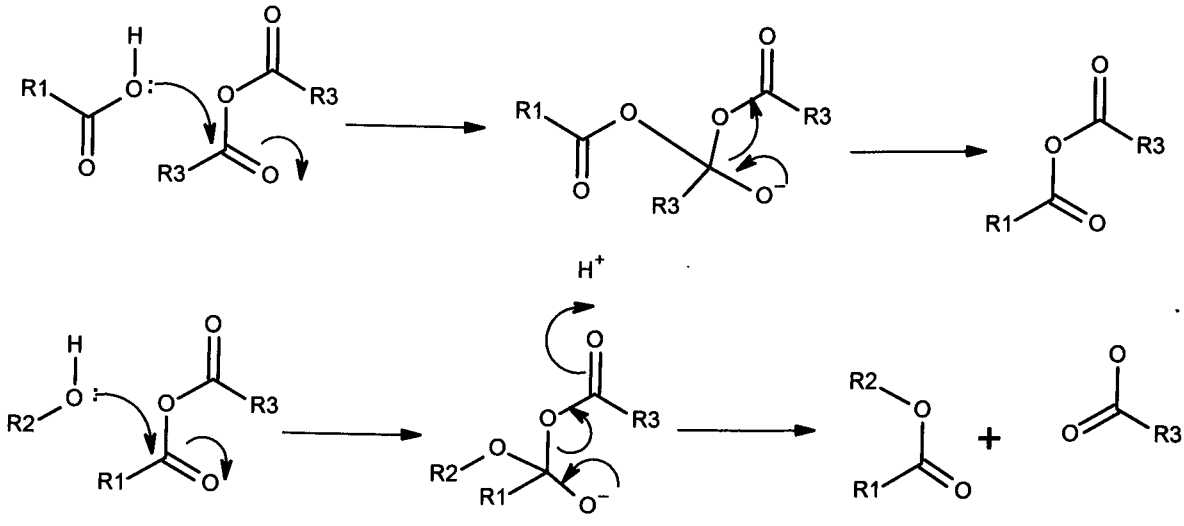

Scheme 3-3: Formation of esters *via* a mixed anhydride

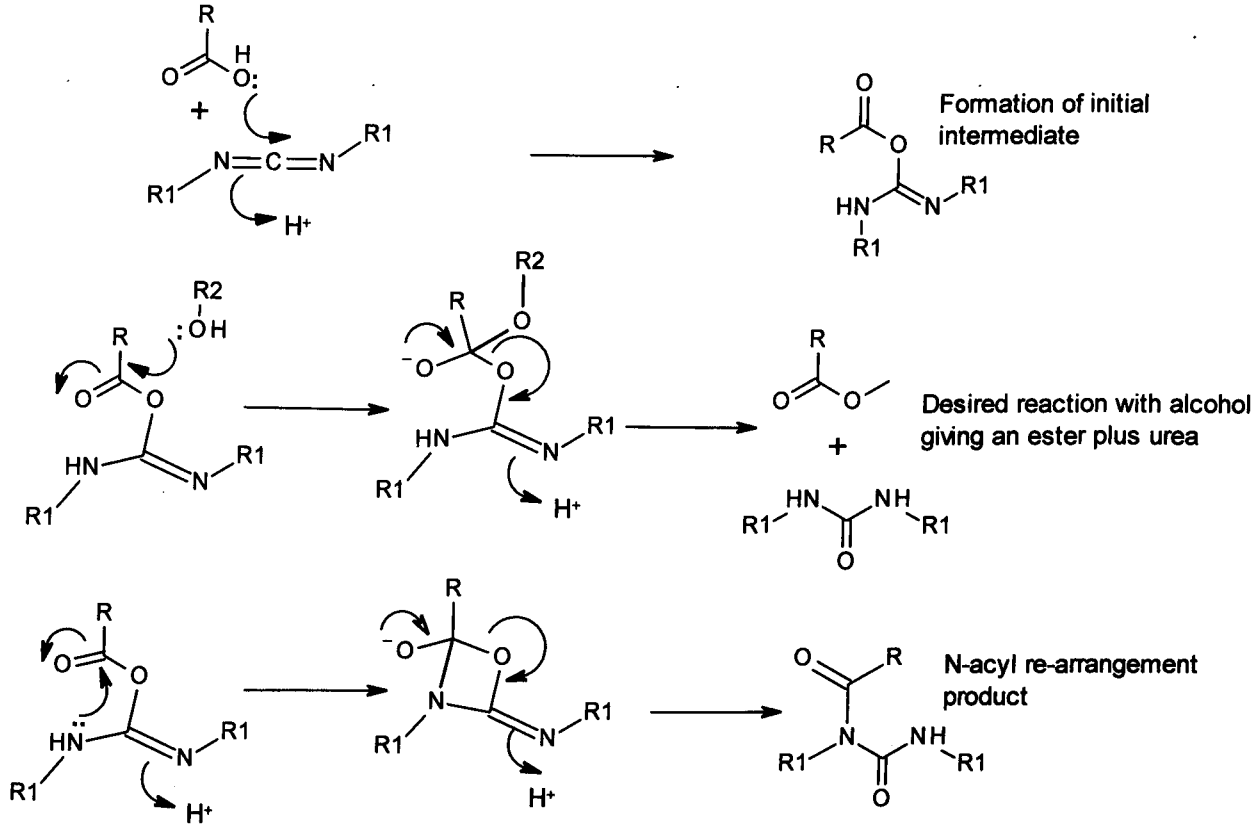

Scheme 3-4: Reaction of a carboxylic acid with a carbodiimide, followed by an alcohol to give an ester, plus N-acyl-rearrangement by-product

3.3.3. Alcohols and Phenols

A reaction of alcohols and phenols that may be suitable for use is that with anhydrides, generating an ester containing the tag, as shown in Scheme 3-5, (for example, trifluoroacetic anhydride, TFAA, where R1 = CF_3–). It may be necessary to carry out the reaction in the presence of base (such as pyridine or triethylamine), to ensure complete reaction, but many possibilities of reagents, offering a range of volatilities and reactivities, are available (see Table 3-1, section 3.3.6).

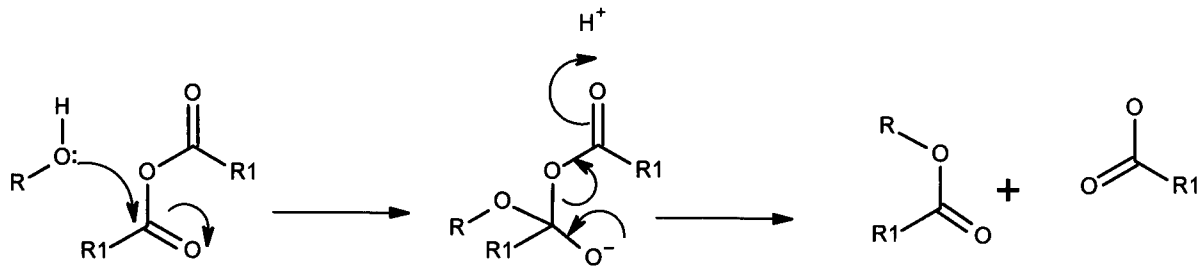

Scheme 3-5: Esterification of an alcohol or phenol with an anhydride to give an ester

3.3.4. Aldehydes and Ketones

Carbonyl groups readily form hydrazones with hydrazine derivatives, such as the crystalline 2,4-dinitrophenylhydrazones. However, if only volatile reagents are to be employed, a better approach is to form an unsubstituted hydrazone with hydrazine itself, followed by further reaction with an electrophilic tagging reagent, such as an anhydride, as shown in Scheme 3-6. Another reagent which may prove useful in tagging these electrophilic groups is diethylzinc (DEZ). This has been used in vapour form to preserve ancient documents (Williams and Kelly, 1976), by reaction with water and the neutralisation of acids. Its role could be to react with electrophilic centres such as carbonyl groups, or previously-introduced halogen atoms. Any water present in the sample will react with DEZ too, and so the sample will require drying

prior to treatment. However, it is possible that DEZ may prove too unreactive, and thus require either extended times, or increased temperatures.

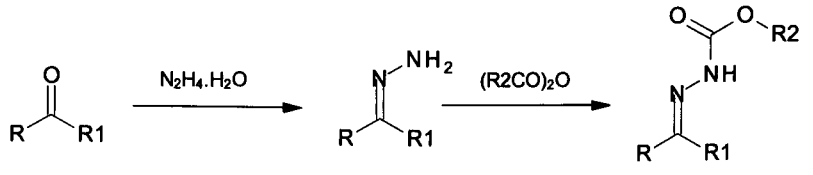

Aldehyde:R1=H
Ketone: R1 = alkyl or aryl

Scheme 3-6: Reaction of carbonyl groups with hydrazine to give a hydrazone, followed by reaction with an anhydride

3.3.5. Amino Acids

Amino acids would be expected to react with anhydrides, to generate an N-acyl derivative, most probably by intermolecular acyl transfer from oxygen to nitrogen. An alternative pathway has been reported (Coleman *et al.*, 1999) when TFAA was used as the acylating reagent, where instead of the expected acyl transfer onto the nitrogen, an oxazolidinone is formed (as shown in Scheme 3-7). For the purposes of introducing a molecular tag, either pathway would be suitable.

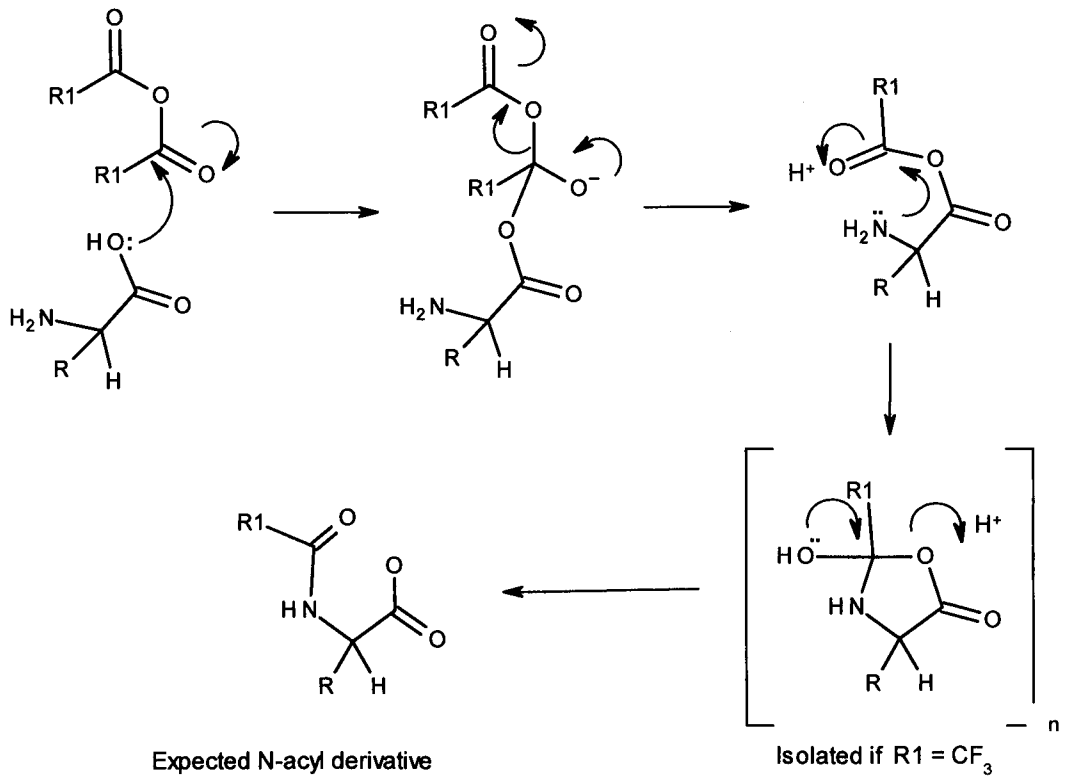

Scheme 3-7: The reactions of amino acids with TFAA

3.3.6. Reagents Suitable for Use in Development of Tagging Methodology

Following this review of potential chemistry, reagents suitable for carrying out the reactions described were selected. Reagents were selected for reactivity (to enable suitable tagging elements and groups to be introduced at ambient temperatures and pressures), volatility (to be usable as vapours, avoiding the need for solvents) and commercial availability. Those chosen for evaluation are listed in Table 3-1.

Compound (and common abbreviation)	mp (°)	bp (°) (760mmHg)	Vapour pressure at 20-25° (mmHg)
Bromine	-7	59	175
Iodine	113	184	0.3
Osmium tetroxide	nd	nd	9.8
Chloroacetic anhydride (CAA)	48-60	203	0.28
Dichloroacetic anhydride (DCA)	29-31	214-216	0.15
Trichloroacetic anhydride (TCA)	nd	221	0.11
Trifluoracetic anhydride (TFAA)	-65	40	nd
Heptafluorobutyric anhydride	nd	108	nd
Pentafluoropropionic anhydride	nd	69-70	nd
Diisopropylcarbodiimide (DIC)	nd	145-148	5.8
Pyridine (Py)	nd	115	22.8
Triethylamine (TEA)	-115	89	52
Hydrazine hydrate	nd	114	20.7
2,2,2-Trichloroethanol (TCE)	nd	152	1.3

Table 3-1: Reagents suitable for use in tagging reactions

Table compiled from www.chemspider.com, www.chemicalbook.com, and www.sigmaaldrich.com: (nd indicates no data found)

3.4. The Use of Terrestrial Models

Samples of meteorites, especially carbonaceous chondrites, are in short supply, and any procedure resulting in their destruction must be minimised. For this reason, development of tagging methodology was carried out using terrestrial models, with the intention of applying the chemistry to meteorite samples only when successfully demonstrated.

3.4.1. Meteorite Samples

Once demonstrated to be effective on terrestrial models, the tagging procedures were to be applied to samples of carbonaceous chondrite. As the meteorite must not be physically processed or treated in any way, these samples were to be small chips or fragments of meteorite, typically no more than 1 mm in any dimension, thus would

be large enough to be easily transported between the storage facility, the apparatus to be used for tagging (see section 3.5) and the analytical laboratories. Chips of carbonaceous chondrites (such as Murchison) of this size are sufficiently heterogeneous in structure to be suitable to demonstrate variability in organic content across the surface.

3.4.2. Choice of Terrestrial Models

The purpose of a model system is to provide a substitute for the valuable meteorite samples, which can be used during evaluation of tagging methodology. Such models, readily available and of little intrinsic value, can be used without concern for wastage. However, to be of any use in development, the model must behave as closely as possible to the eventual target of the methodology, namely chips of carbonaceous chondrite. Models should therefore be in the solid state, of similar size as the meteorite chips (and so able to be handled in a similar way) and contain organic materials with reactivity similar to those contained in carbonaceous chondrites.

Two types of model were evaluated:

- Terrestrial shale, already containing organic material
- Organic standards deposited on inorganic materials with low organic content.

These are discussed in turn in the following sections. The second group contains two types of material, TLC plates, and terrestrial rocks and minerals.

Shale

Terrestrial shale is a common rock which contains macromolecular organic material held within a mineral matrix (Durand, 1980) and so was evaluated as a potential model for carbonaceous chondrites. As a solid rock, with organic material

distributed within its structure, it will act as a model for development of methodology for the manipulation of meteorite samples, and the development of a suitable apparatus and experimental procedure for chemical exposure. However, the organic compounds found within shale are terrestrially-derived, and not therefore typical of those found in meteorite samples, and so their chemical reactions may be different. Shales contain organic materials of varying degrees of maturity, that is, modification following exposure to heat and pressure, divided into several types (for a description, see Tucker, 1991). After this work was completed, Matthewman *et al.*, (2013) studied the pyrolysis of several types of shale, and concluded that Type IV kerogen (such as that found in found in paleosols) gave similar (but not identical) results to samples of Murchison whereas Types I-III were quite different, thus confirming the difficulty of using a terrestrial material as a true chemical model.

In this study, shale was therefore used as a physical model of a carbonaceous chondrite, but not as a predictor for the specific chemistry likely to occur with meteoritic organic materials. Shale was used in a small number of sighting experiments at the beginning of this study, and it use discontinued once study of specific chemical reaction began. Small chips of terrestrial shale (*ca.* 1-2 mm in each dimension) were broken from a larger sample, and used in the experiments described in section 3.6. After exposure to tagging reagents the organic materials present were not extracted; the analysis of the products of reactions of shale were carried out *in situ*.

TLC plates

Thin-Layer Chromatography (TLC) plates, and were used simply as inorganic supports for samples of chemical standards, to enable the reactions of those standards

in the solid state to be investigated. The supports must be low in indigenous organic materials to avoid any interference with the reactions of the standards to be used. The advantage of this approach is that the reactivity of the standard organic materials used is well-characterised, and so appropriate tagging reactions can be selected, whereas with the organic material present in shale, that is not the case.

Organic standards, in solution, were applied to TLC plates (whole plates, or pieces, cut to size), and the solvent allowed to evaporate, leaving an area of the plate coated with a known amount of standard. Experiments using TLC plates are described in section 3.8. TLC was also used as the analytical method to determine whether reactions being investigated had, in fact, occurred. Supporting the test materials on TLC plates for reaction as well as analysis enables the analysis to be carried out in a very simple manner; the TLC plate can merely be transferred to a development tank without the need for further processing or workup.

Rocks and minerals

Organic-free rocks and minerals, however, provide a more representative model for the inorganic supports within carbonaceous chondrites than do TLC plates, despite the advantage of the analytical simplicity of the latter. To analyse products of reactions of standards deposited on rocks or minerals, it is necessary to isolate the reaction products (by removal from the rock or mineral) prior to analysis by TLC. These extra operations add complexity to the process, and so this approach was investigated last. It must be stressed that the role of all these models is only to assess the potential viability of the chemical methods under investigation; demonstration of the method can only come from use with actual meteorite samples.

Samples of rock were typically 1-2 mm in each dimension, prepared by crushing larger samples. Finely-crushed rock, or commercially-available mineral samples were also used. Samples of these materials (typically 50-200 mg) were placed on small glass dishes (using a spatula), before application of solutions of standards, and allowing the solvent to evaporate. All samples for chemical modification were typically supported on glass dishes prior to placement within the apparatus (described in the next section). Samples were not usually fixed to any support (such as SEM stubs, using adhesive pads or aluminium tape), or coated with carbon, except where specifically mentioned in the text.

3.5. Design of Apparatus for Carrying Out Tagging

For the exposure of samples to reactive vapours, two procedures were devised. The first, Procedure A, was used for a small number of experiments, carried out at the beginning of this study, using chips of terrestrial shale, or for a small number of experiments with TLC plates carrying samples of standards.

3.5.1. Procedure A

The samples for exposure, shale chips (1-2 mm in size) or strips cut from TLC plates (about 0.5 cm by 3 cm), were placed in a large glass vial or similar container. The reagent being used was placed in another small vial (*ca.* 100 mg, using a Pasteur pipette for liquids and a spatula for solids). This was then placed inside the vial containing the sample, which was then sealed. For addition of liquid reagents, it proved easier to add the reagent in a controlled way if, rather than being placed inside a small vial, the samples were placed on an upturned vial standing in a shallow dish in a larger container, into which the liquid could be introduced, and the

container sealed. After exposure for the desired time, the sample was removed, and taken for analysis. Excess reagent was disposed of using the appropriate procedure.

3.5.2. Procedure B

Subsequently, a second procedure, Procedure B, was adopted, and used for the majority of experiments. Procedure B had a number of advantages over Procedure A. It allowed controlled addition of reagents (including ozone), the possibility of exposure of a sample to several reagents simultaneously, and also provided a means to decompose excesses of toxic reagents (such as hydrazine hydrate or osmium tetroxide) at the end of the experiment, preventing release into the atmosphere.

Two variants of Procedure B were used; in Procedure B1 a single reagent was delivered to the reaction chamber by bubbling nitrogen through a holding flask, whereas in Procedure B2, reagents were delivered by direct evaporation from watch glasses placed in the reaction chamber. In both variants, solid samples were placed in small (*ca.* 1 cm diameter) watch glasses which were supported in a Petri dish; TLC plates were placed in a dish with higher sides so that they could be stood upright. The dishes were placed in a 1 L round-bottomed, flange-topped glass flask (with an opening of 150 mm diameter) securely mounted onto a flask stand. The flask top was fitted with a number of ground-glass connections, allowing vapours and gases to be passed into the flask, over the surface of the samples inside and then out into a scrubber. The flask was connected to a scrubber using PTFE tubing (which is resistant to attack by most materials). Reactive vapours were generated in two ways:

Procedure B1: Using a flow of nitrogen to introduce vapours

In the first case, vapours were generated by passing nitrogen through a sample of a volatile liquid contained in a smaller (100 or 250 mL) flask, connected using PTFE tubing, to the 1 L flask (as shown in Figure 3-2A). The liquid was introduced into the smaller flask *via* a Pasteur pipette or a syringe, and nitrogen bubbled through, the rate being adjusted by observing the flow rate through the scrubber. This method can only deliver one reagent at a time to the reaction flask; addition of more than one reagent can only be carried out sequentially, or by use of more than one small flask

This procedure was modified for experiments in which samples were exposed to ozone. In these cases, the small flask was disconnected, and the reaction flask attached to an ozone generator, *via* a water bubbler and anti-suck back trap, as shown in Figure 3-2B.

Procedure B2: Vapour production via slow evaporation

Alternatively, reactive vapours could be produced in the 1 L flask by simply allowing samples of volatile liquids to evaporate. In this case, the rotaflo valve from the small flask was closed, or replaced with a stopper, extra watch glasses were placed in the Petri dish, next to the rock or meteorite samples, or TLC plates, the reagent liquid(s) introduced (each into its own watch glass) with a Pasteur pipette, and the flask sealed. This method can allow introduction of more than one reagent at any one time.

Excess vapours remaining at the end of an experiment were swept out by blowing a stream of nitrogen through the flask, and passing the gas stream through a suitable scrubber. The scrubber contents were then disposed of using the appropriate method.

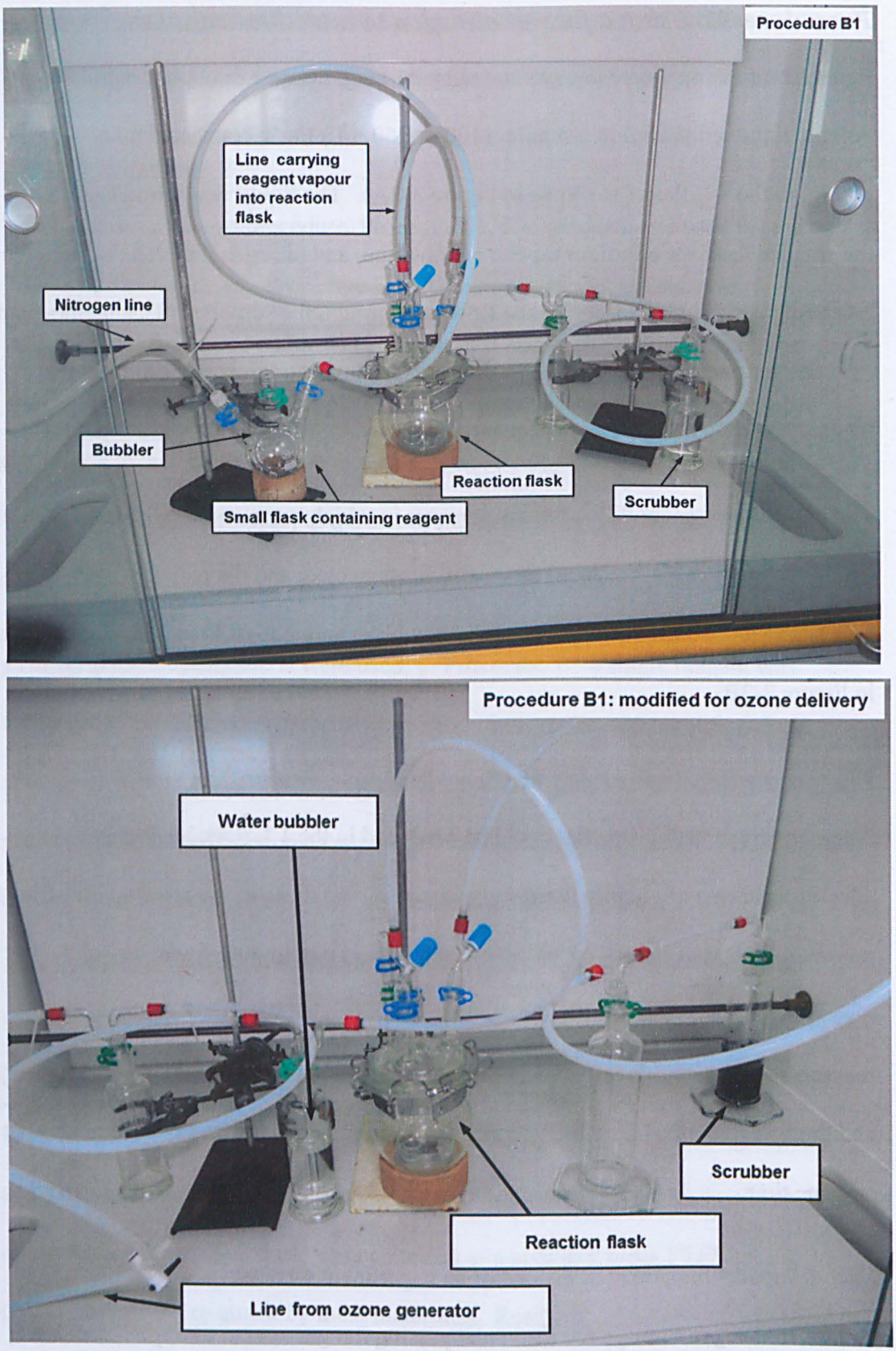

Figure 3-2: Apparatus used in Procedure B1 for delivery of A) vapours, or B) ozone

3.6. Terrestrial Shale Model

As discussed in section 3.4.2, terrestrial shale bears a number of similarities to a carbonaceous chondrite, in that it contains clay minerals (of a similar grain size to the matrix of these meteorites), has undergone a degree of alteration, and contains a significant proportion of organic material. As is an inhomogeneous rock with variable composition, and its organic content is derived from terrestrial organisms, its organic material is only superficially similar to IOM, and may possess significantly different reactivity, according to its source and degree of exposure to heat and pressure (Van Den Berg *et al.*, 1977; Kinney and Leonard, 1961; Matthewman *et al.*, 2013).

A sample of Toarcian shale was used in early studies, to facilitate the development of an experimental methodology for tagging. A complete characterisation of the organic content of this shale (both of soluble or volatile compounds, and of insoluble, macromolecular material) was beyond the scope of this study, and, as any reactions such a terrestrial sample might undergo with tagging reagents could not be considered representative of those typical of a meteorite; its use was primarily in method development. The results obtained in these preliminary studies are described below.

3.6.1. Examination of Terrestrial Shale Before Use

The analytical procedures used to study shale (and all other samples) are described in Chapter 2.

Samples of shale chips were examined using SEM and Raman spectroscopy to provide a baseline analysis prior to any modification. These techniques were chosen

as they can be used on samples without any physical modification, and do not cause any damage to the samples (the samples can be re-analysed after chemical treatment, and its effects assessed).

SEM images showed a heterogeneous surface, made up of micron-scale grains. Strong X-ray signals due to common mineral-forming elements were found throughout as expected. The X-ray signal for carbon was weak, and distributed across the whole of the sample, with no association seen with any specific mineral grains (Figure 3-3).

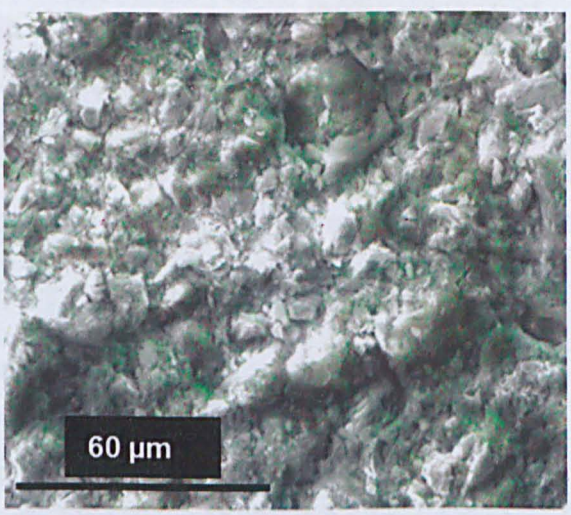

Figure 3-3: SEM image of terrestrial shale overlain with carbon map (shown in green), showing low levels of carbon detected

An image of the sample of shale obtained with the Raman microscope (Figure 3-4) was consistent with that obtained by SEM (Figure 3-3), although inferior (at the point this work was carried out, the use of image stacking, see section 2.1.4, had not yet been developed, and images showed a poor depth of field). Raman spectra taken at points on the surface showed the broad "D" and "G" peaks at *ca.* 1370 and 1600 cm^{-1} respectively, resulting from macromolecular organic material, as

previously reported in other studies of shale (Quirico *et al.*, 2005b; Potgieter-Vermaak *et al.*, 2011), and shown in Figure 3-5.

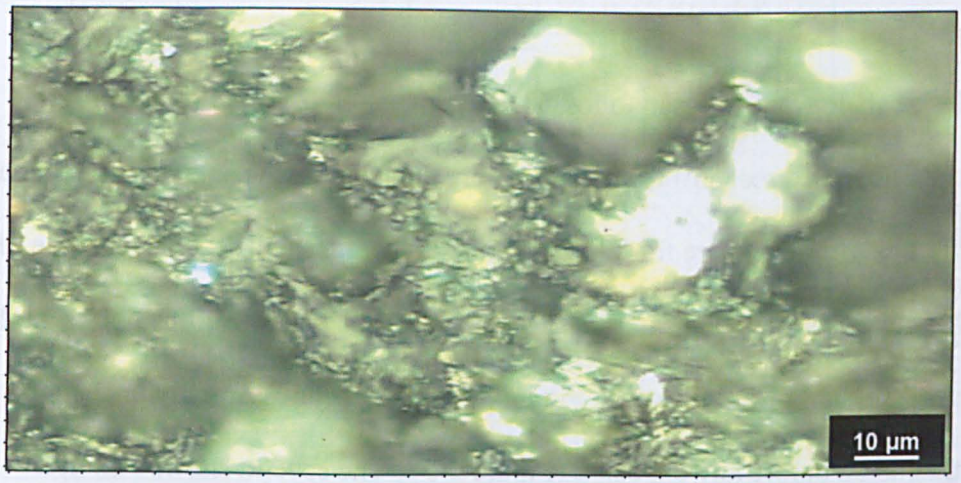

Figure 3-4: Raman microscope image of sample of terrestrial shale

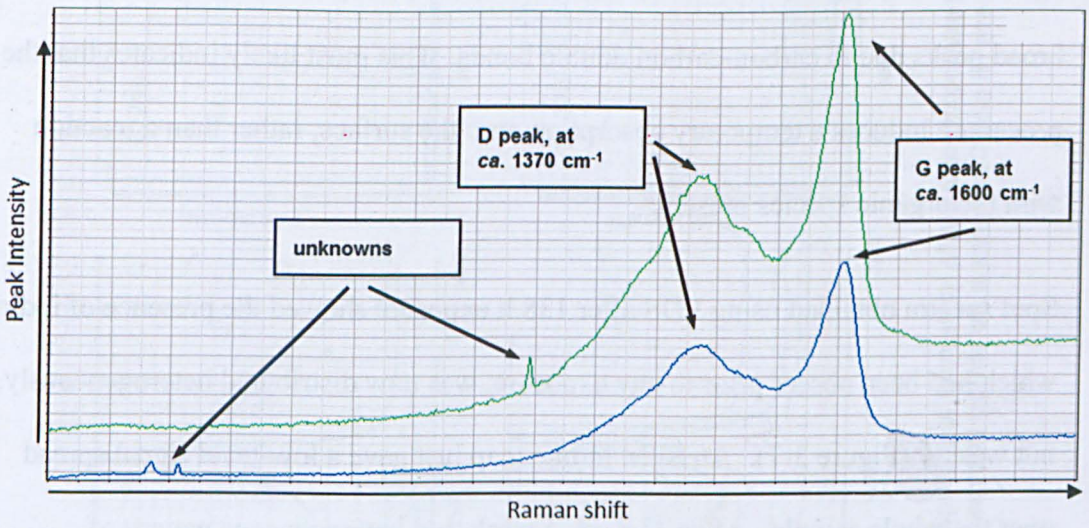

Figure 3-5: Raman spectra of the surface of untreated terrestrial shale (spectra taken at two points shown in different colours)

3.6.2. Exposure of Shale to Tagging Reagents

Procedure A described in section 3.5.1 was used for these initial experiments, in which shale samples were exposed to reagents likely to react with the oxygen-containing functional groups and aromatic ring systems believed to be present in kerogen, (Durand, 1980). The reagents selected for this initial investigation were the halogens, bromine and iodine (to react with aromatic rings), trifluoroacetic

anhydride, TFAA, (to react with nucleophilic centres, such as hydroxyl) and diethyl zinc, DEZ, (to react with electrophilic groups, such as aldehydes).

Iodine

Samples of shale were exposed to iodine, and de-gassed *in vacuo* (to remove any physically absorbed reagent) for *ca.* 4 h before analysis. SEM analysis and Raman spectroscopy after exposure for 8 h, 24h, and 138 h, and finally 27 days. Little, if any change, was seen in the samples. Raman spectra taken at various points on the surface of the sample are shown in Figure 3-6, and appear essentially unchanged from that taken before any exposure (Figure 3-5). The spectra showed no new signals (for example, due to carbon-iodine bonds) or any obvious reduction in the broad peaks due to carbon-carbon double bonds. This most likely indicates that the procedure induces a temporary absorption onto the surface, rather than a reaction with the organic species present.

Spot spectra obtained using EDS after 138 h exposure showed the presence of iodine, which had been absent prior to any exposure, was now distributed heterogeneously, but weakly (Figure 3-7). An SEM iodine map just gave a low-level signal spread over the whole sample. After 27 days, a weak, but heterogeneous pattern of absorption was seen in an element map (see Figure 3-8), but little useful correlation could be made between iodine content and mineral grains. A repeat analysis of this sample (stored in a closed container at ambient temperature) four weeks later showed that the iodine had been lost, presumably desorbed into the atmosphere.

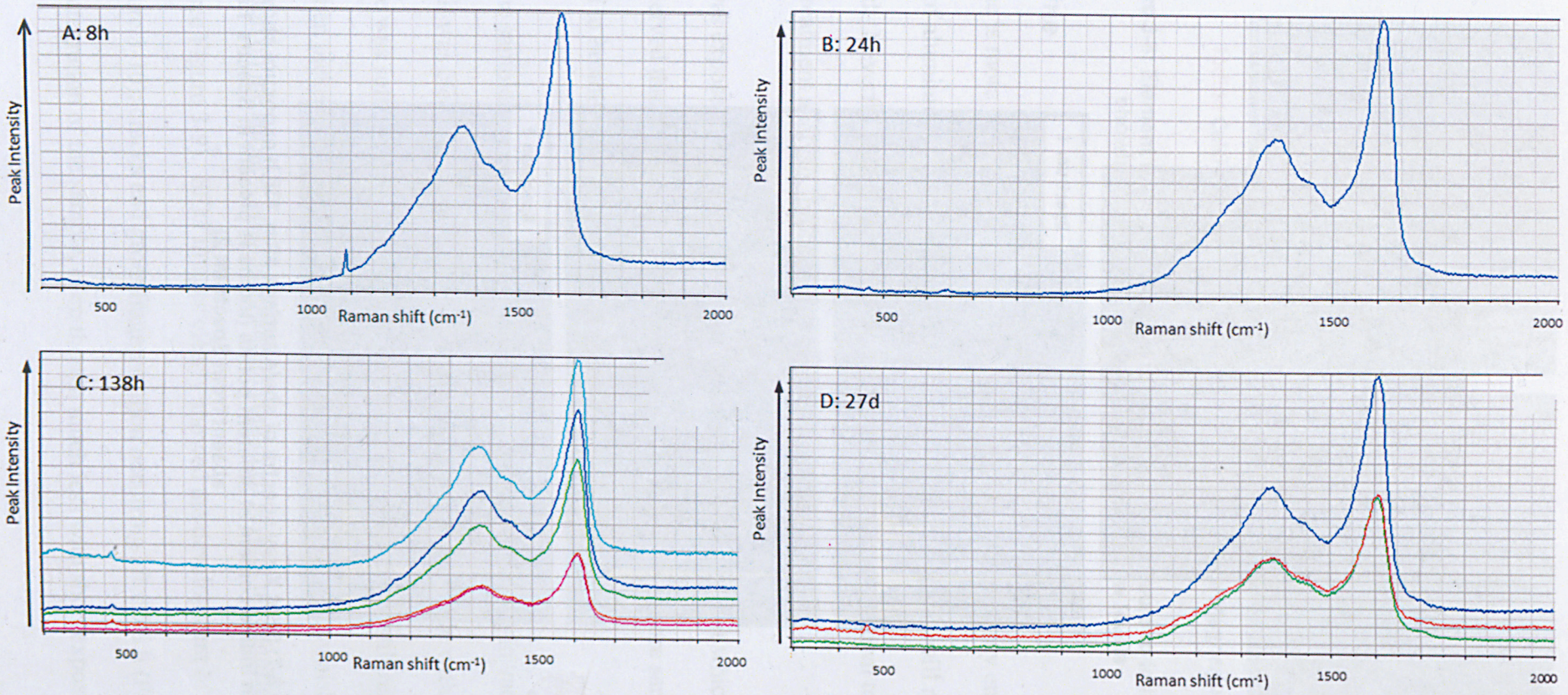

Figure 3-6: Raman spectra of terrestrial shale after exposure to iodine for times up to 27 d. Traces obtained at several points on a sample (C and D) are overlaid in different colours.

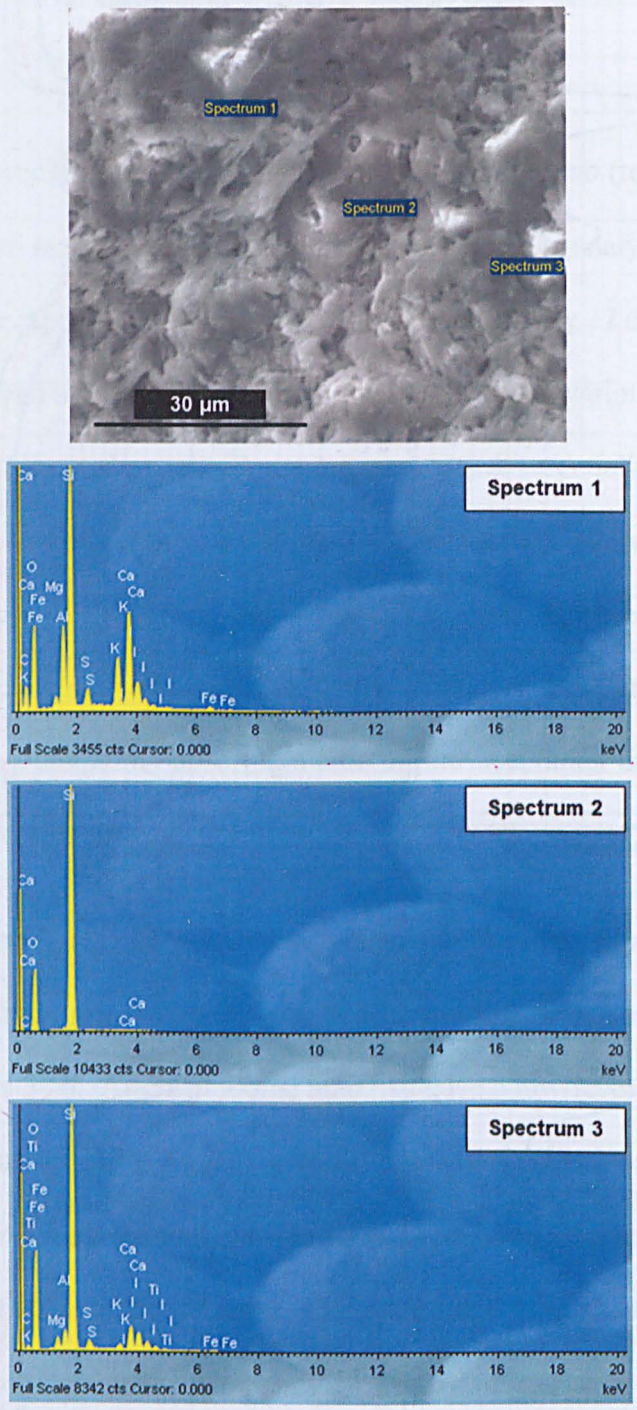

Figure 3-7: Spot X-ray spectra of shale surface after 138 h exposure showing variability in iodine content at different points (iodine is present in Spectra 1 and 3 but absent from Spectrum 2)

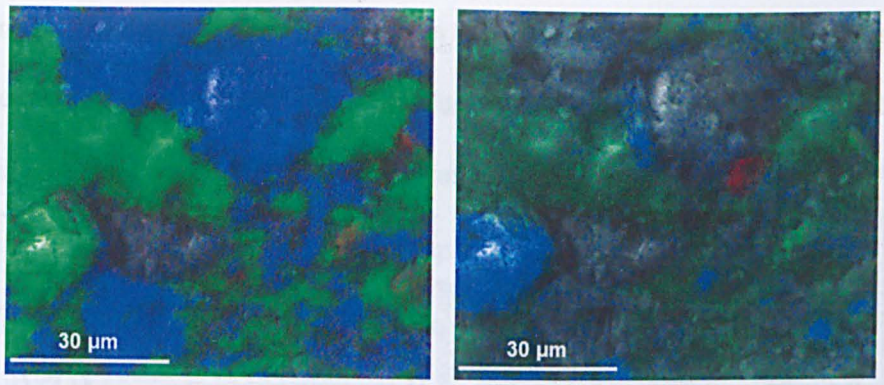

Figure 3-8: Element maps of terrestrial shale following exposure to iodine for 27 d showing heterogeneous distribution, but at low levels

Bromine

Bromine is more volatile than iodine, and more reactive, but its X-ray energy is close to that of aluminium (a common mineral-forming element), and so will not be well-resolved. Nevertheless, if aluminium-containing minerals were shown to be absent in pre-treatment analysis, bromine could be a useful reagent.

Shale was exposed to bromine for up to 5½ h using Procedure A, at which time it was observed that the sample had partially disintegrated. Three more samples were exposed to bromine, for 1, 2 and 4 h respectively.

When the samples were removed for analysis following de-gassing in vacuo for *ca.* 4 h, it was clear that physical damage had occurred. The sample with greatest exposure was soft and crumbly, although those with less exposure still remained intact when picked up. The Raman microscope image showed a brownish colouration on the surface, and the spectrum contained several unidentified broad peaks, (see Figure 3-9). SEM images clearly showed the development of cracks after 4 h (Figure 3-10); cracks and gross fragmentation occurring after 5½ h (Figure 3-11). The disintegration of the sample, even though much less with short exposure times,

clearly makes this approach unsuitable as a method for the detection of organic materials *in situ*, and it was not investigated further.

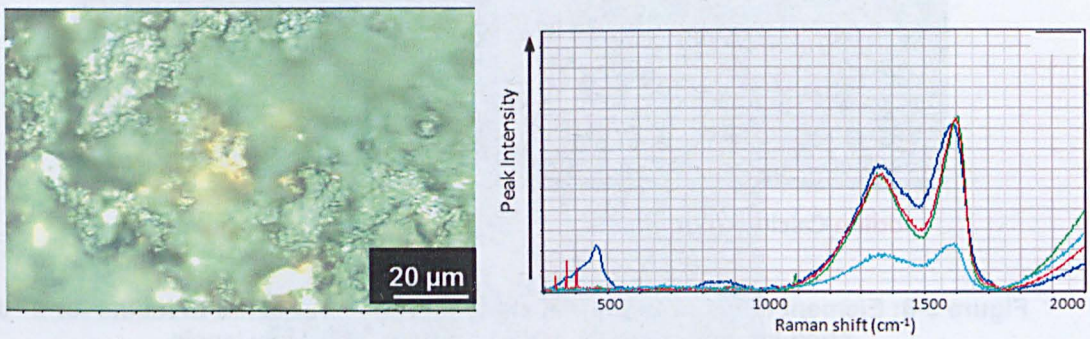

Figure 3-9: Raman image and spectra obtained from shale after exposure to bromine for 5½ h (Raman spectra obtained at different points on the surface are shown in different colours)

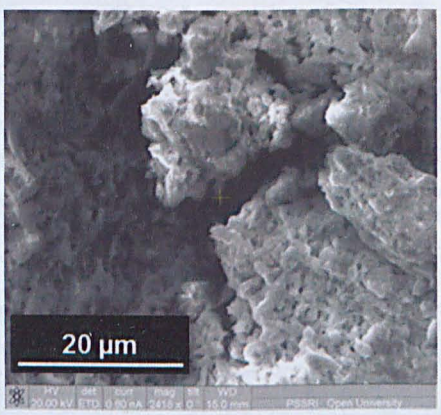

Figure 3-10: SEM image of shale exposed to bromine for 4 h showing partial fragmentation of the sample

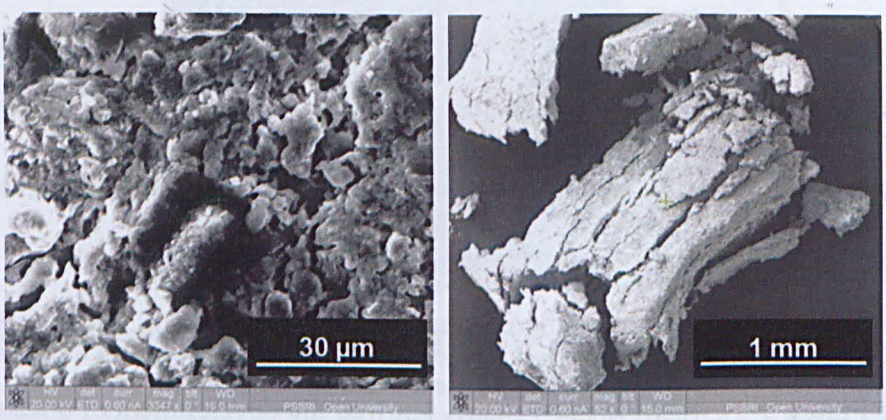

Figure 3-11: SEM images of shale exposed to bromine for 5½ h showing substantial fragmentation of the sample

Trifluoroacetic anhydride (TFAA)

TFAA reacts with nucleophiles (such as alcohols, amines, thiols and acids) forming esters, amides etc., which should be reasonably stable. Furthermore, any TFAA which is physically absorbed onto the sample surface (or which reacts with water to form trifluoroacetic acid) should be easy to remove (as both the acid and anhydride are volatile), thus avoiding spurious background signals.

Samples of shale were dried *in vacuo* for 6 h, to remove any water present, then were exposed to TFAA vapour for up to 4 hours using Procedure A (section 3.5.1) followed by analysis by Raman spectroscopy and SEM/EDS.

After 4 h exposure to TFAA, several brownish spots on the surface of the shale were seen using the Raman microscope; spectra at these points were similar to that of untreated shale (see Figure 3-5), although some weak signals were seen at low Raman shift (as shown in Figure 3-12).

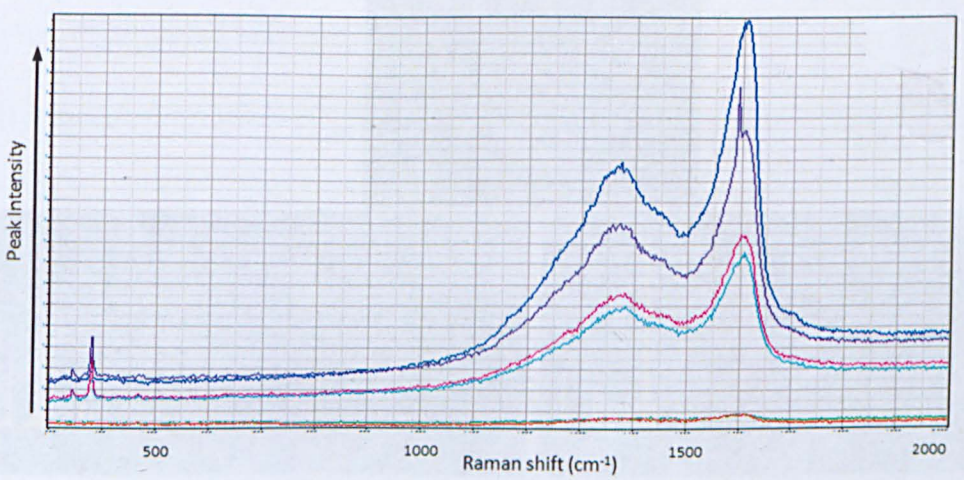

Figure 3-12: Raman spectra of shale exposed to TFAA for 4 h (spectra taken at various points are shown in different colours)

Analysis by EDS showed correlation of fluorine signals in some areas, with calcium, and a slight correlation with absence of silicon and aluminium. In other parts of the

sample, calcium-rich regions showed no fluorine present. The signal due to fluorine was quite weak, although heterogeneously distributed. X-ray spectra showed many areas of high localised fluorine abundance, and although two such areas gave essentially the same X-ray spectrum, a third was quite different, presumably due to differences in the underlying minerals. However, as TFAA also reacts with water (or hydrated minerals), these fluoride concentrations may not relate to tagged organic materials at all. The association of fluorine with different (unidentified) mineralogies is shown in Figure 3-13; areas which contain high levels of fluorine as detected by EDS are highlighted in red. A similar effect, but with areas poor in fluorine is shown in Figure 3-14. The spot spectra show that areas with similar levels of fluorine (high or low) can give different spot spectra. The identities of these minerals were not investigated further, being only a model system.

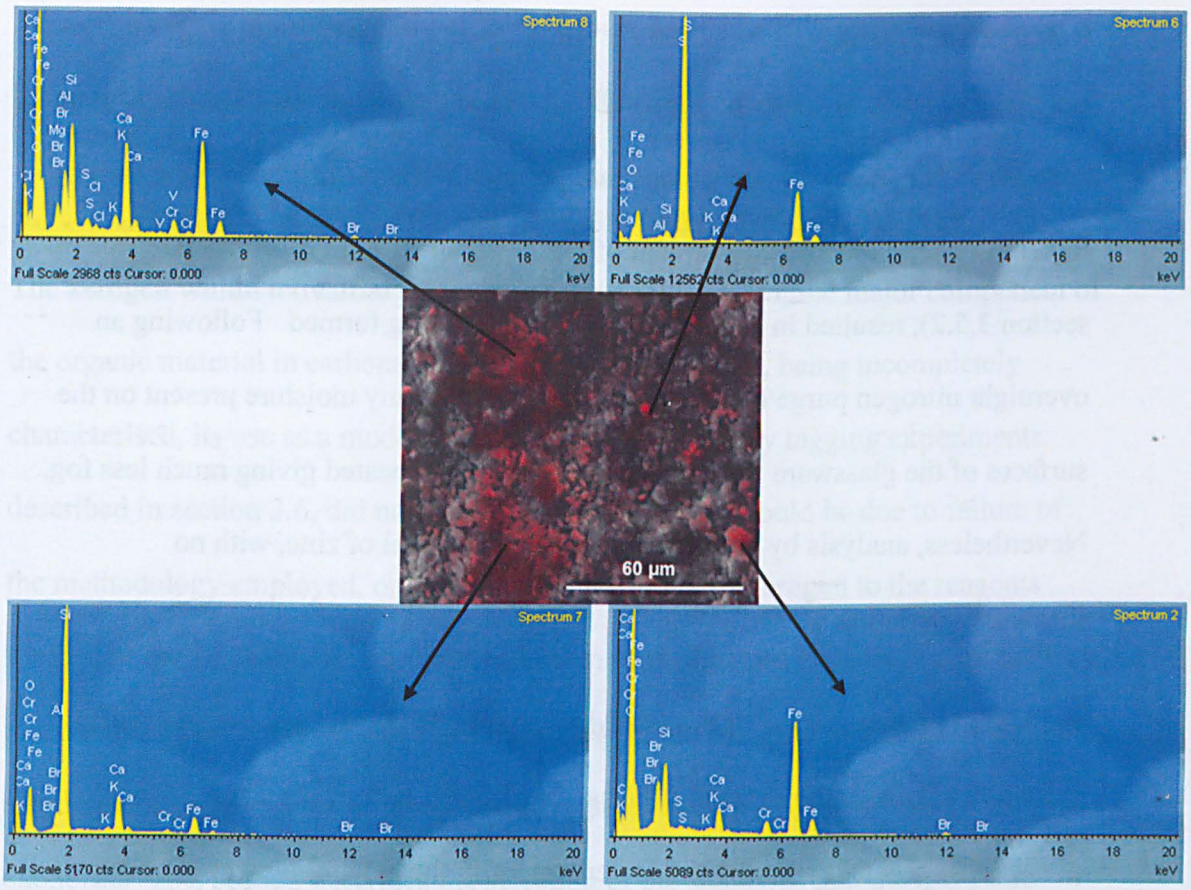

Figure 3-13: Spot X-ray spectra taken of areas containing fluorine (shown in red in element map) show fluorine can be associated with different mineralogies

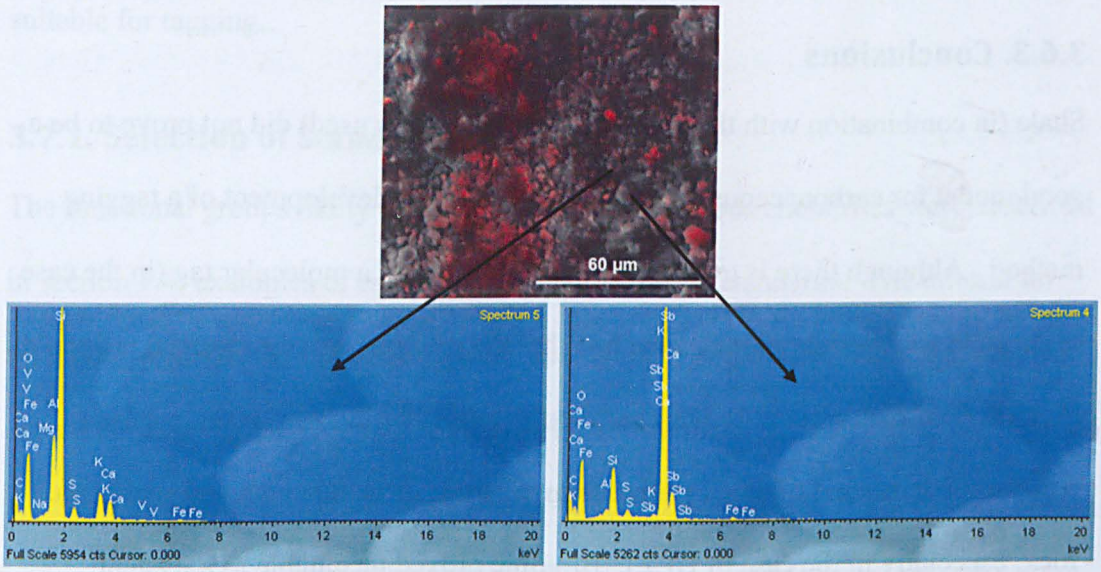

Figure 3-14: Spot X-ray spectra taken of areas low in fluorine (shown as absence of red in element map) show that lack of fluorine can also be associated with different mineralogies

Diethyl zinc (DEZ)

Exposure of shale to DEZ vapour for 2 h at ambient temperature, using Procedure A, gave very little incorporation of zinc and no relationship to mineralogy (shown by EDS). Longer exposure, to a stream of DEZ vapour (using Procedure B1, section 3.5.2), resulted in a fog of zinc hydroxide being formed. Following an overnight nitrogen purge of the apparatus (to remove any moisture present on the surfaces of the glassware used) the experiment was repeated giving much less fog. Nevertheless, analysis by EDS showed a very low level of zinc, with no heterogeneity being seen.

Formation of even a trace of fog would invalidate this procedure, with particles certain to adhere to the sample. SEM showed this was the case, DEZ having presumably reacted with residual water vapour in the reaction vessel. Consequently, this experiment was not investigated further, and the use of DEZ abandoned.

3.6.3. Conclusions

Shale (in combination with the experimental procedures used) did not prove to be a good model for carbonaceous chondrites for use in the development of a tagging method. Although there is evidence of incorporation of a molecular tag (in the case of fluorine, and possibly iodine) the fact that the reacting organic material is not well characterised makes it hard to be confident that the tagging seen is the result of reaction with organic material (rather than minerals or water contained within the rock, especially in the case of DEZ). Bromine proved unsuitable as a reagent, causing physical damage to the sample, as did DEZ, which only showed a reaction with water.

All remaining work was carried out using known organic standards, supported on inorganic materials, and is described in the following sections.

3.7. Chemical Standards for Use on Inorganic Supports

The kerogen within terrestrial shale acts as a model for IOM, the major component of the organic material in carbonaceous chondrites. However, being incompletely characterised, its use as a model is limited. The preliminary tagging experiments, described in section 3.6, did not give good results, which could be due to failure of the methodology employed, or to the lack of reactivity of kerogen to the reagents used. The use of chemical standards of known structure (and therefore predictable reactivity) could enable the effectiveness of tagging to be better evaluated, if these standards can be formulated into an effective physical model of a carbonaceous chondrite. This section describes the selection of the standards and the inorganic materials used as meteorite models, and the development of reaction conditions suitable for tagging.

3.7.1. Selection of Standards

The functional groups likely to be present in carbonaceous chondrites were described in section 1.4; examples of each were chosen for use as standards. The criteria for selection were that the compounds were readily available, stable to storage, and detectable as spots on TLC plates; those selected are listed in Table 3-2.

Functional group	Compound(s) used
Alcohol	Cinnamyl alcohol
Phenol	2-Naphthol
Aldehyde	Benzaldehyde, phenylacetaldehyde
Ketone	Benzophenone, cyclohexanone
Amino acid	Tryptophan, alanine
Carboxylic acid	4-Methoxybenzoic, azelaic, benzoic, cinnamic and tolylacetic acids
Amine	Cyclohexylamine
Polycyclic aromatic hydrocarbon	Phenanthrene, pyrene

Table 3-2: Standard compounds, representing a range of functional groups, selected for use in development of tagging chemistry

3.7.2. Preparation of Solutions

Solutions of these test compounds were prepared by dissolving the compound in a solvent. Dichloromethane was used where possible (to ensure rapid evaporation), but some compounds required more polar solvents such as ethyl acetate, methanol, or even water (for amino acids), in which case the most volatile option was used. Solutions were prepared to a concentration of 10 mg/mL unless the compound was not sufficiently soluble. By successive dilutions, stock solutions of 1.0 and 0.1 mg/mL were also prepared.

3.7.3. Potential Inorganic Supports

Two approaches were employed. In the first, organic standards were deposited on TLC plates. Standards can be deposited on these plates in a very controlled manner using the micropipettes routinely used in TLC analysis, enabling a known volume of solution to be deposited over a desired portion of the plate, giving a known sample loading. Then, following a solid-state reaction, the products, still on the TLC plate, can be analysed chromatographically without any further manipulation, enabling the reactivities of standard compounds to be easily assessed.

However, the coating of a TLC plate is very different, mineralogically, from a carbonaceous chondrite, and so a second set of models was investigated, namely organic standards deposited as a surface coating on organic-poor terrestrial rocks and minerals. In these experiments, a known quantity of standard was loaded by applying a solution of known concentration and allowing it to evaporate. The success of the reaction can be judged by removing the reaction products from the support by dissolving in a suitable solvent, and analysing it by TLC.

These two approaches are discussed in turn in the following two sections.

3.8. The Use of Thin-Layer Chromatography (TLC) Plates as Meteorite Models

In this section, the use of TLC plates is described, both as a support for solid-state tagging reactions, and for analysis of the products of these reactions.

3.8.1. Characterisation of TLC Plates Before Use

Commercially-available TLC plates are prepared by depositing a thin layer of alumina or silica gel onto a thin backing made from glass, plastic or aluminium foil. Only plastic or foil plates were used in this study, as they can be easily cut to size as required. The material of manufacture of the plate does not affect its performance in chromatography. Performance is instead determined by the coating, of which two types, silica gel or alumina, are in common use. The coating often contains a fluorescent additive, to help visualisation of spots. So as not to cause any interference, plates without additive were used in this study.

TLC plates were first examined by SEM. Portions of plastic TLC plates (*ca.* 0.5 cm square) were fixed to an SEM stub with conductive tape and then carbon-coated to

avoid charge accumulation and streaky images, as shown in Figure 3-15A and B, which results in poor-quality images and X-ray spectra. Foil plates gave less charge build-up, but these were more difficult to cut without loss of the coating which was less strongly-bound than for the plastic plates, resulting in greater wastage in obtaining pieces of an appropriate size.

Images acquired of TLC plates coated with silica gel and alumina using the Raman microscope were indistinct, showing only glassy grains. Accompanying spectra (Figure 3-15C and D) were featureless, showing only a rising baseline, and no signals assignable to either silica or alumina could be detected.

These images and spectra show that, as expected, signals arising from organic materials deposited on TLC plates will not be obscured by background.

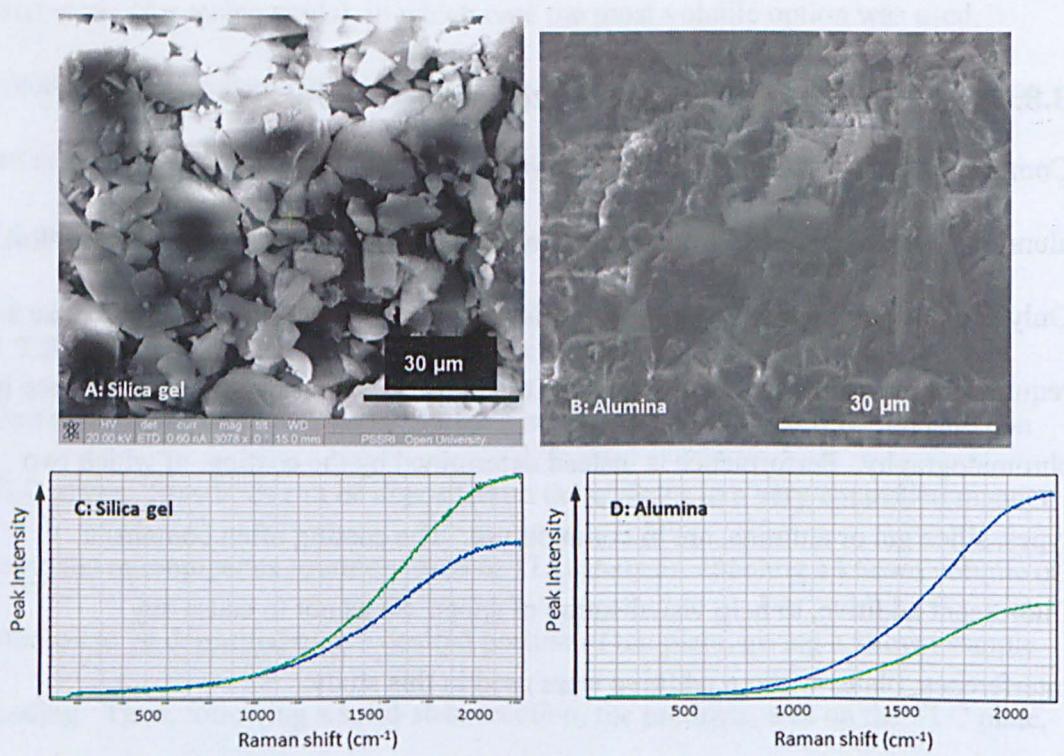

Figure 3-15: SEM images (A, B) and Raman spectra (C, D) of surfaces of TLC plates

3.8.2. Detection of Potential Tags *in situ* on TLC Plates

Prior to any experiments intended to introduce tags, the detectability of elements chosen as tags was evaluated. Solutions of compounds containing potential tags were applied to TLC plates using micropipettes, or a calibrated syringe. Samples of compounds, listed in Table 3-3, were chosen as sources of elements likely to be introduced as tags. (At this point in the project, DEZ was still being considered as a tagging reagent, so zinc chloride was used as a source both of zinc, and chlorine.) Squares (*ca.* 1 cm) were cut from silica-coated foil plates, in duplicate, and solutions of the standards already containing tags were applied to the bottom half of the square (one standard per square) leaving the top half uncoated. The sample loading was *ca.* 1 mg/cm^2

Element	Compound	MW	Mass fraction of element
Br	2-Bromobenzoic acid	201	0.40
I	2-Iodobenzoic acid	248	0.51
F	3-Trifluoromethylbenzoic acid	190	0.30
Zn, Cl	Zinc chloride	136.3	0.48 (Zn) and 0.52 (Cl)

Table 3-3: Compounds used in TLC detection study

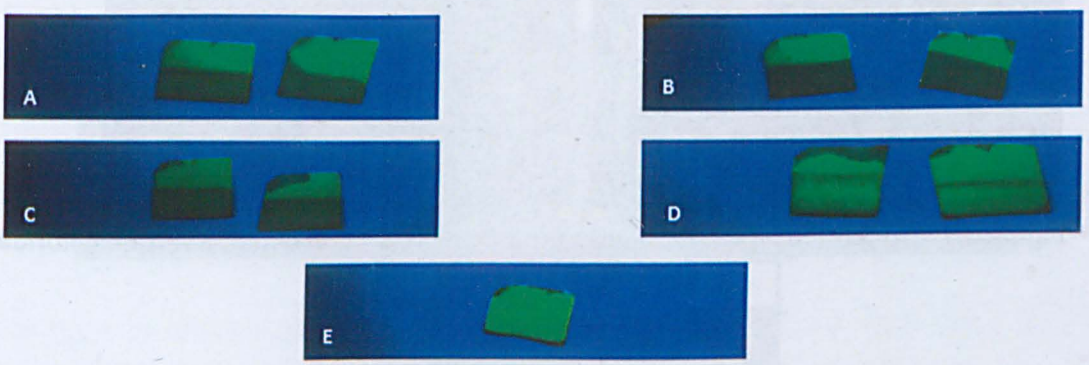

Figure 3-16: Detection of presence of materials on TLC plates with UV light (A: 2-Bromobenzoic acid, B: 2-Iodobenzoic acid, C: 3-Trifluoromethylbenzoic acid, D: Zinc chloride, E: Untreated)

The squares of TLC plate were viewed using UV light. The parts containing the tags could be easily seen as dark regions, although that containing zinc chloride was less distinct (Figure 3-16). The squares were then viewed using the SEM, to attempt detection of the tagging elements, using element maps and spot spectra.

Using EDS, it was possible to detect the presence of both zinc and chlorine on plate D. An SEM image (annotated with the locations of spot spectra), together with an element map are shown in Figure 3-17. The image (Figure 3-17A) shows a portion of the plate, with the grains of silica barely resolved. The element map (Figure 3-17B) shows the presence of both zinc and chlorine on the left-hand side of the image (corresponding to the coated part of the plate), whereas on the uncoated part (seen on the right of the image), levels are low. X-ray spectra taken at the two locations marked on the image illustrate this difference in elemental content (Figure 3-18), zinc and chlorine being detected in spectrum 1, but not in spectrum 2.

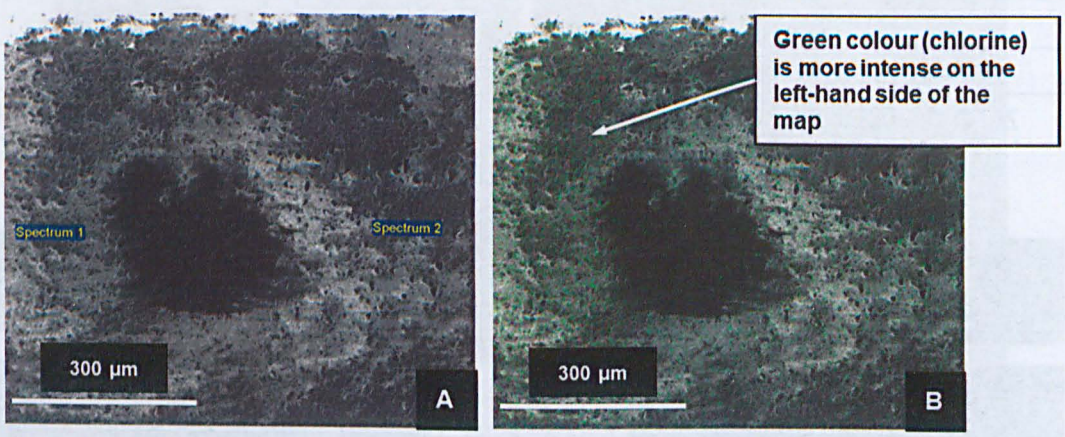

Figure 3-17: A) SEM image, and B) element map of TLC plate containing zinc chloride (chlorine shown in green)

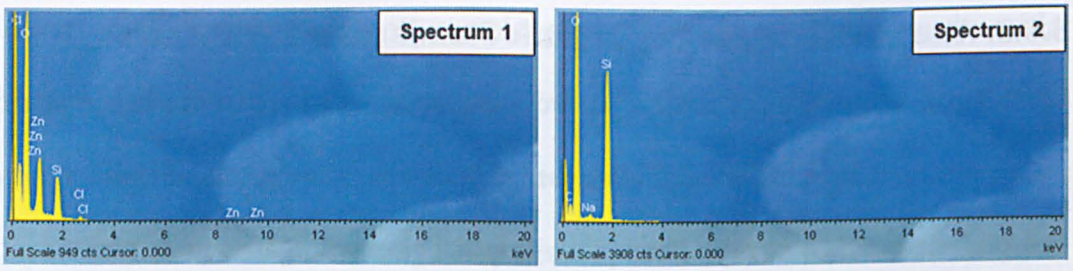

Figure 3-18: EDS spectra at the two locations marked in SEM image showing signals due to chlorine in spectrum 1 but not spectrum 2

Detection of the tagging elements in the other three samples proved difficult. Fluorine and bromine could not be detected by EDS; iodine gave a very weak signal, as shown in Figure 3-19 and Figure 3-20. No signal could be obtained due to any of the tagging compounds when examined by Raman spectroscopy; spectra obtained were equivalent to those of untreated plates (as shown in Figure 3-15C and D).

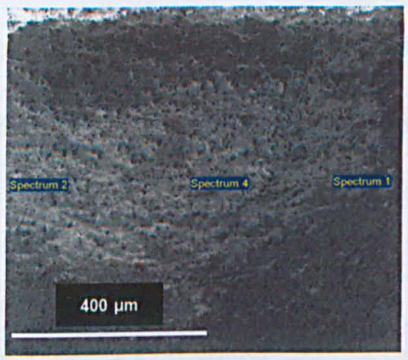

Figure 3-19: SEM image of TLC plate containing iodine

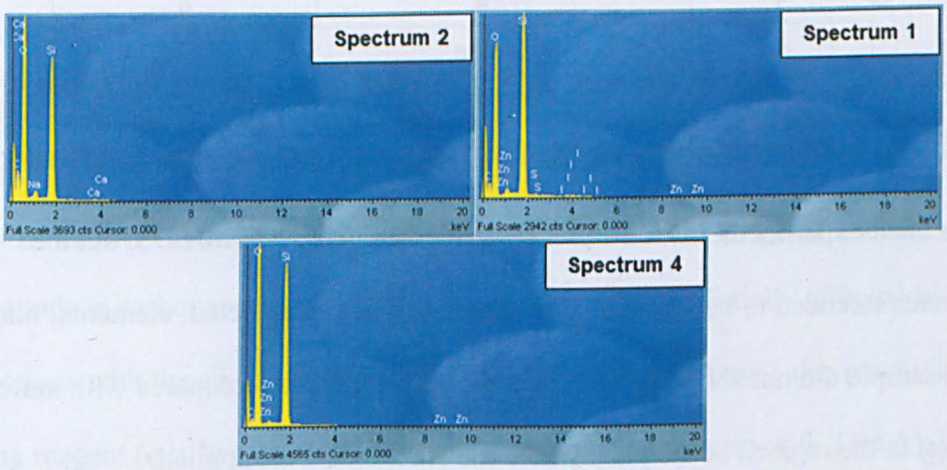

Figure 3-20: EDS spectra showing low levels of iodine (spectrum 1), or none (spectra 2 and 4)

3.8.3. Attempted Tagging of Organic Standards on TLC Plates

Solutions of the standards listed below were applied to strips cut from silica-coated plastic plates (one set of three samples per strip) using micropipettes, to deliver 10 μg of each. The quantity of compound applied gave an organic content of the loaded plate approximately the same as that found in carbonaceous chondrites, namely in the range 3-12% w/w.

Set A: cyclohexanone, alanine, azelaic acid

Set B: phenylacetaldehyde, phenanthrene, cyclohexylamine

The point of application of each standard was marked on the strip using the end of the micropipette, so that its location could be easily found during analysis. These strips, containing three spots per strip were exposed to tagging reagents using Procedure A (section 3.5.1). Reaction conditions are given in Table 3-4, both sets of standards were exposed to each reagent.

Experiment	Reagent	Exposure time (h)
1	Iodine	25
2	TFAA	2
3	TFAA	4
4	Bromine	2.5
5	Bromine	2

Table 3-4: Tagging compounds on TLC plates: Experimental conditions

After each experiment, the TLC plates were examined by SEM/EDS, but the elements intended to be introduced as tags could not be detected; elemental maps for each sample did not show higher levels of these elements (compared with untreated plates) in the regions of the plate where the standards were applied.

In a second series of experiments, samples of standards containing carboxylic acid, hydroxyl or amine functionality were applied to TLC plates, and exposed to TFAA vapour using Procedure B1, described in section 3.5.2. The TLC plates were developed (using DCM), but only in the case of cinnamic acid or 2-naphthol were new spots seen, indicating that a reaction had occurred. However, the TLC plate itself showed evidence of reaction with TFAA (a darkening was seen over the whole surface under UV) which made interpretation of results difficult.

3.8.4. Conclusion

Although TLC plates seemed an attractive approach to both supporting standards for testing, and analysing the results, the data presented above shows that the method has serious drawbacks.

The results show that compounds containing tagging elements, applied directly to TLC plates, are difficult to detect by EDS or Raman. This may also be a consequence of the very high specific surface area of TLC plates, with most of the standard contained within the highly porous structure of silica gel, and thus effectively shielded from the electron beam.

The silica gel or alumina used to make TLC plates possesses a very high specific surface area, and so any standard applied to a TLC plate will form a thin layer over this large surface. Reaction rates may be very different from those for similar compounds in carbonaceous chondrites (as well as being potentially affected by interactions with the silica or alumina). The silica or alumina may also react with the tagging reagent (*e.g.* hydroxyl groups would be expected to react with TFAA), thus giving a high background rendering tagging impossible to detect.

For these reasons, the use of TLC plates as supports for organic standards was discontinued.

3.9. The Use of Organic-Poor Terrestrial Rocks and Minerals to Support Organic Standards

In this section, work carried out with the objective of developing tagging chemistry using standards supported on organic-poor rocks and minerals, followed by analysis of the reaction products by TLC, is described. It should be stressed that the purpose of this work was to define reaction conditions for the tagging of standards, which would therefore act as starting points for the development of similar methods for meteoritic organic materials. There was no intention to fully optimise the conditions, but only to demonstrate that the chosen approach had a good chance of success when applied to precious meteorite samples.

Solutions of organic standards were applied to a sample of terrestrial mineral or rock, allowing the solution to permeate the sample and evaporate, depositing the organic compound between its grains and within its pores. The amount of material added was calculated to approximate the same concentration as organic materials in a carbonaceous chondrite. Samples prepared in this way were exposed to tagging reagents, and the results analysed by TLC. Experimental conditions were modified until a satisfactory degree of reaction was achieved.

3.9.1. Selection of Rock Samples as Supports

In selecting a suitable rock as a support, its porosity was key, so that the solution applied could permeate it and enter the pores within, depositing the organic compound over the internal surfaces. Alternatively, a powdered or crushed single mineral could be used, allowing the solution to wet the fine grains and evaporate,

giving an external coat. (Experiments carried out using minerals (as opposed to rocks) as supports are described in section 3.9.5.) In any case, the support should be essentially free of organic compounds which would interfere with the study. Igneous, or other crystalline rocks are not porous and were not evaluated, neither were rocks with significant organic content, for example, shale. The set of rocks (meeting the criteria of low organic content and suitable porosity) selected for initial investigation is listed in Table 3-5. These rocks were examined by SEM/EDS and Raman spectroscopy, to determine if any would give a background signal (especially that arising from organic content) which would hinder detection of tags.

Sample	Source
Fluvial sandstone	Bradford, England
Ignimbrite	Italy
Arkose	Achiltibuie, Scotland
Greywacke	Leadburn, Scotland
Oolitic limestone	Moreton-in-Marsh England

Table 3-5: Rocks investigated as potential inorganic supports, with their sources

Oolitic limestone, although not showing peaks due to organic materials (such as the D and G peaks in its Raman spectrum), was discarded since it was composed of carbonate, and contains fossil fragments which would give carbon signals when using EDS. Greywacke was well cemented (so non-porous), and also showed several (unidentified) signals in its Raman spectrum, and so was also discarded. Arkose showed little Raman signal, but was also well-cemented, and discarded.

Both sandstone and ignimbrite gave Raman spectra free from peaks due to organic materials, and appeared sufficiently porous, so were investigated further.

Investigation into porosity of potential supports

Small chips (*ca.* 1-2 mm) of sandstone and ignimbrite were weighed, and solvent added carefully *via* a syringe, noting the point at which the sample became saturated. About 0.3 μL/mg could be applied without excess solvent pooling at the base of the sample, and by allowing the solvent to evaporate between applications, a total of 1 μL/mg could easily be added. However, when a solution of pyrene (50 mg/mL) was applied to a fragment of ignimbrite, the solution evaporated on the surface of the sample (without being absorbed into it), rather than within its internal structure, leaving a dusty coating on the surface. When using sandstone however, this problem did not occur; the solution soaked into the sample and evaporated inside it. Sandstone was therefore selected for all future use.

Choice of inorganic supports

Sandstone, is composed largely of quartz, which is only reactive on its surface, where silicon-oxygen bonds are terminated with hydrogen. Bonds in the interior of the crystal (between silicon and oxygen) are strong, and not easily broken. The crystals of quartz making up sandstone have a low specific surface area, so any surface-mediated reactivity was expected to be low (in contrast, for example, with silica gel), and thus was expected to perform satisfactorily as an inert support.

As a comparison, samples of sand (*ca.* 50-70 mesh) and a clay, montmorillonite, both supplied by Aldrich, were also used as supports in some experiments. Sand, also being composed of quartz, would be expected to behave as a similar support to crushed sandstone, although likely to be less porous and have a lower specific surface area.

Montmorillonite has a very high specific surface area (Greene-Kelly, 1964), so the standard will form a thinner layer on it than when deposited on sandstone, and so is likely to react faster. Also, montmorillonite may exert a catalytic effect on the reaction; this effect has been exploited in some organic syntheses (Wallis *et al.*, 2009; Varma, 2002; Montgomery *et al.*, 2011). Catalysis by clays has been proposed as a possible synthetic origin of organic materials in carbonaceous chondrites (Chang and Bunch, 1986; Cairns-Smith and Hartman, 1986) and determining if clays and organic materials are co-located in the rationale for the development of the tagging procedure described in this chapter.

The sand was pre-dried at 600° overnight, whereas neither the sandstone nor the montmorillonite were pre-treated in any way.

3.9.2. Characterisation of Supports before Use

Samples of crushed sandstone, sand and montmorillonite were examined by SEM and Raman spectroscopy, to determine approximate particle sizes, and to confirm absence of signals from organic materials. Images obtained using SEM are shown in Figure 3-21. and those using the Raman microscope in Figure 3-22. These latter set of images, generated using Zerene stacker, do not show much detail, in comparison with those obtained using SEM. Grains of sandstone or sand appear glassy and featureless, whereas montmorillonite gave a very poor quality image. Only sand gave a Raman spectrum, indicating quartz, and is shown in Figure 3-23. The other materials gave no signals. Presumably the quartz present in sandstone is obscured by the surface coatings of the sandstone grains, and so is not detected by the Raman laser.

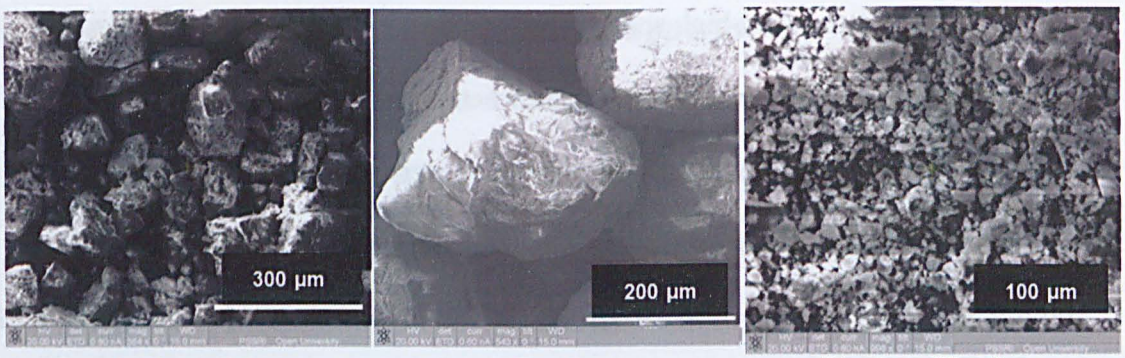

Crushed sandstone **Sand** **Montmorillonite**

Figure 3-21: SEM images of mineral supports

Crushed sandstone **Sand** **Montmorillonite**

Figure 3-22: Stacked images of mineral supports acquired using the Raman microscope

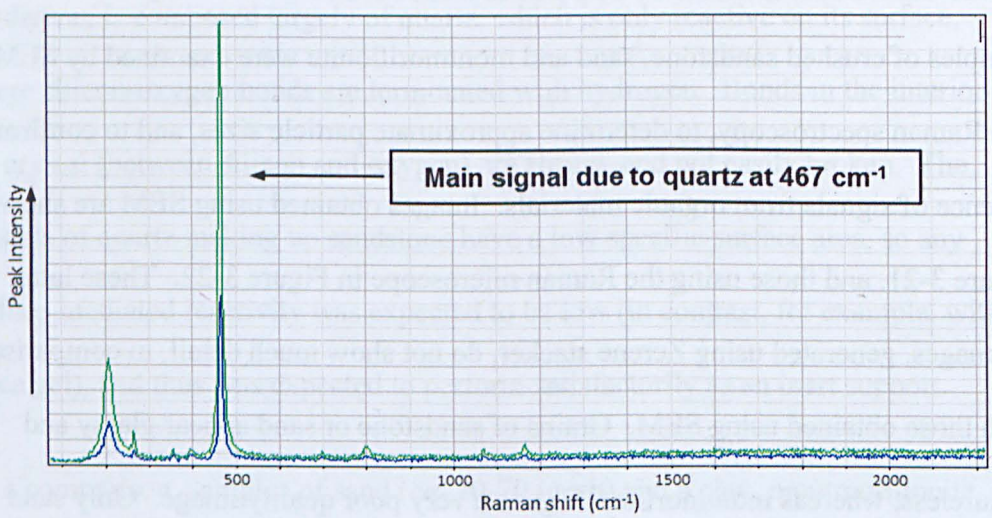

Figure 3-23: Raman spectrum of sand showing signal due to quartz (467 cm^{-1})

3.9.3. Detection of Potential Tags in situ

The objective of the work described in this section is to show that standard compounds containing a potential tagging group or element (as part of their structure), deposited on an inorganic support, can be detected *in situ*. Similar

experiments with standards deposited on TLC plates are described in section 3.8.2. Standard compounds (listed in Table 3-3) were analysed, firstly as neat compounds on microscope slides, then deposited on the surface of rock samples. Detection of elements was attempted by EDS, and functional groups using Raman spectroscopy .

Sample preparation

Organic standards containing a potential tagging element or functional group were listed in section 3.7. Pure samples for analysis by Raman spectroscopy were placed on a microscope slide. Solids were simply applied using a spatula, liquids with a pasteur pipette. When an analyte was applied in solution however, as the solvent evaporated, patches of evaporate formed, and a spectrum was only obtained if the laser struck one of these. In a similar fashion, liquid samples formed small drops under the influence of surface tension.

Samples for SEM were prepared by depositing standards on the surface of crushed sandstone, in the same manner as for standards used in tagging development (section 3.7.3). These samples were then placed on a stub, secured using an adhesive pad.

Raman spectra of neat standards

Spectra were acquired from carboxylic acid, and PAH standards, being compounds representative of those believed to be present in untreated meteorite samples. Example spectra are shown in Figure 3-24; the spectrum shown in Figure 3-24B shows the strong fluorescence obtained in spectra of PAHs. In both cases, as would be expected for a pure standard, a set of sharp signals was obtained. Close structural analogues of these compounds would be expected to give similar, but not identical

spectra, and so a complex molecular structure such as IOM would give many signals, derived from the numerous different functionalities present. Signals due to common functional groups (such as carboxylic acids, or aromatic rings) would be expected to be of similar position in the spectrum (and so form a broad band), the presence of which would indicate the presence of these types of compound.

Raman spectra of compounds supported on rock samples

Crushed sandstone was coated with pyrene (as described in section 3.7.3) and analysed by Raman spectroscopy. Signals due to pyrene were seen, but were not uniformly distributed across the surface, being only seen in isolated spots. This implied that pyrene was present as clumps of crystals, rather than a continuous film. Examination of a sample using an optical microscope, but illuminated with UV, did indeed show isolated spots of fluorescence, indicating the presence of spots of pyrene.

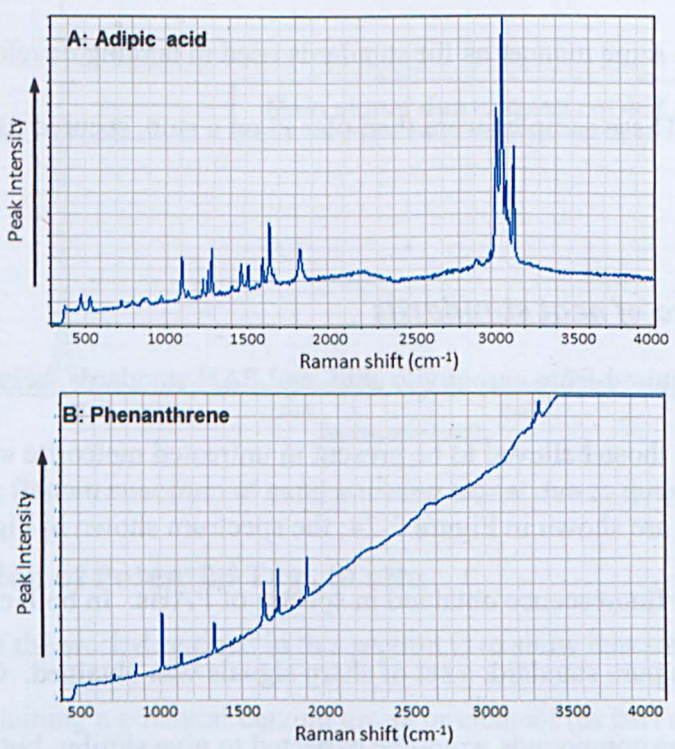

Figure 3-24: Examples of Raman spectra of standard compounds

Detection of standards on rock supports using SEM

The use of SEM/EDS to detect tagging elements was explored by depositing a standard compound containing chlorine onto crushed sandstone and sand, in the same manner as described in section 3.7.3. 2,4-Dichlorobenzoic acid (2,4-DCBA) was applied in solution, to give a sample containing 5% standard by weight, and the material examined by SEM, taking X-ray spectra. The coating of this organic standard was also unevenly spread over the surface of the support, as shown in Figure 3-25. Whereas a chlorine signal was seen at one point (Spectrum 1), no signal was obtained at the other points sampled, and an element map showed only a low level signal due to chlorine. Strong chlorine signals correlated with a deposit of crystalline material, visible in an SEM image (shown in Figure 3-26), indicating this standard had also formed crystalline clumps, rather than a thin film over the surface.

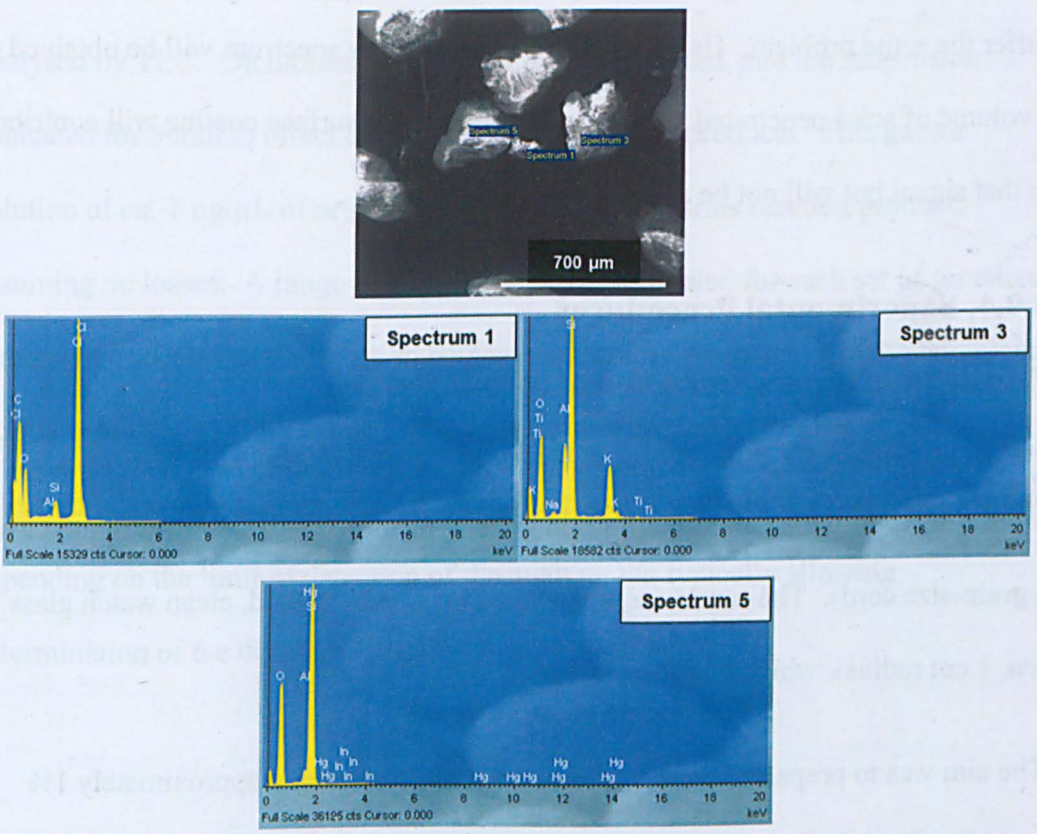

Figure 3-25: X-ray spectra at points on a sample of sandstone containing 2,4-DCBA (chlorine is only detected in spectrum 1)

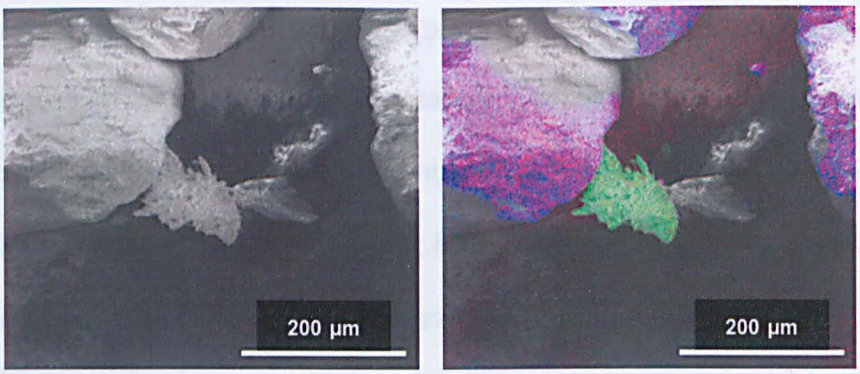

Figure 3-26: Crystals of 2-4-DCBA showing clearly in green (silicon, oxygen, chlorine)

Conclusions

Deposition of standards on rock supports was not uniform. The attempted detection of tagged standards deposited on these supports using both SEM/EDS and Raman has shown that a heterogeneous sample will prove difficult to analyse. A Raman spectrum will only be obtained if the laser strikes the tagged area directly; small regions may be missed altogether. Spot X-ray spectra obtained using the SEM will suffer the same problem. Using EDS, an average X-ray spectrum will be obtained of a volume of solid penetrated by the electron beam; the surface coating will contribute to that signal but will not be a large component of it.

3.9.4. Experimental Procedures

Preparation of sandstone doped with standard

Sandstone chips were prepared by gently breaking up a sample of terrestrial sandstone, to provide a mixture of grain sizes, typically 100-300 µm (estimated using a grain-size card). The sandstone was placed on a pre-weighed, clean watch glass (*ca.* 1 cm radius), which was then re-weighed.

The aim was to prepare a sample of rock fragment containing approximately 1% organic material by weight, distributed throughout its structure, coating external

surfaces and surfaces of internal pores. A solution of organic standard, (typically 10 mg/ml in dichloromethane) was applied at the rate of 1 μL per mg of sandstone, in 2-3 portions, allowing each to evaporate before the next was applied, so that the solution was distributed throughout the sample, which was then allowed to stand for a few minutes to ensure all solvent had evaporated. This procedure gave a sample containing about 1% by weight of organic compound, and therefore an organic layer about 1 μm thick coating the grains (assuming the grain size given above). For some compounds, solubility was too low to enable a 10 mg/ml solution to be prepared, in which case, a more dilute solution was prepared, and correspondingly more applied to the sandstone, resulting in the same loading.

Analysis of reaction products

At the end of the experiment, the sandstone coated with organic compound was analysed by TLC. Dichloromethane (5 μL/mg) was added, and the suspension sonicated for 5 min to effect dissolution of the reaction products. This gave a solution of *ca.* 1 μg/μL of original organic compound, or its reaction product, assuming no losses. A range of TLC eluents was evaluated for each set of functional groups, to obtain a good resolution between reactant and product, whilst maintaining a good spot shape. The solution of reaction product(s) was compared with a selection of standards using TLC, the exact concentrations of the standards depending on the limit of detection of the analyte, but typically allowing determination of the degree of reaction to at least 95%.

3.9.5. Investigation into the Reactions of Standards Supported on Minerals and Rocks

The apparatus used for this study was described in section 3.5. Experiments were carried out to develop tagging reactions for specific classes of organic compounds, using one or more example of each class to evaluate different reaction conditions, with the objective of finding the optimum reaction conditions for each standard. The standards used are the same as those selected for the earlier studies described above, and are listed in Table 3-2. In all reactions, analysis was by TLC, using UV visualisation.

Alcohols and phenols

TFAA reacts with these nucleophilic functional groups to give the respective ester; experimental details are summarised in Table 3-6. Experiments were carried out using cinnamyl alcohol and 2-naphthol as representatives of these classes.

When absorbed onto crushed sandstone, TLC showed near-complete reaction of cinnamyl alcohol with TFAA after 1h exposure using experimental Procedure B1 (section 3.5.2), but no reaction was seen for 2-naphthol (Table 3-6, Entry 1). This result confirms the concern that reaction rates for standards deposited on TLC plates may be significantly different; when supported on silica TLC plates, 2-naphthol had reacted rapidly with TFAA (see section 3.8.3).

Addition of a drop of picoline to a solution of 2-naphthol and TFAA showed complete reaction by TLC. Here, picoline is acting as a catalyst, as, presumably, had the silica gel of the TLC plate.

Procedure B1 was used to expose samples sequentially to a base, followed by TFAA. To minimise reaction between these two reagents, the 1L flask was purged with nitrogen between addition of base and addition of TFAA. With no intermediate purging, and removal of residual base vapour, the flask filled with fumes (presumably the respective trifluoroacetate) on admission of TFAA.

Difficulty was experienced in evaporating pyridine (chosen as being more volatile than picoline) into the evacuated reaction flask (it did not readily volatilise, and required heating), so the more volatile triethylamine was used as base (Table 3-6, Entry 2), after confirming the reaction worked in solution as for picoline. Reaction times were extended to allow compete reaction; triethylamine vapour was blown into the flask using nitrogen for 1.5 h, then excess removed with a nitrogen purge over 2 h. TFAA vapour was then blown through the flask over 1 h. However, TLC showed no reaction (Table 3-6, Entry 3). The reaction was repeated (also using a nitrogen flow to deliver pyridine, instead of triethylamine, (Table 3-6, Entry 4), when *ca.* 95% reaction was seen (Table 3-6, Entry 3) and this was is more successful, being less susceptible to leaks, loss of pressure, or the need to heat liquids to ensure complete evaporation.

However, the effectiveness of this reaction proved to vary between standards (Table 3-6, Entry 5), and although a good degree of reaction was always obtained using cinnamyl alcohol, 2-naphthol typically gave only about 75% reaction (Table 3-6, Entry 6). Nevertheless, that degree of reaction was felt to be sufficient for this stage of the development of the procedure. Use of procedure B2, with both reagents present in the flask simultaneously, gave a poor result (Table 3-6, Entry 7).

Substitution of 2,2-dichloroacetic anhydride (DCAA) for TFAA, using Procedure B2 for the second part of the reaction (due to the much lower volatility of DCAA compared with TFAA, but delivering the pyridine using Procedure B1, as before), gave a good result, with no more than 1% of either 2-naphthol or cinnamyl alcohol remaining after exposure overnight (Table 3-6, Entry 8).

Carboxylic acids

Of the acids selected for use, spots of benzoic and tolylacetic acids proved difficult to visualise using UV, but 3-trifluoromethylbenzoic and iodobenzoic acids contained stronger chromophores, and were satisfactory. These also contained elements for which detection by SEM/EDS could be investigated.

These acids, supported on crushed sandstone, were exposed sequentially to pyridine, TFAA and methanol, in an attempt to form esters *via* a mixed anhydride (as shown in Scheme 3-3). To be able to follow the reactions of carboxylic acids, the TLC method had to be modified to move the residual acid away from the baseline, and thus obtain a good spot shape. Addition of a small quantity of methanol and acetic acid to DCM gave satisfactory results, but as methanol would react with any intermediate anhydride present, the reaction could not easily be monitored. Nevertheless, the carboxylic acid substrates were consumed, and new products seen (about 10-20% remaining unreacted).

Entry	Standard	Base	Time	N_2 purge time	Reagent	Time (h)	Vacuum or N_2 flow	Standard remaining (%)
1	2-Napthol	None	n/a	n/a	TFAA	1	Vacuum	100
	Cinnamyl alcohol							<<5
2	2-Napthol	Et_3N	25 min	20 min	TFAA	0.75	N_2 flow	100
3	2-Napthol	Et_3N	1h 40 min	2 h	TFAA	3	N_2 flow	100
4	2-Napthol	Py	2h	1 h	TFAA	1	N_2 flow	5
5	Cinnamyl alcohol	Py	2h	1 h	TFAA	1	N_2 flow	10
	2-Napthol							50
6	2-Napthol	Py	2h	10 min	TFAA	3	N_2 flow	25
	Cinnamyl alcohol							<1
7	2-Napthol	Py	n/a	n/a	TFAA	2	n/a	>25
8	2-Napthol	Py	2h	1 h	DCAA	22	n/a	<1
	Cinnamyl alcohol							<1

Table 3-6: Reactions carried out between anhydrides and oxygen nucleophiles

Standard	Reagent	Rf standard	Rf product
2-Naphthol	TFAA	0.21	0.79
Cinnamyl alcohol	TFAA	0.15	0.77
Benzylamine	TFAA	Baseline	0.40

Table 3-7: TLC retention factors for standards and reaction products

Notes: All TLC analyses of reactions of alcohols and phenols were carried out using DCM as eluent.

As a simpler alternative to both this reaction and analytical method, esterification mediated by a carbodiimide was investigated, with ethyl acetate used as TLC eluent. Diisopropylcarbodiimide (DIC) was preferred over the more common, but more toxic, dicyclohexylcarbodiimide (DCC). DIC is a liquid at room temperature, and although its vapour pressure is low, solid-state reactions have been reported (Takabayashi *et al.*, 2010). Small-scale solution experiments using 4-methoxy-benzoic acid (MBA) and 2,2,2-trifluoroethanol (TFE) showed a new product was formed, prior to any addition of alcohol, presumed to be either the initial isourea adduct, or its known rearrangement product (see Scheme 3-4). Addition of pyridine accelerated the reaction, with all starting material being consumed after 2 h, so these reagents were then used with samples of standard, using Procedure B2. 4-Methoxy-benzoic acid (MBA) was used as substrate, being easily visualised on a TLC plate, and typical of the likely reactivity of carboxylic acids present in IOM. Experiments were also carried out using acids supported on montmorillonite and sand.

An initial experiment (Table 3-8, Entry 1a/b), using MBA on both crushed sandstone and montmorillonite, was left for 70 h to ensure complete reaction After this time, no starting material could be seen by TLC (both DCM and ethyl acetate were used).

After only 1 h (Table 3-8, Entry 2a/b), again, no starting material could be seen (using either support). In the case of crushed sandstone, two products had formed. Although one of these corresponded to the product seen after 70 h, the other was new. This second product was formed when the experiment was repeated, omitting TFE, and thus is probably either the intermediate, or the acyl isourea as shown in

Scheme 3-4. A comparison of MBA with 2-iodobenzoic and cinnamic acids showed reaction rates were comparable, although MBA reacted the slowest.

Extending the reaction time to overnight (Table 3-8, Entry 4) gave compete reaction; TLC showed one product with no starting material being detected. Two further experiments (Table 3-8, Entries 5 and 6) were carried out to better define the reaction time; only a trace of the undesired product was seen after 4 h, with none after 7 h. In these experiments, unreacted acid was either undetected, or only present in low, unquantified amounts. The limit of detection was re-investigated, and the limit found to be between 0.05 and 0.1 μg for cinnamic acid and MBA, but 0.5 to 0.2 μg for iodobenzoic acid. At low loading, spots were elongated in shape, making comparison difficult. The reaction was repeated, using standard spots to try to quantify the reaction turnover, which was estimated at no less than 95% (Table 3-8, Entry 7). The procedure was repeated using 2,2,2-trichloroethanol (TCE) instead of TFE (Table 3-8, Entry 8), which proved slower to react, presumably due to its lower volatility and therefore lower concentration in the reaction flask.

The reaction was repeated, using both sandstone and sand as supports (Table 3-8, Entry 9). After 18 h, both samples showed greater than 95% turnover, although the sample supported on sand contained more of the other product.

Entry	Acid	Alcohol	Support#	Reaction time (h)	Amount acid remaining (%)	Other spot* (%)
1a	MBA	TFE	SST	70	nd	none
1b			mont		nd	none
2a	MBA	TFE	SST	1	nq	*ca.* 50%
2b			mont		nd	none
3a	MBA	TFE	SST	2	nq	*ca.* 20%
3b	Iodobenzoic				nd	nd
3c	Cinnamic				nd	nd
4	MBA	TFE	SST	16.5	nd	nd
5	MBA	TFE	SST	4	nd	trace
6	MBA	TFE	SST	7	nd	nd
7	MBA	TFE	SST	4	<5	nq
8a	MBA	TCE	SST	3	25-50	*ca.* 20-30
8b				6	5-10	nq
8c				65	nd	nd
9a	MBA	TCE	SST	18	<5	nq
9b			sand		<5	nq, (more than 9a)

Table 3-8: Reactions carried out with acids to give esters

* estimated by comparison of spot density (no standard is available for the other spot)
nq: Not detected nq: Spot seen, but not quantified TLC using both DCM and EtOAc in all cases
#: SST = sandstone; mont = montmorillonite

Standard	Reagent	TLC eluent	Rf standard	Rf product
MBA	DIC/Py/TFE	DCM	Baseline	0.57
MBA	DIC/Py/TFE	Ethyl acetate	0.50	0.67
MBA	DIC/Py	DCM	Baseline	0.23
MBA	DIC/Py	Ethyl acetate	0.50	0.58

Table 3-9: TLC conditions used for following reactions of acids

Ketones, aldehydes and quinones

Standards representative of this group of carbonyl-containing compounds were supported on crushed sandstone and exposed to hydrazine hydrate, using Procedure B2, in order to form the respective hydrazone (reactions are summarised in Table 3-10).

Acetophenone and benzaldehyde gave complete reaction after 2 h (Table 3-10, Entry 1). Benzophenone reacted more slowly (some remaining after 4 h, but complete after overnight, Table 3-10, Entry 2), whereas anthraquinone showed no reaction after 22 h (Table 3-10, Entry 2). Anthraquinone also failed to react when acid catalysts (either acetic acid, or boron trifluoride etherate) were placed in the reaction flask. Subsequent reactions used only aldehydes and ketones, and quinones were not evaluated further. Although TLC (run in both DCM and ethyl acetate) gave good-shaped spots for the staring materials (which ran close together in both systems), no product spot was seen, even when no residual standard could be seen. The product hydrazone had not been extracted from the crushed sandstone using the standard method (see section 3.9.4), (*i.e.* extraction from the sandstone with DCM) . The method was modified, replacing DCM with ethyl acetate, in which the product hydrazone was soluble. The limit of detection of remaining aldehyde or ketone was less than 5%.

Entry	Compound	Reaction time (h)	Amount remaining (%)
1a	Acetophenone	4	nd
1b	Benzaldehyde		nd
1c	Anthraquinone		*ca.* 100
1d	Benzophenone		nq
2a	Acetophenone	22	nd
2b	Benzaldehyde		nd
2c	Anthraquinone		*ca.* 100
2d	Benzophenone		nd

Table 3-10: Reactions carried out between carbonyl compounds and hydrazine hydrate

Standard	Reagent	TLC eluent	Rf standard	Rf product
Acetophenone	Hydrazine hydrate	DCM	0.32	Baseline
Acetophenone	Hydrazine hydrate	Ethyl acetate	0.67	0.35
Benzaldehyde	Hydrazine hydrate	Ethyl acetate	0.64	0.43
Benzophenone	Hydrazine hydrate	Ethyl acetate	0.69	0.61

Table 3-11: TLC conditions used for following reactions of ketones and aldehydes

Tags can be introduced by reacting the hydrazone (produced from the carbonyl compound and hydrazine hydrate) with an anhydride, as for alcohols and phenols. Acetophenone and benzaldehyde were exposed to hydrazine hydrate (a TLC check showed >95% reaction), then, after purging the reaction flask with nitrogen for 30 min, the products of the reaction with hydrazine were treated with TFAA (Table 3-12 Entry 1). TLC showed new products had formed, a more polar TLC system, (EtOAc:MeOH:AcOH 20:1:0.2), being needed to get a good spot shape.

The reaction could not be quantified as no standards of the intermediate hydrazone were available, but residual hydrazone could not be detected. The reaction was repeated using benzophenone, with similar results (Table 3-12 Entry 2), although TLC showed a small quantity of unreacted hydrazone was possibly present. The reactions of benzaldehyde and benzophenone were repeated (Table 3-12, Entries 3 and 4) being the least and most reactive standards used, comparing the reaction on crushed sandstone with that on sand, with a slower reaction seen for the standard when deposited on sand, as found for reactions of carboxylic acids. After exposure of the intermediate hydrazones to TFAA for 2 h, although the amount of intermediate remaining could not be quantified, TLC showed only traces remaining indicating reaction was essentially complete.

Finally, using DCAA instead of TFAA gave the corresponding dichloroacetate (Table 3-12 Entry 5). TLC analysis of the products formed from both benzaldehyde and benzophenone showed no intermediate hydrazone remained after exposure to DCAA for 18 h

Entry	Compound	Support#	Reaction time (h) hydrazine	Amount standard remaining (%)	Second reagent	Reaction time (h) anhydride	Amount hydrazone remaining
1a	Acetophenone	SST	1	<5	TFAA	2	nd
1b	Benzaldehyde	SST	1	<5		2	nd
2	Benzophenone	SST	17.5	2.5	TFAA	3.5	nq
3a	Benzaldehyde	SST	2	<5	TFAA	2	nq
3b		sand		<5			nq
4a	Benzophenone	SST	18	5-10	TFAA	2	nq
4b		sand		ca 50	Not taken further due to incomplete reaction on sand		
5a	Benzaldehyde	SST	2	<5	DCAA	18	nq
5b		sand		<5			nq
5c	Benzophenone	SST	18	5-10			nq

Table 3-12: Reactions carried out between hydrazones and anhydrides

#: SST = sandstone; mont = montmorillonite

Standard used to form hydrazone	Reagent	TLC eluent	Rf standard	Rf intermediate	Rf product
Benzaldehyde	TFAA	DCM:EtOAc 1:1	0.78	0.39	0.48
Benzophenone			0.79	0.65	0.47
Benzaldehyde	DCAA		0.78	0.39	*ca.* 0.55
Benzophenone			0.79	0.65	0.62

Table 3-13: TLC conditions used for following reactions of hydrazones with anhydrides

Amino acids

Tryptophan was used in this study, as it is easily visualised by TLC (no better TLC system was found than the commonly-used n-BuOH:AcOH:water, 4:1:1). Exposure

of a sample of tryptophan, supported on crushed sandstone, to TFAA alone showed little reaction, but if pre-treated with triethylamine, a reaction was seen to occur. No further change was seen on exposure to TFE, indicating that an intermediate mixed anhydride had probably not been formed. The reaction product was extracted with water, to determine the amount or amino acid unreacted (<5% was seen), and with acetonitrile, to remove reaction products (this latter solvent gave the better extraction than water or ethyl acetate).

Entry	Compound	Reaction time (Et_3N)	Reaction time (TFAA)	Amount remaining
1	Tryptophan	1 h	2 h	<5%

Table 3-14: Reaction carried out between an amino acids and TFAA

Standard	TLC eluent	Rf standard	Rf product
Tryptophan	n-BuOH:AcOH:water 4:1:1	ca 0.6	ca 0.85

Table 3-15: TLC conditions developed for following reactions of amino acids with TFAA

Variation in reaction rate with support

The reaction rate was found to vary with the nature of the inorganic support used. The majority of reactions were carried out using crushed sandstone as support. When this was replaced with sand, reactions were found to be slower. Although the sand grains are mineralogically similar to sandstone, they were typically larger than those of crushed sandstone, and likely to be less porous. The larger, less porous grains will therefore have a lower specific surface area, and so the deposited standard will form a thicker layer, which is likely to be the reason for its slower reaction. In contrast, reactions of standards supported on montmorillonite were faster.

3.9.6. Conclusions and summary

Reaction conditions have been defined for the classes of oxygen-containing organic compounds, listed in Table 3-16. Reaction times were found to vary with other substituents as expected, but the conditions listed are all good starting points for investigation of the reactions of actual meteoritic organic materials.

The use of standard compounds deposited on inorganic supports successfully enabled the definition of reaction conditions, as reaction products could be extracted from the support, and analysed by TLC to show reaction had occurred. The non- uniform deposition of standards on these supports made *in situ* detection difficult, as only if a (small) region containing product was examined (by either Raman or SEM) would a product be seen.

Functional group	Final reaction product	TLC eluent	Reaction conditions	Modifications for chlorine reagents
Alcohol and phenol	Ester	DCM and EtOAc	Pyridine for 2 h, N_2 purge (1 h) then TFAA for 3 h	DCAA, reaction was extended to 22 h
Ketone	Acylated hydrazone	EtOAc:MeOH:AcOH 20:1:0.2 and DCM:EtOAc, 1:1	Hydrazine overnight, then TFAA for 3½ h.	DCAA, reaction was extended to 18 h
Aldehyde			Hydrazine for 2 h, then TFAA 2 h	
Carboxylic acid	Ester	EtOAC:MeOH 20:1	DIC/Py and TFE complete after 4 h	With TCE, 80-90% after 6 h, but 100% after 65 h.
Amino acid	Oxazolidinone	BuOH:AcOH:H_2O 4:1:1.	TEA for 1 hr, N_2 purge (30 min) TFAA for 1 h	No chlorine analogue investigated

Table 3-16: Summary of reaction conditions developed for tagging

3.10. Activation of IOM before Tagging

IOM, being insoluble and involatile, may well prove unreactive to the tagging reagents described in the previous section. Based on the current understanding of its structure, (see section 1.4.3) reaction with ozone is likely to result in the generation of oxygen-containing functional groups within the structure of IOM, leading to an increase in its reactivity towards the tagging reagents developed, and enabling it to be tagged using the same chemistry as that suitable for soluble organic compounds. This section describes the development of this activation procedure.

The bulk of the organic material in carbonaceous meteorites, IOM, is believed to consist largely of small aromatic rings systems, linked by branched aliphatic chains. Double bonds and aromatic ring systems, such as those expected to form the bulk of the structure of IOM (Kwok, 2004; Derenne and Robert, 2010) would be expected to react with ozone (Bailey, 1958), to give a variety of oxygen-containing derivatives, such as aldehydes, ketones or carboxylic acids. The tagging chemistry described earlier is designed for such functionality, and so will also be applicable ozone-treated IOM. IOM will probably already contain these functional groups, but ozone treatment should increase their density within the structure, allowing a larger number of tags to be attached (thus making detection easier). The use of gaseous, reactive ozone conforms to the constraints imposed on tagging chemistry described in section 1.7.2, and can also be carried out using the same set of apparatus as developed for that purpose (section 3.5), Procedure B1 being used for all experiments (the apparatus is shown in Figure 3-2B).

3.10.1. Precedents for the Use of Ozone

Chattanooga shale (a Devonian shale, located in Tennessee, from which natural gas is extracted) also contains uranium minerals, the extraction of which is made more difficult by the organic component of the shale cementing the mineral grains together. In an attempt to separate these grains (Kinney and Leonard, 1961), the shale was exposed to ozone gas (no solvent was used) resulting in a partial decomposition of the organic material into lower molecular weight, soluble carboxylic acids. Isolation of the organic material (by demineralisation) followed by treatment with ozone in solution gave a similar result. A similar study has been carried out using meteoritic organic material (again in solution) (Bitz and Nagy, 1967), indicating that the intended procedure, (treatment of meteoritic organic material with ozone in the absence of solvent) is likely to lead to a reaction with IOM, introducing oxygen-containing functionality.

Many reactions of materials in the solid state with gaseous ozone have been reported. Aflatoxin, a toxic compound found in many foodstuffs, and with a structure similar to that proposed for components making up IOM, can be destroyed *in situ* by treatment with gaseous ozone (Inan *et al.*, 2007). The green colouration present in cardamom seeds can be bleached using ozone, the process being accelerated by passing the ozone stream through water (Astrack and Schoenfeld, 1983). In both these examples, there was no work-up, nor decomposition of reactive intermediates. Ozone has also been used as a reagent in the gas phase in chemical synthesis (Winterhalter *et al.*, 2009), to oxidise the double bonds in the terpenoid, β-caryo-phyllene, but in that case, formic acid was used to decompose the reactive ozonide intermediate(s). It has also been used in the elucidation of the structures of complex

biopolymers such as synthetic rubber, (Barnard, 1956), and sporopollenin, a carotenoid polymer (Domínguez *et al.*, 1999), but in both those examples, the reaction was carried out in solution. Taken together, these examples demonstrate sufficient precedent for ozone being potentially useful for reactions of the macromolecular IOM, without need for solvent or further processing of any reactive intermediates.

3.10.2. Ozone Chemistry Background

The reactions of ozone with organic compounds are well-documented in the literature, and are a well-proven technique for use in organic synthesis. Carbon-carbon double bonds react with ozone to give an intermediate trioxolane known as a molozonide, which is not usually isolated, but is rapidly converted into more-stable cyclic peroxide (Criegee, 1975), (Scheme 3-8).

The final products of the reaction depend on the conditions used to decompose this intermediate molozonide, but can result in either the addition of oxygen to form an epoxide, or the cleavage of the double bond to give carbonyl-containing functional groups, (Scheme 3-9).

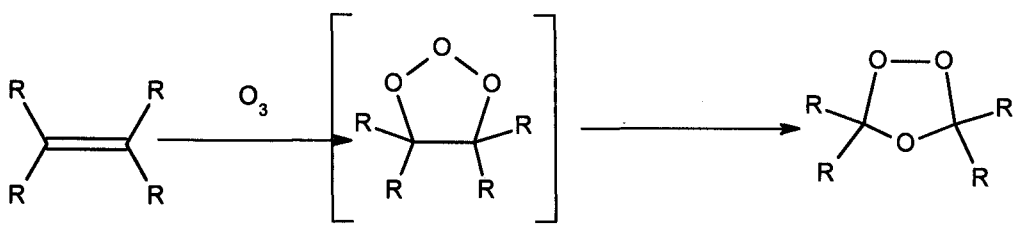

Scheme 3-8: Reaction of ozone with double bonds

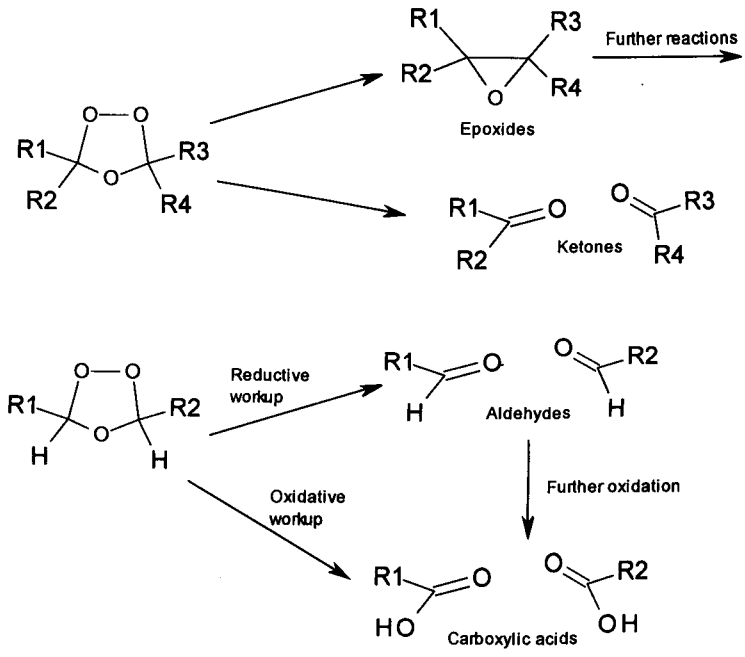

Scheme 3-9: Decomposition pathways for intermediates formed by ozone treatment

IOM is expected to contain a wide range of reactive centres, and so the results of this reaction are impossible to predict specifically. For example, an electron-rich ring system such as furan will be rapidly cleaved, but electron-poor rings, such as pyridine may be unreactive. Polycyclic hydrocarbons will react at the most "double-bond like" regions (Bailey, 1958). Assuming the structure of IOM as shown in Figure 1-3, then the resulting product will be a network of oxygenated functional groups, linked by the original branched aliphatic groups present. The exact nature of these final products is not important, as it is intended to develop conditions for tagging any or all of these oxygen-containing functional groups, and then to use which ever tagging procedure leads to a successful visualisation procedure.

3.10.3. Use of Standards as Models for IOM

As discussed in section 3.4; meteorite samples are in limited supply, and to avoid wastage, terrestrial models were used in the development of an activation procedure.

As models for the complex network of aromatic systems making up IOM, a number of polycyclic aromatic hydrocarbons (PAHs) were selected to study the introduction of oxygen-containing functionality by reaction with ozone. The aromatic systems in IOM are believed to be relatively small, consisting of up to about four rings joined together in various ways. A set of compounds containing a small number of rings was chosen on the basis of commercial availability and lack of toxicity, and is shown in Figure 3-27.

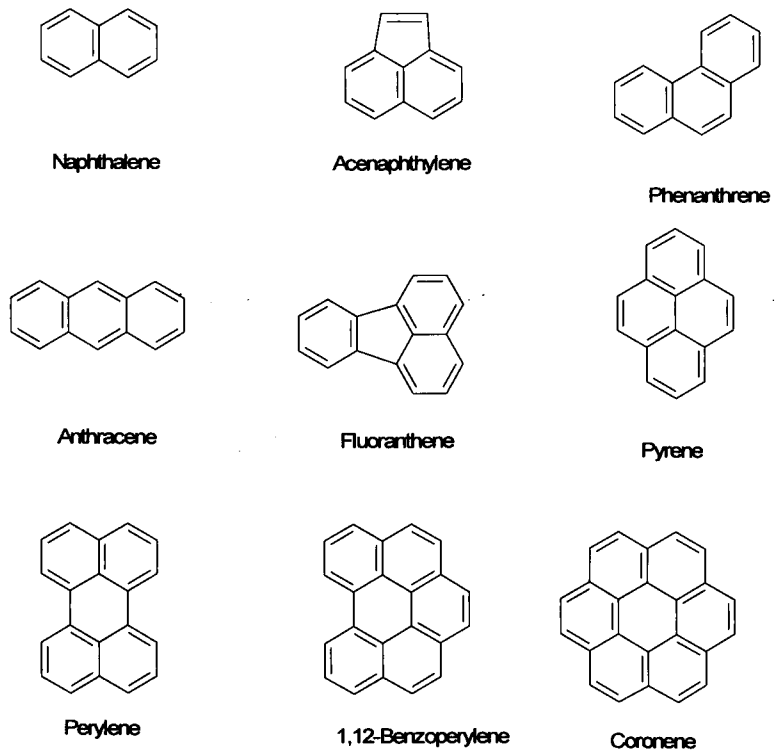

Figure 3-27: Structures of PAHs used as models for IOM

3.10.4. Use of Inorganic Supports

Using a similar methodology to that described for the development of tagging reactions (in section 3.9.4), the standards described above were deposited on

inorganic materials, as a model for IOM in carbonaceous chondrites, where it forms a coating on mineral grains. Three types of support were evaluated:

- on plastic or aluminium TLC plates coated with silica gel
- on glass plates
- on crushed rock samples, or minerals

and are discussed in turn.

3.10.5. Practical Methodology and Details

Hazards of ozone and its reaction products

Ozone is a toxic gas, causing irritation to the airways if inhaled. Reactions generating and using ozone must therefore always be carried out in a fume cupboard, and excess ozone decomposed before release of off-gases to the atmosphere.

The epoxide- or peroxide-containing intermediates formed in reactions with ozone are unstable, and may decompose with some violence (Van Ornum *et al.*, 2006), and so reactions involving this methodology must be carried out with care. Typically, in synthetic chemistry, the reactive intermediates are formed at low temperatures, and decomposed under controlled conditions to give the desired reaction product. In this project however, as the sample of meteorite or analogue is so small (<1 mg, containing, at most, a few per cent organic material), the amount of heat generated by decomposition of the intermediate would be so small as not to pose any hazard.

Generation of ozone

Ozone is generated by exposing oxygen to a high voltage. It is better to use oxygen rather than air, to avoid the formation of oxides of nitrogen.

In all these experiments, ozone was generated by passing a stream of oxygen through a Fischer 502 ozoniser, at a rate of about 50 L/h (as monitored by a flow gauge), using a pressure of about 1 bar, and a current of 1-1.5 A, which is sufficient to generate ozone at a suitable concentration. This device contains a series of high-voltage discharge tubes; as oxygen molecules pass through these tubes they are decomposed to oxygen atoms, which then react with unatomised molecules to give ozone, as shown in Equation 3-1.

$$O_2 \rightarrow 2O \quad O_2 + O \rightarrow O_3$$ **Equation 3-1: Formation of ozone**

Ozone concentration was not measured, but using the calibration provided with the apparatus (for the flow rate of oxygen used) the concentration of ozone in the output stream was approximately 90 g/m^3. The effect of water vapour on the reactivity of ozone has been discussed previously (in section 3.10.2).. In some reactions the ozone was moistened by passing through a bubbler containing purified water; if dry ozone was to be used, the water bubbler was disconnected. Ozone is only slightly soluble in water (of the order of 1 mg/L) but it readily decomposes in solution, so a true solubility cannot be measured. When a water-filled bubbler was used to generate wet ozone, an anti-suck-back trap was placed between the bubbler and the ozoniser, to prevent any possibility of water entering the ozoniser.

Apparatus used for exposure of samples to ozone

The apparatus used for exposing samples to ozone was the same as that used for the development of tagging, where vapours are generated and passed into the reaction flask (Procedure B1, described in section 3.5.2). Ozone was passed into the reaction flask, from the generator, using one of the connections shown in Figure 3-2B.

The gas flow out of the reaction flask was passed *via* an anti-suck-back trap into a scrubber containing aqueous potassium iodide/starch solution. Ozone oxidises iodide to iodine, which reacts with starch to give a strong blue-black colour. Paper impregnated with a mixture of starch and potassium iodide is commonly used as a test for oxidising agents. The absence of any ozone being released to the atmosphere was confirmed by holding a piece of wet starch-iodide paper by the outlet (no black colour developed). In contrast, the presence of ozone in the flask at the end of the experiment could be confirmed using starch-iodide paper, which in every case gave a positive reaction.

The sample was placed in the flask, all valves opened, and the oxygen flow adjusted to 50 L/h. The ozoniser current was increased to *ca.* 1A, and oxygen allowed to flow to through the system until the starch indicator registered the presence of ozone at the outlet. Flow was continued for 10 minutes, after which time the oxygen cylinder was closed, the ozoniser was switched off, and the reaction vessel sealed. The half-life of ozone at room temperature is about 12 h, so unless the sample catalysed decomposition in some way, a large enough concentration of ozone was expected to remain in the reaction flask during the experiment.

3.10.6. Experimental Procedures

Solutions of the PAHs shown in Figure 3-27 were prepared by dissolving each in a suitable solvent. Solutions were prepared in concentrations of 10 mg/mL in DCM, except for coronene, for which the solubility was lower, and only 2.5 mg/mL could be achieved. The extent of reaction was monitored by TLC. For each PAH, TLC plates were prepared containing spots with loadings ranging from 20 to 0.5 μg, which were developed, then examined under UV, to determine the smallest loading

that was clearly visible. With an initial spot size of 10 μg, the smallest proportion of starting material for each compound is listed in Table 3-17.

Compound	Smallest loading detectable (%)
Acenaphthylene	2-5
Anthracene	<1
1,12-Benzoperylene	<<1
Coronene	1-2
Fluoranthene	<<1
Naphthalene	<5
Perylene	1-2
Phenanthrene	<<1
Pyrene	<1

Table 3-17: Minimum loading of PAHs detectable by TLC (expressed as fraction of material initially present)

Reactions on TLC plates

The use of TLC plates to support samples of standard compounds for use in tagging development was described in section 3.8. A similar methodology was used to study the reactions of PAHs with ozone.

Samples of PAHs (10 μg) were applied to silica TLC plates, which were then placed in the reaction flask, and exposed to ozone. After developing, and examination under UV, no change was seen with perylene, even after 70 h, whereas unreacted pyrene and phenanthrene could no longer be seen after only 5 min.

The experiment was extended to the whole set of PAHs. Spots of 10 μg of each (in solution) were applied to silica TLC plates, and exposed to ozone for 1 h. Reactions were repeated with various reaction times to determine the time needed to give complete reaction, experimental data is shown in Table 3-18.

Compound	Amount remaining after 1h (%)	Time taken for complete reaction
Acenaphthylene	<5	20 min
Anthracene	≥10	100 h
1,12-Benzoperylene	*ca.* 10	>140 h
Coronene	≥10	>140 h
Fluoranthene	<1	10 min
Naphthalene	<5	10 min
Perylene	≥10	>140 h
Phenanthrene	<<1	10 min
Pyrene	<1	10 min

Table 3-18: Times taken for reaction of PAHs with ozone

In the development of tagging reactions, it was found that reactions of standards deposited on TLC plates were not a good model for similar reactions of organic materials in carbonaceous chondrites. For that reason, the methodology described in the preceding section was not investigated further, with other inorganic supports being investigated. However, TLC was used as an analytical method, as described in section 3.9.4.

These results show a general reduction in reaction rate with increasing ring size, but as it is the smaller ring systems (containing up to four benzene rings) which are understood to make up the bulk of IOM (Derenne and Robert, 2010), the slow reactions of larger ring systems were not regarded as a drawback. Pyrene was selected as a target molecule for future experiments, as it has a ring size similar to that believed present in IOM, and, with a low limit of detection, reactions can be monitored easily.

Reactions on glass plates

A single reaction using a few crystals of pyrene had shown no reaction by TLC, even after 70 h. To give a large surface area of PAH under test, solutions of pyrene were applied to clean watch glasses and allowed to evaporate, giving a film of solid. Typically about 1 mg solid was deposited in a circle of about 1 cm radius.

Pyrene is a crystalline solid, but IOM forms an amorphous, non-crystalline structure. To better model this physical form, mixtures of pyrene and hydrocarbons were prepared (1:1 pyrene: hydrocarbon) and applied to watch glasses. The hydrocarbons were chosen to be inert (*i.e.* unreactive towards ozone), and solid (eicosane), waxy (heptadecane) or liquid (dodecane) at room temperature. On exposure to ozone, although some of the samples became discoloured, only very small amounts of reaction were seen. The results are summarised in Table 3-19 which show that over the reaction times studied, the physical form of pyrene films on glass seem to have little effect on reactivity.

Entry	Additive	Reaction time (h)	Degree of reaction (% by TLC)
1	None	1	<20
2	Eicosane	1	*ca.* 20
3	Heptadecane	4	*ca.* 40
4	Dodecane	4	*ca.* 20, new spot appeared

Table 3-19: Extent of reactions of pyrene deposited on glass with ozone in the presence of hydrocarbons

Reactions on crushed rock

The use of terrestrial rocks and minerals as substrate supports had proved suitable for the development of tagging methodology. As surface area is proportionately greater for small particles (as particles are divided, so new surfaces are exposed), deposition of substrates onto crushed rock samples allows the exposure of larger surface areas to

reagents, with a likely increase in reaction rates. Solutions of samples under test were therefore applied to crushed sandstone, to give a loading of organic material comparable to that found in carbonaceous chondrites. Following exposure of these samples to the appropriate reagent, the products were dissolved, and analysed by TLC. This methodology was used to study the effect of ozone on pyrene.

A series of experiments was performed, depositing pyrene, with or without added hydrocarbon on crushed sandstone, either small grains (powder, *ca.* 100 μm in size) or as chips measuring about 2 mm. The results of these reactions are summarised in Table 3-20.

When supported on chips, the degree of reaction was similar to that on glass, even with extended reaction times (Table 3-20, Entry 1). It is possible that only the pyrene on the surface of the chip reacted with ozone, and that pyrene deposited inside the sandstone pores did not. The remaining experiments were therefore carried out using crushed sandstone rather than chips. When in the solid state (alone, or with eicosane), the reaction was slower than when present with a liquid or wax (Table 3-20, Entry 2) but reaction was not complete after 6 h, although only about 10% remained after 24 h (in the presence of heptadecane, Table 3-20, Entry 3).

Passing ozone through a water bubbler is known to accelerate its reactions with organic compounds (Astrack and Schoenfeld, 1983). This effect was observed when pyrene, in the presence of hydrocarbons or alone (Table 3-20, Entry 4), was exposed to moist ozone; a complete reaction was seen after 24 h in all cases. When reacted for only 4 h (Table 3-20, Entry 5) the effects of the hydrocarbon additives were apparent; pyrene mixed with heptadecane gave the greatest degree of reaction.

Increasing the reaction time to 16 h (Table 3-20, Entry 6) gave greater than 95% reaction in all cases, with no pyrene being detected in the presence of heptadecane (Table 3-20, Entry 6c).

Entry	Support	Additive	Water bubbler	Reaction time (h)	Degree of reaction (% by TLC).
1a	chips	None	N	1	*ca.* 30
1b	chips	None	N	4	*ca.* 30
1c	chips	none	N	16	*ca.* 30
2a	powder	None	N	6	0
2b	powder	Eicosane			*ca.* 25
2c	powder	Heptadecane			80
2d	powder	Dodecane			*ca.* 50
3a	powder	Heptadecane	N	24	90
3b	powder	Dodecane			30
4a	powder	None	Y	24	>95
4b	powder	Eicosane			>95
4c	powder	Heptadecane			>95
4d	powder	Dodecane			>95
5a	powder	None	Y	4	*ca.* 90
5b	powder	Eicosane			90-95
5c	powder	Heptadecane			>95
5d	powder	Dodecane			*ca.* 90
6a	powder	None	Y	16	>95
6b	powder	Eicosane			>95
6c	powder	Heptadecane			>>95
6d	powder	Dodecane			>95

Table 3-20: Summary of the results of the reactions of pyrene (on crushed sandstone) with ozone

Nature of the product of ozone treatment

When pyrene was treated with ozone, TLC showed disappearance of its spot, but no new spots appeared, apart from streaks near the baseline. The implication is that the structure was decomposed quite extensively, and that the fragments possess no

significant chromophore to allow visualisation by UV. These fragments were not characterised.

Such fragmentation should not prevent this methodology being used to convert IOM into a functionalised derivative. When IOM is subjected to ozone treatment, if the aromatic rings present are similarly fragmented, then the extensive branched aliphatic chains believed to link the aromatic rings will remain unreacted, and a complex network of oxygenated fragments should result, albeit mainly aliphatic rather than aromatic in character. This will still undergo the tagging reactions described in this chapter.

3.11. The Development of Tagging Methodology: Conclusions

A set of chemical methods has been developed, using pure chemical standards as models for the organic compounds present in carbonaceous chondrites, which enable several functional groups to be molecularly tagged. Using this chemistry it should be possible to attach these tags to the respective functional groups present in the actual compounds contained in carbonaceous chondrites.

The chemistry developed was successfully demonstrated using standards present on inorganic supports in the solid state. This chemistry satisfies the constraints outlined in section 1.7.2 to ensure organic materials are not mobilised within the meteorite.

Reaction conditions have also been developed under which the aromatic ring systems (up to four rings in size), believed to be the main component of the molecular framework making up IOM, will react with ozone to give oxygenated derivatives. These derivatives can then be tagged using the chemistry developed should IOM itself prove unreactive.

The use of terrestrial systems as models of carbonaceous chondrites proved partly-successful. Although these model materials were successfully used to support standards for reaction in the solid state, their physical form did not accurately model carbonaceous chondrites.

Organic materials in carbonaceous chondrites are present as coatings, covering the surface of mineral grains (El Amri *et al.*, 2005). Solutions of standards applied to model supports evaporated forming droplets which gave crystalline clumps of organic compound (as seen in SEM images), rather than thin films, and so it was not possible to use EDS or Raman spectroscopy to map the production of tagged standards on the supports. Demonstration of the effectiveness of these techniques would require preparation of tagged and/or activated samples of meteorite. These chemical treatments of meteorite samples are described in the next chapter.

Chapter 4 The Chemical Modification of Murchison

The methodology for both activation and tagging of meteorite samples was described in chapter 3. The aim of activation was to introduce more functionality into the structure of IOM, so that there were more sites available for tagging. As the functional groups acting as the targets for tagging were the same in both activated and unactivated samples, the same reaction conditions would serve to tag both. So that tagging could be carried out on both activated and unactivated samples simultaneously (and therefore directly compared), activation of samples of Murchison was investigated before the tagging of unactivated samples. The results of that work are described in this chapter.

4.1. Characterisation of Samples Before Treatment

Before beginning any chemical treatments, fragments of Murchison were examined using both Raman spectroscopy and SEM to provide a baseline against which possible changes caused by chemical treatments could be judged. Much work has already been carried out investigating the mineralogy of Murchison, (for example, as reviewed in Papike, 1998). Also, Raman spectroscopy has also been used to examine the organic materials present (Quirico *et al.*, 2005a; Busemann *et al.*, 2007), as described in section 2.1.1. The objective of the work described in this section was not to carry out a detailed mineralogical characterisation of the samples using Raman spectroscopy and SEM/EDS, but to evaluate these analytical methods for use in the detection of molecular tags *in situ*.

4.1.1. Samples

The constraints on sample preparation were discussed in section 1.7.2. During this part of the study, small chips of Murchison were used. These chips were not prepared in any way (such as coating, or mounting with epoxy resin), but simply placed on an aluminium stub and held in place on a carbon adhesive pad. These samples were transferred to the Raman microscope stage, and examined without prior removal from the stub.

4.1.2. SEM

The criteria for the selection of tagging elements and reagents were discussed in sections 3.2.3 and 3.3. Initial candidate elements were those that do not commonly occur in rock-forming minerals, and could conveniently be introduced *via* appropriate chemistry, such as chlorine, fluorine, or zinc. The resolution of the EDS detector is 130 eV, so the X-ray emission of candidate elements should ideally be separated by at least this amount from common elements, otherwise good resolution will be difficult. Element maps of the surface of Murchison fragments were generated using SEM/EDS as described in section 2.2.1 to show that any background signal due to these elements would be weak. As expected, the maps obtained were dominated by regions containing elements found in common rock-forming minerals, such as oxygen, silicon, iron and magnesium, often correlating well with distinct grains (Figure 4-1). A map highlighting elements potentially useful as tags (zinc, bromine, and chlorine) is shown in Figure 4-2, showing their signals to be very weak, and not concentrated in any grains. At this stage in the project, the minerals present in Murchison were not identified.

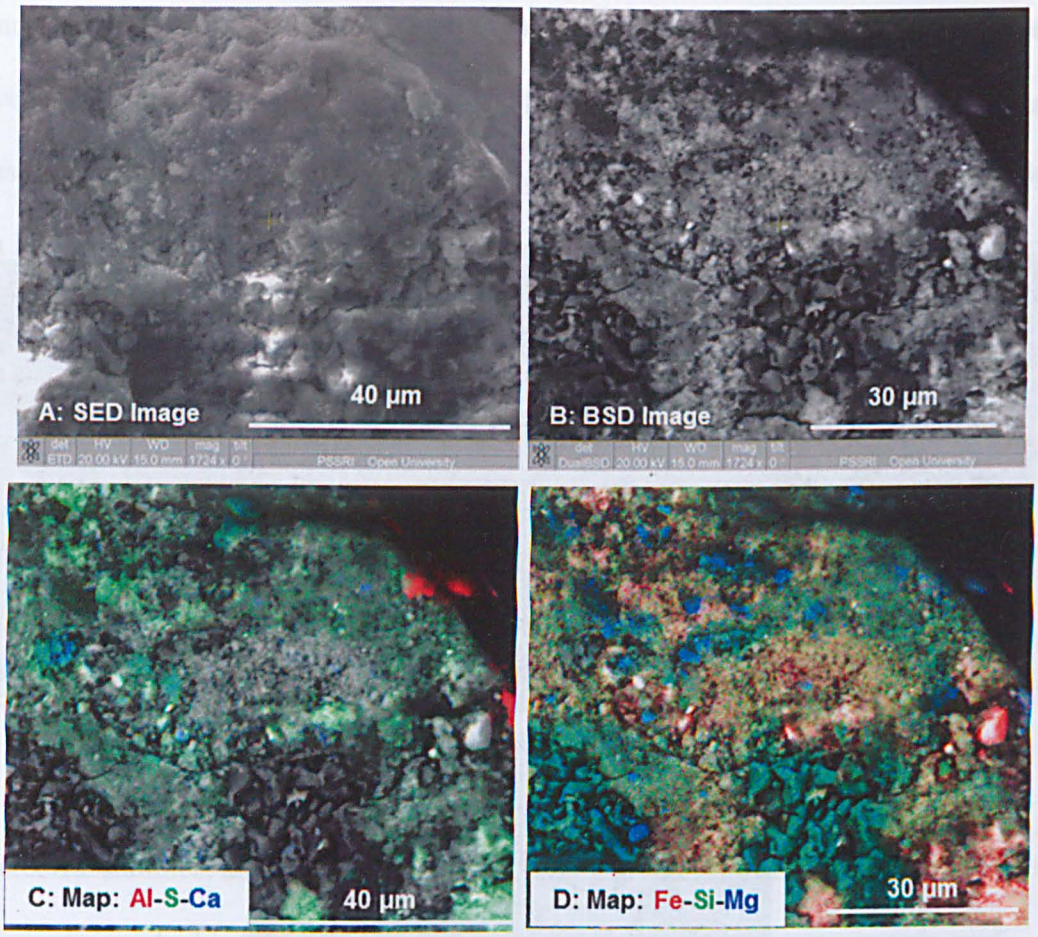

Figure 4-1: Electron images and element maps of a sample of Murchison showing common rock-forming elements

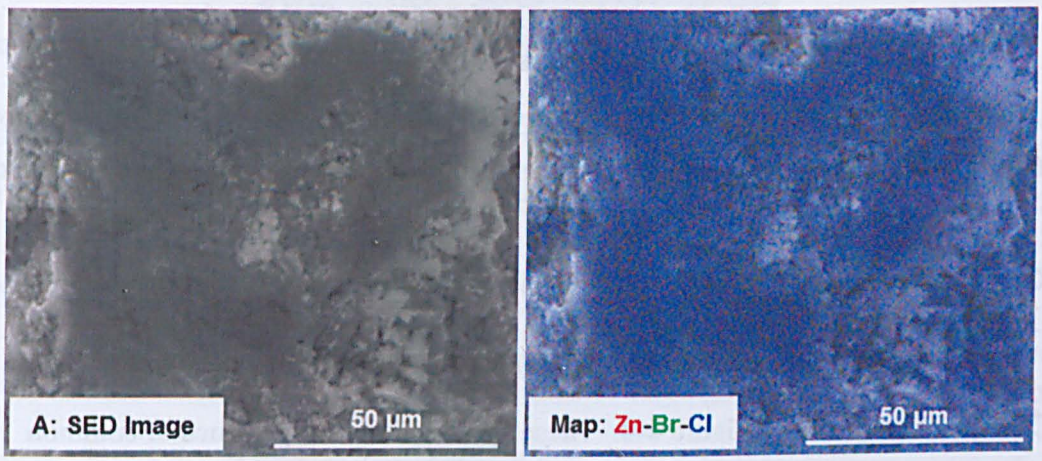

Figure 4-2: Image and map of potential tagging elements in a sample of Murchison showing low-level distribution throughout the sample

In most cases, carbon-rich regions were absent; its signal was very weak, and not correlated with any grains. In a few cases though, regions giving a strong signal were seen (such as that shown in Figure 4-3). In that example, the carbon signal

coincided with a region visible using SED and BSD where it appeared bright, and dark, respectively, most likely a carbon-rich mineral, such as a carbonate, also potentially an interference to the detection of organic compounds before tagging.

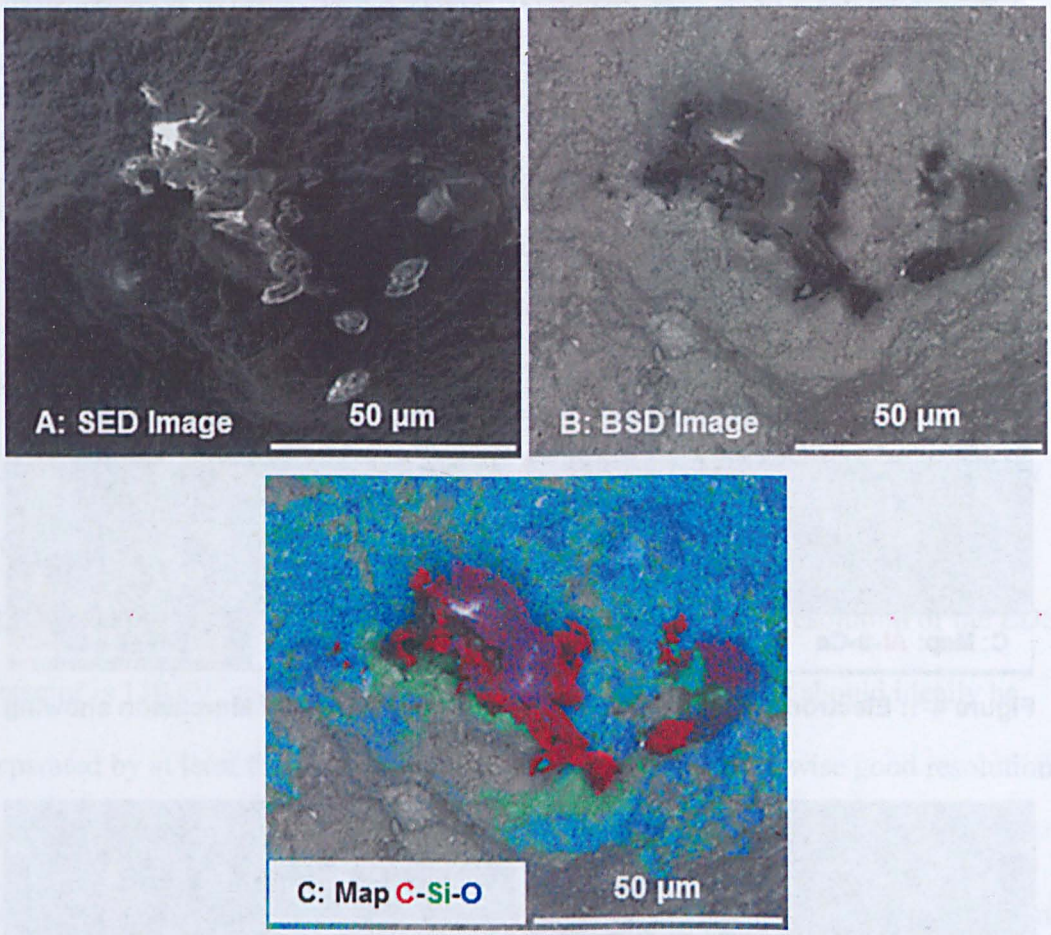

Figure 4-3: Electron images and element map of a carbon-rich portion of a sample of Murchison

X-ray spectra were obtained at various points on this sample, to confirm the presence or absence of individual elements in that specific grain, or region of interest. Examples are shown in Figure 4-4. These spectra show the presence of common elements, such as iron, oxygen, silicon and magnesium, but not elements proposed as potential tags (iodine, chlorine, or zinc). (The use of bromine was discontinued after it was found to cause disintegration of samples, as described in section 3.6.2.) Care must be taken in the use of these spectra however; many elements are poorly resolved, and occasionally the software will interpret a signal from one element for

another. One spectrum (shown in Figure 4-4D) shows this effect, where dysprosium (very unlikely to be present) has been identified. Its Lα line at 6.498 keV is not resolved from the Kα line of iron, at 6.409 keV. Nevertheless, the spectra (presented in Figure 4-4B-E) show that the minerals present in Figure 4-4C and D (containing iron, magnesium, silicon, oxygen and some sulfur) are the same. These are, however, different from those in Figure 4-4B (containing iron and sulfur) and Figure 4-4E (magnesium silicon and oxygen). It is important to remember that depending on the grain size, and the minerals present, these spectra may be due to a mixture of minerals rather than a single mineral (if the grains are smaller than the interaction volume).

In conclusion, EDS is confirmed as a suitable method for *in situ* analysis of tagged meteorite samples, and the detection of elements such as chlorine, or iodine. These elements, resolvable by X-ray spectra from common rock-forming minerals, and proposed as potential tags, are not seen in spot spectra, and appear only as low-level background in element maps. Bromine and zinc, detectable but difficult to resolve from aluminium, proved to be unsuitable as tags (as described in section 3.6.2), and investigation into their use was discontinued.

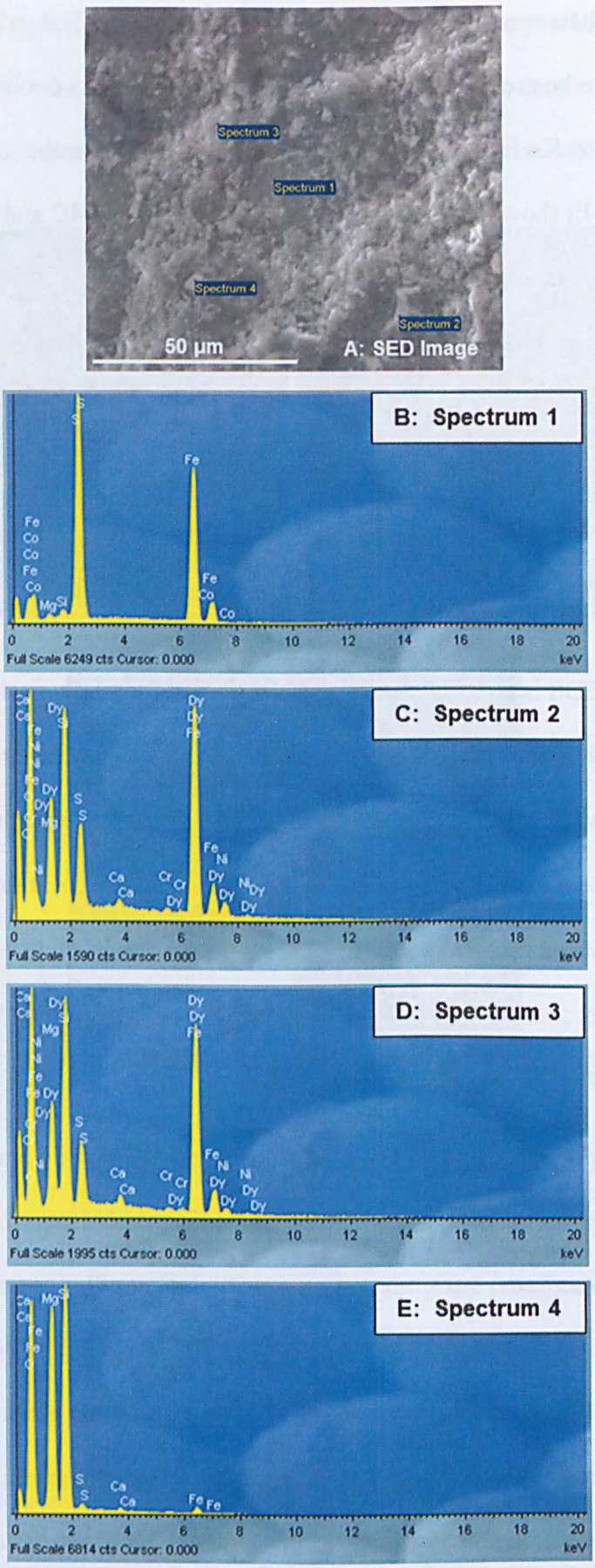

Figure 4-4: SED image and spot spectra obtained from a sample of Murchison showing absence of potential tagging elements

4.1.3. Raman Spectroscopy

Analysis of the surface of the fragment of Murchison using Raman Spectroscopy gave a rather different result from SEM. Whereas the latter showed signals due to elements present in common rock-forming minerals, and little evidence of regions rich in carbon, the Raman signal was dominated by that of aromatic carbon, consisting of the broad D and G peaks indicative of the widespread presence of substituted polyaromatic systems (see the discussion in section 2.1.1), as shown in Figure 4-5C.

Regions, such as that seen to the left of the image in Figure 4-5A, appearing bright and mineral-like in the Raman microscope image, gave simple spectra, such as that shown in Figure 4-5B, which is characteristic of forsterite (identified from library spectra, see Figure 4-6). (The microscope images shown in this section are of relatively flat regions, therefore reasonably well-focused and not needing to be stacked.) The majority of the surface of the fragments however, appeared dark and grainy (such as to the right-hand side of Figure 4-5A, with Raman spectra showing mainly the D and G peaks as shown in Figure 4-5C.

The presence of forsterite, being a major component of Murchison, is not unexpected, but as described by El Amri *et al.* (2005), the spectrum of this mineral is only seen in regions unassociated with organic Raman signals.

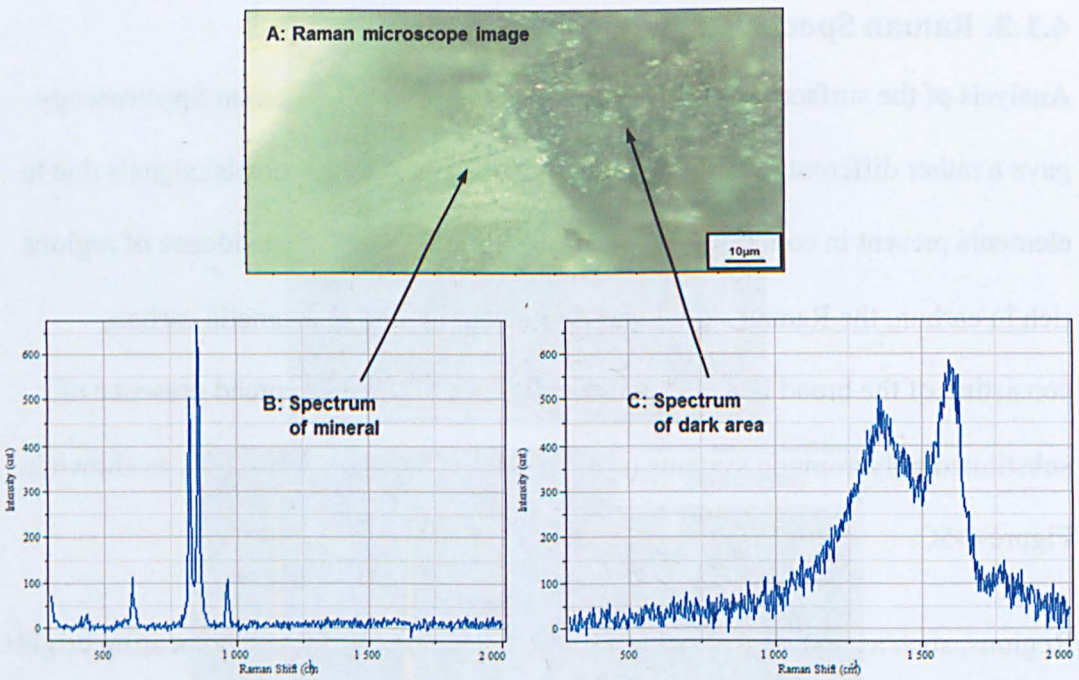

Figure 4-5: Image and spectra obtained from Murchison fragment showing localisation of forsterite and aromatic carbon compounds

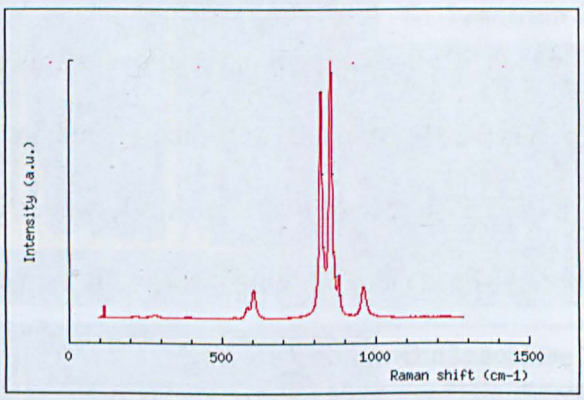

Figure 4-6: Library spectrum of forsterite (Handbook of Minerals Raman Spectra)

These differences in Raman spectra were used to construct maps of the surface composition, using the instrument software as described in section 2.1.1. The strength of signal due to either forsterite or aromatic carbon is represented by colour intensity (the lighter the colour, the higher the intensity), as plotted in the two maps (Figure 4-7B and C). The area covered by the map is defined by the box in the centre of the image of Figure 4-7A. This shows that Raman spectra can be used to locate regions containing organic compounds (at least those giving strong signals due to

aromatic rings) on the surface of a meteorite fragment, particularly when in close proximity to organic-free regions, where the contrast easily seen.

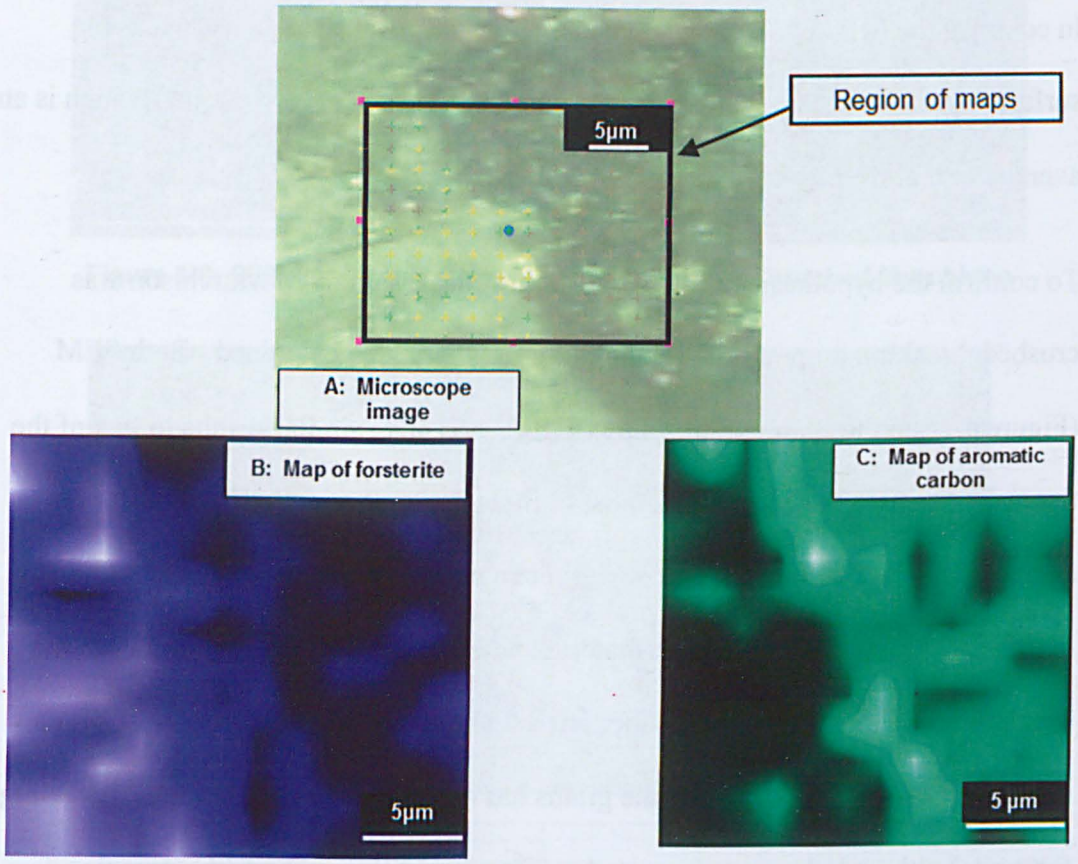

Figure 4-7: Raman microscope image and maps of fragment of Murchison (showing location of forsterite and aromatic carbon compounds)

4.1.4. Distribution of Organic Materials amongst Mineral Grains

El Amri *et al.* (2005) suggested that the mineral grains in the matrix of carbonaceous chondrites are coated with a thin organic coating, which, being black, and opaque is not penetrated by the Raman laser. Consequently, although only a minor proportion of the whole, its signal is dominant in the Raman spectrum.

This proposal is supported by the data presented above. Despite the carbon content of Murchison being only about 2% (Fuchs *et al.*, 1973), signals due to aromatic rings (the D and G peaks) dominate the Raman spectrum of the meteorite surface; the

mineral constituents (although by far the major component) are only seen when free from any organic covering.

In contrast, the SEM electron beam penetrates into the mineral grain, and as the surface layer is only thin, contributes little to the signal detected by EDS (which is an average of that of the whole interaction volume).

To confirm the hypothesis of El Amri *et al.,* (2005) a sample of Murchison was crushed, breaking it up into individual grains, which were examined. Both SEM (Figure 4-8) and Raman spectroscopy (Figure 4-9) gave similar results to that of the uncrushed sample, indicating that most of these grains (typically less than 10 μm in size) are coated with IOM. Most gave spectra similar to that shown in Figure 4-9B in green, indicating carbonaceous material, whereas a minority were similar to the blue spectrum, indicating mainly forsterite, thus supporting the conclusions of El Amri *et al.* (2005). Crushing the grains has created some new surfaces (revealing forsterite) although the organic-coated surfaces are still dominant (the organic material still being attached to forsterite fragments). When the grains were crushed even further, in an attempt to break them open rather than just disaggregate them, the small particles which resulted were smaller than the laser spot size, and so did not give Raman spectra. An SEM image with grain dimensions superimposed is shown in Figure 4-10.

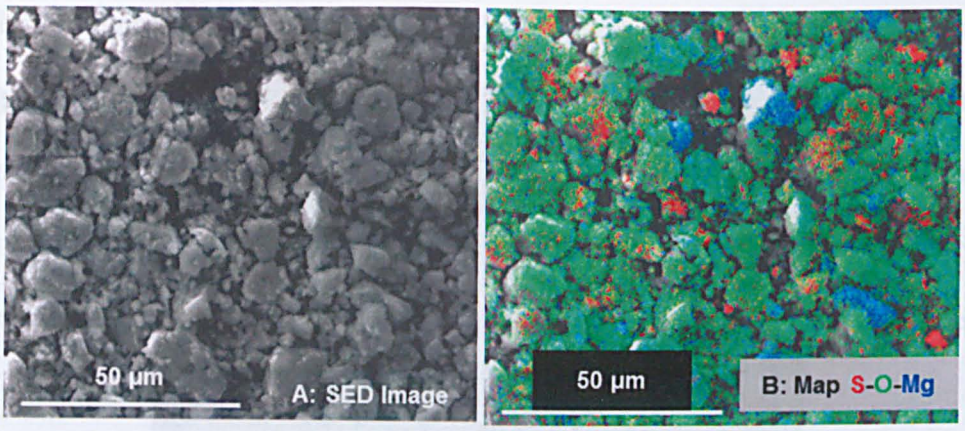

Figure 4-8: SEM image and element map of sample of crushed Murchison

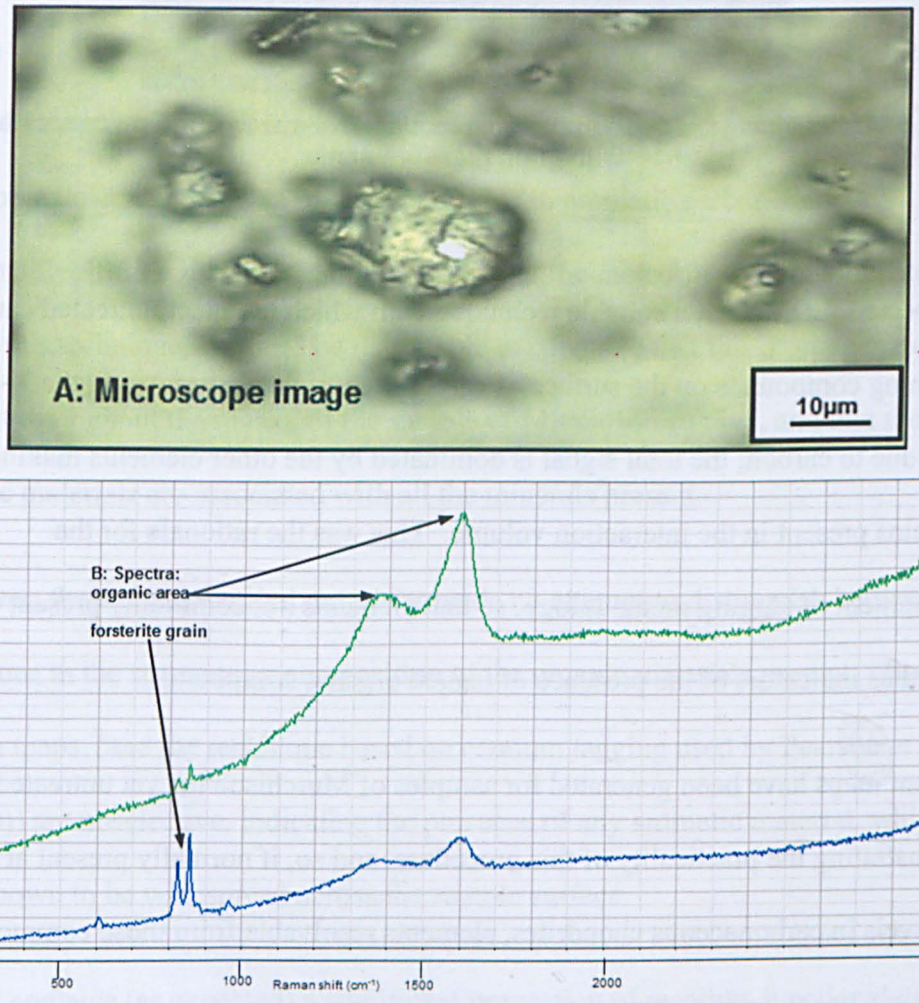

Figure 4-9: Image and Raman spectra acquired from the same sample

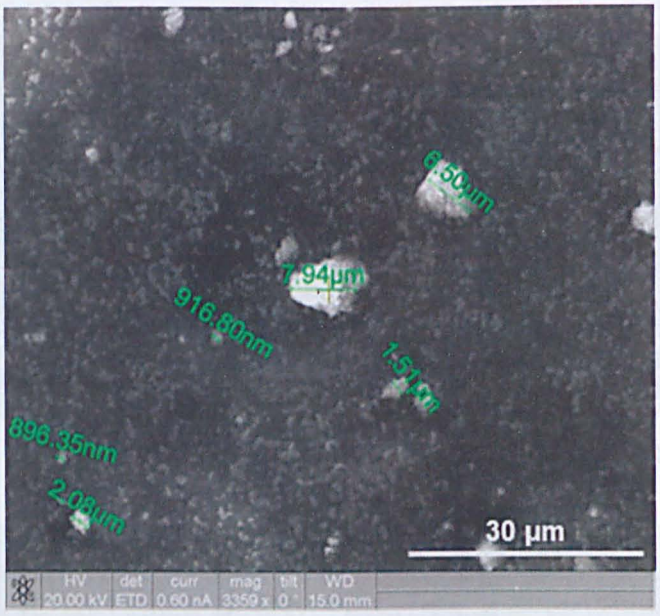

Figure 4-10: SEM image of the sample of Murchison following grinding annotated with with grain measurements

4.1.5. Conclusion

As expected, EDS is not a suitable technique with which to detect untreated carbon-containing compounds on the surface of carbonaceous chondrites, using the X-ray signal due to carbon; the total signal is dominated by the other elements making up the grains present in the interaction volume. This was the rationale for the development of tagging methodology, so that elements not commonly present could be used as indicators of the presence of tagged organic compounds.

Element maps have been generated for samples of Murchison (as yet untreated), demonstrating the practicality of this procedure, and so, if normally present at only low levels in carbonaceous chondrites, elements resolvable from those commonly occurring, are suitable as tags.

Raman spectroscopy has confirmed the earlier observation (El Amri *et al.*, 2005) that carbonaceous chondrites are (at least in part) composed of small mineral grains, coated with macromolecular organic material. Signals due to the underlying minerals are not seen, unless the coating is absent. These grains could, of course,

also be wholly carbonaceous, with no underlying mineral core; Raman spectroscopy, being unable to penetrate the opaque surface layer, cannot distinguish between these alternatives. In organic-rich areas of the sample, the broad peaks due to aromatic rings dominate the Raman spectrum; maps can be generated showing its intensity (as well as that of other components, such as forsterite), thus locating these materials within the meteorite sample.

The abundance of this organic signal has implications for the objective of the project, which is the detection of the distribution of organic materials with respect to co-located minerals. Data returned from Raman maps, unless mineral grains are free from organic coating, shows solely signals due to aromatic carbon, derived, presumably, from IOM, the major component of the meteoritic organic inventory. Using this technique, it would be reasonable to conclude that this organic material is present throughout the matrix of the sample of Murchison studied, and that therefore organic materials are associated with all the minerals present.

However, the analysis carried out so far made no attempt to distinguish between variations in the structure or composition of the organic materials present. Both the Raman maps, (and the technique based on osmium tagging used by Pearson *et al.* (2007b)) are unselective, indicating the presence of any aromatic material, which has been shown to be widespread across the sample surface.

If IOM contains (as expected) a significant proportion of reactive, functional groups, then, following tagging, differences in the organic structure across the surface of the sample may be revealed. Only by developing a tagging methodology which is selective for these functional groups (which is the objective of this project), will any

heterogeneity be revealed, allowing specific associations between minerals and organic materials (if present) to be revealed.

4.2. Exposure of Samples of Murchison to Ozone

Using pyrene as a model, conditions for the reaction of meteoritic organic materials with ozone were developed (see section 3.10), with the aim of derivatising the aromatic components of IOM (by introduction of oxygen-containing functional groups), and increasing the number of sites available for tagging. Although IOM may react somewhat differently from the model PAHs used, the conditions developed provide a valid starting point for this investigation. Based on the current understanding of the composition of IOM, the reaction is expected to lead to a modified IOM structure, consisting of oxygenated aromatic rings, linked together by branched aliphatic chains. These molecular changes would be expected to result in changes in Raman spectra as well as possibly visible changes to the meteorite structure if the physical structure of IOM is altered.

4.2.1. Samples and Procedure

Samples of Murchison (three chips, approximately 1 mm in each dimension) were either supported on aluminium stubs (on a carbon adhesive disc, as used in an SEM), or simply placed on a watch glass, then placed inside the reaction flask and exposed to ozone in the manner described in section 3.5.2 (Procedure B1). Ozone was bubbled through water prior to entering the reaction flask.

A control experiment, using aluminium stubs holding only carbon adhesive discs, or pieces of aluminium sticky tape showed no apparent changes (by SEM) on exposure to ozone, nor was ozone decomposed by contact with these materials (ozone was still present at the end of the experiment, detected by reaction with starch-iodide paper).

In section 3.10.6, the investigation of the effect of ozone on pyrene supported on sandstone was described. In those reactions, complete oxidation of pyrene was observed after 16 h. Reaction times for Murchison samples were chosen to bracket this value, to determine the appropriate exposure required for meteorite samples, rather than models. Reactions of up to 8 hours were carried out during a working day; for times greater than this, samples were left overnight, or for a number of days.

4.2.2. Effects of Exposure of Murchison Fragments to Ozone

In the first experiment, two small fragments of Murchison, previously characterised using SEM and Raman, and fixed to an SEM stub using an adhesive disc, were exposed to moist ozone for 3 h and 19.5 h (overnight) respectively, and then examined by SEM and Raman spectroscopy. Both samples were then returned to the reaction flask and exposed to moist ozone for a further overnight period (16.5 h), and re-analysed (giving total exposure times of 19.5 h and 36 h). The procedure was repeated for a third fragment, for two periods of 16 h. All samples were analysed using both Raman spectroscopy and microscopy, and SEM.

No fragmentation or other visible changes were apparent, using either the Raman microscope or the SEM, when Murchison fragments were exposed to ozone; by comparison of the samples with untreated Murchison chips, no changes in colour or appearance were seen.

Raman spectroscopy

The Raman spectrum showed no apparent change after 3 h (Figure 4-11A); the strong aromatic absorptions between 1200 and 1800 cm^{-1} (the D and G peaks) were still present, although varying in intensity across the surface. In the sample exposed for 19.5 h (Figure 4-11B), additional strong signals between 800 and 850 cm^{-1} were

also seen. These are evident in one spectrum (shown in Figure 4-11B, in green), and are due to forsterite. Such signals were seen in samples of untreated meteorite (section 4.1.3); their presence in this sample merely reflects the heterogeneity of the sample. Similar spectra were obtained for this sample after a total of 36.5 h exposure, except a new signal was seen, at 1010 cm^{-1}, as shown in Figure 4-12, Spectrum 4 (coloured in cyan), which was not present in samples of Murchison prior to exposure to ozone.

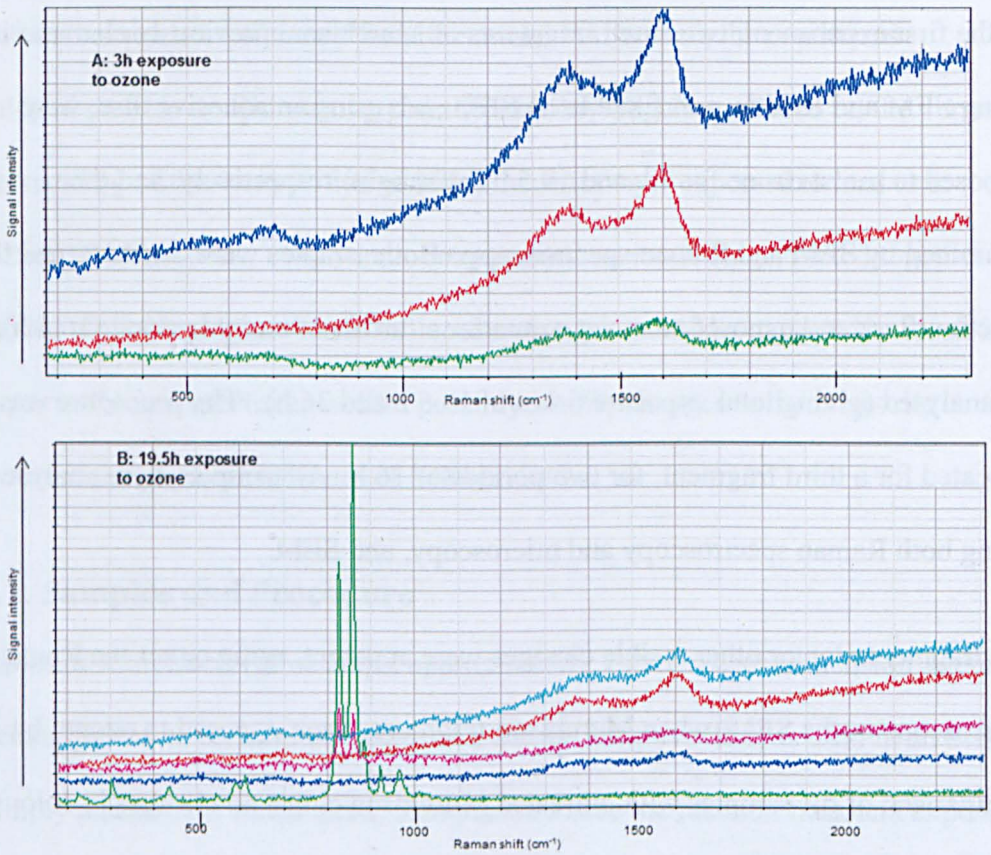

Figure 4-11: Raman spectra of surface of Murchison exposed to ozone for up to 19.5 h (spectra obtained at different locations on the surface are shown in different colours)

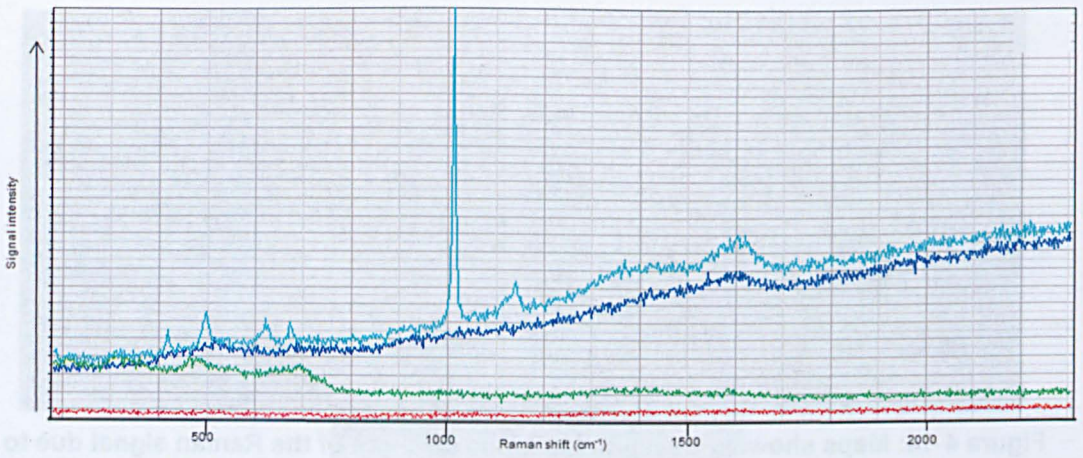

Figure 4-12: Spectra taken on the surface of Murchison sample exposed to ozone for 36.5 h (spectra obtained at different locations on the surface are shown in different colours)

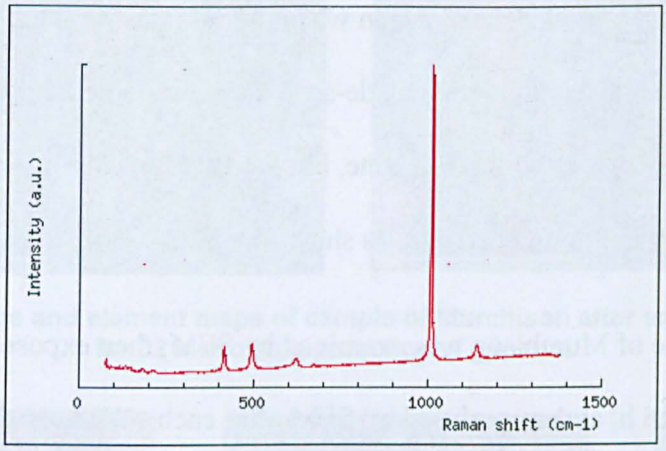

Figure 4-13: Library spectra of gypsum for comparison (Handbook of Minerals Raman Spectra)

The signal at 1010 cm^{-1} was identified from library spectra as being due to gypsum (Figure 4-13). A similar result was obtained for the third sample; gypsum was only detected in the sample after ozone treatment, and not before. However, after ozone treatment, gypsum was not apparent over the whole surface of the fragment; some areas showed practically no changes. The maps shown in Figure 4-14 show gypsum to be widespread in the first region examined, but present in only one small part of the second region (intensity of colour is a function of the ratio of the gypsum signal to that of aromatic carbon).

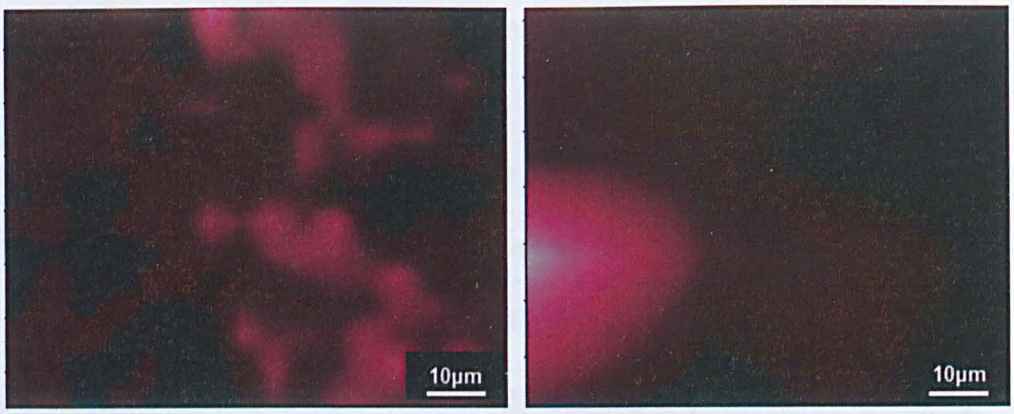

Figure 4-14: Maps showing the variation in the strength of the Raman signal due to gypsum over two areas of the sample

SEM

This heterogeneity was also clearly seen when the samples were examined by SEM (shown in Figure 4-15). Numerous blade-shaped grains could be seen on the surface (in both samples, after exposure to ozone, but not before), which correlated with concentrations of sulfur and calcium, as shown by EDS.

The third sample of Murchison was examined by SEM, then exposed to ozone for two periods of 16 h, and re-analysed by SEM after each. Whereas the volume sampled by the electron beam contained mainly iron, magnesium and silicon prior to ozone exposure, both calcium and sulfur increased in intensity afterwards, their signals being stronger, the longer the exposure to ozone, as seen in Figure 4-16. However, the heterogeneous distribution of gypsum seen by Raman spectroscopy was also seen using EDS. Whereas one region (Region A) showed extensive development of gypsum crystals after exposure to ozone, a second region, (Region B) was largely unchanged (Figure 4-17).

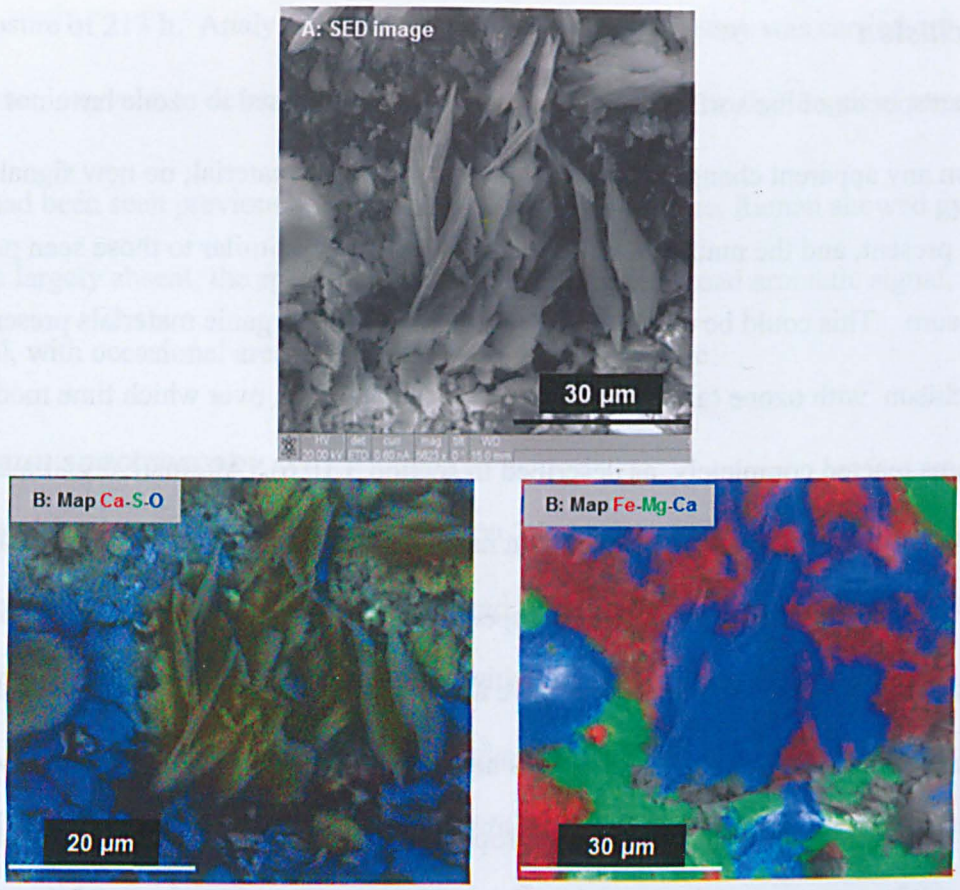

Figure 4-15: Image and element maps of sample of Murchison after exposure to ozone for 32 h showing presence of gypsum

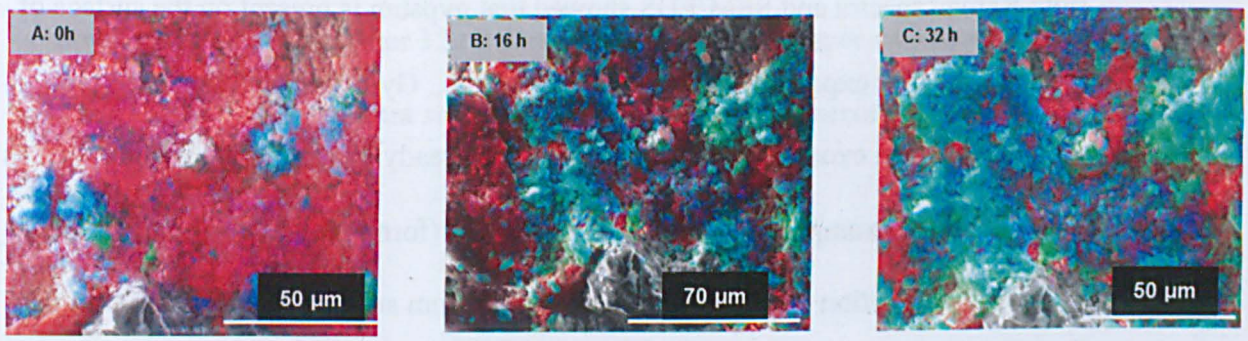

Figure 4-16: Element maps (Fe-Ca-S) of the surface of Murchison sample (Region A) showing increase in calcium and sulfur (gypsum) over time

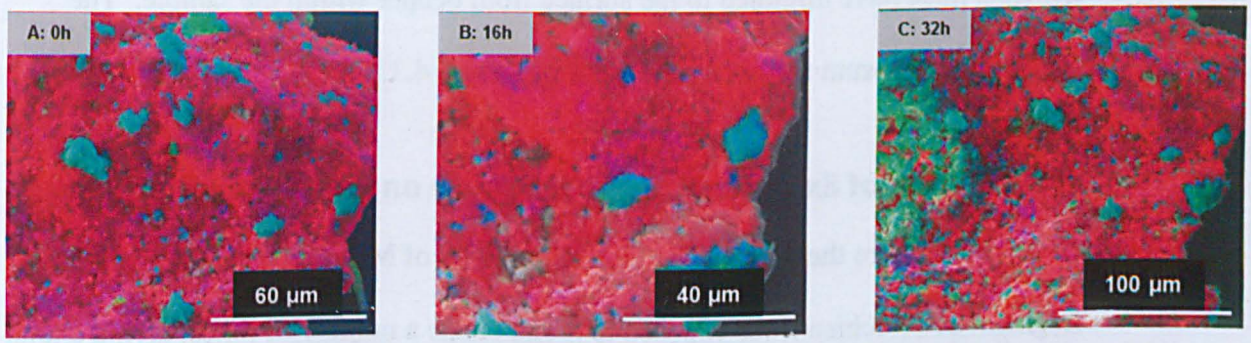

Figure 4-17: Element maps (Fe-Ca-S) of the surface of Murchison sample (Region B) showing no change in calcium and sulfur over time

Conclusion

Raman spectra of the surfaces of Murchison samples exposed to ozone have not shown any apparent change in the signals due to organic material; no new signals were present, and the main D and G peaks appeared very similar to those seen pre-exposure. This could be due to a lack of reaction of the organic materials present in Murchison with ozone (although exposure was up to 32 h, over which time model systems reacted completely, as described in section 3.10.6). Alternatively, it may be that the organic material has reacted, but has not generated products which would give distinctive signals in their Raman spectra. Based on prior determinations of the structure of IOM, it was expected to give a network of oxygenated aromatic systems on exposure to ozone. The fact that this has not been observed indicates its structure may be different from that previously proposed, or possibly, that its reactivity has been modified in some way, by the minerals present in Murchison.

Both Raman spectra and SEM/EDS showed that gypsum is present on the surface of the samples after exposure to ozone, but not before. Gypsum could be formed by reaction between ozone and some other mineral already present in the sample such as reaction of, for example, calcite, with sulfuric acid (formed by oxidation of sulfur), or possibly oxidation of (the rare) oldhamite (calcium sulfide), but EDS showed the absence of both calcium and sulfur in areas where gypsum was later found. These elements must have migrated to the surface from deeper within the sample. The formation of gypsum is discussed further in section 4.3.1.

4.2.3. Effects of Extended Ozone Exposure on Murchison Fragments

To further explore these changes to the mineralogy of Murchison samples, a fourth fragment of Murchison was exposed to moist ozone a number of times, giving a total

exposure of 213 h. Analysis by SEM and Raman spectroscopy was carried out at various intervals, to determine how any changes depended on the length of exposure.

As had been seen previously, prior to any exposure to ozone, Raman showed gypsum to be largely absent; the spectrum was dominated by the broad aromatic signal, as usual, with occasional areas showing peaks due to forsterite.

Raman spectroscopy

Using the methodology described in section 2.3, regions of the surface that could be easily re-located were selected for study and re-examined after each exposure, taking several Raman spectra (of discrete spots within the general area selected for study) each time. A signal at 1010 cm^{-1} (due to gypsum, as seen before), had developed in the first sample after 16 h exposure. In addition, another peak was observed at about 1470 cm^{-1} in one spectrum (Figure 4-18). After 32 h exposure, instances of this new peak were more common, although very localised; a map of the signal at 1470 cm^{-1} is shown in Figure 4-19. After 122 h exposure, another set of spectra was acquired over this region. These spectra showed elevated levels of this second new peak (Figure 4-20).

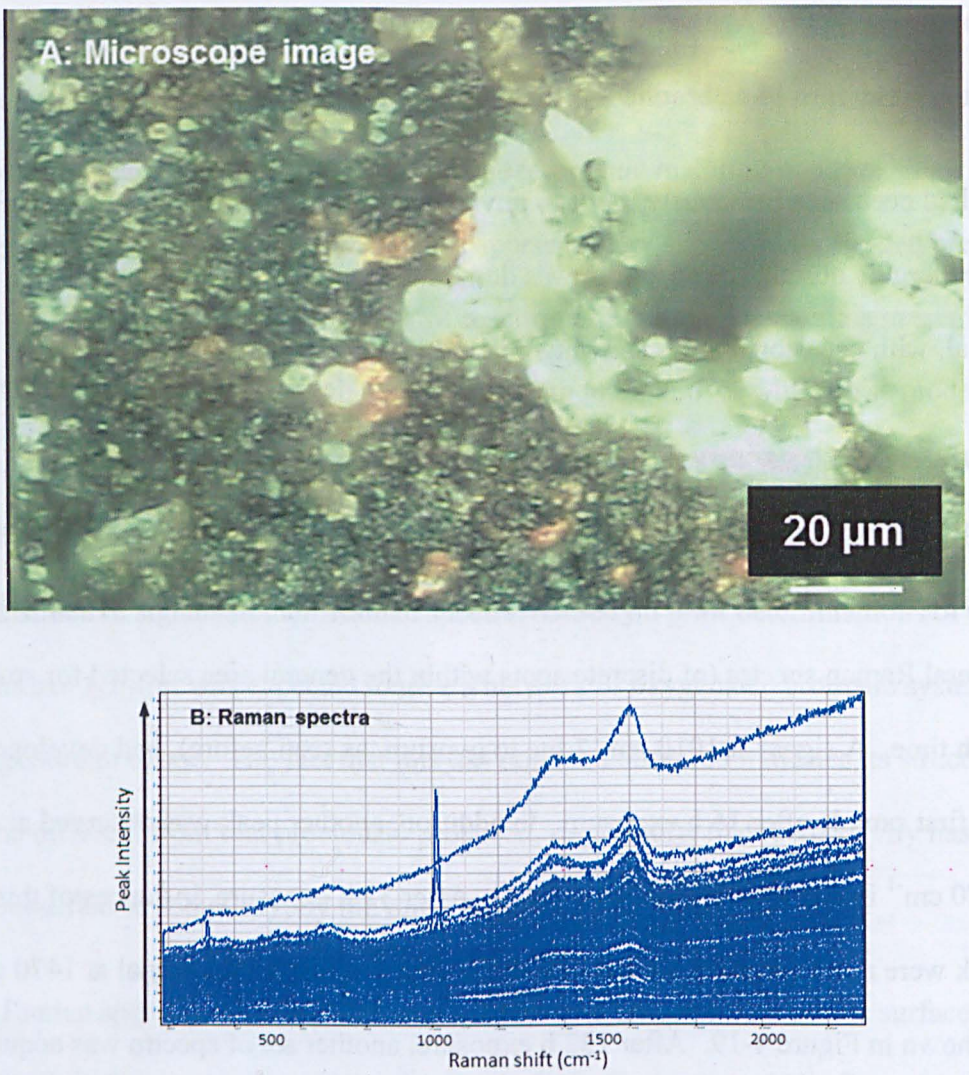

Figure 4-18: Raman analysis (A: Stacked Image, B: Overlay of spectra taken across the surface of a sample of Murchison) after one exposure to ozone

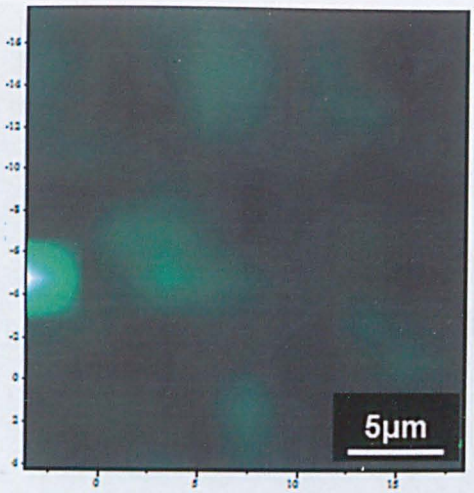

Figure 4-19: Map showing variation across the sample surface, in the signal at 1470 cm^{-1} obtained after 32 h exposure to ozone showing localised concentrations of its source

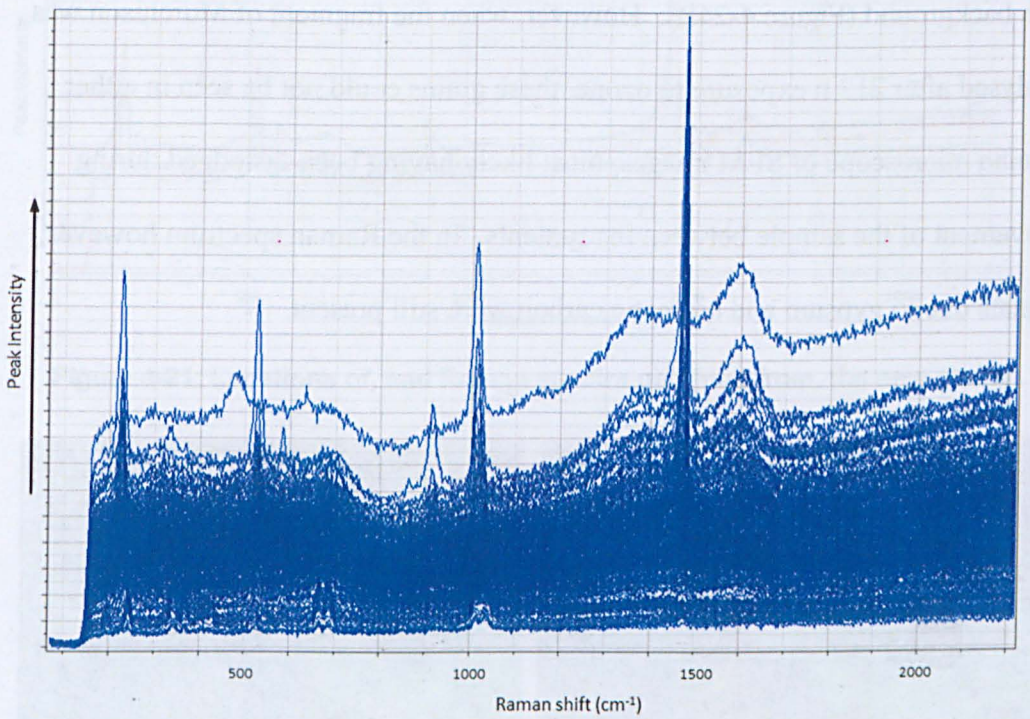

Figure 4-20: Overlay of spectra acquired across the sample surface showing increased intensity of the peak at 1470 cm^{-1} at some points

Identification of the source of the signal at 1470 cm^{-1}

A map of Raman intensity (Figure 4-19) showed this signal was concentrated at a small number of discrete locations which appeared to coincide with individual grains, as shown in Figure 4-21A. Spot spectra acquired of those grains did indeed show this signal, along with several others of a lower intensity, with the broad

signals indicative of aromatic groups (the D and G peaks) being missing. These spectra are shown in Figure 4-21B. Images of this area taken using the Raman microscope were re-examined, and it is clear (see Figure 4-22) that these grains were not present before ozone treatment. SEM images were also acquired of this same area, and compared with those taken prior to ozone exposure (Figure 4-23A).

An X-ray spectrum was acquired of one of these new grains (as indicated in Figure 4-23B), which shows only magnesium and oxygen present (Figure 4-24A). An elemental map of this area shows the grains clearly against the silicon- and iron-rich background (Figure 4-24B). However, when the fragment of Murchison was analysed after 213 h exposure to ozone, these grains could not be seen in either Raman microscope or SEM images, most likely having been dislodged during movement of the sample between instruments. In the Raman spectrum however, signals due to gypsum and aromatic carbon were still present.

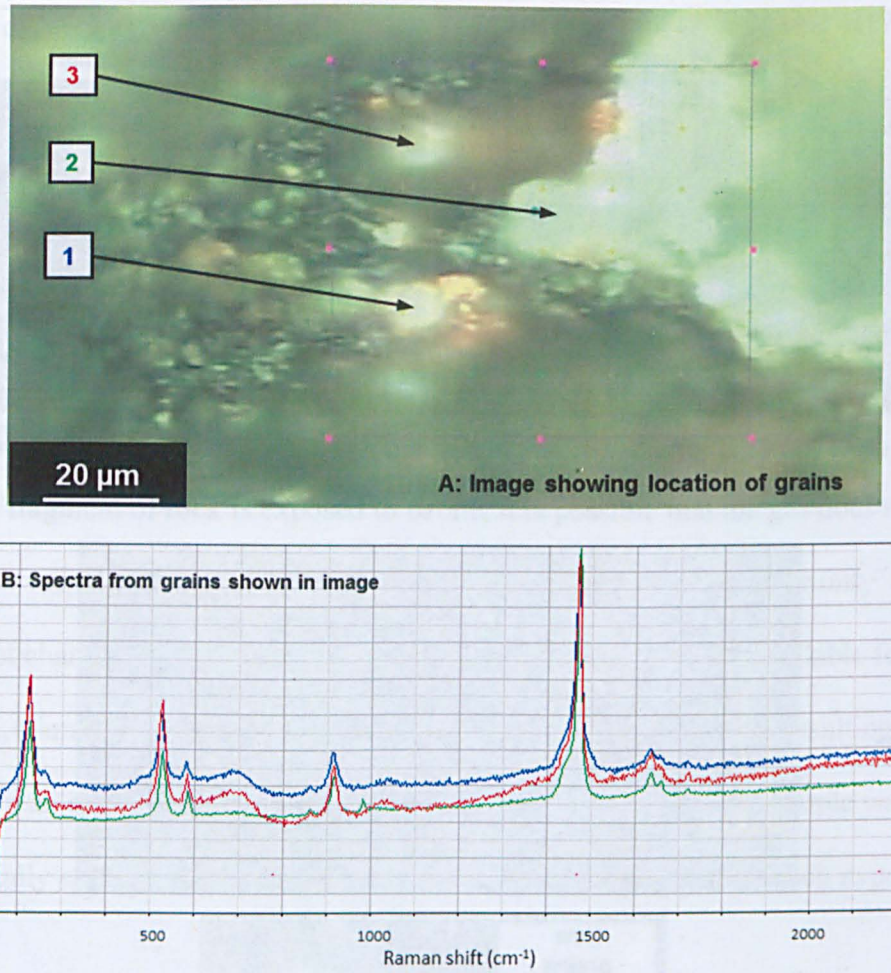

Figure 4-21: Locations of, and Raman spectra obtained from, the new grains

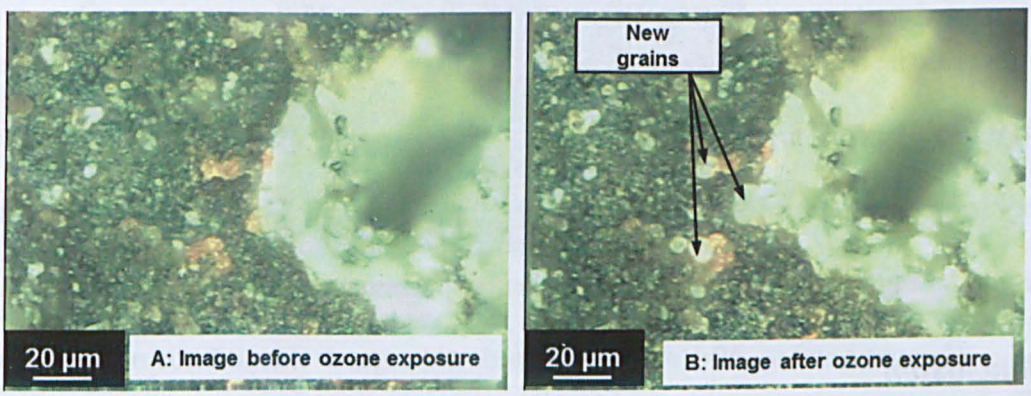

Figure 4-22: Stacked Raman microscope images showing the new grains, present after exposure to ozone, but not before

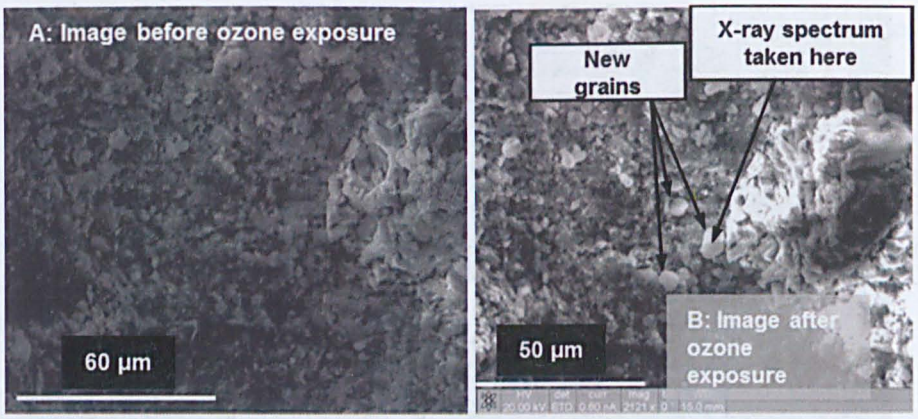

Figure 4-23: SEM images of sample surface A) before and B) after 132 h ozone exposure

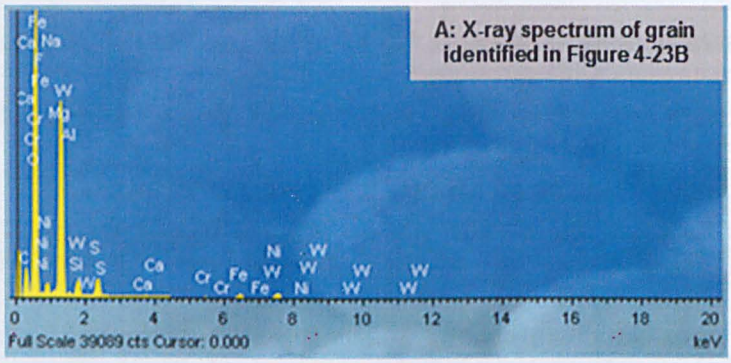

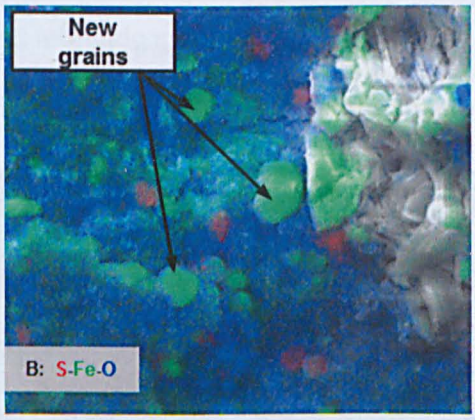

Figure 4-24: A) X-ray spectrum and B) element map of new grains

Conclusion

On extended exposure to ozone, in addition to the development of areas containing gypsum, a new material was formed. This material, giving a distinctive Raman spectrum with a peak at 1470 cm^{-1}, formed small grains, visible both using the Raman microscope and SEM. X-ray spectra of the grains showed the presence of magnesium and oxygen, but no other elements. The grains had not been seen in any

sample of Murchison prior to treatment with ozone, and so have arisen following reaction of ozone with some component of the meteorite sample. Further information on this new material was obtained by treating crushed Murchison with ozone (as described in the next section), with interpretation of both sets of results discussed in section 4.3.2.

4.2.4. The Effect of Ozone on Crushed Murchison

When a fragment of rock is exposed to ozone, it is possible that the gas does not penetrate very deeply within the sample, and that the results seen so far only represent changes at, or close to, the surface. To increase the area available for reaction, a small fragment of Murchison was gently crushed, and the resulting grains placed on an adhesive disk stuck on an aluminium SEM stub. This sample was sequentially exposed to ozone for 17 h then 24 h, and analysed after each exposure.

SEM

Low magnification images of the crushed sample before and after 17 h exposure are shown in Figure 4-25. After exposure to ozone, the grains clearly appear less well-defined, as if fused together. Higher magnification images show the surface of the sample to be covered with spherical objects. These are absent from the areas of the stub free from sample (and were not formed when a blank stub was subjected to the same reaction conditions). Images are shown in Figure 4-26. After a second exposure to ozone, SEM showed the spherical objects to have collapsed, and the sample appeared to be cracking and breaking up (see Figure 4-27). This cracking seemed to depend on the time the sample spent in the electron beam; imaging only part of the sample resulted in the area affected being clearly visible as a square of altered appearance (within the white rectangle highlighted in Figure 4-28).

Elemental maps showed these objects to contain sulfur, with iron and calcium also seen in spot X-ray spectra, as shown in Figure 4-29A and B. After the second exposure to ozone, maps of the structures showed the presence of sulfur and iron, but less calcium (Figure 4-31).

These spheroidal structures are physically reminiscent of the "organized elements" found in meteorite samples, which, at one time, were thought to be evidence of extra-terrestrial life (Fitch *et al.*, 1962; Anders and Fitch, 1962). The iron and sulfur seen in these spheroidal structures may be the mineral troilite (iron (II) sulfide), which was also detected in the investigations into "organised elements". It is possible therefore that the "organised elements" may have arisen by some abiotic oxidative process, analogous to that resulting from exposure to ozone, occurring in the meteoritic samples investigated, but not recognised at the time.

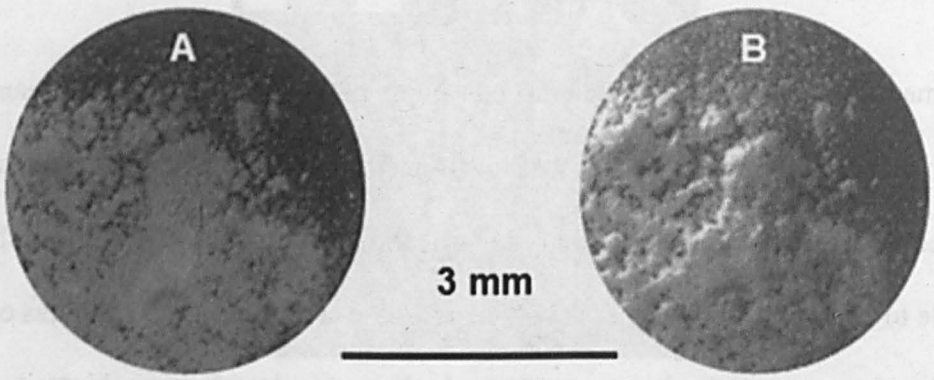

Figure 4-25: Low magnification images A) before and B) after ozone treatment showing development of fused appearance of the sample

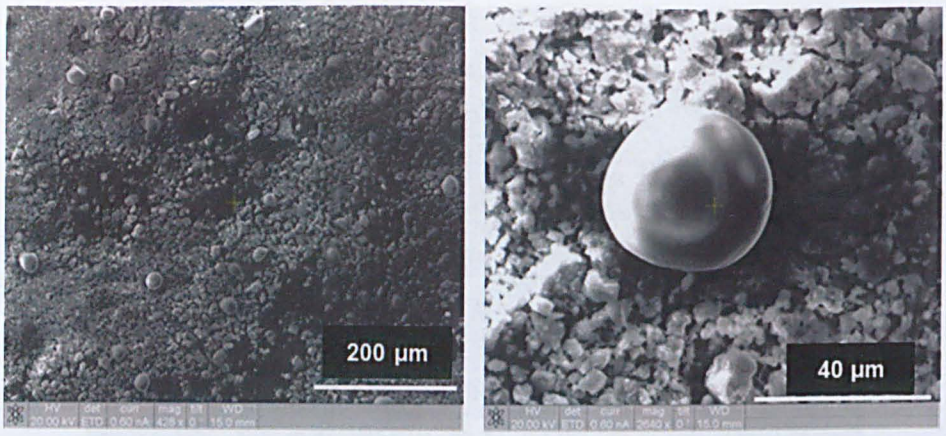

Figure 4-26: Higher-magnification images of spherical objects on the sample surface

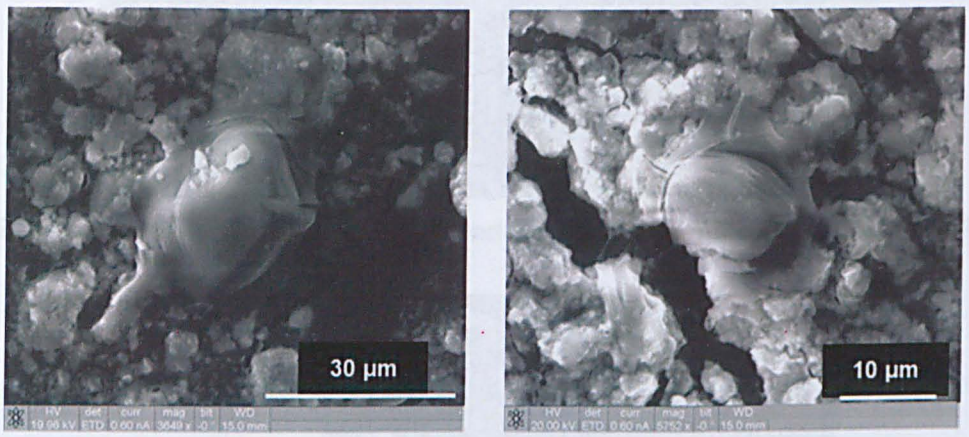

Figure 4-27: SEM images after 41 h exposure to ozone showing cracking of surface and collapse of spherical objects

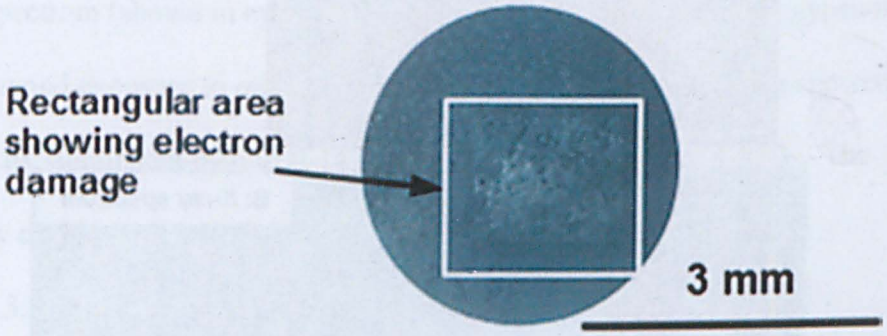

Figure 4-28: Effects of electron beam impact on the sample

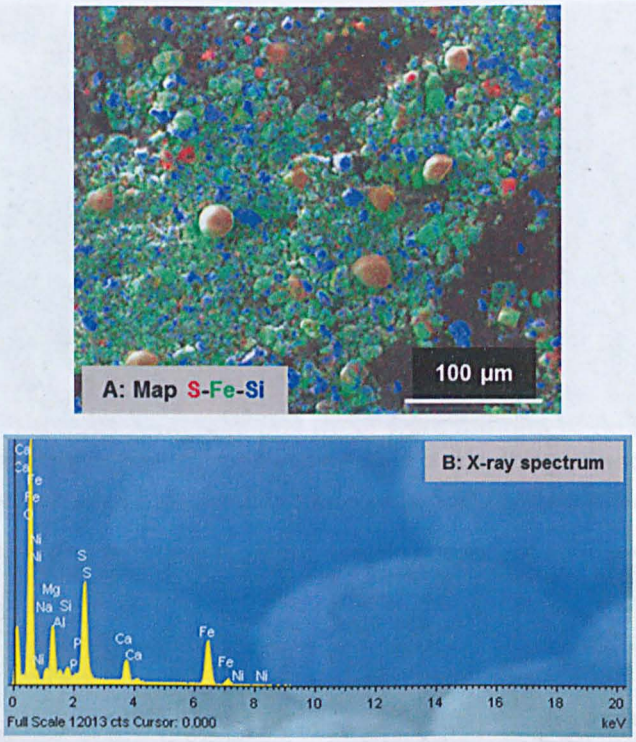

Figure 4-29: A) Element map (S-Fe-Si) and B) X-ray spectrum of spherical object

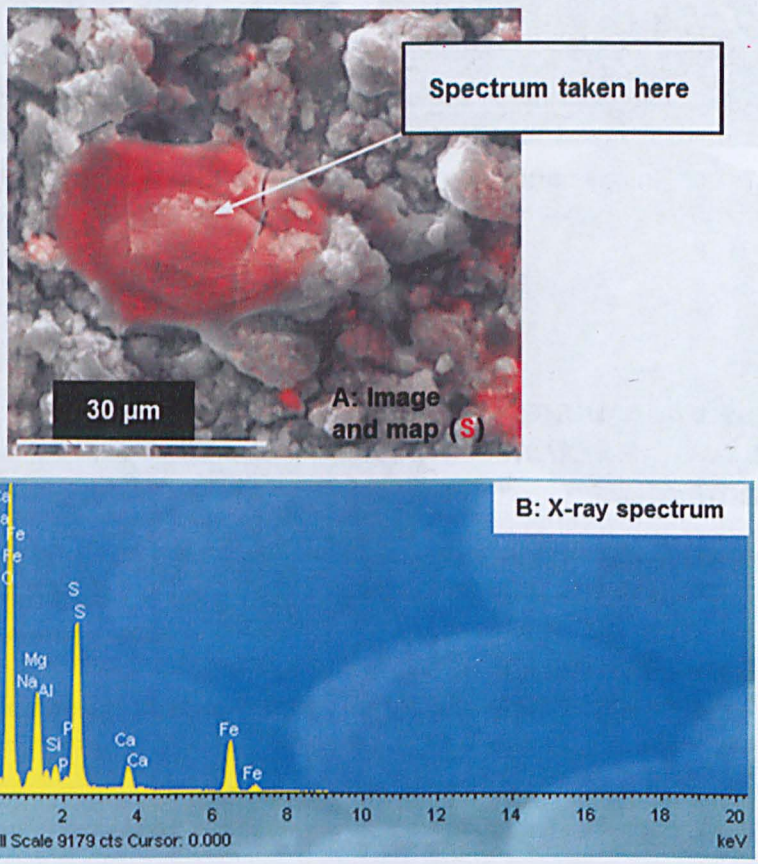

Figure 4-30: A) Element map (S-Fe-Si) and B) X-ray spectrum of collapsed feature (showing no change from that before collapse, as shown in Figure 4-29)

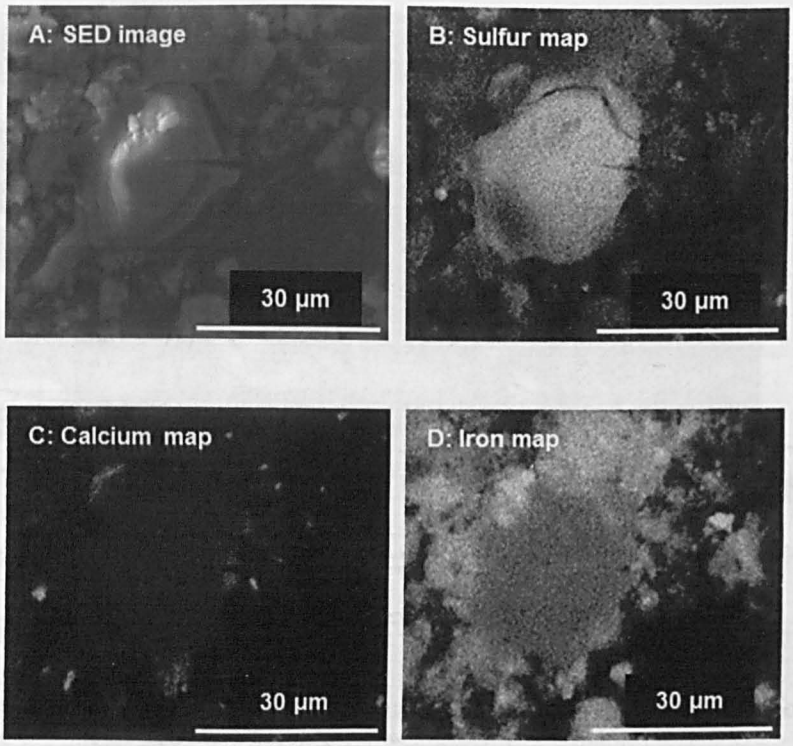

Figure 4-31: Elemental maps of collapsed feature after 41 h exposure to ozone

Raman spectroscopy

Raman spectra taken at various points across the surface of the sample after 17 h ozone treatment were very similar to those before exposure, with gypsum present, but not widespread. Representative spectra are shown in Figure 4-32A, with the bottom spectrum (shown in cyan) showing a peak at 1010 cm^{-1}, due to gypsum. After a second exposure to ozone, making 41 h in total, Raman spectra showed many new signals, dominated by one at 1470 cm^{-1}, as shown in Figure 4-32B . The frequency of this peak is the same as the new mineral grains described in section 4.3.2.

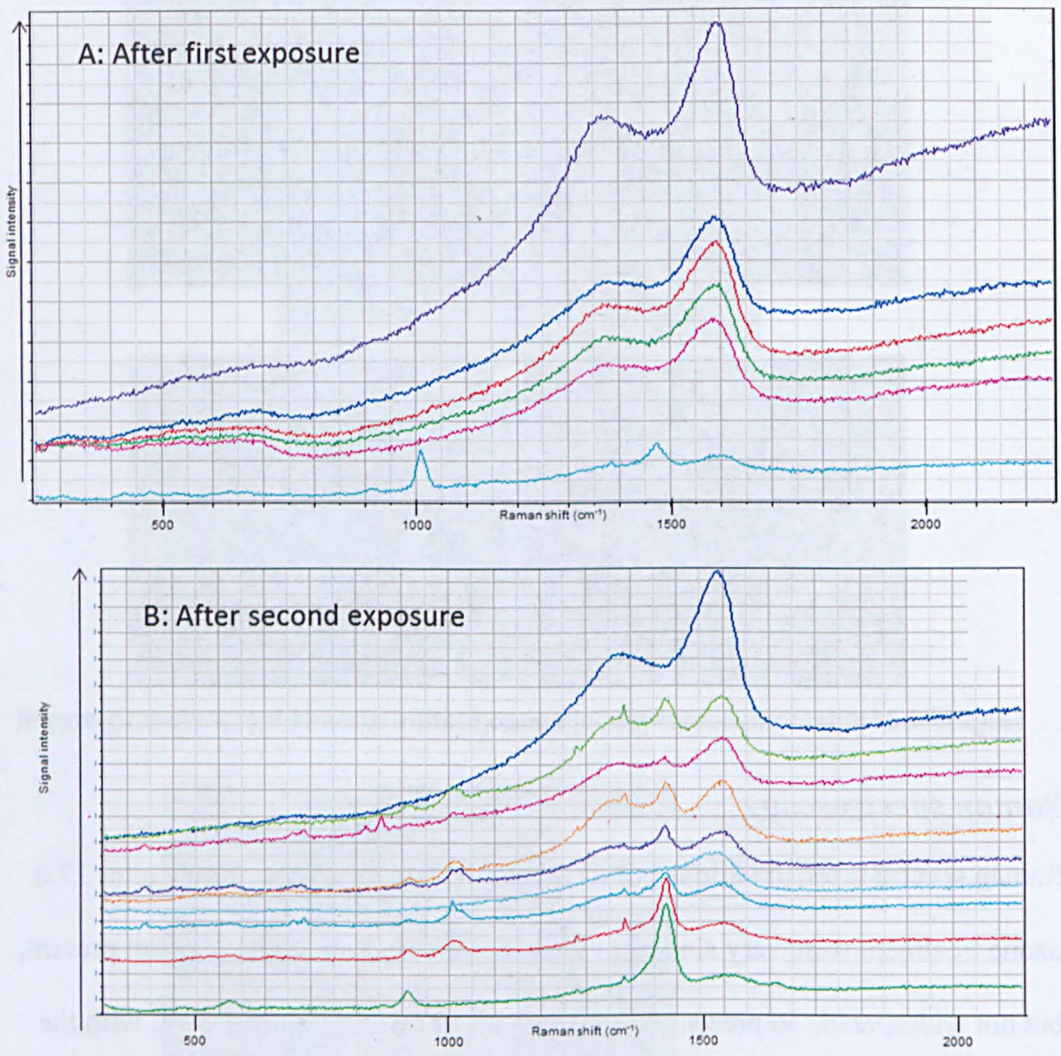

Figure 4-32: Raman spectra after A) first and B) second exposure to ozone. Spectra obtained at various points across the surface are shown in different colours, and show the variability in the strength of the signal at 1470 cm^{-1}.

At this stage, the image-stacking methodology (see section 2.1.4) had not been developed, and so good-quality microscope images were not obtained. However, images, such as that shown in Figure 4-33, clearly show the collapsed features. It seems very likely that the formation of these objects and the appearance of the Raman signal at 1470 cm^{-1} are connected. These results, and others directed towards identification of the grains are discussed in section 4.3.2.

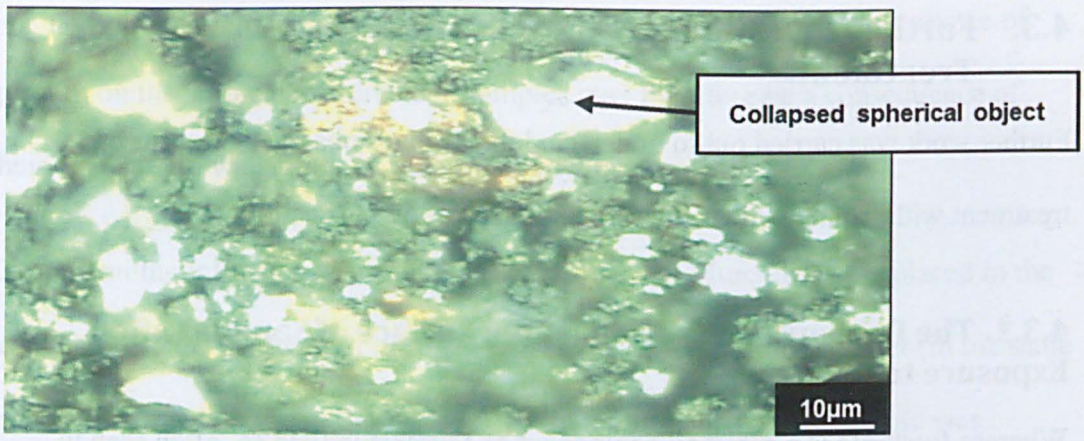

Figure 4-33: Raman microscope image of crushed Murchison, after ozone treatment

Summary

When a Murchison sample was powdered, then exposed to ozone, visible physical changes were clearly seen, in contrast to millimetre-sized fragments, which appeared, by eye, to be unchanged following ozone treatment. The grains appeared to be fused together, and spherical objects had formed on the surface. These objects appeared to be fragile, breaking up on further exposure to ozone, or after extended electron impact. X-ray spectra showed these seemed to contain only sulfur and iron. Well-defined grains of gypsum were not seen. The presence of carbon, which only gives a weak EDS signal, could not be confirmed. Raman spectra showed the presence of a signal at 1470 cm^{-1} (as described in the previous section). In Murchison chips, the signal at 1470 cm^{-1} was identified with newly-formed grains, but in the crushed sample, such grains were not identified. The fragile spherical objects which formed were shown, by their X-ray spectra to be different from those grains, and could not be associated directly with the signal at 1470 cm^{-1}, although it seems likely both are due to ozone treatment in some way.

4.3. Further Investigations into the Changes on Ozone Treatment.

Further work was carried out to understand the changes observed to occur on treatment with ozone; which is described in the following section

4.3.1. The Presence of Gypsum on the Surface of Samples after Exposure to Ozone

Whereas forsterite is a common component of Murchison (and so, often seen in Raman spectra), gypsum is not (Papike, 1998, pp3-217), and had not been seen in Raman spectra obtained (on whole rock) before ozone treatment (see section 4.1.3). Whereas it is conceivable that the sulfate ion of gypsum could have been formed by ozone-mediated oxidation of a metal sulfide (*e.g.* the rare oldhamite), or elemental sulfur (Chanturia *et al.*, 2007; Ivanova *et al.*, 2008), the calcium must have been present in the meteorite sample prior to treatment, in the form of some other mineral, possibly calcite, which would then react to form the gypsum.

However, water-soluble minerals are known to migrate to the surface when meteorite samples are exposed to a damp environment. This may reflect simply pre-existing minerals being mobilised, or the formation of new minerals, but from ions already present in other minerals, and solubilised by water vapour. An example is the appearance of sulfate-containing veins on the surface of Orgueil on storage (Gounelle and Zolensky, 2001). Similar observations have been reported for meteorite samples found in Antarctica (Velbel *et al.*, 1991). Minerals with any water solubility are also (not surprisingly) easily removed when a sample is wetted. Fragments of Sutter's Mill, (a CM2 carbonaceous chondrite which fell in California in 2012), recovered after rain, showed considerably lower calcium and sulfate concentrations that those recovered immediately after its fall (Cooper and

Jenniskens, 2012) indicating a leaching process had occurred. The appearance of gypsum on the surface of Murchison samples may therefore be a consequence of their exposure to water vapour, and not to any reaction with ozone.

To confirm the influence of water, a fresh fragment of Murchison was placed in the reaction flask and a stream of nitrogen passed through the water bubbler (in the same manner as for ozone), then the flask sealed. After seven days, the sample was examined by SEM and Raman spectroscopy. SEM images of this fragment clearly show the appearance of new grains (shown in Figure 4-34B). X-ray maps (Figure 4-35A and B) and spot spectra (Figure 4-35C) confirm the presence of calcium and sulfur as before.

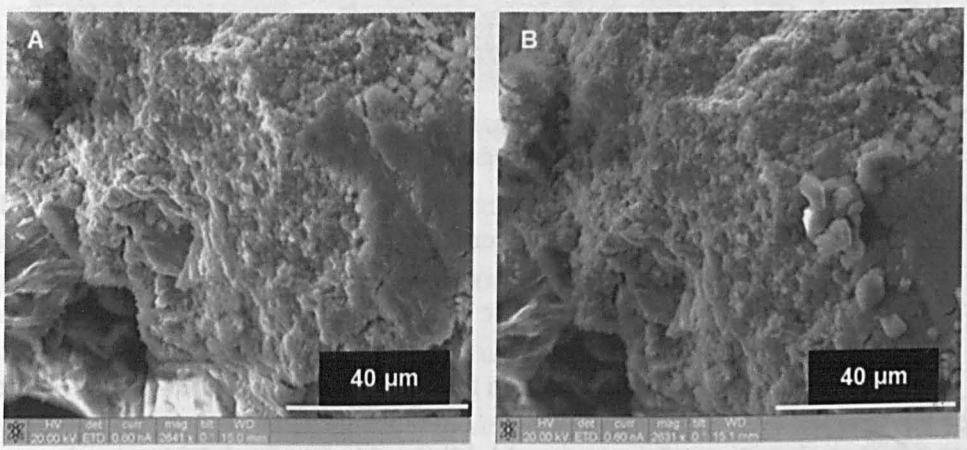

Figure 4-34: SEM images of Murchison fragment A) before and B) after exposure to wet nitrogen showing appearance of new grains of gypsum

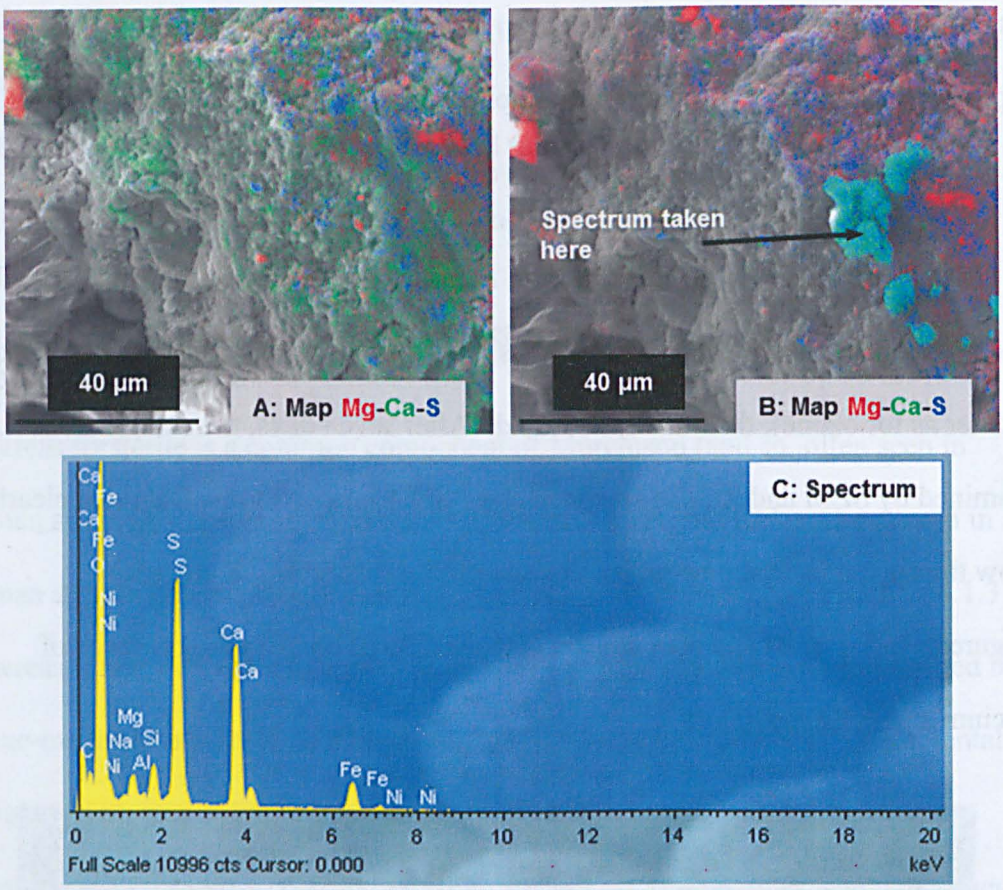

Figure 4-35: Element maps of sample surface A) before and B) after exposure to water, and C) spot spectrum of new mineral grain showing calcium and sulfur

Raman spectra and microscope images were also acquired for this sample. Signals due to gypsum were rare prior to exposure to wet nitrogen, but common afterwards. The presence of gypsum is clearly seen in the Raman map (Figure 4-36C) obtained across the central portion of the image, highlighted in Figure 4-36A. A microscope image (Figure 4-36A) of the central area of this fragment shows a mineral present, but although clearly displayed in the SEM image (Figure 4-36B) was less distinct. The formation of gypsum on the surface of these samples therefore is clearly due to the presence of water vapour, and not to any reaction with ozone. This water vapour is only present in the atmosphere surrounding the meteorite sample (it was not, even partly, immersed in liquid water). The concentration of water in air at ambient temperature varies, being up to about 1.5%; in these experiments, the maximum concentration of water in the ozone stream was likely to have been a similar value.

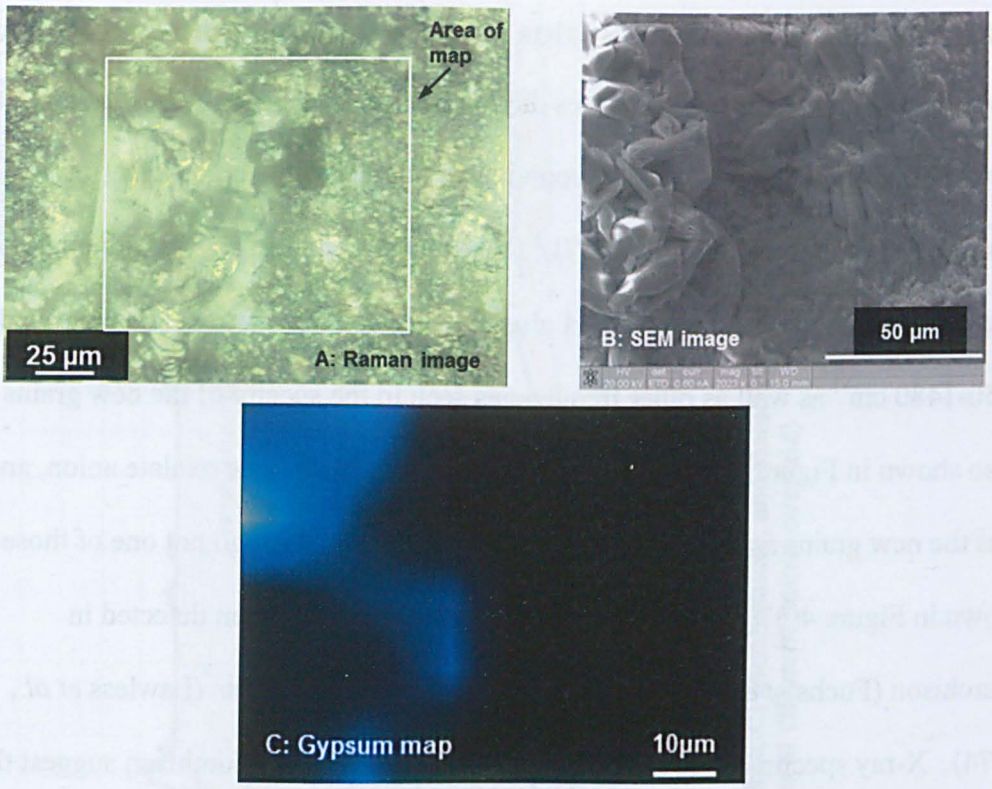

Figure 4-36: A) Raman microscope and B) SEM images of central part of the Murchison fragment, with C) Raman map showing presence of gypsum

However, these results do not distinguish between the two possible mechanisms by which gypsum could have formed on the surface. Gypsum may have been present (as that mineral) in the sample of Murchison, and, by recrystallisation after mobilisation, migrated within the sample, until it reached the surface, and recrystallized as gypsum once more. However, as significant gypsum was not seen prior to treatment, it is possible that it is in fact formed by the action of water vapour from the reaction of calcium and sulfate ions (both present in other minerals). If this is the case, then other new minerals must also have been formed from the counter-ions of calcium and sulfate.

A more extensive mineralogical and petrographical analysis of samples exposed to water vapour (both on the surface, and internally) would be needed to determine which of these two alternatives was the correct mechanism.

4.3.2. Identification of the Grains giving a Raman Signal at 1470 cm^{-1}

A search of Raman spectral databases did not reveal any exact matches for the spectra obtained (Figure 4-22), but contained a number with similarities (for example, those shown in Figure 4-37). The Raman spectra of several minerals (including weddelite, whewellite and glushinskite) contain a strong signal around 1450-1480 cm^{-1} as well as other frequencies seen in the spectra of the new grains (also shown in Figure 4-37). These are minerals containing the oxalate anion, and thus the new grains are likely to be salts of oxalic acid, although not one of those shown in Figure 4-37. The oxalate mineral whewellite has been detected in Murchison (Fuchs *et al.*, 1973) and oxalic acid found in extracts (Lawless *et al.*, 1974). X-ray spectra of the grains formed on the surface of Murchison suggest that the grains are a magnesium mineral (no signals of any other metal were seen). They are not, therefore, the oxalate dihydrate, glushinskite, but may be a magnesium oxalate with a different degree of hydration, which would be expected to give a similar, but not identical Raman spectrum. For example, the spectra of calcium salts of oxalic acid (whewellite and weddelite in Figure 4-37) are somewhat different, even if their chemical compositions are very similar. Another possibility is a mixed salt, with an anion which does not give a Raman signal, for example, carbonate which would be consistent with the X-ray spectrum. Whatever the exact composition of the grains, the data supports identification as an oxalate-containing mineral. These grains presumably formed by reaction of oxalic acid with other minerals in the sample; the oxalic acid is most likely formed by reaction of the organic materials present in the sample with ozone. Possible magnesium-containing minerals are its oxide, hydroxide or carbonate; all of which have both been reported (Papike, 1998), and would be expected to undergo this reaction.

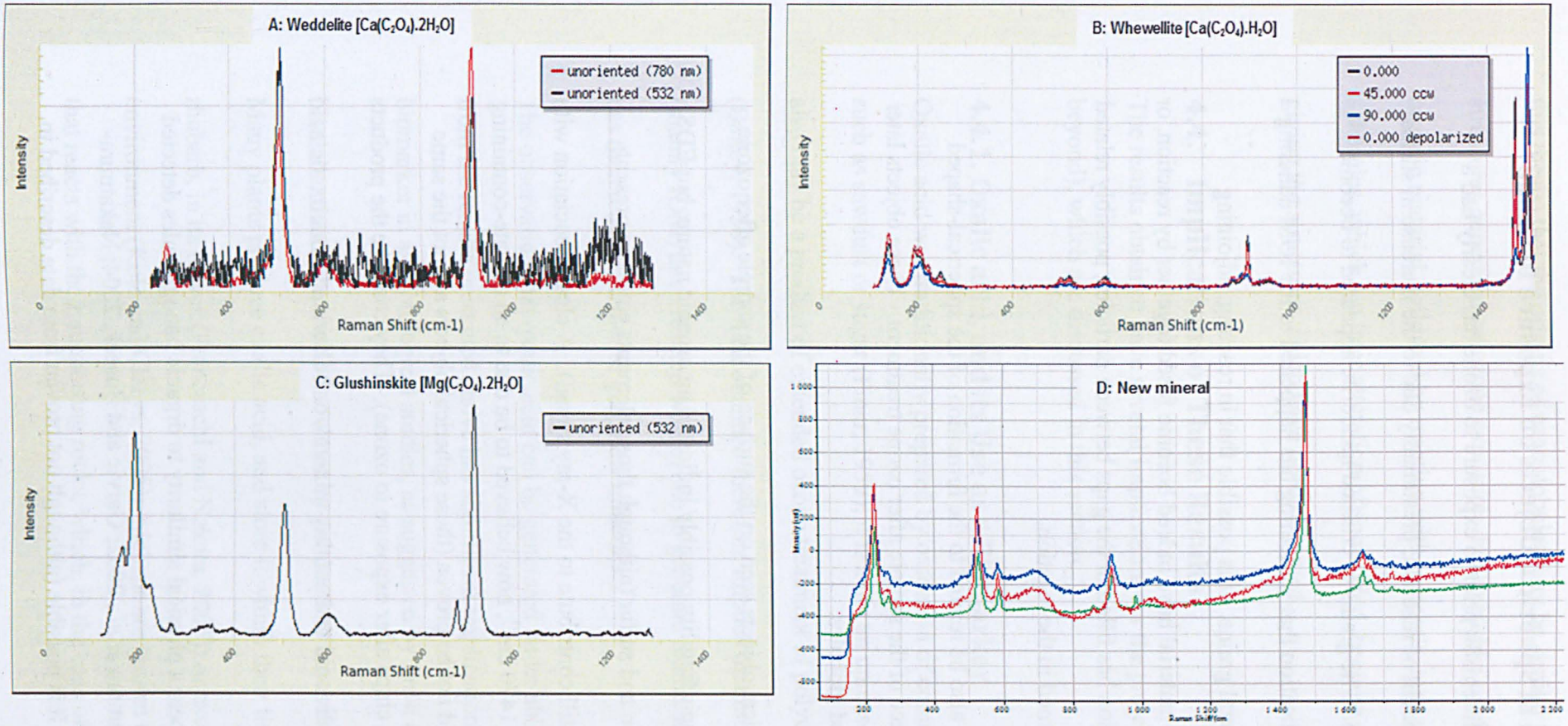

Figure 4-37: Raman spectra of oxalate-containing minerals: A) Weddelite, B) Whewellite, C) Glushinskite, annotated with chemical formulae, and D) Raman spectra of new mineral grains (three spectra at different points overlaid)

4.3.3. The Formation of Spherical Objects on Exposure to Ozone

Crushing the sample of Murchison prior to exposure to ozone has clearly had a significant effect on the extent of reaction, presumably due to the increase in surface area available for reaction. The grains of crushed meteorite appeared to become fused together, a clear indication that something has happened to the IOM adhering to the surfaces of the mineral grains. It is possible that in reacting, adjoining particles of carbonaceous material have indeed become fused together by reaction, or some product of the reaction has filled in the gaps between particles, possibly related to the oxalic acid also formed in the reaction.

The fusing observed may also be related to the formation of the spherical-shaped objects found on the surface of the sample after ozone treatment. These objects later collapsed to form flattened globules.

The nature of these spherical objects seen on the surface of the sample after ozone treatment is not clear. Their fragility possibly indicated an organic nature, but EDS shows the presence of iron and sulfur (although those elements could be present beneath the spheres and still contribute to the X-ray signal). A clear association with the Raman signal seen at 1470 cm^{-1}, now believed to be due to an oxalate-containing magnesium mineral, could not be proven (these spherical objects are not the same grains seen in Murchison chips after exposure to ozone). They could be the products of a reaction between oxalic acid and another mineral, or be derived from oxalic acid itself.

The spherical structures bear a physical similarity to organic nanoglobules detected in some meteorites (Nakamura *et al.*, 2002; Garvie and Buseck, 2004; Nakamura-Messenger *et al.*, 2006). It is possible (although not proven from data described in

this thesis) that the origins of nanoglobules may be similar to that of the spherical structures generated on ozone exposure. For example, oxidation of meteoritic organic material, followed by reaction with minerals, may generate organic-rich spherules, which, on later alteration of some kind, become consolidated in some way, giving the structures which have been observed.

4.4. Implications of These Results

The results obtained have several implications for the project objectives (and beyond), which are discussed in this section.

4.4.1. Oxalic acid, and its Use as a Biomarker

Oxalic acid was traditionally prepared by oxidation of common organic materials, such as sawdust or sugar (Finar, 1959); it is a not an unreasonable assumption that it also may be a product of extended ozone treatment of polyunsaturated systems (Bailey, 1958). The data obtained therefore implies that meteoritic organic materials (mainly IOM) have reacted with ozone to generate oxalic acid, which, in this case, has then reacted further to give new minerals.

The observation that oxalic acid can be generated under abiotic conditions, as seen from the results presented above has significant implications for its use as a biomarker in astrobiological studies, as suggested by Frost *et al.* (2003).

Oxalate minerals are well-known as by-products of terrestrial biological processes. Many plants produce oxalic acid, and store it within their tissues (for example, rhubarb, in its leaves (Franceschi and Nakata, 2005)) or excrete it into the environment (Kolo and Claeys, 2005). Lichens are known to generate oxalic acid that reacts with their supporting rocks, which, in the case of dolomite, will lead to the

production of calcium- and magnesium-containing oxalate minerals (Edwards *et al.*, 2003). In these terrestrial examples, oxalic acid has been formed by biotic processes.

To act as a biomarker, a compound must be formed *exclusively* by biotic processes, at least in the environment under study. If there is any possibility that a proposed biomarker may have had an abiotic source, any proposal of a biotic source is immediately open to question

Based on the known examples of their biotic production mechanisms, oxalate-containing minerals have been proposed as biomarkers, for example, their presence on the surface of Mars has been suggested as being evidence of the existence of life at present, or in the past, (Frost *et al.*, 2003). Raman spectroscopy has been proposed as a means to detect such minerals (Wdowiak *et al.*, 1995a) although to date, no Raman instruments have as yet been deployed on other planets.

Indeed, it is not unreasonable that oxalates may exist on the surface of Mars, formed by a similar mechanism to that observed in this project. Ozone can be generated in many environments (and is, of course, a natural component of the atmosphere of Earth). It has also been detected in the atmosphere of Mars (Novak *et al.*, 2002). Potentially, any aromatic system could react with ozone to give oxalates; meteorites could provide that source of organic materials (Sephton *et al.*, 2002), and indeed, oxidation of meteoritic organic materials has been proposed as a possible source of methane in the atmosphere of Mars (Ott *et al.*, 2012), by, for example, reactions of carbonaceous meteorites on the surface, or during entry through the atmosphere. As other oxidants could also possibly carry out this reaction (such as perchlorate, also detected on the surface of Mars (Hecht *et al.*, 2009)), the use of oxalate minerals as biomarkers in general is likely to be inappropriate.

4.4.2. The Exposure of Meteorite Samples to Water Vapour

Exposure of Murchison to an atmosphere containing water vapour resulted in the formation of grains of gypsum on its surface. These were formed by migration of calcium and sulfate ions, either from pre-existing gypsum, or from other minerals, through the structure of the meteorite sample, and recrystallizing at the surface. The passage of these ions will have affected the structure of the meteorite, as grains dissolved and re-formed elsewhere.

The implication of this observation is that a similar effect could be expected for a meteorite sample exposed to normal atmospheric conditions, for example following a fall, but before collection. Only if the meteorite is surrounded by an impermeable layer (such as a fusion crust), is the penetration of water likely to be prevented. Even though this time might be short, just a few days, the observation was that this is sufficient for gypsum to form. It is very likely therefore, that any minerals with an appreciable solubility in water (such as gypsum), will migrate to the surface of a recently-fallen meteorite. Less-soluble minerals, such as calcite, which will be slower to dissolve and recrystallise, might behave similarly, although more slowly. It is likely therefore that exposure of samples to uncontrolled atmospheres even for durations as short as a day or two (such as during transit from one institution to another) can result in changes to the mineral distribution. The possibility that such minerals are no longer in their original locations, and may have been mobilised by water-mediated recrystallization within a meteorite sample, must not be ignored.

Clearly, any use of moistened ozone in any attempt to activate the structure of IOM towards tagging must be discontinued. Only dry ozone can be used.

4.4.3. The Use of Organic Solvents in Tagging

A similar phenomenon to that discussed in the previous section might be expected to occur with soluble organic materials, if exposed to solvent vapour, which might also migrate to the surface of a meteorite fragment. This is added justification for avoiding the use of solvents when tagging. It is possible however, that reagents used in tagging (described in Chapter 3) might also act as solvents for meteoritic soluble organic materials. This mobilisation could not, of course, occur with the insoluble IOM, and as the level of soluble organic materials present is expected to be low, this is not likely to be a significant problem. If this is indeed the case, even vapour-phase chemistry may result in mobilisation of the soluble organic components, rendering *in situ* detection impossible.

4.4.4. The Distribution of Organic Material in Murchison

The results obtained from samples of crushed Murchison and Murchison chips confirm the observations of El Amri *et al.* (2005) that IOM appears to be widely distributed over the grains making up the matrix of Murchison, possibly even cementing them together, and forming a coat which is not penetrated by the Raman laser. A similar observation was made by Pearson *et al.* (2007b), who detected organic material both within the matrix and within chondrules rims. Raman spectra of samples of Murchison show the signals due to aromatic carbon, (the D and G peaks), over most of its surface, with little apparent variation. Only when a mineral grain protrudes through this coat (or the mineral, for example, in the form of a chondrule, is uncoated) are signals due to minerals (such as forsterite) seen. Thus, unselective methods such as these will be of limited value in detecting structural variation in the organic materials present in carbonaceous chondrites.

Value will be gained however from determining what (if any) variation exists in the structure and composition of the organic material over the sample surface, thus justifying the original project objectives, namely to develop methodology to determine variations in the proportion of different functional groups across the surface, rather than a non-specific, generic method.

4.5. A Structural Interpretation of Changes Occurring on Ozone Treatment

The reaction of ozone with IOM to give a product, macromolecular in structure, but functionalised with groups such as carboxylic acids, does not seem to have occurred as would have been expected. Raman spectra have shown no evidence for this; no new peaks, or broad bands have been seen which would clearly indicate introduction of new functionality. Prolonged exposure of Murchison to ozone also did not result in its complete decomposition of its organic material. Raman spectroscopy still shows a substantial signal due to aromatic carbon, even after over 200 h exposure.

The fact that oxalic acid is generated rapidly, yet substantial aromatic carbon remains even after 200 h (as shown by the Raman spectrum) implies that IOM contains two structural components. One of these reacts rapidly (to give oxalic acid), whereas the other is much less-reactive, and remains even after 200 h exposure. These reactions are not those predicted for IOM with the structure previously proposed (Derenne and Robert, 2010). Ozone treatment of such a structure would be expected to give a network of oxygenated aromatic fragments, linked with aliphatic chains, which was not obtained. Neither would substantial aromatic carbon be expected to remain after ozone treatment.

It is possible that the presence of the minerals in Murchison may have affected its reactivity to give the observed products (although it is hard to rationalise the formation of a less-reactive aromatic component from a structure such as that shown in Figure 1-3).

As reactivity towards ozone distinguishes the two components, it is likely that the difference in reactivity observed is indeed due to a different structure of IOM. For example, the more reactive component could be made up of relatively electron-rich (or less conjugated) unsaturated systems, with the less-reactive component being the opposite.

To try to understand if an interaction with minerals could be the cause of these differences, and to better understand the structure of IOM in whole rock, a set of reactions of isolated IOM with ozone were carried out. These are described in Chapter 5, with further discussion of the structure of IOM presented in Chapter 7.

4.6. Tagging a Meteorite Sample

The intention of this project was to use reaction with ozone to activate meteoritic organic materials, principally IOM, so that the organic materials could be molecularly tagged with atoms or functional groups aiding detection. The results presented above indicate that meteoritic organic material has not reacted as expected, to generate a complex oxygenated macromolecular material, but to give oxalic acid, as well as macromolecular material which seems to be more resistant to reaction.

To check if carboxylic acids were present (but not giving a diagnostic Raman signal), a fragment of Murchison which had been exposed to ozone for 19 h was subjected to the conditions developed in section 3.9.5 for tagging carboxylic acids with chlorine.

After 68 h treatment (a time which should allow the reaction of any organic acids present) the sample was removed from the reaction vessel and kept in an atmosphere of nitrogen before analysis.

Examination of the sample using both the Raman microscope and SEM (Figure 4-38A and B) showed that it was covered in acicular crystals, distributed over the whole surface of the sample; some of which appeared to have broken off and had fallen onto the adhesive pad. A Raman spectrum of a crystal was acquired (Figure 4-39) but its structure could not be identified. It is neither oxalic acid, nor any of the reagents used in tagging (which are all liquids). On examination by EDS, no chlorine could be detected in these crystals, which appeared to be fragile under the electron beam. In Figure 4-40, images are shown before (A) and after (B) mapping; the damage to the crystals is clear. On mapping, a clear distribution of carbon could be seen (Figure 4-40C), but chlorine appeared as a low level, background signal. This material is still unidentified, but may be a derivative of oxalic acid, and so distributed all over the surface

This indicates that either the tagging reaction, although proven with meteorite models, (*e.g.* carboxylic acids supported on rock samples) did not function using a sample of meteorite, or, more likely, that the reaction of IOM with ozone did not introduced the expected functionality into meteoritic organic material. Work to understand if the latter is the case is described in the next chapter.

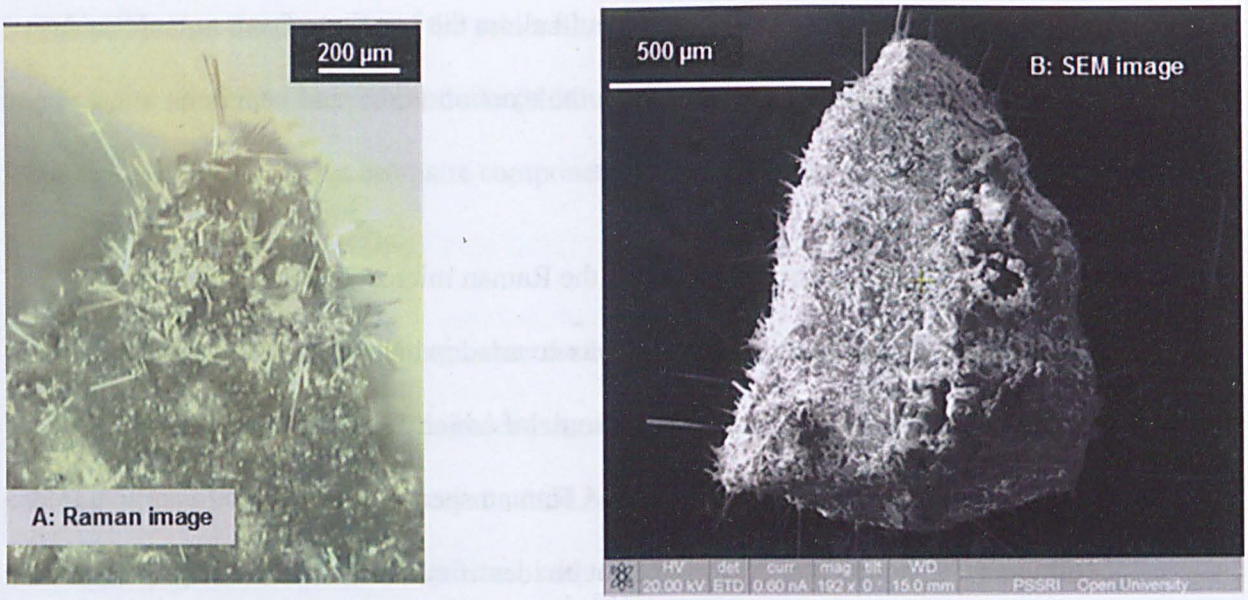

Figure 4-38: A) Raman and B) SEM images of sample of Murchison after ozone activation and tagging showing presence of new crystals

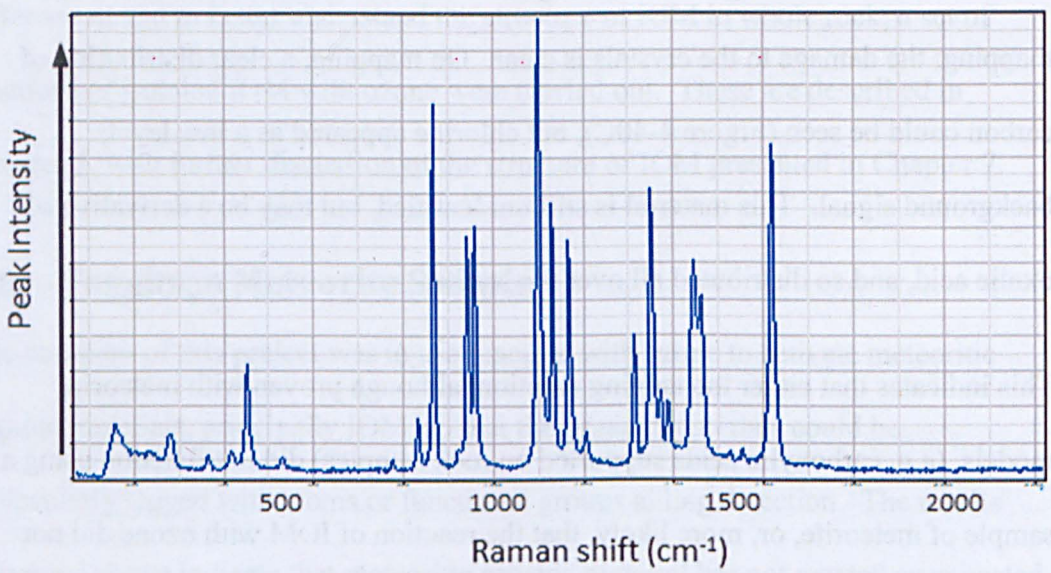

Figure 4-39: Raman spectrum of new crystal

Figure 4-40: SEM images of sample A) before and B) after mapping, and C) carbon map showing damage to new crystals following exposure to the electron beam

4.7. Conclusions

Detection of organic material in Murchison was not difficult; non-specific analysis, by Raman spectroscopy, showed that organic material is widespread over the surface of Murchison samples.

To understand if specific associations of organic materials with minerals exist, or not, it is therefore necessary to develop specific methods for these materials, which is the objective of this project. Selective molecular tagging will enable the distribution of structurally-dissimilar organic components to be determined, and any associations with minerals identified.

Development of such selective tagging methods are reliant on understanding the structure of the organic material being tagged, namely IOM, the major component.

Reaction with ozone was intended to introduce extra functionality into meteoritic organic materials, thus enabling a higher density of tags to be introduced, but the results were not as expected. Rather than giving a functionalised network connected by aliphatic chains, organic materials in samples of Murchison reacted to give oxalic acid, as well as a significant proportion of material apparently resisting further reaction (and showing high levels of signals in its Raman spectra due to aromatic carbon). In addition, the action of water vapour, causing formation of gypsum on the sample surfaces, shows that any future attempt to activate IOM can only use ozone if dry.

This observation may also imply that soluble organic materials (but not the insoluble IOM) may be mobilised by the presence of organic vapours, rendering their detection *in situ* impossible when using the tagging methodology developed, and described in Chapter 3. As IOM is the major component of meteoritic organic materials, tagging methodology is still appropriate for its detection.

This observation, although possibly due to some interaction of the organic and inorganic components of Murchison, is more likely to be due to the structure of IOM differing from that previously supposed. In any case, it is necessary that more information is gained on the structure of IOM so that the mechanisms and outcomes of its reactions with tagging reagents can be predicted. For that reason, IOM isolated from Murchison was studied in a similar way to the whole rock as described in this chapter. This work is described in Chapter 5.

Chapter 5 Analysis and Ozone Treatment of IOM

The results obtained when samples of Murchison were exposed to ozone were described in Chapter 4. As IOM was believed to have a structure composed of small aromatic systems linked by aliphatic chains, based on its predicted reactivity, the formation of oxalic acid as the only identifiable organic product was unexpected. This may be because the actual structure of IOM differs from that proposed, for example as shown in Figure 1-3, as it is hard to see how ozone treatment of such a structure would generate only oxalic acid.

It is also possible that the presence of the minerals making up the majority of the meteorite sample have altered its reactivity in some way. If the structure is as shown in Figure 1-3, it is not clear how the presence of minerals could have had the effect of causing ozone treatment to generate oxalic acid. In addition, after prolonged ozone treatment, a residual part of IOM, resistant to ozone treatment but still containing aromatic carbon (seen in the Raman spectrum) remains; no clear mechanism could be proposed for its formation by some mineral-mediated transformation of a structure such as that shown in Figure 1-3.

To gain more information on the structure and reactivity of IOM in the absence of minerals, the effects of ozone on IOM which had been isolated from Murchison by demineralisation were investigated. The results are reported and discussed in this chapter.

5.1. The Isolation of IOM by Demineralisation

The demineralisation procedures used to isolate IOM from meteorites are based on methods originally employed to isolate organic material (kerogen) from terrestrial

organic-bearing rocks (Durand and Nicaise, 1980) Soluble organic compounds are first removed by extraction with one or more solvents. The first stage of demineralisation is to treat the meteorite sample with dilute mineral acid, to remove minerals such as carbonates and oxides, as well as any silicates which are readily hydrolysed, although the bulk of the silicate minerals survive this procedure. The second stage makes use of the reactivity of silicates, such as olivine, pyroxene or clays, with hydrofluoric acid (HF), the effect of which is to form fluorosilicates, which are soluble in water, or mineral acid (Kline and Fogler, 1981) . As IOM is insoluble in water, it can then be isolated from the solubilised minerals by filtration or centrifugation.

A sample of IOM, previously isolated from Murchison, was available (having been prepared for a previous project). Practical details for the procedures used in its isolation are given in the Appendix.

5.2. Sample Preparation

The sample (designated 2DAB) had been generated by demineralisation using the procedure of Amari *et al.* (1994) and was processed further (as described in the Appendix) to remove remaining minerals, by treatment with hydrochloric acid. This produced a sample designated 2DAH which had the appearance of a free flowing, black powder.

Using a spatula, samples for analysis by SEM were placed on an adhesive pad fixed to an aluminium stub. These samples could also be analysed by Raman spectroscopy, with the stub held in a suitable holder (see section 2.1.2). If only Raman spectroscopy was performed, samples were placed directly onto an aluminium stub (without adhesive, so it could then be re-used). Samples were

exposed to ozone using the apparatus described in section 3.5.2, (Procedure B1), with IOM being placed on aluminium stubs, or watch glasses, before being placed in the reaction flask.

5.3. The Reaction of IOM Isolated from Murchison with Ozone

Sample 2DAH was exposed to ozone in the same manner as the chips of whole-rock Murchison described in Chapter 4. The results obtained are discussed in this section.

5.3.1. Characterisation Before Exposure to Ozone

An examination of 2DAH using both SEM and Raman microscopy showed that the grains forming the majority of the sample 2DAB (prior to treatment with hydrochloric acid) and believed to be magnesium fluoride, had been removed, and that the residue now appeared dark, and amorphous in appearance. Prior to acid treatment, EDS showed strong signals due to co-located magnesium and fluorine against a background of carbon (due to the adhesive pad holding the sample onto the stub), as shown in Figure 5-1B. After acid treatment, the SEM image showed the sample to have become less-fluffy in appearance (Figure 5-2A), and by EDS, only a few small grains containing magnesium and fluorine (showing as cyan in colour) could be seen (Figure 5-2B). Low level signals due to magnesium (and carbon) were seen, but were not well-correlated with individual grains. Other common rock-forming elements were present only at very low levels, and a good-quality element map could not be obtained, indicating that all remaining minerals had substantially been removed. The images acquired using the Raman microscope (Figure 5-3C and D) showed a mass of dark, featureless grains, barely resolved even using the highest magnification objective, with brighter inclusions, probably residual small mineral grains. Raman spectra were obtained (Figure 5-3E), the spectra being dominated by

the D and G peaks, as for whole-rock Murchison, with no new signals having appeared.

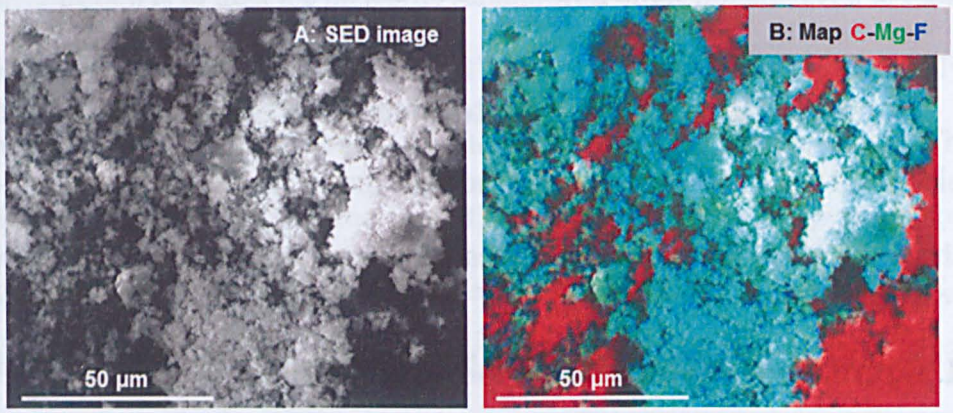

Figure 5-1: A) SEM image and B) element map of sample 2DAB. The map shows fluorine and magnesium co-located (the carbon signal is derived from the adhesive pad)

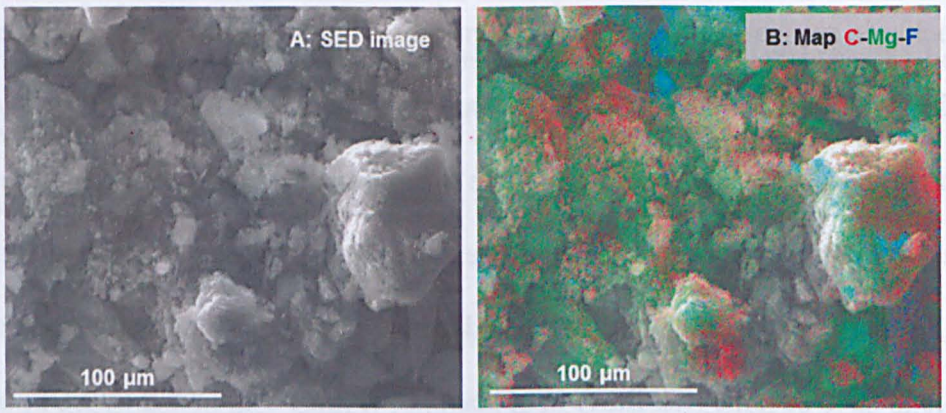

Figure 5-2: A) SEM image and B) element map obtained from sample 2DAH (after acid treatment). The strong signal from magnesium and fluorine seen in the element map has been replaced with a diffuse, low-level signal showing mineral grains have been removed.

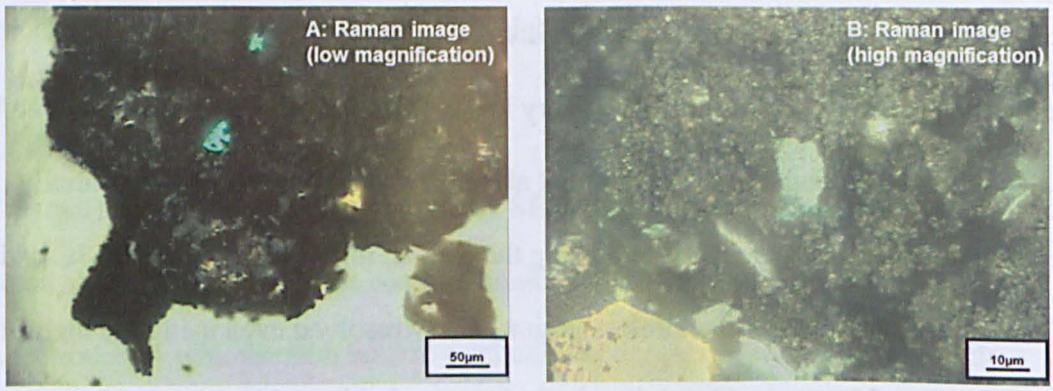

Figure 5-3: Raman microscope images of sample 2DAH at two different magnifications

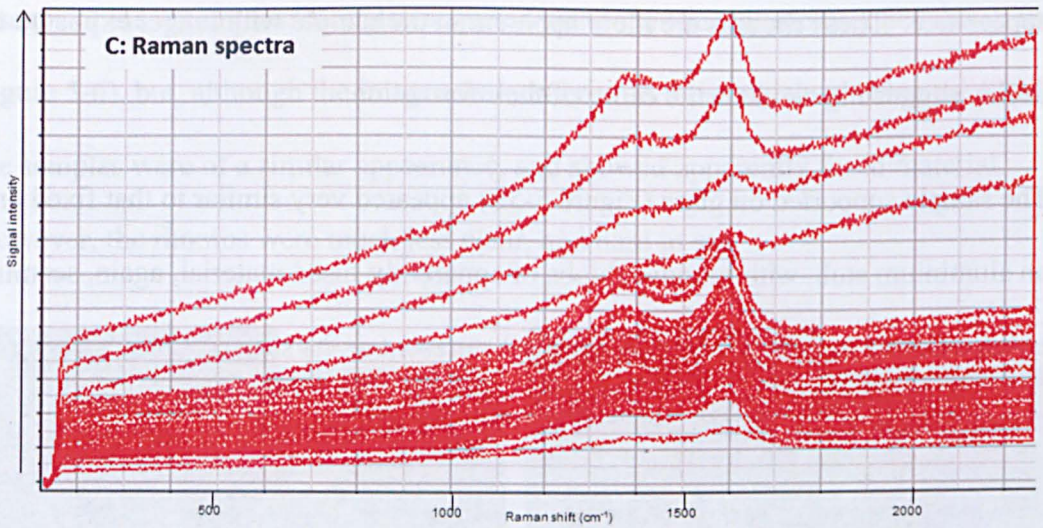

Figure 5-4: Raman spectra of sample 2DAH.

5.3.2. The Effect of Exposure to Ozone

Two portions of sample 2DAH were mounted on adhesive pads fixed to separate aluminium stubs, and were exposed to ozone, the first for 2 h, and the second for 16 h. To confirm any reaction seen was not due to some interaction with the carbon-based adhesive, a third sample was placed on a watch glass, (not mounted on a stub) and also exposed to ozone for 16 h. The three samples were analysed using SEM and Raman microscopy and spectroscopy.

Appearance of the samples after ozone treatment

Whereas the sample exposed for only 2 h did not look to have changed appreciably (by eye), the grains making up both samples exposed to ozone for 16 h appeared to have fused, as if the sample had melted. The samples were examined by SEM and Raman microscopy; both techniques confirmed these changes in appearance. SEM showed the samples after 2 h (Figure 5-5A and B) to still consist of individual particles, which now appeared fused together, whereas after 16 h (Figure 5-5C and D), the particles appeared to have completely fused into one another, with the IOM appearing to have flowed across the sample holder. The SEM images showed what seemed to be crystalline grains, rhombs, embedded in a matrix of amorphous

appearance. These rhombs are more apparent in the sample with longer exposure to ozone, suggesting ozone is the cause of their formation.

The sample supported on glass (Figure 5-5E) appeared very similar to that fixed on an aluminium stub, with roundish blobs of apparently fused material, again, seeming to have flowed across the glass, with rhombs present on its surface. This shows that these changes are not due to any reaction with the adhesive pad.

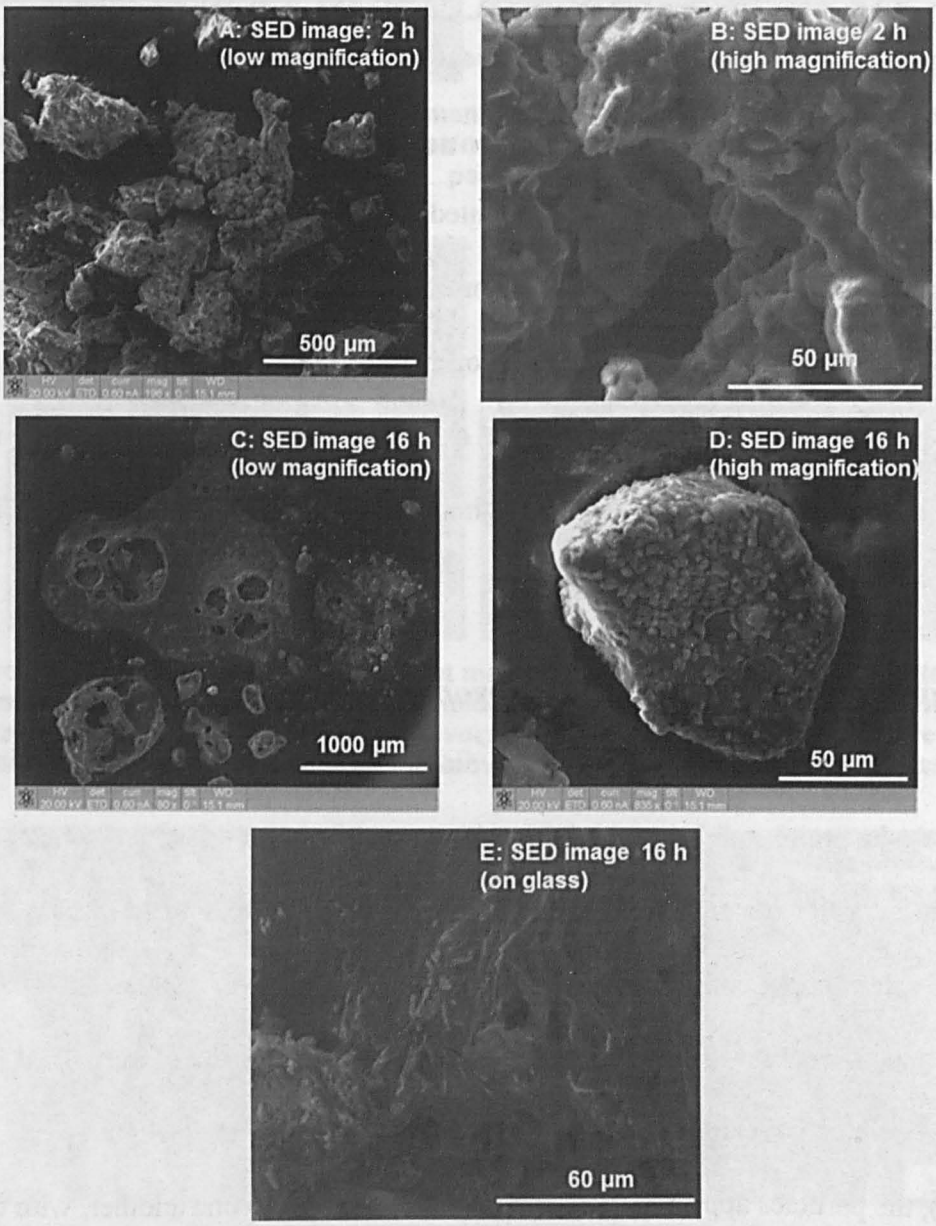

Figure 5-5: SEM images of 2DAH after 2 h (A and B) 16 h (C and D) exposure to ozone, supported on a stub, and after 16 h on glass (E)

Images of these samples were also acquired using the Raman microscope (shown in Figure 5-6), but, although the images were inferior to those obtained using the SEM, the samples were of a similar appearance, and showed apparently fused material. However, the rhombs were much less clear, and hard to see.

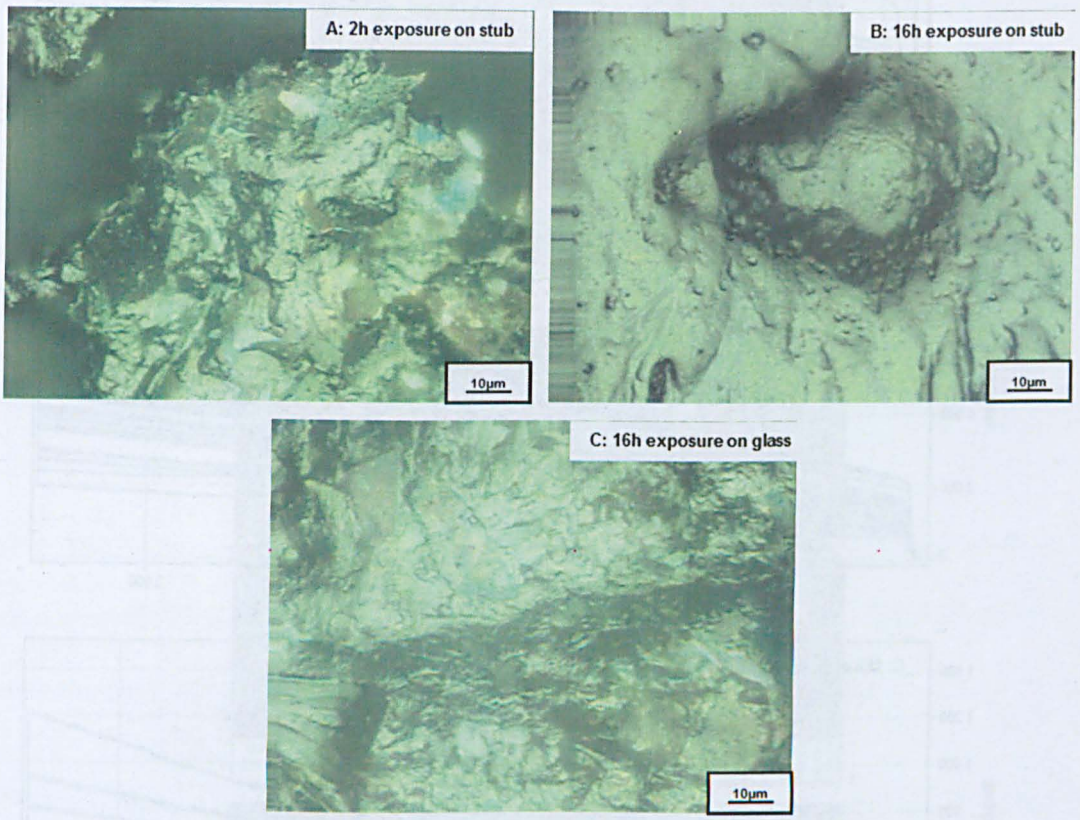

Figure 5-6: Raman microscope images of 2DAH after 2 h (A) 16 h (B) exposure to ozone, supported on a stub, and after 16 h on glass (C)

Raman spectra were acquired from the three samples (Figure 5-7) and all appeared similar, showing the D and G peaks as the dominant features. Signals due to minerals such as gypsum, or the oxalate-containing grain giving a signal at 1470 cm^{-1} (section 4.3.2) were not seen, supporting the previous conclusion that the latter signal was derived from the product of a reaction between oxalic acid and one (or more) of the minerals present in Murchison, and that gypsum (or minerals containing calcium and sulfate from which it was formed) was already present in Murchison (and now removed).

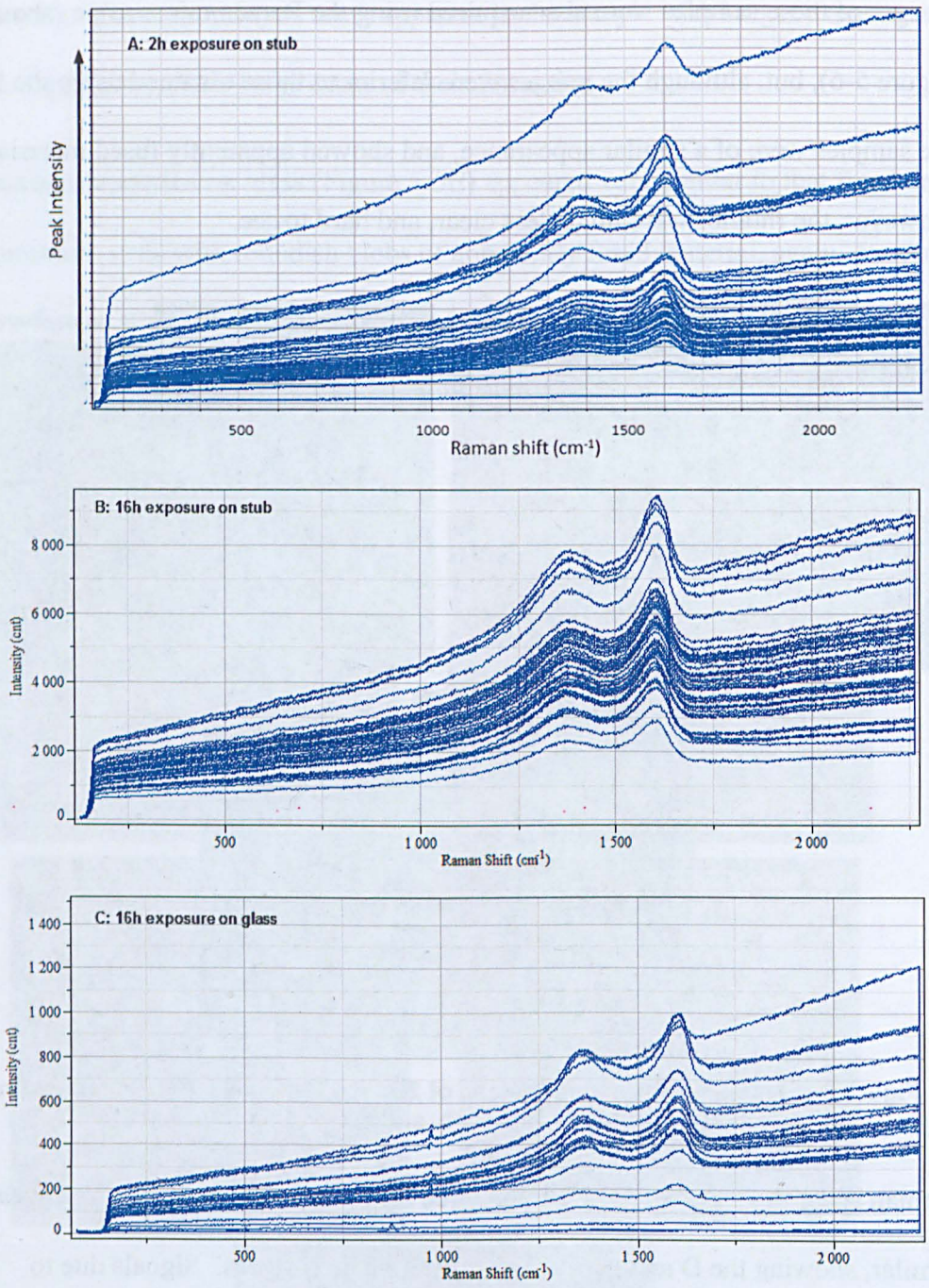

Figure 5-7: Overlays of Raman spectra of demineralised Murchison after exposure to ozone showing no significant new signals despite physical changes

Analysis of the rhombs

Acquisition of an SEM image of a rhomb proved difficult, the structure being unstable in the electron beam. Better images were obtained using FEGSEM (which generates a beam of lower electron energy, as described in section 2.2.2), but disintegration could be seen occurring as the images were being acquired, the rhombs

taking on a honeycombed appearance. Figure 5-8 shows a sequence of images taken over about ten minutes.

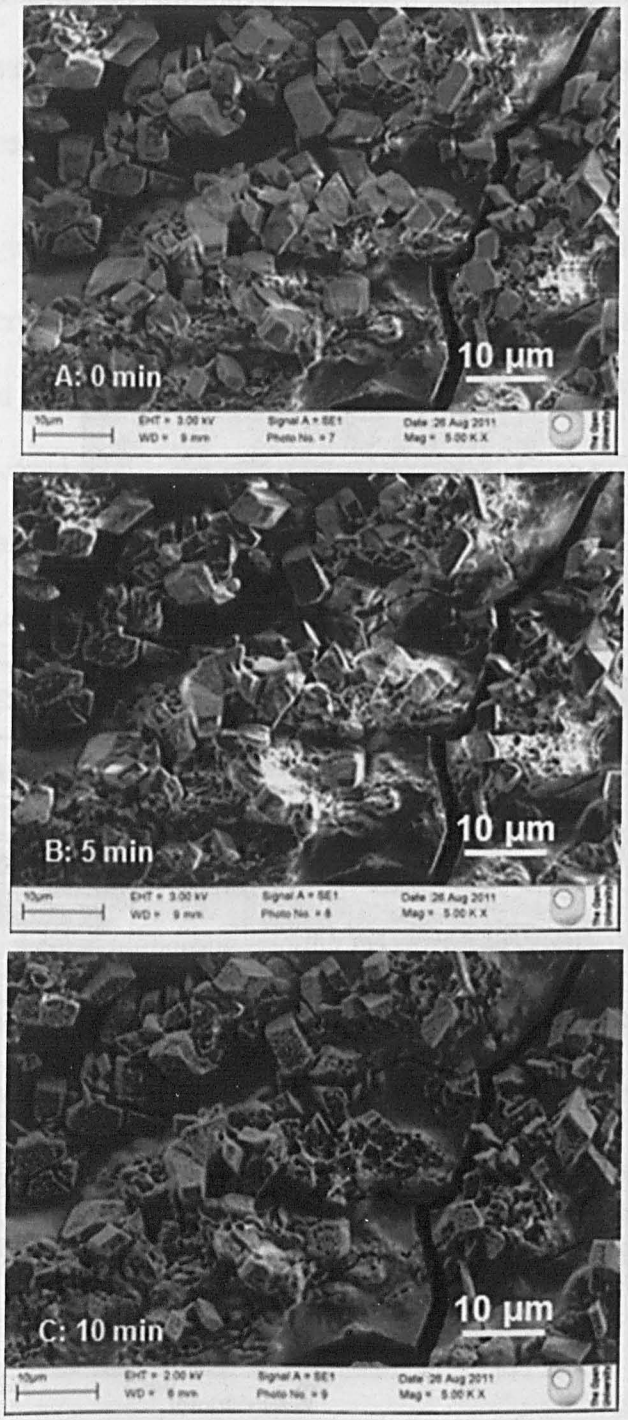

Figure 5-8: FEGSEM images showing increasing effect of electron beam with time, on the rhombs

The sample was re-examined using the Raman microscope, and an area containing rhombs was imaged (Figure 5-9A). The rhombs could be recognised, although the

image was indistinct. A set of Raman spectra was acquired over this region (Figure 5-9B), showing a similar appearance to that obtained previously, being predominately the D and G peaks. A spot spectrum was obtained of one of the rhombs (Figure 5-9) which showed a small peak at 840 cm^{-1} (unidentified at this stage), although the spectrum was still dominated by the signal due to aromatic carbon.

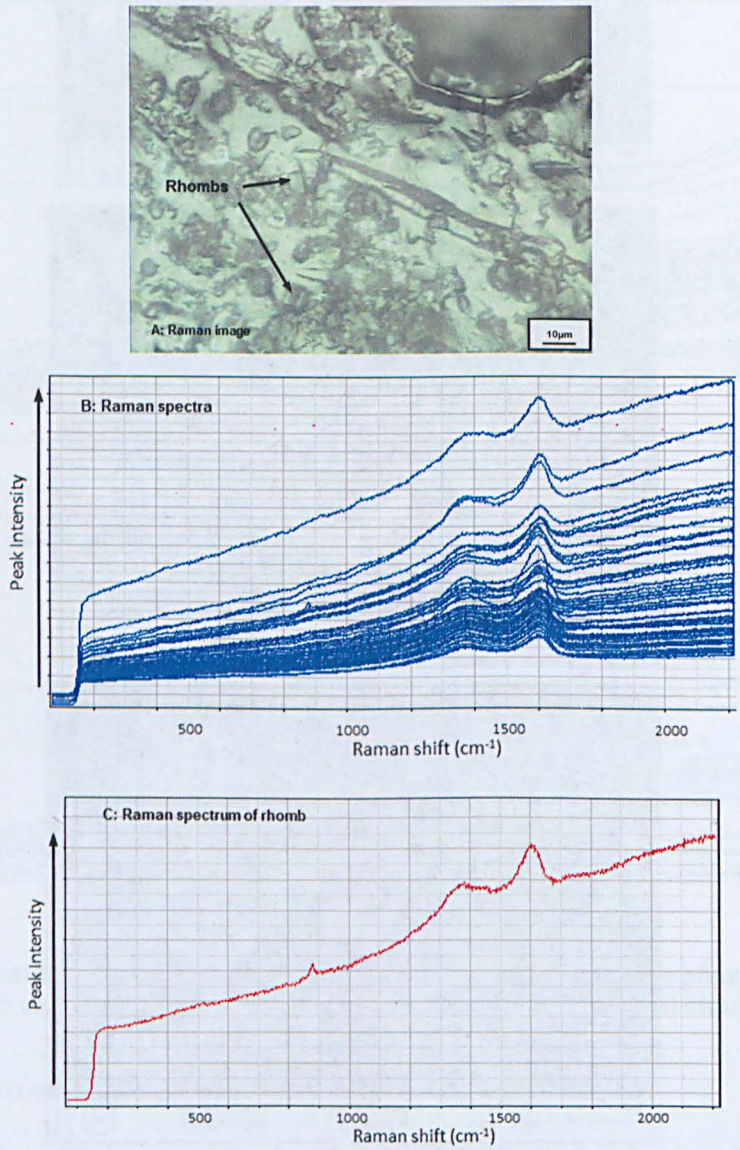

Figure 5-9: Raman microscope image (A) showing rhombs, and Raman spectra of (B) (overlays of several spectra across the sample surface) and (C) of a single rhomb

Stability of IOM after ozone treatment

All three samples were stored at ambient temperature and pressure, in the dark. Reanalysis was carried out after four, six and eight weeks; the sample which had not been exposed to ozone was also monitored, but no changes were seen, in either its spectra or appearance.

In the sample originally exposed to ozone for only two hours, after four weeks storage, acicular crystals had formed on the surface of the adhesive pad (Figure 5-10A and B), although the rhombs present in the bulk of the sample did not seem to have increased in number. These acicular crystals also proved to be fragile in the electron beam; after collecting X-ray data to generate a map (Figure 5-10C), the crystals had clearly been partially destroyed (Figure 5-10D). An EDS element map showed the presence of carbon (in both the sample and the adhesive); the only other element detected in the crystals was oxygen. This, and the fragility of the crystals, indicates they are probably an organic compound.

After a total of six weeks, numerous acicular crystals could be seen on the surface of the adhesive, spread around the sample (Figure 5-11A). No more changes were seen after another two weeks; the image of the sample surface in (Figure 5-11B), after eight weeks storage, appeared similar to that originally acquired.

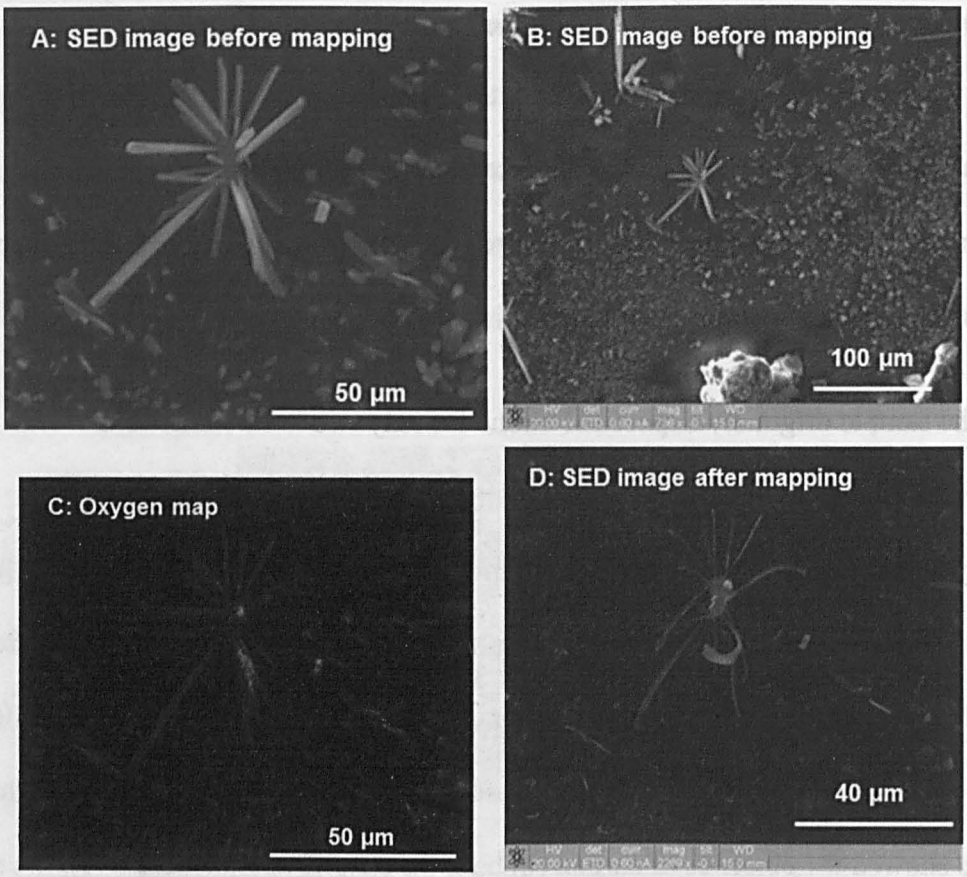

Figure 5-10: SEM images after 4 weeks (A and B), Oxygen map (C) and SEM image after mapping (D), showing damage to the crystals with electron impact

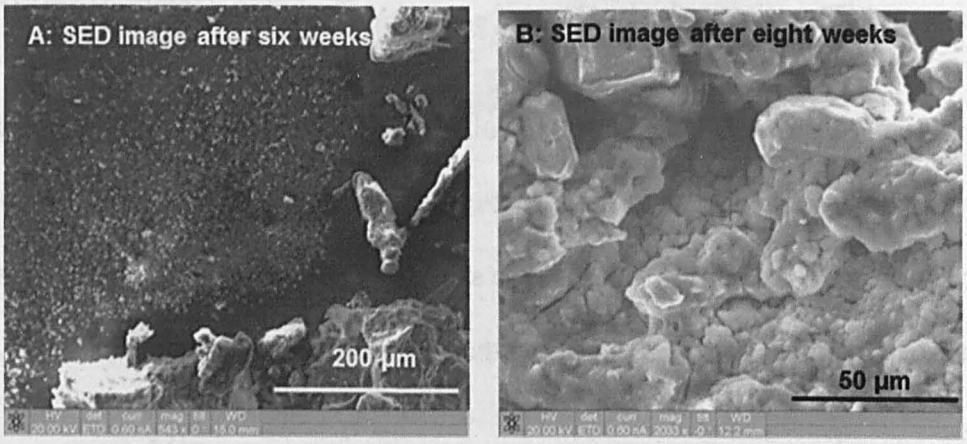

Figure 5-11: SEM images after A) six or B) eight weeks storage showing changes in appearance of the surface

The two samples exposed to ozone for 16 h had shown a greater surface density of rhombs, indicating these were likely to have been formed by reaction of the sample with ozone. After storage for three weeks, the rhombs covered the surface of the whole sample. In Figure 5-12A, the fused nature of the surface is obvious, and the

rhombs can be seen embedded in its structure. These rhombs are clearly seen in the higher magnification image, Figure 5-12B. Acicular crystals were also seen in these samples, being very easy to see in the sample supported on glass. Images taken using an optical microscope (Figure 5-13), show numerous transparent crystals surrounding an opaque spot of IOM.

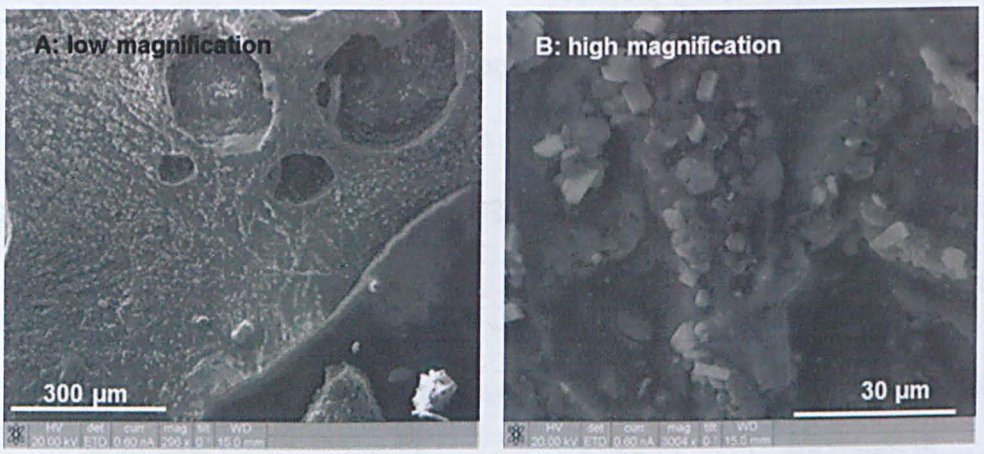

Figure 5-12: Sample of IOM exposed for 16 h and left for 3 weeks

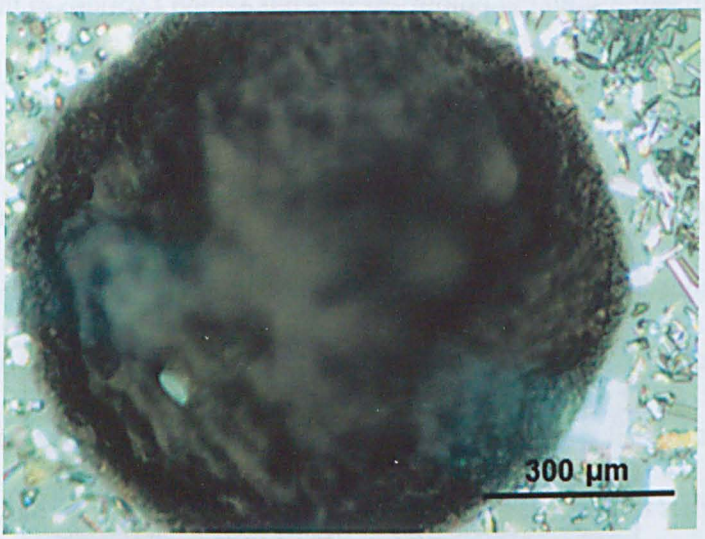

Figure 5-13: Sample on glass under optical microscope (X2.5 and X20 objectives)

The crystals seen in the optical image of this sample appeared to have formed at the edges of the portions of IOM, resting on the glass rather than the organic material. These crystals could easily be located in the Raman image (Figure 5-14) and a

spectrum was acquired (Figure 5-15A). Although this spectrum also contains signals due to aromatic carbon, the peak at 840 cm^{-1} (seen as a weak feature previously, in Figure 5-9C) is strong, indicating this was indeed related to the crystals.

Comparison with a library spectrum (Figure 5-15B) indicated these crystals are likely to be oxalic acid, previously proposed as the source of mineral grains formed in a sample of Murchison on exposure to ozone (section 4.3.2). In this demineralised sample, there is no opportunity for oxalic acid to react with any minerals, and so the grains seen in previous samples (which gave a Raman signal at 1470 cm^{-1}) cannot form.

It seems likely therefore that oxalic acid was generated on exposure to ozone, generating rhombs within the IOM, as it formed. On standing, oxalic acid appears to have recrystallised, giving the colourless crystals which formed on the edges of the particles of IOM.

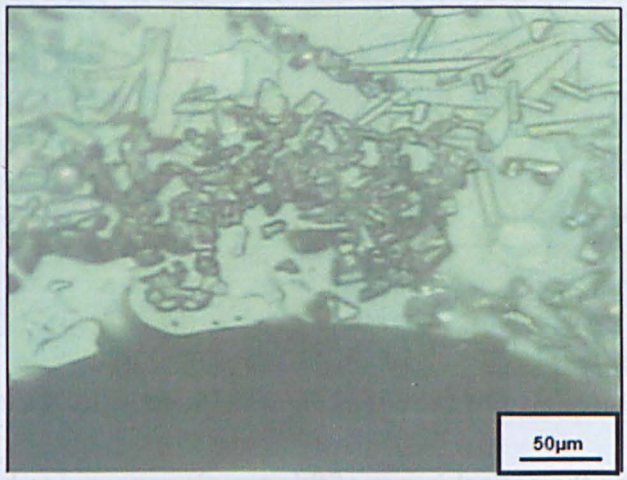

Figure 5-14: Raman microscope image obtained of crystals seen in the sample exposed for 16 h on glass

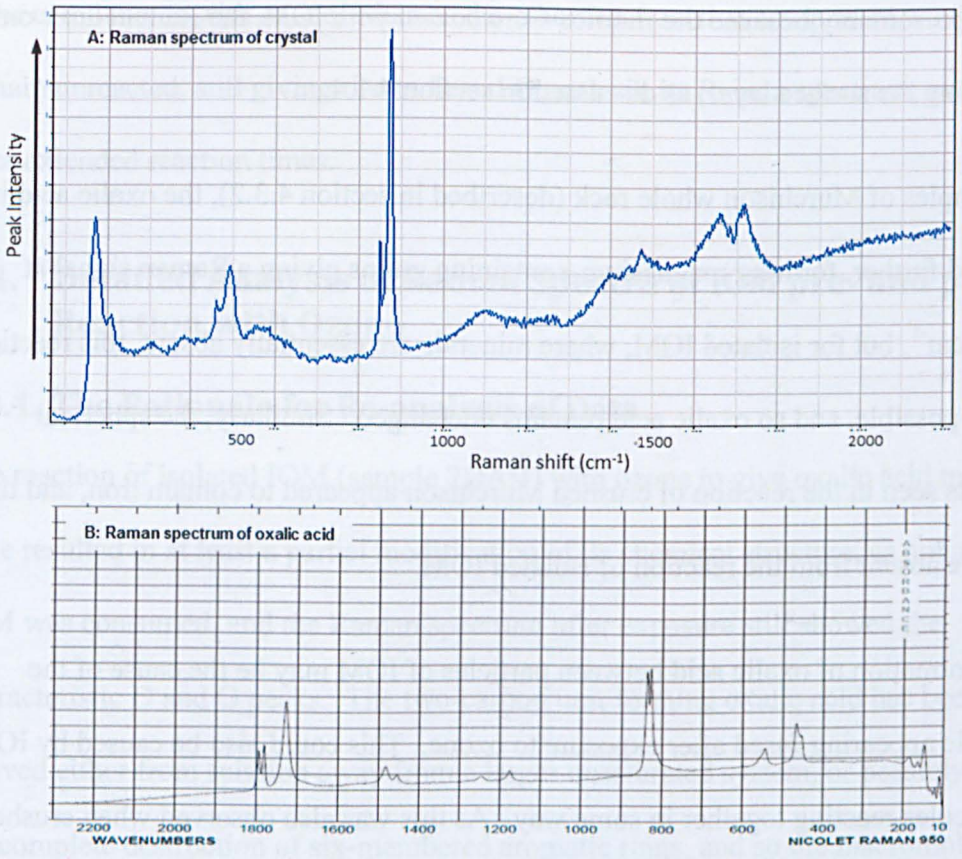

Figure 5-15: Raman spectrum of A) crystal and B) oxalic acid (B, from Sigma Aldrich library, note frequency scale is in opposite direction)

5.3.3. Summary and Conclusion

In the absence of minerals, the effects of ozone on IOM isolated from Murchison could clearly be seen. The grains of organic material appeared to become fused together after only two hours exposure to ozone, and much more so after 16 h. Rhombs appeared on the surface of the samples; these were easily destroyed by electron impact, and so likely to be organic. A Raman spectrum of a rhomb showed a new, weak peak, which is also seen in the spectrum of oxalic acid. On standing, acicular crystals appeared in the samples. These too were fragile, (so also likely to be organic), and gave a Raman spectrum very similar to that of oxalic acid. These results are consistent with the conclusions drawn following the reaction of Murchison whole rock with ozone (see section 4.3). The spectrum of oxalic acid was

weak presumably because the rhombs were coated with IOM, the Raman laser only sampling the surface layer, as discussed in section 4.1.4.

In samples of Murchison whole rock (described in section 4.3.2), the oxalic acid had reacted further, forming magnesium-containing grains giving a Raman signal at 1470 cm^{-1}, but for isolated IOM, where minerals are essentially absent, this reaction is not possible, and so oxalic acid remains unchanged. Similarly, the spherical objects seen in the reaction of crushed Murchison appeared to contain iron, and these too are absent from the reaction of isolated IOM.

The formation of oxalic acid between particles of IOM may be the cause of the sample appearing fused after exposure to ozone. This could also be caused by IOM molecules reacting together in some way. As this was also observed when crushed Murchison was exposed to ozone, the fusing is not likely to be a result of any reaction occurring with the minerals present.

As the chemistry occurring in isolated IOM is the same as that in whole rock, (namely, the formation of oxalic acid) these observations imply that the reaction of IOM with ozone has not been influenced by the minerals present in whole rock Murchison, but only that, in the demineralised samples, there is no scope for the oxalic acid formed to react further. Also, although the main, identifiable product of reaction of IOM with ozone is oxalic acid, Raman spectra (of Murchison whole rock and of isolated IOM, after ozone treatment) indicate that the samples still contain substantial amounts of IOM (or some modified version of it); the Raman spectra are dominated by the D and G peaks. This supports the earlier suggestion (section 4.5) that IOM contains a component that is more reactive towards ozone, and another that is less-so (or unreactive). Oxalic acid would be derived by the reaction of one of

these components with ozone, whereas the other less-reactive component would remain unreacted, still giving rise to D and G peaks in its Raman spectrum, even after extended reaction times.

5.4. Detailed Analysis of Raman Spectra of IOM pre- and post-Reaction with Ozone

5.4.1. The Rationale for Re-analysis of Data

The reaction of isolated IOM (sample 2DAH) with ozone to give oxalic acid must have resulted in at least a partial modification of its chemical structure, as not all the IOM was consumed, and the Raman spectrum after exposure still showed the characteristic D and G peaks. The two-carbon unit forming oxalic acid has been derived either from scission away from a larger unsaturated system, or possibly by the complete destruction of six-membered aromatic rings, and so the macromolecular material remaining cannot have the same structure as before.

The Raman spectrum of IOM after reaction is still dominated by the D and G peaks typical of an extended aromatic system (such as that shown in Figure 1-3 and Figure 1-6), so it seems that, rather than disrupting it completely, reaction with ozone can only have partly modified the structure of IOM. As large, extended conjugated systems are less-reactive to ozone than small ring systems (up to four or five aromatic rings), as described by Bailey, (1958), and in section 3.10.6, this result may indicate that IOM contains a higher proportion of large, extended aromatic systems (and fewer small-ring units) than previously presumed, and suggests that, in fact, IOM may consist of regions of different reactivity, that is some regions more reactive towards ozone (containing small ring-systems), and others less so (an extended, conjugated ring system).

A modified aromatic system would be expected to give a Raman spectrum different from that seen prior to reaction with ozone, but, in a complex Raman spectrum composed of many overlapping signals resulting in broad peaks, such as the D and G peaks of IOM, these differences may only be apparent as changes in the positions of these broad peaks, rather than the appearance of new, distinct, signals. The overall appearance of the spectra before and after treatment would still be similar.

5.4.2. The Effect of Ozone Exposure on the Raman Spectrum of IOM

To determine if any such differences could be seen, Raman spectra generated from isolated IOM before, and after ozone treatment were re-analysed. Using the data processing methods described in section 2.1.2, the positions of the main signals (the D and G peaks) due to aromatic carbon were extracted from the spectra, and plotted on a graph, shown in Figure 5-16. A clear trend was seen, with the frequency of the D peak decreasing, and the G peak increasing, with increasing exposure to ozone. The data for IOM exposed to ozone whilst supported on glass fall into the same region as for IOM fixed with carbon adhesive; the shift in peak position is therefore not caused by some reaction with the adhesive. Other correlations, for example between the areas of the two peaks, or the peak widths, were examined, but were less clear, and were not routinely investigated.

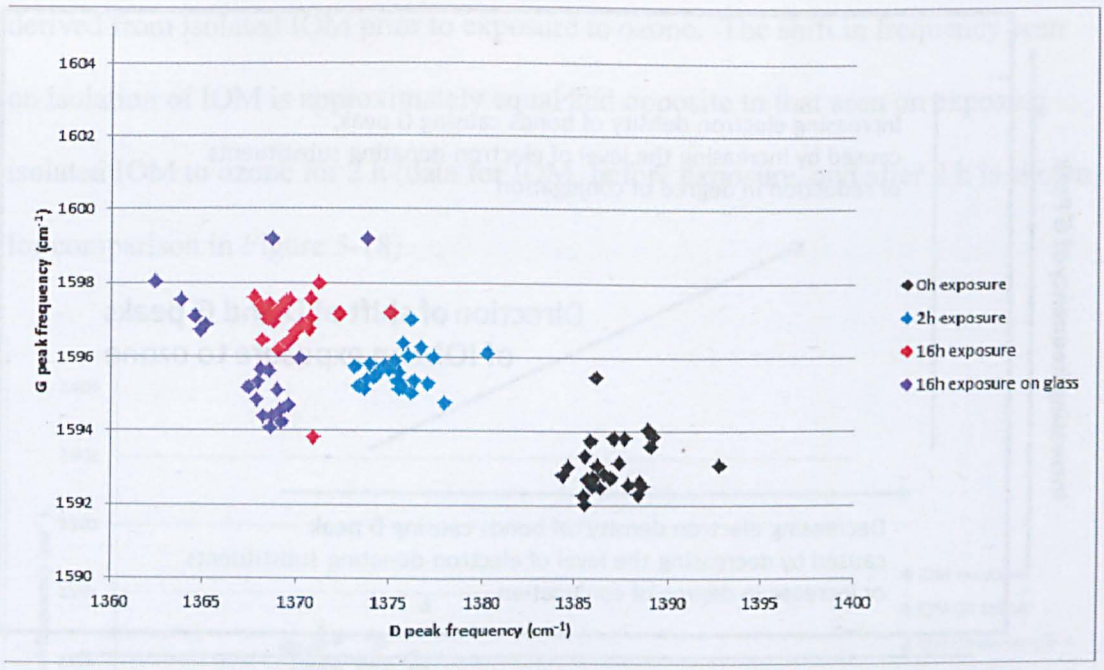

Figure 5-16: Raman peak positions obtained from IOM (2DAH) after exposure to ozone for 0 h, 2 h and 16 h

Interpretation of these changes

The frequency of the bond(s) giving rise to a Raman shift is the same as the shift observed. Thus, if the shift changes (as it does on exposure to ozone), then the frequencies of the bonds giving rise to the Raman peaks have also changed. As the bond strength increases, so its frequency of vibration increases. In organic molecules, an increase in the strength of a bond is caused by increased electron density between the vibrating atoms, and is therefore caused by changes either donating electrons into the bond, by introduction of an electron-donating substituent, or alternatively, reducing the amount by which electron density had previously been reduced (for example, by conjugation into an adjoining unsaturated system). These relationships are shown schematically in Figure 5-17.

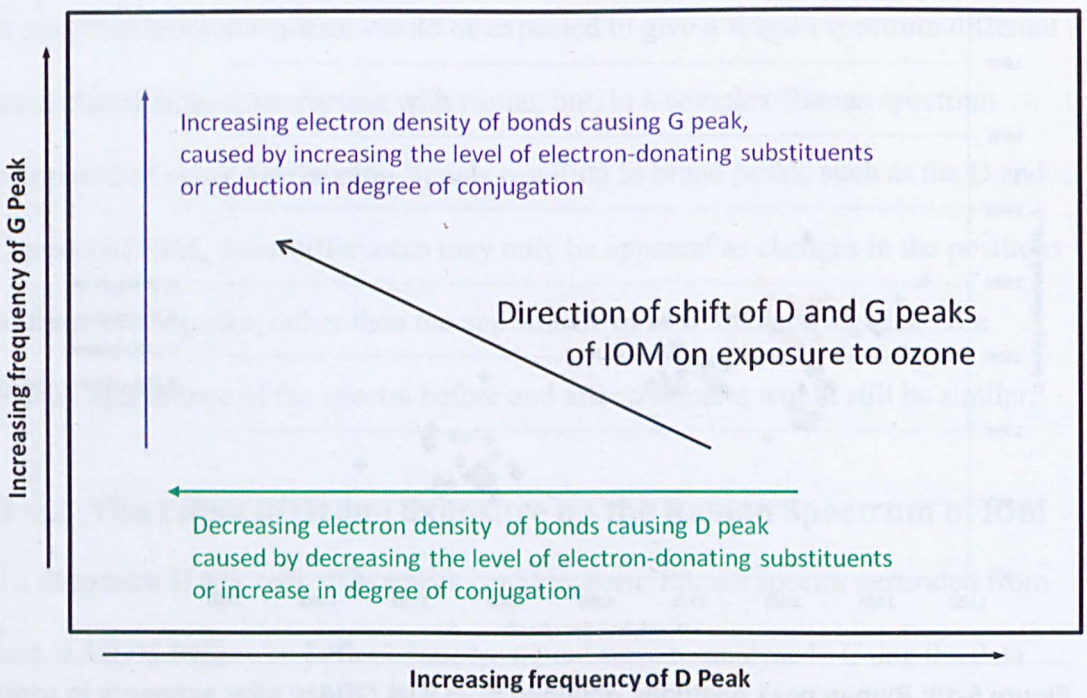

Figure 5-17: Schematic showing the relationships between Raman shift and changes in electron density. Increasing electron donation, or reduced level of conjugation reduces the frequency of bond vibration

Thus, as can be seen in the diagram above, exposure of IOM to ozone has resulted in a shift of its G band to higher frequencies, thus implying an increase in bond strength, whereas the frequency of the D band has decreased, implying a decrease in bond strength. The bonds giving rise to the G bond have therefore undergone an increase in electron-donating substitution (or a decrease in electron-withdrawing), whereas the D bonds have undergone the reverse.

5.4.3. Effect of Ozone Exposure on Raman Spectra of Murchison Whole Rock

To further explore these changes, a similar comparison was carried out, using the data obtained from samples of Murchison whole rock, rather than isolated IOM. Raman spectra of three chips of Murchison (Samples A, B and C, obtained from the OU collection) were processed in the same way as described above, and plotted on a similar graph (Figure 5-18). The result was surprising; although data for the three whole rock samples was similar, it did not lie in the same part of the graph as data

derived from isolated IOM prior to exposure to ozone. The shift in frequency seen on isolation of IOM is approximately equal and opposite to that seen on exposing isolated IOM to ozone for 2 h (data for IOM, before exposure, and after 2 h is shown for comparison in Figure 5-18).

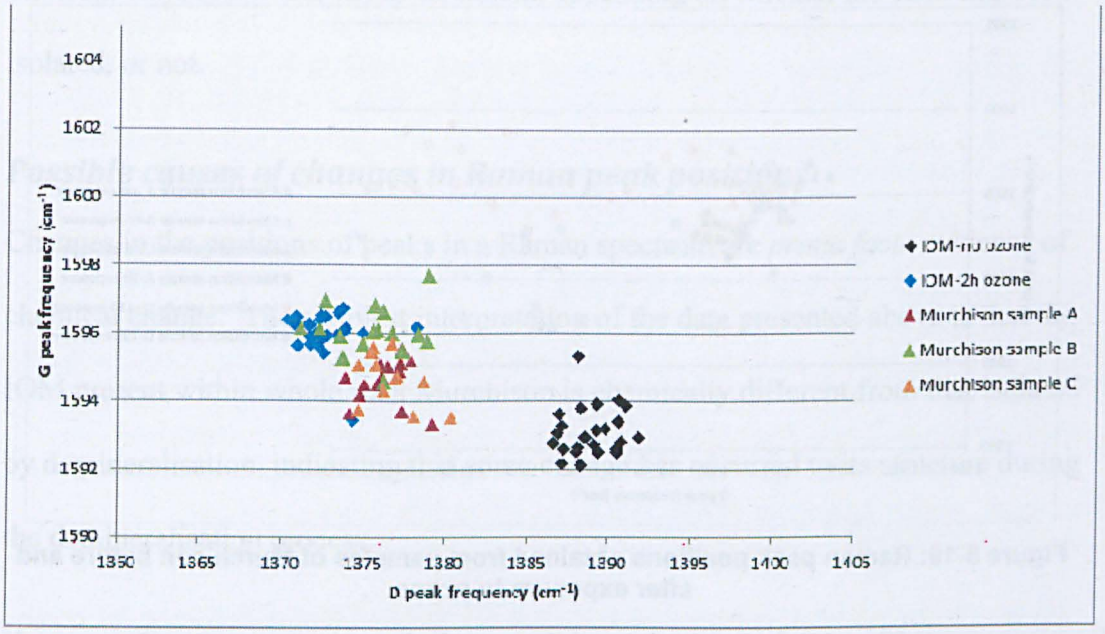

Figure 5-18: Raman peak positions obtained from samples of Murchison, compared with IOM

Another unexpected result was obtained when data obtained following exposure of Murchison fragments to ozone was re-examined. The scatter of this data was rather more pronounced than for the other samples, as spectra were complicated by the presence of peaks such as that at 1470 cm^{-1} (see section 4.3.2), and were rather noisy. However, when the data was plotted (Figure 5-19), it can be seen that the effect of ozone on the Raman signals of organic materials *in situ* within the meteorite has caused the peaks to move broadly in the opposite direction to that seen for isolated IOM, although the changes in the position of the G peak are much less than for the D peak. Not all the fragments shown in Figure 5-18 were exposed to ozone, so a direct comparison of all samples before and after exposure could not be made. Nevertheless, as the samples exposed to ozone for longer times (16-19 h) show

greater shifts in signal positions than that exposed for only 2 h, the differences between samples seem relatively minor in comparison, and the results shown seem to be characteristic of Murchison itself, rather than a specific atypical sub-sample. The shifts seen in all these samples are summarised schematically in Figure 5-20.

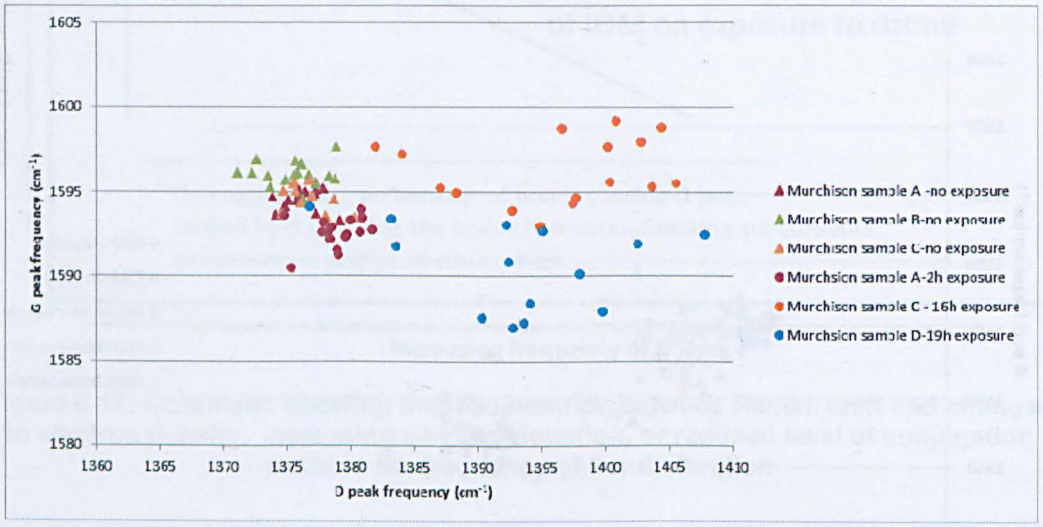

Figure 5-19: Raman peak positions obtained from samples of Murchison before and after exposure to ozone

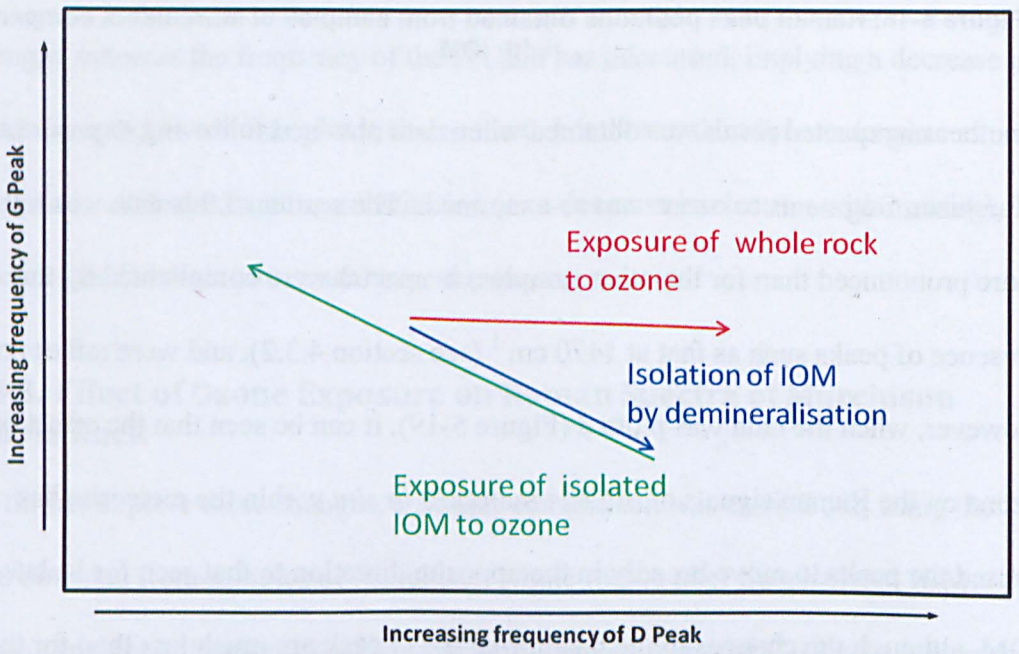

Figure 5-20: Comparison of shifts in Raman spectra on demineralisation and ozone exposure. Peak shifts and sample descriptions are shown in the same colour

5.4.4. Interpretation of these Results

In summary, the data has shown that the positions of the peaks in the Raman spectrum due to organic materials still present in whole rock, and in IOM after isolation, are different, and also, that the positions of the peaks due to IOM change in different ways following ozone treatment, depending on whether the IOM has been isolated, or not.

Possible causes of changes in Raman peak positions

Changes in the positions of peaks in a Raman spectrum are *prima facie* evidence of chemical change. The simplest interpretation of the data presented above is that the IOM present within whole rock Murchison is chemically different from that isolated by demineralisation, indicating that some change has occurred to its structure during the demineralisation process.

However, there are a number of other possible explanations for the effects seen. Murchison is not homogenous, and it is possible that the whole rock sample and the sample of IOM are derived from distinctly different portions of the meteorite. The sample of IOM was prepared from a fragment of Murchison which is no longer available for direct comparison. However, all the samples of Murchison analysed gave very similar results for the positions of the D and G peaks, and behaved similarly on ozone treatment, so possible inhomogeneity is not likely to be the only cause of the differences in reactivity of IOM.

The sample of IOM was prepared about five years ago, and may have changed chemically on storage during that time. No studies of the stability of IOM have been reported in the literature.

It is also possible that the behaviour of IOM is influenced by the presence (or absence) of minerals. An organic molecule may form weak bonds to a solid surface, so that some kind of chemical co-ordination could be created between IOM and the surface of the mineral, altering both the strengths of its component bonds and its reactivity. In the case of IOM though, since the main structural element present is a network of π-systems of various sizes (as described in section 1.4.3), which would not be expected to bond strongly to minerals likely to be present (such as olivine or clays), this seems unlikely. To generate only oxalic acid from a structure such as that shown in Figure 1-3, would require such a modification of its reactivity that is very difficult to see how it could be caused by catalytic effects of minerals. Similarly, the effect of minerals is unlikely to cause the conversion of such a structure into one containing an extended π-system, and so be unreactive towards ozone.

The fact that generation of oxalic acid from IOM on treatment with ozone is unaffected by the presence of minerals was discussed in section 5.3.3. Although there is no proven link, this adds weight to the conclusion that the changes in the positions of the peaks seen in the Raman spectra of samples on reaction with ozone is due to differences in the structure of IOM pre- and post-demineralisation, and not to the presence or absence of minerals.

Structural interpretation of the changes in Raman frequencies

The broad peaks seen in the Raman spectrum of IOM are formed as an envelope of numerous signals of similar frequency formed by the vibrations of the bonds in similar, but not identical, molecular units, as discussed in sections 2.1 and 5.4. A shift in the position of either of these broad bands could then be due to a change in the distribution of bond frequencies, to overall higher or lower energies. Thus a shift

to higher frequency would be caused by an increase in the proportion of stronger bonds (or alternatively, a decrease in the proportion of weaker bonds).

When isolated IOM was exposed to ozone, the G peak shifted to higher frequency, and the D peak to lower. The shift of the G peak to higher frequency could be due to removal of electron withdrawing substituents (such as other unsaturated systems) from the structural subunit from which it is derived. Similarly, the reduction in the frequency of the D peak may be due to the removal of aromatic units with electron-donating substituents (which would be expected to react preferentially with ozone, being relatively electron-rich (Bailey, 1958) The effect on these peaks for IOM still contained within Murchison whole rock is approximately the opposite. The D peak increases in frequency on exposure to ozone whereas the G peak frequency is reduced, although the change is much smaller than for isolated IOM (for which it clearly increases). This means the bonds giving rise to the D peak become stronger on ozone treatment, that is, more electron-rich, as might be expected if substituted with electron-donating substituents, or if electron-withdrawing substituents are removed. The changes occurring to the sources of the G peak are smaller, although opposite.

The changes shown in the positions of the D and G peaks on demineralisation are opposite to those of IOM on treatment with ozone, namely the frequency of the D peak increases, and the G peak decreases. This could imply that these two sets of chemical changes are opposite in nature, but from the evidence obtained so far, more detailed interpretation is not possible.

5.4.5. Conclusions

From the data acquired so far, it seems likely that IOM contains two structural components, or molecular sub-units which have different structures (as noted in section 4.5), that react differently with ozone, with one or both of these components being chemically modified during demineralisation.

This conclusion is similar to that reached by Sephton *et al.* (2003), who proposed that IOM was composed of two components, which they named "Labile Organic Matter" (LOM) and "Refractory Organic Matter" (ROM), based on the behaviour of samples of whole rock meteorite, and isolated IOM, on stepped combustion and hydrous pyrolysis. A similar concept was also discussed by Okumura and Mimura (2011) who named these two components "thermally unstable" and "thermally stable" based on their pyrolytic decomposition profiles. These two terms are equivalent to LOM and ROM, showing the same contrast in reactivity and isotope ratios. This two-component concept is further discussed in section 6.5, and in Chapter 7, when data obtained after demineralisation is presented, and the concept of LOM and ROM is reviewed in terms of the structure of IOM.

Although no data has been obtained specifically to elucidate the structures of these components, their different reactivity towards ozone may be an indicator. Reaction with ozone is faster in unsaturated systems that are more electron-rich, or less-conjugated (Bailey, 1958), and so the more reactive component may possess a higher electron density in its unsaturated bonds, and the less reactive, lower electron density. A possible structural interpretation could be that the less reactive component contains a greater proportion of extended polycyclic aromatic systems, which would be expected to react with ozone to a lesser extent than small ring systems (especially any substituted with electron-donating functional groups).

Studies of the Raman spectra of graphite (described in section 2.1.1) showed that for pure graphite, only the G peak is seen, it being derived from vibrations of the hexagonal carbon lattice. Introduction of disorder to this structure (edge-effects, or substituents) gives rise to the D peak. It may be therefore, that it is the periphery of an extended π-system, functionalised in some way, which reacts with ozone, leaving the interior chemically unreacted, but electronically altered by the changes in the structures adjoining it. The interior of the macromolecule would therefore correspond to the component of IOM which is much less reactive to ozone, with the reactive fringe being the more-reactive component.

In contrast, rather than the macromolecular IOM being composed of regions of different reactivity, but still part of the same molecule, the differences both in the Raman spectra, and in the reactivity of IOM could also result from the reactions of a physical mixture of different types of macromolecule. If IOM in fact consists of two separate types of macromolecule, one of these could be physically shielded by the other, when present in whole-rock, but not so in isolated IOM. For example, if the second component were deposited over the first (as a physical coating, in whole rock) the first component might not be accessible to the Raman laser, nor exposed to ozone. Only following demineralisation would these two components become mixed, so that both were sampled by the laser, and both able to react with ozone.

The Raman evidence also suggests that the structure of IOM has been chemically modified in some way during the demineralisation process. If IOM does in fact contain two components of different reactivity, it could be assumed that it is the more-reactive part which is modified during demineralisation, although at present, there is no evidence to support that association.

In Chapter 3, the methodology for the molecular tagging of organic materials (including IOM) was discussed, which was based on the accepted view of the structure and composition of IOM (as described in section 1.4.3). However, data used to determine the likely structure and composition of IOM is almost wholly based on experiments carried out using IOM isolated from samples of meteorite by demineralisation. If this material has indeed undergone some chemical change during isolation, then it is not unreasonable that analytical data obtained from it is not applicable to IOM still in place within the meteorite.

The best way to determine whether any change does occur to the structure of IOM on demineralisation, would be to obtain a fresh sample of Murchison from which IOM could be isolated. Having samples available of the whole rock, both before any treatment and at every stage during the demineralisation procedure, would enable comparison of these materials to be made, and therefore any changes that might be occurring should be apparent.

The following chapters outline this work; the extraction and acid-treatment of this sample of Murchison is described in Chapter 6, and the fluoride-mediated dissolution of silicates (using two commonly-used procedures) in Chapter 7.

Chapter 6 The Demineralisation of Murchison Part 1: Preliminary Treatments

Results suggesting that the IOM of Murchison has been chemically modified during isolation from the meteorite by demineralisation were presented in the last chapter. To try to understand if this is indeed the case, or whether there is some alternative explanation, a study of the effects of the isolation process itself was undertaken. A fresh sample of Murchison was acquired, providing adequate starting material for all subsequent samples of extracted meteorite, IOM, *etc.* to be derived from a single source, so enabling direct comparisons between samples taken throughout the process. A sufficiently large sample was used so as to minimise the effects of meteorite heterogeneity, including variations in IOM structure, although of course heterogeneity may be on a larger scale. No studies have been reported in which a large number of different fragments of a carbonaceous chondrite (such as Murchison) were investigated, such as might show such a degree of structural variation of IOM, although others (for example, Pearson *et al.*, 2006) have observed heterogeneity when several subsamples were taken.

This investigation into the process of demineralisation is described in the next two chapters. Solvent extraction and treatment with dilute mineral acid are discussed in Chapter 6, and the dissolution of silicates with fluoride in Chapter 7. Practical details of the demineralisation process are described in the Appendix.

It was not an objective of this work to carry out a detailed study to elucidate the structure of IOM, but data collected was compared with that obtained in previously-reported studies, and any conclusions regarding the structure of IOM that could be drawn are also discussed in Chapter 7.

6.1. The Isolation of IOM by Demineralisation

The process of demineralisation was briefly described in section 5.1. One published procedure (Amari *et al.*, 1994), has often been used to isolate IOM from meteorite samples. This method employs repeated treatments with mixtures of hot HF and hydrochloric acid (HCl) to convert silicates to soluble derivatives, followed by more treatments with HCl and boric acid to remove final mineral traces, after which IOM is obtained as an insoluble residue. A second procedure, which is carried out at room temperature and avoids extremes of pH, has been developed (Cody *et al.*, 2002). This method uses a caesium fluoride solution, adjusted to neutral pH, in the presence of a mixture of carbon disulfide and 1,4-dioxane (immiscible with the aqueous solution). As the minerals are dissolved, particles of organic material are released, and collect at the interface of the two immiscible liquids, from which they can be isolated.

6.2. Previous Evidence for Chemical Change in IOM on Demineralisation

There are no published studies specifically investigating the extent of any changes that demineralisation might cause to the structure of meteoritic organic materials. However, the original development of fluoride-ion mediated demineralisation was for use with terrestrial coals and other organic-rich rocks. Investigation into possible modification of the organic materials isolated by this procedure was carried out by Larsen *et al.* (1989).

In those studies, the analysis of the organic materials so isolated was largely limited to non-specific analytical methods, which did not use chromatography or spectroscopy. Non-specific methods are those which return data not specifically related to the structure of the analyte. An example is elemental microanalysis;

clearly all isomeric structures will give the same values, and so these techniques cannot be used to investigate structural change. However, IR and ^{13}C NMR spectra both showed some changes following demineralisation, indicating a chemical change is initiated by fluoride-mediated demineralisation. Since the extent of change could not be determined, Larsen *et al.* (1989) concluded that "It appears that HCl/HF demineralization has little, if any, effect on the macromolecular structure of coals...". This may, in retrospect, have proved misleading to workers studying meteorites and other carbonaceous materials.

In another study (Smith and Kaplan, 1970) of the carbonaceous components present in a range of meteorites (although not including Murchison) it was found that about 50% of the carbon (excluding carbonate) was lost during the demineralisation procedure. In the procedure used, solutions were evaporated to dryness several times, and so any volatile compounds would inevitably have been lost.

Kerridge *et al.* (1987) carried out isotopic analysis of IOM before and after demineralisation. By using deuterium-labelled acids for the demineralisation, they showed that significant hydrogen-deuterium exchange occurred during the procedure, but the extent of exchange also varied between samples (Kerridge *et al.*, 1988). The reaction which they observed could be limited simply to the exchange of acidic protons (as is commonly observed with many species, such as alcohols, phenols *etc.* in an aqueous medium), and involve no more extensive reaction than that. However, this result clearly shows that the insoluble and involatile IOM is capable of reaction in aqueous media, which may have been thought unlikely when these demineralisation methodologies were first designed.

Supported reagents, such as derivatised polystyrene, similarly in solubility and volatility to IOM, are well-known and commonly used in organic synthesis (Clark *et al.*, 1992). Despite being insoluble and involatile, these reagents can still be reactive. Their reactivity derives from a functionalised (more polar) periphery being accessible to other reagents present in solution, probably *via* a thin layer of solvation, even though the bulk of the macromolecule is not solvated, and so out of solution.

In 2012, Ott *et al.* presented work on the UV-mediated decomposition of samples of Murchison, as part of a study to investigate the possibility of generation of methane from meteoritic organic material on the surface of Mars (Ott *et al.*, 2012). Although methane was detected when ground Murchison whole rock was used, none was detected when the experiments were repeated using isolated IOM. This observation could indicate that a component of IOM (which in this case reacts to generate methane) is removed or modified during the demineralisation process, although it is possible that methane, physically bound up in some way within the minerals, is lost on demineralisation.

A study comparing the FTIR spectra of both whole rock samples and isolated IOM (Kebukawa *et al.*, 2013) also showed there were differences in the profiles of the C-H region of the spectra of IOM before and after demineralisation. These changes were interpreted as being caused by an (unidentified) component of the carbonaceous material being lost (which could have been caused by chemical change on demineralisation).

Despite this evidence, IOM isolated following demineralisation has been used many times in studies designed to understand the structure of meteoritic organic material, the assumption being that no significant structural changes would have been caused

by the isolation process (Kebukawa *et al.*, 2013); if significant changes do occur on demineralisation, then the relevance of much of this data to the true structure of IOM still *in situ* within the meteorite must be questioned.

6.3. Demineralisation Part 1A: Solvent Extraction

6.3.1. Procedures

The first stage of the demineralisation procedure is the removal of soluble organic compounds by solvent extraction. A sample of Murchison (supplied by the Field Museum, Chicago, and designated 3M) was extracted to remove organic- and water-soluble species to give sample 3SE; practical details of the procedures used are described in the Appendix. Both samples 3M and 3SE were analysed by Raman spectroscopy, SEM and Pyrolysis-2D-Gas Chromatography-Mass Spectrometry (Py-GCxGC-ToF-MS). The data was compared with that obtained from a previously-extracted sample of Murchison (non-polar compounds had been extracted with supercritical carbon dioxide for another project), designated 1SCE. Samples were also exposed to ozone, and the products analysed using the same techniques. Analytical data from each technique used (both pre-and post-ozone treatment) is presented in this section, followed by an overall conclusion. Samples were prepared for analysis using the same procedures as described in section 5.2. The relationships between these samples (and that used for the experiments described in Chapter 5, are shown graphically in Figure 6-1. (Sample 1M was no longer available for comparison with 3M.)

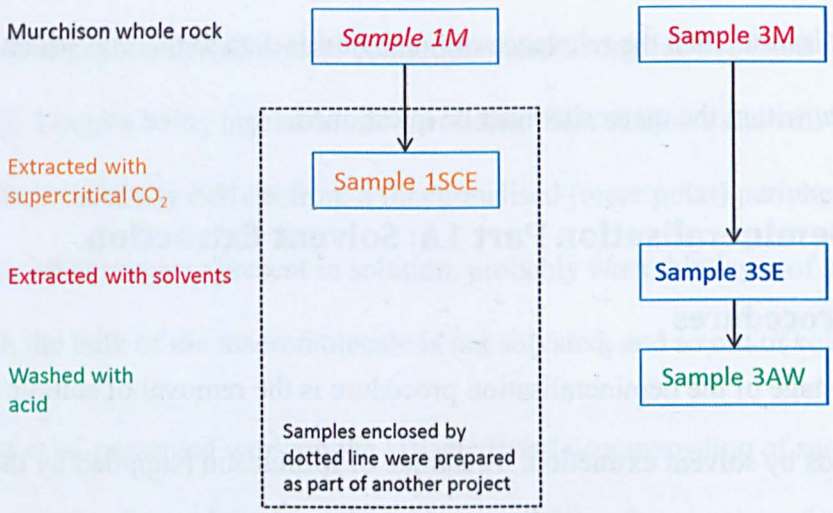

Figure 6-1: Relationships between methodology used to prepare samples from portions of Murchison

6.3.2. Analysis of Untreated Samples

Raman spectroscopy

Samples of Murchison, crushed whole rock, (3M), and after extraction with solvents (3SE), were analysed by Raman spectroscopy, taking a set of spectra across the surface of the sample in the manner discussed in section 2.1.2. Each sample gave a similar spectrum, showing the two broad peaks (D and G) typical of aromatic carbon, as seen in the previous work reported in section 4.1.3. The positions of the D and G peaks, (generated by Labspec software, as discussed in section 2.1.2) are plotted in Figure 6-2. Data for the three fragments of Murchison previously presented (in the work described in section 5.4.3.) is also included. These gave similar, although not identical peak positions, indicating a possible variation in the structure or composition of IOM in different fragments of Murchison. The data shows a rather wide spread of peak frequencies for each sample, but with considerable overlap of those peaks derived from samples with either no extraction or extraction with solvents (*i.e.* following removal of any soluble organic compounds, and water-soluble minerals).

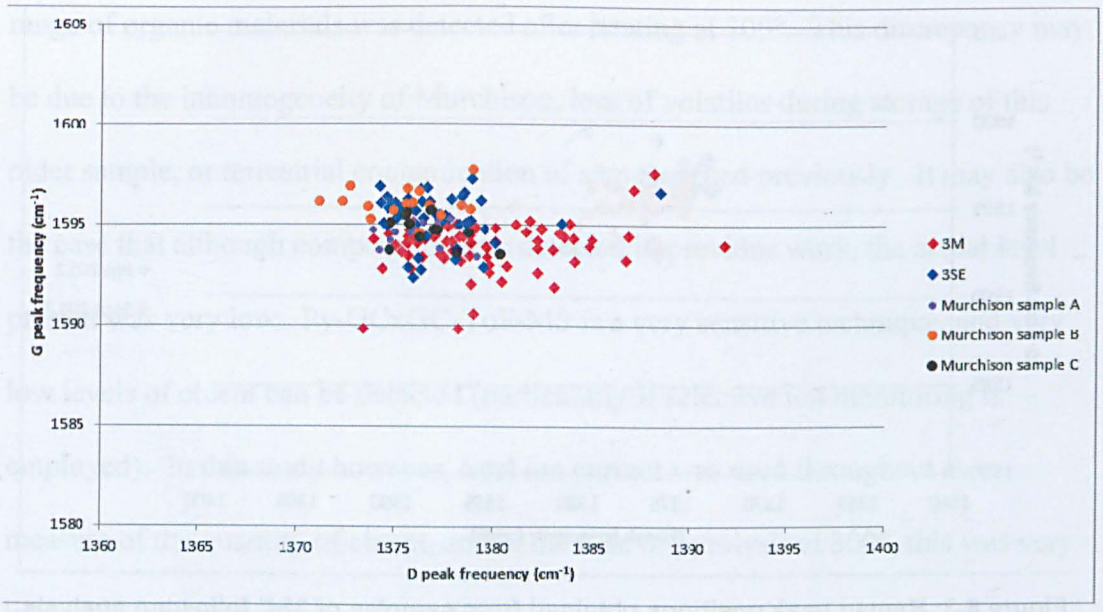

Figure 6-2: Comparisons between the positions of Raman signals obtained from samples of Murchison before and after extraction

These results show that, following solvent extraction, little or no change has occurred in the organic content of Murchison from which the Raman spectrum is derived. Although the extracts were not analysed, nor the amounts of material removed quantified (neither was within the scope of this project), there is no evidence from the Raman data presented that significant levels of organic material have been removed *i.e.* if materials are being removed, then they were present at below the limits of detection of this technique. Neither has any evidence for chemical change been found. The data therefore supports the conclusions that the level of soluble organic material present in Murchison is low, and that no chemical change occurs on solvent extraction.

To check that the samples are stable to storage over the timescale of this study, a sample of 3SE was reanalysed after *ca.* two months (initial analysis late June 2102, re-analysis, early September 2012); the positions of the peaks were essentially unchanged (shown in Figure 6-3).

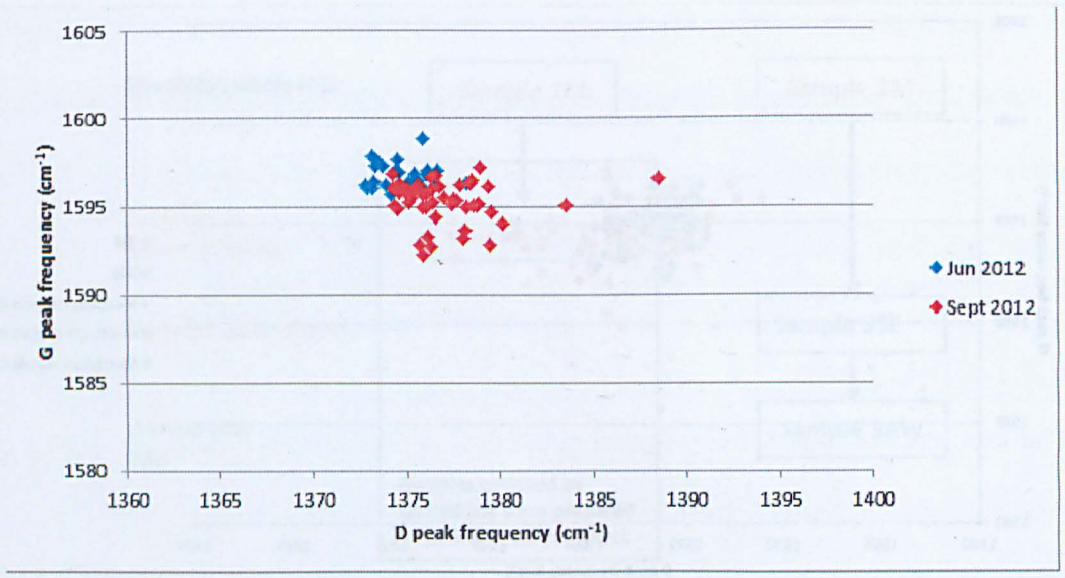

Figure 6-3: Raman peak positions obtained from samples of 3SE following analysis and re-analysis by Raman spectroscopy

Pyrolysis-GCxGC-ToF-MS

Pyrolysis studies were carried out as described in section 2.4.

Results from pyrolysis were analysed in two ways. The variation of TIC with time was used to generate a profile by which the samples could be compared (for example, in a similar way to the fingerprint region of an infra-red spectrum). This profile, although not giving structural information for the compounds detected, enables the comparison of two or more samples. If the profiles are different, the pyrolysates have different compositions, and so the samples must also be different. The identities of the compounds detected were then determined following processing the data to obtain 3D-chromatograms and mass spectra.

Pyrolyses were first carried out at 300°. In previous studies (Pearson, personal communication, 2013), this temperature had been used to remove absorbed compounds and volatile small molecules, which were detected by GCxGC-ToF-MS. However, when sample 1SCE was heated at 300° only trace amounts of pyrolysate were detected. This result is therefore not consistent with the earlier work, where a

range of organic materials was detected after heating at 300°. This discrepancy may be due to the inhomogeneity of Murchison, loss of volatiles during storage of this older sample, or terrestrial contamination of samples used previously. It may also be the case that although compounds were detected in previous work, the actual level present was very low. Py-GCxGC-ToF-MS is a very sensitive technique, and very low levels of eluent can be detected (particularly if selective ion monitoring is employed). In this study however, total ion current was used throughout as a measure of the quantity of eluent, and in the case of pyrolysis at 300°, this was very low.

Fresh samples of Murchison, before and after solvent extraction, gave similar results to 1SCE on pyrolysis at 300°. The TIC traces (Figure 6-4) show no compounds are detected from the extracted sample, 3SE, (blue trace), and only one peak, due to naphthalene, seen in the untreated sample, 3M (red trace). This result shows that any soluble (and volatile) organic compounds contained within 3M are present at below the level of detection of this technique. Solvent extraction would be expected to remove all soluble materials from 3SE, and indeed none were seen.

A possible loss of volatile compounds may have been during the vacuum treatment of part of the sample of Murchison used for solvent extraction (described in the Appendix). However, this procedure, intended to identify any volatile compounds outgassing from asteroids, did not result in significant levels of organic materials being detected (Morse, personal communication, 2013).

Sample 1SCE was also used to compare the effects of pyrolysis at different temperatures. Previous studies investigating the pyrolysis of meteorite samples had used a temperature of about 600° to effect pyrolytic decomposition of the sample

(Pearson *et al.*, 2007a). This temperature is sufficient to break most bonds in organic compounds (Wampler, 2007), and increasing the temperature further does not significantly increase the degree of pyrolytic breakdown (Murae, 1995). A range of temperatures was evaluated to confirm that was the case. Sample 1SCE was pyrolysed at 600°, 650° and 700°; the TIC traces obtained are shown overlaid in Figure 6-5. The three traces show the same profile; new compounds are not formed as the temperature increases, and so the set of compounds generated on pyrolysis is not critically dependent on temperature. The temperature of 600° was adopted for future work to allow comparison with previous work. Samples 3M and 3SE were then subjected to pyrolysis at 600°. The TIC traces (Figure 6-6) were broadly similar in profile both to that obtained for sample 1SCE (compared with 3SE in Figure 6-7), and to each other, the latest eluting peak in each case being naphthalene. The only difference seen between the traces derived from 3M and 3SE was in intensity of signal; this is most likely due to the inhomogeneity of Murchison. Sample 1SCE shows some peaks (highlighted in Figure 6-7) which are not present in 3M or 3SE.

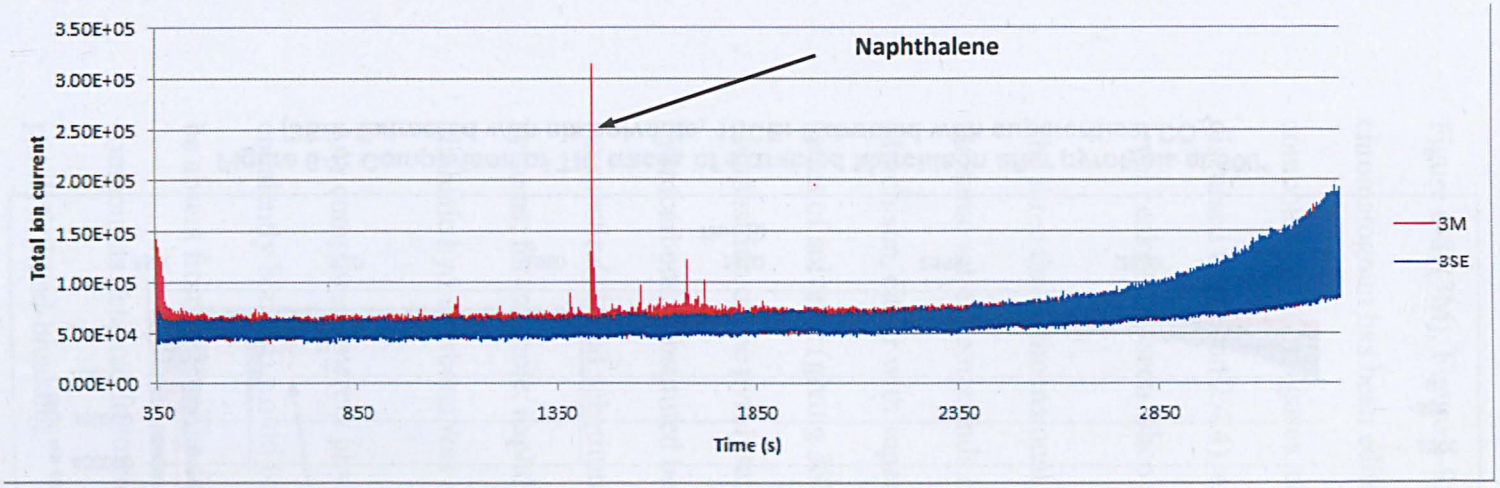

Figure 6-4: TIC traces of 3M and 3SE after pyrolysis at 300° showing naphthalene as major product in 3M

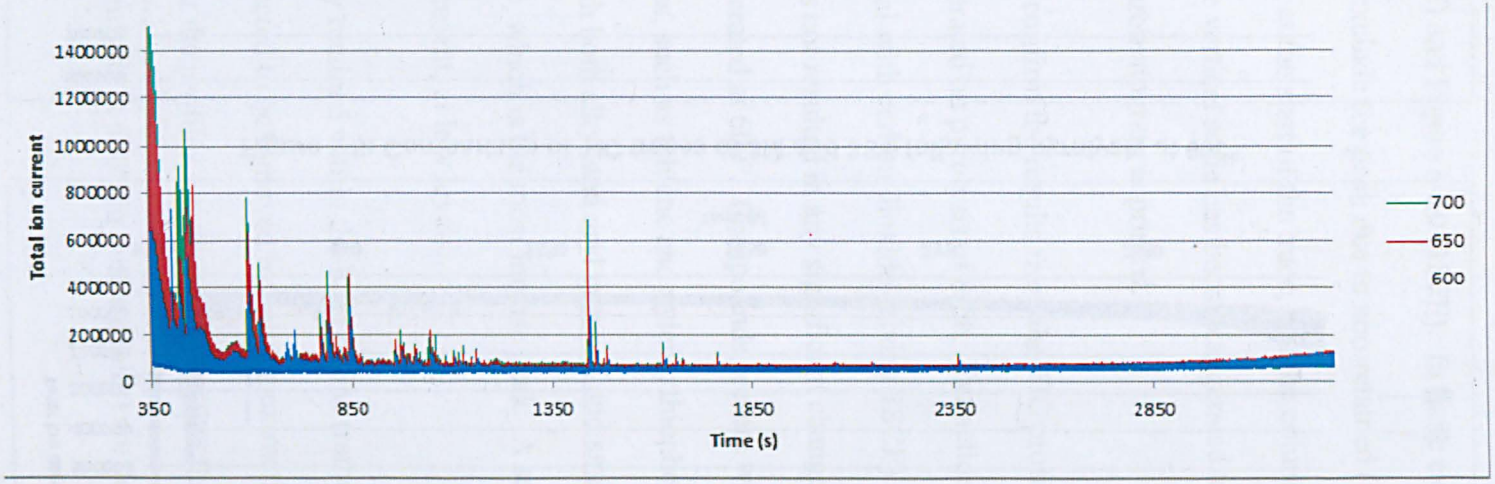

Figure 6-5: Comparison of TIC traces for samples of 1SCE following pyrolysis at different temperatures.

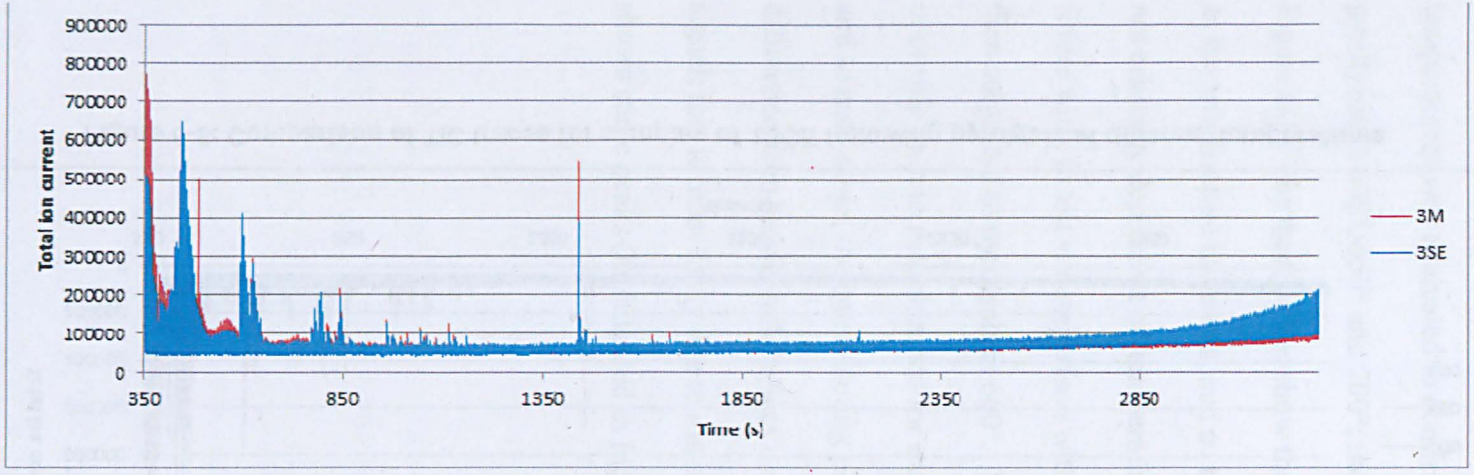

Figure 6-6: Comparison of TIC traces of 3M and 3SE following pyrolysis at 600°

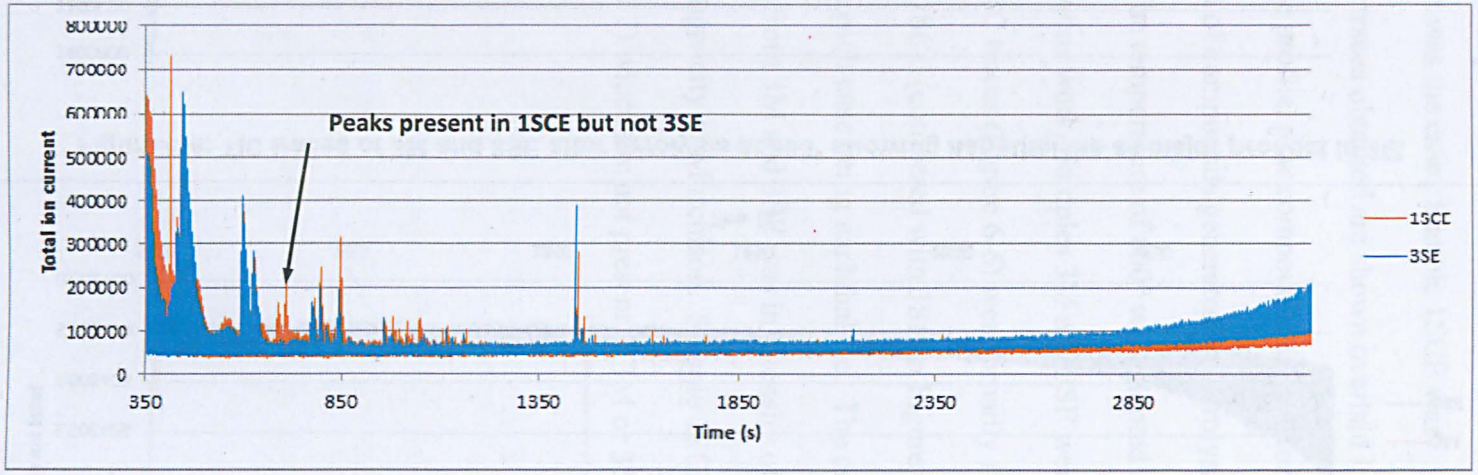

Figure 6-7: Comparison of TIC traces of extracted Murchison after pyrolysis at 600° (3SE: Extracted with six solvents, 1SCE: Extracted with supercritical CO_2)

The identities of compounds generated by pyrolysis can best be determined by examination of the 3D-chromatograms, and the mass spectra of the peaks thus obtained. These are shown below in both contour and oblique presentations in Figure 6-8, (3M), Figure 6-9, (3SE) and Figure 6-10 (1SFE). In these examples, the chromatogram has been edited to exclude the peak due to non-retained (very volatile) compounds, such as gases, eluting at the start of the trace, and the column bleed (as discussed in section 2.4.4), and the vertical scale has been exaggerated to enable low-level peaks to be seen when the chromatogram is printed.

The three three-dimensional plots confirm the results from the TIC profiles, namely the same set of compounds is generated on pyrolysis of each. Extraction of Murchison, either with supercritical with carbon dioxide (giving 1SCE) or with a series of solvents (giving 3SE) has not resulted in any significant change in the composition of the pyrolysate generated at 600°. Compounds present were aliphatic hydrocarbons, substituted benzenes, such as toluene and xylene, thiophenes (unsubstituted, and substituted with both alkyl and aryl groups), and small condensed systems, for example, naphthalene, which is the most intense peak. A sequence of aliphatic hydrocarbons was also present, at low levels.

Any compounds merely physically retained within the IOM of 3M (rather than covalently bonded) would be expected to be removed by solvent extraction (and so be absent from 3SE). The fact that the profiles are similar means that these compounds detected following pyrolysis at 600° (in both samples) are derived from pyrolytic bond-breaking.

The peaks present in 1SCE but not 3SE were examined using the 3D-presentation where it was seen that these peaks had a very short retention time on the second

column, and so lie in the region of solvent bleed, which has been edited from the chromatograms shown in Figure 6-9 and Figure 6-10.

These chromatograms show that the set of compounds generated on pyrolysis either of whole rock Murchison, or of samples after solvent extraction are very similar, with only minor inter-sample variations. This is similar to data previously reported (Watson *et al.*, 2005a; Pearson *et al.*, 2007a; Watson *et al.*, 2007). The results support the conclusion that the set of compounds detected results from the pyrolysis of some component of the IOM present in the samples of Murchison, and that no chemical change has occurred on solvent extraction. The extraction conditions used were chosen to be mild, for example, only being carried out at ambient temperature, using non-reactive solvents, and so changes in IOM were not expected, and indeed, none were seen.

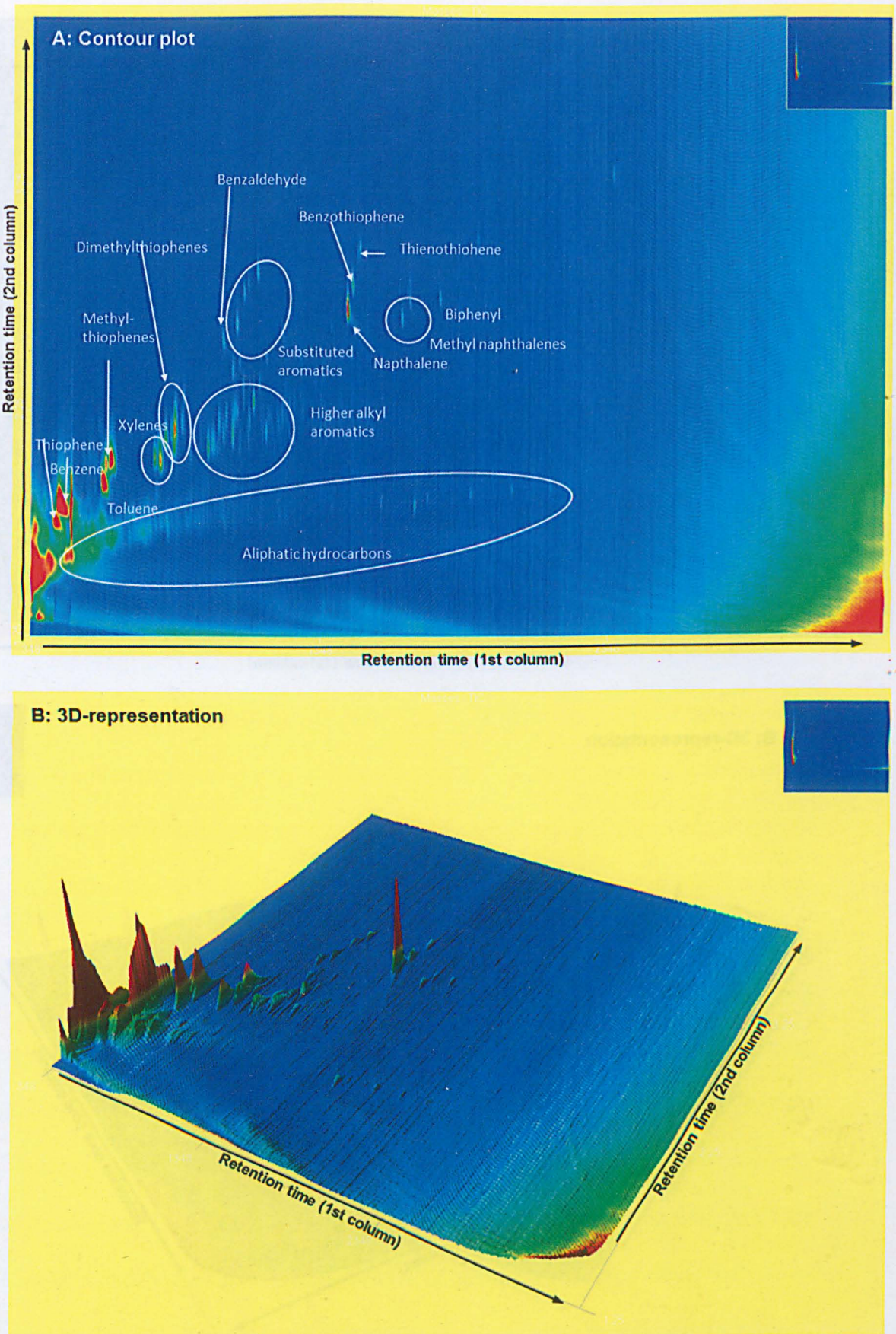

Figure 6-8: 3D-chromatograms of sample 3M after pyrolysis at 600°

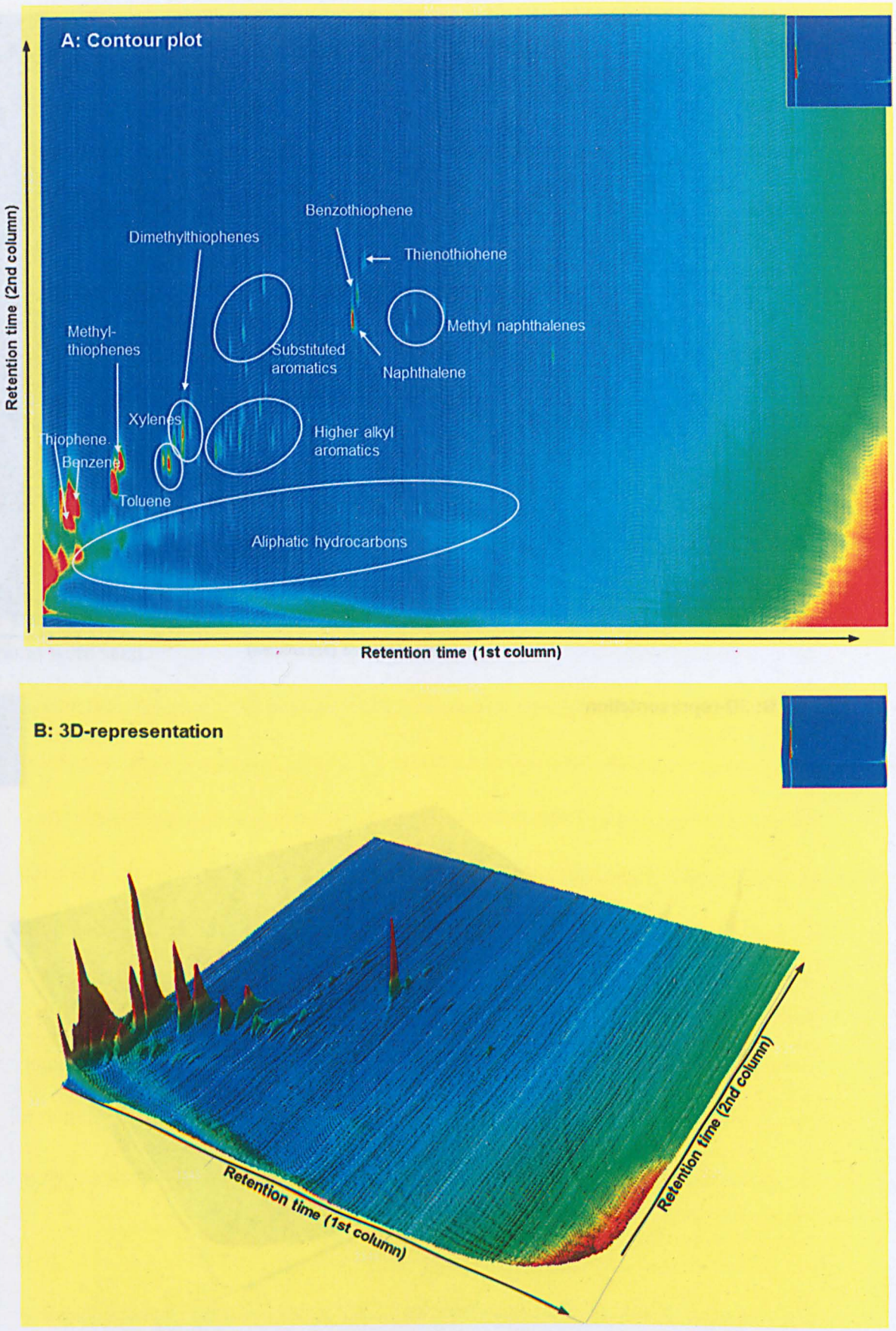

Figure 6-9: 3D-chromatograms of sample 3SE after pyrolysis at 600°

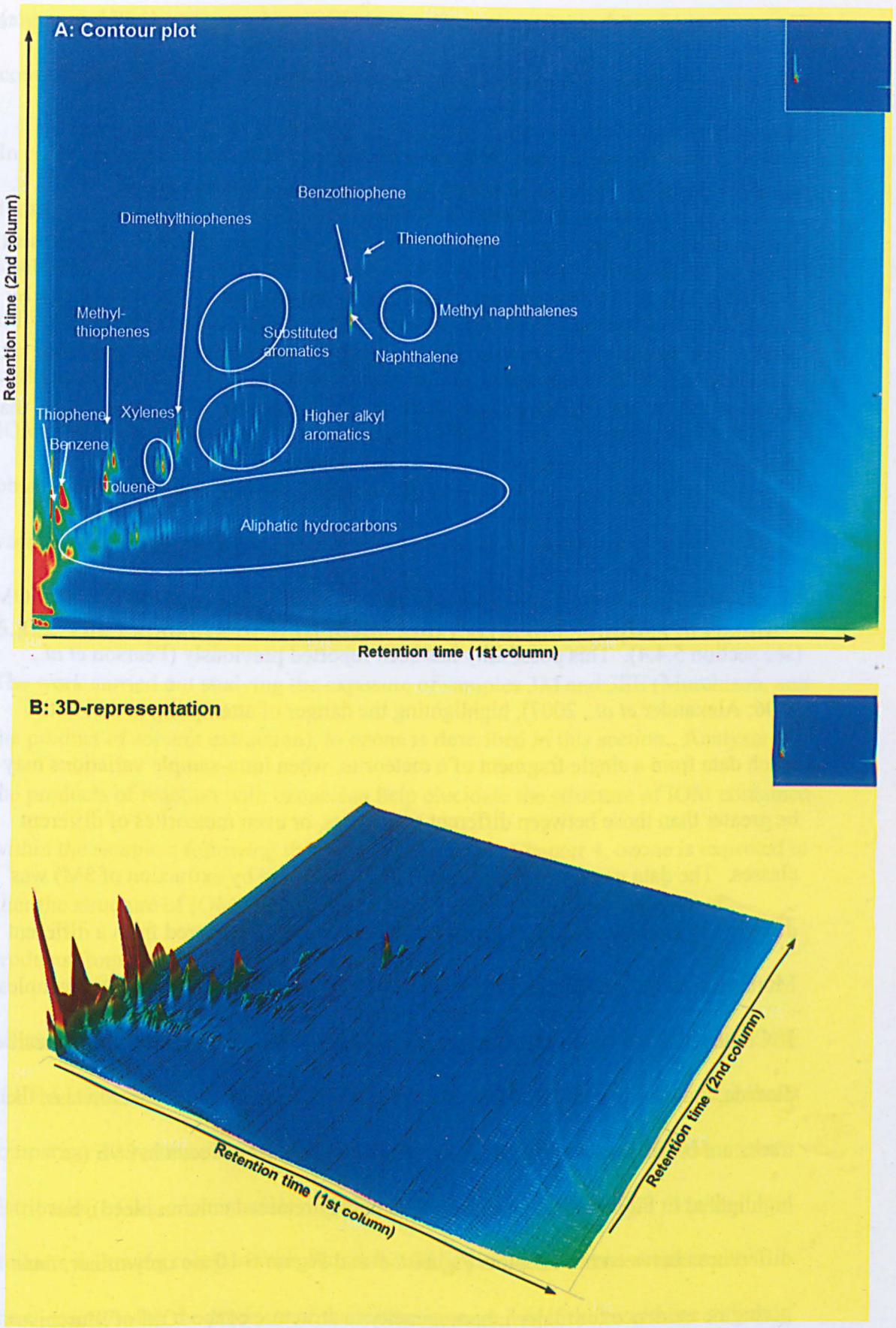

Figure 6-10: 3D-chromatograms of sample 1SCE after pyrolysis at 600°

The composition of the pyrolysate can be used to infer what structural elements go to make up its precursor. The large majority of the compounds seen (identified in Figure 6-8, Figure 6-9, and Figure 6-10) are hydrocarbons (both aliphatic and aromatic) and sulfur-containing heterocycles, such as thiophenes; other functionalities (such as ketones, phenols, ethers or esters) are absent, or only present at very low levels. The functionality proposed in structures of IOM, such as that by Derenne and Robert (2010) (and shown in Figure 1-3) contains largely that latter set of compounds which that are missing from the pyrolysate. It is hard to reconcile that structure with the observations reported in this chapter.

Variation in the composition of Murchison was proposed as a possible explanation for the differences between the reactions with ozone of whole rock and isolated IOM (see section 5.4.4). This possibility has been reported previously (Pearson *et al.*, 2006; Alexander *et al.*, 2007), highlighting the danger of attempting to derive too much data from a single fragment of a meteorite, when intra-sample variations may be greater than those between different meteorites, or even meteorites of different classes. The data generated from sample 3SE, (prepared by extraction of 3M) was directly compared with that obtained from sample 1SCE, prepared from a different Murchison fragment. Figure 6-7 shows the TIC traces of the two extracted samples, 1SCE and 3SE overlaid. The former, having been extracted with supercritical carbon dioxide, may retain polar compounds not soluble in that solvent. Nevertheless, the traces are broadly similar, although 1SCE contains peaks not seen in 3SE (as highlighted in Figure 6-7, and identified as poorly retained column bleed), but differences between the 3D plots Figure 6-9 and Figure 6-10 are only minor, thus giving no evidence for major inhomogeneity in structure of the IOM of Murchison

(although 1M, the precursor to 1SCE, was no longer available for a direct comparative study).

In conclusion, the results obtained using Py-GCxGC-ToF-MS are consistent with those obtained from Raman spectra, in that no chemical change to the organic content of Murchison is detected following solvent extraction. In addition, although different samples of Murchison would be expected to show differences in their composition, pyrolysis indicates a broadly similar composition of that component of IOM which gives rise to a pyrolysate at 600°. This result is consistent with that obtained from Raman spectra of Murchison samples, where little inter-sample variation was seen.

6.3.3. The Exposure of Murchison and Extracted Samples to Ozone

The work carried out studying the exposure of samples 3M and 3SE (Murchison, and the product of solvent extraction), to ozone is described in this section. Analysis of the products of reaction with ozone can help elucidate the structure of IOM contained within the samples; following the results described in Chapter 4, ozone is expected to alter the structure of IOM, which, on pyrolysis, should give a different set of products from that obtained pre-ozone treatment.

Although the exact mechanism of the reaction with ozone is unclear (as the structure of IOM is not fully understood), this reaction can also be used as a chemical probe, comparing the results obtained for a set of samples. If the structure of IOM, or the distribution of organic materials, in general, in each sample is similar, then the products following reaction with ozone should be similar. It is not necessary to know exactly what the products of these reactions are, but if the results are different,

then the organic content of the samples undergoing the reaction must also be different.

The stream of ozone used for previous experiments had been bubbled through a Buchner flask containing water. In future experiments, ozone was used both dry and moist, the expectation being that slower reactions would occur with dry ozone, and so different reaction profiles might be seen if the products could be examined before reactions were complete. Initially, samples of whole rock, (3M) and solvent-extracted (3SE) Murchison were exposed to dry ozone for 1 h, 8 h and 24 h.

Raman spectra

Raman spectra acquired from sample 3M following exposure to dry ozone for 24 h were processed to give the positions of the D and G peaks and are shown in Figure 6-11. The peaks lie in very similar positions to those acquired prior to ozone treatment (shown in Figure 6-2), also with considerable overlap; a substantial shift in peak position has not occurred.

These results differ from those of samples of Murchison whole rock previously exposed to ozone (as discussed in section 5.4.3), for which a shift in peak position was seen. This later set of Raman spectra also did not contain the peak at 1470 cm^{-1}, derived from reaction of the oxalic acid generated by ozone treatment with minerals present in the sample. From the data generated using this most recent sample of Murchison, the conclusion from the Raman data alone would be that no significant change occurs on exposure to ozone. Previous data did not support that claim; lack of any change in the spectrum following exposure to ozone in this case could indicate absence of an organic component which was present in the samples previously used. The difference may also be due to the milder conditions used in this

experiment (use of dry ozone rather than moist) or possibly to the prior exposure of the sample to vacuum, as described in section 6.3.2. This latter explanation is unlikely, as not all the sample used to prepare 3M had been exposed to vacuum (as detailed in the Appendix).

Spectra were not acquired for sample 3SE (but see the discussion in section 6.4.1), Raman spectra of sample 3AW, prepared from 3SE, showed no further changes in its Raman peak positions, indicating that 3SE is very unlikely to be any different.

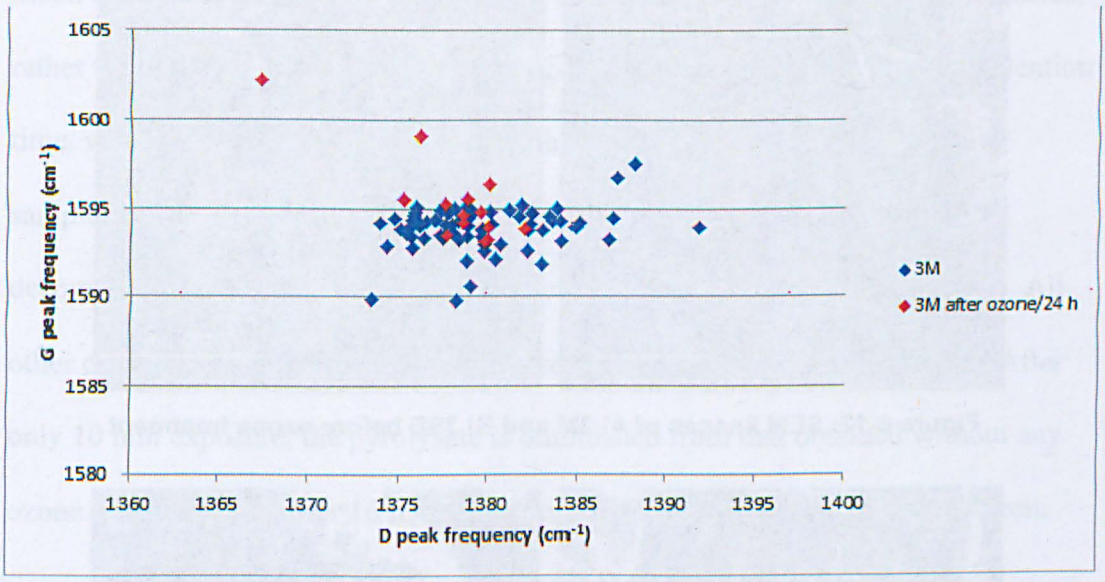

Figure 6-11: Comparison of Raman peak positions for sample 3M before and after exposure to ozone

SEM

Samples of 3M and 3SE were examined using SEM. Images of the two samples (shown in Figure 6-12) appeared very similar, both showing small grains. On treatment with ozone, the appearance did not alter (as shown in Figure 6-13). The grains were still discrete, and there was no sign either of the globules, or the fusing of grains, that had been seen with ozone exposure of a previous sample of crushed Murchison (see section 4.2.4). This confirms the observation from the Raman spectra, that oxalic acid (believed to be the source of both the fused appearance and

the spherical structures) was not present, and adds weight to the suggestion that fusing of grains, and formation of the spherical structures are somehow connected with its formation. These changes are also linked (albeit only circumstantially) with the changes seen in the Raman spectra. Only when oxalic acid was formed (and these physical changes occurred), was a substantial shift in Raman peak positions seen. It seems likely, although there is no proof at present, that all these changes are linked.

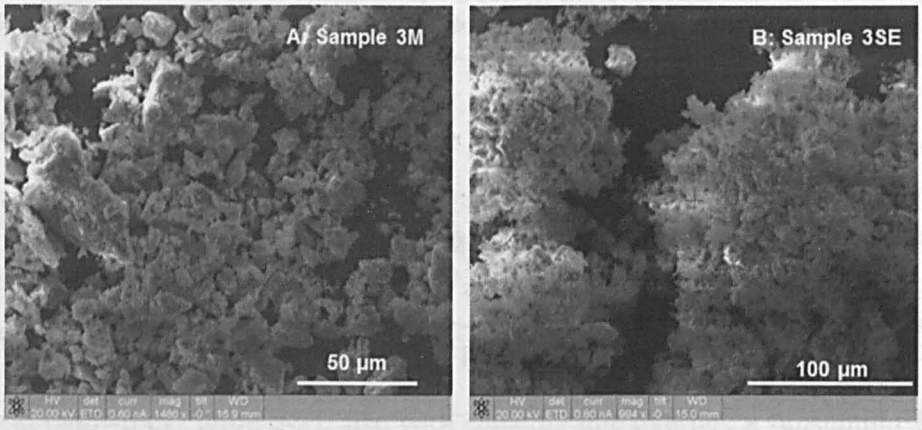

Figure 6-12: SEM images of A) 3M and B) 3SE before ozone treatment

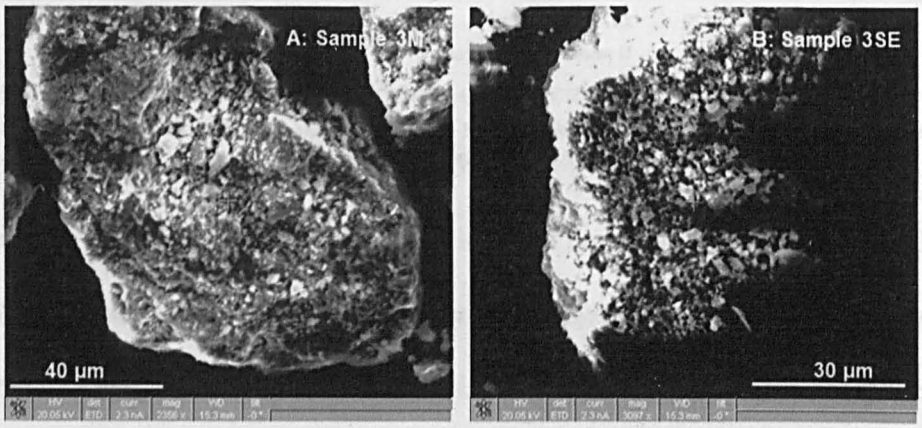

Figure 6-13: SEM images of A) 3M and B) 3SE after ozone treatment

Py-GCxGC-ToF-MS

Previous reactions of Murchison with ozone (described in section 4.2) had employed reaction times of up to *ca.* 40 h, with the goal of maximising the chance of seeing an effect. However, changes in the Raman spectrum of isolated IOM had been seen

after only 2 h, indicating the reaction with ozone was quite fast. To judge the most appropriate time for future use, the sample prepared by supercritical fluid extraction of Murchison (1SCE) was exposed to ozone for a range of times up to 16 h, and the product examined by Py-GCxGC-ToF-MS. Pyrolysis was carried out using the same conditions as described in section 6.3.1; again, no pyrolysate was detected at 300°. The TIC profiles obtained after pyrolysis at 600° are shown in Figure 6-14.

In Figure 6-14, the three TIC traces are overlaid precisely, and show that the effect of moist ozone treatment on sample 1SCE is to reduce the level of pyrolysate detected, rather than to generate new compounds, apart from those eluting with short retention time, which were identified as toluene. The presence of this early peak in the samples obtained after ozone treatment may be due to ozone-mediated decomposition, or possibly due to variation in sample sizes used for pyrolysis. All other peaks eluting later are reduced in size with increasing ozone exposure. After only 10 min exposure, the pyrolysate is diminished from that obtained without any ozone treatment, and after 16 h, the reaction is complete; other pyrolysate is seen.

These results show that the reaction of ozone with the precursor to the pyrolysate is rapid (at least in sample 1SCE); removal of the source of pyrolysis fragments which can be detected by Py-GCxGC-ToF-MS is essentially complete in a few hours. Furthermore, the pyrolysis precursor is not converted into a derivative which gives rise to a different set of detectable products on pyrolysis, with the possible exception of toluene, which was also formed on pyrolysis of samples not exposed to ozone. It is possible that new compounds have been formed, but are not eluted through the GC columns, or not detected by MS. It is also possible that other, undetectable changes to IOM continue on further exposure to ozone, even though no products were seen.

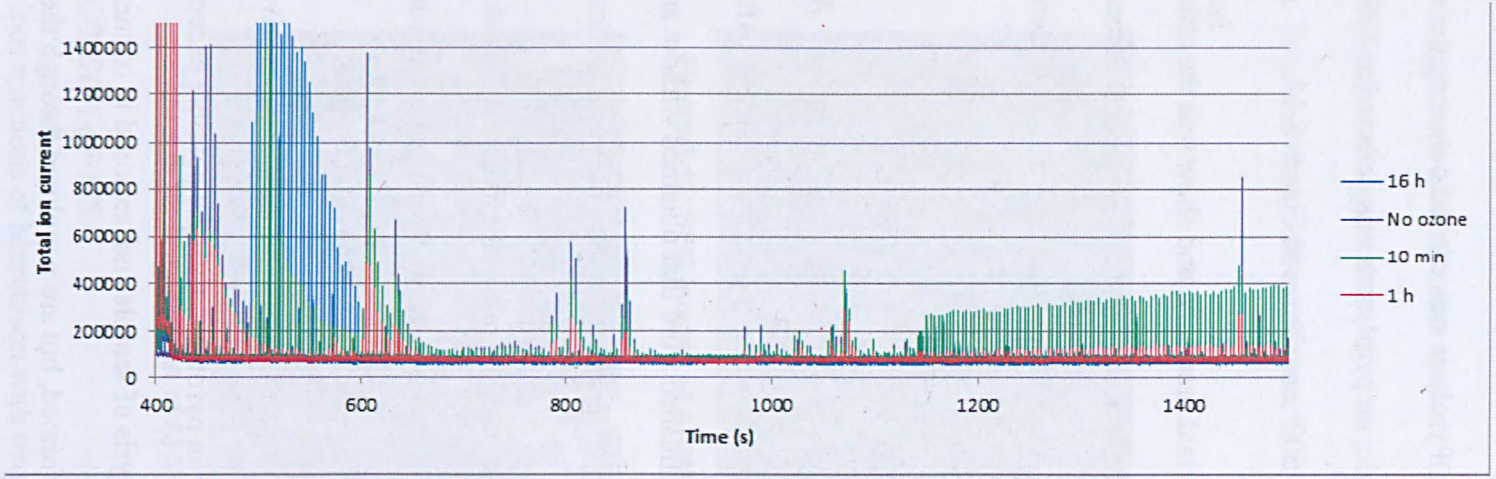

Figure 6-14 TIC traces from pyrolysis at 600° of sample 1SCE exposed to ozone for various times (this chromatogram was produced using a GC method before final optimisation)

Exposure of unextracted Murchison (sample 3M), to dry ozone showed the same behaviour as sample 1SCE (Figure 6-15). No new compounds were detected by Py-GCxGC-ToF-MS; the TIC profiles showed diminishing levels of pyrolysate (including toluene) with increased exposure to ozone. A similar result was seen for the sample following extraction (3SE), treatment with ozone for up to 24 h did not generate any new compounds that were detectable using this technique. TIC traces are shown in

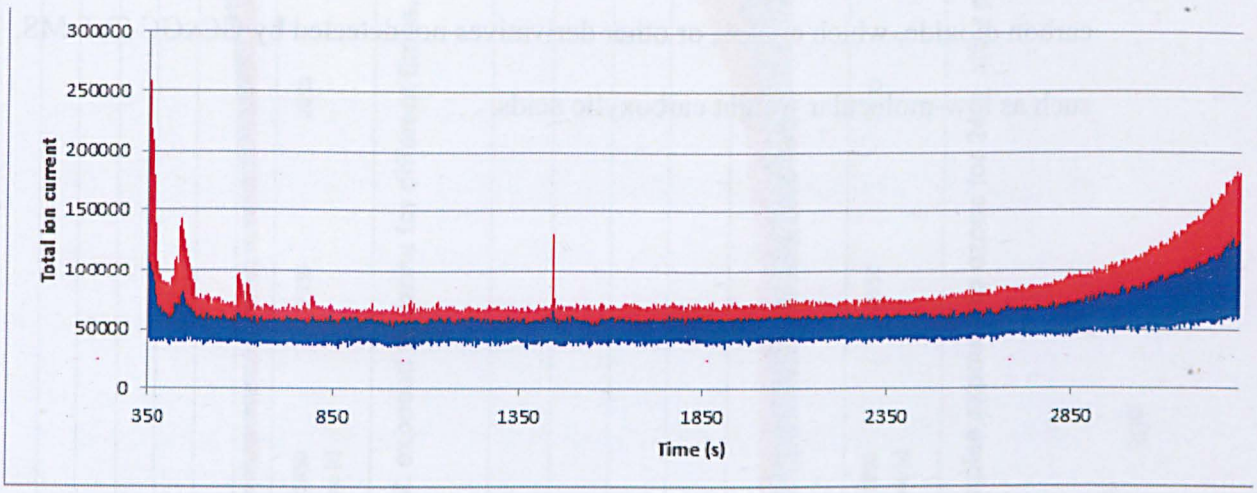

Figure 6-16. As the samples of Murchison pre- and post-extraction have behaved in the same way on ozone treatment, there is still no evidence for any chemical change having occurred during solvent extraction; any soluble organic materials present in 3M are below the level of detection. In this experiment, sample 1SCE has showed the same behaviour as those prepared more recently.

Thus, in summary, reaction with dry ozone has caused a reduction in the level of pyrolysate in all samples, both before and after solvent extraction, with no new compounds being detected. This change occurs without any significant change being seen either in the Raman spectra or the physical appearance of the samples.

Treatment with ozone appears to have either completely removed the component of IOM from which the pyrolysate was derived, or else converted it into some derivative which does not yield a pyrolysate. This is likely to be Labile Organic Material, as proposed by Sephton *et al.*, (2003), introduced in section 5.4.3, and discussed in more detail in the next section. Reaction of this component with ozone at ambient temperature and pressure is rapid, as shown by the data presented in Figure 6-14. LOM is presumably converted into either volatile products, such as carbon dioxide, which escape, or other derivatives not detected by GCxGC-ToF MS, such as low-molecular weight carboxylic acids.

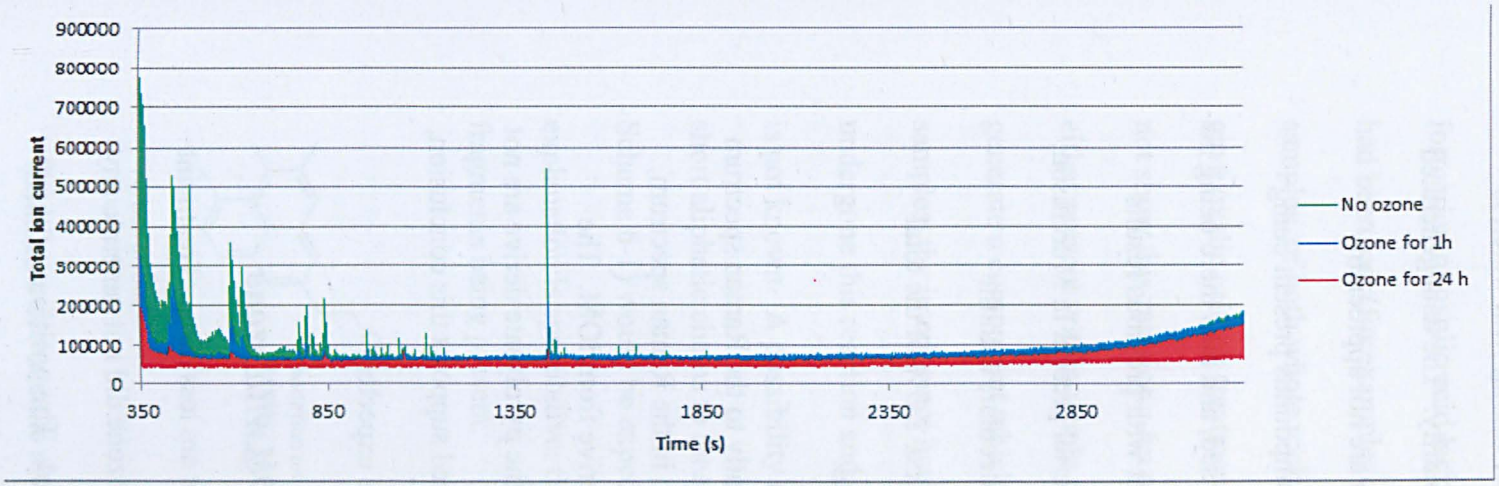

Figure 6-15: Comparison of TIC traces of sample 3M, exposed to ozone for different times, after pyrolysis at 600°

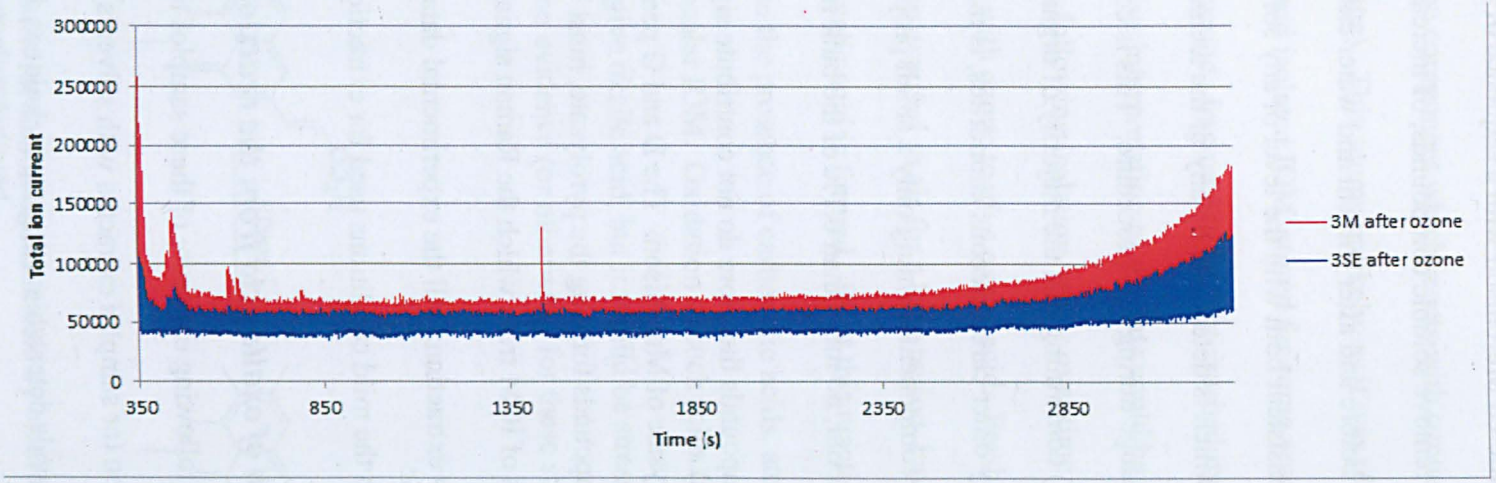

Figure 6-16: Comparison of TIC traces of samples exposed to ozone for 24 h, after pyrolysis at 600°

6.3.4. The Effects of Solvent Extraction: Summary and Conclusion

Soluble compounds present in Murchison

Stirring powdered Murchison with a sequence of solvents, ending with water, is designed to remove soluble compounds, of increasing polarity. The data generated for samples before and after solvent and water extraction are not appreciably different, consistent both with the level of any soluble compounds present being below that which is detectable by any of the techniques used, and also there being no chemical change during this procedure. This is consistent with previous results (section 1.4) confirming that the majority of organic material present in Murchison, and probably other carbonaceous chondrites, is macromolecular, with the extractable component forming only a small proportion, *ca.* 2-5% of the total organic material, no more than 0.1% of the bulk meteorite.

Soluble compounds therefore do not contribute significantly to the Raman spectrum or the pyrolysate of Murchison. The D and G peaks seen in the Raman spectrum, and the compounds forming the pyrolysate, must both derive from IOM. The components of IOM from which the Raman signals and the pyrolysate derive are not modified by extraction. All the experimental data acquired supports this conclusion, which given the mild conditions used for extraction, is as expected.

Formation of oxalic acid from the reaction of IOM with ozone

The results following exposure of these samples to ozone are less clear. Treatment of Murchison (or samples extracted with solvents) with ozone did not generate any new compounds detectable using the techniques described. The positions of the D and G peaks in the Raman spectrum of Murchison, or its extract, did not change significantly following treatment with ozone, nor was the peak indicative of oxalate-

containing minerals (1470 cm^{-1}) seen. This result differs from that obtained with other small chips of Murchison (described in section 5.4.3). At present, the cause of this difference is not known. It could be that the samples which did not show formation of oxalic acid lacked some component which reacts with ozone, and which had been lost (for example, on storage). This seems unlikely, as it was older samples, of both whole rock chips and isolated IOM, stored for some years, which gave oxalic acid on treatment with ozone. In contrast, freshly-crushed meteorite did not show this reaction. An alternative interpretation of the data could be that IOM either present within whole rock, or following isolation, reacts over time with air to generate a component which reacts with ozone to give oxalic acid. Freshly-crushed samples, the interior not having been exposed to air for a long period, have not undergone this reaction and so no oxalic acid is formed. What this reaction might be is not known. A possibility could be the presence of carboxylic acids, attached *via* short aliphatic chains to macromolecular IOM. Oxidation of such acids (as shown in Scheme 6-1) would be expected to give oxalic acid, but it should be stressed that this explanation is speculative; there is no evidence (or otherwise) for these structural fragments being present.

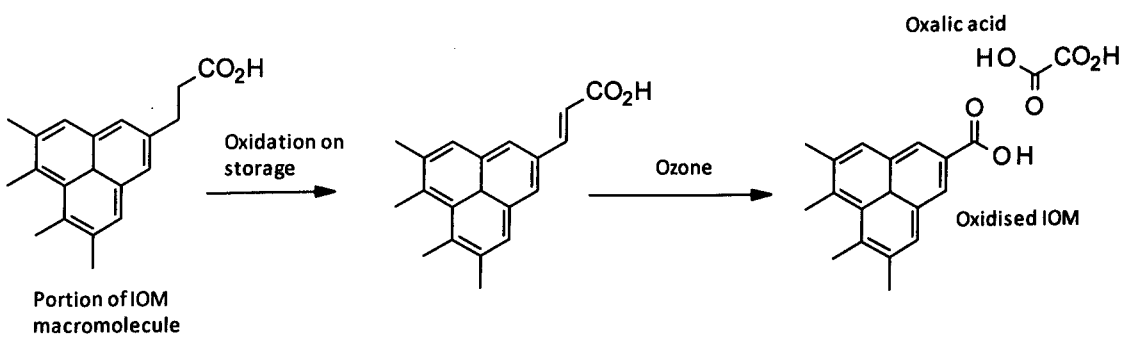

Scheme 6-1: Possible mechanism of formation of oxalic acid by cleavage of an unsaturated acid

The samples which did not show formation of oxalic acid also did not change visually on exposure to ozone, nor did the positions of the D and G peaks in the

Raman spectrum change significantly. Although the evidence is only circumstantial, it may well be possible that these three observations are all due to the decomposition of some component of IOM, such as that shown in Scheme 6-1, resulting in the generation of oxalic acid, with the visible changes caused in some way by its presence. The shift in Raman peak positions seen when oxalic acid was generated is due to some change to its electronic structure following reaction with ozone. When oxalic acid was not generated, this change did not seem to occur.

Alternatively, this difference could result from the heterogeneity of Murchison; the IOM present in the samples recently acquired being genuinely different in structure from that in samples obtained some time ago. If this were the case, then IOM containing the precursor to oxalic acid is distributed throughout Murchison heterogeneously.

The pyrolysis of IOM

When a macromolecule such as IOM is pyrolysed, the compounds which are detected have been generated by breaking apart the molecular structure of the macromolecule, resulting in the liberation of small fragments. These fragments have been generated by bond-breaking within the macromolecule, rather than being discrete molecules, previously having being somehow physically trapped within IOM, and released on heating. They are derived by a reaction (with heat) of a portion of the macromolecule. Thus, this precursor to the pyrolysate will contain, as a part of its overall molecular structure, a number of fragments linked together by covalent bonds, which are broken during pyrolysis.

When the samples were exposed to ozone, this precursor was modified in some way so that it did not decompose to give the pyrolysate when heated to 600°. This

modification could have taken place in a number of ways: (i) the precursor could have been decomposed completely, broken into small fragments which (being volatile) were then lost, (ii), it could have been converted into a derivative which on pyrolysis was decomposed into a set of compounds which were not detected or (iii) it could have been converted into a derivative which did not decompose at all on pyrolysis. A fourth possibility, that the precursor was converted into a derivative which gave a different set of products on pyrolysis, was not the case. The only compounds seen in the pyrolysate were those obtained when untreated samples were pyrolysed, but at much lower levels.

If treatment with ozone had generated small, volatile molecules, (for example carbon dioxide), these would have been difficult to detect, being unretained by the column. Other decomposition products (arising from option (ii) such as oxalic, or other carboxylic acids) might also not be detectable. Oxalic acid would not be expected to be detected in the pyrolysate, being decomposed on heating (Higgins *et al.*, 1997), but detection of stable acids would depend on whether they were eluted through the columns or not. Thus the observations are consistent with any of these three alternatives; alternative chromatography conditions would be required to distinguish between them.

The structure of IOM

In section 5.4.5, the results obtained following treatment of IOM with ozone were interpreted as indication that IOM contained two components. One of these reacted with ozone to give oxalic acid, but the other seemed unreactive. The Raman spectrum obtained after ozone treatment showed considerable aromatic carbon remained, but this component of IOM appeared to have been modified to some extent, not only by ozone treatment, but also by demineralisation.

The results described in this chapter are somewhat different. On exposure to ozone, although the structure of IOM appears to have been modified (in that no detectable pyrolysate is obtained after ozone treatment), oxalic acid was not formed. Again, the Raman spectrum obtained after ozone treatment showed considerable aromatic carbon remained, but in these examples, its structure did not appear to have been modified (as the positions of the D and G peaks did not change). It seems that, whereas the conversion of some component of IOM to oxalic acid results in modification of structure of the IOM which remains, when oxalic acid was not formed, and even though the precursor to the pyrolysate was either modified or decomposed, the IOM which remains appears unreacted; any change in IOM has had little effect on the Raman spectrum. This indicates that the more reactive components of IOM present in the two sets of samples have reacted in different ways, and therefore presumably have different structures.

The differences in the degree of change in the Raman spectrum on ozone treatment of different samples may simply reflect the variability in proportions of these components of IOM between the samples, and indicate that the reactive part is a relatively minor component. It could, however, be due to a more fundamental variation in the composition of IOM.

The two components of IOM, distinguished by their reactivity, could be due to there being a mixture of types of macromolecule, of different structure and different reactivity, or alternatively, of a macromolecule containing regions of different reactivity, in a variable ratio. This second alternative could be represented by a core composed of a condensed aromatic system, effectively a fragment of graphene, with a functionalised (and so more reactive) periphery (of variable extent). The first

alternative therefore would comprise a physical mixture, containing both separate graphene fragments, and macromolecules composed of smaller, functionalised aromatic fragments, covalently linked, but lacking extended condensed π-systems. Whereas reaction of the former with ozone, which if resulting in substantial modification of its reactive periphery, would also give a change in the electronic structure of the underlying core, reaction of the independent macromolecules making up the second alternative, would not. The two types of macromolecule, not being covalently bonded, would be electronically independent, and a change in one would not be expected to exert significant change in the other.

Therefore, although the proposal that IOM contains two components differing in reactivity is supported by the data presented in this chapter, it is possible that the structure of the reactive component may vary considerably, even to the extent of being a separate macromolecule. Nevertheless, in either case, the component which reacts more extensively with ozone, is the same component which decomposes pyrolytically to generate the compounds detected as described in section 6.3.2. However, the set of compounds seen does not correspond to those which would be expected from pyrolytic decomposition of structures such as that proposed for IOM shown in Figure 1-3.

This conclusion is similar to that reached by Sephton *et al.* (2003), who proposed that IOM was composed of two components, which they named "Labile Organic Matter" (LOM) and "Refractory Organic Matter" (ROM), based on the behaviour of samples of whole rock meteorite, and isolated IOM, on stepped combustion and hydrous pyrolysis. This conclusion is further discussed in section 6.5, and in Chapter

7, when data obtained after demineralisation is presented, and the concept of LOM and ROM is reviewed in terms of the structure of IOM.

6.4. Demineralisation Part 1B: Removal of acid-soluble minerals

Following solvent extraction, the sample of Murchison was treated with dilute mineral acid. This procedure, described in the Appendix, serves to remove carbonates and other acid-soluble materials which can interfere in the subsequent fluoride-mediated demineralisation. The sample which resulted, sample 3AW, was analysed using the same techniques as that generated by solvent extraction.

6.4.1. Analysis of Sample 3AW

Raman Spectroscopy

A set of Raman spectra was acquired across the surface of a sample of 3AW; a graph of the positions of the D and G peaks, with comparisons with samples 3M and 3SE is shown in Figure 6-17. This shows a possible subtle shift in peak positions, but still giving considerable overlap with the other samples. This data is consistent with little or no chemical change occurring on treatment with mineral acid.

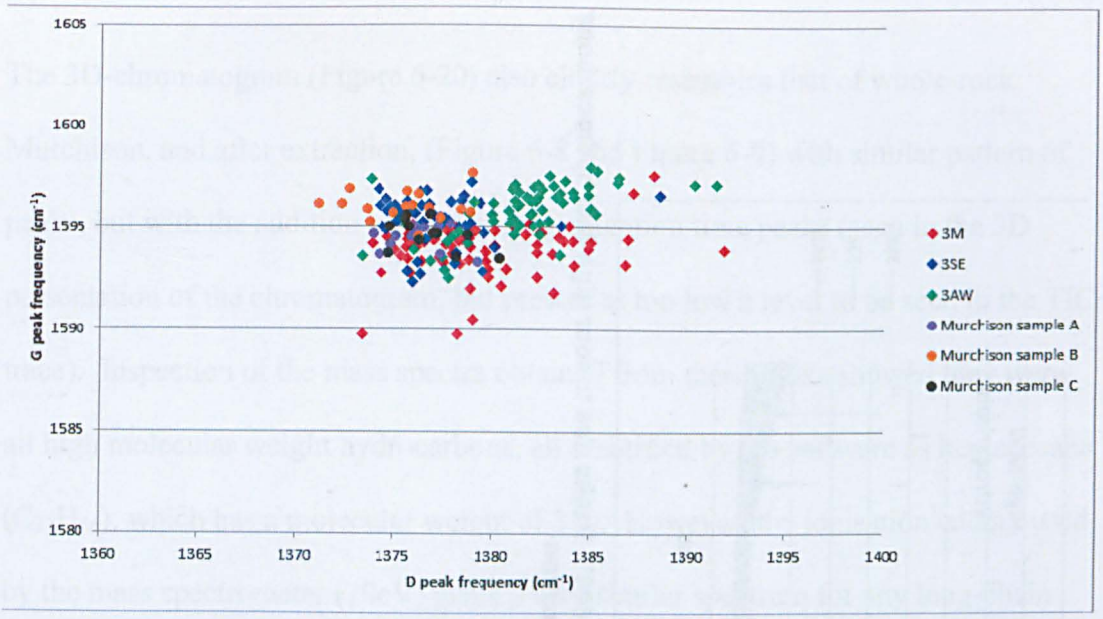

Figure 6-17: Comparison of positions of Raman signals in samples prepared from Murchison.

Py-GCxGC-ToF-MS

Pyrolysis of sample 3AW also gave very similar results (both at 300° and 600°) to those obtained for 3M and 3SE. No pyrolysate was detected at 300°; the TIC trace at 600° is shown in Figure 6-18. Treatment with dilute mineral acid could possibly lead to hydrolysis of esters or similar functional groups. However, the behaviour of sample 3AW was the same as 3SE (and 3M); there was no evidence of any chemical change during treatment with aqueous acid, and no new compounds were generated which could be detected after pyrolysis. Therefore, either the reaction conditions were not sufficient to cause any reaction of the precursor to the pyrolysate, or the functional groups which could undergo such a reaction are not present to any detectable extent.

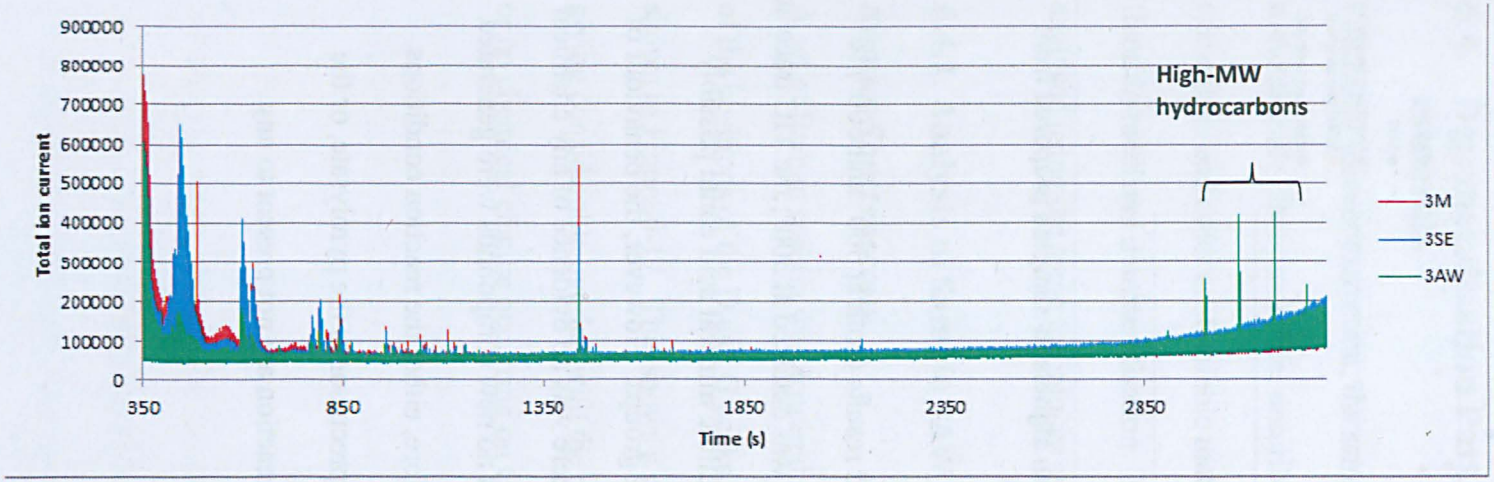

Figure 6-18: Comparison of TIC traces for samples prepared from Murchison following pyrolysis at 600°. Peaks due to four high-MW hydrocarbons can be seen in the trace of 3AW, probably due to contamination

The 3D-chromatogram (Figure 6-20) also closely resembles that of whole-rock Murchison, and after extraction, (Figure 6-8 and Figure 6-9) with similar pattern of peaks, but with the addition of a set of long-retention time peaks (seen in the 3D presentation of the chromatogram, but present at too low a level to be seen in the TIC trace). Inspection of the mass spectra obtained from these peaks showed they were all high molecular weight hydrocarbons, all identified by the software as heptacosane ($C_{27}H_{56}$), which has a molecular weight of 380. However, the ionisation energy used by the mass spectrometer (70eV) gives a very similar spectrum for any long-chain alkane. The molecular ion is usually too low an intensity to detect, as it fragments extremely rapidly, and all that can be seen is a set of ions of progressively lower intensity, separated by 14 mass units. The mass spectrum of one of these peaks is shown in Figure 6-19. Consequently, it is not possible to identify these peaks, other than as a set of long-chain hydrocarbons, or similar molecules for which the molecular ion rapidly decomposes. The origin of these compounds is unclear, but unlikely to have been generated during the extraction process.

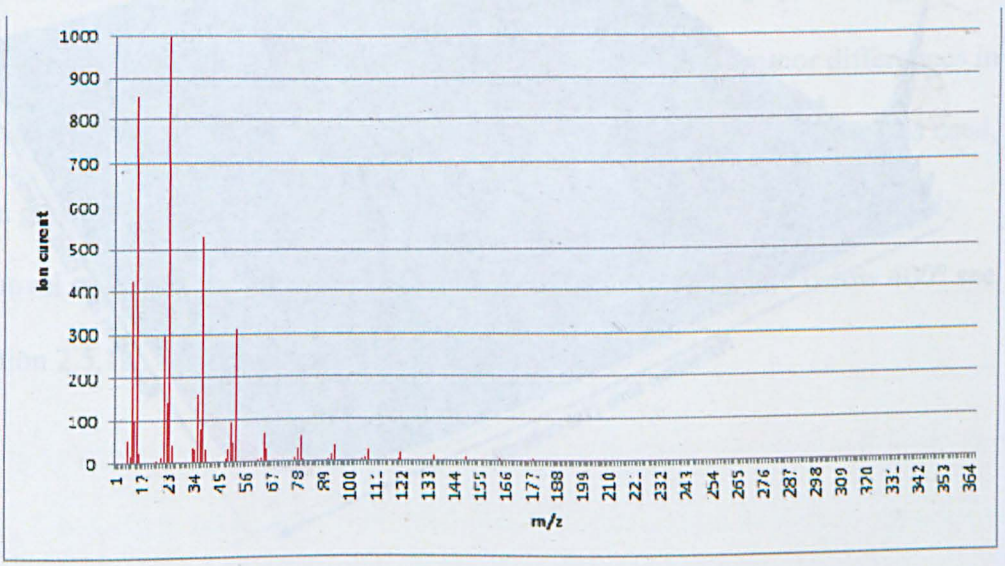

Figure 6-19: Mass spectrum of hydrocarbon peak in 3AW

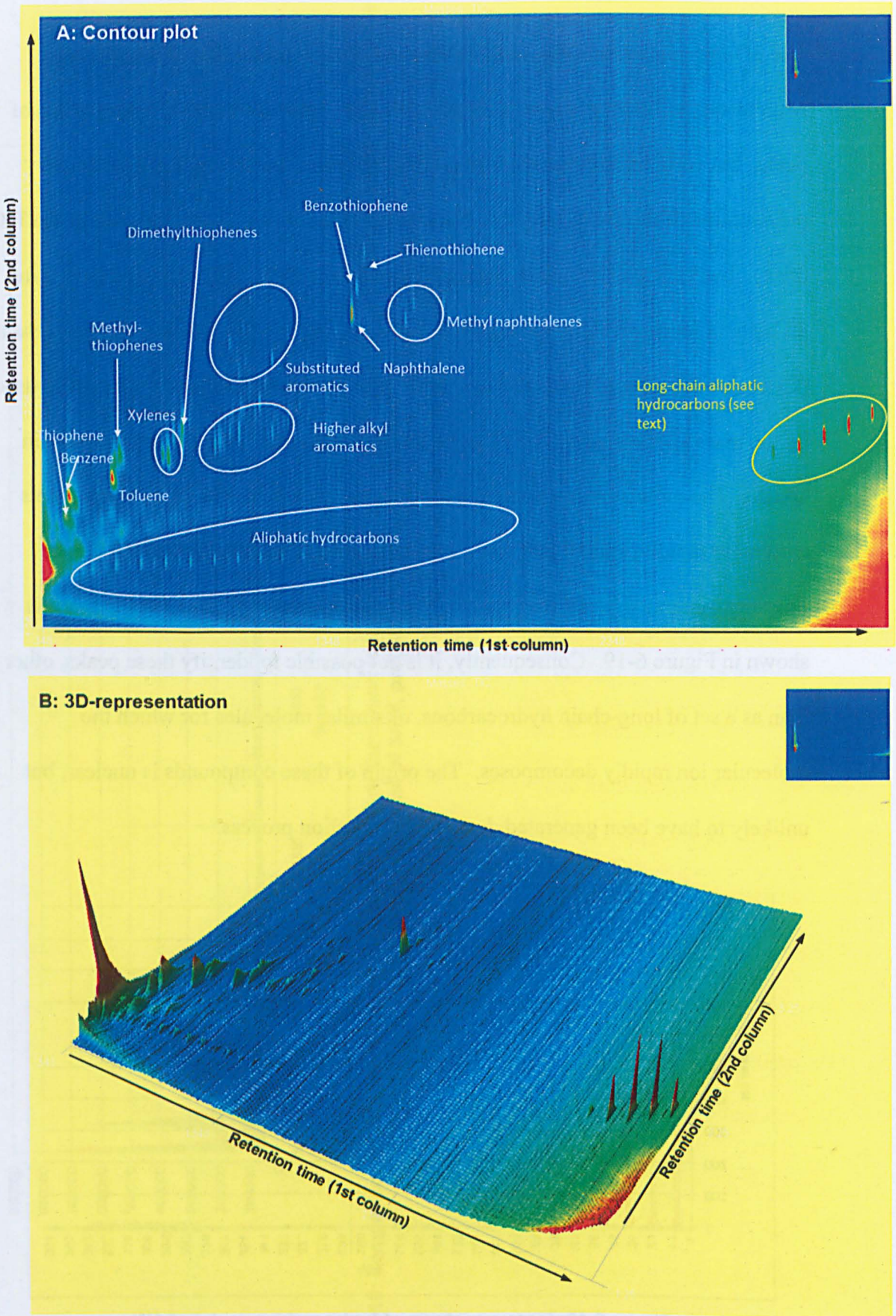

Figure 6-20: 3D-chromatograms of sample 3AW after pyrolysis at 600°

Stepped combustion

In addition to the two techniques discussed above, sample 3AW was also analysed by stepped combustion, as described in section 2.5. Analysis of the organic content of Murchison by stepped combustion has been reported by Sephton *et al.* (2003). A similar experiment (see section 2.5.2 for a description of the methodology), was performed using sample 3AW; the results of both experiments are shown in Figure 6-21.

Data reported for Murchison whole rock (by Sephton *et al.*, 2003) shows carbon dioxide is formed as the sample is combusted over a range from about 200° to 800°, with the maximum occurring between 400° and 600°. 3AW differs from this in that the majority of the carbon dioxide formation above 500° is much-reduced or absent. This is because carbonates and other minerals, (which combust or decompose in this temperature range) have been removed by acid treatment, with the exception of the trace of isotope-heavy material seen at high temperatures in both samples (possibly silicon carbide, removal of which by acid would not be expected). The materials present combusting at a lower temperature have remained largely unchanged (the release profile and isotopic signatures are very similar). The minor differences in profile in the region 200-400° may be due to the different temperature steps used, the data generated (by Sephton *et al.*, 2003) being at higher resolution, or possibly removal of minerals (such as some carbonates) which decompose below 400° see section 2.5.1.

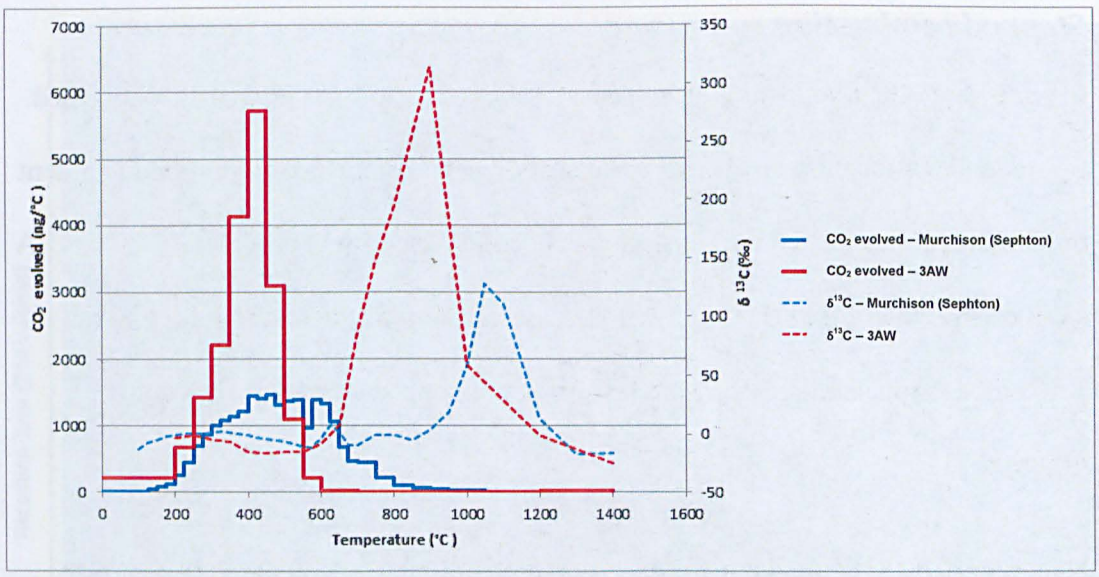

Figure 6-21: Comparison of profile of carbon combustion between bulk Murchison, and acid-washed sample showing quantities of CO_2 evolved, and isotopic ratios.

6.4.2. Treatment of Sample 3AW with Ozone

Sample 3AW was treated with ozone in the same manner as samples 3M and 3SE, with the addition of exposure to moist ozone for up to 96 h. This last experiment was intended to assess the result of such forcing conditions.

Raman spectroscopy

A plot of the positions of the D and G peaks seen in the Raman spectrum showed a slight difference following ozone treatment, as shown in Figure 6-22. Data from a sample exposed to moist ozone for up to 96 h is shown in Figure 6-23. This shows that, in this sample, even with such a long exposure to ozone, very little change in peak position is seen. The set of spectra obtained from this sample is shown in Figure 6-24. Although this shows the presence of gypsum, and of forsterite (revealed by the decomposition of IOM possibly coating the grains (El Amri *et al.*, 2005), no evidence of the oxalate-containing mineral (at 1470 cm^{-1}) was seen, although a few of the spectra contained other, unidentified peaks. This shows that the lack of formation of oxalic acid in other samples is not a consequence of the use of dry ozone.

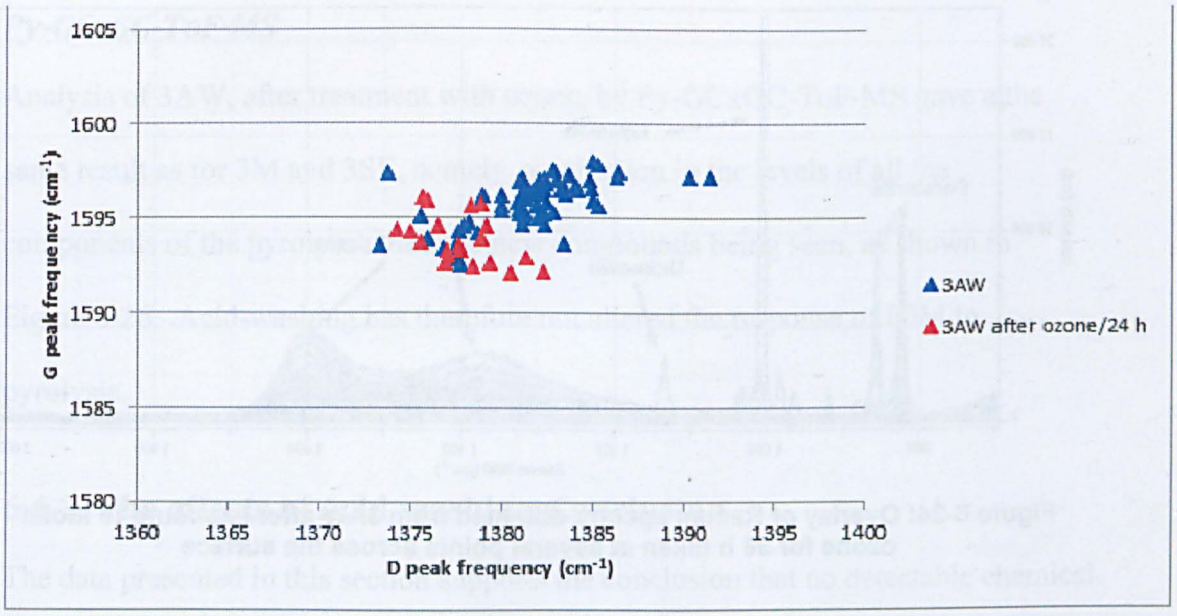

Figure 6-22: Raman peak positions for sample 3AW before and after exposure to ozone

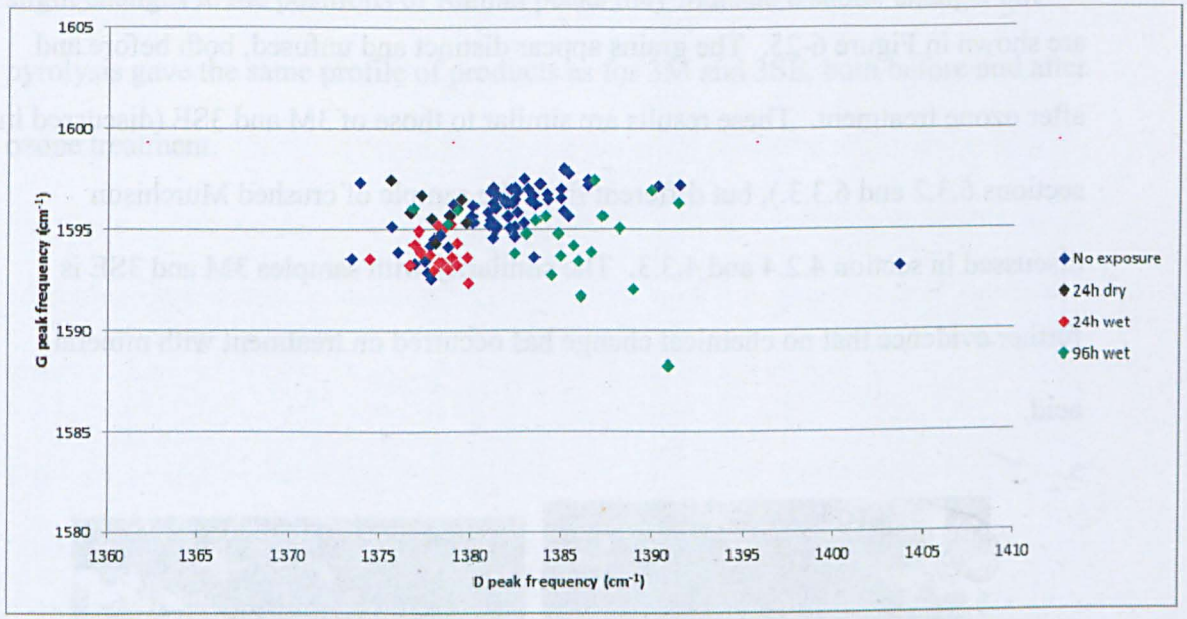

Figure 6-23: Comparison of position of peaks in Raman spectra of sample 3AW following exposure to ozone for up to 96 h

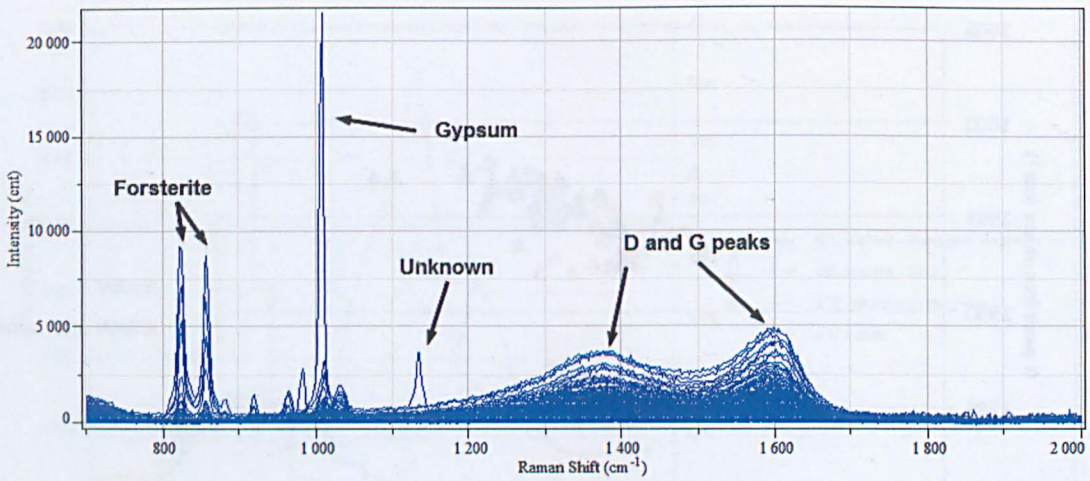

Figure 6-24: Overlay of Raman spectra obtained from 3AW after exposure to moist ozone for 96 h taken at several points across the surface

SEM

Sample 3AW was examined by SEM both before and after ozone treatment; images are shown in Figure 6-25. The grains appear distinct and unfused, both before and after ozone treatment. These results are similar to those of 3M and 3SE (discussed in sections 6.3.2 and 6.3.3.), but different from the sample of crushed Murchison discussed in section 4.2.4 and 4.3.3. The similarity with samples 3M and 3SE is further evidence that no chemical change has occurred on treatment with mineral acid.

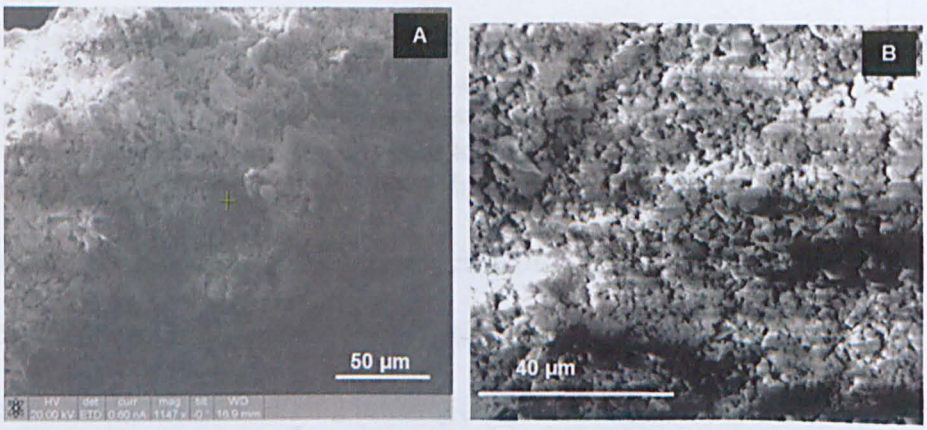

Figure 6-25: SEM images of 3AW A) before and B) after exposure to ozone

Py-GCxGC-ToF-MS

Analysis of 3AW, after treatment with ozone, by Py-GCxGC-ToF-MS gave a the same result as for 3M and 3SE, namely, a reduction in the levels of all the components of the pyrolysate, and no new compounds being seen, as shown in Figure 6-26. Acid-washing has therefore not altered the response of IOM to pyrolysis.

6.4.3. The effects of Acid-washing: Conclusion

The data presented in this section supports the conclusion that no detectable chemical change occurs to the sample following treatment with dilute mineral acid. Very slight changes in the positions of Raman peaks may indicate a subtle change, but pyrolysis gave the same profile of products as for 3M and 3SE, both before and after ozone treatment.

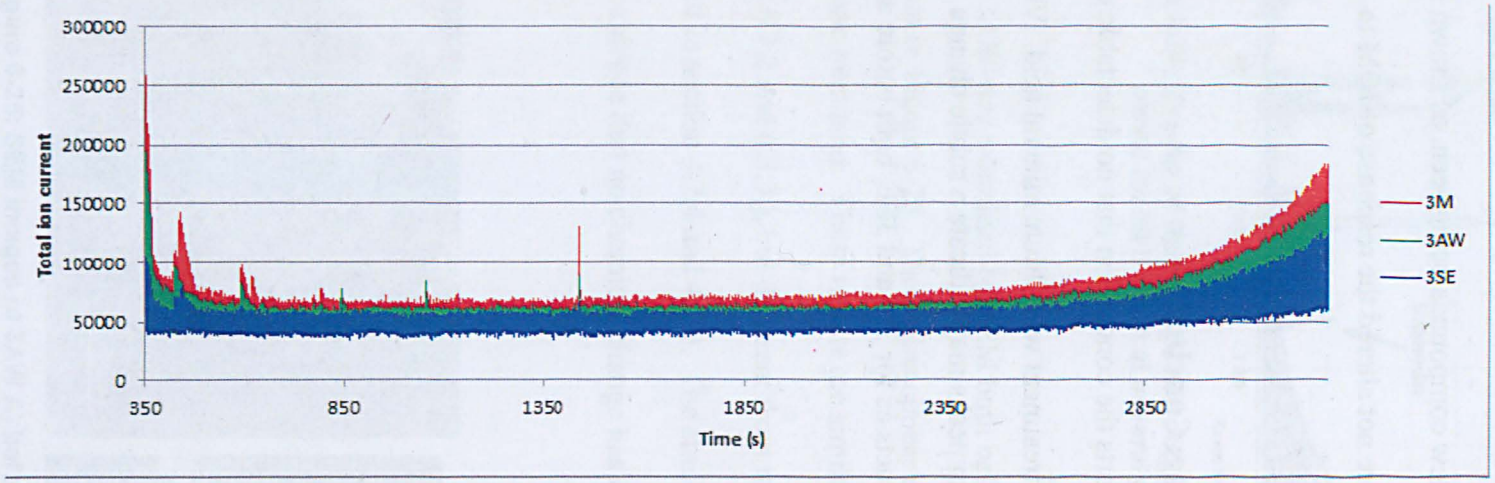

Figure 6-26: Comparison of TIC traces for pyrolysis of samples exposed to ozone for 24 h

6.5. Demineralisation Part 1: Conclusions

The goal of the work presented in this chapter was to assess the effect of the first two stages of demineralisation, namely solvent extraction and acid-washing. The data generated showed no detectable chemical change had occurred to the structure of IOM during either of these procedures. The data also supports previous studies (such as those reviewed by Gilmour, (2005)), in that the level of volatile or soluble organic materials in Murchison is low (and so not detected by the methods used). The Raman spectra of the samples and the products generated on pyrolysis are therefore derived from IOM.

The data also gives a better understanding of the structure and reactivity of IOM, building on the results obtained and described in Chapter 4 and 5. All the results obtained indicate that IOM contains two components, one being more reactive, and one less so. The proportions of these components vary from sample to sample, along with a possible structural variation in the more reactive component, which could be a separate macromolecule, or part of a larger, heterogeneous system.

The sample of meteorite used for demineralisation behaved somewhat differently from those used for the work described in Chapter 4. On treatment with ozone, oxalic acid has been generated from of other samples of Murchison (whole rock, or extracted), but none was seen in this latest sample. This fragment of Murchison therefore lacks the precursor to oxalic acid, which could be either some discrete compound, or part of the more reactive component of IOM. The evidence supports the latter alternative; all samples of Murchison used have either been stored for some time, or exposed to vacuum, allowing loss of volatiles (although no likely precursor to oxalic acid was detected in the latter case). If the precursor to oxalic acid is

present within the structure of IOM, then either IOM is modified on storage to generate this precursor, or it is heterogeneously distributed within the meteorite.

On pyrolysis, the reactive component yields a set of (largely) aromatic compounds, which are separated and detected by GCxGC-ToF-MS. These compounds are largely hydrocarbons and sulfur-containing heterocycles, and are not compounds which might be expected from decomposition of structures such as that proposed for IOM shown in Figure 1-3, (which contain many oxygen-substituted sub-units). On treatment with ozone, this reactive component is converted into a derivative which does not give a detectable pyrolysate. Although the actual composition and/or molecular structure of this precursor may vary from sample to sample, the profiles of the products of pyrolysis of the samples were all very similar.

The removal of the pyrolysate precursor on exposure to ozone occurs over a relatively short time, but even after 96 h exposure, the D and G peaks are still the dominant feature of the Raman spectrum. These must therefore derive largely from the less-reactive component. The actual position of the D and G peaks in untreated whole rock presumably represents a weighted average of peak positions of the two individual components. The Raman spectrum of IOM only changed slightly on exposure of the samples 3M and 3SE to ozone (in contrast to previous data), which is consistent with the proportions of the components of IOM varying from sample to sample, due to the heterogeneity of Murchison. In this example, modification of the more reactive component does not seem to have had an effect on the less-reactive, indicating they may be separate macromolecules, in contrast to the sample used for the work discussed in Chapter 5. In both examples however, the level of pyrolysate was lowered with ozone exposure, resulting eventually there being none detected.

These results support the proposal of Sephton *et al.* (2003) that IOM contains two components. The more reactive component is comparable with Sephton's LOM, and the less reactive with ROM.

The process of demineralisation continues with removal of silicates by treatment with fluoride-containing solutions. This is discussed in Chapter 7. Data generated from that procedure is discussed, including a structural interpretation of the composition of IOM.

Chapter 7 The Demineralisation of Murchison Part 2: Fluoride Treatments

The first two stages of demineralisation, solvent extraction and acid washing, were discussed in Chapter 6. The data obtained supported the suggestion that IOM comprises two components with differing reactivity, but also showed that neither of these components was affected by solvent extraction or acid-washing. All data obtained relating to IOM was the same, either before or after those treatments.

The next two stages of demineralisation are discussed in this chapter, namely treatment with fluoride to convert insoluble silicates into soluble minerals (such as fluorosilicates) followed by a further treatment with hydrochloric acid to remove any minerals remaining. The data generated from those procedures is reported, and the results discussed, both in relation to the objectives of this project, and to wider implications for the study of meteorites.

The preparation of sample 3AW was discussed in Chapter 6, with practical details being described in the Appendix. This sample was processed further, using two methods of demineralisation, as described below.

Each sample prepared was given a number, relating to the sample of Murchison used to prepare it, and a suffix, denoting its position in the demineralisation process. The sample designations are listed in Table 7-1, and the relationships between the samples shown graphically in Figure 7-1. Samples derived from 1M and 2M were prepared as part of a previous project; those samples shown in italics were no longer available.

Suffix	Significance
M	Murchison whole rock
SCE	Extracted with supercritical CO_2
SE	Extracted with organic solvents and water
AW	Treated with dilute mineral acid
DC	Demineralised using the procedure of Cody *et al.* (2002)
DA	Demineralised the procedure of Amari *et al.* (1994)
DAB	Treated with borate
DAH, DCH	Further treated with 6M HCl

Table 7-1: Abbreviations used as sample designations in this study

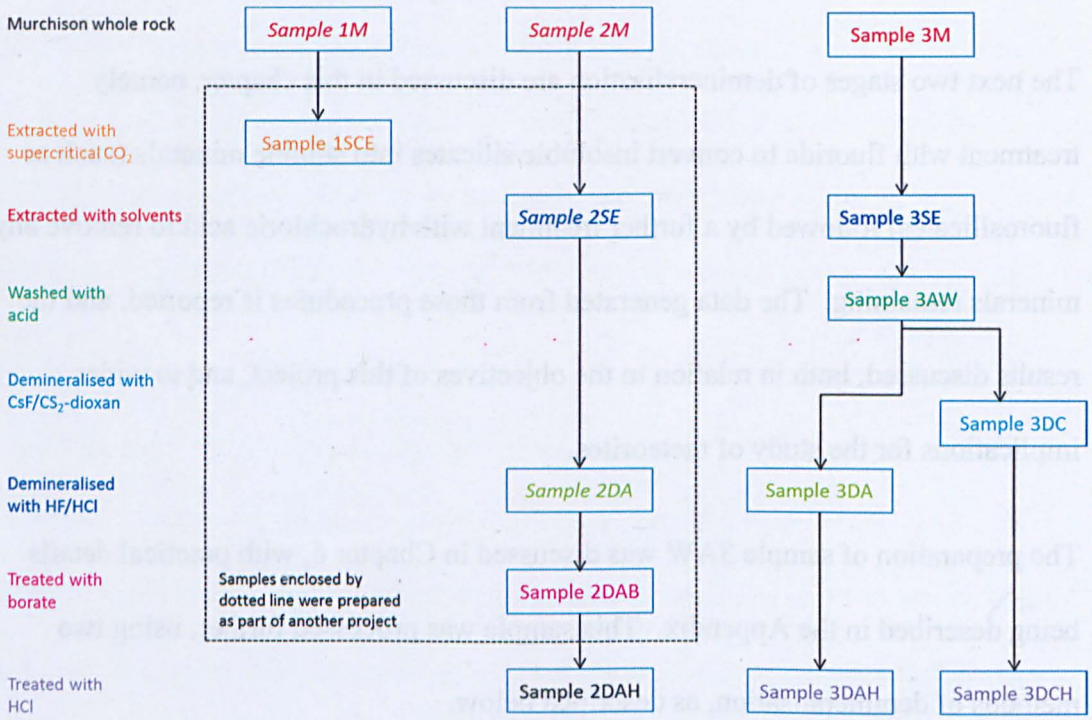

Figure 7-1: The relationships between samples prepared from fragments of Murchison

7.1. Demineralisation Part 2; Fluoride Treatments

A sample of IOM was isolated from acid-washed Murchison, 3AW using each of the procedures of Amari *et al.*(1994) , and Cody *et al.* (2002), and designated 3DA and 3DC respectively. Data generated from these samples was compared with that from sample 2DAH prepared previously (also using the method of Amari *et al.* (1994)). The analysis and reactions of 2DAH were described in Chapter 5, and all preparative procedures are described in the Appendix.

7.1.1. SEM

Both 3DA and 3DC, were examined by SEM. Sample 3DA (Figure 7-2) appeared to contain mostly small organic grains, but discrete mineral grains could clearly be seen. Sample 3DC was composed of aggregates of grains (Figure 7-3), also showing the presence of minerals (including caesium salts, remaining from the demineralisation process).

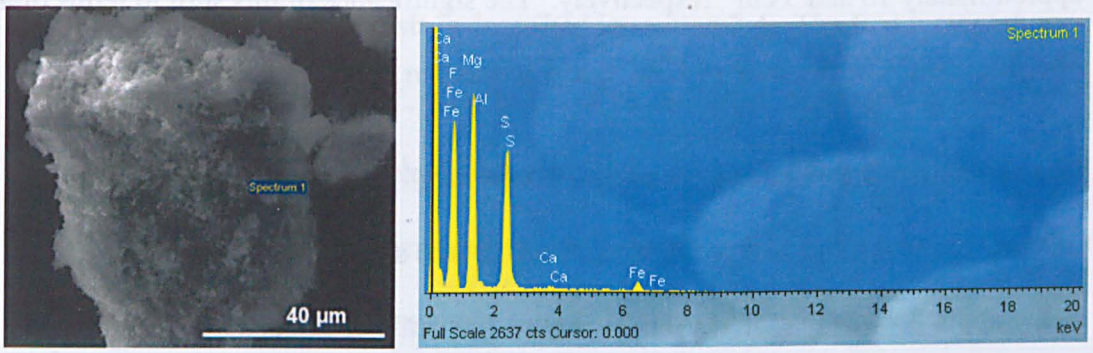

Figure 7-2: SEM images and X-ray spectra obtained from sample 3DA

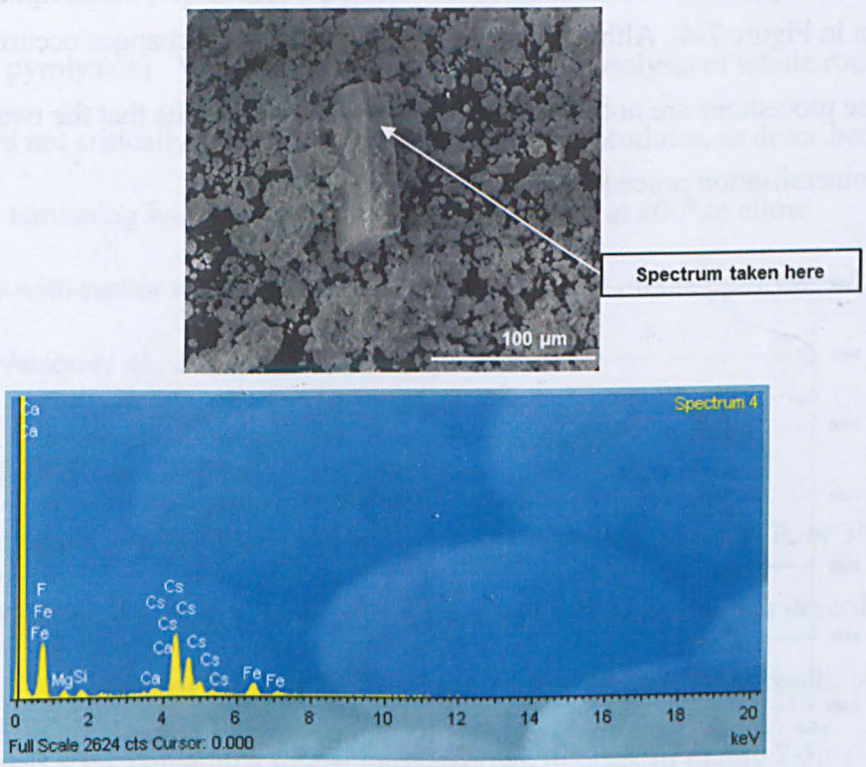

Figure 7-3: SEM images and X-ray spectra obtained from sample 3DC

7.1.2. Raman Spectra

Raman spectra of the samples obtained after fluoride treatment (2DAH, 3DA and 3DC), plus that of acid-washed Murchison (3AW) were compared; the positions of the D and G peaks are plotted in Figure 7-4. The differences between 2DAH and 3AW were similar to those described in section 5.4; on demineralisation, the D peak moved to higher frequency, and the G peak to lower, with the average shift being approximately 10 and 5 cm^{-1} respectively. The significance of this shift in terms of a possible change in structure of IOM was discussed in section 5.4.4.

The shifts in peak positions for sample 3DA (isolated using the same method as 2DAH) were in the same directions as 2DAH, but to a lesser magnitude, that of 3DA being about 20% of that of 2DAH. However, the shifts of frequencies of sample 3DC, although similar in extent to 3DA, were in the opposite direction, as can be seen in Figure 7-4. Although the nature of the chemical changes occurring during these procedures are not known, it seems from these results that the two demineralisation procedures have had a different effect.

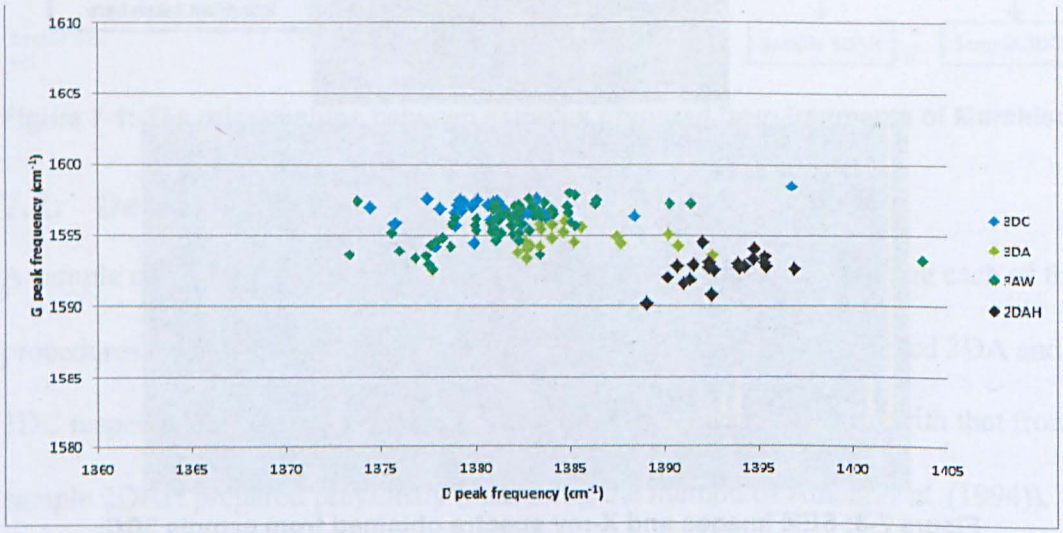

Figure 7-4: Raman peak positions of IOM isolated using different procedures

7.1.3. Py-GCxGC-ToF-MS

Results from pyrolysis (as in previous experiments, described in section 6.3.2) were presented in two ways. The variation of each total ion current (TIC) with time was used to generate a profile by which the samples could be compared, in the manner of a fingerprint. The identities of the compounds were then determined using ChromaTof software.

The science underlying pyrolysis is described in section 2.4. The first temperature step in the sequence used, 300°, was chosen to be sufficient to remove physically-retained or absorbed compounds, but not to cause any pyrolytic decomposition (*via* breaking of bonds). This temperature is also the maximum that the primary GC oven reaches during the temperature ramp.

The second temperature step causes a pyrolytic decomposition of the sample, (generating a pyrolysate). Variation in the temperature of pyrolysis of whole rock Murchison did not critically affect the profile of pyrolysate products, as described in section 6.3.1; remaining work was therefore also carried out at 600° to allow comparability with earlier work, and that previously reported on the pyrolysis of Murchison (Watson *et al.*, 2007).

Pyrolysis of 2DAH at 300°

Whereas unprocessed, extracted or acid-washed Murchison (samples 1SCE, or 3M, 3SE and 3AW) showed no appreciable pyrolysate when heated at 300° (as described in section 6.3.1), a sample of isolated IOM, 2DAH, gave a very different result. A strong signal was seen, containing many peaks, (shown in black in Figure 7-5, expanded to clearly show the corresponding lack of signal arising from 1SCE, which is shown in orange).

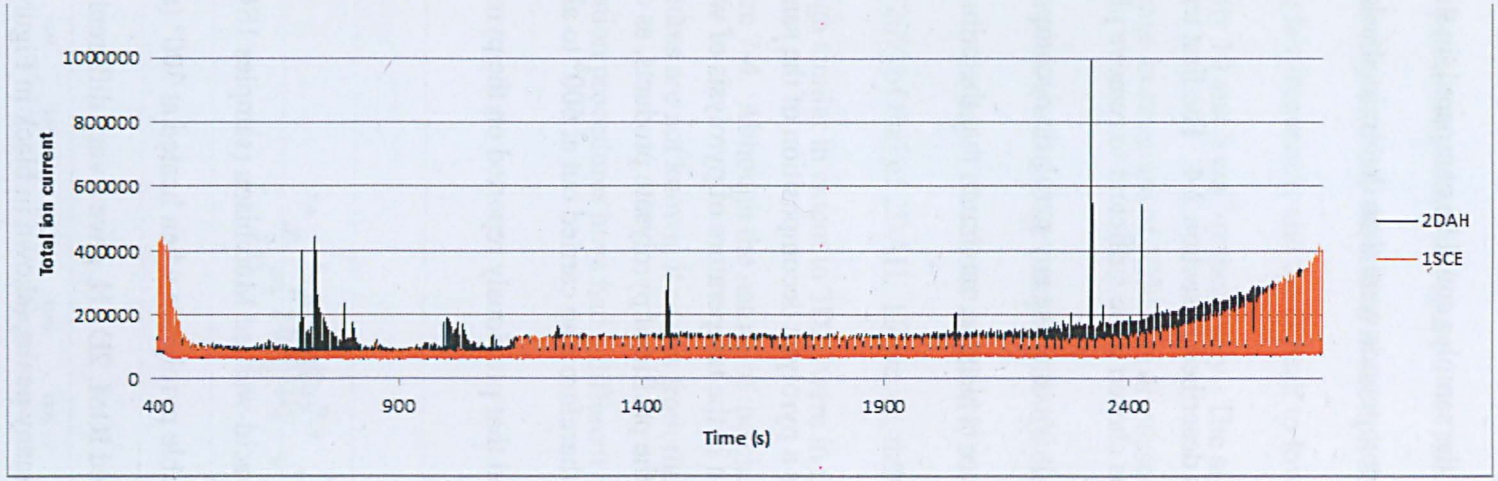

Figure 7-5: Comparison of TIC traces of samples 1SCE and 2DAH obtained following pyrolysis at 300°

It is possible that the higher level of pyrolysate seen was merely due to the organic content of 2DAH being higher than for undemineralised samples (such as 1SCE), resulting in easier detection. However, the heights of the early (non-retained) peaks of 2DAH and 1SCE were comparable, and, when the chromatograms were displayed as 3D plots (from which the non-retained peaks and solvent bleed can be filtered, and any small peaks, if present, would be visible), compounds seen in 2DAH were not present in 1SCE, even at low levels (Figure 7-7 and Figure 7-8). Therefore, the observation that significant pyrolysate is obtained from the demineralised sample, 2DAH when heated at 300°, but not from any of the undemineralised samples, indicates that the compounds observed must have either been generated during the demineralisation process, or possibly by decomposition of this sample of isolated IOM on storage.

Identification of the products of pyrolysis of 2DAH at 300

The 3D-chromatogram of 2DAH following pyrolysis at 300° is shown in Figure 7-8. This shows hydrocarbons similar to those seen in undemineralised samples when pyrolysed at 600° (and discussed in section 6.3.2), both a series of aliphatic hydrocarbons, as well as substituted benzenes, naphthalene, and other, larger aromatic systems (such as phenanthrene). Two compounds, t-butyl phenol and 5-bromo-4-hydroxy-*m*-cymene were not seen previously in samples of unprocessed Murchison, but now gave strong peaks. The mass spectrum and structure of the latter are shown in Figure 7-6. The source of this compound is unknown; no reagents containing bromine have been used. Sulfur-containing heterocycles (thiophene, and substituted derivatives), which were seen in all undemineralised samples when pyrolysed at 600° (section 6.3.1), were absent, although elemental sulfur was seen.

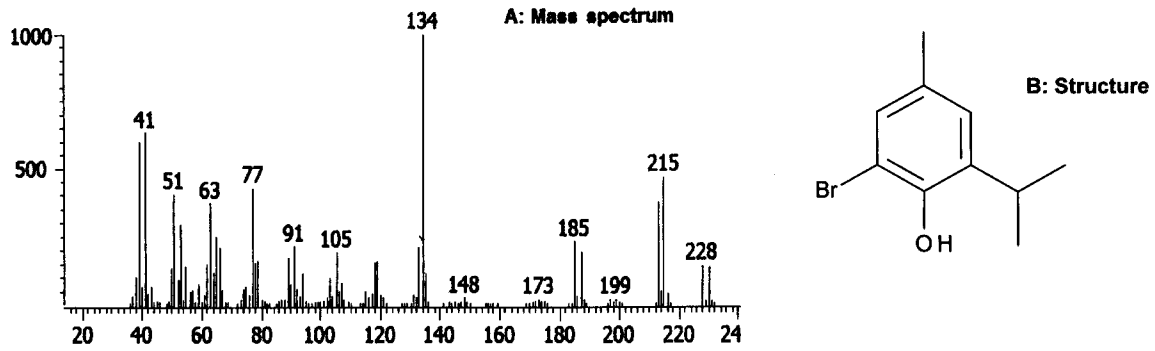

Figure 7-6: Mass spectrum (A) and structure (B) of 5-bromo-4-hydroxy-*m*-cymene

In contrast, the low levels of compounds formed from 1SCE on pyrolysis at 300° are clearly seen in Figure 7-7; the only compounds clearly identified were naphthalene (always the major component of pyrolysate), styrene and benzaldehyde, as well as a set of aliphatic hydrocarbons.

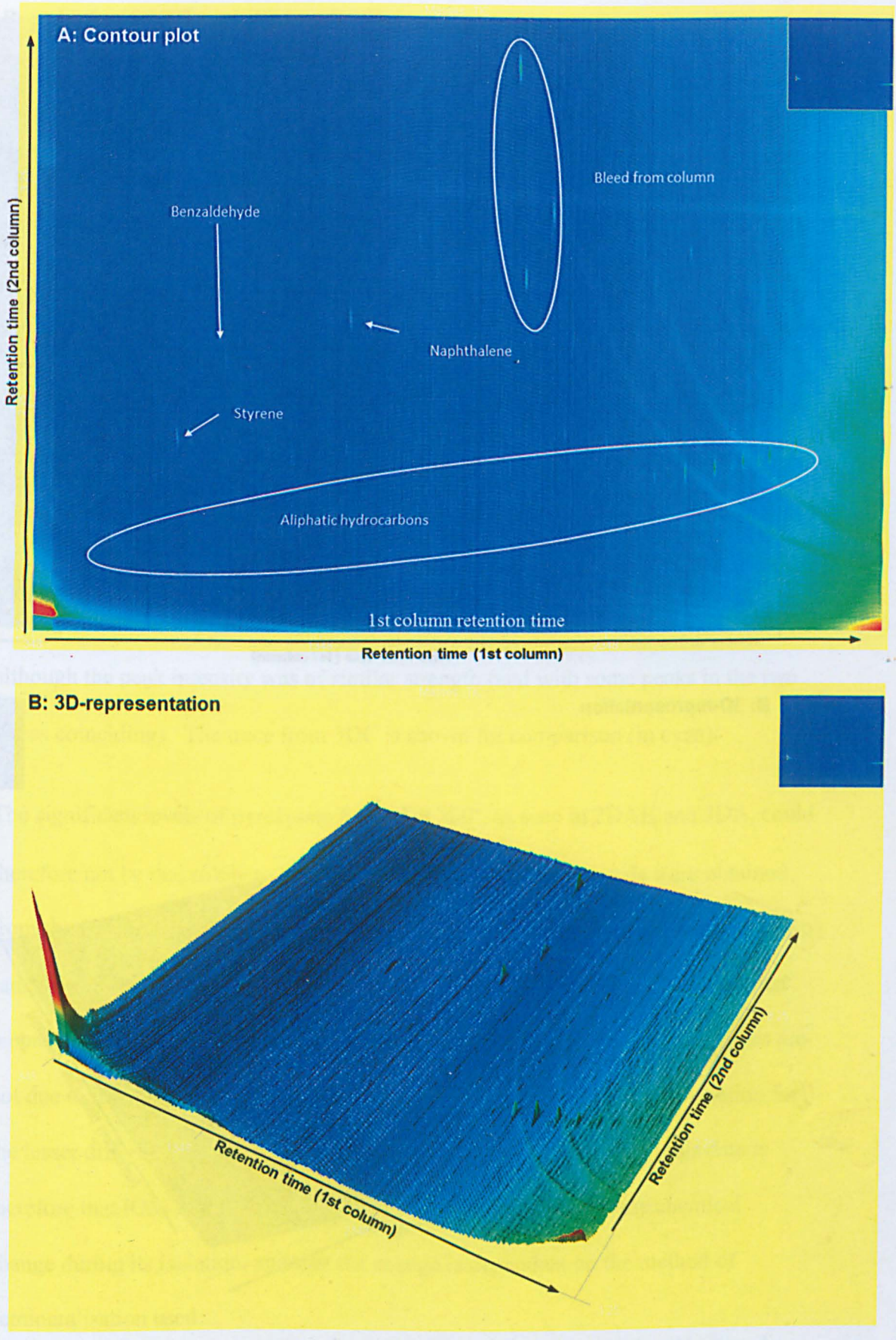

Figure 7-7: 3D-chromatograms of 1SCE after pyrolysis at 300°

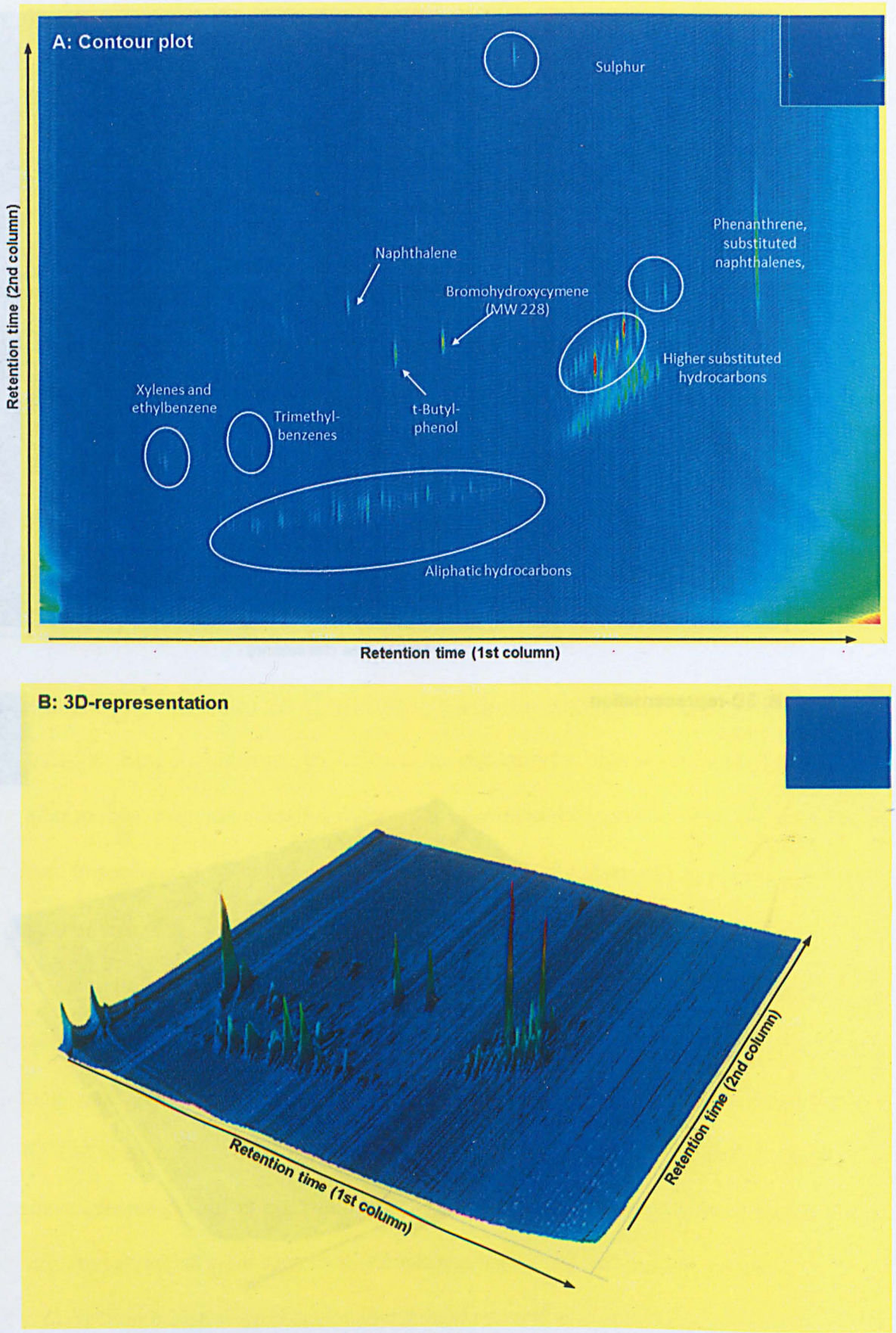

Figure 7-8: 3D-chromatograms of 2DAH after pyrolysis at 300°

Pyrolysis of 3DC and 3DA at 300°

The two freshly-isolated samples of IOM (3DC and 3DA) were then pyrolysed at 300°, and the TIC traces compared. Each was carried out in duplicate, so any sub-sample differences seen are likely to be due to sample heterogeneity.

The sample isolated using the method of Cody *et al.*(2002) (3DC) showed a very low level of pyrolysate. In one sub-sample, pyrolysate was almost undetectable (shown in green in Figure 7-9), and so quite different from sample 2DAH (black trace). The second sub-sample of 3DC (blue trace) gave only minimal pyrolysate.

The sample of IOM isolated using the method of Amari *et al.*(1994) (3DA), gave a very different result (shown in Figure 7-10). A substantial set of compounds was seen (green trace) which was not the same as that derived from 2DAH (black trace), although the peak intensity was of similar strength (and with some peaks in the two traces coinciding). The trace from 3DC is shown for comparison (in cyan).

The significant levels of pyrolysate formed at 300°, as seen in 2DAH and 3DA, could therefore not be due solely to changes on storage, as a similar levels were obtained from the freshly-prepared 3DA, as from the much older 2DAH. The fact that the two samples prepared using the method of Amari *et al.* (1994) are similar, whereas that prepared by the method of Cody *et al.* (2002)is not, implies that these differences are not due to inhomogeneities in Murchison, although that could be the explanation for the lesser differences between 2DAH and 3DA. The conclusion from this data is therefore that IOM isolated by demineralisation has undergone some chemical change during its isolation, and that the change is dependent on the method of demineralisation used.

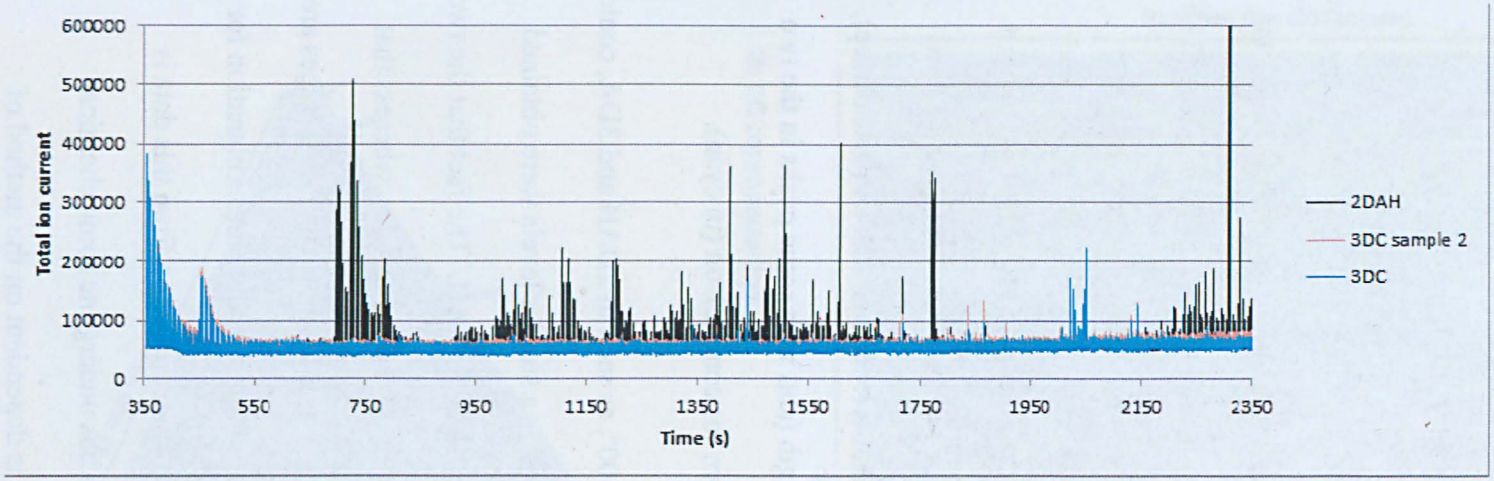

Figure 7-9: Comparison of TIC traces of samples of 2DAH and 3DC after pyrolysis at 300°

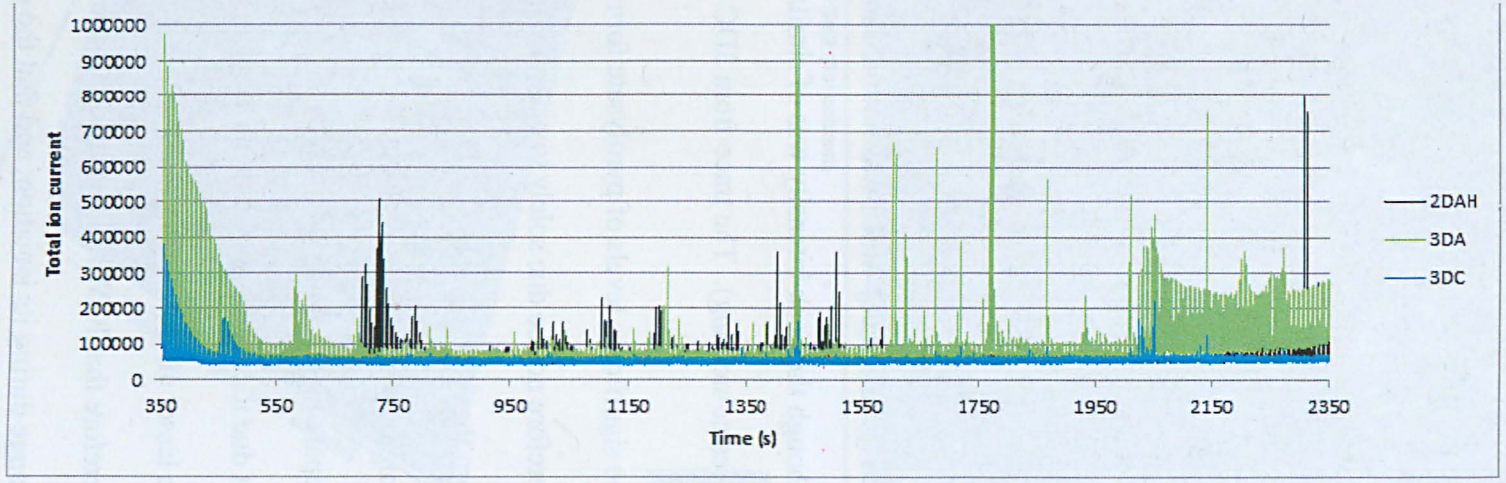

Figure 7-10: Comparison of TIC traces from IOM after pyrolysis at 300°

Identification of the products of pyrolysis of 3DA and 3DC at 300°

The 3D-chromatograms derived from samples 3DC and 3DA are shown in Figure 7-11 and Figure 7-12 respectively. Expansion of the scale of Figure 7-11 to show the low levels of compounds present in the pyrolysate of 3DC gives a noisy chromatogram, but naphthalene and aliphatic hydrocarbons can be seen. Substituted aromatic hydrocarbons and thiophenes are present at low levels, as well as elemental sulfur. The chromatogram derived from 3DA, is quite different from both 2DAH and 3DC. The compounds which had been detected in 3DC are all present, including phenols and bromohydroxycymene, but also the thiophenes are identifiable, which were not seen in 2DAH (although only present at low levels).

In addition, sample 3DA showed a very large, wide peak centred at a retention time of about 3000 s (and clearly seen in Figure 7-12 as a wide band). This effect (also seen in a duplicate sample) seems to result from decomposition of some portion of the pyrolysate on-column, giving low-molecular weight compounds (as shown by MS), and probably due to the presence of sulfur in sample 3DA. Displaying the chromatogram, selected for oligomeric sulfur ions (multiples of 32) shows this to be the case, as shown in Figure 7-13A and B (the y-axis is the same for both traces). Significant sulfur would not be expected to be present in 3DC; sulfur is soluble in carbon disulfide, and so would be expected to dissolve in the organic solvent mixture used in the isolation method developed by Cody *et al.* (2002)(which contains carbon disulfide), and thus be lost. As sulfur is not soluble in aqueous acid, it would not be lost when IOM was isolated using the method of Amari *et al.* (1994)

Sulfur is also seen in the chromatogram of 2DAH, but at much lower levels than in 3DA, which may represent different conditions used in the isolation methods, or a lower level present in the sample of Murchison used.

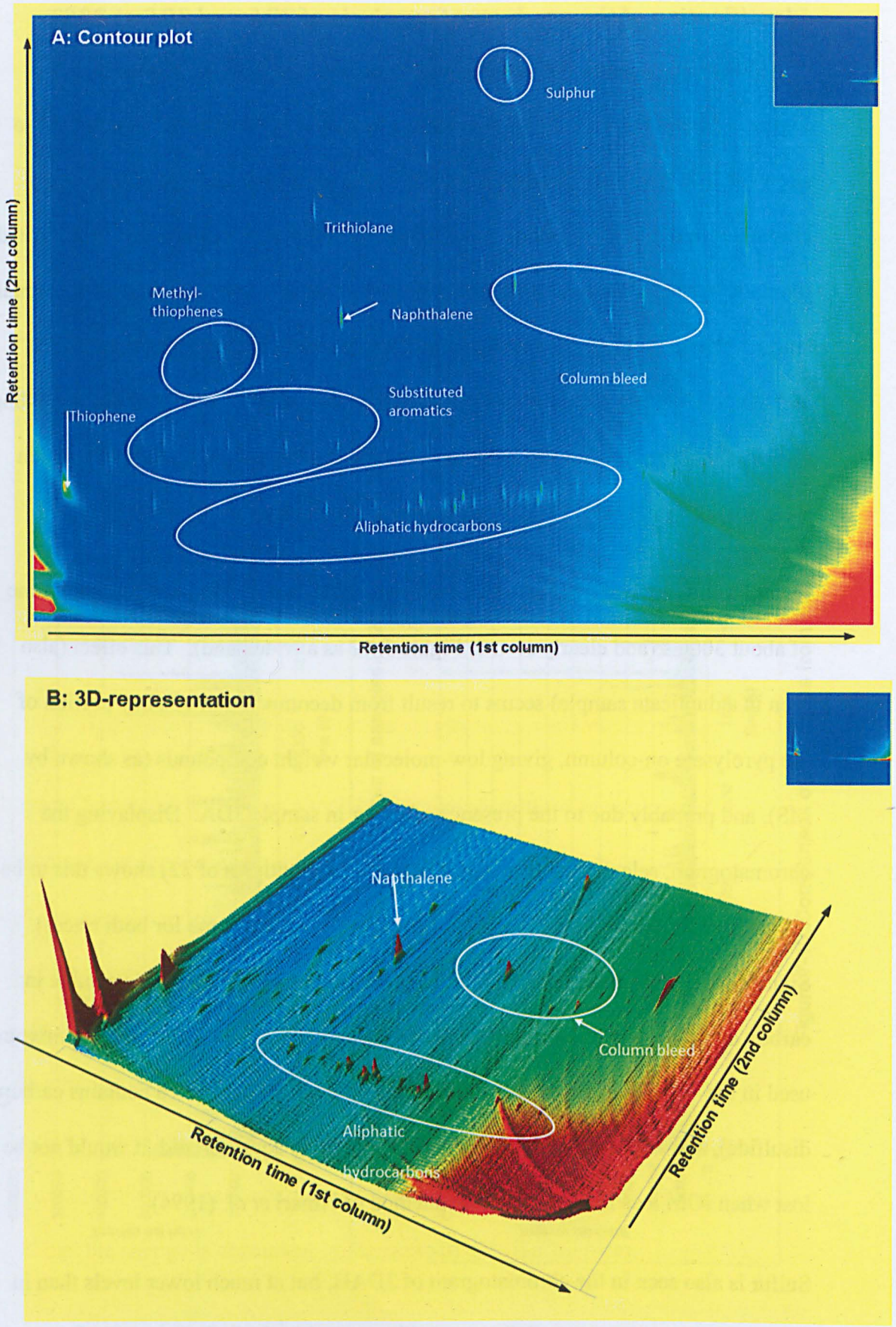

Figure 7-11: 3D-chromatograms of 3DC after pyrolysis at 300°

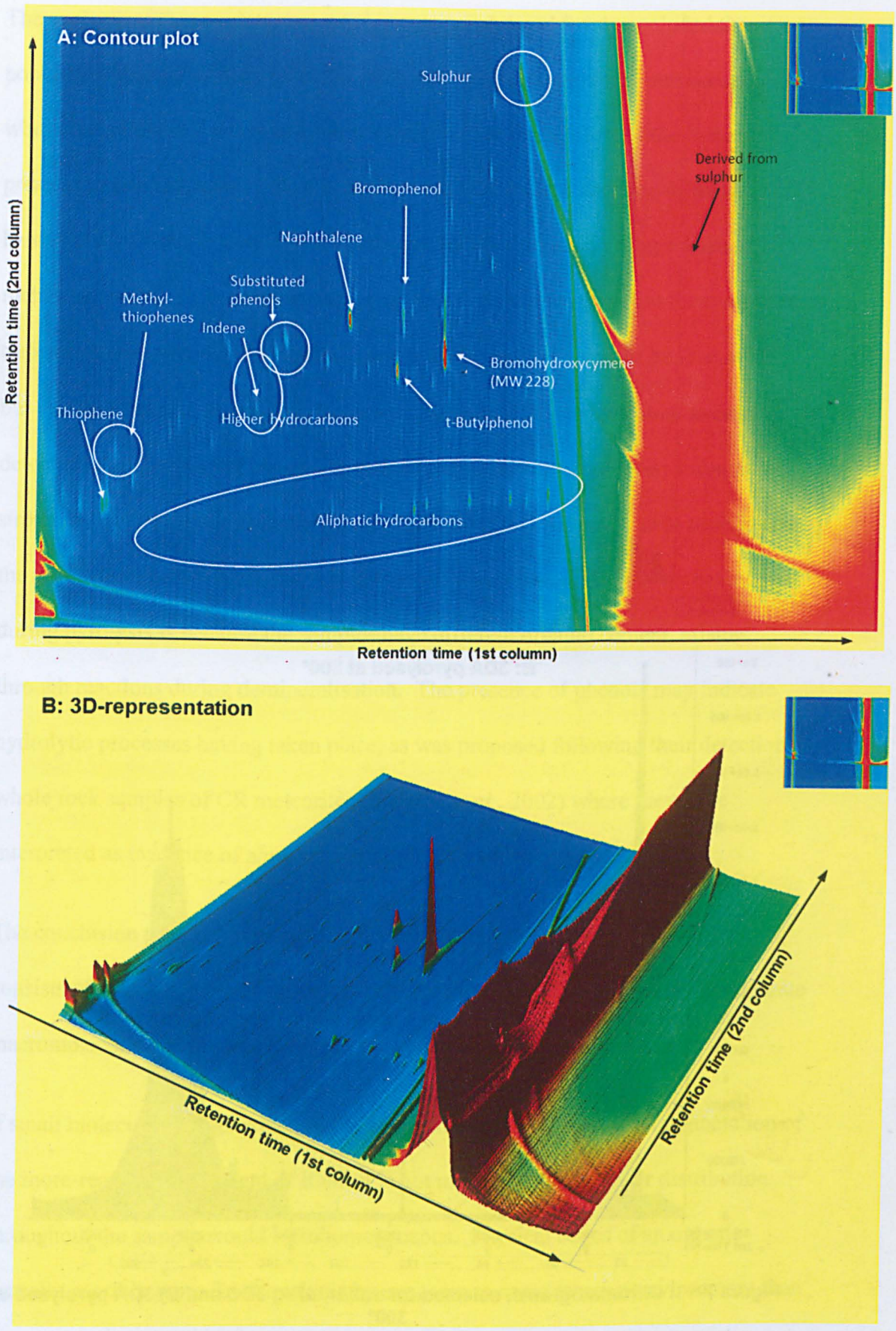

Figure 7-12: 3D-chromatograms of 3DA after pyrolysis at 300°

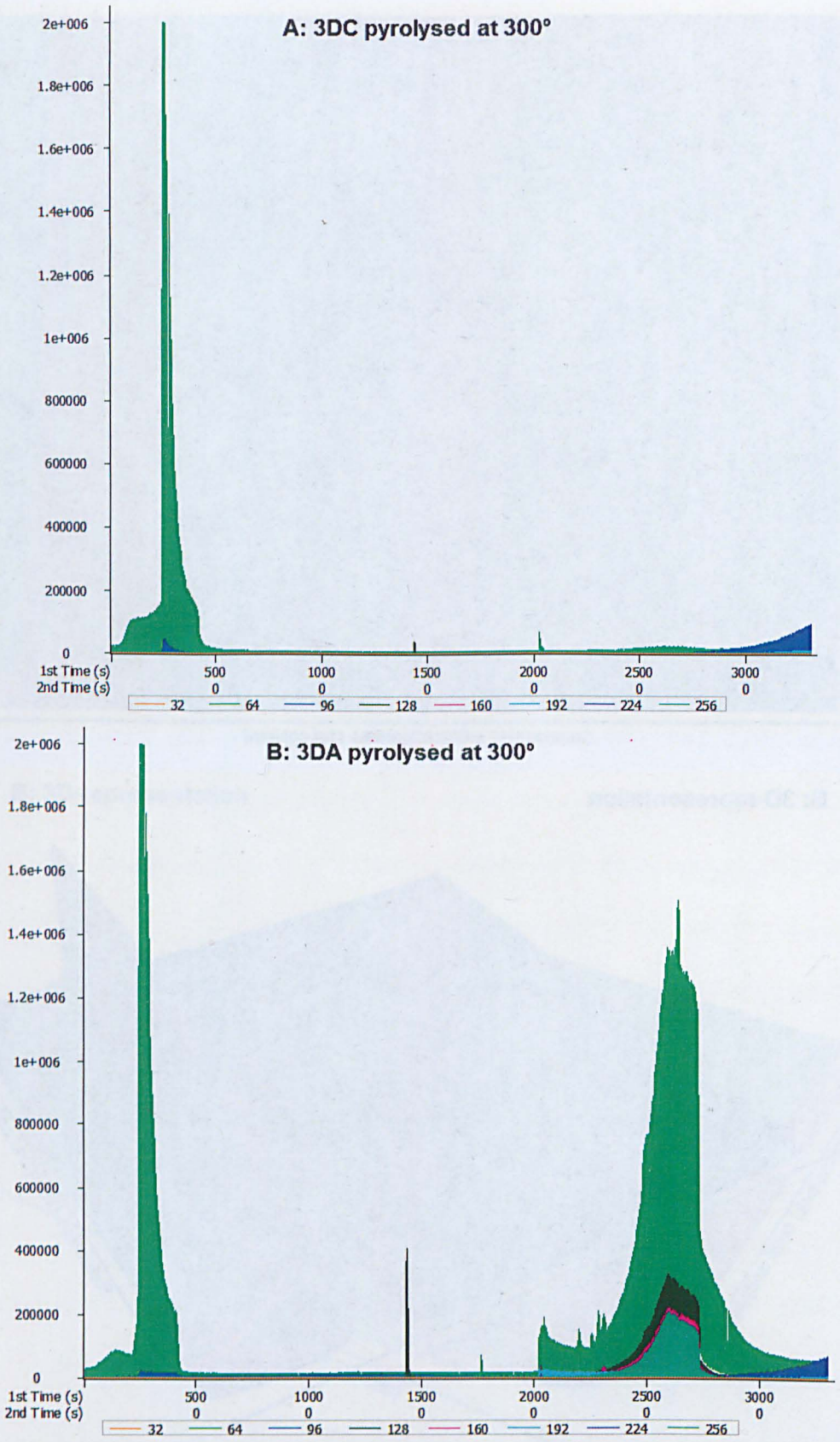

Figure 7-13: Chromatograms, selected for sulfur, of A) 3DC and B) 3DA pyrolysed at 300°

The analysis of Raman data presented in sections 4.4 and 5.4.4 concluded that it was possible (although unlikely) that the differences in peak positions seen between whole rock and demineralised samples could be due to an effect of the minerals present (or absent), rather than a difference in the chemical structure of IOM. It is hard to rationalise the presence of minerals with the prevention of pyrolysis of meteorite at 300°. It is possible that organic materials present within the sample are trapped in some way by the minerals, and not allowed to escape on heating at 300°, but that only when the sample is demineralised would they be released, and then detected. Any binding of organic materials with minerals is not likely to be so strong, as the very large macromolecules forming IOM will not be able to fit inside the sheet structure of clays. It is much more likely that the difference in behaviour during pyrolysis is because the samples have different organic content, arising through reactions during demineralisation. The presence of phenols may indicate hydrolytic processes having taken place, as was proposed following their detection in whole rock samples of CR meteorites (Pearson *et al.*, 2002) where they were interpreted as evidence of aqueous alteration on the meteorite parent body.

The conclusion previously reached (and discussed in section 6.5) was that IOM consists of two components, one more reactive than the other, which may be separate macromolecules, or discrete parts of the same macromolecular structure.

If small molecules are generated in the demineralisation process, by fragmentation of the more-reactive component of IOM, it is not unreasonable that their distribution throughout the sample would be inhomogeneous. Physical edges of an organic particle, possibly more functionalised by exposure to some reactive environment than the molecular interior, but also now more exposed to the reaction medium than

portions well within the interior of the organic particles, would be more easily decomposed and fragments lost than interior portions. The proportions of more- and less- reactive portions of the IOM molecule are also likely to vary considerably from particle to particle, or between individual macromolecules, also contributing to variation in levels of decomposition products.

Samples 3DC and 3DA contain substantially different concentrations of compounds generated following demineralisation, there being considerably less material in 3DC (and therefore detected following pyrolysis at 300°). This could be due to the same effect as the absence of significant sulfur in 3DC, namely the presence of the organic solvent (a mixture of carbon disulfide and 1,4-dioxan) in the demineralisation mixture developed by Cody *et al* (2002). Whereas the molecules broken away during fluoride-ion mediated demineralisation using the method of Amari *et al.* (1994) remain physically trapped in IOM (and released on pyrolysis at 300°), those formed in the method of Cody *et al.* (2002) are extracted into the organic solvent layer and lost. Alternatively, it is possible that the latter method may have generated products which are retained within the IOM and released at 300°, but not detected using this analytical technique, or there had been no reaction generating any small molecules at all. The absence of sulfur, however (which would be expected to be formed during demineralisation under both sets of conditions) indicates that extraction into the organic solvent is more likely.

Pyrolysis of 2DAH at 600°

As in the previous section, TIC traces were used to compare the pyrolysis profiles of the samples, and then, 3D-chromatograms used to identify the products of pyrolysis. In contrast to the results obtained on pyrolysis at 300° (when sample 1SCE showed

very little pyrolysate), at 600°, both samples 1SCE and 2DAH gave strong signals, but the TIC profiles were different; these are shown in Figure 7-14. The blue trace (2DAH) shows many peaks in common with the orange trace (1SCE), although some peaks are present in one sample but not the other. The organic material present in the two samples is therefore likely to be different in structure.

Identification of the products of pyrolysis of 2DAH at 600°

The 3D-chromatogram obtained from 2DAH is shown in Figure 7-15, and is similar to that obtained for the undemineralised samples previously discussed (see Figures 6-7 to 6-9 and 6-19). In common with 1SCE (as well as the recently prepared samples 3M, 3SE and 3AW), the pyrolysate contains aliphatic hydrocarbons, substituted aromatic benzenes and other aromatic hydrocarbons, naphthalene again being a major component. In addition, the hydrocarbons styrene, indene and phenanthrene were detected. It also contains both phenol, and t-butyl phenol, which were not seen in the undemineralised samples, as well as elemental sulfur.

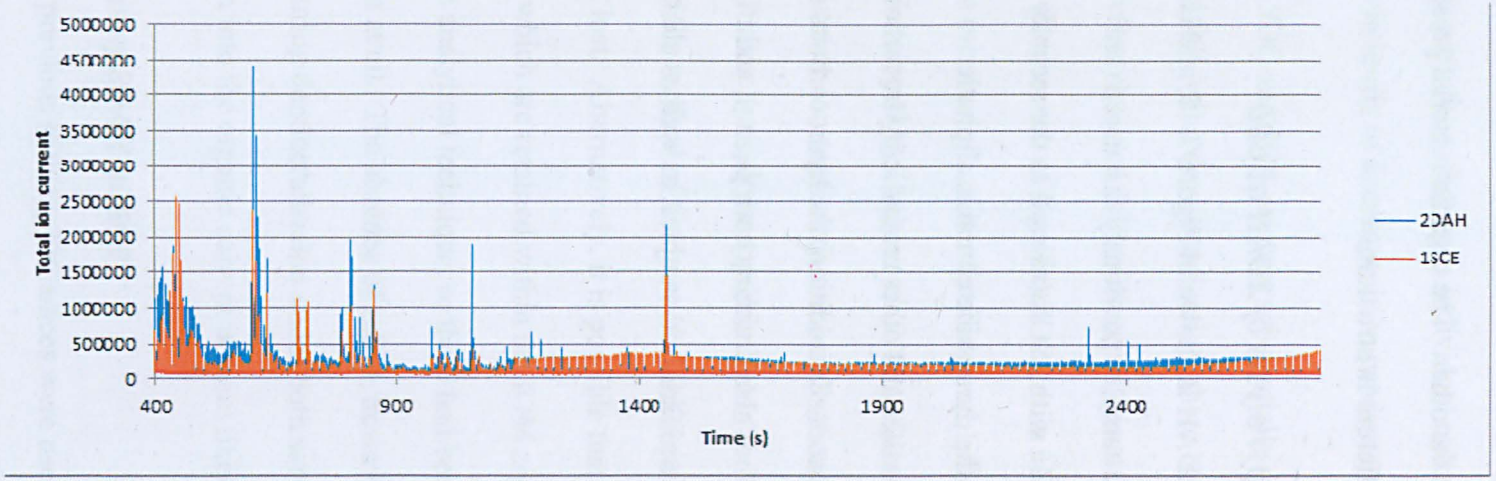

Figure 7-14: Comparison of TIC traces of 1SCE and 2DAH after pyrolysis at 600°

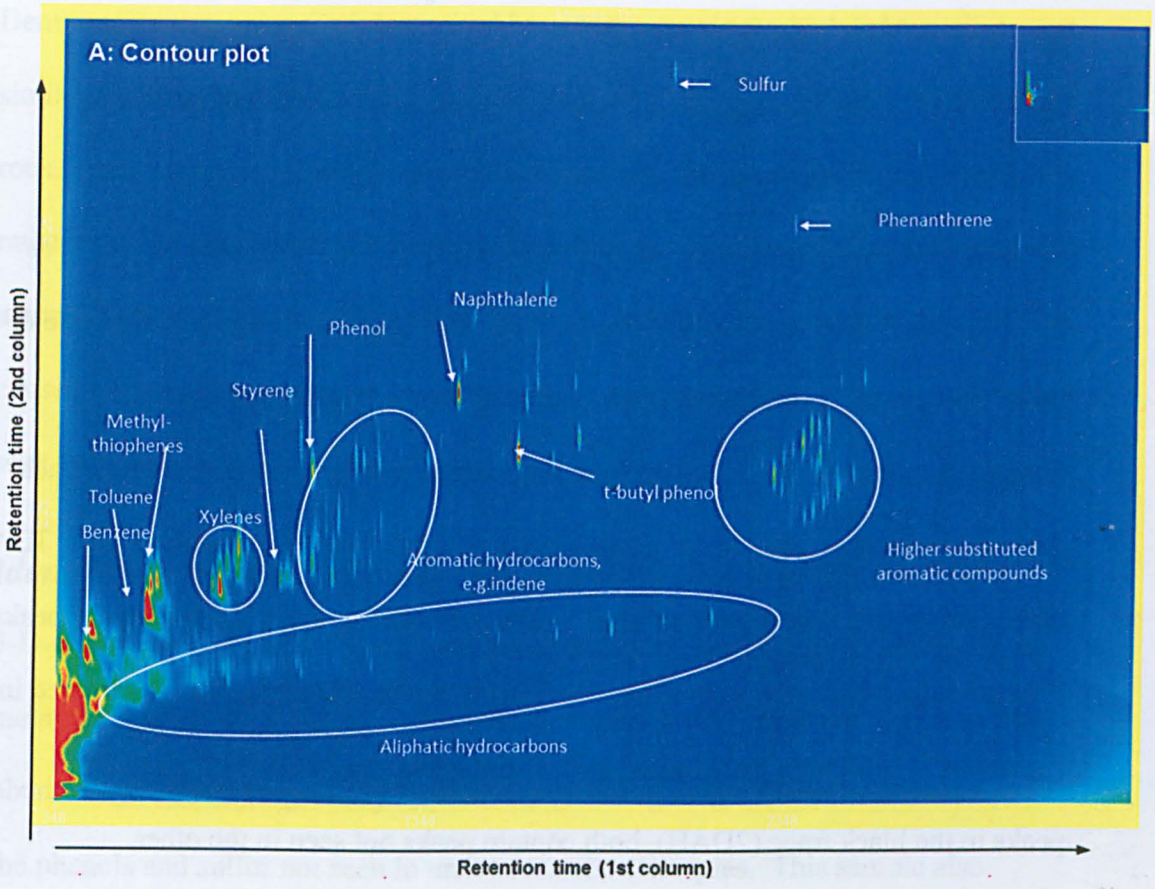

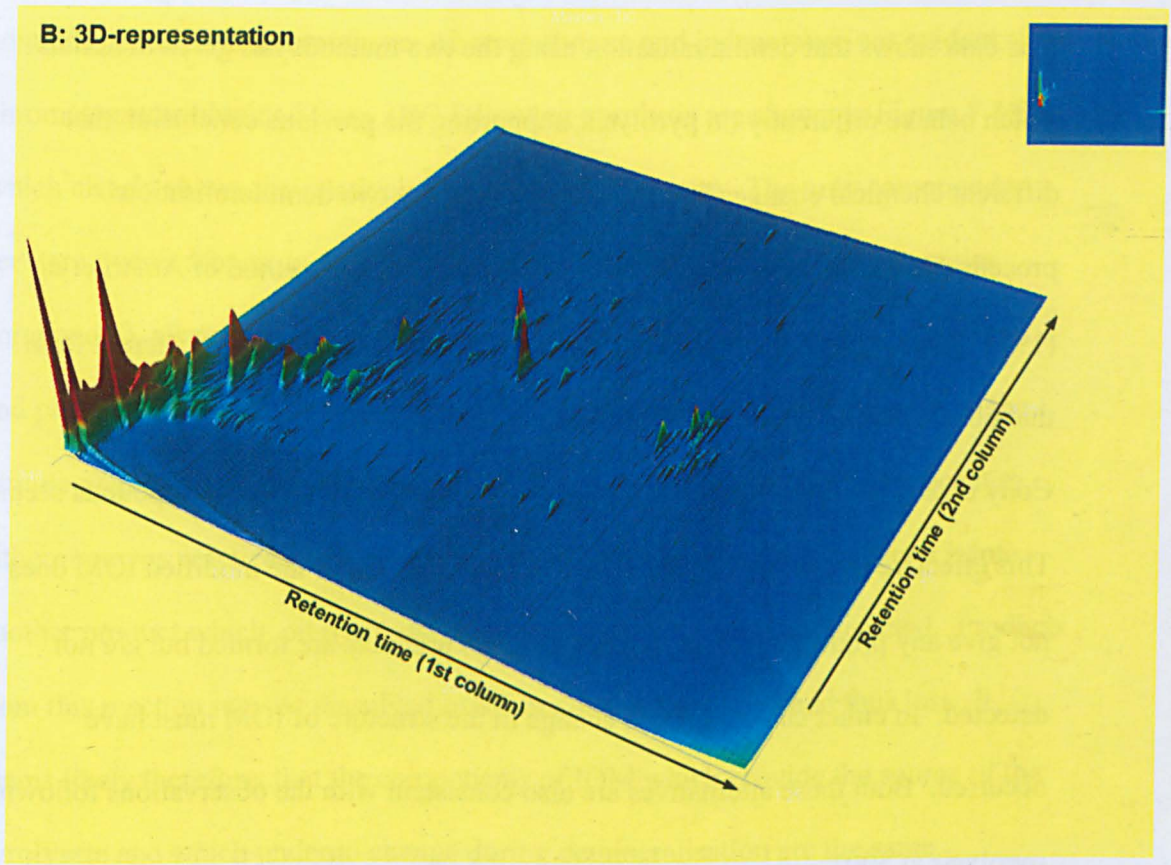

Figure 7-15: 3D-chromatograms for 2DAH pyrolysed at 600°

Pyrolysis of 3DC and 3DA at 600°

The two freshly isolated samples of IOM, 3DC and 3DA, were also subjected to pyrolysis at 600°. Although the differences in their Raman spectra (discussed previously) were small, their behaviour on pyrolysis at 600° was quite different, as shown in the TIC traces shown in Figure 7-16. The green trace shows the profile of 3AW, (the sample of acid washed Murchison used for demineralisation) for comparison. 3DC (the cyan trace), shows a similar profile to 3AW, but gave much reduced levels of pyrolysate, all peaks present in 3DC being also seen in 3AW. 3DA (pale green trace) gave a very different profile, containing many high-intensity peaks. This behaviour is similar to that seen for 2DAH; the two TIC traces are compared in Figure 7-17. Although many peaks seen in the green trace (3DA) correspond to peaks in the black trace (2DAH), both contain peaks not seen in the other.

This data shows that demineralisation using the two methods has given materials which behave differently on pyrolysis, supporting the previous conclusion that different chemical changes have occurred during the two demineralisation procedures. On pyrolysis at 600°, IOM isolated using the method of Amari *et al.* (1994) gives a substantial pyrolysate, the components of which are different from that obtained from whole rock. In contrast, IOM isolated using the method of Cody *et al.* (2002) gives a much reduced pyrolysate, with no new compounds seen. This effective lack of pyrolysate at 600° means that, either the modified IOM does not give any product on pyrolysis, or pyrolysis products are formed but are not detected. In either case, chemical change in the structure of IOM must have occurred. Both these alternatives are also consistent with the observations following pyrolysis at 300°.

Demineralisation using Cody's method has given a product which behaves in a similar way on pyrolysis to that produced by ozone treatment of Murchison whole rock. Both these procedures have resulted in a reduction in the levels of pyrolysate, rather than the generation of a new, unique set of products (and thus diagnostic of the actual chemistry occurring); however, it is not necessarily the case that the changes caused by these procedures are the same, but just that their products behave the same way on pyrolysis.

Identification of the products of pyrolysis of 3DA and 3DC at 600°

3-D-chromatograms of the pyrolysate obtained from the sample prepared using the method of Amari *et al.* (1994) are shown in Figure 7-18. These are similar to those obtained for 2DAH (Figure 7-15), showing the same range of hydrocarbons, and also the phenols and sulfur not seen in undemineralised samples. This sample also contains pyrene and fluoranthene, whereas styrene and indene were not evident. The chromatograms obtained from 3DC following pyrolysis are shown in Figure 7-19, which clearly shows the relatively low level of pyrolysate. The only compounds seen are hydrocarbons, mostly substituted benzenes and naphthalene (the major component), all present at low levels. The larger hydrocarbons, sulfur, thiophenes and phenols seen in 3DA are not detected. The very low level of pyrolysate in the sample prepared by the method of Cody *et al.* (2002) indicates that that procedure either removes practically all of the precursor to the pyrolysate, or converts it into another product which, on pyrolysis, gives products which are not detected. Products from this reaction may be dissolved in the organic solvent used and thus lost. It seems likely therefore, that the components of IOM which provide the source of the pyrolysate and which undergo change during demineralisation are the same.

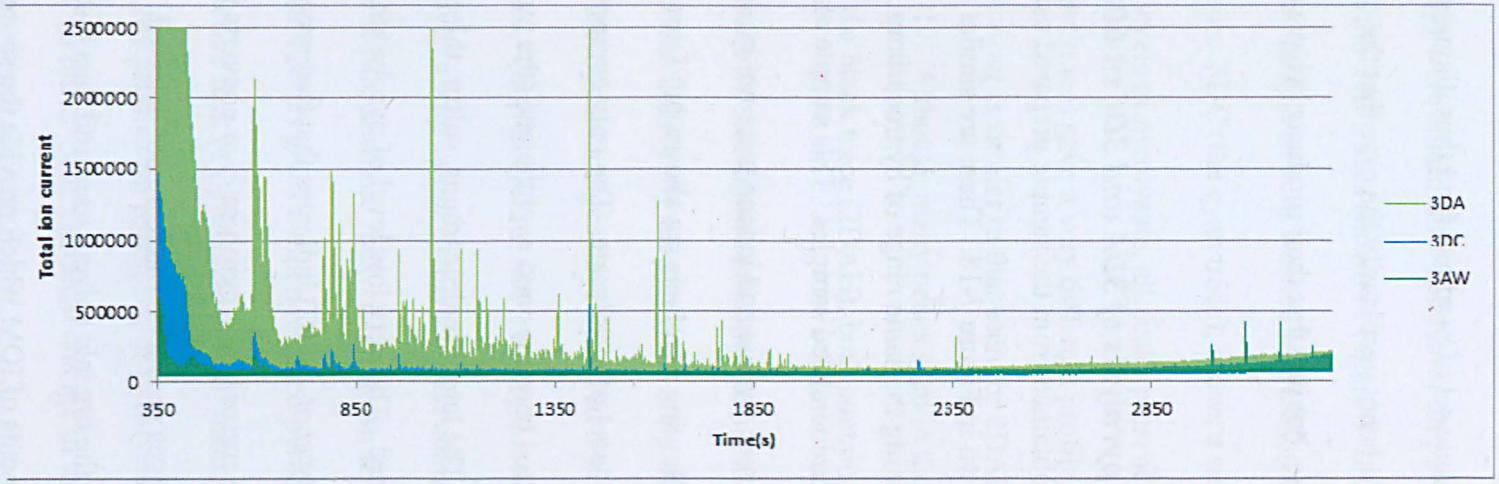

Figure 7-16: Comparison of the TIC traces from pyrolyses of IOM samples 3DA and 3DC with that from 3AW

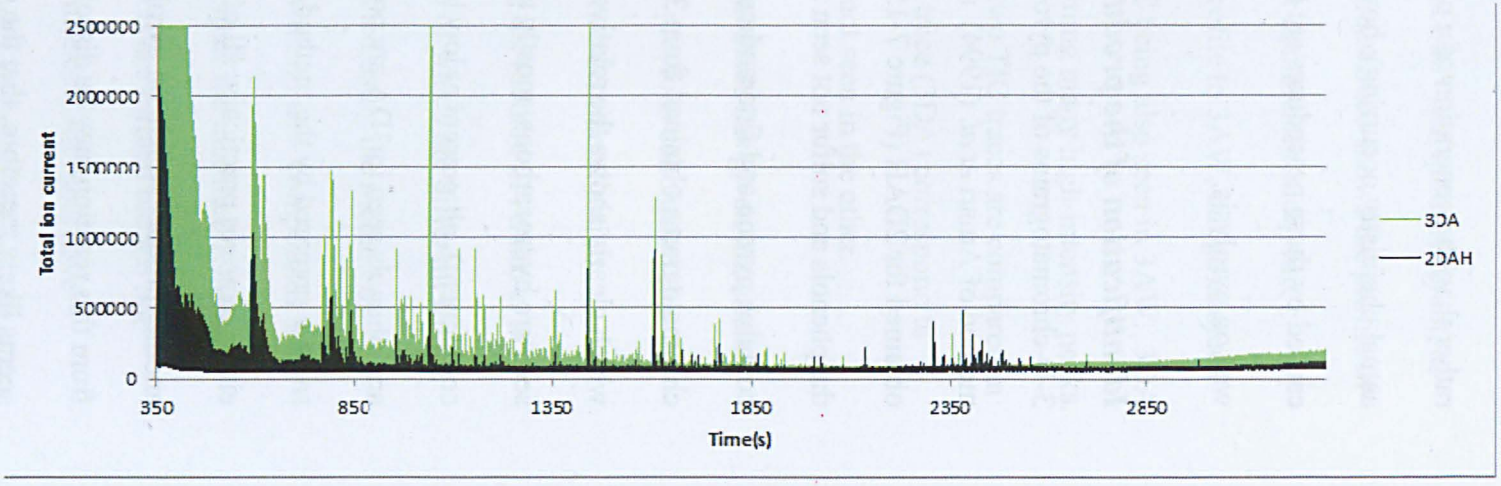

Figure 7-17: Comparison of TIC traces of IOM prepared by the method of Amari *et al.* (1994)

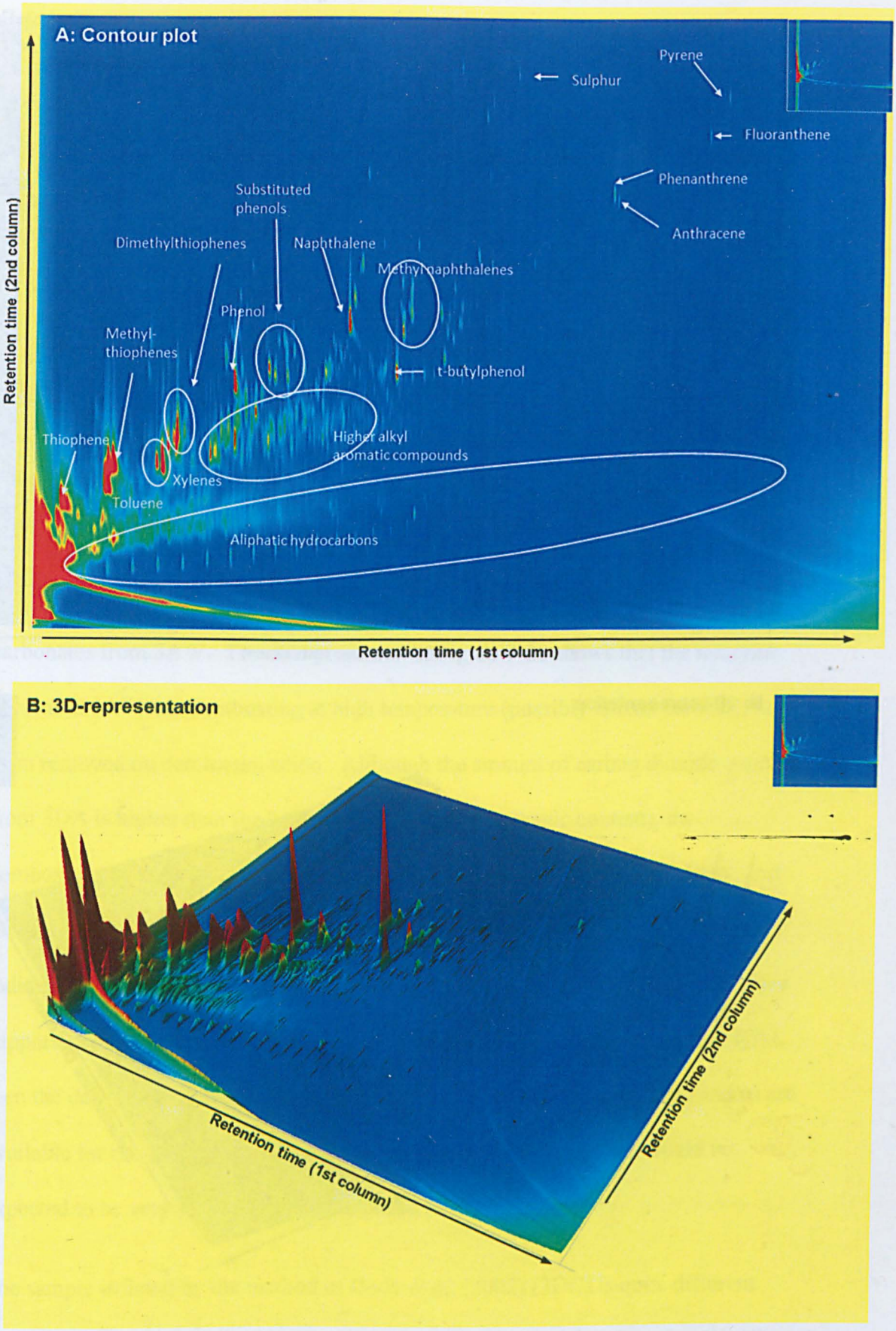

Figure 7-18: 3D-chromatograms of Sample 3DA after pyrolysis at 600°

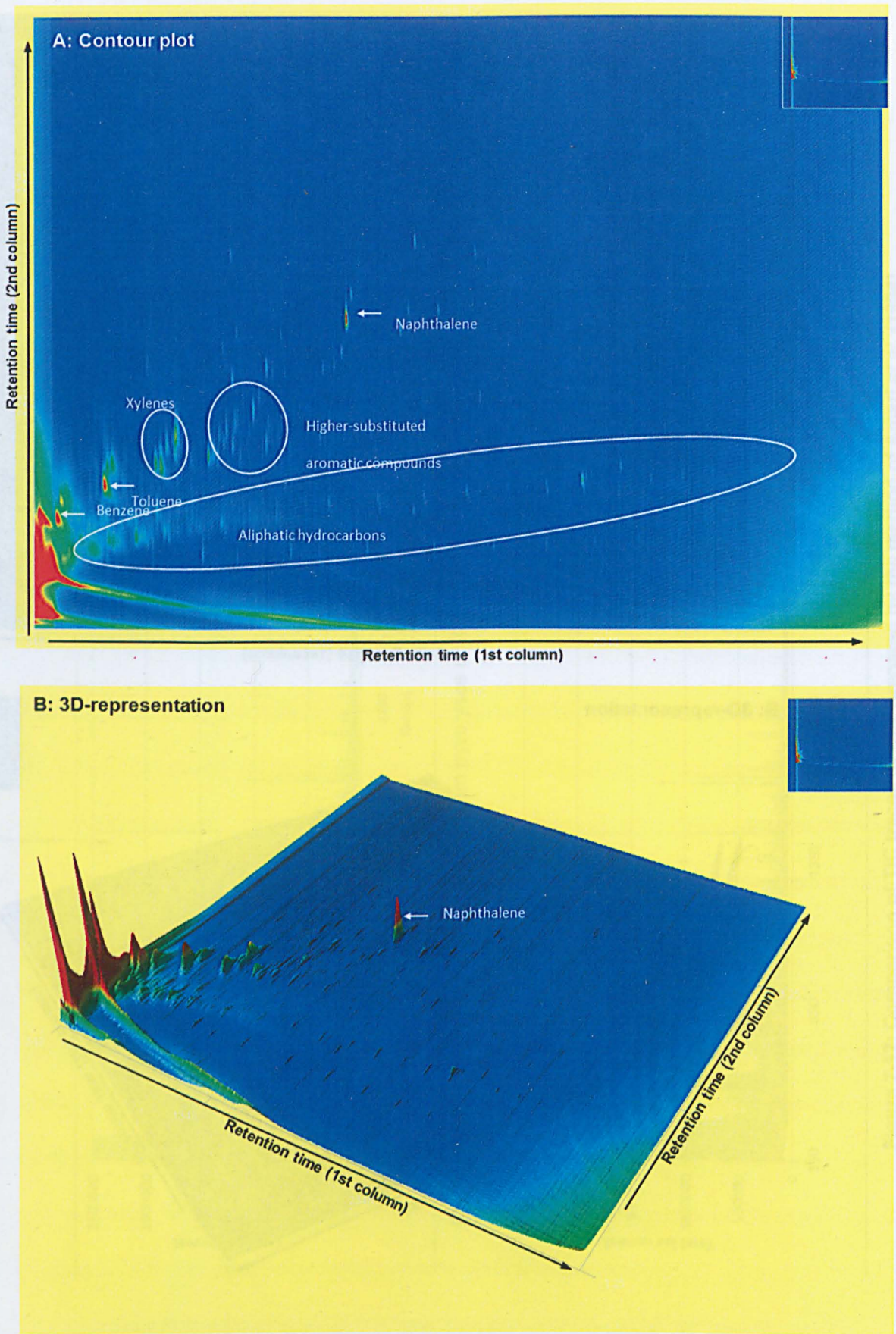

Figure 7-19: 3D-chromatograms of Sample 3DC after pyrolysis at 600°

7.1.4. Stepped Combustion

The two samples 3DA and 3DC were also compared using stepped combustion. Differences in the organic content of samples might be expected to alter their combustion profiles somewhat less than, for example, the removal of minerals (which generally combust at significantly higher temperatures than organic compounds). However, the IOM isolated using the method of Cody *et al.* (2002) (3DC) shows a very different profile from both that prepared using the method of Amari *et al.* (1994) (3DA), and the undemineralised but extracted and acid-washed Murchison (3AW).

The combustion profile of sample 3AW was compared with unextracted, whole rock Murchison in section 6.4.1, where differences were seen, due to the removal of carbonates from 3AW. The data presented in Figure 7-20 shows that the material present in 3AW and combusting at high temperature (possibly silicon carbide), has been removed on demineralisation. Although the amount of carbon dioxide evolved from 3DA is higher than for 3AW, (due to its higher organic content), the combustion profiles (both of CO_2 evolved and the isotope signature) for 3AW, and for IOM isolated by the method of Amari *et al.*(1994) (3DA) are very similar, indicating the proportions of combusting materials have remained unchanged. This supports the conclusion that, if the Amari method results in decomposition of IOM, then the decomposition products are retained within its physical structure, and so are available for combustion. The combustion profile of such a mixture would be expected to be very similar to undecomposed IOM.

The sample isolated by the method of Cody *et al.* (2002) (3DC) is quite different. Figure 7-21 shows a line graph normalised to maximum peak height rather than the conventional histogram because for these samples, the histograms overlap, and are

unclear. This appears to show that part of the component of the IOM present in the whole rock meteorite, and in the sample demineralised using the method of Amari *et al.* (1994), which gives rise to the maximum output on combustion, has been removed. This profile is consistent with the conclusion that the products of decomposition of IOM have also been removed physically, by extraction into the organic solvents used in the demineralisation process. If IOM had been converted into a derivative which gave undetected products on pyrolysis, but still remained in place, either physically or as part of the IOM molecule, then a profile resembling that of 3DA would have been expected. The fact that this was not seen implies that a proportion of the organic content of 3DC has been physically lost.

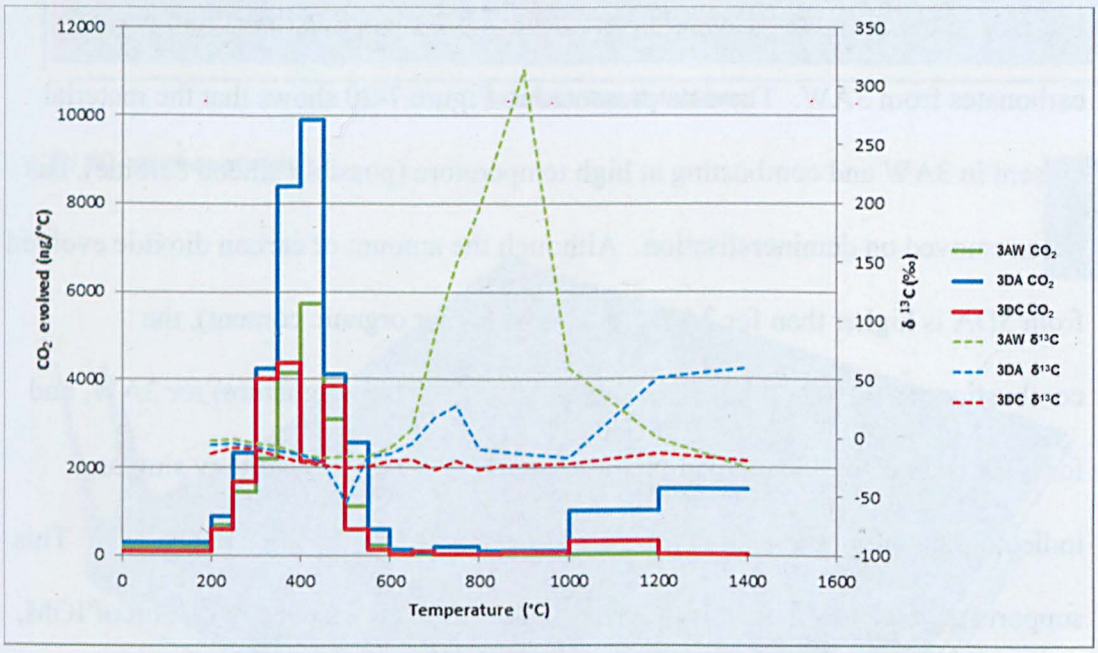

Figure 7-20: Stepped combustion of samples of IOM: CO_2 and isotope data

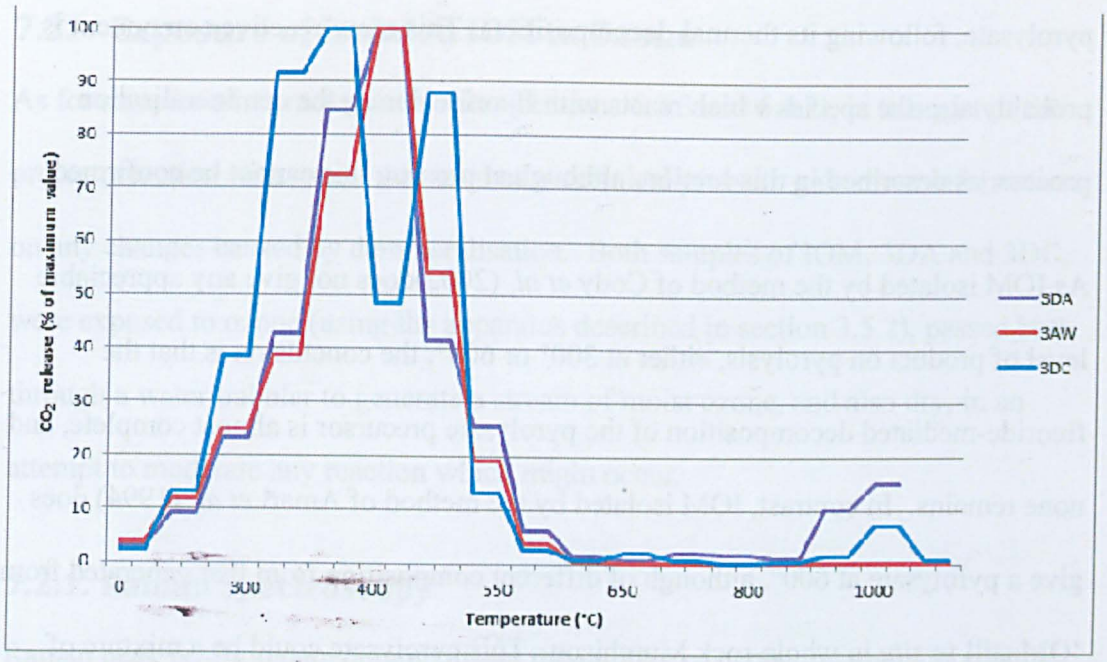

Figure 7-21: Traces obtained from stepped combustion of acid-washed Murchison and IOM prepared using both methods normalised to maximum CO_2 outputs in each case.

7.1.5. Conclusion

The data presented in this section supports the proposal that the chemical structure of IOM has been modified by both processes of demineralisation. The data suggests that both fluoride treatments result in the removal of part of the macromolecular structure of IOM, resulting in a set of small molecules being generated. Using the method of Amari *et al* (1994)., these compounds are physically trapped within the particles of IOM, but are released on pyrolysis at 300°. Using the method of Cody *et al.*(2002), the compounds are extracted into the organic solvents used during demineralisation, and are lost.

Stepped combustion supports this conclusion; materials combusting at *ca.* 400-450° in both whole rock Murchison, and IOM isolated by the method of Amari *et al.* (1994) are largely absent from IOM isolated using the method of Cody *et al.* (2002)

Results from the pyrolysis of Murchison whole rock samples (discussed in section 6.3.2) showed that only one component of IOM provided the source of this

pyrolysate, following its thermal decomposition. This more-reactive component is probably also the species which reacts with fluoride during the demineralisation process, as described in this section, although at present, this cannot be confirmed.

As IOM isolated by the method of Cody *et al.* (2002)does not give any appreciable level of product on pyrolysis, either at 300° or 600°, the conclusion is that the fluoride-mediated decomposition of the pyrolysate precursor is almost complete, and none remains. In contrast, IOM isolated by the method of Amari *et al.* (1994) does give a pyrolysate at 600°, although of different composition from that generated from IOM still *in situ* in whole-rock Murchison. This pyrolysate could be a mixture of compounds still physically retained (within the particles of IOM), even after pyrolysis at 300°, or those generated by pyrolysis of remaining IOM, or from pyrolysis (that is, a reaction, rather than just physical release) of the physically retained compounds, at 600°. The profiles of the products of pyrolysis at 600° of the two samples of IOM isolated by Amari's method are different, indicating that the reactions of IOM on demineralisation have given somewhat different products, again possibly because the reaction conditions used for demineralisation, although similar, were not identical. These differences could also be due to variations in the composition of the fragments of Murchison used in their preparation, and of the IOM present within them. These results are discussed further in section 7.5.

7.2. Exposure of Isolated IOM to Ozone

As for samples of extracted meteorite, (sections 6.3.3 and 6.4.2), in this part of the project, reaction with ozone was used as a chemical probe to gain more information on any changes caused by demineralisation. Both samples of IOM, 3DA and 3DC, were exposed to ozone (using the apparatus described in section 3.5.2), passed both through a water bubbler to generate a stream of moist ozone, and also dry, in an attempt to moderate any reaction which might occur.

7.2.1. Raman Spectroscopy

Raman peak position data obtained from the product of ozone treatment of sample 3DA, prepared by the method of Amari *et al.* (1994) is shown in Figure 7-22. This shows a shift in the positions of the main signal, which is greater for the sample exposed to wet ozone, than to dry (as would be expected, moist ozone being more reactive than dry). This direction of peak shift is opposite to that seen on formation of 3DA from sample 3AW (as shown in Figure 7-4), but the same as that seen for sample 2DAH on exposure to ozone (shown in Figure 7-24, and discussed in section 5.4).

The corresponding data for sample 3DC, prepared using the procedure of Cody *et al.*, (2002) is shown in Figure 7-23. Whereas the position of the D peak moved to lower frequency in both samples, the position of the G peak increased in frequency in sample 3DA, but decreased in frequency in sample 3DC.

This effect could be due to a difference in reactivity of the macromolecular IOM that remains after demineralisation in each sample. Alternatively, as compounds liberated from IOM by fluoride treatment are still present in 3DA (but believed to have been removed from 3DC) the changes in Raman peak shift may reflect that in

3DA, ozone is reacting with both IOM and these liberated compounds, but in 3DC, with IOM alone. Whatever reaction is occurring, the fact that the two samples of IOM isolated from Murchison using the two methods have behaved differently on treatment with ozone supports the proposal that their compositions are different.

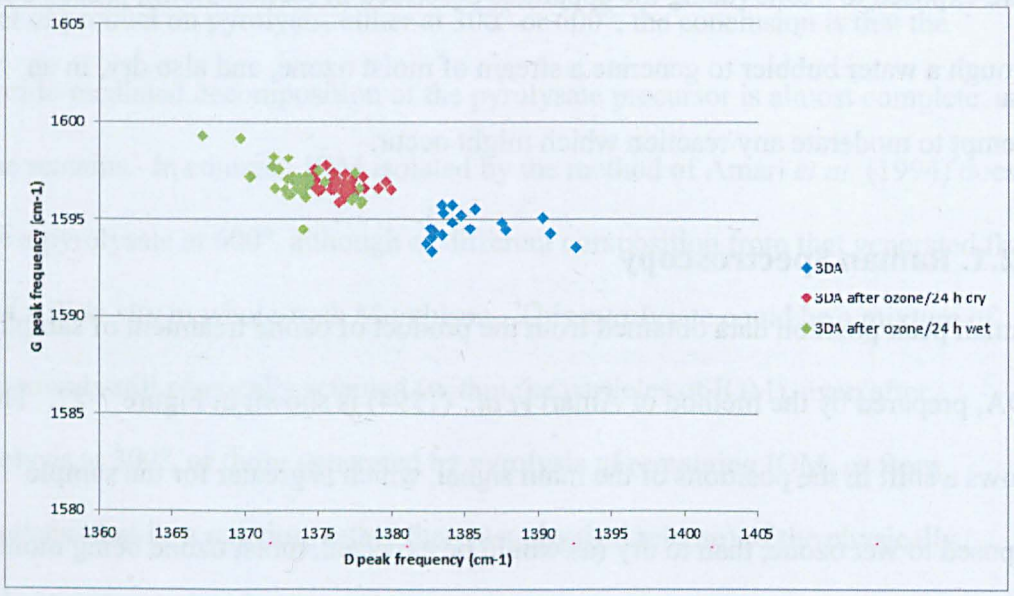

Figure 7-22: Raman peak positions for sample 3DA before and after ozone treatment

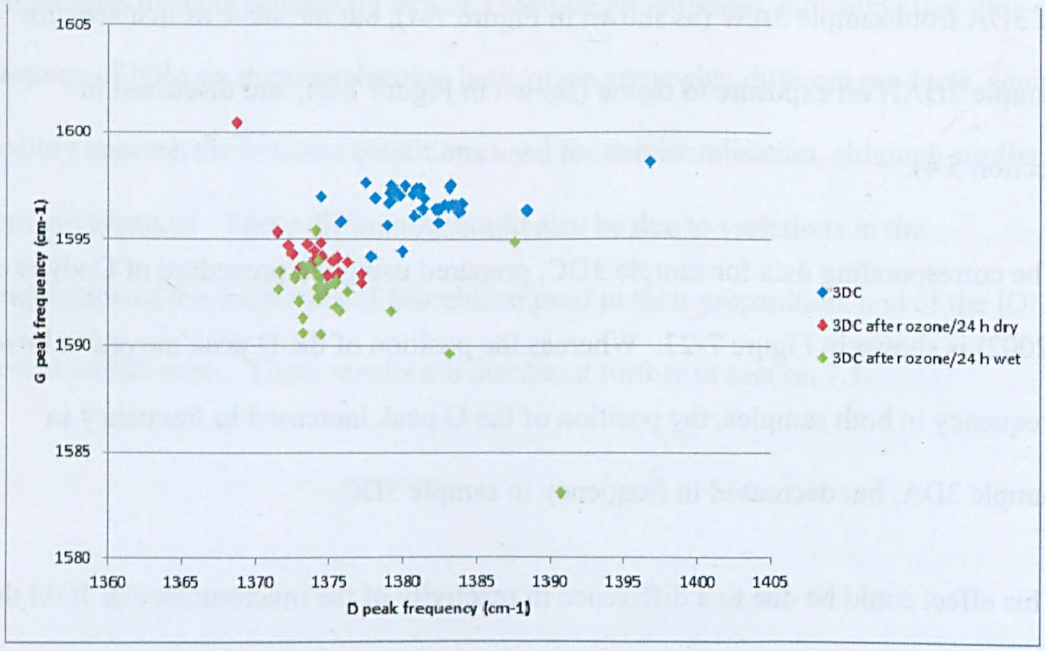

Figure 7-23: Raman peak positions for sample 3DC before and after ozone treatment

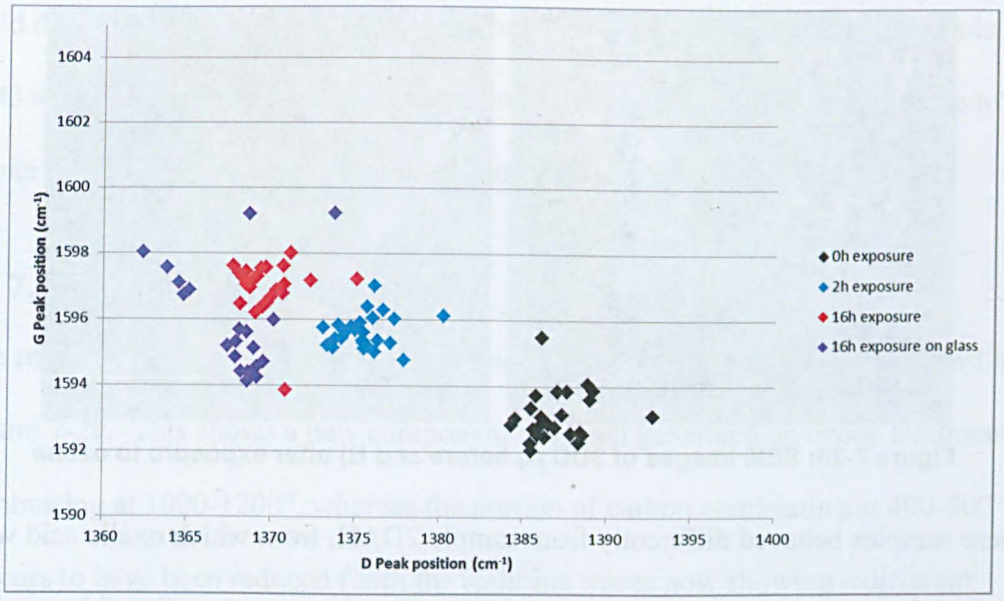

Figure 7-24: Raman peak positions for sample 2DAH after exposure to ozone

7.2.2. SEM

When the sample of isolated IOM 2DAH was exposed to ozone, significant physical changes occurred, with the grains of IOM becoming fused together, and rhombs appearing on its surface (see section 5.3.2). In contrast, when both 3DA and 3DC were exposed to ozone and then examined by SEM, neither fusing nor rhombs were seen in either Figure 7-25 or Figure 7-26.

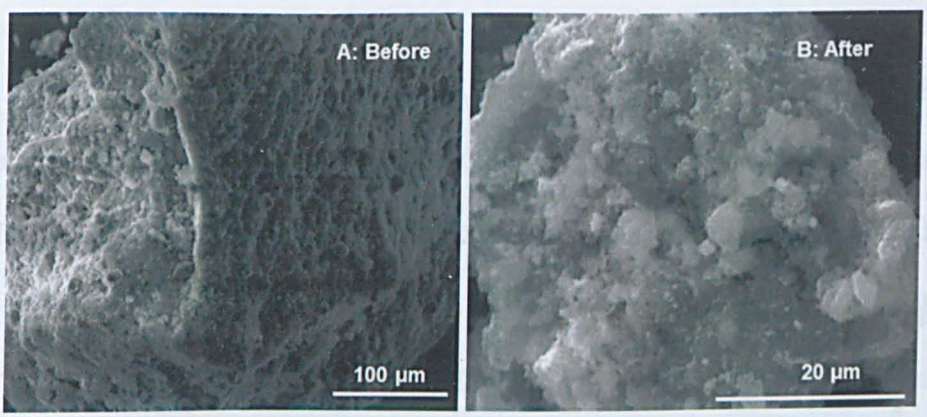

Figure 7-25: SEM images of 3DA A) before and B) after exposure to ozone

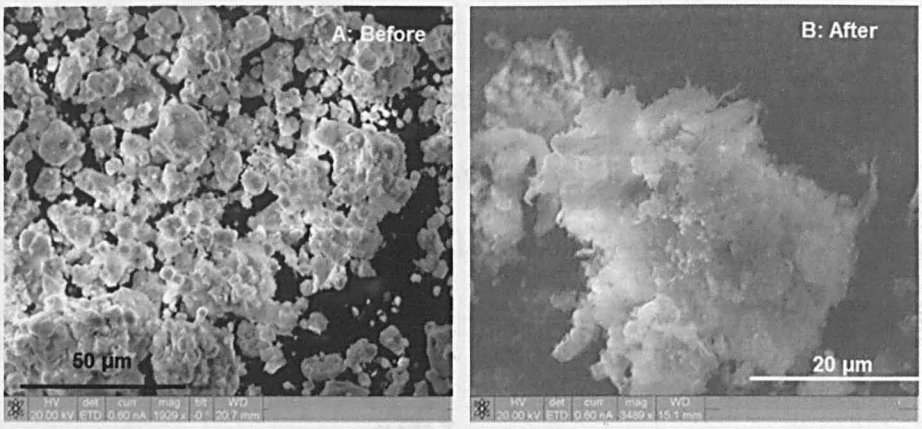

Figure 7-26: SEM images of 3DC A) before and B) after exposure to ozone

These samples behaved differently from sample 2DAH, from which oxalic acid was generated on exposure to ozone (section 5.3.2). The absence of oxalic acid was also seen following exposure to ozone of the precursor to these two samples, 3AW (section 6.4.2). That result was rationalised by the suggestion that the organic precursor to the formation of oxalic acid was missing from the sample of Murchison used for this study (3M), and so it is expected that oxalic acid would not be generated following ozone treatment of either 3DA or 3DC. That organic precursor could be a structural component present in IOM in some samples, but not others, or some other molecule which has been lost from 3M.

7.2.3. Py-GCxGC-ToF-MS

The samples generated by exposure of 3DA and 3DC to dry ozone for 24 h were pyrolysed and the products examined by GCxGC-ToF-MS. As seen previously with samples before demineralisation (section 6.3.3), ozone treatment again resulted in a reduction in the amount of pyrolysate with no new compounds being detected (Figure 7-27). The result of ozone treatment of IOM isolated by the method of Amari *et al.* (1994) has therefore been the same as for that organic materials present in whole rock meteorite; the source of the pyrolysate from both has either been removed, that is, physically lost, or else converted to a derivative which does not

yield detectable products on pyrolysis. The level of pyrolysis products in sample 3DC was already low prior to ozone treatment; afterwards, even after exposure to ozone for only one hour, no pyrolysate could be seen (Figure 7-28).

7.2.4. Stepped Combustion

The result of stepped combustion of sample 3DA after ozone treatment is shown in Figure 7-29. This shows a new component has been generated on ozone treatment, combusting at 1000-1200°, whereas the portion of carbon combusting at 400-500° appears to have been reduced (with the resulting traces now showing a different shape). Amari *et al.* (1994) developed their demineralisation method in order to isolate pre-solar grains, and so it is possible that this high-temperature component merely results from the inhomogeneity of the sample, and is due to a small grain of some mineral being present in the sample, and remaining after oxidation (the sample size is *ca.* 0.3 mg, so may be unrepresentative of the bulk). The isotope data shows that this may be the case, its $\delta^{13}C$ being similar for both samples, and more positive (by about 80‰), than that for carbonaceous materials combusting below 400°. The isotopic ratio and combustion temperature are those expected for presolar grains of silicon carbide, present in Murchison (Sephton *et al.*, 2003).

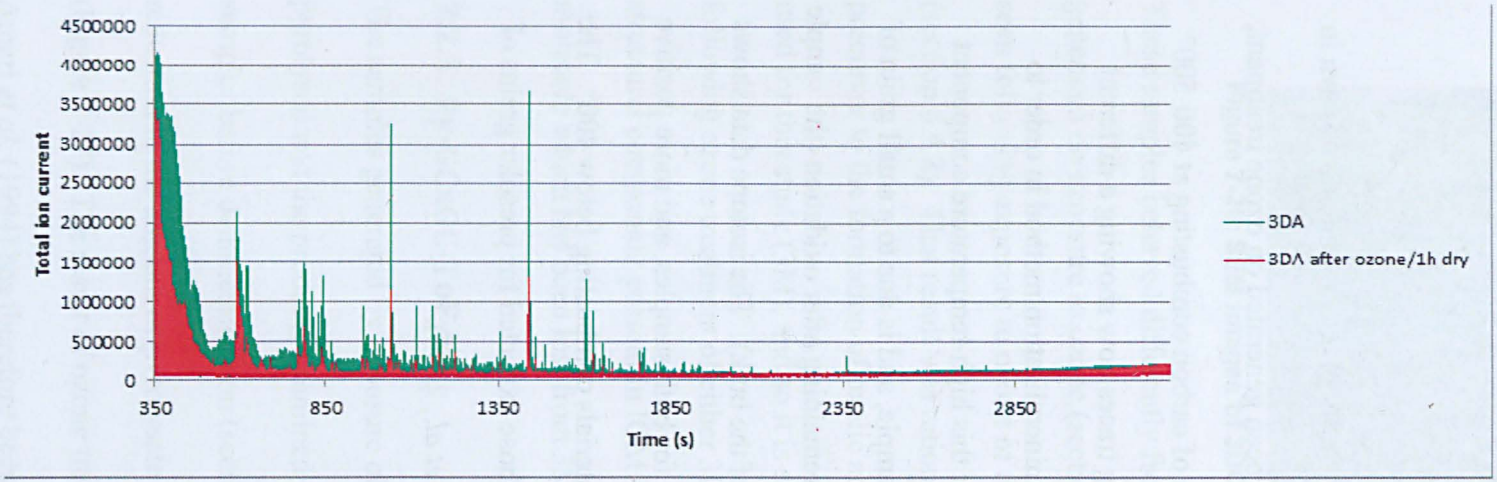

Figure 7-27: Effect of exposure to ozone on TIC trace of sample 3DA

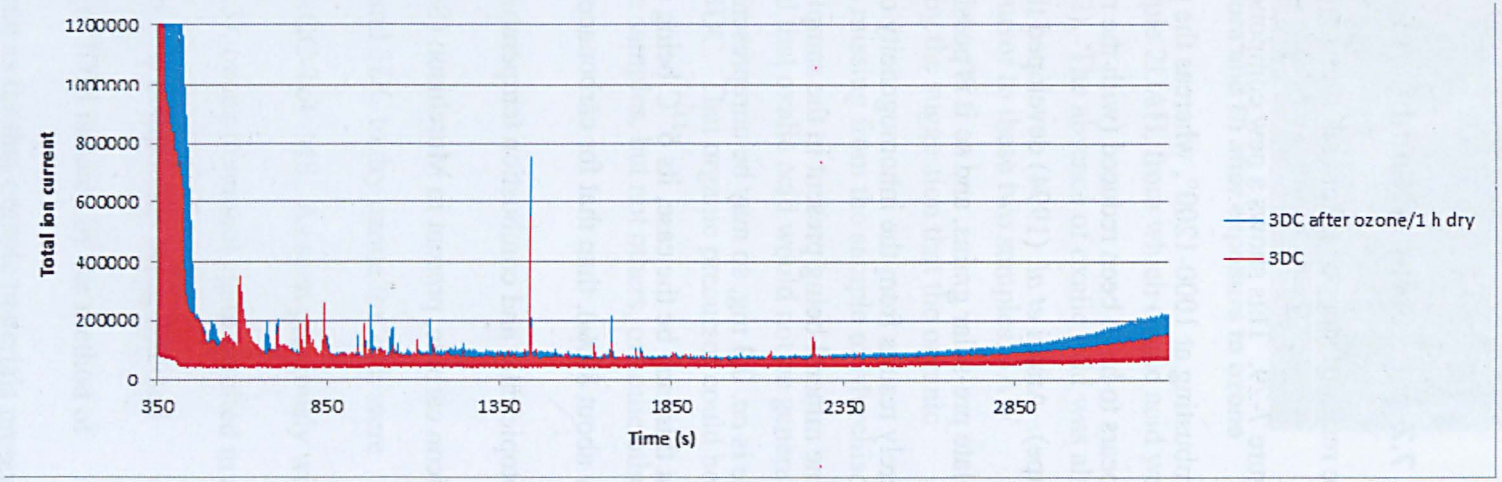

Figure 7-28: Effect of exposure to ozone on TIC trace of sample 3DC

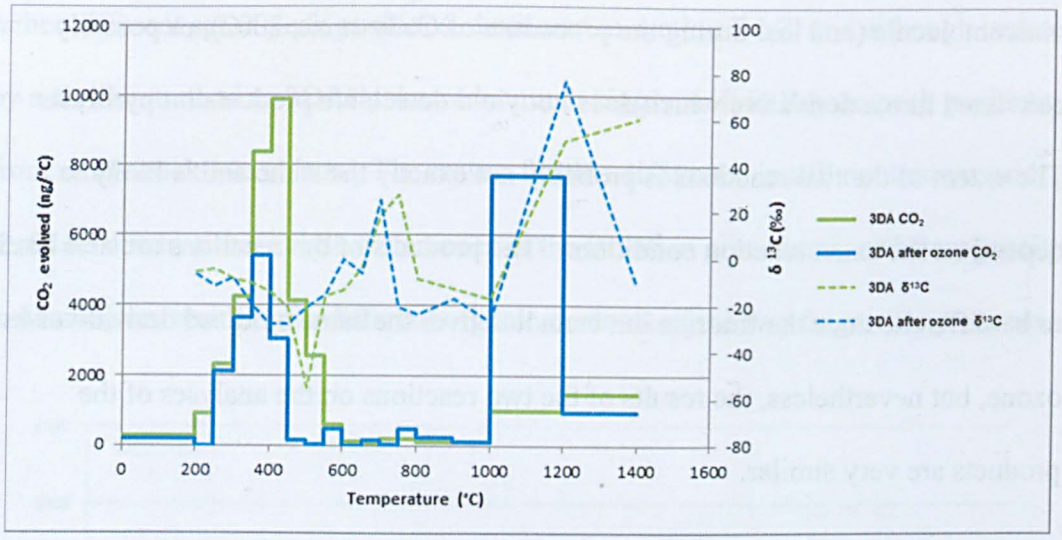

Figure 7-29: Stepped combustion of sample 3DA before and after ozone treatment

In section 7.1, it was noted that the effects of the fluoride-containing solution used in the procedure of Cody *et al.*(2002) (to isolate sample 3DC), and of ozone treatment on the organic material contained within whole rock Murchison, 3AW, were the same. Both resulted in a reduction of the level of pyrolysate, with no new compounds being seen. As the two reactions gave the same analytical result, it was proposed that treatment with ozone has a similar chemical effect to that of fluoride.

The effect of fluoride treatment, as shown by the result of stepped combustion of 3DC (Figure 7-20), was to remove a portion of IOM. In that sample, the products of this reaction were lost into the organic solvent used in the demineralisation process. In sample 3DA, this loss did not occur, and the products of the reaction were physically trapped in the IOM, and thus available for combustion. The effect seen following ozone treatment of 3DA is similar (Figure 7-29), although the proportion of organic compounds combusting at about 400° has been slightly depleted, this is to a smaller degree than was the case for 3DC.

This result again suggests that it is the same component of IOM which reacts with both fluoride and ozone, with the product either being physically detached from the

macromolecule (and lost during the procedure of Cody *et al.*, 2002), or possibly converted into a derivative which does not yield detectable products on pyrolysis. The extent of the two reactions is probably not exactly the same and is likely to depend on the exact reaction conditions. The products of the reactions are also likely to be different since the fluoride ion cannot deliver the same oxidised derivatives as ozone, but nevertheless, the results of the two reactions on the analyses of the products are very similar.

7.3. Effect of Acid Treatment on 3DA and 3DC

Both 3DA and 3DC were treated with 6M hydrochloric acid to remove any remaining acid-soluble minerals, and to determine if any further changes in the structure of IOM occurred. The method used is described in the Appendix, and is essentially the final stage in the process developed by Amari *et al.* (1994) The samples generated were designated 3DAH and 3DCH, prepared from 3DA and 3DC respectively.

7.3.1. Raman spectra

Raman spectra of these two samples showed a small shift in signal position following acid treatment, (the peak positions are plotted in Figure 7-30), but are still quite different from that seen for the sample prepared earlier (2DAH). The positions of the G peaks in the Raman spectra of both 3DA and 3DC have decreased in frequency, but whereas the D peak of 3DC has moved to slightly higher frequency, that of 3DA has decreased. The net effect of these changes was that the D and G peaks of 3DAH and 3DCH now have very similar positions. These changes are small, and possibly not significant, but could represent another example of a difference in reactivity of IOM isolated by the two methods. Sample 2DAH, also shown in Figure 7-30, gave a

rather different set of peak positions, discussed in section 7.1.2, and although isolated by a similar method to 3DAH, showed a much bigger shift in Raman peak positions from whole rock Murchison. The reason for this difference is still not known, and could be due to either subtle differences in the isolation procedures, or heterogeneity in Murchison, resulting in different organic contents of the two fragments processed.

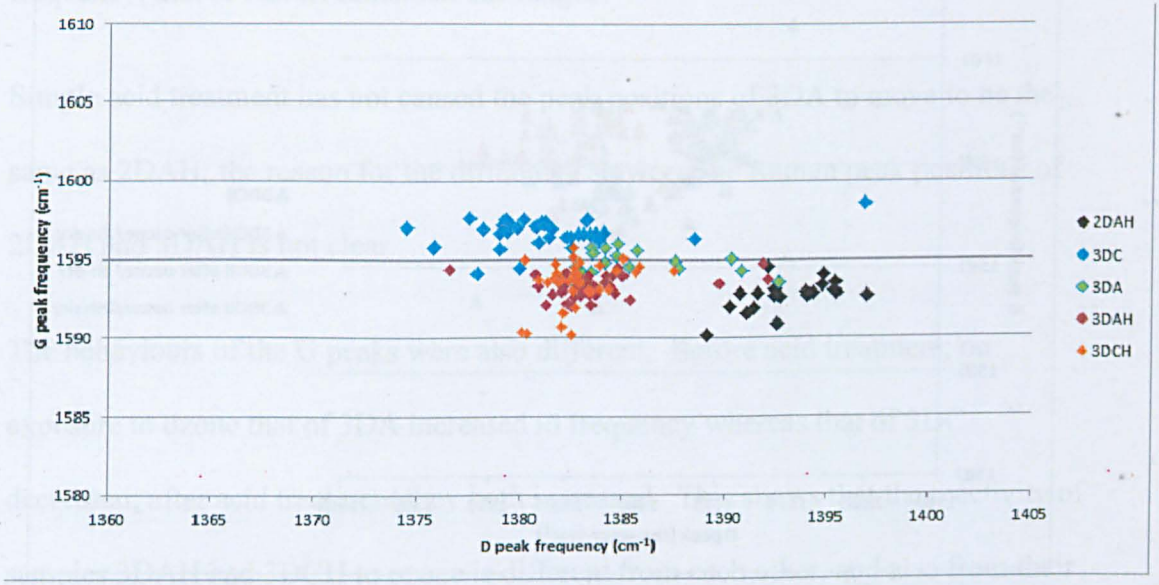

Figure 7-30: Raman peak positions of samples before and after treatment with 6M HCl

7.3.2. Treatment with Ozone

The two samples 3DAH and 3DCH were also exposed to dry ozone for up to 24 h, and the positions of the peaks in the Raman spectra plotted, as shown in Figure 7-31 and Figure 7-32.

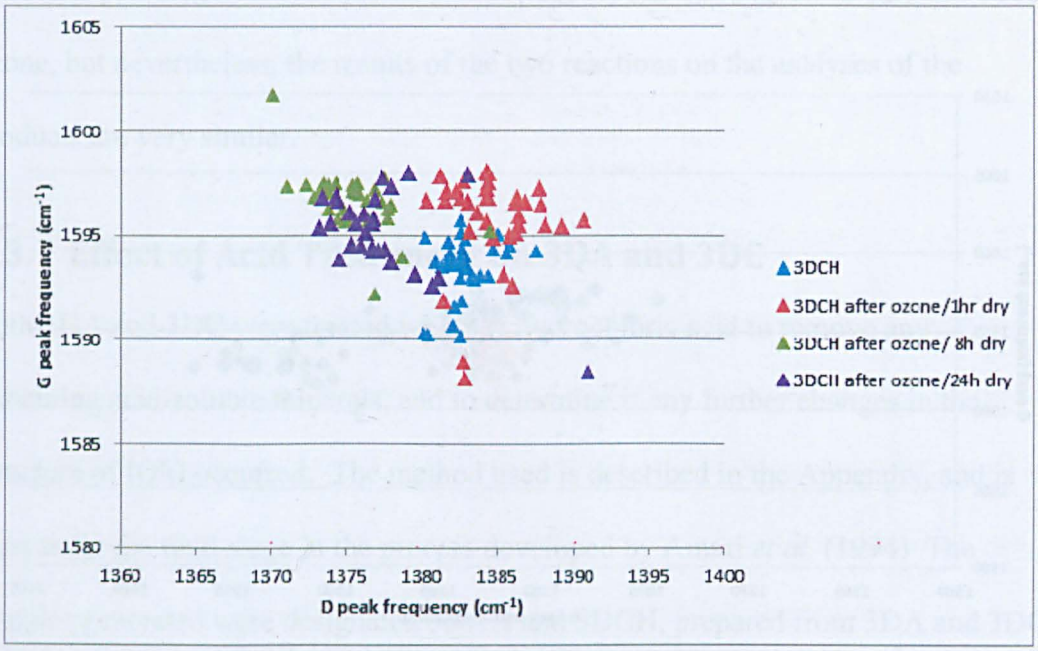

Figure 7-31: Raman peak positions of sample of 3DCH after exposure to ozone

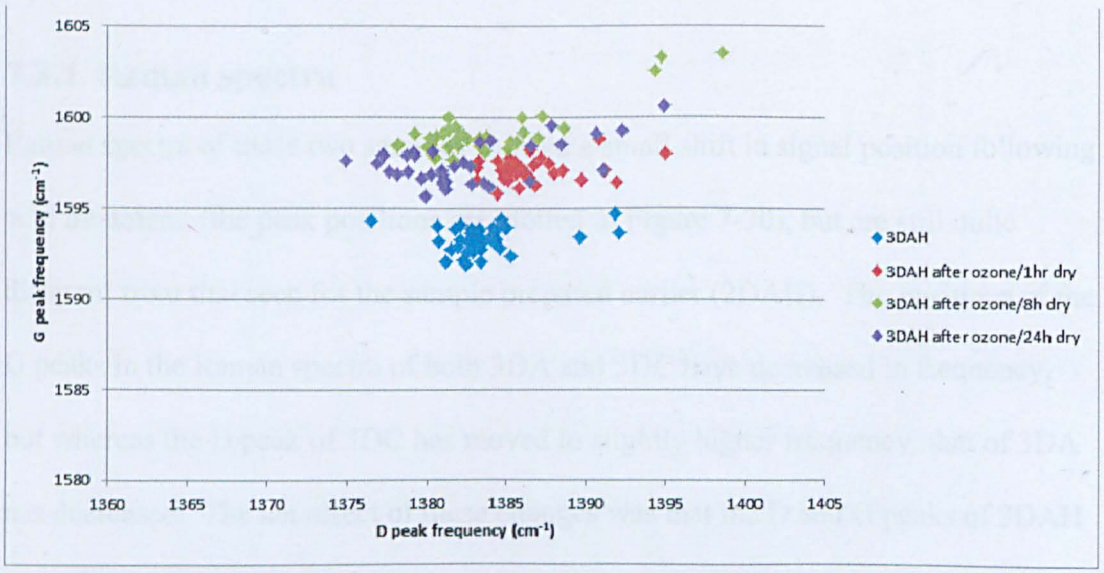

Figure 7-32: Raman peak positions of samples of 3DAH after exposure to ozone

The behaviour of the two samples on exposure to ozone following acid treatment (3DAH and 3DCH) differs from that seen before (3DA and 3DC, discussed in section 7.2). Before acid treatment, after exposure to ozone, the D peaks of 3DA and 3DC both moved to lower frequency, as shown in Figure 7-22 and Figure 7-23. After acid treatment however, although the D peak of 3DCH again moved to lower frequency, that of 3DAH remained unchanged.

Simple acid treatment has not caused the peak positions of 3DA to move to be the same as 2DAH; the reason for the difference between the Raman peak positions of 2DAH and 3DAH is not clear.

The behaviours of the G peaks were also different. Before acid treatment, on exposure to ozone that of 3DA increased in frequency whereas that of 3DC decreased; after acid treatment they both increased. This shows that the reactivity of samples 3DAH and 3DCH to ozone is different from each other, and also from their respective sources, prior to acid treatment. Whatever these changes may actually be, they represent more evidence that the structures of 3DA and 3DC are different, as they have reacted differently with acid to give distinct products.

7.4. Summary: The Effect of Demineralisation and the Structure of IOM

The experimental and analytical data presented in Chapters 4, 5 and 6, and in the first part of this chapter, generated from Raman spectra, SEM, Py-GCxGC-ToF-MS and stepped combustion of samples of Murchison and isolated IOM, before and after exposure to ozone, is consistent with the following conclusions:

- The reactivity of IOM is consistent with previous proposals (Sephton *et al.*, 2003; Okumura and Mimura, 2011) that it is composed of two components of different reactivity, one being more reactive than the other.
- Treatment of either whole rock or isolated IOM with ozone results in reaction of the more-reactive component, to give products such as oxalic acid (although this was not formed in all samples investigated). The less-reactive component may also react with ozone to some extent, although is still present after reactions lasting several days.
- Pyrolysis of IOM results in generation of a set of small molecules derived from decomposition of the more reactive component. No new compounds (that could be detected with the analytical methods used) are formed on pyrolysis of material exposed to ozone. In fact, the level of pyrolysate generated from IOM following exposure to ozone, is reduced substantially.
- IOM is altered chemically by the demineralisation methods developed by Amari *et al.* (1994) and Cody *et al* (2002), but in different ways. In the method of Amari *et al.* (1994), after isolation, IOM contains sulfur and small organic molecules, which are released on heating at 300°, whereas practically none are seen in IOM isolated using the method of Cody *et al.*(2002). In the

latter case, these compounds are probably extracted into the organic phase, and thus lost.

- The composition (and thus the reactivity) of IOM, even if derived from a single meteorite may vary from sample to sample. The ratio of the two components is likely to vary, as is the exact structure of each, particularly the fragments incorporated into the more-reactive component.
- The two components of IOM may be separate macromolecules, or part of a larger, single structure, containing regions of distinct reactivity. The results obtained do not distinguish between these alternatives.

All the data generated supports the proposal that IOM present in Murchison contains two components, one less-reactive, and the other more so. A good model for the less-reactive component could be an extensive delocalised π-bonded network of fused aromatic rings. Such systems are less reactive to ozone than smaller aromatic systems (Bailey, 1958), and give Raman spectra dominated by the D and G bands seen in most samples (Wang *et al.*, 1990). The more-reactive component could be composed of smaller aromatic systems, which being less-delocalised, would be more reactive (Pryor *et al.*, 1983). This component could also contain other functional groups (acids, esters, ketones etc.) which would give reactivity towards the conditions used during demineralisation, and may approximate to the structure proposed by Derenne and Robert (2010), and shown in Figure 1-3.

The data also supports the proposal that the structure of IOM is modified chemically during the demineralisation processes used to isolate it from whole rock meteorite samples. Furthermore, the two processes studied alter the structure (and reactivity) in different ways.

These conclusions, and their impacts on both the objectives of this project, and the wider study of meteorites, are discussed in the remainder of this chapter.

7.5. The Effect of Fluoride-Ion Mediated Demineralisation

Treatment of Murchison with fluoride, to remove minerals, has resulted in chemical modification of the resulting IOM. The two methods used gave products which differed in the results obtained from all analytical techniques used, indicating that the chemical structures of the products also differed.

7.5.1. Summary of Evidence for Chemical Change

A sample of IOM isolated using the method of Amari *et al.* (1994) (3DA) behaved similarly, but not identically, to one prepared previously (2DAH), for example, pyrolysis gave similar, but not identical products. This could be due to differences in the severity of the reaction conditions used in the preparation, and thus the degree of chemical change, or due to the inhomogeneity of Murchison, or possibly, to the different storage history of the fragments used.

Pyrolysis of 2DAH and 3DA at 300° gave a set of products that were similar, but not identical to that seen at 600° (for example, lacking sulfur-containing heterocycles such as thiophenes). These compounds seem to have been formed by reaction of the more reactive component of IOM with the demineralisation reagents, and have then been physically retained within the structure of IOM to be released on heating. Stepped combustion of sample 3DA gave a similar profile to Murchison following acid-treatment (3AW), implying little change in combustion profile following demineralisation by the Amari procedure. The Raman spectra of samples of IOM isolated using the method of Amari *et al.* (1994)show an increase in the frequency of the D peak, and a decrease in the frequency of the G peak, compared with whole

rock Murchison. These changes presumably reflect the reactions of the IOM with fluoride, and are discussed in this section.

Demineralisation of Murchison using the method of Cody *et al* (2002). gave a sample of IOM which gave different analytical results. During demineralisation, the reaction of fluoride with whole-rock IOM may be similar to that using the method of Amari *et al.* (1994), but any small molecules generated are removed by extraction into the immiscible organic solvent used in this procedure. Thus the sample of IOM so obtained would contain no physically-trapped organic component. This is evinced by the absence of any significant amount of pyrolysate being obtained at either 300° or 600°. Any of the more reactive component of IOM remaining after demineralisation must therefore have been converted into a derivative which either gave no pyrolysate, or a pyrolysate was not detected by the GCxGC-ToF-MS analysis used in this study. Stepped combustion supports the former alternative, showing a reduction in the amount of combustible carbon at 400-450°, consistent with the removal of a component of IOM, rather than just its derivatisation. This sample also gave a different Raman spectrum from that prepared by the method of Amari *et al.*(1994), the changes in the frequency of both the D and G peak being opposite in direction.

On treatment with mineral acid, 3DA and 3DC showed changes in the positions of the peaks in their Raman spectra so that although different before acid treatment, were similar afterwards.

On ozone treatment, the IOM prepared using the method of Amari *et al.* (1994)(2DAH), showed a shift of peaks in the Raman spectrum back in the opposite direction from that seen on demineralisation; the D peak moved to lower frequency,

and the G peak to higher. This could indicate the removal of peripheral electron-withdrawing substituents from the π-system generating the spectrum (giving an increase in Raman frequency) or an oxidation during ozone treatment, leading to the introduction of electron-donating groups. Pyrolysis shows the same effect as seen for whole-rock Murchison following treatment with ozone, that is significant reduction in the amount of pyrolysate. This shows that again, after ozone treatment, the more reactive component of IOM present may have been removed, or converted into a derivative which does not yield detectable products on pyrolysis.

Samples 3DA and 3DC also performed differently from one another following exposure to ozone. Although both samples of IOM showed the same direction of change in frequency of the D peak (to a lower value), the G peak of the sample prepared by the method of Cody *et al.* (2002) decreased in frequency (the sample prepared using the method of Amari *et al.* (1994) showed an increase in frequency). This could possibly be caused by oxidation of the condensed aromatic core of IOM if the peripheral substituents have been completely removed, as was indicated by stepped combustion. Oxalic acid was not seen following ozone treatment of these samples.

Finally, samples 3DAH and 3DCH, after treatment with ozone showed different shifts in their Raman peak positions. Whereas the two samples had given similar spectra before ozone treatment, afterwards, their peak positions moved in directions different from one another, and from the samples prior to acid treatment.

As was stated earlier (in section 6.2), previous published work using IOM had been carried out with the assumption that the demineralisation process does not affect its structure, and data generated from samples of demineralised IOM has been taken to

be indicative of IOM still present within a meteorite sample. For example, Derrene and Robert (2010) proposed a possible structure for IOM which is not supported by data from pyrolysis (when only hydrocarbons and thiophenes were seen, and oxygen-containing functional groups, such as ketones, esters and ethers, were not). The data presented in this chapter indicates that the fluoride-containing reaction mixtures used for demineralisation have resulted in a chemical modification of IOM as minerals were dissolved. Thus any models or theories based on the structure of IOM derived from results obtained from IOM isolated by acid-dissolution techniques, may be incorrect. The chemical changes which might occur on treatment with fluoride is discussed in the next section.

7.5.2. The Mechanism of Chemical Change during Demineralisation

The data presented in this chapter all supports the conclusion that, although IOM is unchanged by solvent extraction, it is changed chemically by the fluoride-ion mediated demineralisation processes, and that the changes caused by the two methods investigated are different. This section contains a discussion of the reactivity of the reagent systems used, and the chemistry that IOM might be expected to undergo during demineralisation.

The two demineralisation procedures are intended to remove silicon-containing minerals, by converting them into soluble derivatives by reaction with HF (Kline and Fogler, 1981) whilst leaving IOM unchanged. IOM is not soluble in the reagents used, and so the residue that remains after treatment is of significantly higher organic content (although still containing some minerals, for which further processing is needed to completely remove). The method of Amari *et al.* (1994) involves the use of repeated treatments with a mixture of hydrofluoric and hydrochloric acids, which

dissolve most of the silicate-containing minerals, leaving IOM suspended in the aqueous mixture. The method of Cody *et al.* (2002) employs a biphasic mixture, of aqueous caesium fluoride adjusted to pH7, and a mixture of carbon disulfide and 1,4-dioxan. As the fluoride attacks the silicate minerals, organic materials are released from the solid matrix and collect at the interface.

7.5.3. Chemistry Occurring During Demineralisation

During demineralisation, fluorosilicate ions are formed by the reaction of metal silicates (*e.g.* olivine and pyroxene), which make up the bulk of the meteorite, with HF. The silicates are decomposed into other salts, which will dissolve as the reaction proceeds, or on subsequent acid treatment.

A simple equation can be written, for example, in the case of forsterite:

$$Mg_2SiO_4 + 8HF \rightarrow Mg(SiF_6) + MgF_2 + 4H_2O$$

Equation 7-1: The reaction of forsterite with HF

The reaction media used are not, however, simple solutions of acids. Hydrofluoric acid is a weak acid (its pKa is about 3.2) and so is largely undissociated in aqueous solution, and does not react as hydrated fluoride ion, but as molecular HF (Kline and Fogler, 1981). The high concentrations of the solutions used also result in their properties differing from simple aqueous ionic solutions, especially the method developed by Cody *et al.* (2002). The fluoride-containing solution (in the Cody method) is prepared from aqueous caesium fluoride, and the pH adjusted to 7 with HF. This avoids acid-mediated hydrolysis of IOM, but as the solution of caesium fluoride used is very concentrated (a saturated solution contains about 90% by weight of caesium fluoride), there is a maximum of only two molecules of water per ion of fluoride and five per ion of caesium.

Theoretical studies have shown (Kemp and Gordon, 2005) that the maximum level of solvation for fluoride is about 15 molecules of water, and this solvation process is very exothermic, and therefore favoured. The fluoride present in these systems therefore is under-solvated with respect to optimum; fluoride that is deficient in this way is referred to as "naked" and often shows reactivity quite different from that of its fully-solvated aqueous analogue (Craig and Brooker, 2000), acting as a strong nucleophile or base.

Furthermore, the procedure of Cody *et al.*(2002) uses a mixture of carbon disulfide and 1,4-dioxan as an immiscible organic phase to simplify separation of IOM, which collects at the interface as the minerals dissolve. Whereas 1,4-dioxan is not likely to react under these conditions, carbon disulfide potentially could. Reactions have been reported involving carbon disulfide in the presence of fluoride ion (Rüdiger and Seppelt, 1997a; Rüdiger and Seppelt, 1997b). In the presence of naked fluoride, carbon disulfide is converted into the nucleophilic F-CS-S- ion which will attack electrophilic centres, eventually forming trifluoromethyl thioethers and other sulfur derivatives, as shown in Scheme 7-1.

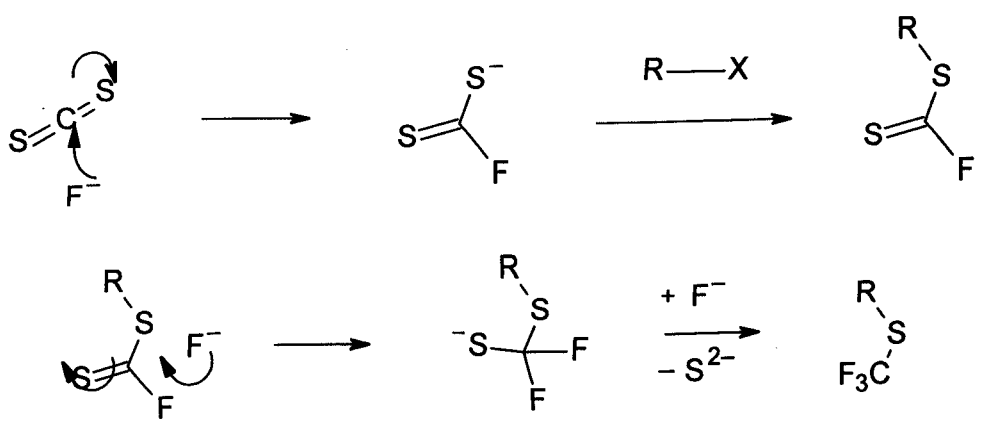

Scheme 7-1: The reactions of carbon disulfide and naked fluoride

Whereas therefore, use of this demineralisation mixture is apparently a more gentle procedure, involving ambient temperatures and neutral conditions, the presence of highly-reactive fluoride and carbon disulfide may in fact lead to more reactions with IOM than the acidic HF-HCl mixture originally developed for demineralisation. Thus, although only the reaction conditions developed by Amari *et al.* (1994) employ low pH, potentially causing hydrolysis, both sets of conditions use, to a certain extent, under-hydrated, partly-naked fluoride.

7.5.4. Potential Reactions of IOM with Fluoride Ion

As the structure of IOM is not well-characterised, it is hard to make good predictions of the reactions it will undergo. However, if the compounds detected following pyrolysis at 300° have indeed been formed by reaction of IOM with fluoride, their identities should indicate the types of reactions occurring. Products of nucleophilic attack by fluoride, and the F-CS-S$^-$ ion would be expected, with the latter perhaps reacting further as described above to give trifluoromethyl derivatives. These could be formed from, for example, ethers, by displacement of the alkoxy group. To generate the small fragments detected by GCxGC-ToF-MS however, substituents present on macromolecular IOM must be displaced. For example, this may occur *via* an S_NAr mechanism, as shown in Scheme 7-2. An extensively delocalised macromolecular core may be able to stabilise the intermediate anion (normally an electron-withdrawing group such as nitro would carry out this function).

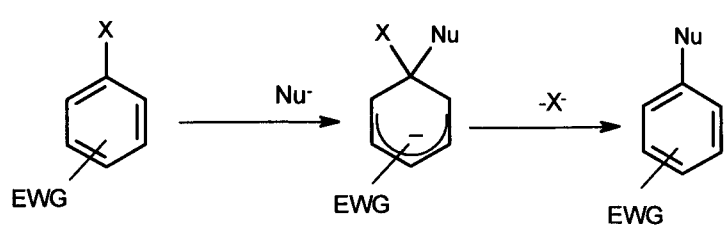

Scheme 7-2: S_NAr displacement of fragments from an aromatic core

Phenols were also observed in the pyrolysate of samples of IOM isolated by the method of Amari *et al.* (1994) These could be generated by reactions similar to that shown in Scheme 7-2 with hydroxide (from the water present) acting as a nucleophile, in association with the basic fluoride ion.

7.5.5. Evidence for Reactions with Fluoride

Any compounds containing fluorine atoms, or a trifluoromethyl group, present in the pyrolysate of IOM at 300° would be good evidence for fluoride-mediated decomposition. The chromatograms of both samples 3DA and 3DC, following pyrolysis at 300° and 600°were selected to display only the ions with m/z=69, indicative of CF_3 (as well as other isomeric species).

There was much stronger signal in the chromatogram for sample 3DA at 600° (Figure 7-36), than in the corresponding sample of 3DC (Figure 7-35) although at 300°, neither sample showed much evidence of this ion (Figure 7-33 and Figure 7-34). The lower level of signal in the two chromatograms at 300°, and in sample 3DC at 600° gives rise to a much noisier image. However, the small peaks present in the both chromatograms at 300° and in 3DC at 600° were identified as hydrocarbons. Those in the chromatogram of 3DA at 600° were identified from their mass spectra as fluorocarbon analogues, which may have resulted from reactions with fluoride, or be contamination from the PTFE apparatus used to prepare this sample.

These results have therefore not shown any good evidence for significant levels of formation of fluorinated compounds from decomposition of IOM, although it is possible that the organic solvent layer from the method of Cody *et al.* (2002) contains such compounds.

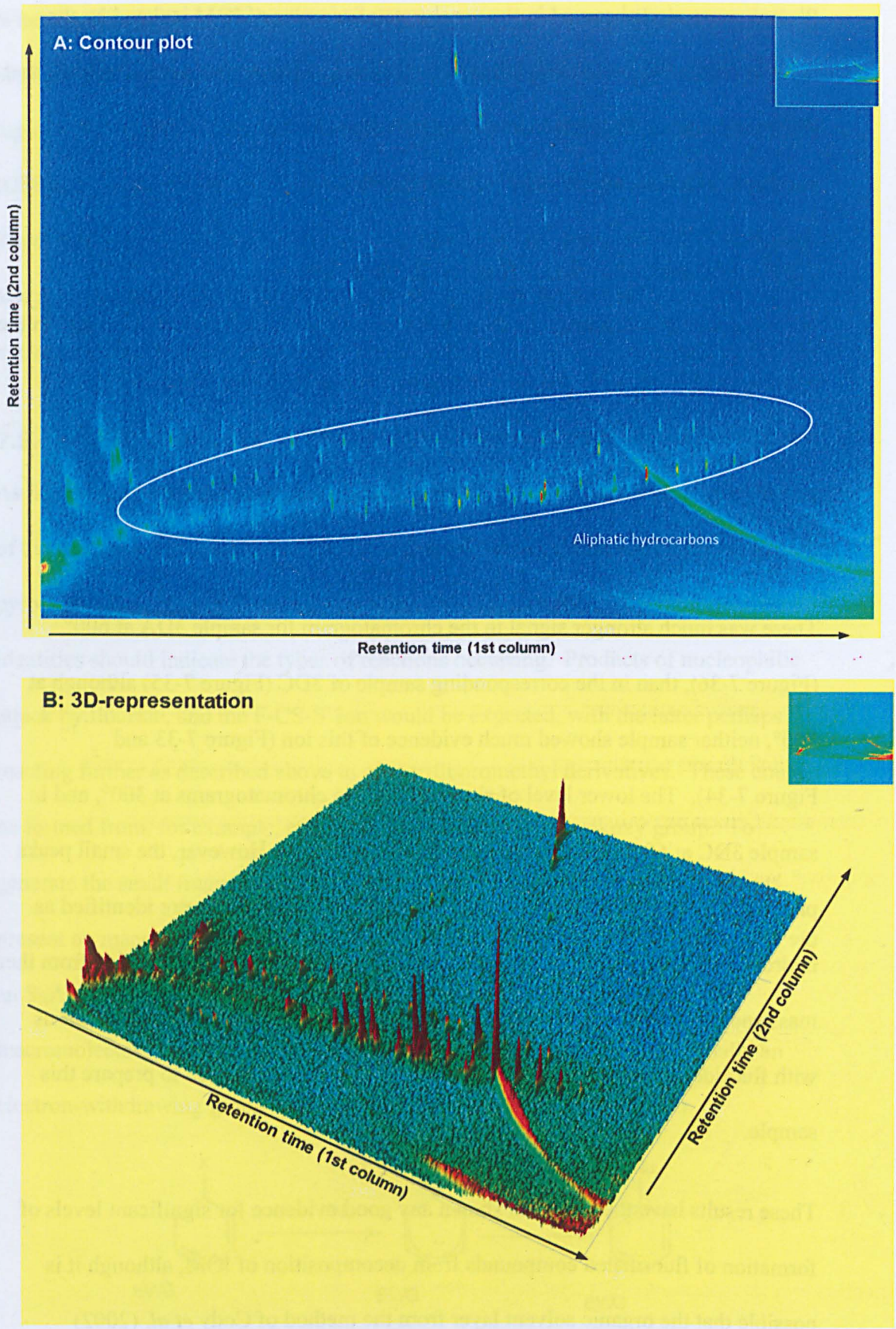

Figure 7-33: 3D-chromatograms of sample 3DC after pyrolysis at 300° (showing m/z=69)

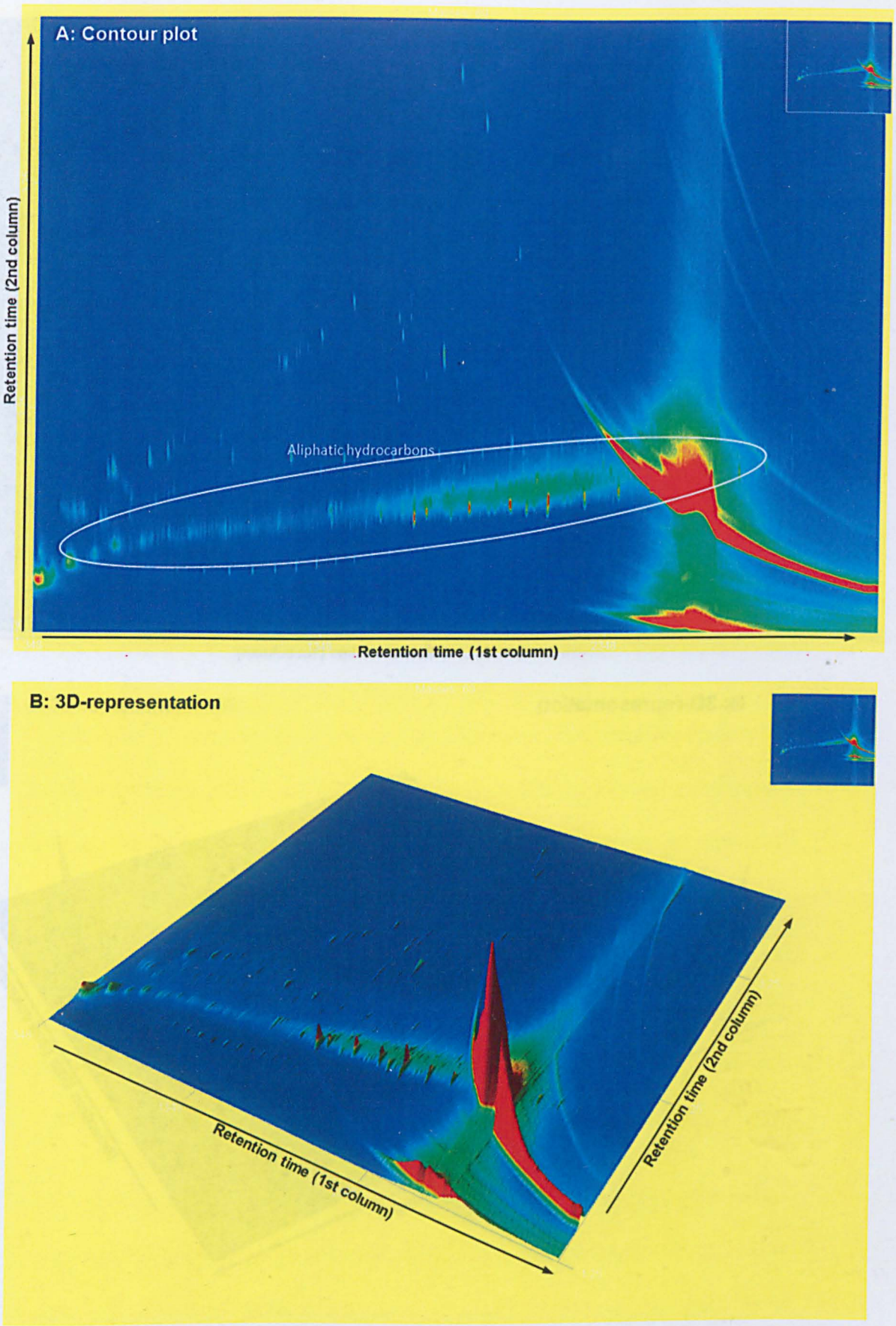

Figure 7-34: 3D-chromatograms of sample 3DA after pyrolysis at 300°(showing m/z=69)

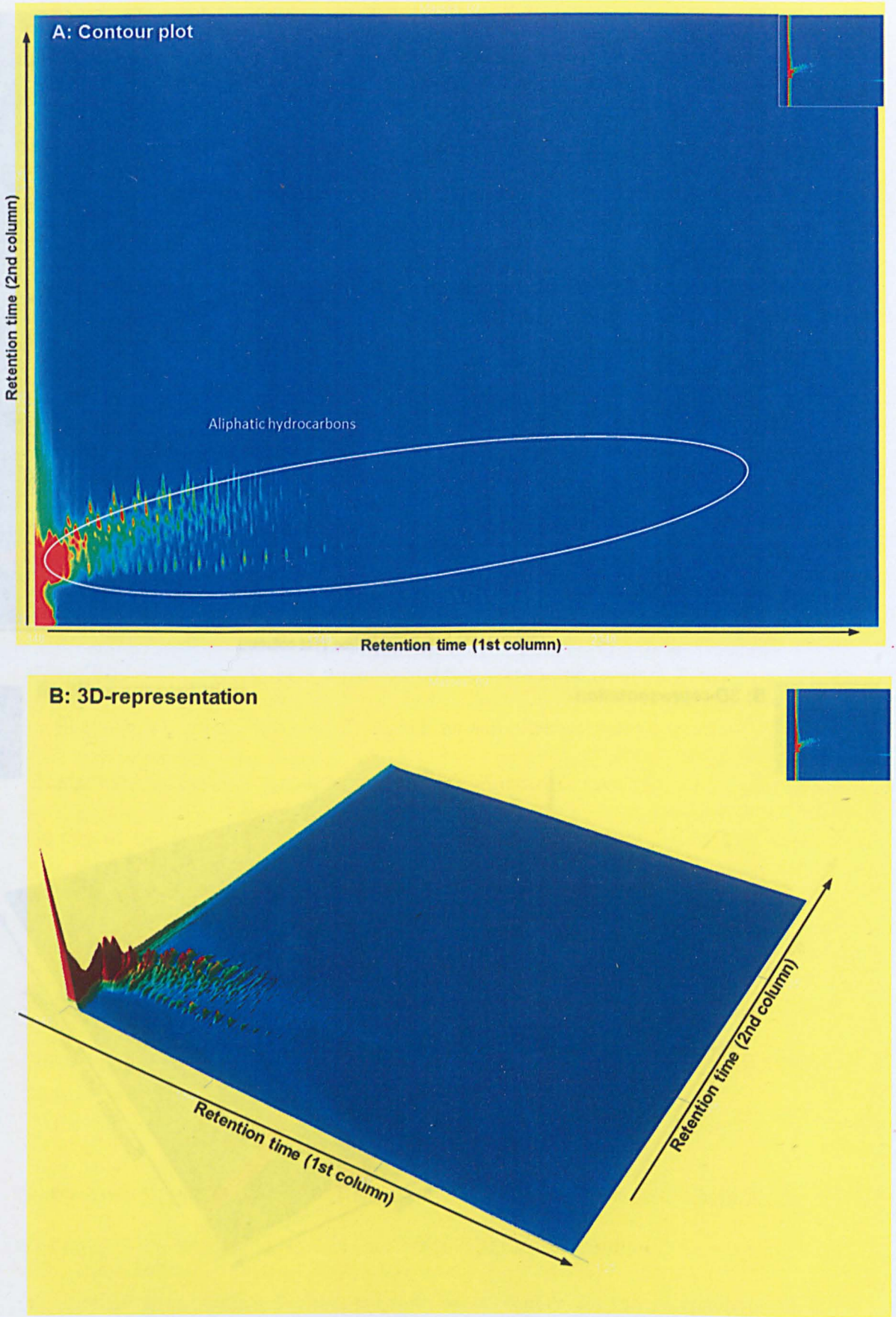

Figure 7-35: 3D-chromatograms of sample 3DC after pyrolysis at 600° (showing m/z=69)

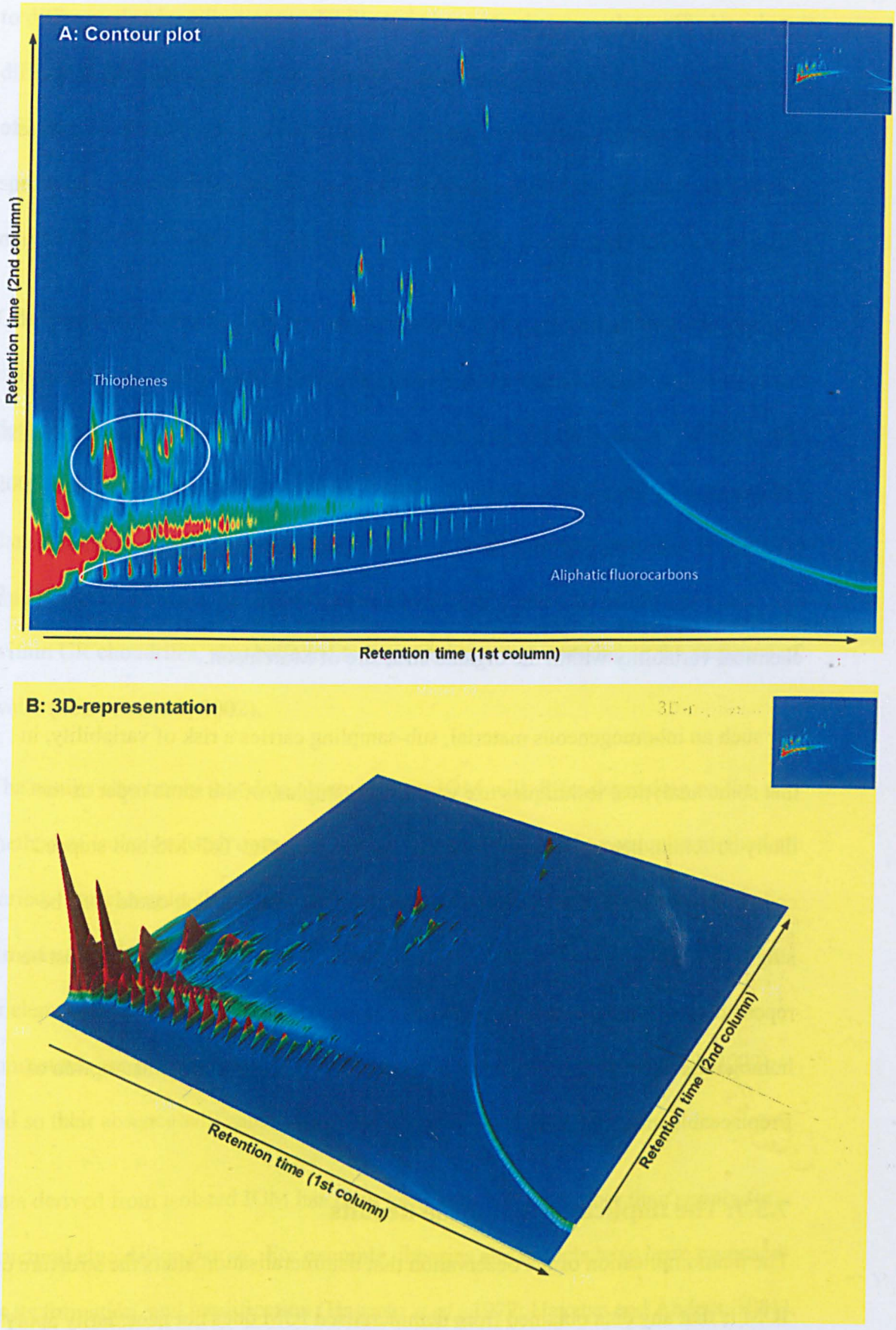

Figure 7-36: 3D-chromatograms of sample 3DA after pyrolysis at 600°(showing m/z=69)

7.5.6. The Heterogeneity of Murchison

Murchison is an inherently heterogeneous meteorite, being composed of grains of many different compositions in a great range of sizes. Analysis of small samples is certain to suffer from lack of reproducibility to some extent due to sample variation (Pearson *et al.*, 2006).

This was observed in this study in a number of ways. Pyrolysis of samples derived from two fragments of Murchison at 300° showed no evidence of weakly-bound organic materials, whereas this has been found in previous studies (Pearson, personal communication, 2013). The sample from which IOM was isolated showed no evidence of oxalic acid formation on treatment with ozone, whereas several other samples, treated in similar ways, did. These results are strong evidence of significant chemical variability within the organic structure of Murchison.

For such an inhomogeneous material, sub-sampling carries a risk of variability, in that some analytical techniques use very small samples, of the same order as the likely structural heterogeneity. Examples are Py- GCxGC-ToF-MS and stepped combustion; both require samples of less than a milligram, which could well be single grains of material. To ensure truly representative results, analyses must be repeated many times on separate sub-samples, or larger samples effectively homogenised before sampling. Both these methods increase the consumption of irreplaceable meteorite samples.

7.5.7. The Implications of these Results

The main implication of the observation that demineralisation alters the structure of IOM is that any data obtained from demineralised IOM does not necessarily apply to that still in place within a meteorite. The Raman spectrum of IOM has been shown

to differ on demineralisation; an FTIR study has also shown such an effect, with different infra-red spectra being obtained from isolated IOM and whole rock samples of a single meteorite (Kebukawa *et al.*, 2013). It is not unreasonable to assume other spectra (such as NMR) will differ too, and so conclusions drawn from those spectra may not be valid when applied to IOM present within a meteorite.

Other data, such as elemental analysis will also clearly not be the same, and, for example, the degree of oxygenation, interpreted from such data (for example, two determinations reviewed by Gilmour (2005), and from NMR (Cody and Alexander, 2005)) may be incorrect. In particular, aqueous processing during demineralisation may introduce oxygen-containing functionality, such as the phenols seen in IOM by Py-GCxGC ToF-MS. Similar oxygen-containing compounds have been found within CR chondrites, also believed to have undergone processing in the presence of water (Pearson *et al.*, 2002).

The results also imply that data obtained from IOM will differ depending on the method of isolation used, or even if the reaction conditions of a particular method are varied. For example, the compounds present in IOM isolated using the method of Amari *et al.* (1994) (both organic, plus sulfur), will contribute to an NMR spectrum or elemental analysis (although no longer part of the macromolecule); these compounds are not present in IOM isolated using the method of Cody *et al.*(2002); and so their absence will cause any data generated to be different.

Data derived from isolated IOM has been used in many ways other than simply for structural elucidation *per se*. For example, theories and models have been proposed for its formation, and modification (Hayatsu *et al.*, 1977; Hayatsu and Anders, 1981), and several reviewed by Alexander *et al.* (1998), which have contributed to the

current understanding of the formation and evolution of the Solar system. The structure of IOM, and in particular its isotopic ratios are used to develop these theories, and if the data available were incorrect, then the reasoning in these studies may be erroneous.

Analytical data derived from meteoritic organic materials, and the variation between different meteorite classes are also used as evidence for the processes which may have operated on the meteorite parent bodies (Alexander *et al.*, 1998). If those studies were carried out on IOM modified during isolation, and the structure of the organic material actually present in meteorites was not the same as that from which the data has been generated, then any conclusions drawn could be questioned.

However, although this study has shown that changes occur to the structure of IOM on isolation, without further work (discussed in section 7.6 onwards), it is not clear how significant these changes are. For example, the data has shown that the component of IOM acting as the precursor to the pyrolysate is lost on demineralisation using the method of Cody *et al.* (2002), but the proportion of this component, as a fraction of IOM, is not known. Only if it only forms an insignificant portion of the structure of IOM would data obtained after demineralisation be valid for organic material in place within a meteorite sample. However, as the effects of these changes are apparent using a number of quite different methods and analytical techniques, the changes are not likely to be quantitatively insignificant.

7.5.8. Conclusion

Although the outcome of the action of fluoride appears to be similar to that of pyrolysis or hydrous pyrolysis (Sephton, 2012), the mechanism of reaction must be different. Whatever this mechanism may be, it is clear from the data presented in

this chapter that IOM is chemically modified during demineralisation. Molecular fragments containing aromatic rings are broken away from the macromolecular structure of IOM in some way, and the ions or radicals which are generated become protonated in the reaction mixture (water supplying the protons). If an organic solvent is present during demineralisation, these fragments are lost, otherwise they are retained, physically trapped within the IOM.

When experiments described earlier in this thesis gave unexpected results, based on the then currently-accepted structure of IOM, the possibility that its actual structure might be different became apparent. The work described in this chapter supports that conclusion (although elucidation of the structure of IOM was not an original objective of this study). Work therefore remains to be carried out to assess the nature and extent of the fluoride-induced modification to IOM, and to understand what its original, unreacted structure is. Once that structure is understood, then the mechanism of its reaction with ozone (and with the set of tagging reagents) will be easier to determine.

To avoid any chance that the structure of IOM is modified during its isolation, alternative isolation methods should be developed. Possible approaches are discussed in the following section.

7.6. Alternative Isolation Methodologies for IOM

7.6.1. Avoiding isolation of IOM

The uncertainty over the structure of IOM will be resolved if IOM still in place within a meteorite sample can be sufficiently analysed (that is, without isolation) to determine its structure. That is likely to be difficult, as organic material only forms about 2-5% of a carbonaceous chondrite, and so any signal obtained will be

correspondingly weak. Furthermore, the presence of minerals may not act merely as an inert diluent, but could actively interfere with analysis. For example, paramagnetic minerals (containing iron, for example) will broaden NMR signals, possibly to the point where no meaningful spectrum can be obtained (Larsen *et al.*, 1989), and so some method of isolation is needed.

7.6.2. Alternative Chemical Methods of Isolation

Unless a method can be found to analyse IOM *in situ*, then separation from the mineral component is necessary, using a method which will not chemically alter IOM.

The chemical methods used could be modified in such a way that minerals were still dissolved, but reactions of the organic material were minimised. Possibly, use of more dilute solutions would have this effect; if fluoride ions were fully solvated, their reactivity towards IOM would be less. The reaction could also be carried out at low temperature; if the temperature dependence of the various rates of reactions occurring were favourable, organic reactions might be minimised.

A procedure has been developed using tetrafluoroborate (Robl and Davis, 1993), which may be less aggressive towards organic materials, and although used for terrestrial systems, does not seem to have been used in meteoritic applications.

7.6.3. Non-Chemical Isolation

A possible physical separation method could be by density. If a meteorite sample is finely ground, so that the mineral fragments are physically removed from the organic component, then it should be possible to use density-separation methods to isolate organic material free from mineral contamination. Minerals are generally much

denser than organic solids, so suspension in liquid of an appropriate density would separate them. It may also be possible to fractionate IOM in some way, based on macromolecule size. Many such methods have been used in previous studies (again, derived from those developed for terrestrial systems) and have been reviewed by Durand and Nicaise (1980). Such physical methods have not been used to isolate IOM from meteorite samples, although they have been used to purify samples already substantially demineralised by fluoride treatments (Ott *et al.*, 1981; Kerridge *et al.*, 1987).

Once isolated from the meteoritic minerals, then non-modified IOM could be analysed by all the techniques already used to study it. One difficulty may be that organic material may be stuck firmly onto its underlying mineral, so that all organic grains retain a thin sliver of mineral on crushing. This may be minimised by, for example, agitation of the mixture by ultrasound, use of a non-reactive surfactant, or more extensive milling. For example, particles of drug substance can be reduced in size to below 1 μm by specialist milling techniques used in the pharmaceutical industry (Peltonen and Hirvonen, 2010).

7.7. Conclusions: The Structure and Formation of IOM

The data presented in this thesis has indicated that the structure of IOM is not likely to be similar to that suggested previously (Derenne and Robert, 2010), as was originally assumed at the start of this work. Possible structural interpretations of the data generated in this study, and previously, is discussed in this final section, including potential mechanisms of formation of IOM, consistent with that data.

7.7.1. The Structure of IOM

Kerridge *et al.* (1987) had noted that combustion data obtained from isolated IOM indicated the presence of more than one structural component. The concept of IOM being composed of two distinct (although possibly structurally-related) components was proposed by Sephton *et al.*, (2003) who named them LOM (labile organic matter) and ROM (refractory organic matter). This concept is explored further, using the data generated in this study to clarify the nature of this structural difference and therefore the reactivities of the components.

The argument put forward by Sephton *et al.* is based on results obtained from stepped combustion of samples of whole rock, and also of isolated IOM both before and after hydrous pyrolysis. It should be noted however, that data generated using isolated IOM cannot be directly related to that of organic materials still present in whole rock, as the IOM would have reacted (as demonstrated earlier) with the fluoride used for demineralisation, in some way, depending on the method used.

In stepped combustion (see section 2.5), samples are oxidised at increasing temperatures, with the amount and isotope ratios of the product gases determined by mass spectrometry. Their data showed that the range of combustion temperatures of IOM is much less after hydrous pyrolysis than before (the carbon combusting at lower temperatures having been lost).

The implication is that hydrous pyrolysis has removed a component of IOM (*i.e.* LOM) by high-temperature hydrolysis. Hydrous pyrolysis involves heating samples at over 300° for extended times in the presence of water, as a model for processes occurring within the parent bodies of some carbonaceous chondrites. It is not unreasonable that decomposition of IOM could occur under these conditions, and

this is in fact what was seen. Products of these reactions were separated and analysed (for example, by GC MS), and the compounds generated identified. Sephton *et al.* (2003) noted that after hydrous pyrolysis, the residue (ROM) is isotopically lighter than the IOM before reaction, implying that the LOM which had been decomposed was isotopically heavier.

This concept was also discussed by Okumura and Mimura (2011) who named these two components "thermally unstable" and "thermally stable" based on their pyrolytic decomposition profiles. These two terms are equivalent to LOM and ROM, showing the same contrast in reactivity and isotope ratios.

Those results, taken together with the data generated in this study, enable the properties of the two components of IOM to be collated, allowing at least a partial proposal for possible structures.

LOM is more reactive than ROM, being decomposed by the action of ozone (section 7.2.3), pyrolysis at 600° (section 7.1.3) and other temperatures (Okumura and Mimura, 2011), and hydrous pyrolysis (Sephton *et al.*, 2003). The decomposition fragments have been identified as a range of small molecules, including many aromatic structures, containing up to four rings. This maximum ring size is often quoted in the literature, (for example, by Derenne and Robert, 2010). Larger ring systems, such as benzoperylene and coronene have been detected (by Sephton *et al.*, 2004a) following hydropyrolysis. These larger systems may have resulted from hydrogenolysis of an extended, condensed ring system of ROM, rather than decomposition of LOM. ("Hydrogenolysis" is the term used to describe cleavage of single bonds by addition of hydrogen, rather "hydrogenation", which reserved for the addition of hydrogen across a double bond, with a single bond

remaining.) The GC conditions used by Sephton et al were comparable to those used in this study.

TEM has been used to directly measure the physical size of condensed aromatic systems (Remusat *et al.*, 2005b; Derenne *et al.*, 2005) but again, these results were obtained using IOM isolated by demineralisation, and so not necessarily representative of that IOM present in the whole rock meteorite. In particular, graphite-like stacks of π-systems may be physically disrupted by the solvent extractions and fluoride treatments used during demineralisation.

Chemical methods (such as reactions with tetramethylammonium hydroxide, TMAH, (Remusat *et al.*, 2005b; Watson *et al.*, 2010) or ruthenium tetroxide (Remusat *et al.*, 2005a), have been previously used to modify IOM, and generate data on its structure extrapolated following identification of the reaction products. If, as is likely, these reactions were carried out on IOM already modified by isolation, extrapolation back to the structure of native, unmodified IOM could be very difficult. Understanding the results obtained from these procedures is further complicated by the fact that small molecules, disconnected from the macromolecular LOM during the demineralisation process, may still remain physically trapped, and contribute to its subsequent behaviour (analytical or in reactions). When demineralisation is carried out in the presence of an organic solvent (such as using the method of Cody *et al.*(2002)) however, these small molecules are removed by that solvent, and different results would be expected.

Okumura and Mimura (2011) conducted a series of pyrolyses (of IOM isolated from Murchison) at increasing temperatures, obtaining elemental analyses after each step. This showed that in the sample they used, on pyrolysis the C:H ratio increased from

100:65 to 100:18. The implication of this result is that the material remaining at the end of the experiment (ROM) contains proportionately more carbon and less hydrogen than that at the start (LOM plus ROM). A structural interpretation of this result is that ROM contains mostly extended polycyclic carbon ring systems, whereas LOM is significantly more functionalised, containing smaller ring systems. (The C:H ratio of a polycyclic system decreases with its ring size, as the bonds to hydrogen, only present on the periphery, become relatively fewer.) This is also consistent with the Raman data acquired in this study. Although changes occur to the positions of the main peaks during the various chemical treatments described (as LOM reacts in various ways), the material remaining, assumed to correspond to ROM, still gives a Raman spectrum dominated by signals due to aromatic carbon (the D and G peaks), indicating that ROM is a largely a condensed π-system. Okumura and Mimura (2011).

The component consisting of an extended π-system may be linked with the presence of noble gases in IOM. These gases are believed to be trapped within a carbonaceous component (often named "Q") for which a structure has not yet been determined (Lewis *et al.*, 1975; Verchovsky *et al.*, 2012). Pyridine has been found to liberate noble gases from this carbonaceous component (Marrocchi *et al.*, 2005), the π-π interactions between pyridine and the carbonaceous material presumably being sufficiently strong as to disrupt the layers present in the latter, liberating noble gases trapped between the sheets of these large, stacked condensed ring systems.

This effect may also be useful in developing a mild method of isolating IOM. If pyridine, or another aromatic solvent such as toluene, were present during demineralisation, it is possible that the solvent would penetrate the layered structure,

acting to prise apart the stacked layers, facilitating their separation from any mineral support.

In their paper, Sephton *et al.* (2003) do not speculate on the structure of LOM and ROM, or how they are structurally related. Two alternatives are possible: (i) that they are separate macromolecules that physically co-exist, or (ii) that LOM and ROM are distinct regions of a larger macromolecule, chemically bonded together. The data generated by Sephton *et al.* (2003)does not distinguish between these alternatives, although Okumura and Mimura (2011) suggested that LOM acted as linkages between fragments of ROM, forming a single macromolecule composed of both components. In either case, the ratio of LOM to ROM could vary, as could the exact structure of either component. These ratios are likely to vary from sample to sample of Murchison, reflecting its origin, heterogeneity, and extraterrestrial sample history, and of course also show variation between different meteorites.

Although much of the data discussed in this study could indicate either possibility for the relationship of LOM and ROM, the effect of chemical change on the position of Raman peaks may indicate which is more likely.

If LOM and ROM are structurally distinct and so form separate molecules, changes in the structure of one are not likely to affect the spectra of the other. When Murchison whole rock (3M) and samples derived from it (3SE and 3AW) were treated with ozone, the positions of peaks in the Raman spectra were not affected significantly, whereas the precursor of the pyrolysate formed at 600° appeared to have been decomposed (section 6.3.2). These results indicate that LOM reacting with ozone is structurally distinct from ROM, giving rise to the Raman spectrum. In contrast, when 2DAH, and other samples of Murchison whole rock (sections 4.2

and 5.3) were treated with ozone, not only was LOM decomposed leading to reduction in the level of pyrolysate, but the positions of peaks in the Raman spectra after treatment were significantly different. Those results would be explained better if LOM and ROM were part of the same macromolecule, so that when LOM was decomposed, giving a reduction in pyrolysate, the covalently-linked ROM was electronically-modified (for example, by loss of conjugation) leading to a change in its Raman spectrum. In addition, in those cases only, treatment with ozone caused formation of oxalic acid. It may be therefore, that oxalic acid results from oxidation of a variant of LOM which is covalently bonded to ROM. This may be formed by some modification over time of ROM, as discussed in section 6.3.4 (these examples were all from samples prepared some time ago).

The work presented in this thesis therefore supports the previous proposals of a multi-component structure for IOM, particularly that developed by Sephton *et al.* (2003). In addition, the results obtained here can be used to give a structural basis to this proposal. The reactive labile component (LOM) is composed of small, aromatic rings systems, linked together by aliphatic chains, and is responsible for the majority of reactions of IOM that have been observed. It reacts with ozone, the reagents used for demineralisation, and no doubt also with reagents used by other investigators (for example, ruthenium tetroxide). The less reactive, refractory component (ROM) is made up of an extended π-system formed from condensed six-membered aromatic rings, and responsible for the D and G peaks seen in Raman spectra. Although less reactive, it may be this component which partially decomposes on hydropyrolysis giving larger ring systems than those typically seen (Sephton *et al.*, 2005).

Although the data does not always distinguish between the two components being distinct macromolecules, physically mixed, or parts of the same macromolecule and covalently bonded, some examples may show evidence of one or either alternative. If no changes in the Raman spectrum are seen on reaction of LOM, then the two components are probably not covalently bonded. Changes in the Raman spectrum could be due to a contribution from the modification of LOM, but alternatively could indicate the two components are electronically linked, and thus part of the same macromolecule. However, in either case, the ratios of the two components could vary, both within a single meteorite, and across different meteorites or classes.

7.7.2. Formation of IOM

The formation of IOM could have occurred in a number of ways, as reviewed in section 1.5. The structure of IOM proposed in the previous section, however, requires that two distinct types of IOM are formed, and later mixed, or that one is somehow modified to give the other, for example, the possible scenarios discussed by Sephton *et al.* (2004b). This section discusses how such structures might be expected to be formed, given the understanding of synthetic processes operating as a meteorite parent body forms, and which were reviewed in Chapter 1.

Polycyclic carbon-based molecules such as those proposed by Kwok (2004), and shown in Figure 1-6, can be formed in the outflow of carbon-rich stars (section 1.5.3). Being composed of stellar carbon, they would be expected to be isotopically light (Croat *et al.*, 2005). These carbonaceous macromolecules could be deposited onto grains, and possibly, as they stack together, could trap other atoms between the layers of carbon (*e.g.* noble gases (Marrocchi *et al.*, 2005)). Thus these macromolecules could be a model for ROM.

Functionalisation of such molecules, by reaction in the gas phase or on grains, with atoms or reactive molecules, or by post-accretionary aqueous processing would modify the molecular periphery (Wdowiak *et al.*, 1995b). A central core of ROM with a reactive fringe of smaller, more reactive molecular units (LOM) around the periphery is therefore one model for IOM. In this case, the ratio of LOM to ROM would be expected to be variable within a carbonaceous grain, depending on how extensive the derivatisation reactions were, or to what extent the ROM was exposed to the reactive environment. If parent-body aqueous processing were the cause of the functionalisation, it would be expected that the ratio of LOM to ROM would vary within carbonaceous particles of IOM; molecules at the edges would be more-functionalised, whereas those deeper within being more protected, and therefore potentially, less-functionalised. Such a functionalisation could also develop in unprotected sample, for example on storage.

The alternative scenario, in which LOM and ROM are separate macromolecules, requires a separate process of formation of LOM. These discrete molecules would arise from small molecules such as acetylene, building up by condensation into larger structures (Morgan *et al.*, 1991), being functionalised by reaction with reactive atoms or molecules, to give the components making up molecules such as those proposed by Derrene and Robert (2010), and shown in Figure 1-3. Larger cyclic systems can also be formed from reactions of methane or carbon dioxide (Gilmour *et al.*, 2002), and well as many other synthetic scenarios (such as Miller-Urey (Khare and Sagan, 1973) or Fischer-Tropsch (Studier *et al.*, 1972; Hayatsu and Anders, 1981; Hayatsu *et al.*, 1983) type reactions). Other possibilities, such as progressively building up large molecules from small (such as formaldehyde) have also been proposed (Cody *et al.*, 2011). Once formed, the LOM would need to become physically mixed with

unfunctionalised ROM before accretion into a meteorite parent body. Clearly this mixing could result in a range of final ratios between the two components.

It is possible, of course, that both these alternatives take place, and IOM contains both types of LOM and ROM. In addition, the possibility suggested by Okumura and Mimura (2011) gives an intermediate structure, where LOM fragments act as links between regions corresponding to ROM. In that case, although ROM and LOM would be part of the same macromolecule, they could react as if they were not, particularly if the linkages were by aliphatic chains, conveying no electronic connectivity between the fragments.

A possible unified formation scenario is that isotopically-light carbonaceous grains coalesce, derived from polycyclic molecules generated in carbon-rich stars, either as homogenous particles, or deposited onto mineral grains. These could build up to give a multi-layered structure, coating the mineral grains (along with ices) found in the matrix of carbonaceous chondrites. This structure could become functionalised by reaction at its molecular periphery, by reactive atoms prior to accretion or solution chemistry within a parent body, or, alternatively become coated with functionalised molecules during the pre-accretion phase (with the isotopic ratio increasing as ^{13}C atoms are incorporated). In either case ROM-rich regions would be enclosed by LOM-rich, either as a physical coat of separate molecules, or as a functionalised molecular periphery.

Processing on a parent body could serve to either increase or to decrease the proportions of LOM to ROM. Immersed in organic-rich fluids, ROM could become more highly-functionalised, creating a region of LOM at the edges of the macromolecule. Alternatively, the fluids present may act more like those seen in

hydrous pyrolysis (Sephton *et al.*, 2003) or fluoride mediated demineralisation (section 7.1), in removing a pre-existing functionalised periphery, increasing the proportion of ROM and releasing smaller molecules into the fluid.

Thus in this second scenario, the process operating on the parent body is the generation of ROM, whereas in the first it is generation of LOM. Small (soluble) molecules could therefore be generated by solution chemistry operating on parent bodies during the time when temperatures are sufficient to allow liquids to exist, generated by decomposition of LOM. Meteorites which experienced longer periods of warmth, or more extreme conditions, might contain more extensively decomposed LOM, giving an increase in the relative proportion of ROM. It may be therefore, that rather than ROM resulting from a graphitisation of organic material, building up aromatic rings from acyclic precursors, it is the non-graphite-like material already present which is destroyed. Molecules thus generated may become redistributed within the parent body, if, for example, differential solubility could cause their physical separation, in a manner similar to chromatography (Wing and Bada, 1991). As liberated small molecules may easily be lost, for example, by vaporisation at the surface of a parent body, evidence of their previous existence, and of this formation scenario, may be difficult to find.

7.7.3. Conclusion

It is clear that much work needs to be done to resolve the uncertainties surrounding data obtained from isolated IOM. Confirmation, or otherwise, of the results described in this study is important, as the continued use of suspect data in the investigation into meteoritic origins could lead to much wasted effort. Quantification of the degree of chemical change with fluoride treatment (which may be quite low,

but could be quite extensive) would confirm the applicability of data already acquired.

If the degree of change in the structure of IOM on demineralisation is not trivial, then effort must be directed towards the elucidation of its structure, and towards finding methods of isolation which do not cause chemical change.

Determining whether there are two distinct populations of IOM macromolecules, or whether all IOM contains both refractory cores and reactive peripheries will add greatly to our understanding of how this molecule formed, and would also require non-chemical methods of isolation of IOM. Generating new analytical data from IOM which has not been chemically modified (therefore allowing a direct comparison with data derived from IOM that has) must be a priority.

Chapter 8 Overall Summary and Conclusion

8.1. Progress Against Objectives

8.1.1. Chemical Tagging and Activation

The main objective of this study was to develop a set of reactions which would then be used to attach chemical tags to the organic materials contained within samples of carbonaceous chondrite. The purpose of these tags was to help increase the detectability of meteoritic organic materials, which would be detected by a set of analytical techniques, adapted for use *in situ*.

To achieve this objective, and to preserve valuable stocks of meteorites, model systems were set up. The purpose of these models was twofold. Firstly, they were to act as supports for test organic compounds, in the development of tagging chemistry, and secondly, as a model of a carbonaceous chondrite, to test analytical methodology adapted to detect tagged compounds *in situ*. This was partly successful. The models enabled development of chemistry, applicable to the tagging of organic materials in the solid state, without the need to use precious meteorite samples. Tagging chemistry was developed for a number of functional groups, namely alcohols, phenols, carboxylic acids, amino acids, aldehydes and ketones (as described in Chapter 3), with which suitable tags containing fluorine or chlorine were covalently attached to the target molecules.

The same methodology used to develop procedures for tagging was also used to develop suitable reactions of polycyclic aromatic hydrocarbons (PAHs), analogues of meteoritic IOM, with ozone. The purpose of this reaction was to introduce oxygen-containing functionality into these molecules, which could then be tagged using the chemistry developed earlier. If the density of oxygen-containing functional groups

were to be increased, then a corresponding increase in tag density should be achievable, increasing the ease of detection.

Conditions were developed (optimised using pyrene as a representative PAH) under which hydrocarbons of up to four rings reacted with ozone to give oxygenated derivatives over a reaction time of several hours. This objective was also met (and is described in Chapter 3).

8.1.2. Detection of Tagged Compounds *in situ*

The models did not provide suitable analogues for the demonstration of *in situ* analytical methodology. It proved difficult to satisfactorily mimic the distribution of organic materials in carbonaceous chondrites, namely spread as a thin film coating mineral grains, (as proposed by El Amri *et al.*, 2005). Organic standards applied in solutions to inorganic supports formed droplets on evaporation, leading to deposition of compounds as crystalline clumps, rather than as a uniform coating.

Detection of organic materials *in situ* was planned using, initially, SEM/EDS and Raman spectroscopy, the former to detect tagging elements, and the latter, functional groups. To facilitate the use of these two techniques in tandem, methods for locating features in a sample using both methodologies were required, such as the use of existing features or platinum markers (although this method carries the danger of introducing spurious platinum or gallium atoms). This objective was successfully met (see Chapter 2). Raman microscope images were processed to give images in focus, which, in conjunction with marking a surface by ion-milling, could be used to locate features using both the Raman microscope and SEM. Thus analytical data from both instruments could be generated on areas of interest (such as single grains), even though the sample had to be moved between analytical laboratories. This

methodology was used to analyse features formed on the surfaces of meteorite samples, described in Chapter 4.

Raman mapping, as described in Chapters 2 and 3 was successfully used to show the distribution of materials on the surface of a sample. This could be used, for example, to highlight the distribution of a mineral, by plotting the strength of its characteristic signal(s). For organic materials, the broad peaks between 1200 and 1800 cm^{-1} could be used to distinguish organic-rich areas from those containing minerals. The presence of these signals over most of the surface indicated a widespread presence of IOM, with only relatively small mineral regions being detectable by Raman spectroscopy. The use of mapping to show more subtle variations in Raman signal (such as the positions of maximum signal due to aromatic carbon), was not demonstrated, but by using the ratios of signal strength at appropriate positions in the spectrum, this should be possible. SEM was, as expected, suitable for mapping the presence of elements across a surface, although carbon gives a poor response, and so is not easily detected.

8.1.3. The Activation of IOM

The work set out in the earlier part of this thesis was intended to use molecular tagging to introduce detectable atoms or functional groups into the organic materials present in carbonaceous chondrites. Part of that methodology was the activation of IOM, the introduction of oxygen-containing functionality using ozone. Those reactions, described in Chapter 4 gave unexpected results, including changes to the mineralogy of the samples, and the formation of oxalic acid from reaction of IOM.

The ozone used for those reactions was passed through a water bubbler to increase its reactivity. The presence of water caused gypsum to be mobilised within the sample,

which would negate attempts to detect organic compounds *in situ.* If the use of ozone is to be continued, the use of water must be discontinued.

The action of ozone, to cause the formation of oxalic acid, was unexpected, but was not seen in reactions of all samples. The rate of reaction with ozone was also faster than expected. In studies with isolated IOM, complete consumption of the active component of IOM was complete in a few hours, with no difference in reaction profile seen at shorter reaction times (just less-complete reactions). The temperature of reaction may therefore have been too high, causing extensive decomposition of the IOM structure, rather than a partial functionalisation. More successful reactions might result from being carried out at a lower temperature, for which a new reaction vessel (incorporating cooling) would need to be built.

These results indicated that it was likely that IOM was composed of two components, of differing reactivity. One component reacts rapidly with ozone, and the other does not, as substantial amounts of aromatic carbon were detected (by Raman spectroscopy) even after many hours exposure to ozone. This did not seem consistent with previous work, which indicated IOM was composed of small-ring systems, linked by aliphatic chains (Derenne and Robert, 2010), and thus raised the possibility that the actual structure of IOM was different from that assumed. It was also possible that the different reactivity was due to an interaction of some kind with the minerals making up the bulk of the meteorite.

8.1.4. The Structure and Reactivity of Isolated IOM

This result prompted a re-assessment of the project scope, which was extended to the investigation of this possible role of meteoritic minerals in the reaction with ozone. The reaction of isolated IOM with ozone (described in Chapter 5) caused changes in

its structure and appearance, which when analysed in detail (by measuring changes in the positions of the main peaks seen in Raman spectra) showed that the IOM present within the meteorite sample had reacted in a different way from that isolated following demineralisation. It was possible that this difference was due to the presence (or absence) of minerals, or, that IOM reacts with the fluoride-ion containing reaction mixtures used in its isolation, with more evidence being gathered to show that the latter was the case. The proposal that IOM was composed of two components with differing reactivity towards ozone was given weight by these results, with it seeming likely that one of the two components reacted with both ozone and fluoride ion (during demineralisation), whereas the other either did not, or reacted to a much lesser degree.

This observation prompted a new objective, namely to investigate the isolation of IOM, and to determine whether any chemical changes had in fact occurred on isolation. The original project objectives had been based on an understanding of the structure of IOM (and therefore its reactivity), and based on data derived largely from isolated IOM. If its structure were modified by the isolation process, then the assumed structure may not be correct, and the activation chemistry used (described in Chapter 4) may have been inappropriate.

This final objective was satisfactorily met (as described in Chapters 6 and 7). IOM was isolated and studied; the data generated showed not only that its structure was modified by the two isolation processes used, but the modification was different in the two methods. Evidence for this reaction was reviewed in Chapter 7, and a structural basis for the results seen was discussed. The concept of a two-component structure for IOM (proposed by Sephton *et al.*, 2003) can be met by one component

being unreactive, and similar in structure to a fragment of graphene, consisting largely of polycyclic aromatic systems. The other component, the more reactive, would consist of smaller ring systems, being more reactive towards ozone and fluoride, and capable of generating the compounds seen on pyrolysis of IOM (such as small aromatic systems, thiophenes etc.). These two components might exist as part of the same macromolecule, with the reactive part forming a functionalised periphery of an unreactive centre. Alternatively, both components could exist as discrete macromolecules, physically mixed in some way. In either case, the ratio of the two components could differ from sample to sample. Solutions to the problem of analysis of IOM, and possible methods for its isolation without modification were also discussed, as a means towards determining if these proposed structures for IOM are correct.

8.2. Work Needed to Complete Objectives

The tagging chemistry was designed to introduce detectable atoms and functional groups into oxygen-containing organic compounds. To confirm its applicability, samples of carbonaceous chondrites should next be subjected to the set of reaction conditions developed for tagging each functional group (described in Chapter 3), and analysed using both Raman spectroscopy and SEM/EDS. Features of interest on the meteorite surface (located using both techniques) can be analysed both before and after attempted tagging.

Introduction of new elements in tags (such as chlorine) should be detectable using EDS, whereas functional groups may be detectable using Raman. Usually however, Raman spectra were dominated by the signals due to aromatic carbon, the D and G peaks, and it is quite possible that little change will be seen following tagging,

other than shifts in the positions of the main peaks. The positions of these peaks can be measured (perhaps by developing more accurate estimation of peak maxima), and plotted on graphs. Methods of mapping using peak positions could also be developed. Other analytical methods might be developed.

Should the attempted tagging be unsuccessful, a less-specific chemical method (such as the use of osmium tetroxide) should be re-evaluated. This methodology, although proven, was not originally investigated as part of this study, as the objective was to seek functional-group specific tagging methods, which osmium tetroxide does not provide.

Osmium is detectable by EDS, but, as its tetroxide most likely reacts with the double bonds present in the aromatic structure of IOM, its use as a tag should also cause changes in the Raman spectrum. If the degree of reaction is significant, changes in, for example the positions or ratio of areas of the D and G peaks could be used to generate maps indicating the areas which have been tagged.

Once a modified tagging process is demonstrated, then samples of tagged meteorite can be investigated to determine if associations between tagged organic materials and specific inorganic, (*i.e.* mineral), components can be identified, the original objective of this study.

Appendix: Demineralisation: Practical Details

Three fragments of Murchison were processed to yield a number of samples, the studies of which are described and discussed in Chapters 5 to 7. The majority of these samples were prepared from a fragment of Murchison, supplied by the Field Museum, Chicago. Before that fragment was acquired, samples left from a previous project were used. Their preparation, although not carried out as part of this project, is included in this Appendix for completeness. The relationships between these samples are shown in Figure A-1 (samples shown in italics were no longer available).

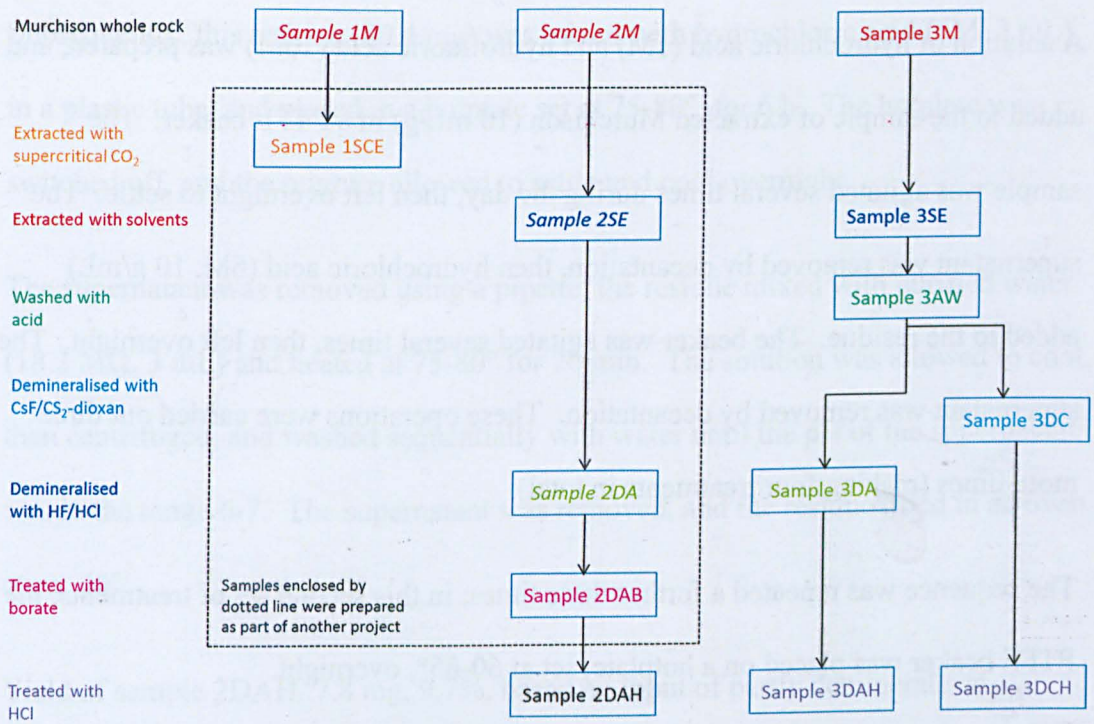

Figure A-1: The relationships between samples prepared from fragments of Murchison

A1. Preparation of Sample 1SCE

Sample 1SCE was prepared (as part of a previous project) by extraction of a fragment of Murchison using supercritical carbon dioxide.

The sample, 1SCE, had been stored in a vial, in the dark, for approximately five years before use.

A2. Preparation of Samples 2DAB and 2DAH

Sample 2DAB had also been prepared as part of a previous project, following the method of Amari *et al.* (1994).

A sample of crushed Murchison was extracted with a mixture of dichloromethane and methanol, 93:7 (Distol or Certified grade), in an ultrasound bath at 0° for 25 min, then the supernatant was removed with a pipette. This was repeated three times, and the residue dried in an oven for at least 1 day.

A solution of hydrochloric acid (1M) and hydrofluoric acid (10M) was prepared, and added to the sample of extracted Murchison (10 mL/g) in a PTFE beaker. The sample was agitated several times during the day, then left overnight to settle. The supernatant was removed by decantation, then hydrochloric acid (6M, 10 g/mL) added to the residue. The beaker was agitated several times, then left overnight. The supernatant was removed by decantation. These operations were carried out three more times (making four treatments in total).

The sequence was repeated a further three times; in this second set of treatments, the PTFE beaker was placed on a hotplate, set at 60-65°, overnight.

A solution of hydrochloric acid (6M) and boric acid (0.6M) was prepared, and added to the residue from the HF-HCl treatments (10 g/mL). The sample was agitated several times during the day, then left overnight to settle. The supernatant was removed by decantation. These operations were carried out three more times (making four treatments in total).

A solution of hydrochloric acid (6M) and hydrofluoric acid (2M) was prepared, and added to the residue from the HF-HCl treatments (10 g/mL). The sample was agitated several times during the day, then left overnight to settle. The supernatant was removed by decantation.

Finally, the residue was treated with a solution of hydrochloric acid (0.1M), and the beaker placed on a hotplate set at 120° for *ca* 24 h.

The mixture was decanted, washed with distilled water and dried. This sample, 2DAB, was stored in a vial, and kept in the dark for about five years before use in this project.

Subsequently, this residue (80.4 mg) was mixed with hydrochloric acid (6M, 3 mL) in a plastic tube, and placed in a hotplate set at 75-80°, for 6 h. The hotplate was switched off, and the mixture allowed to settle and cool overnight.

The supernatant was removed using a pipette, the residue mixed with purified water (18.2 MΩ, 3 mL) and heated at 75-80° for 20 min. The solution was allowed to cool, then centrifuged, and washed sequentially with water until the pH of the supernatant was in the range 6-7. The supernatant was removed, and the residue dried in an oven at *ca.* 40°.

Yield of sample 2DAH, 7.8 mg, 9.7%, based on input of partly demineralised residue, 2DAB.

A3. Extraction of Murchison Sample 3M Using a Range of Solvents

Experimental Preparation

An agate pestle and mortar (mortar *ca.* 10 cm diameter, 50 mL capacity) was cleaned by grinding a few grams of pre-roasted (at 600^0 for 2 h, then cooled to ambient) sand (Aldrich, 50-70 mesh) suspended in a few millilitres of purified (18.2 MΩ) water. This was repeated twice, then the mortar and pestle rinsed with purified water (to remove traces of sand), then methanol and finally dichloromethane before being allowed to dry.

A single sample of Murchison, *ca.* 5 g was requested from the Field Museum, Chicago, USA for this work. During transit, the sample had broken into two large fragments, plus some some debris. The two large fragments were exposed to high vacuum (*ca.* 10^{-9} torr) at *ca* 50-100^0 to remove volatiles (to provide data for another study outside this thesis). The mass loss on exposure to vacuum, which includes any physical losses, was 3.55 %.

Sample	Weight (g)
Total supplied	5.026
Two fragments before degassing	4.7875
Two fragments after degassing	4.6202
Loss	0.1673
Remainder of sample (not degassed)	0.2385
Sample recombined for remaining work (Sample 3M)	4.8587

Table A2: Weights of samples of Murchison after degassing

The degassed fragments were combined with the other small fragments from the Field Museum making a total of 4.8587 g. The sample was ground in portions in the mortar to give a particle size of approximately 100 μm (confirmed by SEM images),

and the portions combined and thoroughly mixed to homogenise them. A portion of this whole rock material (0.2730 g) was retained for analysis (sample 3M, as described in section 6.3).

Extraction with Solvents

The remaining portion of crushed meteorite, 3M (4.5857 g) was extracted with a series of solvents (of increasing polarity and boiling point) to remove any soluble compounds (organic or inorganic). To maximise the removal of organic compounds, solvents were selected across a range of polarities. Solvents from each class of polarity were selected with as low boiling point as possible to simplify eventual concentration of extracts, if needed. High-purity grades were chosen for each, to minimise the possibility of any high-boiling residues or other potential contaminants. The meteorite was stirred in each solvent in a three-necked flask (100 mL capacity) through which a gentle stream of nitrogen (filtered through a 1 μm in-line filter fitted to a PTFE line) had been allowed to flow for *ca.* 10 min. The suspension was stirred magnetically (with a PTFE-coated stirrer-bar) at ambient temperature (typically 19-20^0) for 20-21 h. The suspension was filtered through a sintered funnel fitted with a glass-fibre disc (Whatman GF/A, 1.6 μm retention) into a pre-rinsed Buchner funnel. The round-bottomed flask was rinsed with a little solvent to remove any residual solid, using this to wash the solid on the filter, and the filtrate collected together in a single portion. The filtrate was retained for possible future use. The filter residue was dried by sucking air (screened with a larger glass-fibre disc) through it for 30-60 min, then returned to the flask for extraction with the next solvent after sub-sampling. The set of solvents used is listed in Table A3.

Solvent	Dielectric constant	Boiling point (°C)	Grade	Purity (%)[a]
n-Pentane	1.8	36	For residue analysis	>99.0
Carbon disulfide	2.6	46	Purified by redistillation	>99.9
Dichloromethane	9.1	42	Chromasolv	>99.9
Acetone	20.7	56	Pesticide residue analysis	*ca* 99.8%
Methanol	32.6	65	Anhydrous	99.8

Table A3: Organic solvents used for the extraction of Murchison (sample 3M)

Notes:

a: All materials were obtained from Sigma-Aldrich; full specifications are available in their catalogue (http://www.sigmaaldrich.com/catalog)

Dipolar aprotic solvents were not selected, as their complete removal would be difficult (owing to their high boiling-points) and previous work (Schmitt-Kopplin *et al.*, 2010) had shown these solvents had minimal extractive effect.

After extraction using this set of organic solvents, the process was repeated using purified water (18.2 MΩ). In this case, following filtration, the solid residue was washed with a little methanol to displace water, and a little diethyl ether, and dried *in vacuo*, yielding sample 3SE, 4.2062 g. A sub-sample was retained for analysis, leaving 4.1078 g for processing.

A4. Demineralisation of Murchison after Extraction

Demineralisation involves treating the meteorite with a sequence of inorganic reagents which react with silicate minerals to give soluble derivatives. The first stage of demineralisation is to treat the meteorite with dilute mineral acid, to remove minerals such as carbonates and oxides, as well as any silicates which are readily hydrolysed. The second stage employs the reactivity of silicates with hydrofluoric acid (HF). This is one of the few reagents to readily react with silicates (even silica, or glass) to form fluorosilicates, which are soluble in water, or mineral acid.

One published procedure (Amari *et al.*, 1994) has often been used to isolate IOM. This method employs repeated treatments with mixtures of hot HF and hydrochloric

acid (HCl) to convert all silicates to soluble derivatives, followed by more treatments with HCl and boric acid to remove final mineral traces. IOM remains as an insoluble residue at the end of this procedure. A second procedure, which is carried out at room temperature and avoids extremes of pH, has more-recently been developed (Cody *et al.*, 2002). This method also uses a fluoride-containing solution together with an immiscible organic mixture. As the mineral is dissolved, particles of organic material are released, and collect at the interface of the two immiscible liquids.

Safety Considerations

Hydrofluoric acid, although not a strong acid, causes severe burns which are difficult to treat. At all times when handling this reagent, appropriate safety measures were employed. As this reagent reacts with silicates, including glass, only materials made from plastic or PTFE were allowed to come into contact with it. All residues were made basic with aqueous sodium carbonate, and disposed of following approved procedures.

When it was necessary to separate solids from suspensions, mixtures containing flammable solvents were separated by filtration. Only aqueous mixtures were separated by centrifugation, which, in the absence of a nitrogen blanketing system, presents a hazard of explosion.

Carbon disulfide has an extremely low auto-ignition temperature (90°), and precautions were taken to ensure its vapour did not come into contact with potential ignition sources.

Preliminary Acid Treatment

The meteorite residue obtained from solvent extraction (sample 3SE, 4.1078 g) was mixed with hydrochloric acid (2M, 40 mL) and left to stand, under nitrogen, at ambient temperature for 20 h. The suspension was filtered through a glass-fibre pad, using purified water (18.2 MΩ, 10 mL) for transfer and washing. The residue was washed with further purified water (2 x 10 mL), and pulled dry on the filter. Without further drying, this solid (totalling 2.32 g) was used for the next stage of demineralisation; (a sample was retained for analysis, 3AW (section 6.4)).

Demineralisation Procedure 1 (Amari *et al.* 1994)

A solution containing hydrochloric (HCl) and hydrofluoric (HF) acids was prepared from the concentrated acids and purified water; details are given in Table A4.

Component	Vol (mL)	Conc (% w/w)	Density (g/mL)	Acid (g)	Water (g)	Total (g)	mMol	Molarity
HCl	7	36	1.12	2.8	5.0	2.8 (acid)	77	1
HF	29	48	1.15	16.0	17.3	16.0 (acid)	800	10
Water	48		1.0	0	48	70.3 (water)	3905	49

Table A4: Components of the HF-HCl mixture as used by Amari *et al.*(1994)

Approximately half the solid from solvent extraction and acid washing (sample 3AW, 1.17 g) was treated with a portion of this acid mixture (20 mL), mixed well, and left to stand at ambient temperature for 20 h. The supernatant was removed using a plastic pipette, and the residue treated with HCl (6 M, 20 mL), the suspension mixed, and left for 20 h. After settling, the supernatant was removed.

This sequence of alternating treatments with HF/HCl and HCl was repeated a further four times (making five treatments in total).

After removal of the final portion of HCl, the solid residue was transferred into a plastic centrifuge tube using purified water (20 mL), centrifuged (2500 rpm for 5 min), and the supernatant removed using a plastic pipette. The solid was similarly treated with HCl (2 M, 20 mL), then portions of purified water (20 mL) until the pH of the supernatant was 5-6 (three washes were required). The final wash was removed with a pipette, the tube allowed to drain, and the solid dried to constant weight *in vacuo* at room temperature, giving sample 3DA.

The yield of sample 3DA was 0.1818g (8.7 % of Murchison after solvent extraction (3SE)).

A portion of sample 3DA (0.1524 g) was suspended in HCl (6 M, 3 mL) in a closed glass tube, and placed in a heating block set at 65°, for 20 h. After settling, the supernatant was removed, and the residue washed with portions of purified water (18.2 MΩ, 5 mL), removing the supernatant after centrifugation, until the pH reached 5-7 (five washes were required). The wash was removed, the solid allowed to drain, and dried, *in vacuo* at room temperature to constant weight, giving sample 3DAH.

The yield of sample 3DAH was 21.8 mg (1.25 %, of Murchison after solvent extraction (3SE)).

Demineralisation Procedure 2 (Cody *et al.* 2002)

A saturated solution of caesium fluoride (CsF) in water (43 g CsF in 10 mL water) was prepared, giving a solution with a density measured as 2.9 g/mL.

A portion of 15 mL (43.5 g) was taken, equivalent to 35.3 g CsF and 8.2 g water, and the pH adjusted to 5-7 by carefully adding aqueous hydrofluoric acid (48%w/w,

10 mL was required). The composition of this solution is given in Table A5, and the overall molar ratios in Table A6.

The density of this solution was measured at 2.18 g/mL.

Compound	MW	Weight (g)	Moles
Water	18	8.2	0.46
Caesium fluoride	152	35.3	0.23
HF 48%	20	10 mL x 1.15 g/mL = 11.5 g (5.5 g HF, 6.0 g H_2O)	0.28 HF 0.33 H_2O

Table A5: Composition of the fluoride-containing solution used in the method of Cody *et al.* (2002).

Ion/molecule	Moles
Cs	0.23
F	0.51
Water	0.77

Table A6: Molar composition of the aqueous solution used in the method of Cody *et al.* (2002)

Approximately half of the solid prepared by solvent extraction and acid washing, (sample 3AW, 1.12 g,) was mixed with 20 mL of the HF-CsF solution, followed by 10 mL carbon disulfide and 10 mL 1,4-dioxan. The mixture was stirred overnight at ambient temperature, then left to settle. The upper organic, and the lower aqueous layers were returned to the reaction vessel, after separating the interfacial layer. This procedure was repeated twice more, the interfacial layers being removed and combined at each stage, returning any organic or aqueous layers which separated, to the reaction vessel. If necessary, a few mL of either dioxane-carbon disulfide or water were used to effect the transfer of the lower layer (which contained insoluble mineral residue).

The combined interfacial suspension was washed, transferred to a centrifuge tube, and washed with a mixture of water:dioxane:carbon disulphide (1:1:1, 7.5 mL in

total), then water (5 mL) and hydrochloric acid (2M, 5 mL). The solid was washed with water until the pH of the supernatant was 5-7 (five washes were required). The supernatant was removed, the solid allowed to drain, and the solid dried to constant weight *in vacuo* at room temperature giving sample 3DC.

The yield of sample 3DC was 0.4183 g (21.1 % of Murchison after solvent extraction (3SE)).

A portion of sample 3DC (0.2470 g) was suspended in HCl (6M, 5 mL) in a closed glass tube, and placed in a heating block set at 65°, for 20 h. After settling, the supernatant was removed, and the residue washed with portions of purified water (18.2 MΩ, 5 mL), removing the supernatant after centrifugation, until the pH reached 5-7 (five washes were required). The wash was removed, the solid allowed to drain, and dried, *in vacuo* at room temperature to constant weight, giving sample 3DCH.

The yield of sample 3DCH was 26.2 mg (2.23 % of Murchison after solvent extraction (3SE)).

References

ALEXANDER, C. M. O'D. (2001) Inherited material from the Protosolar cloud: Composition and Origin. *Phil. Trans. Roy. Soc. London,* 359, 1973-1989.

ALEXANDER, C. M. O'D., FOGEL, M., YABUTA, H. & CODY, G. D. (2007) The origin and evolution of chondrites recorded in the elemental and isotopic compositions of their macromolecular organic matter. *Geochim. Cosmochim. Acta,* 71, 4380-4403.

ALEXANDER, C. M. O'D., RUSSELL, S. S., ARDEN, J. W., ASH, R. D., GRADY, M. M. & PILLINGER, C. T. (1998) The origin of chondritic macromolecular organic matter: A carbon and nitrogen isotope study. *Meteorit. Planet. Sci.,* 33, 603-622.

ALLAMANDOLA, L. J. (2008) Chemical Evolution in the Interstellar Medium: Feedstock of Solar Systems. *in* ZAIKOWSKI, L. & FRIEDRICH, J. M. (Eds.) *Chemical Evolution: Chemical Change across Space and Time.* Washington, American Chemical Society.

ALLAMANDOLA, L. J., BERNSTEIN, M. P., SANDFORD, S. A. & WALKER, R. L. (1999) Evolution of interstellar ices. *Space Sci. Rev.,* 90, 219-232.

ALPHER, R. A., BETHE, H. & GAMOW, G. (1948) The Origin of Chemical Elements. *Phys. Rev.,* 73, 803-804.

AMARI, S., LEWIS, R. S. & ANDERS, E. (1994) Interstellar grains in meteorites: I. Isolation of SiC, graphite and diamond; size distributions of SiC and graphite. *Geochim. Cosmochim. Acta,* 58, 459-470.

ANDERS, E., DUFRESNE, E. R., HAYATSU, R., CAVAILLE, A., DUFRESNE, A. & FITCH, F. W. (1964) Contaminated Meteorite. *Science,* 146, 1157-1161.

ANDERS, E. & EBIHARA, M. (1982) Solar-system abundances of the elements. *Geochim. Cosmochim. Acta,* 46, 2363-2380.

ANDERS, E. & FITCH, F. W. (1962) Search for Organized Elements in Carbonaceous Chondrites. *Science,* 138, 1392-1399.

ANDRÉ, P., WARD-THOMPSON, D. & BARSONY, M. (2000) From Prestellar cores to Protostars: The Initial Conditions of Star Formation. *in* MANNINGS, V., BOSS, A. P. & RUSSELL, S. S. (Eds.) *Protostars and Planets IV.* Tuscon, University of Arizona Press.

ASTRACK, A. & SCHOENFELD, C. G. (1983) Ozonolysis of whole cardamom seeds. US Patent 4376130.

BADA, J. L. (2004) How life began on Earth: a status report. *Earth Planet. Sci. Lett.,* 226, 1-15.

BADA, J. L. & LAZCANO, A. (2003) Prebiotic Soup - Revisiting the Miller Experiment. *Science,* 300, 745-746.

BAILEY, P. S. (1958) The reactions of ozone with organic compounds. *Chem. Rev.,* 58, 925-1010.

BARBER, D. J. (1981) Matrix phyllosilicates and associated minerals in C2M carbonaceous chondrites. *Geochim. Cosmochim. Acta,* 45, 945-970.

BARNARD, D. (1956) Ozonolytic Degradation of Interpolymers of Natural Rubber with Methyl Methacrylate and Styrene. *J. Polymer Res.,* 22, 213-216.

BARUCCI, M. A. & FULCHIGNONI, M. (1989) Unified Asteroid Taxonomy. *in* LAGERKVIST, C. I., RICKMAN, H. & LINDBLAND, B. A. (Eds.) *Asteroids, Comets and Meteorites III.* Uppsala, Universitet Uppsala.

BELLOCHE, A., GARROD, R. T., MÜLLER, H. S. P., MENTEN, K. M., COMITO, C. & SCHILKE, P. (2009) Increased complexity in interstellar chemistry: detection and chemical modeling of ethyl formate and n-propyl cyanide in Sagittarius B2(N). *Astronomy and Astrophysics,* 499, 215-232.

BERNAL, J. D. (1957) The Origins of Life. *Nature,* 180, 1220.

BERNARD, S., BEYSSAC, O. & BENZERARA, K. (2008) Raman Mapping Using Advanced Line-Scanning Systems: Geological Applications. *Appl. Spectr.*, 62, 1180-1188.

BERNATOWICZ, T. J., CROAT, T. K. & DAULTON, T. L. (2006) Origin and Evolution of Carbonaceous Presolar Grains in Stellar Environments. *in* LAURETTA, D. S. & McSWEEN, H. Y. (Eds.) *Meteorites and the Early Solar System II.* Tucson, University of Arizona Press.

BERNSTEIN, M. P., MOORE, M. H., ELSILA, J. E., SANDFORD, S. A., ALLAMANDOLA, L. J. & ZARE, R. N. (2003) Side group addition to the polycyclic aromatic hydrocarbon coronene by proton irradiation in cosmic ice analogs. *Astrophys. J.*, 582, L25-L29.

BERNSTEIN, M. P., SANDFORD, S. A., ALLAMANDOLA, L. J. & CHANG, S. (1995) Organic compounds produced by photolysis of realistic interstellar and cometary ice analogs containing methanol. *Astrophys. J.*, 454, 327-344.

BITZ, M. C. & NAGY, B. (1967) Ozonolysis of "polymer-type" material in coal, kerogen, and in the Orgueil meteorite: a preliminary report. *Proc. Natl. Acad. Sci.*, 56, 1383-1390.

BLANCO, A., CAPPELLO, D., FONTI, S., IENTILE, A. & OROFINO, V. (1999) Processing of Amorphous Carbon Grains Produced in Hydrogen-Rich Atmosphere. *Adv. Space Res.*, 24, 443-447.

BLAND, P. A., JACKSON, M. D., COKER, R. F., COHEN, B. A., WEBBER, J. B. W., LEE, M. R., DUFFY, C. M., CHATER, R. J., ARKADANI, M. G., McPHAIL, D. S., McCOMB, D. W. & BENEDIX, G. K. (2009) Why aqueous alteration in asteroids was isochemical: High porosity ≠ high permeability. *Earth Planet. Sci. Lett.*, 287, 559-568.

BONAL, L., BOUROT-DENISE, M., QUIRICO, E., MONTAGNAC, G. & LEWIN, E. (2007) Organic matter and metamorphic history of CO chondrites. *Geochim. Cosmochim. Acta,* 71, 1605-1623.

BONAL, L., QUIRICO, E., BOUROT-DENISE, M. & MONTAGNAC, G. (2006) Determination of the petrologic type of CV3 chondrites by Raman spectroscopy of included organic matter. *Geochim. Cosmochim. Acta,* 70, 1849-1863.

BOSS, A. P. (1993) Evolution of the Solar Nebula. II. Thermal Structure during Nebula Formation. *Astrophys. J.*, 417, 351-367.

BOSS, A. P. (1996) A Concise Guide to Chondrule formation. *in* HEWINS, R. H., JONES, R. H. & SCOTT, E. R. D. (Eds.) *Chondrules and the Protoplanetary disk.* Cambridge, CUP.

BOSS, A. P. (1998) Temperatures in Protoplanetary Disks. *Ann. Rev. Earth Planet. Sci.*, 26, 53-80.

BOSS, A. P. (2004) Evolution of the Solar Nebula: VI. Mixing and Transport of Isotopic Heterogenity. *Astrophys. J.*, 616, 1265-1277.

BOSS, A. P. & GOSWAMI, J. N. (2006) Presolar Cloud Collapse and the Formation and Early Evolution of the Solar Nebula. *in* LAURETTA, D. S. & McSWEEN, H. Y., JR (Eds.) *Meteorites and the Early Solar System II.* Tucson, University of Arizona Press.

BOTTA, O. & BADA, J. L. (2002) Extraterrestrial organic compounds in meteorites. *Surveys in Geophysics,* 23, 411-467.

BREARLEY, A. J. (2005) Nebular versus Parent-Body Processing. *in* DAVIS, A. M. (Ed.) *Treatise on Geochemistry Vol 1.* Oxford, Elsevier.

BRESLOW, R. (2011) A likely possible origin of homochirality in amino acids and sugars on prebiotic earth. *Tetrahedron Letters,* 52, 2028-2032.

BRIGGS, M. H. & MAMIKUNIAN, G. (1963) Organic Constituents of the Carbonaceous Chondrites. *Space Sci. Rev.*, 1, 647-682.

BROOKS, J. B., ALLEY, C. C. & LIDDLE, J. A. (1974) Simultaneous Esterification of Carboxyl and Hydroxyl Groups with Alcohols and Heptafluorobutyric Anhydride for Analysis by Gas Chromatography. *Anal. Chem.*, 46, 1930-1934.

BUNCH, T. E. & CHANG, S. (1980) Carbonaceous chondrites: II. Carbonaceous chondrite phyllosilicates and light element geochemistry as indicators of parent body processes and surface conditions. *Geochim. Cosmochim. Acta,* 44, 1543-1577.

BURBIDGE, E. M., BURBIDGE, G. R., FOWLER, W. A. & HOYLE, F. (1957) Synthesis of the Elements in Stars. *Rev. Mod. Phys.,* 29, 547-654.

BUSEMANN, H., ALEXANDER, C. M. O'D. & NITTLER, L. R. (2007) Characterization of insoluble organic matter in primitive meteorites by microRaman spectroscopy. *Meteorit. Planet. Sci.,* 42, 1387-1416.

CAIRNS-SMITH, A. G. & HARTMAN, H. (Eds.) (1986) *Clay minerals and the origin of life,* Cambridge, Cambridge University Press.

CAMERON, A. G. W. (1955) Origin of anomalous abundances of the elements in giant stars. *Astrophys. J.,* 121, 144-160.

CAMERON, A. G. W. (1962) The Formation of the Sun and Planets. *Icarus,* 1, 13-69.

CAMERON, A. G. W. (1995) The first ten million years in the solar nebula. *Meteoritics,* 30, 133-161.

CARR, J. S. & NAJITA, J. R. (2008) Organic Molecules and Water in the Planet Formation region of Young Circumstellar Disks. *Science,* 319, 504-506.

CASSEN, P. & BOSS, A. P. (1988) Protostellar collapse, dust grains and solar-system formation. *in* KERRIDGE, J. F. (Ed.) *Meteorites and the Early Solar System.* Tucson, University of Arizona Press.

CASTIGLIONI, C., MAPELLI, C., NEGRI, F. & ZERBI, G. (2001a) Origin of the *D* line in the Raman spectrum of graphite: A study based on Raman frequencies and intensities of polycyclic aromatic hydrocarbon molecules. *J. Chem. Phys.,* 114, 963-974.

CASTIGLIONI, C., NEGRI, F., RIGOLIO, M. & ZERBI, G. (2001b) Raman activation in disordered graphites of the A'_1 symmetry forbidden $k \neq 0$ phonon: The origin of the D line. *J. Chem. Phys.,* 115, 3769-3778.

CATALDO, F., BRUCATO, J. R. & KEHEYAN, Y. (2005) Chirality in pre-biotic molecules and the phenomenon of photo- and radioracemization. *J. Physics: Conf. Ser.,* 6, 139-148.

CHANG, S. & BUNCH, T. E. (1986) Clays and Organic matter in meteorites. *in* CAIRNS-SMITH, A. G. & HARTMAN, H. (Eds.) *Clay minerals and the origins of life.* Cambridge, Cambridge University Press.

CHANTURIA, V. A., IVANOVA, T. A., KHABAROVA, I. A. & RYAZANTSEV, M. V. (2007) Mineral Dressing. Effect of Ozone on physico-chemical and flotation properties of surface of pyrrhotite under the nanosecond electromagnetic pulse treatment. *J. Mining Sci.,* 43, 83-90.

CHAPMAN, C. R. (1976) Asteroids as meteorite parent-bodies: the astronomical perspective. *Geochim. Cosmochim. Acta,* 40, 701-719.

CHIAR, J. E., TIELENS, A. G. G. M., WHITTET, D. C. B., SCHUTTE, W. A., BOOGERT, A. C. A., LUTZ, D., van DISHOECK, E. F. & BERNSTEIN, M. P. (2000) The composition and distribution of dust along the line of sight toward the galactic centre. *Astrophys. J.,* 537, 749-762.

CLARK, J. H., KYBETT, A. P. & MACQUARRIE, D. J. (1992) *Supported Reagents - Preparation, Analysis and Applications,* VCH.

CLEMMETT, S. J., MESSENGER, S., THOMAS-KEPRTA, K. L., GIBSON, E. K. & ROSS, D. K. (2012a) *In situ* Mapping of the Organic Matter in Carbonaceous Chondrites and Mineral Relationships. *75th Meteoritical Society Conference. Abstract 5370*

CLEMMETT, S. J., THOMAS-KEPRTA, K. L. & NAKAMURA-MESSENGER, K. (2012b) The spatial distribution of Organic Matter and Mineralogical relationships in carbonaceous chondrites. *43rd Lunar and Planetary Science Conference. Abstract 2889*

CODY, G. D. & ALEXANDER, C. M. O'D. (2005) NMR studies of chemical structural variation of insoluble organic matter from different carbonaceous chondrite groups. *Geochim. Cosmochim. Acta,* 69, 1085-1097.

CODY, G. D., ALEXANDER, C. M. O'D. & TERA, F. (2002) Solid state (^{1}H and ^{13}C) nuclear magnetic resonance spectroscopy of insoluble organic residue in the Murchison meteorite: A self-consistent quantitative analysis. *Geochim. Cosmochim. Acta,* 66, 1851-1865.

CODY, G. D., HEYING, E., ALEXANDER, C. M. O'D., NITTLER, L. R., KILCOYNE, A. L. D., SANDFORD, S. A. & STROUD, R. M. (2011) Establishing a molecular relationship between chondritic and cometary organic solids. *Proc. Natl. Acad. Sci.,* 108, 19171-19176.

COLEMAN, M. J., GOODYEAR, M. D., LATHAM, D. W. S. & WHITEHEAD, A. J. (1999) A convenient method for the N-acylation and esterification of hindered amino acids: Synthesis of ultra short acting opioid agonist, remifentanil. *Synlett,* 1923-1924.

CONSOLMAGNO, G. J. (2000) Lithification Scenarios for Ordinary Chondrites. *Meteorit. Planet. Sci.,* 35, A45.

COOPER, G. & JENNISKENS, P. (2012) Water soluble organic and inorganic anions in Sutter's Mill. *75th Meteoritical Society Conference. Abstract 5399*

CRAIG, J. D. C. & BROOKER, M. H. (2000) On the Nature of Fluoride Ion Hydration. *J. Solution Chem.,* 29, 879-888.

CRIEGEE, R. (1975) Mechanism of Ozonolysis. *Angew Chem Int Ed Engl,* 87, 745.

CROAT, T. K., STADERMANN, F. J. & BERNATOWICZ, T. J. (2005) Presolar graphite from AGB stars: Microstructure and s-Process Enrichment. *Astrophys. J.,* 631, 976-987.

d'HENDECOURT, L. B., ALLAMANDOLA, L. J. & GREENBERG, J. M. (1985) Time dependent chemistry in dense molecular clouds. I Grain surface reactions, gas/grain interactions and infrared spectroscopy. *Astronomy and Astrophysics,* 152, 130-150.

DERENNE, S. & ROBERT, F. (2010) Model of molecular structure of the insoluble organic matter isolated from Murchison meteorite. *Meteorit. Planet. Sci.,* 45, 1461-1475.

DERENNE, S., ROBERT, F., BINET, L., GOURIER, D., ROUZARD, J.-N. & LARGEAU, C. (2002) Use of Combined Spectroscopic and Microscopic Tools for deciphering the Chemical Structure and Origin of the Insoluble Organic Matter in the Orgueil and Murchison Meteorites. *33rd Lunar and Planetary Science Conference. Abstract 1182*

DERENNE, S., ROUZAUD, J.-N., CLINARD, C. & ROBERT, F. (2005) Size discontinuity between interstellar and chondritic aromatic structures: A high-resolution transmission electron microscope study. *Geochim. Cosmochim. Acta,* 69, 3911-3918.

DEYRUP, C. L., CHANG, S.-M., WEINTRAUB, R. A. & MOYE, H. A. (1985) Simultaneous Esterification and Acylation of Pesticides for Analysis by Gas Chromatography. 1. derivatisation of Glyphosate and (Aminomethyl)phosphonic Acid with Fluorinated Alcohols-Perfluorinated Anhydrides. *J. Agric. Food Chem.,* 33, 944-947.

DICKIE, R. A., HAMMOND, J. S., DEVRIES, J. E. & HOLUBKA, J. W. (1982) Surface Derivatization of Hydroxyl Function Acrylic Copolymers for Characterisation by X-ray Photoelectron Spectroscopy. *Anal. Chem.,* 54, 2045-2049.

DOMÍNGUEZ, E., MERCADO, J. A., QUESADA, M. A. & HEREDIA, A. (1999) Pollen sporopollenin: degradation and structural elucidation. *Sex. Plant Reprod.,* 12, 171-178.

DRAINE, B. T. & SALPETER, E. E. (1979) Destruction Mechanisms for Interstellar Dust. *Astrophys. J.,* 231, 438-455.

DULEY, W. W. & WILLIAMS, D. A. (1984) *Interstellar Chemistry,* London, Academic Press.

DURAND, B. (Ed.) (1980) *Kerogen: Insoluble organic matter from sedimentary rocks,* Paris, Editions Technip.

DURAND, B. & NICAISE, G. (1980) Procedures for kerogen isolation. *in* DURAND, B. (Ed.) *Kerogen, Insoluble Organic Matter from Sedimentary Rocks.* Paris, Editions Technip.

EBEL, D. S. (2006) Condensation of Rocky Material in Astrophysical Environments. *in* LAURETTA, D. S. & McSWEEN, H. Y., JR (Eds.) *Meteorites and the Early Solar System II.* Tucson, University of Arizona Press.

EDWARDS, H. G. M., SEAWARD, M. R. D., ATTWOOD, S. J., LITTLE, S. J., De OLIVEIRA, L. F. C. & TRETIACH, M. (2003) FT-Raman spectroscopy of lichens on dolomitic rocks: an assessment of metal oxalate formation. *Analyst,* 128, 1218-1221.

EHRENFREUD, P. & CHARNLEY, S. B. (2000) Organic Molecules in the Interstellar Medium, Comets and Meteorites: A Voyage from Dark Clouds to the Early Earth. *Ann. Rev. Astro. Astrophys.,* 38, 427-483.

El AMRI, C., MAUREL, M.-C., SAGON, G. & BARON, M.-H. (2005) The micro-distribution of carbonaceous matter in the murchison meteorite as investigated by Raman imaging. *Spectro. Acta A,* 61, 2049-2056.

ELSILA, J. E., GLAVIN, D. P. & DWORKIN, J. P. (2009) Cometary glycine detected in samples returned by Stardust. *Meteorit. Planet. Sci.,* 44, 1323-1330.

EVERHART, D. S. & REILLEY, C. N. (1981) Chemical Derivatization in Electron Spectroscopy for Chemical Analysis of Surface Functional Groups Introduced on Low-Density Polyethylene Film. *Anal. Chem.,* 53, 665-676.

FERRARI, A. C., MEYER, J. C., SCARDACI, V., CASIRAGHI, C., LAZZERI, M., MAURI, F., PISCANEC, S., JIANG, D., NOVOSELOV, K. S., ROTH, S. & GEIM, A. K. (2006) Raman Spectrum of Graphene and Graphene layers. *Phys. Rev. Lett.,* 97, 187401 1-4.

FINAR, I. L. (1959) *Organic Chemistry Volume 1: Fundmental Principles,* Longmans.

FITCH, F., SCHWARCZ, H. P. & ANDERS, E. (1962) "Organized Elements" in carbonaceous Chondrites. *Nature,* 193, 1123-1125.

FITCH, F. W. & ANDERS, E. (1963) Organized Element: Possibe Identification in Orgueil Meteorite. *Science,* 140, 1097-1100.

FLYNN, G. J., KELLER, L. P., WIRICK, S. & JACOBSEN, C. (2008) Organic matter in interplanetary dust particles. *in* KWOK, S. & SANDFORD, S. (Eds.) *Organic Matter in Space.*

FLYNN, G. J., WIRICK, S., KELLER, L. P., JACOBSEN, C. & SANDFORD, S. A. (2010) Organic coatings on individual grains in CP IDPs: Implications for the formation mechanism of pre-biotic organic matter and for grain sticking in the early Solar System. *41st Lunar and Planetary Science Conference. Abstract 1079*

FRANCESCHI, V. R. & NAKATA, P. A. (2005) Calcium Oxalate in Plants: Formation and Function. *Ann. Rev. Plant Biol.,* 56, 41-71.

FRENKLACH, M. & FEIGELSON, E. D. (1989) Formation of Polycyclic aromatic hydrocarbons in circumstellar envelopes. *Astrophys. J.,* 341, 372-384.

FROST, R. L., YANG, J. & DING, Z. (2003) Raman and FTIR spectroscopy of natural oxalates: Implications for the evidence of life on Mars. *Chin. Sci. Bull.,* 48, 1844-1852.

FUCHS, L. H., OLSEN, E. & JENSEN, K. J. (1973) Mineralogy, Mineral-Chemistry, and Compositon of the Murchison (C2) Meteorite. *Smithsonian Contributions to the Sciences,* 1-39.

GAFFEY, M. J. & McCORD, T. B. (1979) Mineralogical and petrological characterizations of asteroid surface materials. *in* GEHRELS, T. (Ed.) *Asteroids.* Tucson, University of Arizona Press.

GAINES, S. M., EGLINGTON, G. & RULLKÖTTER, J. (2009) *Echoes of Life: What Fossil Molecules Reveal About Earth History,* Oxford, OUP.

GARVIE, L. A. J. & BUSECK, P. R. (2004) Nanosized carbon-rich grains in carbonaceous chondrite meteorites. *Earth Planet. Sci. Lett.,* 224, 431-439.

GEIM, A. K. & NOVOSELOV, K. S. (2007) The rise of graphene. *Nature Materials,* 6, 183-191.

GEISS, J. & REEVES, H. (1981) Deuterium in the Solar System. *Astronomy and Astrophysics,* 93, 189-199.

GIELEN, C., CAMI, J., BOUWMAN, J., PEETERS, E. & MIN, M. (2011) Carbonaceous molecules in the oxygen-rich circumstellar environment of binary post-AGB stars. *Astronomy and Astrophysics,* 536, A54 1-9.

GILMOUR, I. (2005) Structural and Isotopic Analysis of Organic Matter in Carbonaceous Chondrites. *in* DAVIS, A. M. (Ed.) *Treatise on Geochemistry Vol 1.* Oxford, Elsevier.

GILMOUR, I., HILL, H. G. M., PEARSON, V. K., SEPHTON, M. A. & NUTH, J. A. (2002) Production of high molecular weight organic compounds on the surfaces of amorphous iron silicate catalysts: Implications for organic synthesis in the solar nebula. *33rd Lunar and Planetary Science Conference. Abstract 1613*

GOLDSTEIN, J. I., NEWBURY, D. E., ECHLIN, P., JOY, D. C., FIORI, C. & LIFSHIN, E. (1981) *Scanning Electron Microscopy and X-Ray Microanalysis,* New York, Plenum.

GORIELY, S., BAUSWEIN, A. & JANKA, H.-T. (2011) R-Process Nucleosynthesis in Dynamically Ejected Matter of Neutron Star Mergers. *Astrophys. J. Letters,* 738, L32 1-6.

GOUNELLE, M. & ZOLENSKY, M. E. (2001) A terrestrial origin for sulfate veins in CI1 chondrites. *Meteorit. Planet. Sci.,* 36, 1321-1329.

GRADY, M. M., VERCHOVSKY, A. B., FRANCHI, I. A., WRIGHT, I. P. & PILLINGER, C. T. (2002) Light element geochemistry of the Tagish Lake CI2 chondrite: Comparsion with CI1 and CM2 meteorites. *Meteorit. Planet. Sci.,* 37, 713-735.

GRAEDEL, T. E., LANGER, W. D. & FRERKING, M. A. (1982) The Kinetic Chemistry of Dense Interstellar Clouds. *Astrophys. J. Suppl. Series,* 48, 321-368.

GREENE-KELLY, R. (1964) The Specific Surface Areas of Montmorillonites. *Clay Min. Bull.,* 5, 392-400.

GROSSMAN, L. & LARIMER, J. W. (1974) Early Chemical History of the Solar System. *Rev. Geophys. Space Phys.,* 12, 71-101.

HAMILTON, P. B. (1965) Amino-acids on Hands. *Nature,* 205, 284-285.

HARTGERS, W. A., SINNINGHE DAMSTE, J. S. & De LEEUW, J. W. (1994) Geochemical significance of alkylbenzene distributions in flash pyrolysates of kerogens, coals and asphaltenes. *Geochim. Cosmochim. Acta,* 58, 1759-1775.

HASEGAWA, T. I., HERBST, E. & LEUNG, C. M. (1992) Models of gas-grain chemistry in dense interstellar clouds with complex organic molecules. *Astrophys. J. Suppl. Series,* 82, 167-195.

HAYATSU, R. & ANDERS, E. (1981) Organic Compounds in Meteorites and their Origins. *Top. Curr. Chem. Cosmo. Geo. Chem.,* 99, 1-39.

HAYATSU, R., MATSUOKA, S., SCOTT, R. G., STUDIER, M. H. & ANDERS, E. (1977) Origin of organic matter in the early solar system-VII. The organic polymer in carbonaceous chondrites. *Geochim. Cosmochim. Acta,* 41, 1325-1339.

HAYATSU, R., SCOTT, R. G. & WINANS, R. E. (1983) Comparative structural study of meteoritic polymer with terrestrial geopolymers coal and kerogen. *Meteoritics,* 18, 310.

HAYES, J. M. (1967) Organic constituents of meteorites - a review. *Geochim. Cosmochim. Acta,* 31, 1395-1440.

HAZEN, R. M., PAPINEAU, D., BLEEKER, W., DOWNS, R. T., FERRY, J. M., McCOY, T. J., SVERJENSKY, D. A. & YANG, H. (2008) Mineral Evolution. *American Mineralogist,* 93, 1693-1720.

HECHT, M. H., KOUNAVES, S. P., QUINN, R. C., WEST, S. J., YOUNG, S. M. M., MING, D. W., CATLING, D. C., CLARK, B. C., BOYNTON, W. V., HOFFMAN, J., DeFLORES, L. P., GOSPODINOVA, K., KAPIT, J. & SMITH, P. H. (2009) Detection of Perchlorate and the Soluble Chemistry of Martian Soil at the Phoenix Lander Site. *Science,* 325, 64-67.

HELLING, C., JØRGENSEN, U. G., PLEZ, B. & JOHNSON, H. R. (1996) Formation of PAHs, polyynes and other macromolecules in the photosphere of stars. *Astronomy and Astrophysics,* 315, 194-203.

HERBST, E. (1985) Gas-phase carbon chemistry in Dense Clouds. *in* BLACK, D. C. & MATTHEWS, M. S. (Eds.) *Protostars and Planets II.* Tucson, University of Arizona Press.

HERBST, E. (1995) Chemistry in the interstellar medium. *Ann. Rev. Phys. Chem.,* 46, 27-53.

HEVEY, P. J. & SANDERS, I. S. (2006) A model for planetesimal meltdown by ^{26}Al and its implications for meteorite parent bodies. *Meteorit. Planet. Sci.,* 41, 95-106.

HIGGINS, J., ZHOU, X., LIU, R. & HUANG, T. T.-S. (1997) Theoretical Study of Thermal Decomposition Mechanim of Oxalic Acid. *J. Phys. Chem. A,* 101, 2702-2708.

HOLMLID, L. (2009) Light in Condensed Matter in the Upper Atmosphere as the Origin of Homochirality: Circularly Polarized Light from Rydberg Matter. *Astrobiology,* 9, 535-542.

HOPPE, P. (2006) NanoSIMS: A new tool in cosmochemistry. *Appl. Surface Sci.,* 252, 7102-7106.

HUA, X., WANG, J. & BUSECK, P. R. (2002) Fine-grained rims in the Allan Hills 81002 and Lewis Cliff 90500 CM2 meteorites: Their origin and modification. *Meteorit. Planet. Sci.,* 37, 229-244.

HUANG, Y., ALEXANDRE, M. R. & WANG, Y. (2007) Structure and isotopic ratios of aliphatic side chains in the insoluble organic matter of the Murchison carbonaceous chondrite. *Earth Planet. Sci. Lett.,* 259, 517-525.

HUSS, G. R. (1988) The Role of Pre-solar dust in the formation of the Solar System. *Earth, Moon and Planets,* 40, 165-211.

HUTH, M., PORRATI, F., SCHWALB, C., WINHOLD, M., SACHSER, R., DUKIC, M., ADAMS, J. & FANTNER, G. (2012) Focused electron beam induced deposition: A perspective. *Beilsten J. Nanotechnol.,* 3, 597-619.

INAN, F., PALA, M. & DOYMAZ, I. (2007) Use of ozone in detoxification of aflatoxin B_1 in red pepper. *J. Stored Prod. Res.,* 43, 425-429.

IRVINE, W. M. & KNACKE, R. F. (1989) The Chemistry of Interstellar Gas and Grains. *in* ATREYA, S. K., POLLACK, J. B. & MATTHEWS, M. S. (Eds.) *Origin and Evolution of Planetary and Satellite Atmospheres.* Tucson, University of Arizona Press.

IRVINE, W. M., SCHLOERB, F. P., HJALMARSON, Å. & HERBST, E. (1985) The Chemical State of Dense Interstellar Clouds: An Overview. *in* BLACK, D. C. & MATTHEWS, M. S. (Eds.) *Protostars and Planets II.* Tucson, University of Arizona Press.

IVANOVA, T. A., BUNIN, I. Z. & KHABAROVA, I. A. (2008) On the Characteristic Properties of Oxidation of Sulfide Minerals Exposed to Nanosecond Electromagnetic Pulses. *Bull. Russ. Acad. Sci. Physics,* 72, 1326-1329.

JAFFE, B. (1976) *Crucibles: The Story of Chemistry,* New York, Dover Publishing Inc.

JAVAUX, E. J., MARSHALL, C. P. & BEKKER, A. (2010) Organic-walled microfossils in 3.2-billion-year-old shallow-marine siliciclastic deposits. *Nature,* 463, 934-939.

JEANS, J. H. (1902) The Stability of a Spherical Nebula. *Phil. Trans. Roy. Soc. London,* 199, 1-53.

JEON, H. & SHIPLEY, G. G. (2000) Membrane transport structure function and biogenesis. *J. Biol. Chem.,* 275, 30465-30470.

JIN, L. & SUI, N. (2010) The evolution of the Solar Nebula I. Evolution of the Global Properties and Planet Masses. *Astrophys. J.,* 710, 1179-1194.

JONES, A. P. (1997) The Lifecycle of Interstellar Dust. *in* PENDLETON, Y. J. & TIELENS, A. G. G. M. (Eds.) *From Stardust to Planetesimals.* San Francisco, Astronomical Society of the Pacific.

KEBUKAWA, Y., ALEXANDER, C. M. O'D. & CODY, G. D. (2011) Compositional diversity in insoluble organic matter in type 1, 2 and 3 chondrites as detected by infrared spectroscopy. *Geochim. Cosmochim. Acta,* 75, 3530-3541.

KEBUKAWA, Y., ALEXANDER, C. M. O'D. & CODY, G. D. (2013) Comparison of FTIR Spectra of Buk and Acid-Residual Organic Matter in Chondrites. *76th Annual Meteoritical Society Meeting. Abstract1589*

KEBUKAWA, Y., CODY, G. D. & ALEXANDER, C. M. O'D. (2010) Compositional Diversity of Organic Matter in Type 1, 2 and 3 Chondrites by Infrared Spectroscopy. *41st Lunar and Planetary Science Conference. Abstract 2047*

KEBUKAWA, Y., ISHIKAWA, M., NAKASHIMA, S., NAKAMURA, T. & ZOLENSKY, M. E. (2007) Infrared microspectroscopic mapping of organic matter in Tagish Lake meteorite for studying organic evolution during aqueous alteration. *38th Lunar and Planetary Science Conference. Abstract 1450*

KEMP, D. D. & GORDON, M. S. (2005) Theoretical study of the solvation of fluorine and chlorine anions by water. *J. Phys. Chem. A,* 109, 7688-7699.

KERRIDGE, J. F., CHANG, S. & SHIPP, R. (1987) Isotopic Characterisation of kerogen-like material in the Murchison carbonaceous chondrite. *Geochim. Cosmochim. Acta,* 51, 2527-2540.

KERRIDGE, J. F., CHANG, S. & SHIPP, R. (1988) Deuterium exchange during acid-demineralisation. *Geochim. Cosmochim. Acta,* 52, 2251-2255.

KHARE, B. N. & SAGAN, C. (1973) Red clouds in Reducing Atmospheres. *Icarus,* 20, 311-321.

KINNEY, C. R. & LEONARD, J. T. (1961) Ozonization of Chattanooga Uraniferous Black Shale. *J. Chem. Eng. Data,* 6, 474-476.

KITAJIMA, F., KOTSUGI, M., OHKOCHI, T., NARAOKA, H., ISHIBASHI, Y., ABE, M., FUJIMURA, A., OKAZAKI, R., YADA, T., NAKAMURA, T., NOGUCHI, T., NAGAO, K., TSUCHIYAMA, A., YURIMOTO, H., EBIHARA, M., MUKAI, T., SANDFORD, S. A., OKADA, T., SHIRAI, K., UENO, M., YOSHIKAWA, M. & KAWAGUCHI, J. (2011) A Preliminary Micro-spectroscopic Analysis of the Carbonaceous Matter in the Particles Recovered by the Hayabusa Mission. *74th Annual Meteoritical Society Meeting. Abstract 5341*

KLINE, W. E. & FOGLER, H. S. (1981) Dissolution of Silicate Minerals by Hydrofluoric Acid. *Industrial and Engineering Chemistry Fundamentals,* 20, 155-161.

KOLO, K. & CLAEYS, P. (2005) In vitro formation of Ca-oxalates and the mineral glushinskite by fungal interaction with carbonate substrates and seawater. *Biogeosciences,* 2, 277-293.

KRING, D. A. (1991) High temperature rims around chondrules in primitive chondrites:evidence for fluctuating conditions in the solar nebula. *Earth Planet. Sci. Lett.,* 105, 65-80.

KROT, A. N. & BIZZARRO, M. (2009) Chronology of meteorites and the early solar system. *Geochim. Cosmochim. Acta,* 73, 4919-4921.

KROT, A. N., KEIL, K., SCOTT, E. R. D., GOODRICH, C. A. & WEISBERG, M. K. (2005) Classification of Meteorites. *in* DAVIS, A. M. (Ed.) *Treatise on Geochemistry Vol 1.* Oxford, Elsevier.

KROTO, H. W., HEATH, J. R., O'BRIEN, S. C., CURL, R. F. & SMALLEY, R. E. (1985) C_{60}: Buckminsterfullerene. *Nature,* 318, 162-163.

KUAN, Y.-J., CHARNLEY, S. B., HUANG, H.-C., TSENG, W.-L. & KISIEL, Z. (2003) Interstellar Glycine. *Astrophys. J.,* 593, 848-867.

KUBOTA, K. (2001) From tumor biology to clinical PET: A review of positron emission tomography (PET) in oncology. *Ann. Nucl. Med.,* 15, 471-486.

KWOK, S. (2004) The synthesis of organic and inorganic compounds in evolved stars. *Nature,* 430, 985-990.

LADA, C. J. & LADA, E. A. (2003) Embedded Clusters in Molecular Clouds. *Ann. Rev. Astro. Astrophys.*, 41, 57-115.

LANGER, W. D., van DISHOECK, E. F., BERGIN, E. A., BLAKE, G. A., TIELENS, A. G. G. M., VELUSAMY, T. & WHITTETT, D. C. B. (2000) Chemical Evolution of Protostellar Matter *in* MANNINGS, V., BOSS, A. P. & RUSSELL, S. S. (Eds.) *Protostars and Planets IV.* Tuscon, University of Arizona Press.

LARNØY, E., EIKENES, M. & MILITZ, H. (2011) Detection of chlorine-labelled chitosan in Scots Pine by energy-dispersive X-ray spectroscopy. *Wood Sci. Technol.*, 45, 103-110.

LARSEN, J. W., PAN, C.-S. & SHAWVER, S. (1989) Effect of Demineralization on the Macromolecular Structure of Coals. *Energy and Fuels,* 3, 557-561.

LAWLESS, J. G. & YUEN, G. U. (1979) Quantification of monocarboxylic acids in the Murchison carbonaceous meteorite. *Nature,* 282, 396-398.

LAWLESS, J. G., ZEITMAN, B., PEREIRA, W. E., SUMMONS, R. E. & DUFFIELD, A. M. (1974) Dicarboxylic acids in the Murchison meteorite. *Nature,* 251, 40-41.

LEE, C.-W., KIM, J.-K., MOON, E.-S., MINH, Y. C. & KANG, H. (2009) Formation of Glycine on Ultraviolet-Irradiated Interstellar ice-analog films and implications for interstellar amino acids. *Astrophys. J.,* 697, 428-435.

LEWIS, R. S., SRINIVASAN, B. & ANDERS, E. (1975) Host Phase of a Strange Xenon Component in Allende. *Science,* 190, 1251-1262.

LEYTON, P. (2012) The role of minerals on prebiotic synthesis Comment on "Formamide and the origin of life" by R. Saladino *et al. Phys. Life Revs.*, 9, 116-117.

LODDERS, K. (2003) Solar System Abundances and Condensation Temperatures of the Elements. *Astrophys. J.,* 591, 1220-1247.

LODDERS, K. (2008) Circumstellar Chemistry and Dust from Dead Stars in Meteorites. *in* ZAIKOWSKI, L. & FRIEDRICH, J. M. (Eds.) *Chemical Evolution across Space and Time.* Washington, American Chemical Society.

LODDERS, K. & FEGLEY, B., JR (1999) Condensation Chemistry of Circumstellar Grains. *in* LE BERTRE, T., LÈBRE, A. & WAELKENS, C. (Eds.) *Asymptotic Giant Branch Stars.* International Astronomical Union.

LODDERS, K. & OSBORNE, R. (1999) Perspectives on the Comet-Asteroid-Meteorite link. *Space Sci. Rev.*, 90, 289-297.

LONG, D. A. (2002) *The Raman Effect - A Unified Treatment of the Theory of Raman Scattering by Molecules,* Chichester, Wiley.

MACKINTOSH, R., STANNARD, R., EVANS, T., FIRTH, L. & SCHUTZ, B. (2005) *Cosmology and the Universe (S357 Block 4),* Milton Keynes, The Open University.

MACPHERSON, G. J. (2005) Calcium-Aluminium-Rich Inclusions in Chondritic Meteorites. *in* DAVIS, A. M. (Ed.) *Treatise on Geochemistry Vol 1.* Oxford, Elsevier.

MARROCCHI, Y., DERENNE, S., MARTY, B. & ROBERT, F. (2005) Interlayer trapping of noble gases in insoluble organic matter of primitive meteorites. *Earth Planet. Sci. Lett.*, 236, 569-578.

MARTINS, Z., WATSON, J. S., SEPHTON, M. A., BOTTA, O., EHRENFREUD, P. & GILMOUR, I. (2006) Free dicarboxylic and aromatic acids in the carbonaceous chondrites Murchison and Orgueil. *Meteorit. Planet. Sci.*, 41, 1073-1080.

MASON, B. (1962) The Classification of Chondritic Meteorites. *Am. Mus. Novitates*, 1-20.

MASON, B. (1963) The Carbonaceous Chondrites. *Space Sci. Rev.*, 1, 621-646.

MATTHEWMAN, R., MARTINS, Z. & SEPHTON, M. A. (2013) Type IV Kerogens as Analogues for Organic Macromolecular Materials in Aqueously Altered Carbonaceous Chondrites. *Astrobiology,* 13, 324-333.

McCREERY, R. L. (2000) *Raman Spectroscopy for Chemical Analysis,* New York, Wiley Interscience.

McSWEEN, H. Y., JR (1999) *Meteorites and Their Parent Planets,* Cambridge, Cambridge University Press.

MENDYBAEV, R. A., BECKETT, J. R., GROSSMAN, L., STOLPER, E., COOPER, R. F. & BRADLEY, J. P. (2002) Volatilization kinetics of silicon carbide in reducing gases: An experimental study with applications to the survival of presolar grains in the solar nebula. *Geochim. Cosmochim. Acta,* 66, 661-682.

MENNELLA, V., COLANGELI, L., BRUCATO, J. R., EPIFANI, E., PALOMBA, E., PALUMBO, P. & ROTUNDI, A. (1999) Carbonaceous Grain Processing in Space and in the Laboratory. *Adv. Space Res.,* 24, 439-442.

MERRILL, P. W. (1952) Spectroscopic observations of stars of Class S. *Astrophys. J.,* 116, 21-26.

MESSENGER, S., SANDFORD, S. & BROWNLEE, D. (2006) The Population of Starting Materials Available for Solar System Construction. *in* LAURETTA, D. S. & McSWEEN, H. Y., JR (Eds.) *Meteorites and the Early Solar System II.* Tucson, University of Arizona Press.

METZLER, K., BISCHOFF, A. & STÖFFLER, D. (1992) Accretionary dust mantles in CM chondrites: Evidence for solar nebula processes. *Geochim. Cosmochim. Acta,* 56, 2873-2897.

MILLAR, T. J., BENNETT, A. & HERBST, E. (1989) Deuterium Fractionation in Dense Interstellar Clouds. *Astrophys. J.,* 340, 906-920.

MILODOWSKI, A. E. & MORGAN, D. J. (1980) Identification and estimation of carbonate minerals at low levels by CO_2 analysis. *Nature,* 286, 248-249.

MOLDOVEANU, S. C. (1998) *Analytical Pyrolysis of Natural Organic Polymers,* Amsterdam, Elsevier.

MONTGOMERY, W., TUFF, J., KOHN, S. C. & JONES, R. L. (2011) Reactions between organic acids and montmorillonite clay under Earth-forming conditions. *Chem. Geol.,* 283, 171-176.

MORGAN, W. A., FEIGELSON, E. D., WANG, H. & FRENKLACH, M. (1991) A New Mechanism for the Formation of Meteoritic Kerogen-Like Material *Science,* 252, 109-112.

MORLOK, A., BISCHOFF, A., STEPHAN, T., FLOSS, C., ZINNER, E. & JESSBERGER, E. K. (2006) Brecciation and chemical heterogeneities of CI chondrites. *Geochim. Cosmochim. Acta,* 70, 5371-5394.

MOSELEY, H. G. J. (1913) XCIII. The High-frequency spectra of the elements. *Philosophical Magazine Series 6,* 26, 1024-34.

MUIRHEAD, D. K., PARNELL, J., TAYLOR, C. & BOWDEN, S. A. (2012) A kinetic model for the thermal evolution of sedimentary and meteoritic organic carbon using Raman spectroscopy. *J. Anal. Appl. Pyrolysis,* 96, 153-161.

MURAE, T. (1995) Characterization of extraterrestrial high-molecular-weight organic matter by pyrolysis-gas chromatography/mass spectrometry. *J. Anal. Appl. Pyrolysis,* 32, 65-73.

NAGY, B., MEINSCHEIN, W. G. & HENNESSY, D. J. (1961) Mass Spectroscopic Analysis of the Orgueil Meteorite: Evidence for Biogenic Hydrocarbons. *Ann. New York Acad. Sci.,* 93, 27-35.

NAKAMURA-MESSENGER, K., MESSENGER, S., KELLER, L. P., CLEMETT, S. J. & ZOLENSKY, M. E. (2006) Organic Globules in the Tagish Lake Meteorite: Remnants of the Protosolar Disk. *Science,* 314, 1439-1442.

NAKAMURA, K., ZOLENSKY, M. E., TOMITA, S., NAKASHIMA, S. & TOMEOKA, K. (2002) Hollow organic globules in the Tagish Lake meteorite as possible products of primitive organic reactions. *Int. J. Astrobiol.,* 1, 179-189.

NICHOLS, R. H., JR (2006) Chronological Constraints on Planetesimal Accretion. *in* LAURETTA, D. S. & McSWEEN, H. Y., JR (Eds.) *Meteorites and the Early Solar System II.* Tucson, University of Arizona Press.

NOVAK, R. E., MUMMA, M. J., DISANTI, M. A., DELLO RUSSO, N. & MAGEE-SAUER, K. (2002) Mapping of Ozone and Water in the Atmosphere of Mars near the 1997 Aphelion. *Icarus,* 158, 14-23.

NOVOSELOV, K. S., JIANG, D., SCHEDIN, F., BOOTH, T. J., KHOTKEVICH, V. V., MOROZOV, S. V. & GEIM, A. K. (2005) Two-dimensional atomic crystals. *Proc. Natl. Acad. Sci.*, 102, 10451-10453.

NUTH, J. A., III, CHARNLEY, S. B. & JOHNSON, N. M. (2006) Chemical Processes in the Interstellar Medium: Source of the Gas and Dust in the Primitive Solar Nebula. *in* LAURETTA, D. S. & McSWEEN, H. Y., JR (Eds.) *Meteorites and the Early Solar System II.* Tucson, University of Arizona Press.

NUTH, J. A., III & JOHNSON, N. M. (2012) Transformation of Graphitic and Amorphous Carbon Dust to Complex Organic Molecules in a Massive Carbon Cycle in Protostellar Nebulae. *75th Meteoritical Society Conference. Abstract 5070*

OKUMURA, F. & MIMURA, K. (2011) Gradual and stepwise pyrolyses of insouble organic matter from the Murchison meteorite revealing chemical structure and isotopic distribution. *Geochim. Cosmochim. Acta,* 75, 7063-7080.

OTT, U., KEPPLER, F., VIGANO, I., MCLEOD, A., FRÜCHTL, M. & RÖCKMANN, T. (2012) UV-radiation induced methane emission from Murchison - possible implications for methane in the Martian atmosphere. *75th Meteoritical Society Meeting. Abstract 5133*

OTT, U., MACK, R. & CHANG, S. (1981) Noble-gas-rich separates from the Allende meteorite. *Geochim. Cosmochim. Acta,* 45, 1751-1788.

PALME, H. & JONES, A. (2005) Solar System Abundances of the Elements. *in* DAVIS, A. M. (Ed.) *Treatise on Geochemistry Vol 1.* Oxford, Elsevier.

PAPIKE, J. J. (Ed.) (1998) *Planetary Materials,* Washington DC, Mineralogical Society of America.

PARKER, E. T., CLEAVES, H. J., DWORKIN, J. P., GLAVIN, D. P., CALLAHAN, M. P., AUBREY, A., LAZCANO, A. & BADA, J. L. (2011) Primordial synthesis of amines and amino acids in a 1958 Miller H_2S-rich spark discharge experiment. *Proc. Natl. Acad. Sci.,* 108, 5526-5531.

PASCOLI, G. & POLLEUX, A. (2000) Condensation and growth of hydrogenated carbon clusters in carbon-rich stars. *Astronomy and Astrophysics,* 359, 799-810.

PEARSON, V. K., GREENWOOD, R. C., MORGAN, G. H., TURNER, D., RAADE, G., ROALDSET, E. & GILMOUR, I. (2007a) Organic constitution of the CO3 chondrites and implications for asteroidal processes. *38th Lunar and Planetary Science Conference. Abstract 1846*

PEARSON, V. K., KEARSLEY, A. T., SEPHTON, M. A. & GILMOUR, I. (2007b) The labelling of meteoritic organic material using osmium tetroxide vapour impregnation. *Planet. Space Sci.,* 55, 1310-1318.

PEARSON, V. K., SEPHTON, M. A., FRANCHI, I. A., GIBSON, J. M. & GILMOUR, I. (2006) Carbon and nitrogen in carbonaceous chondrites: Elemental abundances and stable isotopic compositions. *Meteorit. Planet. Sci.,* 41, 1899-1918.

PEARSON, V. K., SEPHTON, M. A. & GILMOUR, I. (2002) Organic indicators of alteration in the CR chondrites. *33rd Lunar and Planetary Science Conference. Abstract 1670*

PEARSON, V. K., WILSON, R. C. & GILMOUR, I. (2009) Extraterrerestrial Organic Matter as recorded in Meteorites. *in* BASIUK, V. A. (Ed.) *Astrobiology: Emergence, Search and Detection of Life.*

PELTONEN, L. & HIRVONEN, J. (2010) Pharmaceutical nanocrystals by nanomilling: critical process parameters, particle fracturing and stabilization methods. *J. Pharm. Pharm.,* 62, 1569-1579.

PETTINI, M. & BOWEN, D. V. (2001) A New measurement of the Primordial Abundance of Deuterium: Toward convergence with the Baryon Density from the Cosmic Microwave Background? *Astrophys. J.,* 560, 41-48.

PIPER, J. (2008) Use of Software to Enhance Depth of Field and Improve Focus in Photomicrography. *Microscopy and Analysis,* 22, 15-19.

PIZZARELLO, S. (2006) The Chemistry of Life's Origin: A Carbonaceous Meteorite Perspective. *Acc. Chem. Res.,* 39, 231-237.

PIZZARELLO, S., HUANG, Y. & ALEXANDRE, M. R. (2008) Molecular asymmetry in extraterrestrial chemistry: Insights from a pristine meteorite. *Proc. Natl. Acad. Sci.*, 105, 3700-3704.

PIZZARELLO, S., SCHRADER, D. L., MONROE, A. A. & LAURETTA, D. S. (2012) Large enantiomeric excesses in primitive meteorites and the diverse effects of water in cosmochemical evolution. *Proc. Natl. Acad. Sci.*, 109, 11949-11954.

POTGIETER-VERMAAK, S., MALEDI, N., WAGNER, N., van HEERDEN, J. H. P., van GRIEKEN, R. & POTGIETER, J. H. (2011) Raman spectroscopy for the analysis of coal: a review. *J. Raman Spectrosc.*, 42, 123-129.

PRASAD, S. S. & HUNTRESS, W. T., JR (1980a) A Model for Gas phase chemistry in interstellar clouds. II. Nonequilibrium effects and effects of temperature and activation energies. *Astrophys. J.*, 239, 151-165.

PRASAD, S. S. & HUNTRESS, W. T., JR (1980b) A Model for Gas Phase Chemistry in Interstellar Clouds: I. The basic model, library of chemical reactions and chemistry among C, N, and O Compounds. *Astrophys. J. Suppl. Series*, 43, 1-35.

PRASAD, S. S. & HUNTRESS, W. T., JR (1982) Sulfur chemistry in dense interstellar clouds. *Astrophys. J.*, 260, 590-598.

PRINN, R. G. (1993) Chemistry and Evolution of Gaseous Circumstellar disks. *in* LEVY, E. H. & LUNINE, J. I. (Eds.) *Protostars and Planets III.* Tucson, University of Arizona Press.

PRINN, R. G. & FEGLEY, B., JR (1987) The atmospheres of Venus, Mars and Earth: A critical comparison. *Ann. Rev. Earth Planet. Sci.*, 15, 171-212.

PRYOR, W. A., GLEICHER, G. J. & CHURCH, D. F. (1983) Reaction of Polycyclic Aromatic Hydrocarbons with Ozone. Linear Free-Energy Relationships and Tests of Likely Rate-Determining Steps Using Simple Molecular Orbital Correlations. *J. Org. Chem.*, 48, 4198-4202.

PYE, K. & KRINSLEY, D. H. (1984) Petrographic Examination of Sedimentary Rocks in the SEM using Backscattered Electron Detectors. *J. Sed. Pet.*, 54, 877-888.

QUIRICO, E. & BONAL, L. (2004) An infrared study of the matrices of CI1 and CM2 Chondrites. *35th Lunar and Planetary Science Conference. Abstract 1803*

QUIRICO, E., BORG, J., RAYNAL, P.-I., MONTAGNAC, G. & d'HENDECOURT, L. (2005a) A micro-Raman survey of 10 IDPs and 6 carbonaceous chondrites. *Planet. Space Sci.*, 53, 1443-1448.

QUIRICO, E., MONTAGNAC, G., ROUZAUD, J.-N., BONAL, L., BOUROT-DENISE, M., DUBER, S. & REYNARD, B. (2009) Precursor and metamorphic condition effects on Raman spectra of poorly ordered carbonaceous matter in chondrites and coals. *Earth Planet. Sci. Lett.*, 287, 185-193.

QUIRICO, E., RAYNAL, P.-I. & BOUROT-DENISE, M. (2003) Metamorphic grade of organic matter in six unequilibrated ordinary chondrites. *Meteorit. Planet. Sci.*, 38, 795-811.

QUIRICO, E., ROUZAUD, J.-N., BONAL, L. & MONTAGNAC, G. (2005b) Maturation grade of coals as revealed by Raman spectroscopy: Progress and problems. *Spectro. Acta A*, 61, 2368-2377.

REIMER, L. (1998) *Scanning Electron Microscopy - Physics of Image Formation and Microanalysis,* Berlin, Springer Verlag.

REMUSAT, L., DERENNE, S. & ROBERT, F. (2005a) New insight on aliphatic linkages in the macromolecular organic fraction of Orgueil and Murchison meteorites through ruthenium tetroxide oxidation. *Geochim. Cosmochim. Acta*, 69, 4377-4386.

REMUSAT, L., DERENNE, S., ROBERT, F. & KNICKER, H. (2005b) New pyrolyic and spectroscopic data on Orgueil and Murchison insoluble organic matter: A different origin than soluble. *Geochim. Cosmochim. Acta*, 69, 3919-3932.

REMUSAT, L., ROBERT, F., MEIBOM, A., MOSTEFAOUI, S., DELPOUX, O., BINET, L., GOURIER, D. & DERENNE, S. (2009) Proto-planetary disk chemistry recorded by D-Rich Organic radicals in carbonaceous chondrites. *Astrophys. J.*, 698, 2087-2092.

ROBL, T. L. & DAVIS, B. H. (1993) Comparison of the HF-HCl and HF-BF_3 maceration techniques and the chemistry of resultant organic concentrates. *Org. Geochem.*, 20, 24-255.

RUBIN, R. H., SWENSON, G. W., JR, BENSON, R. C., TIGELAAR, H. L. & FLYGARE, W. H. (1971) Microwave detection of interstellar formamide. *Astrophys. J.*, 169, L39-L44.

RÜDIGER, S. & SEPPELT, K. (1997a) On reaction sof carbon disulphide induced by "naked" fluoride Part 1: Reactions with fluoroaromatics. *J. Fluorine Chem.*, 82, 25-28.

RÜDIGER, S. & SEPPELT, K. (1997b) On reactions of carbon disulphide induced by "naked" fluoride Part 2: reactions with 2-H-heptafluoropropane, hexafluoropropene and bis (2,2,2-trifluoroethyl)amine. *J. Fluorine Chem.*, 82, 29-32.

RYAN, S., HASWELL, C. & KOLB, I. (2002) *The Life and Death of Stars,* Milton Keynes, The Open University.

SALADINO, R., CRESTINI, C., COSSETTI, C., Di MAURO, E. & DEAMER, D. (2011) Catalytic effects of Murchison Material: Prebiotic Synthesis and Degradation of RNA Precursors. *Orig. Life Evol. Biosphere,* 41, 437-451.

SALADINO, R., CRESTINI, C., PINO, S., COSTANZO, G. & Di MAURO, E. (2012a) Formamide and the origin of life. *Phys. Life Revs.*, 9, 84-104.

SALADINO, R., CRESTINI, C., PINO, S., COSTANZO, G. & Di MAURO, E. (2012b) Formamide in non-life/life transition. *Phys. Life Revs.*, 9, 121-123.

SANDFORD, S. A. (1996) The inventory of interstellar materials available for the formation of the solar system. *Meteorit. Planet. Sci.*, 31, 449-476.

SANDFORD, S. A., ALÉON, J., ALEXANDER, C. M. O'D., ARAKI, T., BAJT, S., BARATTA, G. A., BORG, J., BRADLEY, J. P., BROWNLEE, D. E., BRUCATO, J. R., BURCHELL, M. J., BUSEMANN, H., BUTTERWORTH, A., CLEMETT, S. J., CODY, G., COLANGELI, L., COOPER, G., d'HENDECOURT, L., DJOUADI, Z., DWORKIN, J. P., FERRINI, G., FLECKENSTEIN, H., FLYNN, G. J., FRANCHI, I. A., FRIES, M., GILLES, M. K., GLAVIN, D. P., GOUNELLE, M., GROSSEMY, F., JACOBSEN, C., KELLER, L. P., KILCOYNE, A. L. D., LEITNER, J., MATRAJT, G., MEIBOM, A., MENNELLA, V., MOSTEFAOUI, S., NITTLER, L. R., PALUMBO, M. E., PAPANASTASSIOU, D. A., ROBERT, F., ROTUNDI, A., SNEAD, C. J., SPENCER, M. K., STADERMANN, F. J., STEELE, A., STEPHAN, T., TSOU, P., TYLISZCZAK, T., WESTPHAL, A. J., WIRICK, S., WOPENKA, B., YABUTA, H., ZARE, R. N. & ZOLENSKY, M. E. (2006) Organics captured from Comet 81P/Wild 2 by the Stardust Spacecraft. *Science,* 314, 1720-1724.

SCHMITT-KOPPLIN, P., GABELICA, Z., GOUGEON, R. D., FEKETE, A., KANAWATI, B., HARIR, M., GEBEFUEGI, I., ECKEL, G. & HERTKORN, N. (2010) High molecular diversity of extraterrestrial organic matter in Murchison meteorite revealed 40 years after its fall. *Proc. Natl. Acad. Sci.*, 107, 2763-2768.

SCHÖLER, H. F., NKUSI, G., NIEDAN, V. W., MÜLLER, G. & SPITTHOFF, B. (2005) Screening of organic halogens and identification of chlorinated benzoic acids in carbonaceous meteorites. *Chemosphere,* 60, 1505-1512.

SCHÜTT, H.-W. (2003) Chemical Atomism and Chemical Classification. *in* NYE, M. J. (Ed.) *The Cambridge History of Science.* Cambridge, Cambridge University Press.

SCHUTTE, W. A., ALLAMANDOLA, L. J. & SANDFORD, S. A. (1993) An Experimental Study of the Organic Molecules Produced in Cometary and Interstellar Ice Analogs by Thermal Formaldehyde Reactions. *Icarus,* 104, 118-137.

SCOTT, E. R. D. & KROT, A. N. (2005) Chondrites and their components. *in* DAVIS, A. M. (Ed.) *Treatise on Geochemistry Vol 1.* Oxford, Elsevier.

SEARS, D. W. G., BENOIT, P. H. & JIE, L. (1993) Two chondrule groups each with distinctive rims in Murchison recognised by cathodoluminescence. *Meteoritics,* 28, 669-675.

SELLGREN, K., BROOKE, T. Y., SMITH, R. G. & GEBALLE, T. R. (1995) A new 3.25 micron absorption feature towards Monoceros R2/IRS 3. *Astrophys. J.,* 449, L69-L72.

SEPHTON, M. A. (2002) Organic compounds in carbonaceous meteorites. *Nat. Prod. Rep.,* 19, 292-311.

SEPHTON, M. A. (2005) Organic matter in carbonaceous meteorites: past, present and future research. *Phil. Trans. Roy. Soc. London,* 363, 2729-2742.

SEPHTON, M. A. (2012) Pyrolysis and Mass Spectrometry Studies of Meteoritic Organic Matter. *Mass Spec. Reviews,* 31, 560-569.

SEPHTON, M. A., LOVE, G. D., MEREDITH, W., SNAPE, C. E., SUN, C.-G. & WATSON, J. S. (2005) Hydropyrolysis: A new technique for the analysis of macromolecular material in meteorites. *Planet. Space Sci.,* 53, 1280-1286.

SEPHTON, M. A., LOVE, G. D., WATSON, J. S., VERCHOVSKY, A. B., WRIGHT, I. P., SNAPE, C. E. & GILMOUR, I. (2004a) Hydropyrolysis of insoluble carbonaceous matter in the Murchison meteorite: New insights into its macromolecular structure. *Geochim. Cosmochim. Acta,* 68, 1385-1393.

SEPHTON, M. A., PILLINGER, C. T. & GILMOUR, I. (1994) Pyrolysis typing of meteoritic organic matter. *25th Lunar and Planetary Science Conference. Abstract 1247*

SEPHTON, M. A., PILLINGER, C. T. & GILMOUR, I. (2001) Normal alkanes in meteorites: molecular $\delta^{13}C$ values indicate an origin by terrestrial contamination. *Precambrian research,* 106, 47-58.

SEPHTON, M. A., VERCHOVSKY, A. B., BLAND, P. A., GILMOUR, I., GRADY, M. M. & WRIGHT, I. P. (2003) Investigating the variations in carbon and nitrogen isotopes in carbonaceous chondrites. *Geochim. Cosmochim. Acta,* 67, 2093-2108.

SEPHTON, M. A., VERCHOVSKY, A. B. & WRIGHT, I. P. (2004b) Carbon and nitrogen isotope ratios in meteoritic organic matter. *Int. J. Astrobiol.,* 3, 221-227.

SEPHTON, M. A., WRIGHT, I. P., GILMOUR, I., DE LEEUW, J. W., GRADY, M. M. & PILLINGER, C. T. (2002) High molecular weight organic matter in Martian meteorites. *Planet. Space Sci.,* 50, 711-716.

SHALABIEA, O. M. & GREENBERG, J. M. (1994) Two key processes in dust/gas chemical modelling: photoprocessing of grain mantles and explosive desorption. *Astronomy and Astrophysics,* 290, 266-278.

SHU, F. H., ADAMS, F. C. & LIZANO, S. (1987) Star formation in molecular clouds: Observation and Theory. *Ann. Rev. Astro. Astrophys.,* 25, 23-81.

SIEBENMORGEN, R. & KRÜGEL, E. (2010) The destruction and survival of polycyclic aromatic hydrocarbons in the disks of T Tauri stars. *Astronomy and Astrophysics,* 511, A6 1-8.

SIMAKOV, M. B. & KUZICHEVA, E. A. (2005) Abiogenic photochemical synthesis on surface of meteorites and other small space bodies. *Adv. Space Res.,* 36, 190-194.

SIMAKOV, M. B., KUZICHEVA, E. A., ANTROPOV, E. A. & DODONOVA, N. Y. (2002) Abiogenic synthesis of nucleotides on the surface of small space bodies with high energy particles. *Adv. Space Res.,* 30, 1489-1494.

SKINNER, W. R. (1989) Compaction and Lithification of Chondrites. *20th Lunar and Planetary Science Conference. Abstract 1026*

SMITH, J. W. & KAPLAN, I. R. (1970) Endogenous Carbon in Carbonaceous Meteorites. *Science,* 167, 1367-1370.

SNOW, T. P. (2001) The unidentified diffuse interstellar bands as evidence for large organic molecules in the interstellar medium. *Spectro. Acta A,* 57, 615-626.

SNYDER, L. E., LOVAS, F. J., HOLLIS, J. M., FRIEDEL, D. N., JEWELL, P. R., REMIJAN, A., ILYUSHIN, V. V., ALEKSEEV, E. A. & DYUBKO, S. F. (2005) A Rigorous Attempt to Verify Interstellar Glycine. *Astrophys. J.,* 619, 914-930.

SPENCER, M. K., HAMMOND, M. R. & ZARE, R. N. (2008) Laser mass spectrometric detection of extraterrestrial aromatic molecules: Mini-review and examination of pulsed heating effects. *Proc. Natl. Acad. Sci.,* 105, 18096-18101.

STAUNTON, J. & WEISSMAN, K. J. (2001) Polyketide biosynthesis: a millennium review. *Nat. Prod. Rep.,* 18, 380-416.

STUDIER, M. H., HAYATSU, R. & ANDERS, E. (1972) Origin of organic matter in early solar system-V. Further studies of meteoritic hydrocarbons and a discussion of their origin. *Geochim. Cosmochim. Acta,* 36, 189-215.

SZATHMÁRY, E. (2005) In search of the simplest cell. *Nature,* 433, 469-470.

TAKABAYASHI, S., OKAMOTO, K., MOTOYAMA, H., NAKATANI, T., SAKAUE, H. & TAKAHAGI, T. (2010) X-ray photoelectron analysis of surface functional groups on diamond-like carbon films by gas-phase chemical derivatization method. *Surf. Interface Anal.,* 42, 77-87.

TAKAHAGI, T. & ISHITANI, A. (1988) XPS Study on the Surface Structure of Carbon Fibres using Chemical Modification and C1s Line Shape Analysis. *Carbon,* 26, 389-396.

TIELENS, A. G. G. M. (2005) *The Physics and Chemistry of the Interstellar Medium,* Cambridge, Cambridge University Press.

TRAVIS, B. J. & SCHUBERT, G. (2005) Hydrothermal convection in carbonaceous chondrite bodies. *Earth Planet. Sci. Lett.,* 240, 234-250.

TUCKER, M. E. (1991) *Sedimentary Petrology,* Durham, Blackwell Science Ltd.

TYTLER, D., O'MEARA, J. M., SUZUKI, N. & LUBIN, D. (2000) Review of Big Bang Nucleosynthesis and Primordial Abundances. *Physica Scripta,* T85, 12-31.

UDENFRIEND, S., STEIN, S., BÖHLEN, P., DAIRMAN, W., LEIMGRUBER, W. & WEIGELE, M. (1972) Fluorescamine: A Reagent for Assay of Amino Acids, Peptides, Proteins and Primary Amies in the Picomole Range. *Science,* 178, 871-872.

van den BERG, M. L. J., MULDER, G. J., De LEEUW, J. W. & SCHENCK, P. A. (1977) Investigations into the structure of kerogen-I. Low temperature ozonolysis of Messel shale kerogen. *Geochim. Cosmochim. Acta,* 41, 903-908.

van DISHOECK, E. F. (2004) ISO Spectroscopy of Gas and Dust: From Molecular Clouds to Protoplanetary disks. *Ann. Rev. Astro. Astrophys.,* 42, 119-167.

van DISHOECK, E. F., BLAKE, G. A., DRAINE, B. T. & LUNINE, J. I. (1993) The chemical evolution of protostellar and protoplanetary matter. *in* LEVY, E. H. & LUNINE, J. I. (Eds.) *Protostars and Planets III.* Tucson, University of Arizona Press.

van ORNUM, S. G., CHAMPEAU, R. M. & PARIZA, R. (2006) Ozonolysis Applications in Drug Synthesis. *Chem. Rev.,* 106, 2990-3001.

van SCHMUS, W. & WOOD, J. A. (1967) A chemical-petrologic classification of the chondritic meteorites. *Geochim. Cosmochim. Acta,* 31, 747-765.

VARMA, R. S. (2002) Clay and clay-supported reagents in organic synthesis. *Tetrahedron,* 58, 1235-1255.

VELBEL, M. A., LONG, D. T. & GOODING, J. L. (1991) Terrestrial weathering of Antarctic stone meteorites: Formation of Mg-carbonates on ordinary chondrites. *Geochim. Cosmochim. Acta,* 55, 67-76.

VERCHOVSKY, A. B., FISENKO, A. V., SEMJONOVA, L. F. & PILLINGER, C. T. (1997) Heterogenous distribution of Xe-HL within Presolar Diamonds. *60th Meteoritical Society Meeting. Abstract 5217*

VERCHOVSKY, A. B., PEARSON, V. K., FISENKO, A. V., SEMENOVA, L. F., SEPHTON, M. A. & WRIGHT, I. P. (2012) Separation of Q from Carbon in CR meteorites during stepped combustion. *43rd Lunar and Planetary Science Conference. Abstract 2645*

WALLIS, P. J., GATES, W. P., PATTI, A. F., SCOTT, J. L. & TEOH, E. (2009) Assessing and improving the catalytic activity of K-10 montmorillonite. *Green Chem,* 9.

WAMPLER, T. P. (Ed.) (2007) *Applied Pyrolysis Handbook,* Boca Raton, CRC Press.

WANG, Y., ALSMEYER, D. C. & McCREERY, R. L. (1990) Raman Spectroscopy of Carbon Materials: Structural Basis of Observed Spectra. *Chem. Mater.,* 2, 557-563.

WATSON, J. S., PEARSON, V. K., GILMOUR, I., PILLINGER, C. T., TURNER, D., PERKINS, R. & MORGAN, G. H. (2005a) Pyrolysis-GCxGC-TOFMS to Characterise Carbonaceous Chondrites. *36th Lunar and Planetary Science Conference. Abstract 1829*

WATSON, J. S., PEARSON, V. K., GILMOUR, I. & SEPHTON, M. A. (2003) Contamination by sesquiterpenoid derivatives in the Orgueil carbonaceous chondrite. *Org. Geochem.*, 34, 37-47.

WATSON, J. S., PEARSON, V. K., SEPHTON, M. A. & GILMOUR, I. (2004) Molecular, isotopic and in situ analytical approaches to the study of meteoritic organic material. *Int. J. Astrobiol.*, 3, 107-116.

WATSON, J. S., SEPHTON, M. A. & GILMOUR, I. (2005b) Macromolecular organic acids in the Murchison meteorite. *36th Lunar and Planetary Science Conference. Abstract 1842*

WATSON, J. S., SEPHTON, M. A. & GILMOUR, I. (2010) Thermolysis of the Murchison meteorite: identification of oxygen bound and occluded units in the organic macromolecule. *Int. J. Astrobiol.*, 9, 201-208.

WATSON, J. S., TURNER, D. C., GILMOUR, I., SEPHTON, M. A. & MORGAN, G. H. (2007) Application of GCxGC-TOFMS in the analysis of Meteoritic Organic Macromolecules. *23rd International Meeting on Organic Geochemistry.* Torquay.

WATSON, J. T. & SPARKMAN, O. D. (2007) *Introduction to Mass Spectrometry,* Hoboken, NJ, Wiley.

WDOWIAK, T. J., AGRESTI, D. G. & MIROV, S. B. (1995a) A Laser Raman Spectrometer System Suitable for Incorporation into Lander Spacecraft. *26th Lunar and Planetary Science Conference. Abstract 1473*

WDOWIAK, T. J., LEE, W., CRONIN, J., BEEGLE, L. W. & ROBINSON, M. S. (1995b) Plasma processing of interstellar PAHs into solar system kerogen. *Planet. Space Sci.*, 43, 1175-1182.

WEIDENSCHILLING, S. J. (2011) Initial sizes of planetesimals and accretion of the asteroids. *Icarus,* 214, 671-684.

WICKRAMASINGHE, C. (2009) Life on Earth: Did it come from other Planets? *J. Cosmology,* 1, 76-80.

WIIK, H. B. (1956) The chemical composition of some stony meteorites. *Geochim. Cosmochim. Acta,* 9, 279-289.

WILLIAMS, A. & IBRAHIM, I. T. (1981) Carbodiimide Chemistry: Recent Advances. *Chem. Rev.*, 81, 589-636.

WILLIAMS, J. C. & KELLY, G. B., JR (1976) Method of Deacidifying Paper. US Patent 3969549.

WILLIAMS, J. P., BLITZ, L. & MCKEE, C. F. (2000) The structure and evolution of molecular clouds: From clumps to cores to the IMF. *in* MANNINGS, V., BOSS, A. P. & RUSSELL, S. S. (Eds.) *Protostars and Planets IV.* Tucson, University of Arizona Press.

WILSON, R. (2009) Organic Material in Micrometeorites: Processes Affecting its Delivery to Planetary Environments. Ph.D Thesis, *PSSRI,* Milton Keynes, Open University.

WING, M. R. & BADA, J. L. (1991) Geochromatography on the parent body of the carbonaceous chondrite Ivuna. *Geochim. Cosmochim. Acta,* 55, 2937-2942.

WINTERHALTER, R., HERRMANN, F., KANAWATI, B., NGUYEN, T. L., PEETERS, J., VEREECKEN, L. & MOORTGAT, G. (2009) The gas-phase ozonolysis of β-caryophyllene (C15H24). Part I: an experimental study. *Phys. Chem. Chem. Phys.*, 11, 4152-4172.

WIRICK, S., FLYNN, G. J., JACOBSEN, C. & KELLER, L. P. (2006) Organics in the Murchison Meteorite using Carbon XANES Spectroscopy. *37th Lunar and Planetary Science Conference. Abstract 1418*

WOOD, J. A. & MORFILL, G. E. (1988) A review of solar nebula models. *in* KERRIDGE, J. F. (Ed.) *Meteorites and the Early Solar System.* Tucson, University of Arizona Press.

WOPENKA, B. & PASTERIS, J. D. (1993) Structural characterization of kerogens to granulite-facies graphite: Applicability of Raman microprobe spectroscopy. *American Mineralogist,* 78, 533-557.

WRIGHT, I. P., BOYD, S. R., FRANCHI, I. A. & PILLINGER, C. T. (1988) High-precision determination of nitrogen stable isotope ratios at the sub-nanomole level. *J. Phys. E: Sci. Instrum.,* 21, 865-875.

WRIGHT, I. P. & PILLINGER, C. T. (1988) Carbon Isotopic Analysis of Small Samples by Use of Stepped-Heating Extraction and Static Mass Spectrometry. *in* SHANKS, W. C., III & CRISS, R. E. (Eds.) *New Frontiers in Stable Isotopic Research: Laser Probes, Ion Probes and Small-Sample Analysis.*

YUEN, G. U. & KVENVOLDEN, K. A. (1973) Monocarboxylic Acids in Murray and Murchison Carbonaceous Chondrites. *Nature,* 246, 301-303.

YURIMOTO, H., ABE, K.-I., ABE, M., EBIHARA, M., FUJIMURA, A., HASHIGUCHI, M., HASHIZUME, K., IRELAND, T. R., ITOH, S., KATAYAMA, J., KATO, C., KAWAGUCHI, J., KAWASAKI, N., KITAJIMA, F., KOBAYASHI, S., MEIKE, T., MUKAI, T., NAGAO, K., NAKAMURA, T., NARAOKA, H., NOGUCHI, T., OKAZAKI, R., PARK, C., SAKAMOTO, N., SETO, Y., TAKEI, M., TSUCHIYAMA, A., UESUGI, M., WAKAKI, S., YADA, T., YAMAMOTO, K., YOSHIKAWA, M. & ZOLENSKY, M. E. (2011) Oxygen Isotopic Compositions of Asteroidal Materials Returned from Itokawa by the Hayabusa Mission. *Science,* 333, 1116-1120.

ZEGA, T. J., NITTLER, L. R., BUSEMANN, H., HOPPE, P. & STROUD, R. M. (2007) Coordinated isotopic and mineralogic analyses of planetary materials enabled by in situ lift-out with a focused ion beam scanning electron microscope. *Meteorit. Planet. Sci.,* 42, 1373-1386.

ZINNER, E. (2005) Presolar Grains. *in* DAVIS, A. M. (Ed.) *Treatise on Geochemistry Vol 1.* Oxford, Elsevier.

ZOLENSKY, M., BARRETT, R. & BROWNING, L. (1993) Mineralogy and composition of matrix and chondrule rims in carbonaceous chondrites. *Geochim. Cosmochim. Acta,* 57, 3123-3148.